DEPARTMENT OF THE NAVY · NAVAL POSTGRADUATE SCHOOL

LEVEL II

Proceedings

V/STOL AIRCRAFT
AERODYNAMICS

Volume II

Sponsored by

DDC

RECEIVE

JAN 8 1980

A
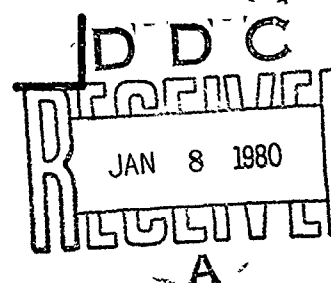
NAVAL AIR DEVELOPMENT CENTER

16 to 18 MAY 1979

NAVAL POSTGRADUATE SCHOOL

MONTEREY, CALIFORNIA

80 1

(6)

PROCEEDINGS OF A WORKSHOP

ON

V/STOL AIRCRAFT AERODYNAMICS

VOLUME II

HELD AT
NAVAL POSTGRADUATE SCHOOL
MONTEREY, CALIFORNIA,

MAY 16 - 18, 1979

(10) CHAIRMEN: C. HENDERSON, NADC
M. F. PLATZER, NPS

(11) 18 May '79   (12) 472

251 450

TABLE OF CONTENTS

OVERVIEW SESSION

---

[x] This presentation was based on a movie and therefore is not included
     in the proceedings.

MAIN PRESENTATIONS

VOLUME I

B. Session II:

Aerodynamics of VSTOL Aircraft in Hovering Flight

Chairman: Robert Weinraub, Naval Air Systems Command

x) Not submitted for publication

Contents:

→ next page

x) Not submitted for publication

viii

FOREWORD AND ACKNOWLEDGMENT

A Workshop on V/STOL Aircraft Aerodynamics, sponsored by the Naval Air Development Center, was held at the Naval Postgraduate School during May 16-18, 1979 for the purpose of information exchange, status review and identification of critical problems by technical specialists working in the fields of V/STOL aircraft aerodynamics, propulsion and flight mechanics.

The proceedings of the workshop contain the papers presented in the five sessions and a transcript of the panel discussion. It is hoped that this information will prove useful not only to the relatively small group of specialists working in the field of V/STOL aircraft aerodynamics but will also provide helpful stimulus to others who wish to inform themselves about this challenging frontier in aeronautical engineering.

A number of people contributed to the success of this workshop whose contributions are gratefully acknowledged. Mr. C. J. Mazza, Naval Air Development Center, initiated and supported this meeting. RADM T. F. Dedman, Superintendent of the Naval Postgraduate School, gave the welcome address which was very much appreciated. Sincere thanks are extended to the many participants, including our friends from the United Kingdom and Canada, and to the session chairmen for their individual contributions. Finally, we are much indebted to Mmes. Evelyn Basham and Janice Cicconi for their help in organizing the workshop, transcribing the tapes and assembling the written material.

C. HENDERSON
Naval Air Development Center

M. F. PLATZER
Naval Postgraduate School

LIST OF PARTICIPANTS

D. Adler
Israel Institute of Technology
Technion City, Haifa 32000
Israel

K. Aoyagi
Research Engineer
NASA Ames Research Center
Moffett Field, California 94035

H. Arnaiz
NASA Dryden Flight Research Center
P.O. Box 273
Edwards, California 93523

R. O. Bailey
Aircraft Aerodynamics Branch
NASA Ames Research Center
Moffett Field, California 94035

A. J. Baker
Computational Mechanics Consultants, Inc.
3601-A Chapman Highway
Knoxville, Tennessee 37920

J. P. Barrack
NASA Ames Research Center
Moffett Field, California 94035

T. D. Beatty
Vought Corporation
P.O. Box 5907
Dallas, Texas 75222

D. P. Bencze
Aircraft Aerodynamics Branch
NASA Ames Research Center
Moffett Field, California 94035

M. D. Betzina
Aerospace Engineer
Aeromechanics Laboratory
U.S. Army Research & Technology Laboratories
NASA Ames Research Center
Moffett Field, California 94035

Paul M. Bevilaqua
Rockwell International
Columbus, Ohio 43218

W. W. Bower
McDonnell-Douglas Research Laboratories
P.O. Box 516
St. Louis, Missouri 63166

A. L. Byrnes
Lockheed-California Company
Burbank, California 91520

R. L. Carmichael
Aircraft Aerodynamics Branch
NASA Ames Research Center
Moffett Field, California 94035

Y. T. Chin
Lockheed-California Company
Department 75/41
Bldg 63G, Plant A-1
P.O. Box 551
Burbank, California 91520

S. J. Craig
Systems Tech., Inc.
Hawthorne, California 90250

R. G. Culpepper
NASA Langley Research Center
Hampton, Virginia 23665

J. V. Davis
Naval Air Systems Command
PMA 269
Washington, DC 20361

J. T. DeLany
D/71-6
Rockwell International
Columbus Aircraft Division
4300 E. Fifth Avenue
P.O. Box 1259
Columbus, Ohio 43218

J. H. Diedrich
NASA-Lewis Research Center
Cleveland, Ohio 44135

M. E. Dillenius
Research Engineer
Nielsen Engineering & Research, Inc.
Mountain View, California 94043

L. Duke
NASA Dryden Flight Research Center
P.O. Box 273
Edwards, California 93523

T. Duvvuri
Duvvuri Research Associates
651 Windsor Circle
Chula Vista, California 92010

J. C. Erickson, Jr.
Aerodynamic Research Department
Calspan Corporation
Advanced Technology Center
Buffalo, New York 14225

L. L. Erickson
Aircraft Aerodynamics Branch
U.S. Army Research & Technology Labs.
Moffett Field, California 94035

M. Falarski
Aerospace Engineer
NASA Ames Research Center
Moffett Field, California 94035

R. Fearn
Department of Engineering Sciences
University of Florida
Gainesville, Florida 32611

W. H. Foley
Aerodynamics Engineering Manager
General Dynamics Corporation
P.O. Box 748
Fort Worth, Texas 76101

R. J. Furey
David Taylor Naval Ship Research
  and Development Center
Bethesda, Maryland 20084

D. B. Garland
Senior Engineer
The De Havilland Aircraft
  of Canada, Ltd.
Downsview, Ontario M3K 1Y5

D. P. Gleiter
Naval Air Development Center
Warminster, Pennsylvania 18974

R. Greene
ASD/XRU
Wright-Patterson AFB, Ohio 45433

D. L. Hammond
AFFDL/FXB
Wright-Patterson AFB, Ohio 45433

J. D. Hawk
NASA Lewis Research Center
Cleveland, Ohio   44135

C. Henderson
Flight Dynamics, Code 6053
Naval Air Development Center
Warminster, Pennsylvania   18974

D. Hickey
NASA Ames Research Center
Moffett Field, California   94035

W. G. Hill, Jr.
Research Department, A-08-35
Grumman Aerospace Corporation
Bethpage, New York   11714

R. C. Jenkins
Research Department, A-08-35
Grumman Aerospace Corporation
Bethpage, New York   11714

J. Katz
Mail Stop 247-1
NASA Ames Research Center
Moffett Field, California   94035

G. Kidwell
NASA Ames Research Center
Moffett Field, California   94035

R. J. Kita
Grumman Aerospace Corporation
Bethpage, New York   11714

P. G. Knott
British Aerospace, Warton Division
Wind Tunnel Department
Warton Aerodome
Preston, Lancashire PRY1AX
England

D. Koenig
Mail Stop 247-1
NASA Ames Research Center
Moffett Field, California   94035

D. R. Kotansky
Section Chief, Aerodynamics
McDonnell Douglas Corporation
McDonnell Aircraft Company
P.O. Box 516
St. Louis, Missouri   63166

S. S. Kress
Vought Corporation
P.O. Box 5907
Dallas, Texas 75222

R. Kuhn
AMPAC Corporation
2640 Amy Drive
Norristown, Pennsylvania 19403

D. Lacey
David W. Taylor Naval Ship Research
  and Development Center
Bethesda, Maryland 20014

R. J. Laib
Code 034Le
Naval Postgraduate School
Monterey, California 93940

B. A. Lampkin
Mail Stop 237-9
NASA Ames Research Center
Moffett Field, California 94035

J. A. Laughrey
Air Force Flight Dynamics Laboratory
AFFDL-FXM
Wright-Patterson AFB, Ohio 45433

D. Levine
Mailstop 247-1
NASA Ames Research Center
Moffett Field, California 94035

E. L. Lewis
Code 03APAJ
Naval Air Systems Command Headquarters
Washington, DC 20361

R. B. Lowry
AFFDL/FXB
Wright-Patterson AFB, Ohio 45433

J. R. Lummus
Senior Engineer
General Dynamics Corporation
Fort Worth Division
Fort Worth, Texas 76100

C. J. Martin
David W. Taylor Naval Ship Research
  and Development Center
Bethesda, Maryland 20014

H. McMahon
Georgia Institute of Technology
School of Aerospace Engineering
Atlanta, Georgia   30332

M. R. Mendenhall
Nielsen Engineering & Research, Inc.
510 Clyde Avenue
Mountain View, California   94043

L. D. Miller
Lockheed-California Company
Burbank, California   91520

W. T. Miller
Naval Air Development Center
Warminster, Pennsylvania   18925

R. D. Murphy
Naval Air Systems Command
Washington, DC   20361

T. C. Nark
Boeing Aerospace Company
P.O. Box 3999
Seattle, Washington   98124

W. P. Nelms
Aircraft Aerodynamic Branch
NASA Ames Research Center
Moffett Field, California   94035

J. H. Nichols
David W. Taylor Naval Ship Research
  and Development Center
Bethesda, Maryland   20014

M. E. Omar
Boeing Aerospace Company
P.O. Box 3999
Seattle, Washington   98124

W. Painter
NASA Dryden Flight Research Center
P.O. Box 273
Edwards, California   93523

R. E. Palmer
Naval Air Development Center
Warminster, Pennsylvania   18974

J. W. Paulson, Jr.,
Mail Stop 286
NASA Langley Research Center
Hampton, Virginia 23665

S. Perkins
Nielsen Engineering & Research, Inc.
510 Clyde Avenue
Mountain View, California 94043

R. Perkins
Deputy Chief V/STOL Project Office
Naval Air Systems Command
Washington, DC 20361

M. F. Platzer
Code 67P1
Department of Aeronautics
Naval Postgraduate School
Monterey, California 93940

H. C. Quigley
NASA Ames Research Center
Moffett Field, California 94035

D. Renselaer
Rockwell International
Los Angeles, California 90009

V. Rossow
Mail Stop 247-1
NASA Ames Research Center
Moffett Field, California 94035

A. Rubel
Research Department
Grumman Aerospace Corporation
Bethpage, New York 11714

R. L. Schaeffer
David W. Taylor Naval Ship Research
  and Development Center
Bethesda, Maryland 20014

P. R. Scheurich, Jr.
David W. Taylor Naval Ship Research
  and Development Center
Bethesda, Maryland 20014

D. B. Schoelerman
Vought Corporation
P.O. Box 5907
Dallas, Texas 75222

A. Sim
NASA Dryden Flight Research Center
Edwards, California 93523

C. W. Smith
Engineering Specialist
General Dynamics Corporation
Fort Worth Division
Fort Worth, Texas 76100

E. Snowden
General Dynamics
Fort Worth Division
Fort Worth, Texas 76100

E. D. Spong
Branch Chief, Propulsion
Dept. 343, Bldg. 32/2
McDonnell Aircraft Company
P.O. Box 516
St. Louis, Missouri 63166

V. R. Stewart
Member of Technical Staff
Rockwell International, Columbus
4300 E. Fifth Avenue
Columbus, Ohio 43218

N. O. Stockman
NASA Lewis Research Center
Cleveland, Ohio 44135

S. C. Stumpfl
U.S. Air Force Flight Dynamics Lab.
Wright-Patterson AFB, Ohio 45433

J. Syberg
Boeing Military Airplane Development
Boeing Aerospace Company
P.O. Box 3994
Seattle, Washington 98124

D. Tavella
Joint Institute of Aerodynamics
  and Acoustics
Stanford, California 94305

T. H. Thompson
PMA 269T
Naval Air Systems Command
Washington, DC 20361

R. H. Traudt
Air Force Systems Command   AFSC-XRL
Bolling Air Force Base
Washington, DC 20332

G. Vander Plaats
NASA Ames Research Center
Moffett Field, California 94035

R. F. Vomaske
Mail Stop 237-9
NASA Ames Research Center
Moffett Field, California 94035

S. A. Walker
U.S. Air Force Aeronautical Systems Division
Wright-Patterson AFB, Ohio 45433

R. Weinraub
AIR-5301
Naval Air Systems Command
Department of the Navy
Washington, DC 20361

R. Whitehead
Office of Naval Research
Department of the Navy
800 N. Quincy Street
Arlington, Virginia 22217

P. Whitten
General Dynamics Corporation
Fort Worth Division
Fort Worth, Texas 76100

F. W. Wilson
Code 1613
David W. Taylor Naval Ship Research
  and Development Center
Bethesda, Maryland 20014

J. Wilson
Air Force Office of Scientific Research
AFOSR-NA, Building 410
Bolling Air Force Base
Washington, DC 20332

W. Woodrey
General Dynamics Corporation
Fort Worth Division
Fort Worth, Texas 76100

P. T. Wooler
Aerosciences Research
Department 3811, Zone 82
Northrop Corporation, Aircraft Group
3901 W. Broadway
Hawthorne, California 90250

K. T. Yen
Naval Air Development Center
Warminster, Pennsylvania 18974

A. Zalay
Lockheed MIssile and Space Company
Huntsville Research & Engineering Center
P.O. Box 1103
Huntsville Alabama 35800

H. Ziegler
Northrop Corporation
Aircraft Division
3901 W. Broadway
Hawthorne, California 90250

SESSION IV

PROPULSION SYSTEM/AIRFRAME INTERACTIONS

Chairman:

Norbert Stockman
NASA-Lewis Research Center

RECENT APPLICATIONS OF THEORETICAL ANALYSIS

TO V/STOL INLET DESIGN

by Norbert O. Stockman

National Aeronautics and Space Administration
Lewis Research Center
Cleveland, Ohio 44135

ABSTRACT

The theoretical analysis methods, potential flow, and boundary layer, used at Lewis are briefly described. Recent application to Navy V/STOL aircraft, both fixed and tilt nacelle configurations, are presented. A new three-dimensional inlet analysis computer program will be described and preliminary results presented. Finally, a suggested approach to optimum design of inlets for high angle-of-attack operation is discussed.

INTRODUCTION

Current configurations being considered for subsonic V/STOL aircraft give rise to a variety of problem areas for the propulsion system inlets, for example, high angle-of-attack, extremely short inlets, wide range of operating conditions, and three-dimensional geometries. A rational evaluation of the viability of the proposed configurations requires analytical tools capable of investigating specific problems associated with the inlets and other components of the various configurations. One such analytical tool is the Lewis method for analyzing the potential and viscous flow in subsonic inlets. The axisymmetric version of this method (documented in refs. 1 and 2) has been successfully applied to various aspects of V/STOL inlet design and analysis over the past several years (refs. 3 to 7). The more recent two-dimensional version of the method for potential flow is documented in reference 8 and applied to V/STOL inlets and nozzles in reference 9. The new three-dimensional version is described in reference 10 and documented in reference 11.

This paper will present a brief description of the axisymmetric potential flow and boundary layer analysis methods. Then application of this method to inlet problems arising from both tilt-nacelle and fixed-nacelle V/STOL aircraft configurations will be illustrated. Next, the new three-dimensional inlet potential flow analysis will be described and preliminary results will be presented. Finally, an approach to the design of optimum subsonic inlets will be suggested.

SYMBOLS

A   area

a   speed of sound

C_f skin friction coefficient

D   fan diameter

ℓ inlet length

M   Mach number

m_b boundary-layer bleed mass flow rate

S   surface distance

V   velocity

$\dot{W}$ inlet mass flow rate

α inlet incidence angle (angle of attack)

β inlet yaw angle

δ^*	boundary-layer displacement thickness
θ	circumferential coordinate
ρ	density

Subscripts:

cor	corrected for local supersonic flow
de	diffuser exit
i	incompressible
s	static conditions
T	throat
t	total (stagnation) conditions
tip	fan tip
$\left.\begin{array}{c} 0 \\ \infty \end{array}\right\}$	free stream
*	critical conditions (i.e., at Mach 1)

AXISYMMETRIC ANALYSIS METHOD

The basic problem to be solved is to calculate the compressible potential and, when desired, the viscous flow in an arbitrary axisymmetric inlet at any combination of operating conditions of inlet mass flow rate, W, free-stream velocity V_∞, and inlet incidence angle, α (fig. 1). At nonzero incidence angle the flow in and around the inlet is three-dimensional. At the present time there is no exact practical compressible viscous flow method of solution (computer program) capable of handling this inlet problem. Therefore, the problem is solved in several steps (fig. 1) as follows:

1. Geometry representation

2. Incompressible potential flow basic solutions

3. Combined solutions with compressibility correction

4. Boundary layer calculations

Geometry

The inlet is assumed to be axisymmetric and is represented by its meridional profile. This profile is broken into segments at convenient tangent points as shown in figure 1.

The geometry program prepares coordinate-point input for efficient use of the potential flow program.

Potential Flow

The Douglas-Neumann program (refs. 12 and 13) is used for calculating the incompressible potential flow in the form of three independent basic solutions: a static solution ($V_\infty = 0$), an axisymmetric streamflow solution ($V_\infty \neq 0$, $\alpha = 0$) and a pure crossflow (or angle of attack) solution ($V_\infty \neq 0$, $\alpha = 90^\circ$). These three basic solutions are combined into a solution of interest having arbitrary flow conditions of V_∞, α, and mass flow $\dot{W}$ (fig. 1). Thus, once the basic flow solutions are obtained for a specified geometry, any solution of interest for that geometry can be obtained without repeating the more time-consuming potential flow calculations.

The velocity obtained by the linear combination is incompressible and is corrected for compressibility by the Lieblein-Stockman compressibility correction (ref. 13).

$$V = V_i \left(\frac{\rho_t}{\bar{\rho}_s}\right)^{V_i/\bar{V}_i} \tag{1}$$

where all the terms on the right hand side are obtained from the incompressible flow solution or the input flow conditions. This correction requires no alteration of the inlet geometry and it can handle local sonic and supersonic velocities. If the local velocity is supersonic it is further corrected (since it is, in effect, based on the wrong relation between area and velocity) by the following empirical formula

$$V_{cor} = a_* \left[1 + \left(\frac{V}{a_*} - 1\right)^{\frac{\sqrt{1.2}}{A_*/A}} \right] \tag{2}$$

where V_{cor} is the corrected supersonic velocity; V is the supersonic velocity obtained from equation (1); a_* is the critical velocity (i.e., the velocity at Mach 1); and A_*/A is the sonic-to-local area ratio and can be obtained from

$$\frac{A_*}{A} = \frac{V}{a_*} \left[1.2 - 0.2 \left(\frac{V}{a_*}\right)^2 \right]^{2.5} \tag{3}$$

Boundary Layer

In cases where the boundary layer behavior is required the surface Mach number distributions obtained from the potential flow solution are used as input to the Herring-Mellor axisymmetric compressible boundary layer program. Reference 2 contains a complete documentation of the boundary layer program and references to the original sources. The program calculates boundary layer profiles, displacement thickness δ^*, skin friction coefficient C_f, etc., at each station, and also predicts transition from laminar to turbulent flow. Separation (whether laminar or turbulent) is predicted when C_f is zero. The boundary layer calculation can handle bleed, as will be illustrated later, and is currently being revised to handle tangential blowing.

In cases where the boundary layer is relatively thick the accuracy of both the potential flow and the boundary layer calculations can be improved by adding the displacement thickness δ^* to the geometry and repeating all the calculations. The greatest improvement in accuracy will be seen in the diffuser. Some users have automated the δ^* addition including an iterative loop, adding a new δ^* each iteration until satisfactory convergence is attained.

A common use of the boundary layer calculation is to obtain inlet separation bounds. A separation bound is a plot of angle of attack at incipient separation versus the ratio of throat-to-free-stream velocity. To facilitate finding the separation bound the combination routine and the boundary layer routine have been combined and an automatic α sweep incorporated. Thus, for a given V_T and V_0 the α at incipient separation can be found in one computer run.

Comparison with Experiment

To indicate the accuracy of the method of obtaining the compressible potential flow a comparison of the analysis with experiment is given in figure 2. There it can be seen that the agreement is quite good even in the region of supersonic flow. Although the agreement is not always this good, this is a typical case. Several additional comparisons are given in reference 4.

APPLICATIONS TO SUBSONIC V/STOL AIRCRAFT

Two types of aircraft currently under consideration for subsonic V/STOL missions are the fixed-nacelle deflected thrust configuration and the tilt nacelle configuration. The analysis method will be applied to two inlet problems arising from each of these configurations.

Fixed Nacelle

A possible fixed nacelle configuration is shown in figure 3. The problems to be addressed herein (taken from ref. 14) are related to the shortness of the fixed nacelle inlet. The combined requirements of engine location and pilot visibility lead to the need for very short inlets.

Short inlets usually have no diffuser, thus the fan face is at the throat and the throat Mach number is lower than for a conventional inlet. The lower throat Mach number is unfavorable for cruise since it requires a larger throat diameter which tends to result in larger nacelle maximum diameter. To reduce the needed maximum diameter the inlet lip must be made thinner. In brief, short inlets tend to need thin inlet lips.

Short, thin inlets give rise to two problems that will be discussed: thin inlet lips have higher peak surface velocities on the lip at low speed conditions than inlets with thicker lips and short inlets have greater velocity and flow angle distortion at the fan face at angle of attack than longer inlets.

Inlet Lip Peak Velocity. - The higher peak surface velocities on a thin inlet lip increase the probability of boundary layer separation. Therefore it is worthwhile to try to reduce these peak velocities. The peak velocities are higher because the reduced lip surface area of the short thin inlet requires a higher loading (i.e., a lower pressure) to turn the flow into the inlet. This high loading, and thus the peak velocity, can be reduced by providing additional lip surface area. This additional area can be obtained without an increase in overall inlet thickness by inserting a slot in the inlet cowl which in effect creates an additional lip as shown in figure 4. The geometry inset of figure 4 shows both the original unslotted short inlet lip and the same lip slotted.

The potential flow calculations have been used to determine the velocity distributions on both the slotted and unslotted inlets (fig. 4). Since the slot is a flow passage a new flow condition in addition to $\dot{W}$, V_∞, and α must be specified to obtain a practical solution. For the case shown on figure 4 which is a static case (i.e., $V_\infty = 0$) the additional condition was the Kutta condition prescribed at the trailing (lower) edge of the slat (B on fig. 4). The results of figure 4 show that the peak velocity of the unslotted lip can be reduced significantly by the use of the slot. It was assumed that the lowest peaks on the slat and main lip would occur when those peaks were equal; therefore the goal in the design procedure was to obtain equal peaks as seen on figure 4.

The potential flow program has been used to investigate the effect of slot and slat variables such as slot area distribution and slat wall contour in order to arrive at promising designs. Several such designs have been built and will be tested in the Lewis 9×15 low speed wind tunnel.

Fan Blade Incidence Angle. - Another problem with short inlets is that there is not sufficient length to smooth out circumferential velocity and flow angle gradients induced by inlet angle of attack. These circumferential gradients produce changes in fan blade incidence and, hence, fluctuating loads on the rotating fan blades. The variation of fan blade incidence might limit the allowable range of thrust modulation and the fluctuating loads might produce intolerable fan blade stress. In either case, it is desirable to predict the change in fan blade incidence as an aid in short inlet design. The potential flow analysis has been used to predict the change in blade incidence for short inlets of two different lengths and the results are shown for the blade tip on figure 5. It can be seen that incidence variations reach $\pm 4^{o}$ for an inlet length to diameter ratio $\ell/D = 0.05$. Variations that large are probably intolerable. The effect of increasing inlet length to $\ell/D = 0.25$ is also shown in figure 5. The flow angle variation has been reduced to $\pm 1.5^{o}$, a more acceptable range. The distortion shown on figure 5 is for an angle of attack of 45° and a V_{∞} of 35 knots. The distortion will be lower at lower angle of attack and/or lower V_{∞}.

Tilt Nacelle

Another approach to subsonic V/STOL is the tilt nacelle. A tilt nacelle airplane in the approach configuration is shown in figure 6. As can be seen the inlet is exposed to very high angles of attack. Two problems associated with high angle of attack will be discussed: wake ingestion from the leeward side of the inlet and control of internal flow separation on the windward side by boundary layer bleed.

Wake Ingestion. - In a recent wind tunnel test of a tilt nacelle inlet unanticipated high fan blade stresses were measured at high angle of attack and very low free-stream velocity. Usually fan blade stress is a minimum at a low free-stream velocity. It was conjectured that the inlet was ingesting vorticity shed from the leeward side of the inlet. This conjecture was qualitatively verified by flow-visualization tests of a simple inlet model in a small wind tunnel.

To get a quantitative feel for the phenomenon, flow fields were obtained from the potential flow program. Some three-dimensional streamlines are shown on figure 7 for a throat-to-free-stream velocity ratio of 10 and an inlet angle of attack of 90°. It can be clearly seen that the rear stagnation point is off the body and that flow ingestion from the rear (leeward) side of the inlet occurs. If the free-stream velocity is high enough to produce a wake, that wake will probably be ingested. Further calculation indicates that as V_{T}/V_{0} decreases, the stagnation point moves toward the body and for this inlet occurs on the body at a V_{T}/V_{0} of about 5.1. Thus for a given inlet geometry a range of flow conditions over which rear wake ingestion is likely to occur could be determined.

Boundary Layer Bleed. - Internal boundary layer separation on the windward side of this inlet is another problem arising in a tilt nacelle inlet. If changing the inlet geometry is prevented by other constraints (e.g., cruise requirements) then it may be necessary to control the boundary layer to prevent separation. One method of control is to bleed off part of the boundary layer. This bleeding can be handled by the boundary layer calculations and an example is shown in figure 8. There the skin friction distribution on the internal surface of the windward cowl is shown. When the skin friction becomes zero, the boundary layer separates as shown for the no bleed case. The bleed curve shows that a relatively small amount of bleed can "control" the boundary layer and prevent separation. In this case, the bleed extended circumferentially over 120°. The circumferential extent of bleed required can be estimated by comparing the circumferential distribution of the diffusion velocity ratio with the diffusion limit as shown in the inset.

THREE-DIMENSIONAL INLET ANALYSIS

Many inlets proposed for subsonic V/STOL aircraft are fully three-dimensional as opposed to axisymmetric. Most of these cannot adequately be analyzed with an axisymmetric program. An example is the scoop inlet shown on figure 9. Other examples are curved centerline (S-duct) inlets, nonround inlets, inlets with canted highlight plans. Therefore a three-dimensional inlet program was recently acquired under contract (ref. 10).

The three-dimensional method is essentially the same as the axisymmetric method previously described. Four basic flow solutions are obtained (instead of three) since a solution of interest now consists of four conditions: inlet mass flow, free-stream velocity, angle of attack, and angle of yaw.

Preliminary results for a rather coarse paneling are shown on figure 10 for the scoop inlet. The scoop inlet was originally conceived as a noise suppression device. However, wind tunnel tests (ref. 17) indicated improved angle-of-attack performance over a baseline inlet of the same lip shape. The reason for the improvement can be seen on the pressure plots of figure 10. The windward lip ($\theta = 0^o$) is less highly loaded than the leeward lip ($\theta = 180^o$). Thus at 0° angle of attack the inlet is effectively operating at a negative angle of attack giving a greater angle-of-attack margin than a nonscoop inlet having the same lip shape.

These examples are just a few of many current investigations using the potential flow and boundary layer programs. Next a method of using the program to design optimum inlets will be discussed.

OPTIMUM INLET DESIGN

In reference 15 a method is proposed for obtaining the optimum internal lip and diffuser wall shape for subsonic inlets that must operate under a variety of flow conditions. Briefly, the method consists of comparing inlet operating requirements with estimated inlet separation characteristics to identify the most critical inlet operating condition. This critical condition is taken to be the design point and is defined by the values of inlet mass flow, free-stream velocity, and inlet angle of attack. An optimum inlet design is then obtained at the design point flow condition. By an optimum inlet is meant the shortest, thinnest, most efficient inlet with attached flow that satisfies the operating requirements.

In reference 15 the approach to optimizing the inlet is to optimize the flow distributions over the inlet surfaces. The optimum flow distribution recommended are a high flat top velocity distribution on the inlet lip to turn the flow quickly into the inlet and a low, flat bottom skin friction distribution on the diffuser wall to diffuse the flow rapidly and efficiently to the velocity required at the fan face. Sample optimum flow distributions are shown on figure 11. The limit on peak velocity marked on figure 11(b) is the empirical Mach number or diffusion limit for separation-free operation (ref. 16). A safety margin is recommended below the flat roof top velocity and the limit. The lower limit on skin friction (fig. 11(c)) is, of course, zero and a safety margin is recommended here also. The safety margins allow for inaccuracies in the calculation and unanticipated operating excursions. Refinements to the recommended optimum distributions and extension of the optimum design method are discussed in reference 15.

CONCLUDING REMARKS

The theoretical analysis methods, potential flow, and boundary layer, used at Lewis have been described. Recent application to subsonic V/STOL aircraft, both fixed- and tilt-nacelle configurations have been presented. A recently-suggested approach to optimum inlet design has been discussed. A new three-dimensional inlet analysis computer program has been described and preliminary results presented.

The computer programs for axisymmetric geometries have proved useful for many years and, in fact, have already exceeded their initially-expected period of usefulness. The three-dimensional version is expected to be equally long-lived. Even when three-dimensional exact compressible-flow programs become available the approximate programs will still be used for many calculations, especially preliminary screening, because of their computational efficiency and relative ease of use.

REFERENCES

1. Stockman, N. O.; and Farrell, C. A., Jr.: Improved Computer Programs for Calculating Potential Flow in Propulsion System Inlets. NASA TM-73728, 1977.

2. Albers, J. A.; and Gregg, J. L.: Computer Program for Calculating Laminar, Transitional, and Turbulent Boundary Layers for a Compressible Axisymmetric Flow. NASA TN D-7521, 1974.

3. Stockman, N. O.: Potential and Viscous Flow Prediction in V/STOL Propulsion System Inlets. Prediction Methods for Jet V/STOL Propulsion Aerodynamics, Vol. II, M. F. Platzer, ed., Naval Air Systems Command, 1975, pp. 722-742.

4. Stockman, N. O.: Potential and Viscous Flow in VTOL, STOL, or CTOL Propulsion System Inlets. AIAA Paper 75-1186, Sep. 1975.

5. Boles, M. A.; Luidens, R. W.; and Stockman, N. O.: Theoretical Flow Characteristics of Inlets for Tilting-Nacelle VTOL Aircraft. NASA TP-1205, 1978.

6. Hawk, J. D.; and Stockman, N. O.: Theoretical Study of VTOL Tilt-Nacelle Axisymmetric Inlet Geometries. NASA TP-1380, 1979.

7. Chou, D. C.; Luidens, R. W.; and Stockman, N. O.: Prediction of Boundary-Layer Flow Separation in V/STOL Engine Inlets. J. Aircr., vol. 15, no. 8, Aug. 1978, pp. 474-481.

8. Hawk, J. D.; Stockman, N. O.; and Farrell, C. A., Jr.: Computer Programs for Calculating Two-Dimensional Potential Flow in and About Propulsion System Inlets. NASA TM-78930, 1978.

9. Hawk, J. D.: Theoretical Fan Velocity Distortion Due to Inlets and Nozzles. NASA TM-79150, 1979.

10. Hess, J. L.; and Stockman, N. O.: An Efficient User-Oriented Method for Calculating Compressible Flow About Three-Dimensional Inlets. AIAA Paper 79-0081, Jan. 1979.

11. Hess, J. L.; Mack, D. P.; and Stockman, N. O.: An Efficient User-Oriented Method for Calculating Compressible Flow About Three-Dimensional Inlets. (Douglas Aircraft Co., Inc.; NASA Contract NAS3-21135.) NASA CR-159578, 1979.

12. Hess, J. L.; and Smith, A. M. O.: Calculation of Potential Flow About Arbitrary Bodies. Progress in Aeronautical Sciences, Vol. 8, D. Kuchemann, ed., Pergamon Press, 1967, pp. 1-138.

13. Hess, J. L.; and Martin, R. P., Jr.: Improved Solution for Potential Flow About Arbitrary Axisymmetric Bodies by the Use of a Higher-Order Surface Source Method. (MDC-J6627-01, Douglas Aircraft Co., Inc.; NASA Contract NAS3-18018.) NASA CR-134694, 1974.

14. Woollett, R. R.: Design Criteria for Short V/STOL Inlets. Paper to be published.

15. Luidens, R. W.; Stockman, N. O.; and Diedrich, J. H.: An Approach to Optimum Subsonic Inlet Design. ASME Paper 79-GT-51, Mar. 1979.

16. Boles, M. A.; and Stockman, N. O.: Use of Experimental Separation Limits in the Theoretical Design of V/STOL Inlets. J. Aircr., vol. 16, no. 1, Jan. 1978, pp. 29-34.

17. Abbott, J. M.; and Dietrich, D. A.: Aerodynamic and Directional Acoustic Performance of a Scoop Inlet. NASA TP-1028, 1977.
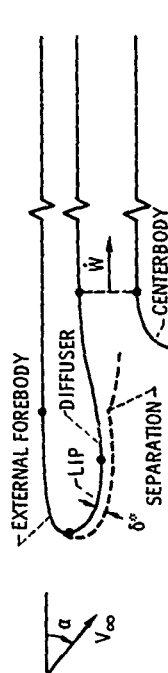
GEOMETRY REPRESENTATION
INCOMPRESSIBLE POTENTIAL FLOW
COMPRESSIBILITY CORRECTION
BOUNDARY LAYER CALCULATIONS
PROFILES, δ^*, ETC., TRANSITION, SEPARATION

Figure 1. – Axisymmetric inlet analysis.

CS-74215

597
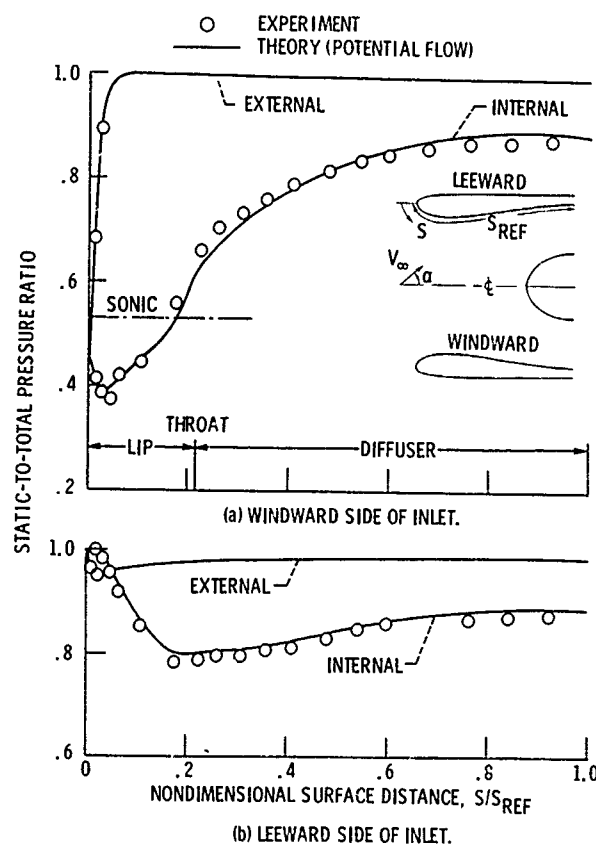
Figure 2. - Comparison of theory with experiment.
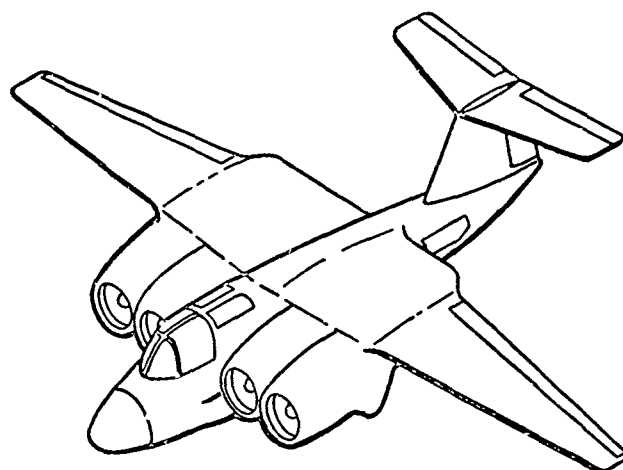
Figure 3. - Possible fixed nacelle V/STOL aircraft.
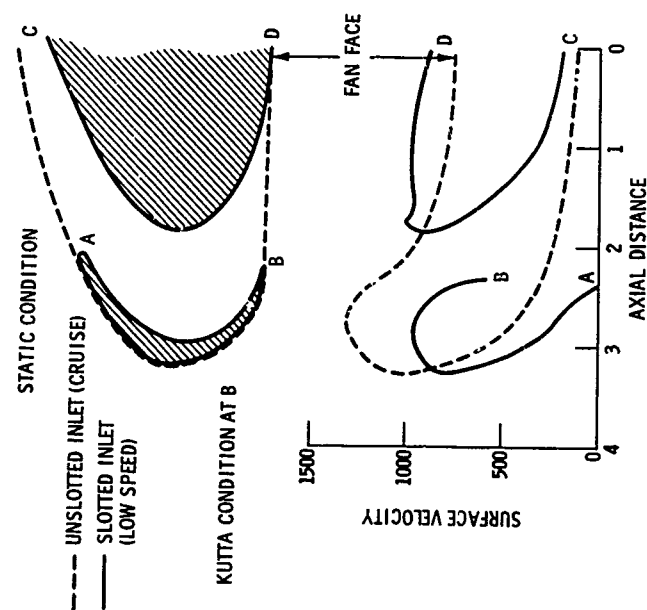
Figure 4. – Effect of slot on inlet surface velocity.

STATIC CONDITION

--- UNSLOTTED INLET (CRUISE)

SLOTTED INLET (LOW SPEED)

KUTTA CONDITION AT B

FAN FACE

SURFACE VELOCITY

AXIAL DISTANCE

$V_{tip} = 1000$ ft/sec

180^0

270^0

90^0

$\theta = 0^0$

D

L

$V_\infty = 35$ kts
$\alpha = 45^0$

CHANGE IN BLADE TIP INCIDENCE ANGLE, deg

L/D

0.25

.05

θ, deg
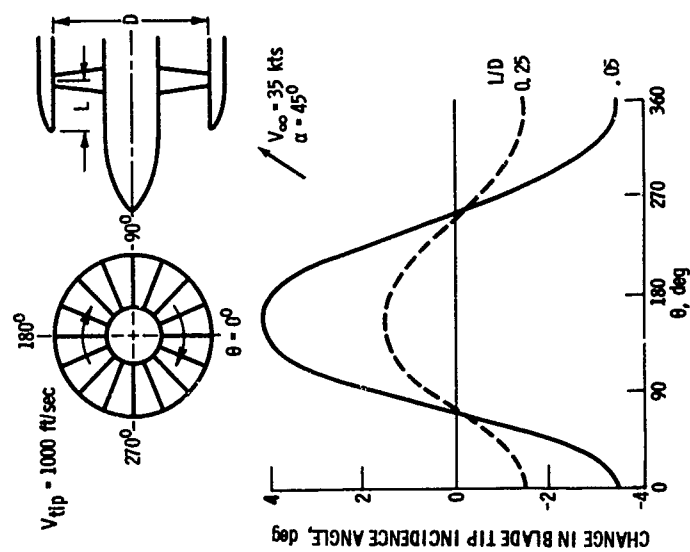
Figure 5. - Fan inflow distortion at angle of attack.
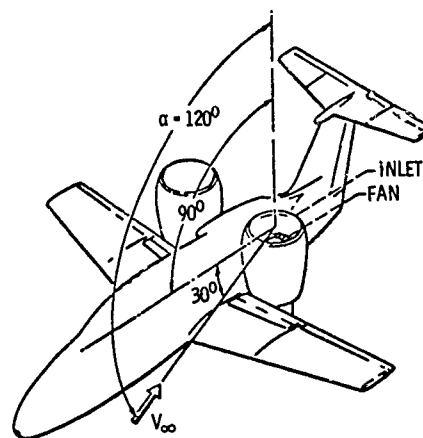
LANDING CONFIGURATION

Figure 6. - Possible tilt-nacelle V/STOL aircraft.

(a) 3-D FLOW FIELD.

(b) LEEWARD LIP DETAIL.
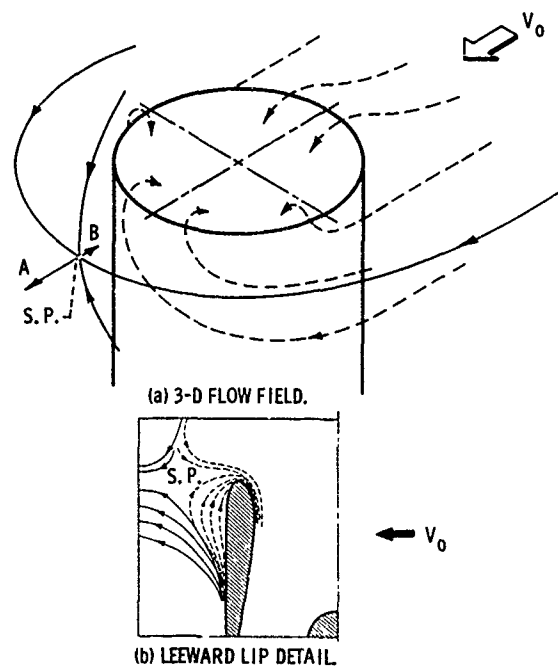
Figure 7. – Flow field of tilt-nacelle inlet. $V_T/V_0 = 10$, $\alpha = 90^0$.
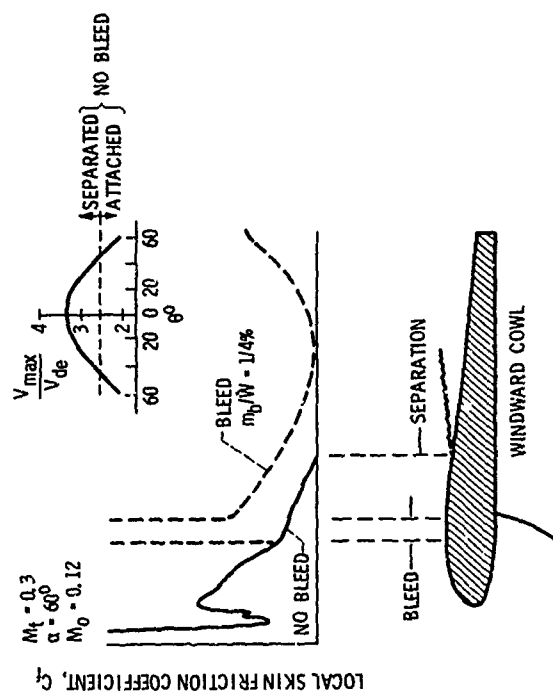
Figure 8. – Effect of boundary-layer bleed on inlet separation.
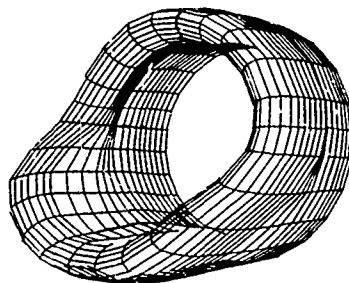
Figure 9. - Three-dimensional scoop inlet.
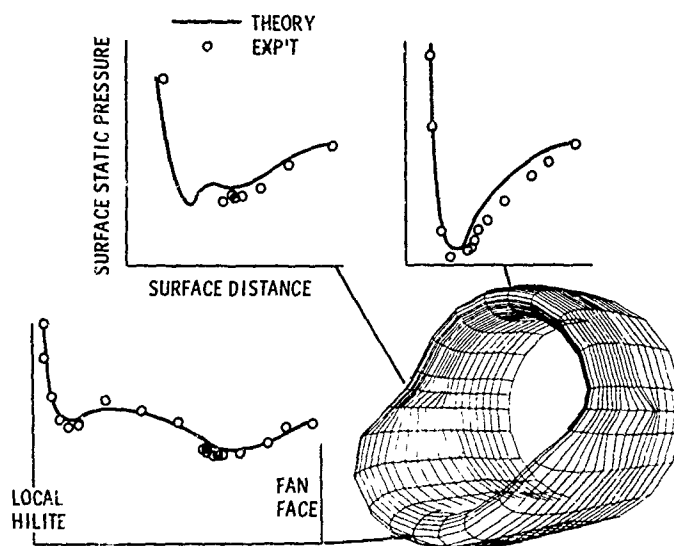
Figure 10. - Comparison of 3-D theory and experiment, scoop inlet. $V_T/V_\infty = 1.7$, $\alpha = 0$, $\beta = 0$.

(a) LIP.

(b) DIFFUSER.
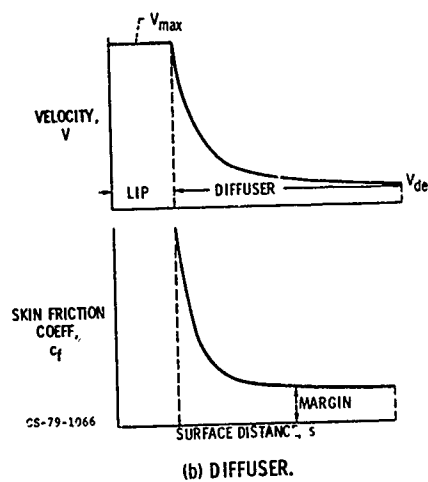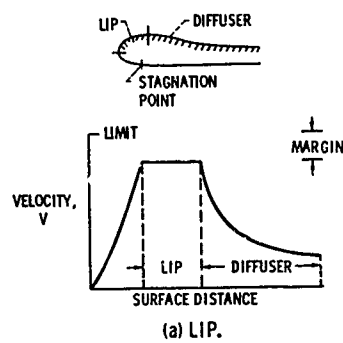
Figure 11. - Optimum flow distributions.

CS-79-1966

INLET OPERATING CHARACTERISTICS
AT HIGH ANGLES OF ATTACK

by
J. Syberg
Boeing Military Airplane Development
Boeing Aerospace Company

ABSTRACT

Full scale and one-third scale models of an asymmetric, high-contraction-ratio inlet were tested with fan at low forward speeds and high angles of attack to define the limits for safe and controllable operation. For the full scale inlet/nacelle these limits were found to be determined by a sudden change in the inlet flow pattern, which caused a significant drop in the measured net thrust as well as a sharp increase in the fan blade vibratory stresses. This change in flow pattern is associated with boundary layer separation in the inlet. When the angle of attack is increased at constant freestream velocity and inlet airflow, a value is reached where a small separation is formed in the diffuser of the inlet. When the angle of attack is increased beyond this point the separation grows in size and moves forward in the inlet. As the angle of attack is further increased, the flow suddenly becomes very unsteady and the separation now appears to originate at or near the hilite of the inlet lip. This sudden change is associated with high fan blade stresses and a loss in thrust and thus constitutes the operating limit.

Whereas the boundaries for onset of separation in the diffuser were found to improve with increasing model size, the lip separation occurred at less severe operating conditions on the large inlet than on the small inlet. This phenomenon, for which no satisfactory explanation has been found, resulted in more restrictive operating limits for the full scale inlet than expected.

NOMENCLATURE

A_H	Inlet hilite area
A_{TH}	Inlet throat area
DISC	Max-min total pressure differential at compressor face divided by average total pressure
DISF	Max-min total pressure differential at fan face (ignoring the outer 2.1 cm annulus) divided by average total pressure
L	Radial distance measured from inlet wall at fan face station
M_{TH}	Throat Mach number
P	Static pressure
PT	Total pressure
PTAV	Area weighted average total pressure
PTO	Free stream total pressure
R_{FAN}	Fan tip radius
R_H	Local hilite radius referenced to fan centerline
R_{TH}	Local throat radius referenced to fan centerline
S	Surface distance along cowl wall measured from hilite
V_0	Tunnel velocity
$V_0/\sqrt{\theta}$	Tunnel velocity corrected to standard temperature
WK1A	Fan face airflow corrected to standard sea-level conditions and divided by fan face area
Y	Radial distance at the fan nozzle rake station
α	Inlet angle of attack

INTRODUCTION

Various concepts have been studied as candidates for the Navy Type A V/STOL airplane. Some of these configurations, such as the aircraft illustrated in Figure 1, achieve powered lift by rotating the nacelles in the vertical plane during takeoff and landing. This scheme presents a special challenge to the inlet designer since the inlets during these maneuvers will be exposed to much higher angles of attack than normally experienced on a conventional subsonic airplane.

This potential inlet design problem has been the subject of various analytical and experimental studies over the last three to four years. As a result, the general performance characteristics of high-contraction-ratio, fixed-geometry inlets designed for high-angle-of-attack operation are well understood and can be estimated with reasonable accuracy using various analytical/empirical prediction techniques; see for example References 1-4.

The objective of the present paper is to discuss the experimentally observed operating limits for a full scale tilt nacelle propulsion system and compare these results with similar findings on a 1/3 scale inlet with powered fan.

The wind tunnel test of the full scale inlet was funded by NASA-Ames Research Center, Reference 5, while the 1/3 scale model program was funded by NASA-Lewis Research Center, Reference 6.

STATEMENT OF PROBLEM

During low-speed maneuvers the main function of the inlet is to supply flow with low total-pressure distortion and high total-pressure recovery to the fan. The primary source of distortion in a subsonic inlet is separation of the boundary layer. As illustrated in Figure 2, separation can occur both when the inlet airflow, i.e., throat Mach number, is too high and when it is too low:

At high throat Mach numbers local pockets of supersonic flow tend to develop on the inlet cowl. The peak Mach number in this supersonic region will increase with angle of attack and, for high angles of attack, also with forward speed. When the shock waves, or adverse pressure gradients, become sufficiently strong, the flow separates away from the cowl surface, leading to increases in distortion and reductions in recovery. Once the inlet is separated, the distortion will increase rapidly with throat Mach number, angle of attack, and forward speed. Thus, the separation boundary is usually considered to be the inlet operating limit.

Boundary layer separation in the inlet can also occur when the inlet throat Mach number is too low. This seems to be contradictory to the fact that the overall adverse pressure gradients in the inlet decrease

with decreasing airflow. However, the local velocity is also decreasing with decreasing airflow making the boundary layer more sensitive to an adverse pressure gradient. This increased sensitivity can, under certain free stream conditions, dominate the favorable change in pressure gradient such that the inlet boundary layer eventually separates. When separated flow is present at the fan face, the minimum total pressure is approximately equal to the local static pressure. Low airflow rates imply a small difference between the total and static pressures. Thus, the distortion tends to be relatively low. It follows that if the separation can be restricted to very low throat Mach numbers, the fan performance may not be significantly degraded and the blade stresses may be acceptable while operating with separated flow in the inlet.

The topic of the present paper is the effects of the latter boundary layer separation on the inlet operating characteristics as determined in a full scale experimental program. Also included is a discussion of a significant difference in inlet operation between 1/3 scale and full scale models for which a satisfactory explanation has yet to be found.

TEST APPARATUS

A schematic of the test inlet is shown in Figure 3. The design incorporates some unique features. A cross-section taken in a radial plane at the upper (leeward during angle-of-attack operation) part of the inlet shows a fairly conventional cowl, while a similar cut at the lower (windward) part of the inlet reveals much thicker and blunter contours. The purpose of the asymmetry is to take advantage of the operating characteristics of the airplane; i.e., the inlet is subjected only to positive angles of attack. At a positive angle of attack the windward stagnation point moves outboard, increasing the internal pressure gradients, while the leeward stagnation point moves inboard reducing the internal pressure gradients. Thus for the windward cowl the operating condition becomes increasingly severe with angle of attack and free stream velocity. For the leeward cowl, the worst condition is ground static operation at maximum airflow.

The cowl contours are circular in any cross-section normal to the fan centerline. The asymmetric cowl therefore has a curved centerline. Another feature of the cowl is that the wall curvature is everywhere continuous. This is considered important since near the cowl lip the flow attains transonic velocities at angle of attack, and potential flow analyses have indicated that at such velocities a continuous wall curvature distribution helps to maintain smooth pressure gradients.

Referenced to the fan centerline, the local contraction ratio $(R_H/R_{TH})^2$ for the leeward cowl is 1.30. For the windward cowl the local contraction ratio is 1.76. The overall area contraction ratio (A_H/A_{TH}) for the asymmetric design is 1.50. The inlet length is approximately 80% of the fan face diameter.

The full scale inlet was tested with engine in the NASA-Ames 40 by 80-foot wind tunnel. Model schematic and photos are shown in Figure 4. The engine used for the test consists of a Hamilton Standard 1.4 m (55 in.) variable pitch fan driven by a Lycoming T55-L-11A 2800 KW (3750 hp) gas turbine core engine. With this engine the fan pressure ratio is 1.14 and the bypass ratio 17:1. The fan is driven through a 4.75:1 reduction gear box producing a maximum fan speed of 3365 rpm. Appropriate cowlings and fairings were provided to assemble the propulsion system components into a wind tunnel test article that simulated the tilting nacelle on a proposed Navy V/STOL airplane. Performance and force balance data were obtained at free stream velocities ranging from 0 to 82 m/s (0-160 knots) and inlet angles of attack ranging from 0 to 120 degrees.

The one-third scale inlet was tested with fan in the NASA-Lewis 9 by 15-foot Low Speed Wind Tunnel, see Figure 5. The fan is a single stage 0.508 m (20 in.) diameter design with a pressure ratio and tip speed representative of the Type A V/STOL aircraft application. The fan nozzle exit area was sized to duplicate as closely as possible the operati.g line (pressure ratio versus airflow) of the full scale variable pitch fan. The fan, which has 15 rotor blades and 25 stator blades, is driven by a four-stage turbine powered by high-pressure, heated air delivered to the turbine through flow passages in the model support strut.

Further details of the two wind tunnel models and tests can be found in References 5 and 6.

TEST RESULTS

The primary objective of the full scale inlet test program was to establish the range of nacelle tilt angles, freestream velocities, and inlet airflows for which the inlet can provide pressure recoveries and distortion levels that result in acceptable fan/engine operating characteristics and fan blade stress levels. Since these limits are related to the size and intensity of inlet flow separation an important first step was to determine the conditions at which the initial onset of boundary layer separation occurs in the inlet.

Separation Boundaries
The separation boundaries were determined primarily by varying inlet angle of attack at constant power setting and forward speed. The root-mean-square (RMS) value of a dynamic pressure output from a high-frequency transducer (PDF1) was plotted on-line versus angle of attack on an x-y plotter. This transducer was located close to the windward side cowl wall immediately upstream of the fan. A sudden increase in the RMS-level was usually indicative of the onset of separation. Steady state data points were then recorded at angles of attack near this point of increasing turbulence. Traces of the RMS-level versus angle of attack for one of the forward speed conditions tested are shown in Figure 6 to illustrate the test technique. Following the test the steady state data points were analyzed to determine which points indicate the presence of

boundary layer separation and which points show attached flow. This judgement was based on the fan face total pressure profiles near the windward side cowl wall. Typical profiles recorded on either side of the separation boundary are shown in Figure 7.

The analysis of the fan face rake profiles provided a large number of data points recorded near the onset of separation, i.e., either barely attached or just separated. From these results it was possible to construct the separation boundaries shown in Figure 8. For a given airflow the boundary layer will be attached when the inlet is operated below the corresponding separation boundary and separated when operated above the line.

Similar separation boundaries were developed in Reference 6 for the 1/3 scale model. A comparison of the full scale and the 1/3 scale inlet separation boundaries are shown in Figure 9. To facilitate the comparison, the boundaries are here shown as inlet angle of attack versus fan face corrected airflow for two forward speeds. As expected, the separation-free operating range for the full scale inlet is significantly larger than that for the 1/3 scale model. As shown in Reference 2, this difference can be attributed to the difference in Reynolds number between the two model scales.

Operating Limits

The operating limits for the full scale tilt-nacelle inlet were determined by increasing α (or reducing the airflow) beyond the separation boundary until excessive fan blade stresses and/or changes in the core engine flow distortion were observed. Figure 10 shows some of the inlet and engine parameters measured during a test run in which the angle of attack was varied at constant power setting and wind tunnel speed. The power setting was adjusted to provide an inlet airflow of approximately 100 kg/sm^2 (20.5 lb/sec ft^2). The tunnel speed was 45 m/s (87 knots) during this run. The procedure was to increase α until the safe operating limit was reached and then reduce α without changing the power setting until the flow conditions were back to normal.

Figure 10 shows a discontinuity in all of the aerodynamic parameters when α reaches a value of 81°, i.e., 8° beyond the onset of separation. The fan face recovery drops from about 0.996 to 0.981 while the fan face distortion increases from 6% to 9%. The core engine total pressure recovery and distortion also deteriorate at this condition. It is significant that the sudden change in flow pattern causes a large reduction (about 15%) in inlet airflow which is the primary reason for the 20% reduction in the thrust measured with the force balance system. As illustrated in Figure 10, a rather large hysteresis is also associated with this flow phenomenon: It is necessary to reduce α to 75° before high performance operation is restored.

The pressure profiles measured in the inlet provide a clue to the abrupt change in performance. The static pressure profiles for the

windward side of the inlet lip and diffuser are shown in Figure 11 for the data points recorded during increasing α, i.e., $\alpha = 70^{\circ}$, 73°, 79° and 81°. The corresponding fan face total pressure profiles on the windward rake are shown in Figure 12. At the onset of separation ($\alpha = 73^{\circ}$), the separation seems to originate in the aft end of the diffuser as judged by the change in the static pressure profile, see Figure 11. When α is increased the leading edge of the separation moves forward in the diffuser. The discontinuity occurring at $\alpha = 81^{\circ}$ is caused by the diffuser separation suddenly changing into a lip separation originating at the inlet hilite region ($S/R_{FAN} = 0$). This lip separation results in a large low-pressure region at the fan face as evidenced by Figure 12. It should be noted that the flow was observed to be very unsteady during conditions with lip separation explaining the non-uniform profiles measured during these conditions. The circumferential extent of the low-pressure region is illustrated by the fan face total pressure isobar plots in Figure 13. Nearly 50% of the fan face area is affected by the lip separation.

The fan nozzle total pressure profiles measured during this test run are shown in Figure 14. The effect of the diffuser separation ($\alpha = 79^{\circ}$) on the windward rake profile is quite small, whereas a large pressure drop is seen when the lip separation is present ($\alpha = 81^{\circ}$). The leeward side rake is not affected by the inlet separations.

The fan blade bending and torsional stresses were monitored and recorded with various strain gauges during the wind tunnel test. Figure 15 shows a summary of the results obtained during the lip separation investigation. The blade vibratory stress increases as the angle of attack is increased beyond the value where the onset of diffuser separation occurs. A dramatic rise in stress is seen when the separation jumps forward to the lip. The high stress, which in this case is slightly above the endurance limit for the fan blades, persists until the angle of attack is decreased sufficiently to remove the lip separation.

Due to the abrupt loss in thrust and increase in fan blade stresses associated with the lip separation phenomenon it appears that this flow condition should be avoided in flight. The operating limit can therefore be defined as the point where the separation jumps from the diffuser to the inlet hilite.

Since the boundaries for the onset of diffuser separation have already been established (Figure 8) the operating limits can be defined by determining the additional reduction in airflow (or increase in α) required for lip separation to occur. Figure 16 shows the results of this study. In this figure, the estimated locations of the leading edge of the separation are plotted versus α or WK1A. In two of the four runs shown, lip separation was experienced at the conditions indicated. In the other two runs the lip separation was intentionally avoided by using various on-line instrumentation to warn against this high-stress condition. It is believed that the last data points (lowest airflows) were recorded just prior to the occurrence of lip separation.

The leading edge stations of the diffuser separations were obtained by studying the aft diffuser static pressure profiles as illustrated in Figure 17. The leading edge may be defined as the point where the slope of the pressure profile deviates significantly from that of the attached pressure profile at the same station. Although this method is somewhat subjective, especially due to the relatively large spacing between the pressure taps in this region of the inlet, it does provide an indication of the location of the separation.

Referring back to Figure 16, it is interesting to note that the change in flow pattern from diffuser separation to lip separation seems to take place when the separation reaches station $S/R_{FAN} = .85 - .90$. The change in inlet airflow from on-set of diffuser separation to on-set of lip separation is in the order of 10 kg/sm^2 (2 $lb/sec\ ft^2$). This is much less than that found on the 1/3 scale inlet model tested in the NASA Lewis 9- by 15-foot wind tunnel. Figure 18 shows a comparison between the full scale and the 1/3 scale inlet models. On the smaller inlet the change in separation location per unit of airflow was smaller and the separation could be pushed farther forward before the lip separation occurred, thereby providing a much greater margin between the diffuser separation boundary and the lip separation boundary. Consequently, the operating limit, when defined as the point where lip separation occurs, is actually better for the small scale inlet even though the full scale inlet diffuser separation occurs at a lower airflow (due to the higher Reynolds number).

A thorough study of the data from the two tests was conducted to provide an understanding of this unexpected difference between model and full scale boundary layer separation characteristics. Comparisons of the static pressure profiles showed that a small, but perhaps very significant difference in pressure profile develops in the windward side hilite region at high angles of attack. This difference is illustrated in Figure 19. At V_0 = 74 m/s, α = 45°, WK1A = 120 kg/sm^2, the model and full scale pressure profiles agree reasonably well throughout the inlet although a small shift in the location of the minimum pressure is apparent. At V_0 = 40 m/s, α = 90°, WK1A = 148 kg/sm^2, the full scale profile has changed dramatically in the hilite region from a smooth profile with the minimum pressure inside the hilite to a "pointed" profile with the minimum pressure right at the hilite.

This pointed lip pressure profile was found to occur only on the full scale inlet and only at severe operating conditions. Figure 20 shows the band of free stream conditions separating the smooth profiles from the pointed profiles. Below the band the profiles are relatively smooth and similar to those observed on the 1/3 scale model. Above the band the full scale inlet profiles are pointed with the minimum pressure always occurring at the hilite.

Only a few test runs were devoted to investigating the lip separation phenomenon due to the high fan blade stresses (see Figure 15). As

indicated in Figure 20, all of these runs were conducted in the region of free stream conditions where the full scale inlet lip pressure profiles differ from the 1/3 scale inlet profiles by being "pointed" at the hilite (at inlet mass flows where the lip boundary layer is still attached). The possibility thus exists that the unexpected difference in separation progression between the full scale and the 1/3 scale inlets is related to the pointed lip pressure profiles.

The pointed profile is not well understood. Local deformation of the fiberglass lip is considered unlikely since eight aluminum girders were installed in the hollow lip to prevent buckling. The formation of a local laminar separation bubble is a distinct possibility but it remains to be explained why such a bubble would occur so consistently on the full scale inlet and never on the 1/3 scale inlet, and why it always would originate at the hilite. It appears that a more in-depth experimental study with sophisticated instrumentation for measurement of the very thin lip boundary layers will be required to answer these questions.

CONCLUDING REMARKS

The test results described in this paper point out that it is not always correct to assume that small scale inlet model testing will provide conservative data:

If the operating limit is defined as the point where boundary layer separation is first noticed at the fan face then the full scale inlet will have a substantially larger operating envelope than the 1/3 scale model. If, however, boundary layer separation is allowed up to the point where the fan blade stresses exceed their endurance limit, which seems to take place when the separation reaches the inlet lip, then the 1/3 scale inlet appears to provide the largest operating range.

This surprising result is associated with a difference in the rate of progression of the diffuser separation between the two inlet models and with the sudden occurrence of a lip separation on the full scale inlet.

To provide a more complete understanding of the inlet flow characteristics during high angle of attack operation it is recommended that detail boundary layer instrumentation as well as flow visualization methods be incorporated in future tests of this type. High-frequency static pressure transducers installed along the windward side cowl surface from the hilite region to the aft end of the diffuser should also be considered.

REFERENCES

1. M. A. Boles and N. O. Stockman, "Use of Experimental Separation Limits in the Theoretical Design of V/STOL Inlets", AIAA Paper 77-878, July 1977.

2. J. Koncsek and J. Syberg, "Fan Inlet for a V/STOL Airplane", AIAA Paper 77-802, July 1977.

3. R. J. Shaw, R. C. Williams and J. L. Koncsek, "V/STOL Inlet Nacelle Aerodynamics and its Relation to Fan Blade Stresses", NASA TM-78899, July 1978.

4. R. W. Luidens, N. O. Stockman, and J. H. Diedrich, "An Approach to Optimum Subsonic Inlet Design", NASA TM-79051, March 1979.

5. J. Syberg, "Low Speed Test of a High-Bypass Ratio Propulsion System with an Asymmetric Inlet Designed for a Tilt-Nacelle V/STOL Airplane", NASA CR-152072, January 1978.

6. J. L. Koncsek and R. J. Shaw, "Operating Characteristics of an Inlet Model Tested with a 0.5 Meter Powered Fan at High Angles of Attack", NASA CR-135270, September 1977.
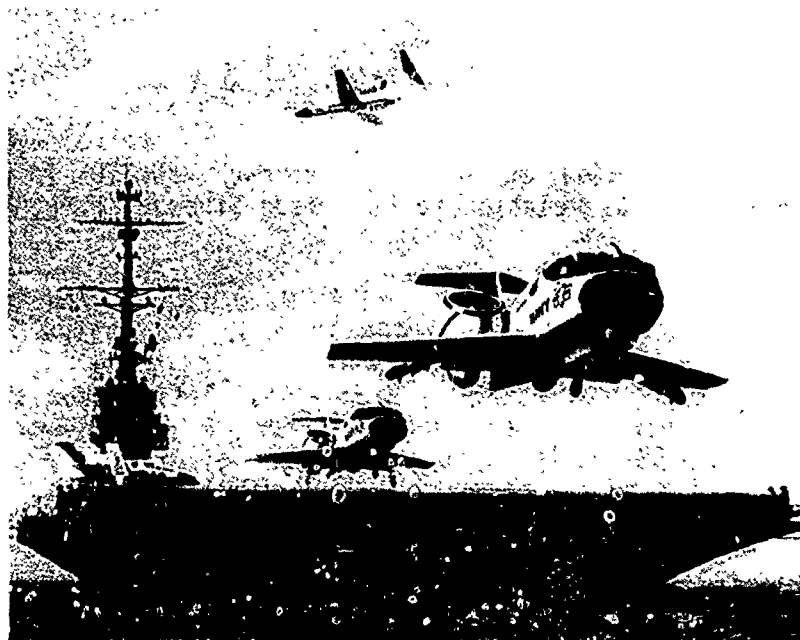
Figure 1. Tilt-Nacelle Lift-Cruise Fan Concept
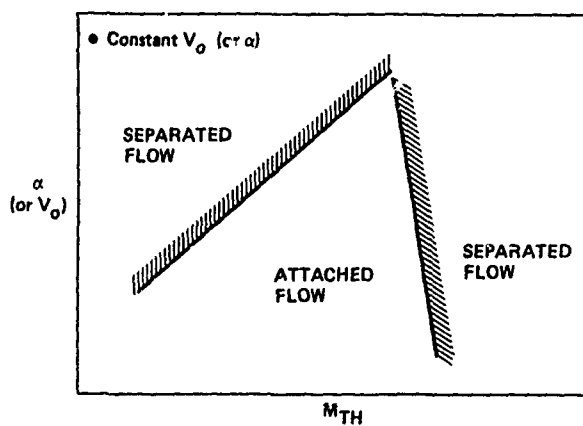
Figure 2. Inlet Separation Boundaries
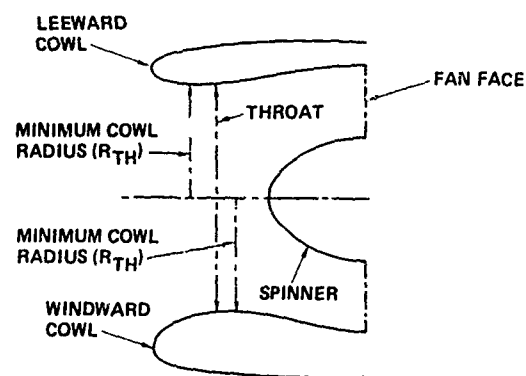
Figure 3. Inlet Schematic

618

2.90m 1.00m

1.304m

A_FAN = 1.206 m² CORE NOZZLE

COMPRESSOR INLET

A = 1.064 m²

A = 0.25 m²

FAN FAN DUCT CORE ENGINE

FAN NOZZLE

INLET FAN COWL

1.113m

a. NACELLE SCHEMATIC

b. NACELLE INSTALLED IN NASA AMES 40- by 80-ft WIND TUNNEL

Figure 4. Full Scale Test Model

TURBINE DRIVE AIR SUPPLY LINES

STATORS (25 BLADES)

MODEL SUPPORT STRUT

ROTORS (15 BLADES)

FAN ₵

TURBINE

VARIABLE AREA EXHAUST NOZZLE

a. INLET AND FAN ASSEMBLY

b. INLET AND FAN INSTALLED IN NASA LEWIS LOW-SPEED WIND TUNNEL

Figure 5. 1/3-Scale Test Model

POINT	V_o (m/s)	WKIA (kg/sm^2)
1	55.5	90
2	55.2	90
3	55.0	86
4	54.5	106
5	54.2	105
6	54.1	105
7	53.2	127
8	52.9	126
9	52.3	142
10	51.9	140
11	51.6	140
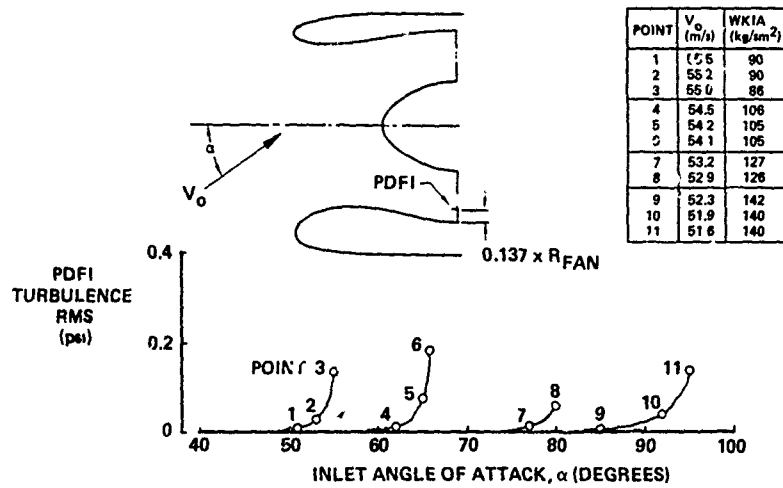
Figure 6. On-Line Display of Inlet Boundary Layer Separation

Symbol	V_o (m/s)	α (deg)	WKIA (kg/sm^2)
o	51.9	92	139.3
□	51.7	95	138.5
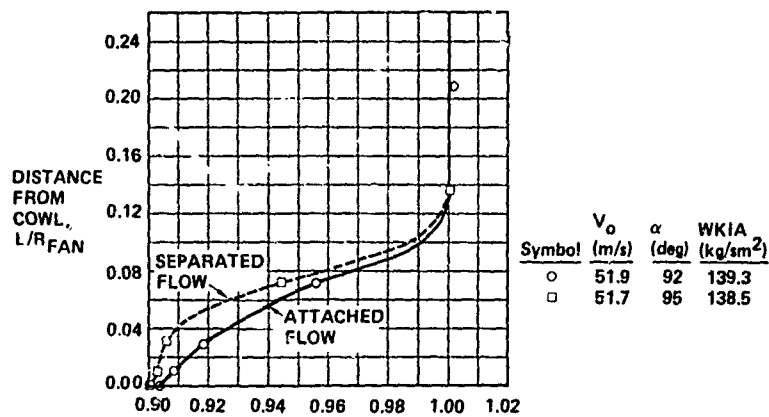
Figure 7. Fan Face Total Pressure Profiles, Windward Rake
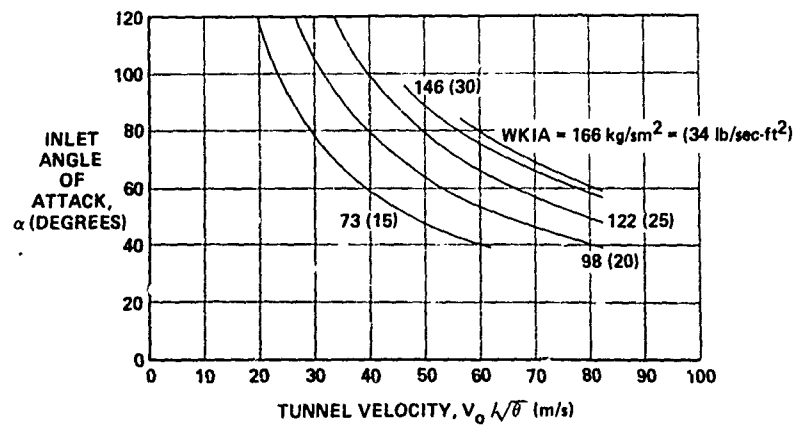
Figure 8. Separation Boundaries
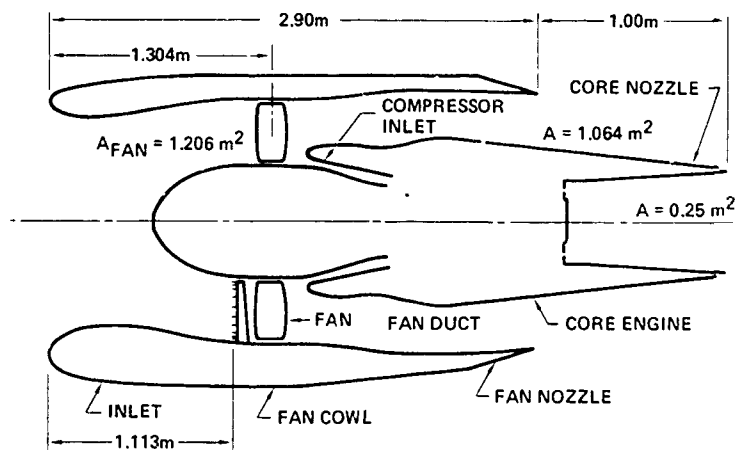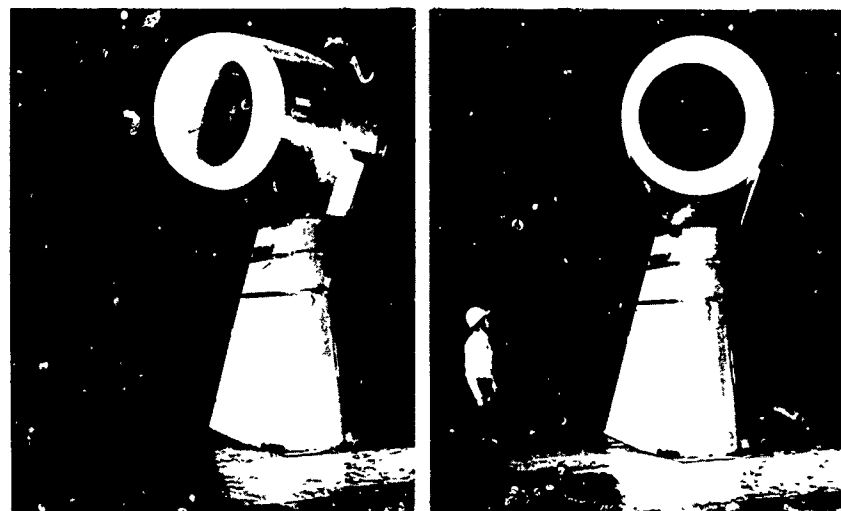
2.90m

1.304m

$A_{FAN} = 1.206 \text{ m}^2$

COMPRESSOR INLET

CORE NOZZLE

1.00m

$A = 1.064 \text{ m}^2$

$A = 0.25 \text{ m}^2$

FAN   FAN DUCT   CORE ENGINE

INLET   FAN COWL   FAN NOZZLE

1.113m

a. NACELLE SCHEMATIC

b. NACELLE INSTALLED IN NASA AMES 40- by 80-ft WIND TUNNEL

Figure 4. Full Scale Test Model

TURBINE DRIVE AIR SUPPLY LINES

STATORS (25 BLADES)

ROTORS (15 BLADES)

MODEL SUPPORT STRUT

FAN ₵

TURBINE

VARIABLE AREA EXHAUST NOZZLE
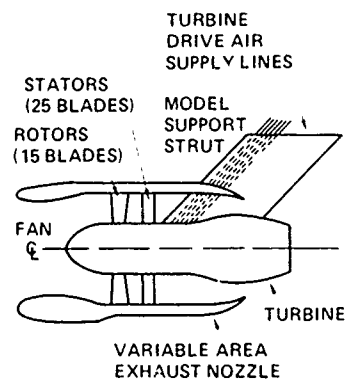
a. INLET AND FAN ASSEMBLY
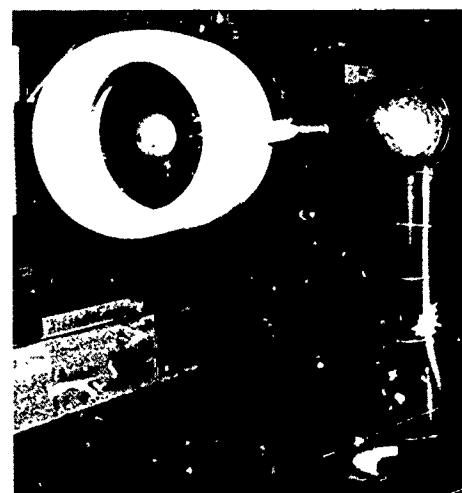
b. INLET AND FAN INSTALLED IN NASA LEWIS LOW-SPEED WIND TUNNEL

Figure 5. 1/3-Scale Test Model
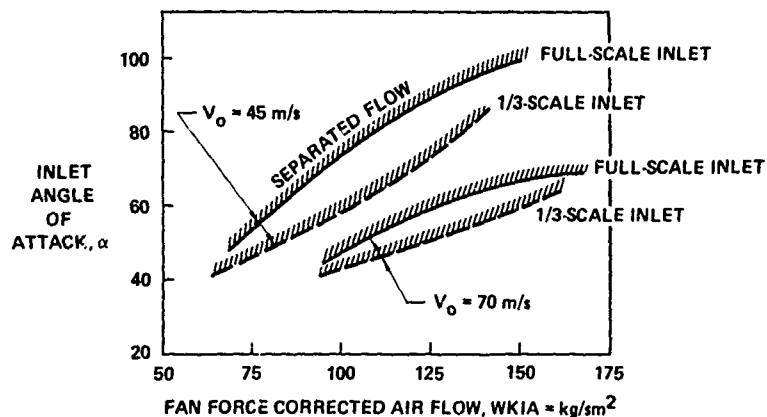
Figure 9. Separation Boundaries for Full-Scale and 1/3-Scale Tilt-Nacelle Inlets
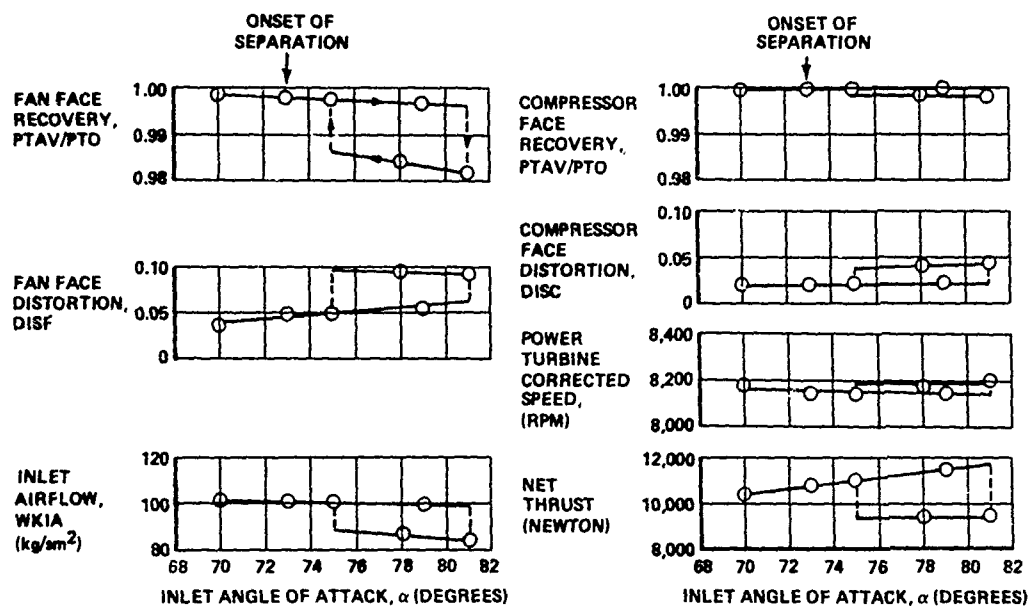
Figure 10. Performance Characteristics During Separation— V_O = 45 m/s, WKIA = 100 kg/sm^2
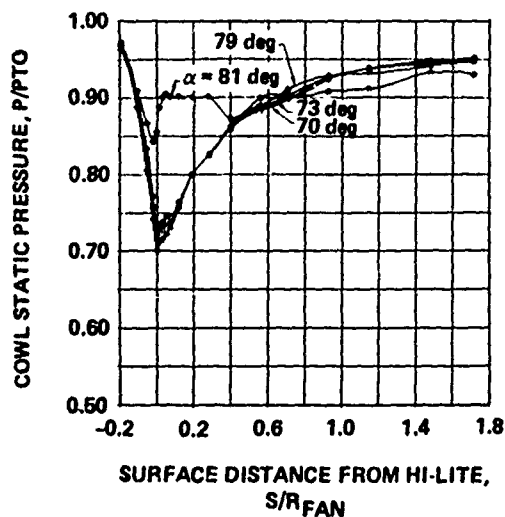
Figure 11. Windward Cowl Static Pressure Profiles—
V_O = 45 m/s, WKIA = 100 kg/sm^2
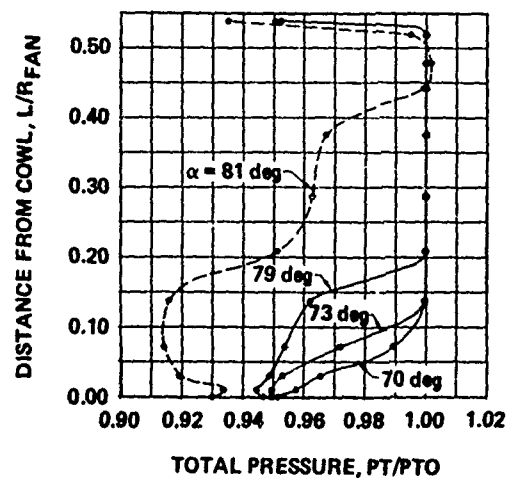
Figure 12. Fan Face Total Pressure Profiles, Windward Rake—V_O = 45 m/s, WKIA = 100 kg/sm^2

	PT/PTO		PT/PTO
1	0.9950	6	0.9200
2	0.9900	7	0.9000
3	0.9800	8	0.8600
4	0.9600	9	0.8200
5	0.9400	0	0.7800

$\alpha = 73$ deg $\alpha = 79$ deg $\alpha = 81$ deg

VIEW LOOKING AFT
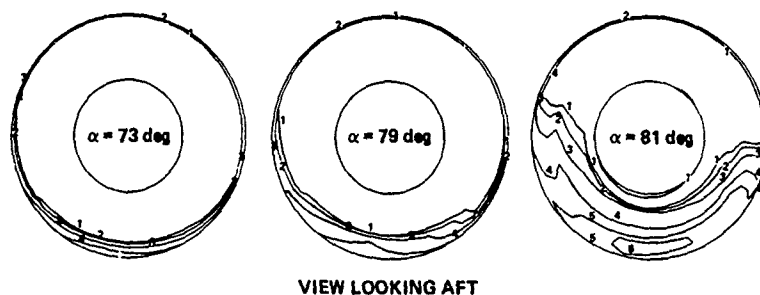
Figure 13. Fan Face Total Pressure Maps—V_O = 45 m/s, WKIA = 100 kg/sm^2

Symbol	α (deg)
	70
	73
	79
	81

Symbol	α (deg)
	70
	73
	79
	81

FAN NOZZLE PRESSURE RATIO, PT/PTO
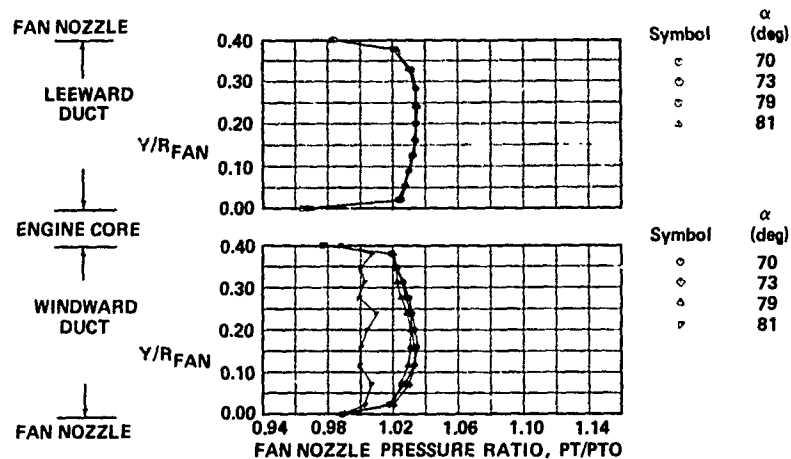
Figure 14. Fan Nozzle Total Pressure Profiles—V_O = 45 m/s, WKIA = 100 kg/sm^2

- V_o = 45 m/s
- WKIA = 100 kg/sm^2

NOTE: Stress values are based on an average of the peak readings from three bending guages mounted 36.2 cm from the tip of blades 1, 6, and 7.

BLADE VIBRATORY STRESS (N/m^2 x 10^{-6})

INLET ANGLE OF ATTACK, α (DEGREES)
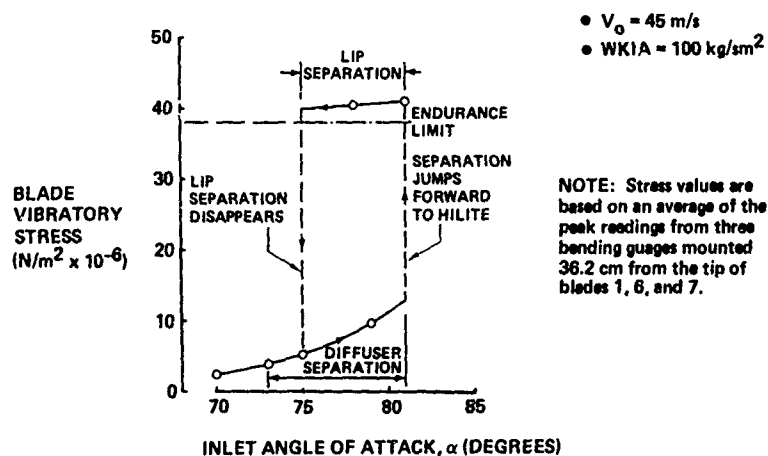
Figure 15. Fan Blade Vibratory Stress During Lip Separation

622
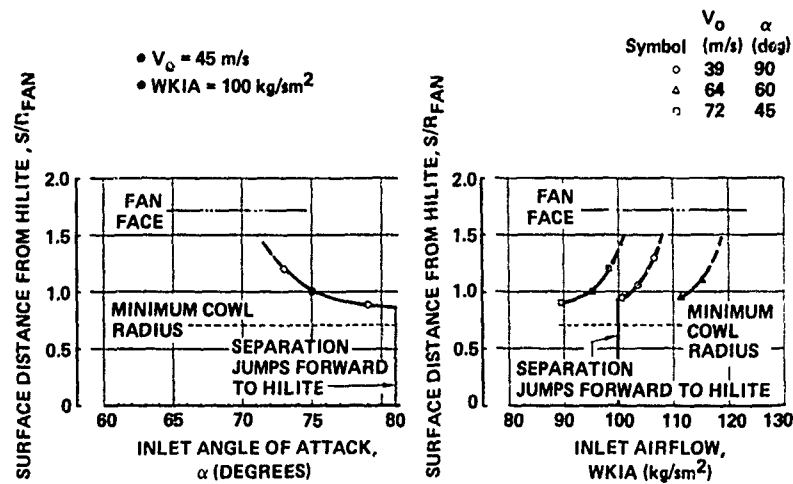
Figure 16. Estimated Location of Leading Edge of Separation in Windward Plane
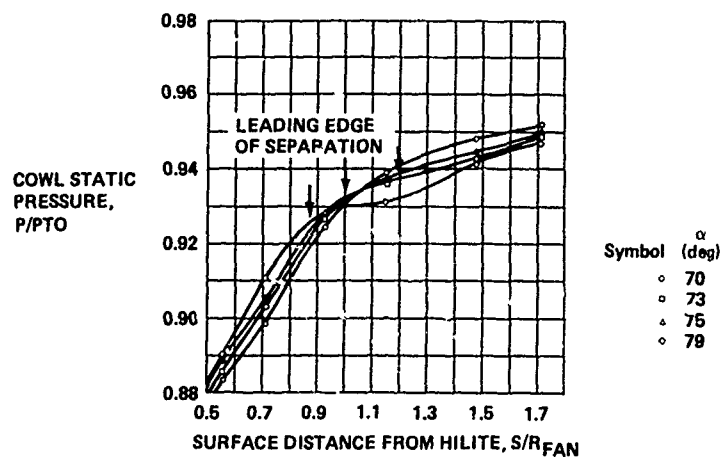
Figure 17. Static Pressure Profiles with Diffuser Separation—$V_O = 45$ m/s, $WKIA = 100$ kg/sm^2
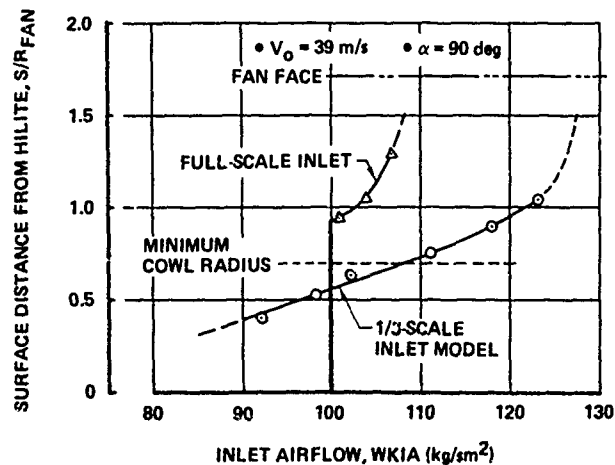
Figure 18. Diffuser Separation Characteristics in Small- and Large-Scale Inlet Models

623
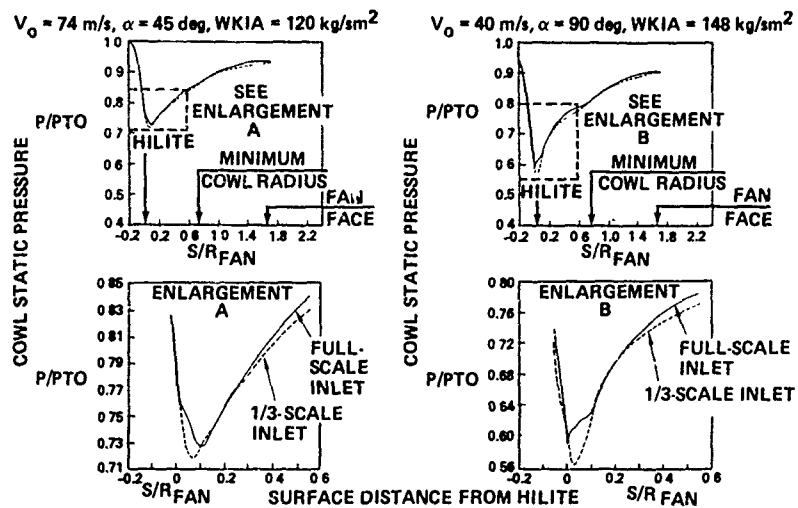
Figure 19. Comparison of Full Scale and 1/3-Scale Inlet Lip Pressure Profiles
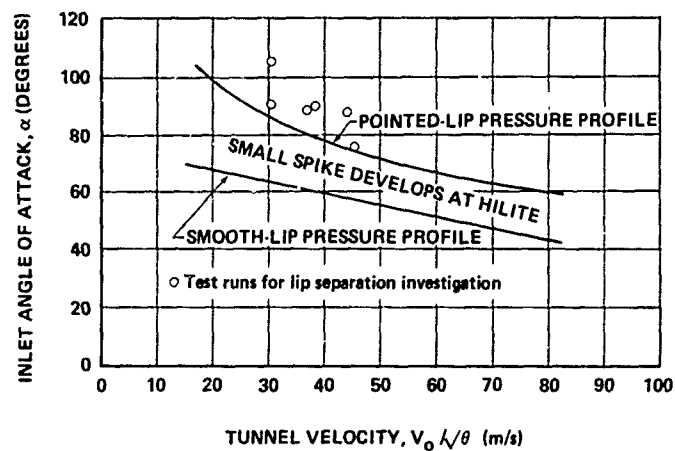
Figure 20. Regions Characterizing Full-Scale Inlet Lip Pressure Profile

LOW SPEED DEVELOPMENT OF THE SUPERSONIC

XFV-12A V/STOL INLET

J. T. DeLany

Rockwell International

ABSTRACT

Inlet performance and pressure distribution of the supersonic XFV-12A
V/STOL technology prototype were initially investigated with a 0.2 scale
model in static and low speed wind tunnel tests. The model simulated the
complete forebody of the XFV-12A including the primary inlet with porous
ramps fixed in the takeoff position, the inlet ramp bleed system, the
auxiliary inlet with adjustable doors and a canard with fully blown aug-
menter surfaces. The internal trifurcated duct lines simulated the air-
craft design. A 40-probe steady-state total pressure rake was used to
obtain engine face pressure distributions. Additionally, a few high-
response total pressure probes were used to obtain local turbulence at
selected spatial locations. Wind tunnel tests were conducted in the
4.9 x 4.3m (16' x 14') V/STOL section of NACAL, the Rockwell International
wind tunnel facility in Columbus, Ohio. The model was tested at takeoff
and landing speeds at angles of attack up to 30° and sideslip angles of
25°. Test results indicated good recovery and distortion characteristics
over the range of variables tested, with the static recovery goal of 96%
achieved in initial tests. Augmenter operation had a negligible effect
on inlet characteristics. Pressure distribution plots at the simulated
engine face indicate an unusual, but benign pressure profile. Limited
correlation data from tests of a one-sixth scale XFV-12A model at NASA
Ames and from full scale static tests of XFV-12A #1 at NASA Langley are
presented.

Currently under development for the U. S. Navy, the XFV-12A V/STOL technology prototype, Figure 1, embodies the thrust augmented wing principle for maximizing lifting efficiency using a basic turbofan engine. The augmenters in the wing and canard entrain large amounts of ambient air, producing greater lifting force than attainable with the engine alone, while providing a benign footprint. With the augmenter closed, Figure 2, the XFV-12A is the prototype of a multi-mission supersonic fighter capable of Mach 2+ speeds.

The wide speed range of operation, with the additional requirement of noninterference between the inlet and augmenter, represented the inlet design challenge. The resulting design concept is both conventional and innovative. The primary inlets are conventional two-dimensional vertical ramp supersonic inlets. Vertical rather than horizontal ramp orientation was selected for better integration with the bifurcated duct leading to the single turbofan engine and to provide a greater degree of canard shielding to minimize nearfield reingestion. To minimize costs, the prototype inlets are F-4A inlets which were modified to match F401 engine airflow requirements, to obtain additional supersonic flow turning and to provide higher Mach number potential.

The large auxiliary inlet was placed on top, rather than what would be a more conventional location in the sides of the inlet cowls, to minimize reingestion and FOD, and to minimize interaction with the canard augmenter. The result is a trifurcated inlet for V/STOL operation which closes to become a somewhat unconventionally contoured bifurcated inlet for high speed flight.

To obtain early experimental verification of the trifurcated inlet concept, an inexpensive scale model, Figure 3, was fabricated, primarily of wood. Based on engine airflow and the simulated engine face diameter, the scale was 0.2, sufficently large for detailed flow studies. An ejector was used to induce flow through the model. Results of initial static tests answered several fundamental questions:

(1) Inlet recovery matched the predicted values of 96%, Figure 4.

(2) Benign engine face distortion patterns were obtained, Figure 5.

(3) The effect on the inlet of the canard augmenter is negligible, Figure 6. (In subsequent tests it was likewise established that the inlet proximity has no effect on augmenter performance.)

As tested in the first test, the model did not quite represent what were later to become the lines of the XFV-12A. Nevertheless, it served to establish the efficacy of the trifurcated inlet concept for static/lift-off operation.

Early full scale validation of the concept was obtained in 1975 when the forward fuselage of the XFV-12A, as it progressed through assembly, was moved temporarily to the engineering engine test cell at the Columbus Plant where it was mated to an afterburning F401 engine, Figure 7. Engine operation, at all power settings including afterburning, was unaffected by inlet geometry variations including positioning of the inlet ramps in the fully closed (supersonic) position and partial closure of the auxiliary inlet. Auxiliary door operation was checked during these tests by close visual observation. Smooth operation of the doors, shown in Figure 8, was obtained by proper balance of spring stiffness and seal friction. The doors open during the engine start cycle, and are fully and stably open at engine idle. Measured inlet recovery was noticeably higher than the model data, as seen in Figure 9, apparently reflecting the improved lines of the actual aircraft inlet as well as beneficial Reynolds number (scale) effect. In the distortion patterns obtained from the full scale tests, the flow defect noted in the model distortion patterns was absent. As the defect was also absent in tests of 0.168 scale model, to be discussed later, it was attributed to a model peculiarity, scale effects having been eliminated. The full scale and model patterns are shown in Figure 10. Full scale turbulence, obtained using a single probe, shown in Figure 11, indicates comparatively low levels. With the completion of the full scale engine inlet integration test, the first phase of the model development program, which was concerned primarily with verification of the trifurcated inlet concept's ability to deliver the estimated level of performance at satisfactory distortion levels, was completed.

Low speed wind tunnel tests, using the 0.2 scale low speed model shown in Figure 3, were conducted in the 4.9 x 4.3 meter (16 x 14 foot) V/STOL section of the Columbus Plant NACAL facility. The purpose of these tests was to investigate the inlet characteristics under high angle of attack and sideslip conditions. A photograph of the model in the test section at high angle of attack is shown in Figure 12. These tests, which simulated speeds up to 34 m/s (66 kts), were conducted to the attitude limits achieveable with the comparatively large model in the test section. As shown in Figure 13, recovery and distortion were satisfactory up to approximately 30° angle of attack and 25° of sideslip. This was considered significant because of the high angles realized during the landing mode as well as under cross wind conditions.

Results of other tests in this series established that canard deflections, simulating roll and yaw control positions, had no effect on inlet performance. They also provided door position optimization information, Figure 14.

Prior to the initiation of a high speed model program, the low speed model was modified by the addition of bellmouth inlet lips as shown in Figure 15. Tests with this configuration were intended to obtain inlet distortion patterns which might be typical of high speed cruise flight. While the patterns were comparatively benign, they were noticeably different from those obtained in subsequent high speed model tests. A

fallout of these tests was the isolation of the diffuser losses from the lip losses. As seen in Figure 16, the diffuser and lips were about equal contributors, indicating that some improvement could be obtained by blunting of the inlet lips, as expected. It should be noted that under static conditions, approximately 45% of the engine airflow demand is satisfied by the primary inlet and 55% by the auxiliary inlet. This was obtained by removing the bellmouth lips, closing the auxiliary doors and calibrating the primary inlet ducts. Then with the auxiliary inlets open, using the throat static pressure, the flow entering the main inlets was determined. From this information, the momentum of each inlet stream could be calculated. At maximum flow, the inlet velocity is approximately 82 m/s (M = 0.24).

A new model, designed to withstand transonic testing loads, was constructed at 0.168 scale, sufficiently large based on tests of other models with high response pressure instrumentation, yet small enough to test to desired angles of attack in the transonic/supersonic tunnels under consideration. This model has been tested to date in the NASA Ames 14 foot transonic tunnel. The model is shown installed in the tunnel in Figure 17. Although the tests were conducted up to the limit Mach number of the tunnel, only the low speed portion is discussed in this paper for comparison with other static and low speed tests. The static performance comparison is shown in Figure 9 which shows that the recovery data, like that of the 0.2 scale model, is slightly less than that of the full scale aircraft. These data are also shown in Figure 18, which also compares the pressure recovery obtained with the auxiliary inlet doors closed. This curve, more than any other, shows the tremendous benefit of the auxiliary inlet system.

A stability assessment, conducted by the engine manufacturer, based on the inlet distortion characteristics as measured by high response pressure instrumentation, indicated satisfactory inlet/engine compatibility throughout the low speed regime.

As presented in Figure 9, full scale aircraft operation, with all augmenters operating, resulted in pressure recovery and distortion data similar to early full scale testing results as expected. Even under certain tests at NASA Langley, see Figure 19, in which the aircraft was deliberately maintained in a high reingestion environment, engine operation was satisfactory.

Conclusions:

1. Static inlet performance of the trifurcated inlet of the XFV-12A is excellent.

2. Inlet performance at low speeds is satisfactory within the range of angle of attack and sideslip conditions tested.

3. Early model data, even with premature configuration details, was useful in establishing the acceptability of the trifurcated inlet concept.

FIGURE 1. XFV-12A

629
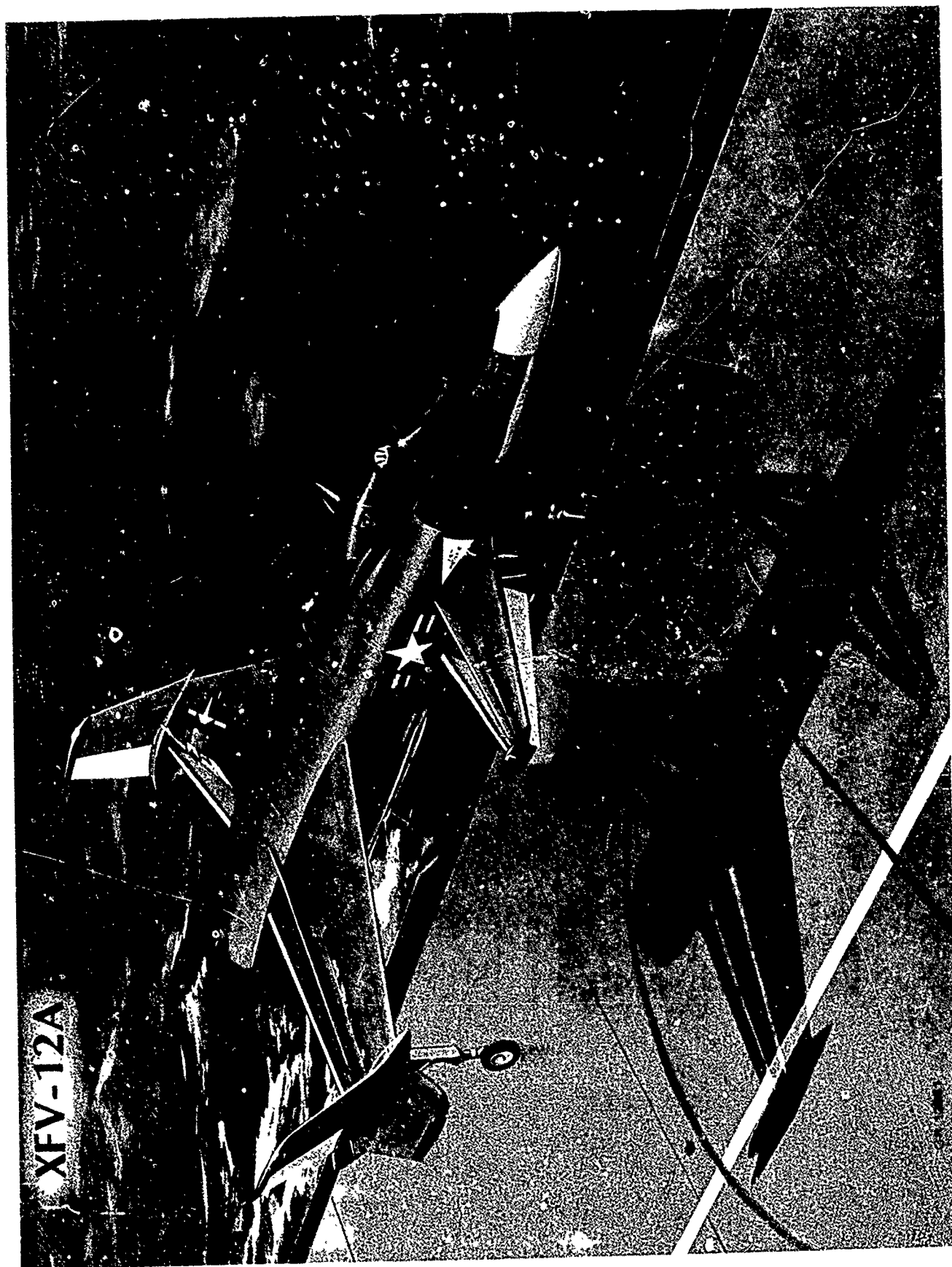
FIGURE 2. XFV-12A IN FLIGHT (ARTIST'S CONCEPTION)
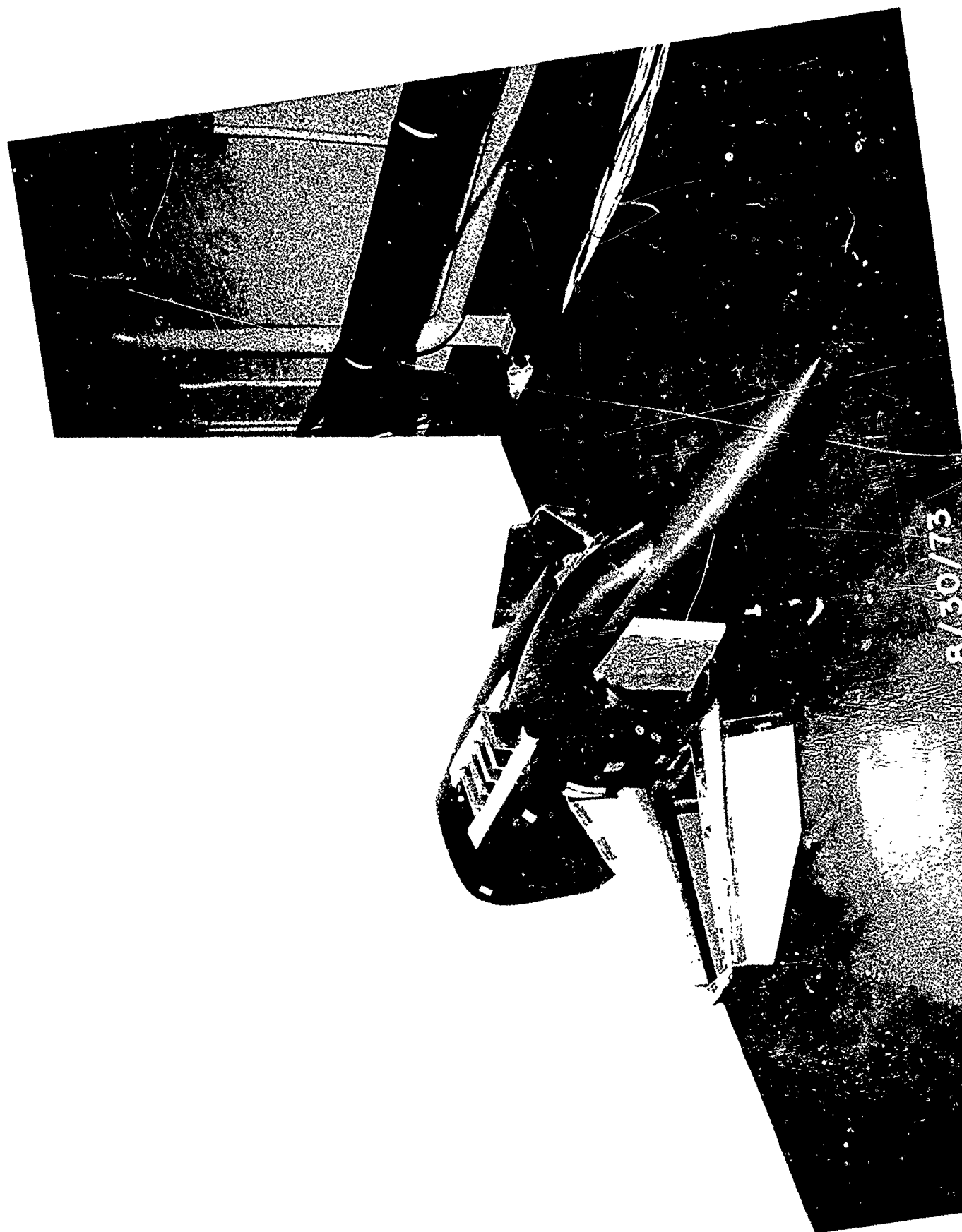
FIGURE 3. LOW SPEED INLET MODEL

H356-93-9A   8/30/73

FIGURE 4. MODEL RECOVERY

632

TOP

Hub
Perimeter

Fan
Perimeter

$P_{TL}/P_{TL,\ AVG}$	
0.96	= —··—··—
0.98	= ············
1.00	= — — —
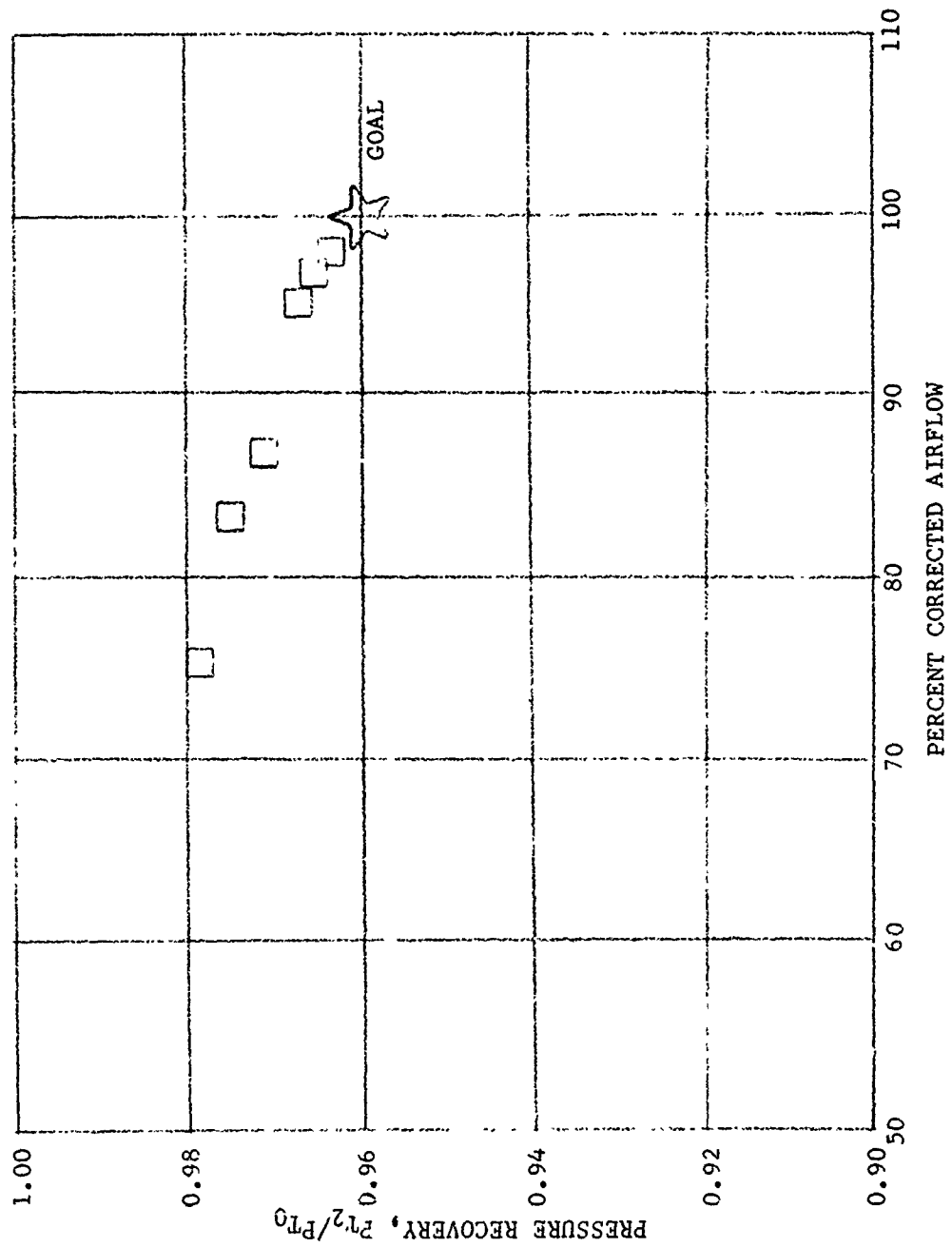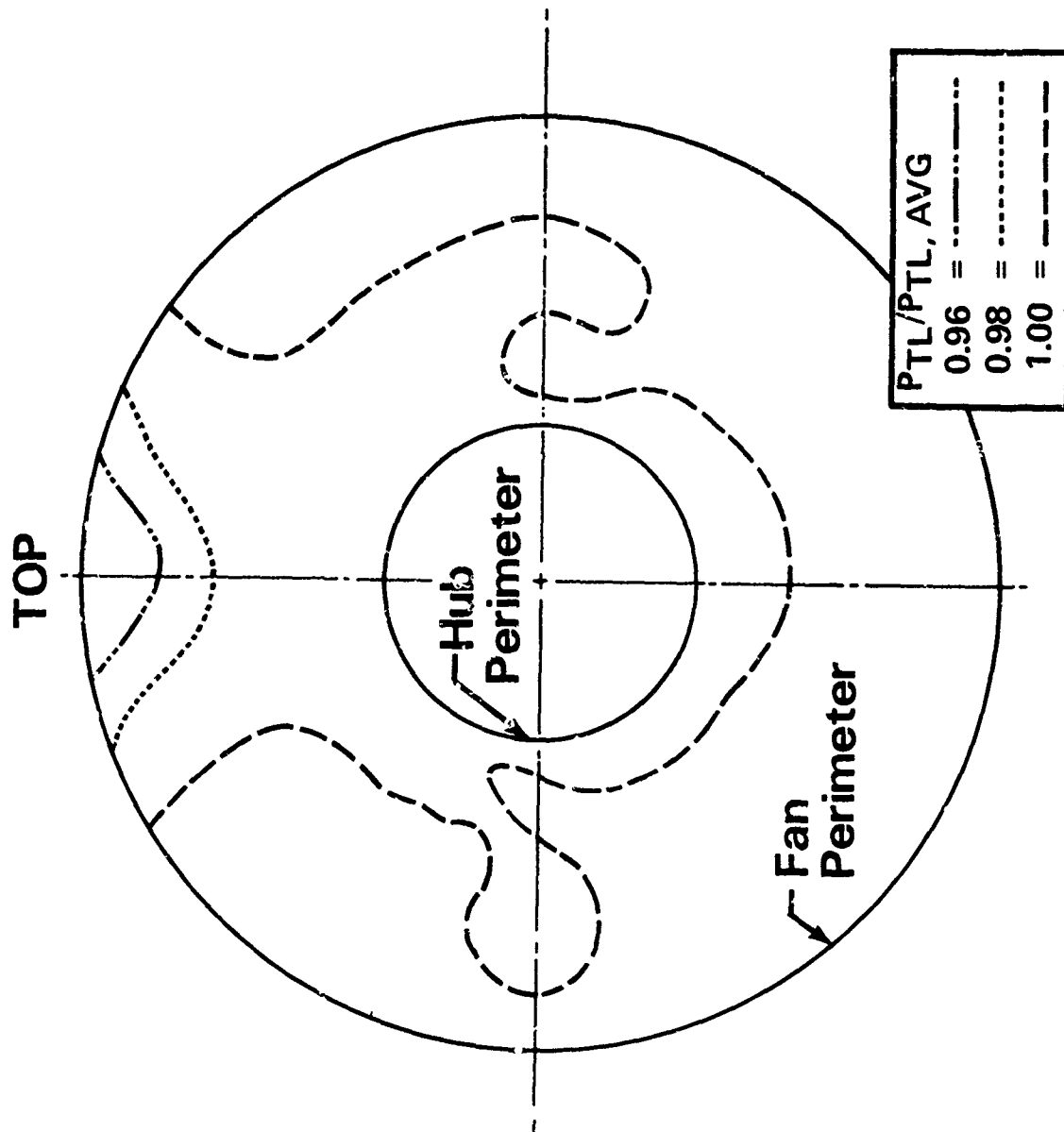
FIGURE 5.   MODEL DISTORTION
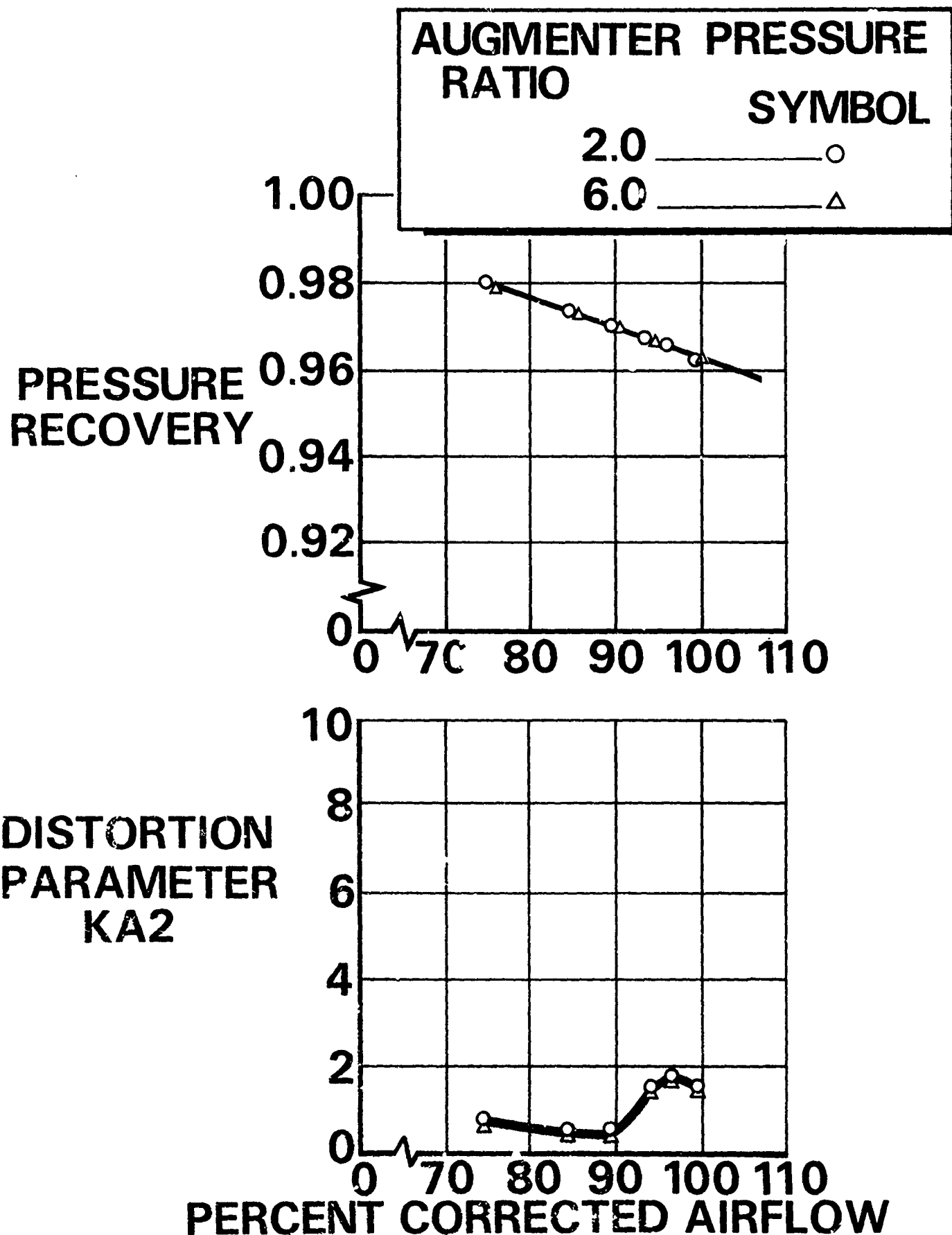
FIGURE 6. EFFECT OF AUGMENTER
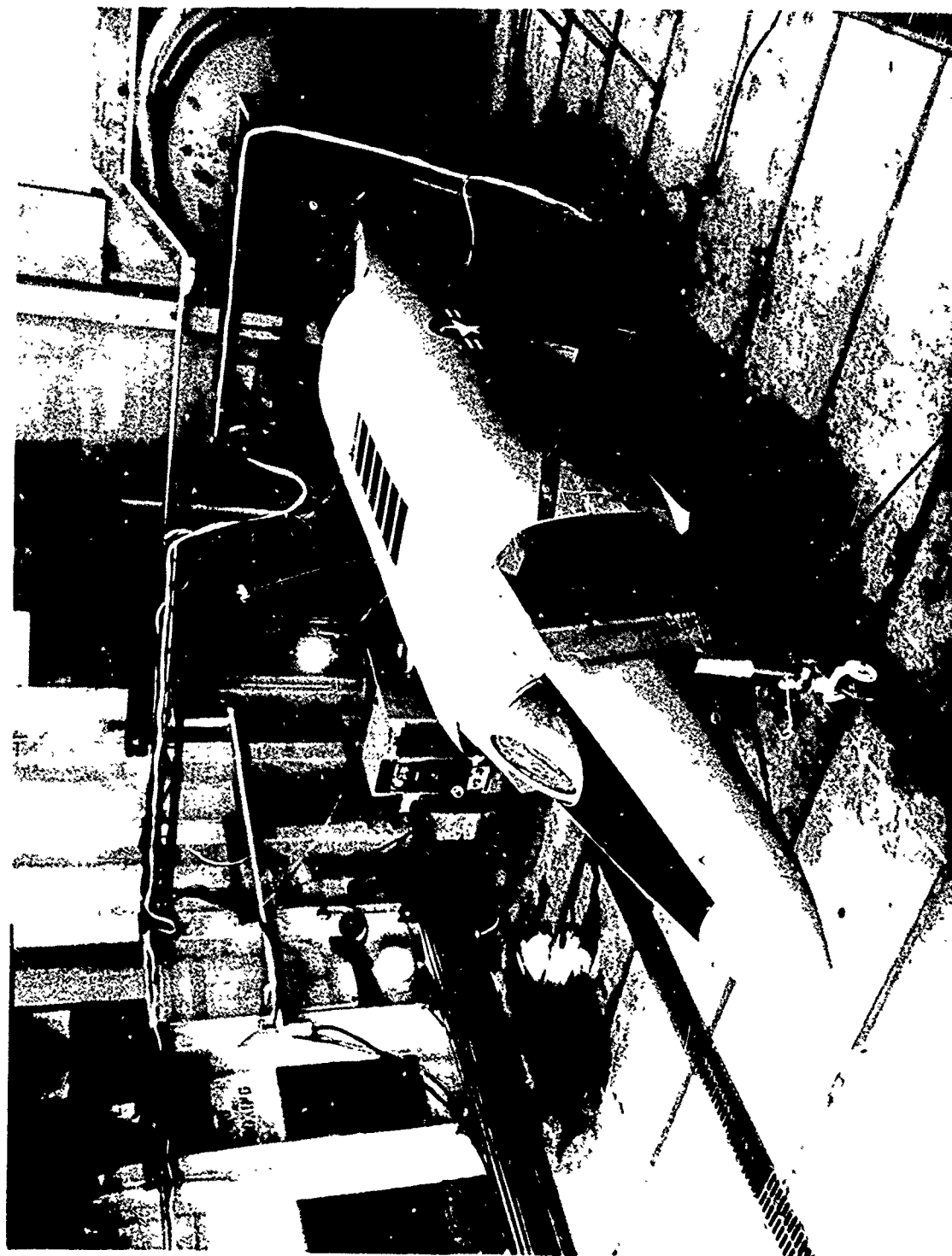
FIGURE 7. INLET/ENGINE INTEGRATION TEST

FIGURE 8. AUXILIARY INLET

SYMBOL	SCALE	ARTICLE	SITE	TEST NO.	RUN NO.
O	0.168	Model	Ames	233-1-14	82
△	0.2	Model	CAD	241	9
□	Full	Forebody	CAD	13	-
◇	Full	XFV-12A #1	CAD	24	-
▷	Full	XFV-12A #1	CAD	28	-
0	Full	XFV-12A #1	Langley	38	-
(	Full	XFV-12A #1	Langley	42	-

Vertical axes: P_{T2}/P_{T0} (1.00, .96, .92, .88, .84), KA_2 (6, 4, 2, 0)

Horizontal axis: % Design Corrected Airflow, % W_{DES} (50, 60, 70, 80, 90, 100, 110)

INLET DATA CORRELATION
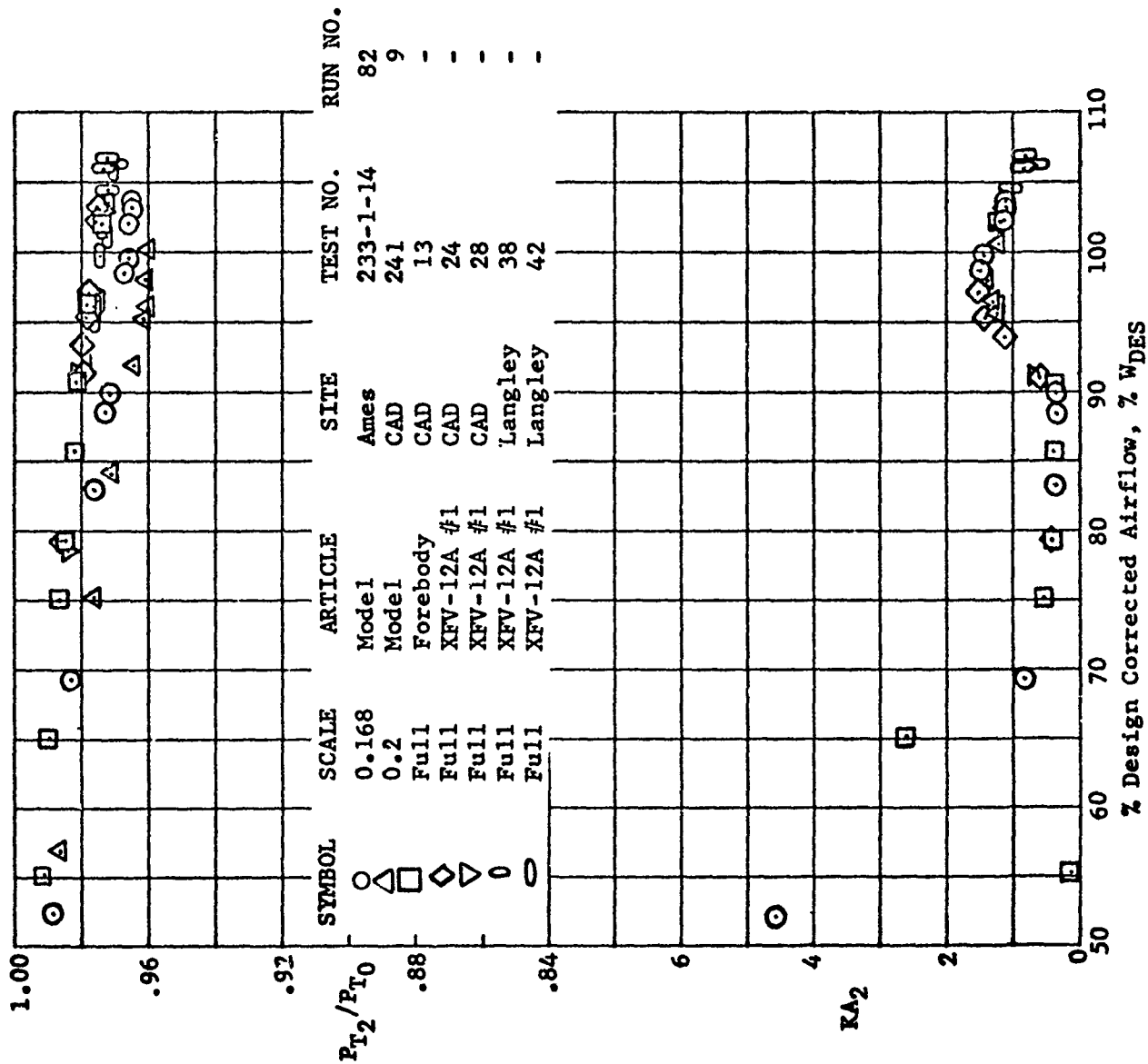
PRESSURE DISTRIBUTION - STATIC CONDITIONS

XFV-12A TEST

%WDES = 103.1
PT2/PTO = 0.977
KA2   = 1.10

82/12
%WDES = 103.7
PT2/PTO = 0.966
KA2   = 1.10

PHASE I AMES TEST
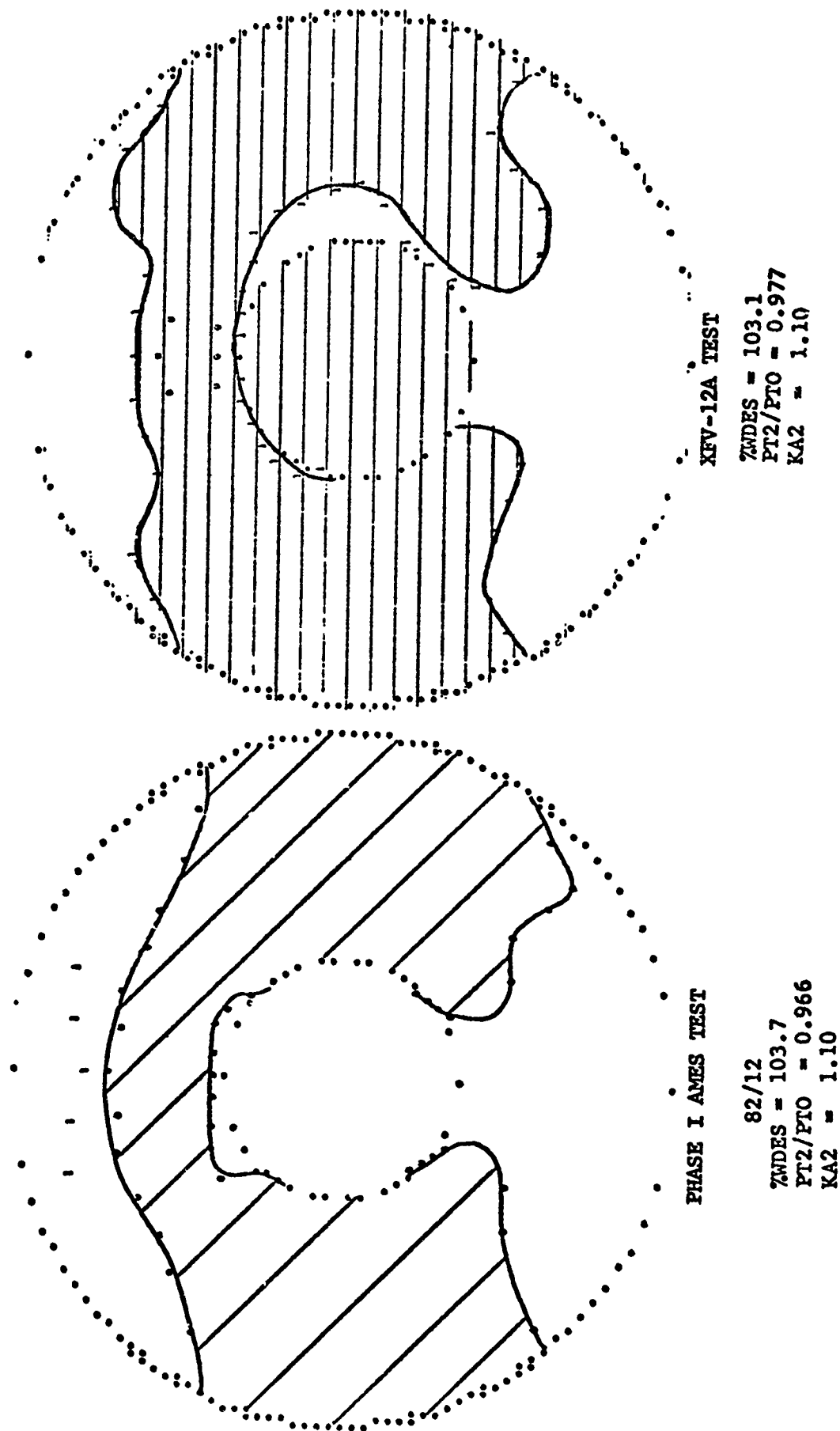
FIGURE 10. ENGINE FACE DISTORTION COMPARISON

Turbulence Measured by Single Probe on 0° (TDC) Rake,

at D/OD = 0.552, during CAD Tests

○ Test 11 ~ Second Ramp Angle = 17°, FOD Screens on

□ Test 12 ~ Second Ramp Angle = 11°, 30', FOD Screens off
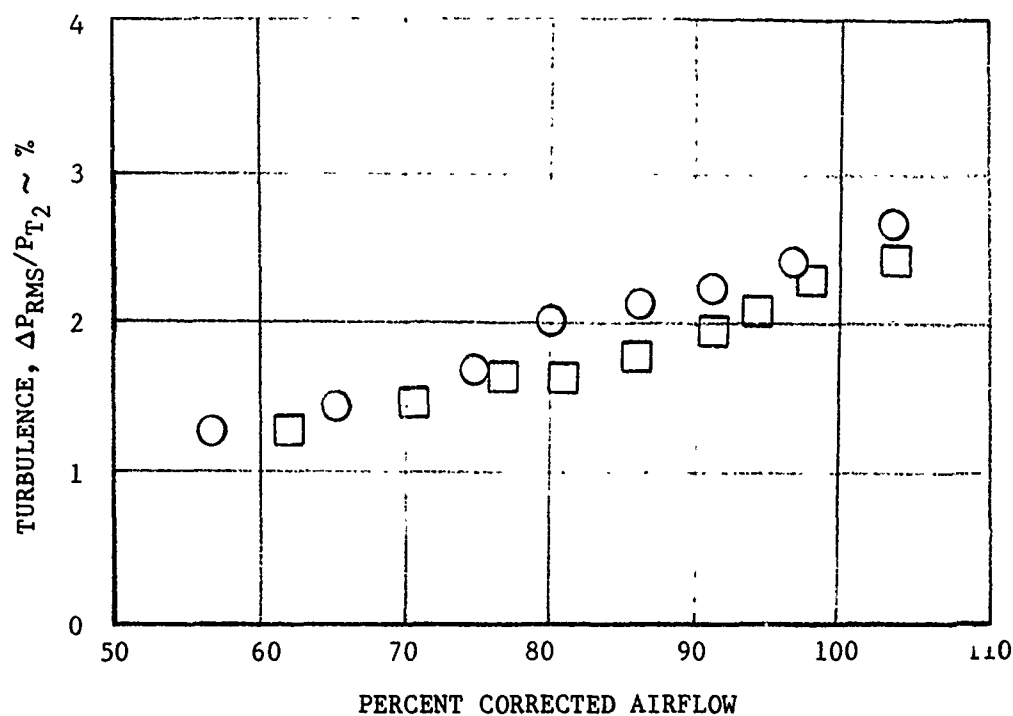
FIGURE 11. TURBULENCE

H356-93-47B⎿   9/10/
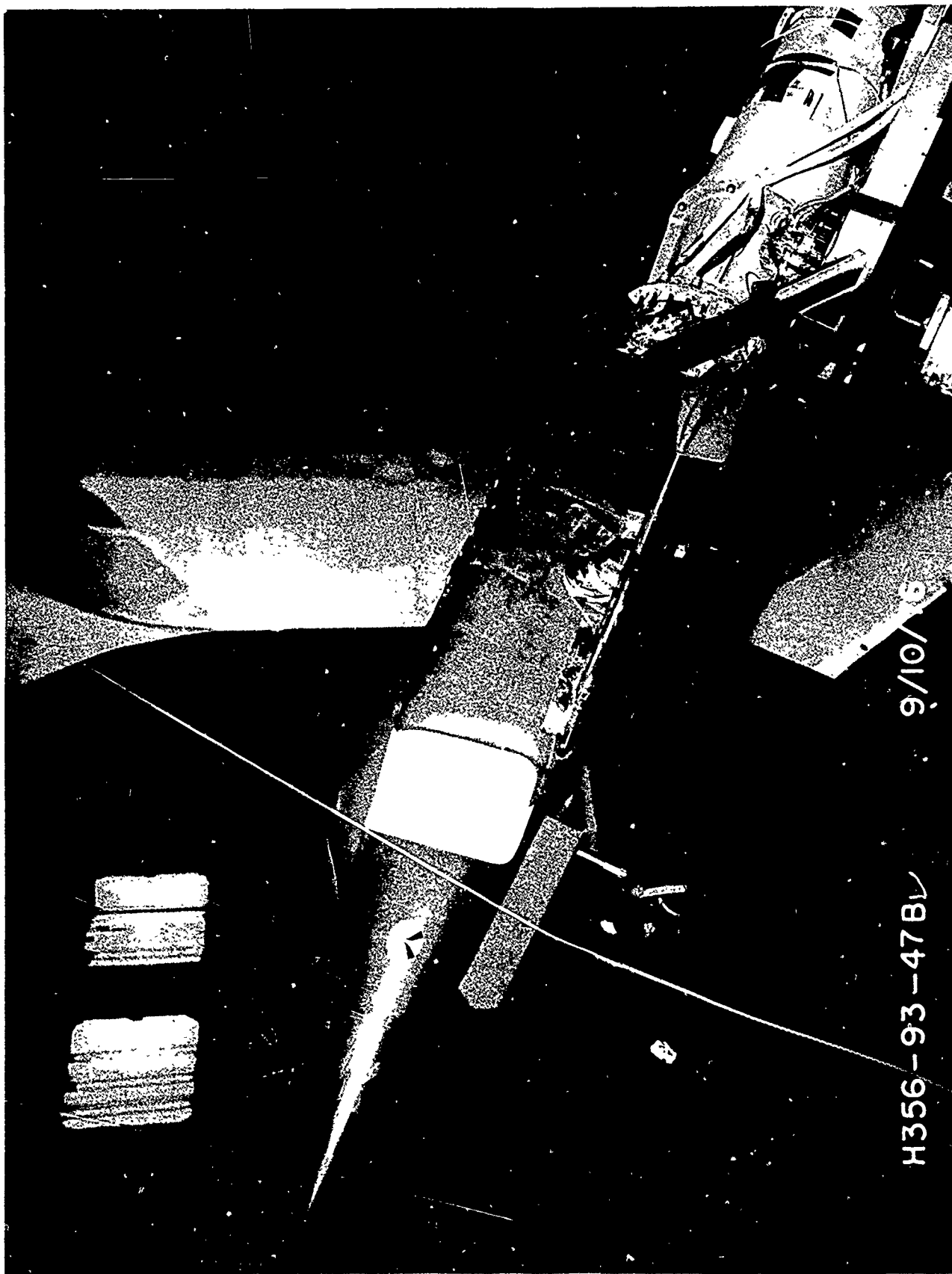
FIGURE 12.   LOW SPEED INLET MODEL AT ANGLE OF ATTACK
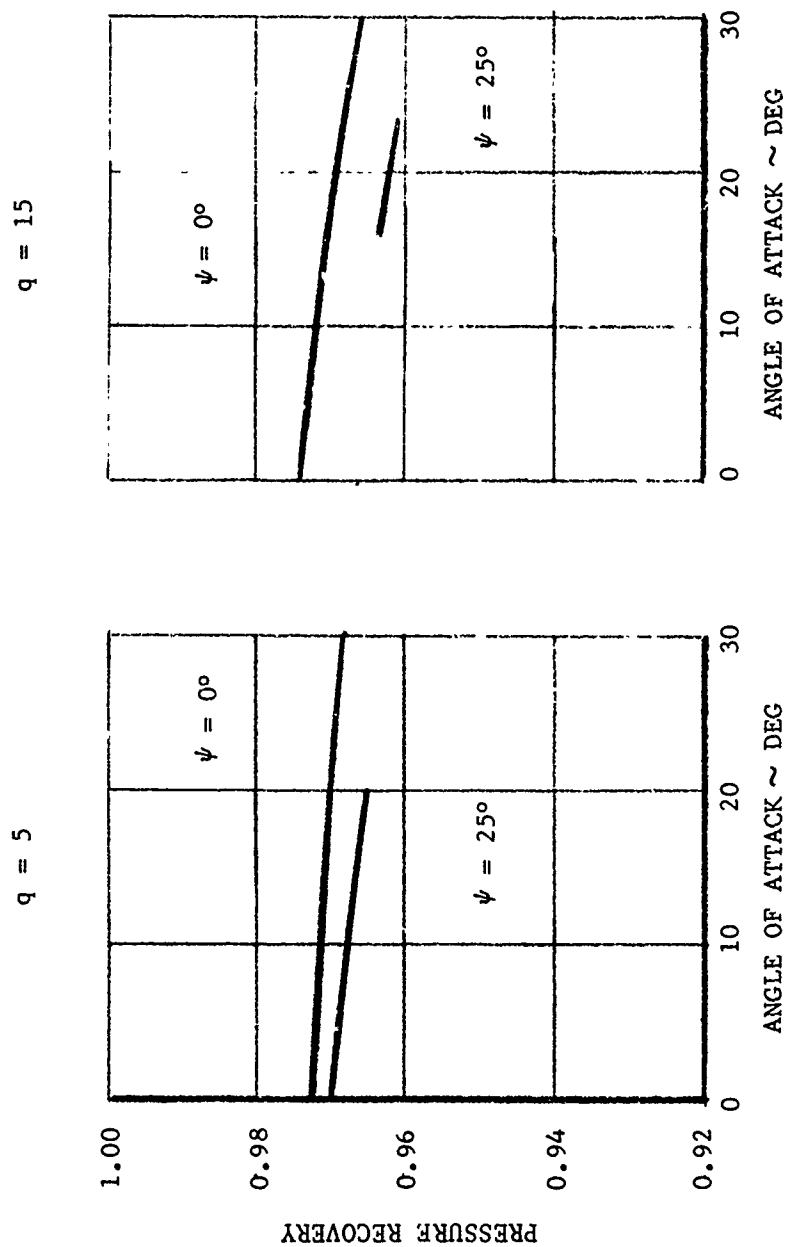
FIGURE 13. EFFECT OF PITCH AND SIDESLIP
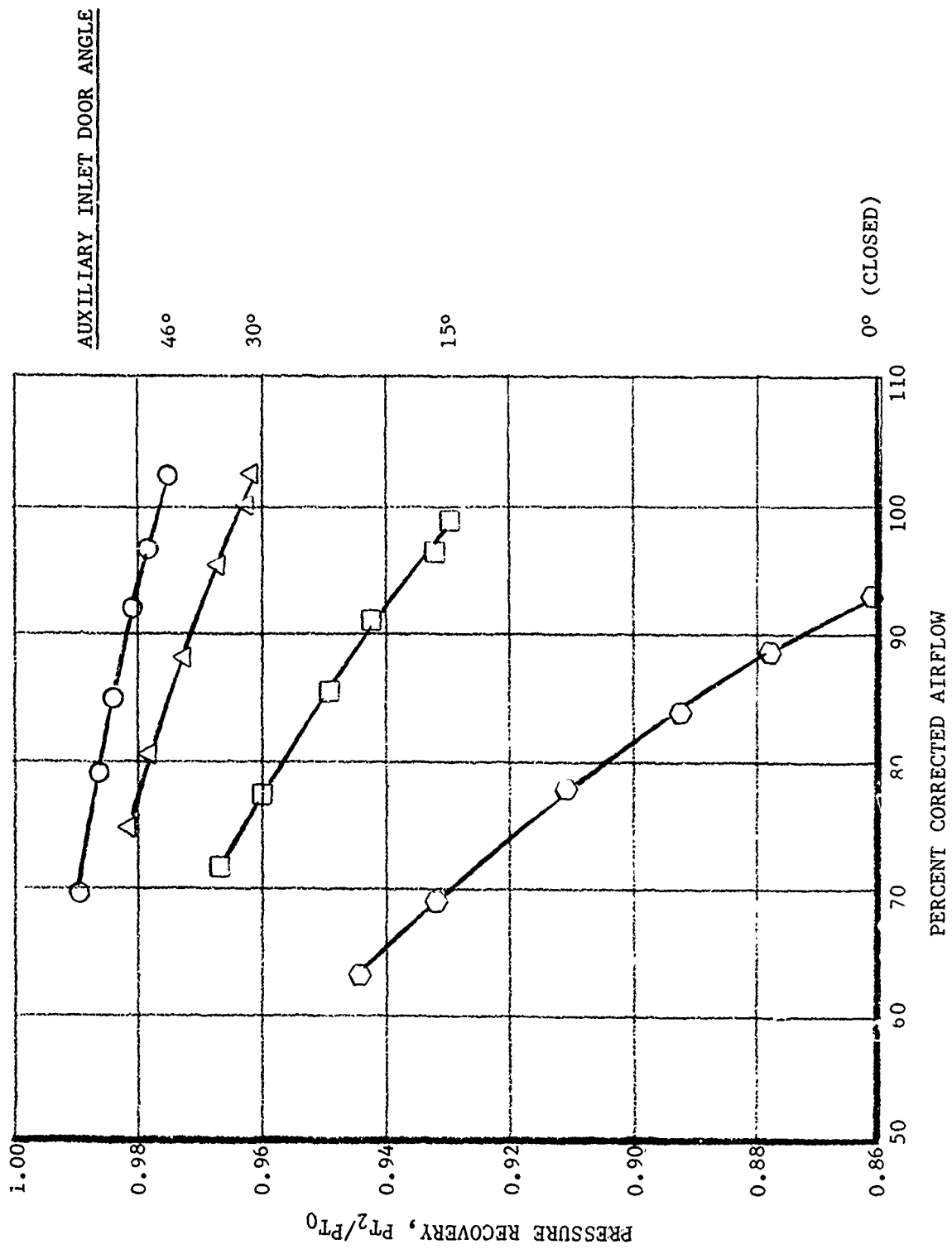
FIGURE 14. DOOR ANGLE

642
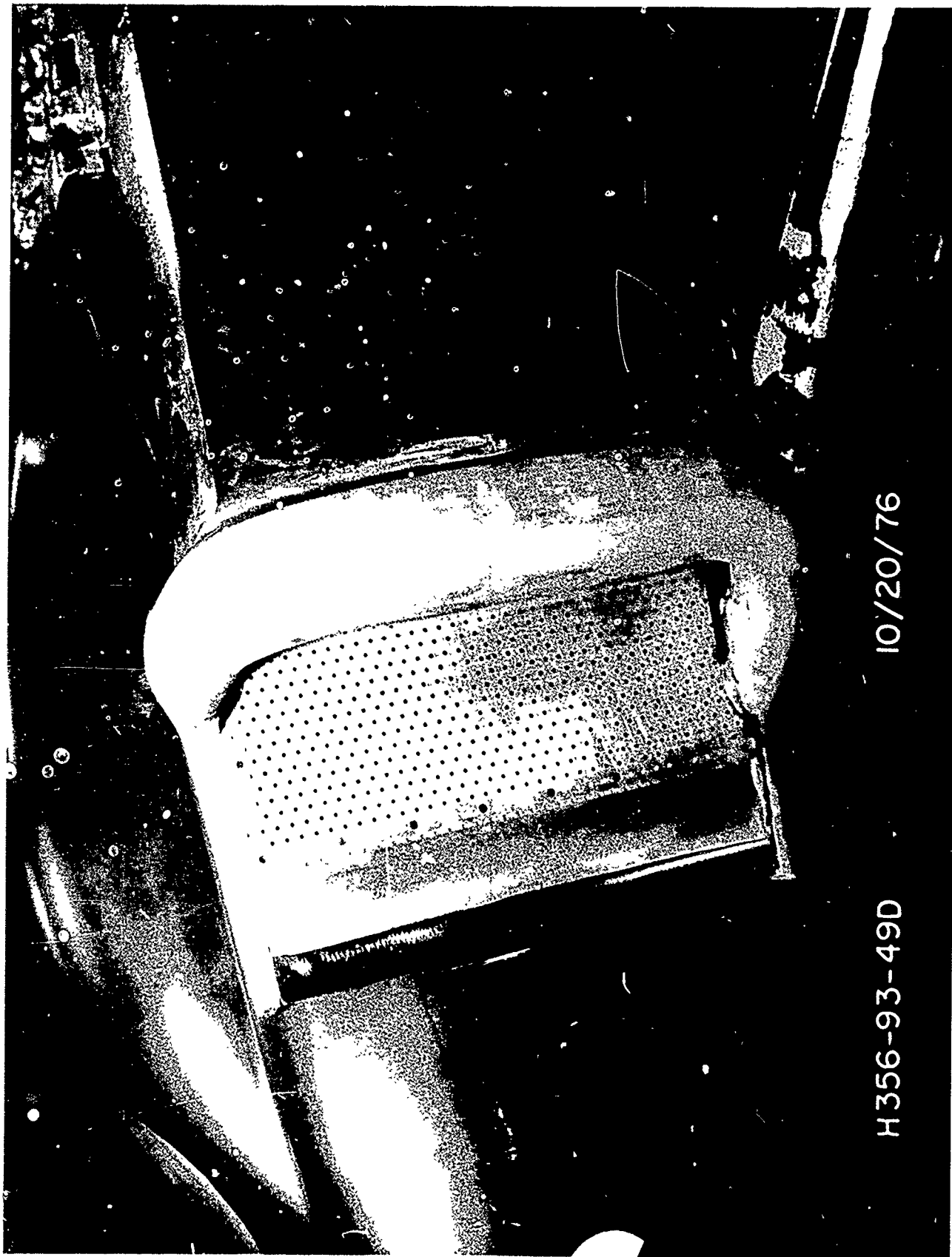
FIGURE 15. BELLMOUTH INLETS

H356-93-49D   10/20/76

0.2 SCALE MODEL DATA

○ WITH BELLMOUTH LIPS
△ WITHOUT BELLMOUTH LIPS

PERCENT CORRECTED AIRFLOW

PRESSURE RECOVERY, P_{T_2}/P_{T_0}
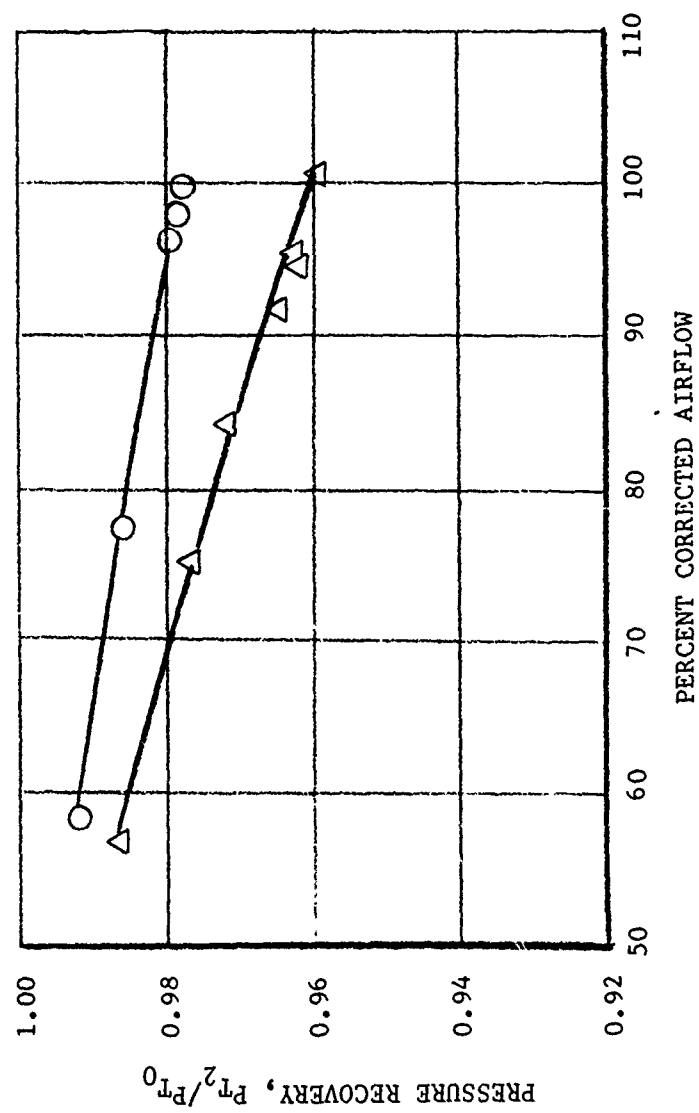
FIGURE 16. RECOVERY COMPARISON WITH AND WITHOUT BELLMOUTH
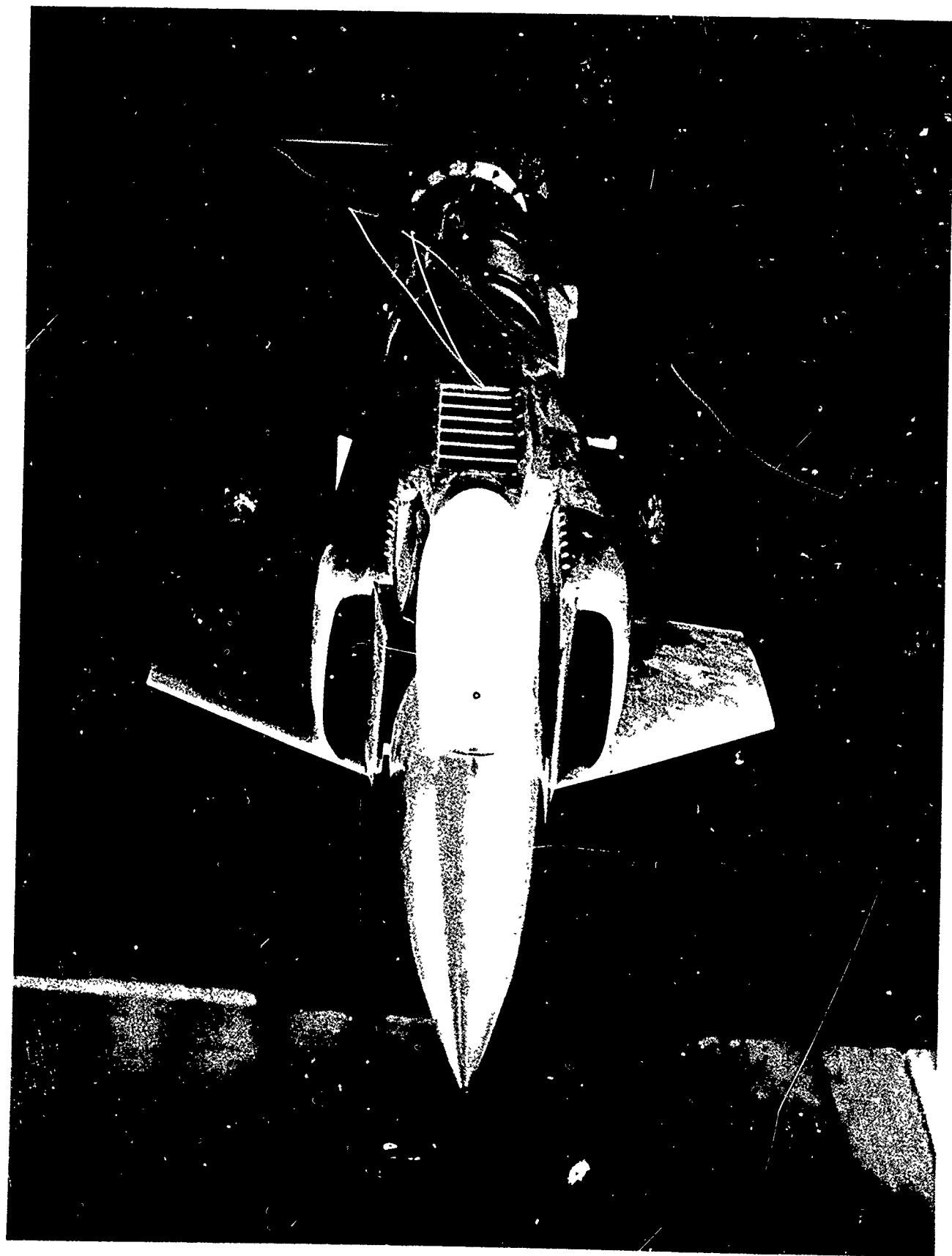
FIGURE 17. 0.168 SCALE MODEL IN AMES TUNNEL
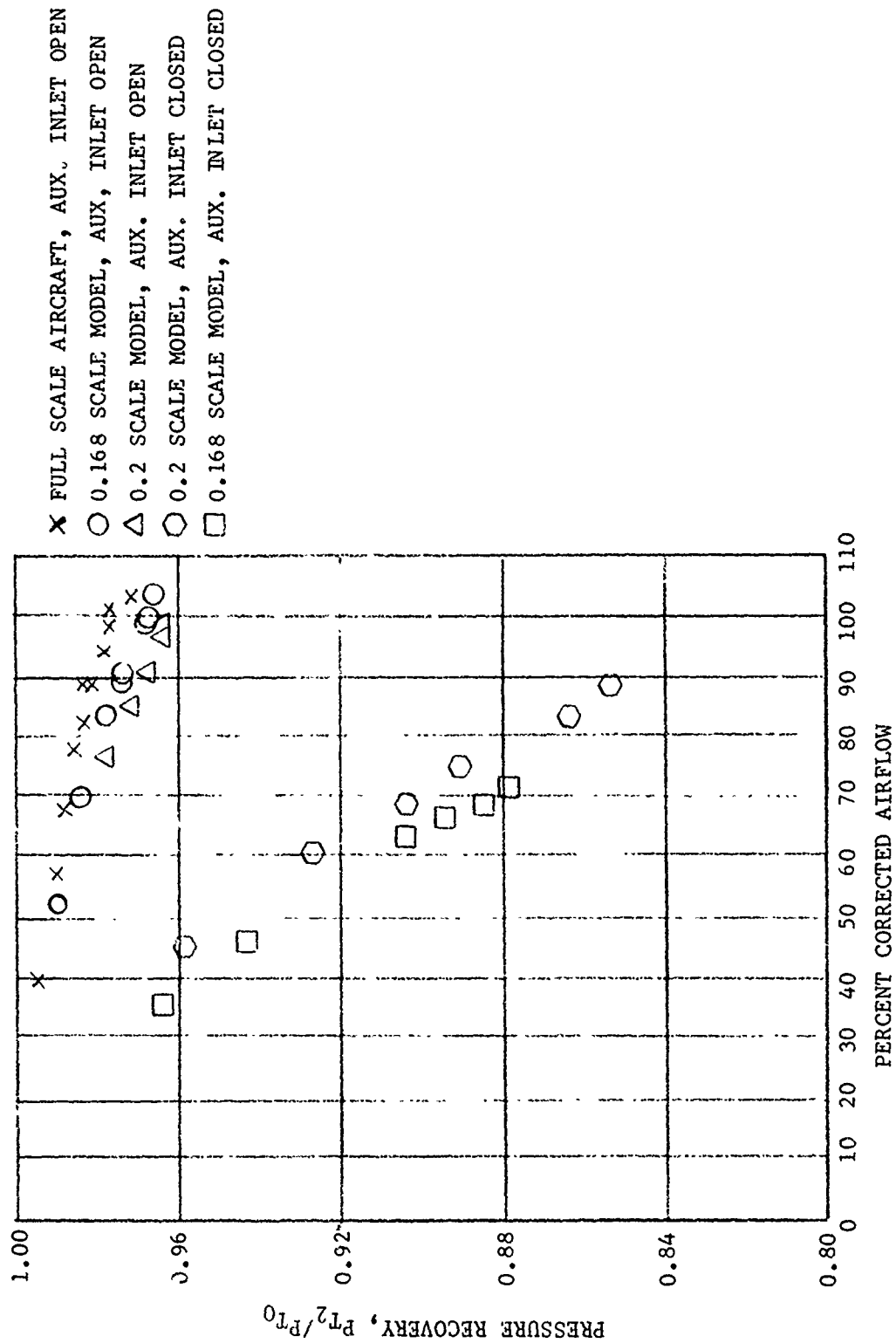
FIGURE 18. RECOVERY @ M = 0
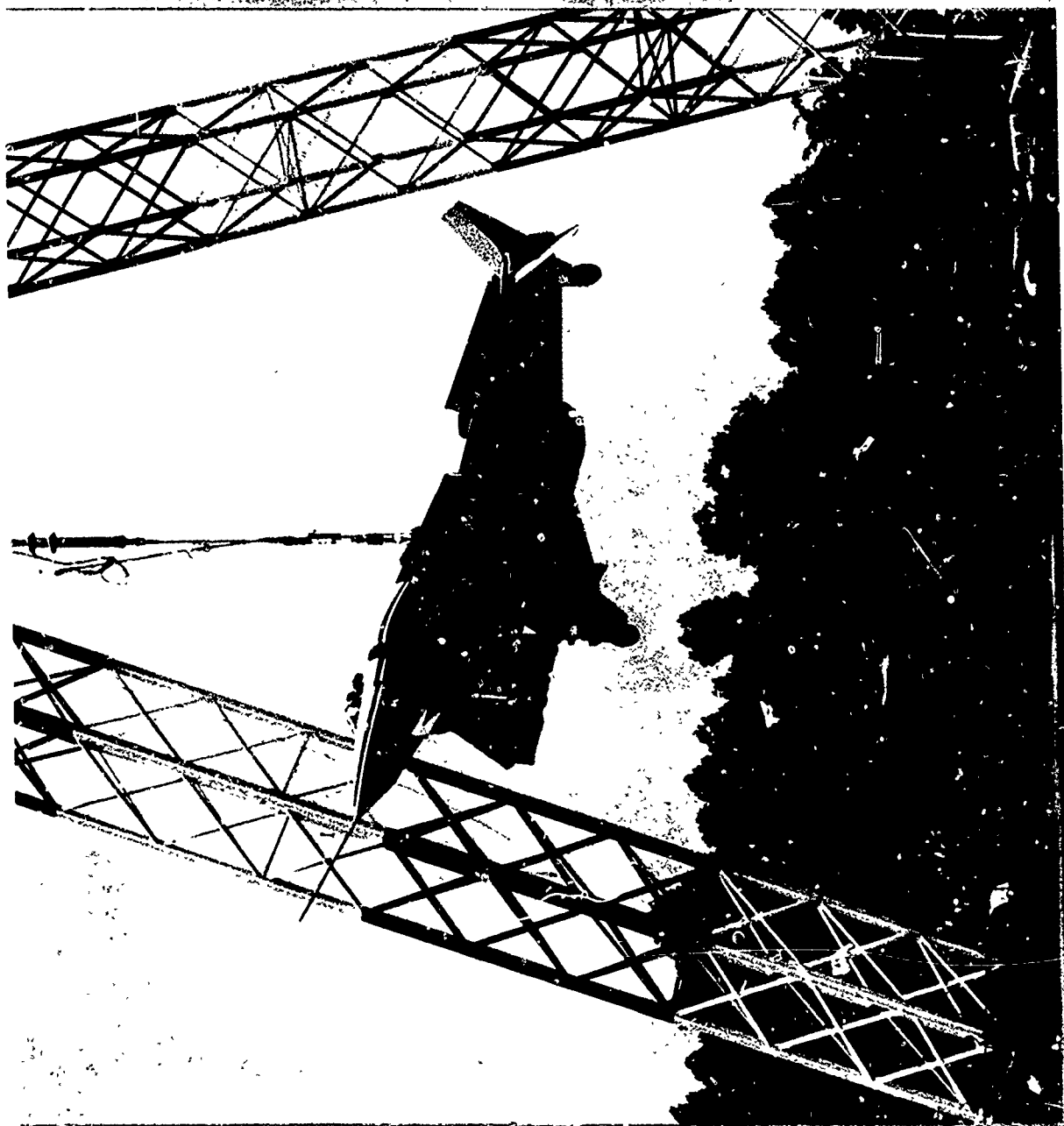
FIGURE 19. XFV-12A ON NASA LANGLEY GANTRY

SUBSONIC VTOL INLET EXPERIMENTAL RESULTS

Richard R. Burley

Albert L. Johns

and

James H. Diedrich

NASA-Lewis Research Center

Cleveland, Ohio

ABSTRACT

Inlets for tile-nacelle VTOL aircraft must operate up to angles of
attack of 120° without internal flow separation. Test results on
12 in. dia. and 20 in. dia. model inlets are presented. The
effectiveness of the following variables on achieving high angle
of attack capability are reported: Lip countraction ratio,
centerbody location, leading edge profile, and lip and diffuser
boundary layer control by blowing. (The variables are listed
in order of increasing effectiveness.) The effects of inlet
blowing on fan blade stresses are also presented.

SUBSONIC VTOL INLET EXPERIMENTAL RESULTS

R. R. Burley, A. L. Johns and J. H. Diedrich

NASA-Lewis Research Center

Cleveland, Ohio

INTRODUCTION

The operating conditions encountered by VTOL aircraft during
takeoff and landing present a hostile environment to the inlet.
For tilt nacelle aircraft, inflow angles up to 120° can occur.
As a general guideline, the inlets should be designed to avoid
internal flow separation in order to avoid the potentially dis-
continuous thrust loss and high fan blade stresses. The inlets
and nacelles should be as low drag and light weight (i.e., thin
and short) as possible so as to present the minimum penalty to
the aircraft and its mission. As inlets become thinner, the
angle of attack at which flow separation occurs becomes less.
Hence, the inlet surfaces are designed by the landing and
takeoff condition (refer to N. Stockman paper). At Lewis,
we are exploring ways to prevent inlet flow separation to
enable the use of a thinner inlet than might normally be used.
This paper will present some recent experimental results that
increase the flow separation angle on VTOL inlets. The topics
discussed will be the effect of inlet lip contraction ratio
(thickness), centerbody location, inlet leading edge profile,
blowing boundary layer control on the lip and diffuser, and the
effects of inlet blowing on fan blade stresses.

EXPERIMENTAL RESULTS

All of the experiments were performed in the Lewis Research
Center 9x15 foot Low Speed Wind Tunnel. Two basic types of
systems were used in the tests: a 12-inch diameter vacuum
system and a 20-inch diameter fan system. The 12-inch diameter
vacuum system experiments will be discussed first. Figure 1
shows the 12-inch diameter vacuum system installed in the test
section of the 9x15 foot wind tunnel. The entire apparatus
rotates in a horizontal plane to vary the angle of attack. The
inlets are mounted on the front of the apparatus as shown.

Effect of Contraction Ratio: Figure 2 shows the results of the experiment to study the effect of contraction ratio on flow separation incidence angle. A conventional fixed centerbody was used for these tests. The plot shows the incidence angle α versus the ratio of throat velocity to freestream velocity V_T/V_o. This parameter has been found to collapse the incompressible flow inlet separation data. Each curve is the bou.dary between attached and separated flow. The local contraction ratio is defined in the inset on figure 2 as $(R_{h1}/R_t)^2$--or lip thickness. The tests were conducted holding the flow rate and tunnel velocity fixed, and increasing the angle of attack until the inlet separated. Separation was determined by monitoring the static and total pressure at the end of the diffuser in the location of the compressor face. For a given contraction ratio, the data indicate that the separation angle increases as the ratio V_t/V_o increases until the flow compressibility effects becomer. dominant. This occurs at about a throat Mach number of 0.5. At a specified value of V_T/V_o, the separation angle increases with increasing contraction ratio, as expected.

Effect of Centerbody Location: The next experiment studied the effect of centerbody location on separation angle using an inlet having a contraction ratio of 1.46. The results are shown on figure 3 and the incidence angle α is plotted versus the center-body axial position X/L for various throat Mach numbers. The origin of the position coordinate is the minimum passage area without the centerbody. The inset shows the range of centerbody locations tested. The centerbody was mounted on an actuator and was continuously variable over the range shown. An optimum centerbody length occurred within the range of lengths investigated. The improvements in separation angle compared to the shortest centerbody position ranged from $20°$ for $M_T = 0.30$ to $5°$ for $M_T-0.70$.

That is, the centerbody location producing the higher separation is considerably further forward than the centerbody in the previous figure. The variation in centerbody position causes change in the area distribution in the flow passage of the inlet. We are in the process of analyzing the test results now to obtain a better understanding of the basic flow mechanisms involved. Reference 1 presents additional data.

Scarf Inlets: Changing the inlet leading edge profile can affect the separation limits of inlets. Figure 4 presents data for a scarf inlet where the lower lip is extended forward beyond the upper lip and the profile is at a constant angle as shown in the inset. The separation angle is plotted against the ratio V_t/V_o and data are shown for the scarf inlet and for an unscarfed baseline inlet. The figure indicates the improvements possible by using

the scarf concept. Our experiments (ref. 2) have investigated another profile contour and the one shown exhibited the best performance. Decreasing the extension of the lower lip reduces the benefits in separation angle a corresponding amount. A word of caution is appropriate here, the static performance of the scarf inlet is less than that of the conventional baseline inlet. At static conditions the upper lip is aerodynamically so highly loaded that separation occurs. At low forward speeds and zero angle of attack the upper lip is still more highly loaded than the lower lip when the flow is all attached. Increasing the angle of attack first equalizes the loading on the upper and lower lips and loads the lower lip until it separates.

The next series of experiments were performed using a 20-inch diameter fan mounted as shown in figure 5. The model rotates in a horizontal plane and pivots about the support post shown in the figure. The fan was driven by a compressed air turbine. The turbine air being supplied through the vertical post.

Effect of Lip Blowing: A 1.46 contraction ratio inlet was fitted with a lip blowing slot for boundary layer control as shown on figure 6. The slot height for this particular experiment was 0.020 inches and the angular extent of the slot was 120°. The figure shows the incidence angle α plotted versus the throat to freestream velocity ratio V_t/V_0 for a baseline no blowing inlet and this lip blowing inlet. The results show that there is a sizeable improvement in the separation characteristics of the inlet for a blowing pressure ratio P_b/P_0 of 1.4. For example, for a value of V_t/V_0 of 2, α increases from 45° for the baseline inlet to approximately 70° for the inlet with blowing. This is a sizeable improvement in angle. The amount of blowing boundary layer control mass flow was approximately 6% of the inlet mass flow at the blowing pressure ratio of 1.4. Increasing the slot height to 0.060 inches gave essentially the same separation characteristics shown. Approximately 6% of the inlet mass flow was required at a blowing pressure ratio of only 1.1. This raises the possibility that the fan could be used as the source of pressurized air for the boundary layer control system.

Effect of Diffuser Blowing: An unsymmetrical inlet having a lower lip contraction ratio $(R_{hl}/R_T)^2$ of 1.69 and an upper lip contraction ratio of 1.32 was fitted with a blowing boundary layer control system in the diffuser as shown in the inset in figure 7. The blowing slot height extended for 120° and has a slot height of 0.012 inches. Figure 7 is a plot of the incidence angle α, versus the throat to free stream velocity ratio V_t/V_0.

Data are presented for a baseline (no blowing) inlet and the diffuser blowing inlet with a blowing pressure ratio of 1.4. There is a sizeable improvement in the separation boundary as shown. For example at a V_t/V_0 of 2 the separation angle increased from 50° without blowing to 85° with blowing. This is similar to the lip blowing results that were discussed previously. Data used in this test series were obtained at freestream velocities of 60, 80, 110 and 125 knots. The amount of blowing boundary layer control mass flow was approximately 6% of the inlet mass flow at a blowing pressure of 1.4.

Comparison of Inlets: Figure 8 compares the effectiveness of the various inlet designs for improving the separation angle characteristics of inlets. The data are plotted as a function of the separation angle versus the inlet contraction ratio for specified values of V_0 and V_t. The baseline configuration (solid line) was developed from data on basic inlets with short centerbodies. Increasing lip contraction ratio (thickness) increases separation angle. Optimizing centerbody length gives a small improvement while the lip and diffuser blowing and scarfing concepts give sizeable improvements.

Blade Stresses: Figure 9 depicts the fan blade stresses obtained from 20-inch diameter fan tests. The figure was obtained from an on-line trace of the signals from strain gages attached to the blade root. The inlets were conventional type without blowing slots. The data represent the first flatwise bending mode of the blade and depict the blade stress in percent of limit stress versus inlet rotational speed as a percent of the design value. The figure was plotted for data taken at a freestream velocity of 120 knots and α of 60°. The blade stresses start at low values and gradually build up with increasing inlet rotational speed. This stress buildup is due to the increase in the intensity of the distortion induced by the flow separation within the inlet as fan rotational speed and hence flow velocity in the inlet increases. For the 1.76 contraction ratio inlet, when the flow becomes attached, the stresses reduce. The blade stress for the 1.46 contraction ratio inlet continues to increase indicating that this inlet remains separated. The spike on the 1.76 contraction ratio inlet data curve is due to a harmonic resonance between the blade natural frequency in bending and the rotational frequency of the rotor. Figure 10 shows the effect of blowing boundary layer control on the magnitude of the blade bending stresses. The data were obtained from tests on a 1.69 contraction ratio inlet at a forward velocity of 125 knots and angle of attack of 55°. The top curve illustrates the typical pattern obtained from the

baseline inlet without blowing and the harmonic resonance peaks are clearly evident. The addition of blowing boundary control reduced the magnitude of the stresses dramatically. Data are also shown for 120° circumferential blowing slots. Thus the inlet separation behavior is improved which reduces the blade stresses.

CONCLUDING REMARKS

The various experimental results discussed illustrate a number of ways to improve the inlet separation characteristics, and reduce fan blade stresses. For the blowing boundary layer control concept the penalty for the required blowing needs to be evaluated. Future experiments will include boundary layer control by suction, vortex generators and slats.

REFERENCES

1. B.rley, R. R., "Effect of Lip and Centerbody Geometry on Aerodynamic Performance of Inlets for Tilting-Nacelle VTOL Aircraft" AIAA 79-0381.

2. Abbott, J. M., "Aerodynamic Performance of Scarf Inlets" NASA TM 79055, January 1979.

NASA
C-77-4496
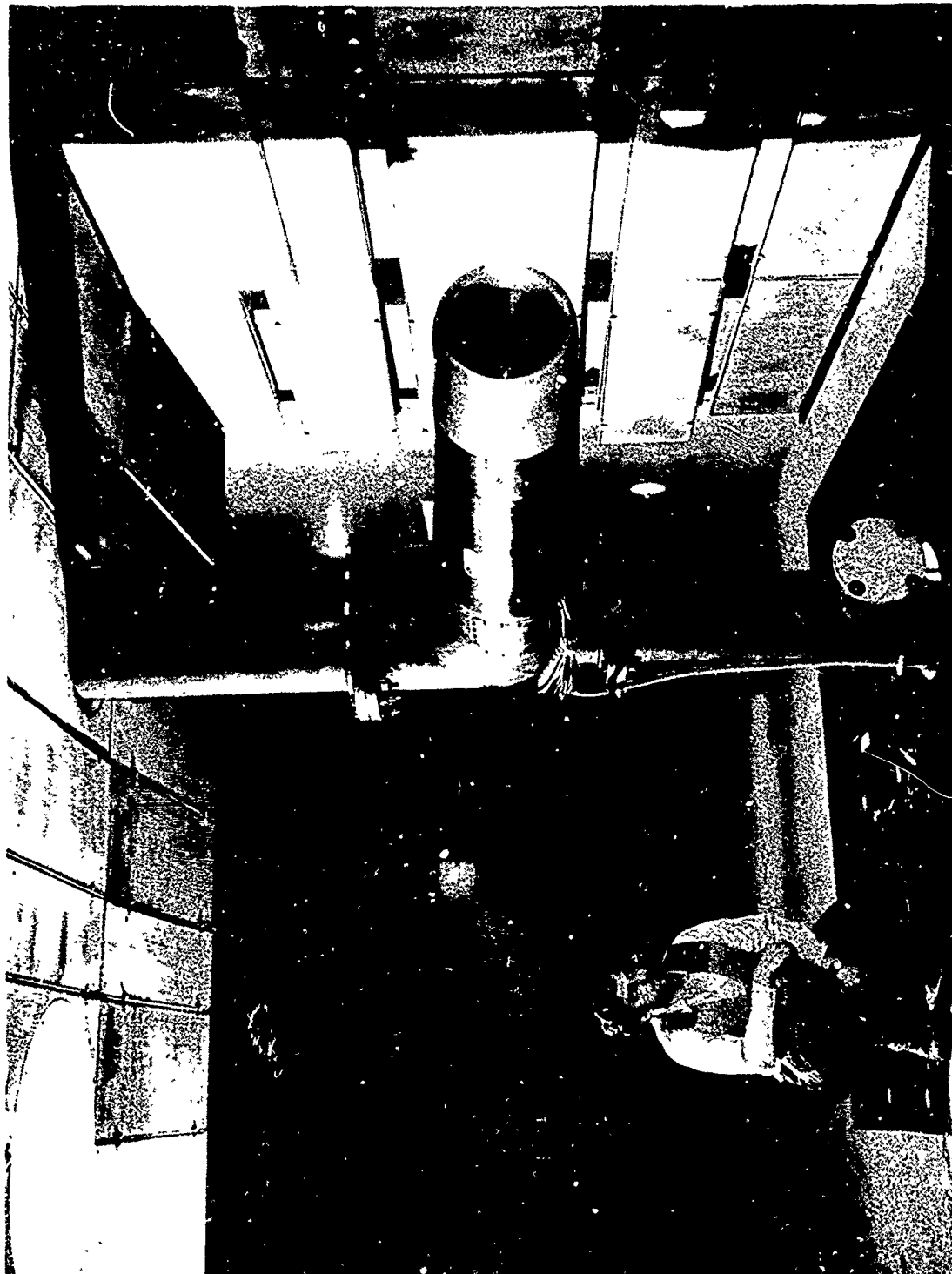
FIGURE 1 - 12 INCH D. INLET MODEL - LEWIS 9X15 WIND TUNNEL

FIGURE 2. EFFECT OF CONTRACTION RATIO
$V_0 = 41$ M/SEC (80 KT.)
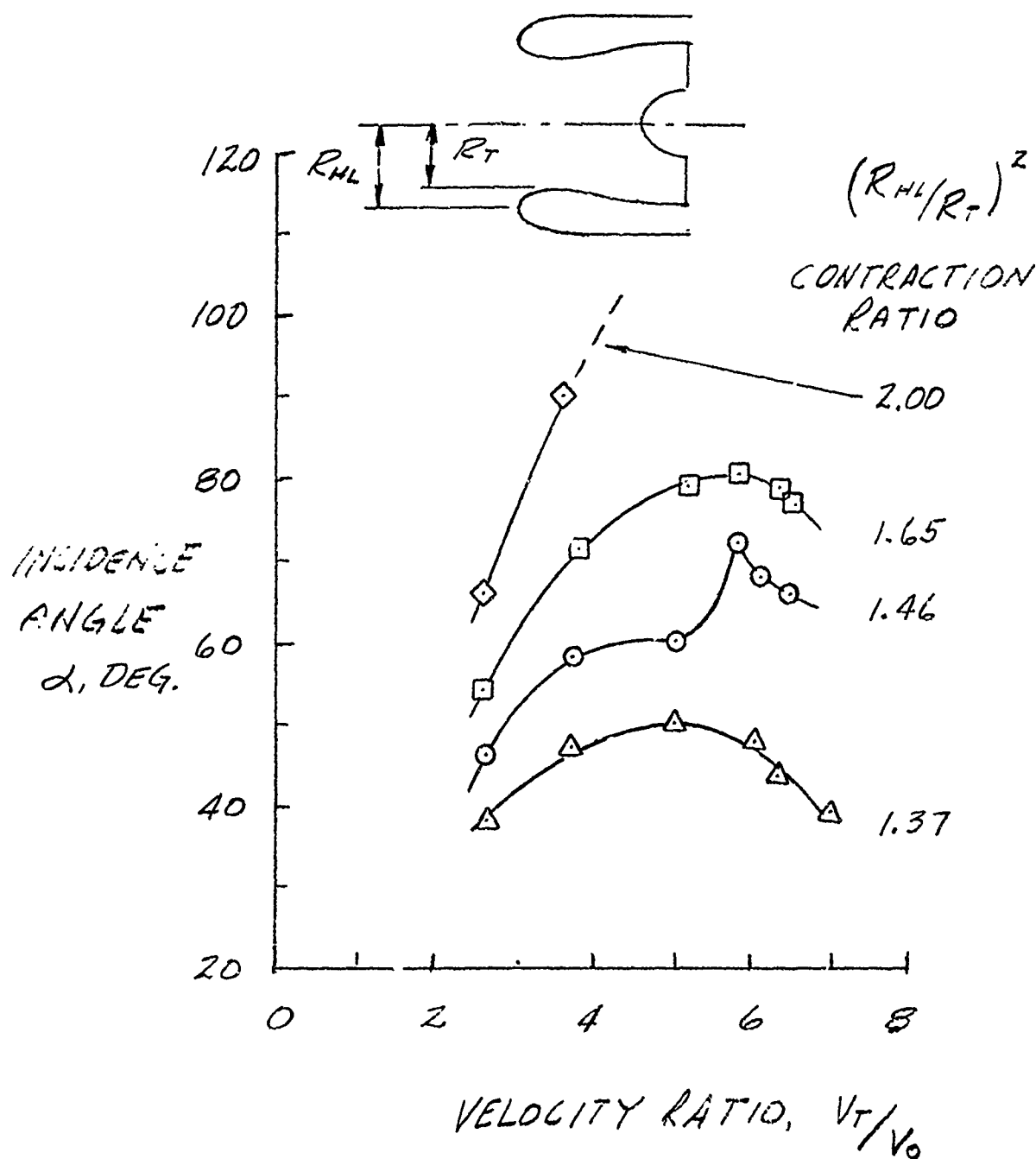
FIGURE 3.   EFFECT OF CENTERBODY LOCATION

$V_0 - 41 \, m/sec \, (80 \, kt), \, (R_{Hu}/R_T)^2 = 1.46$

$\underline{M_T}$
0.70
0.60
0.45
0.30

INCIDENCE ANGLE α, Deg.

CENTERBODY LOCATION, (X/L)
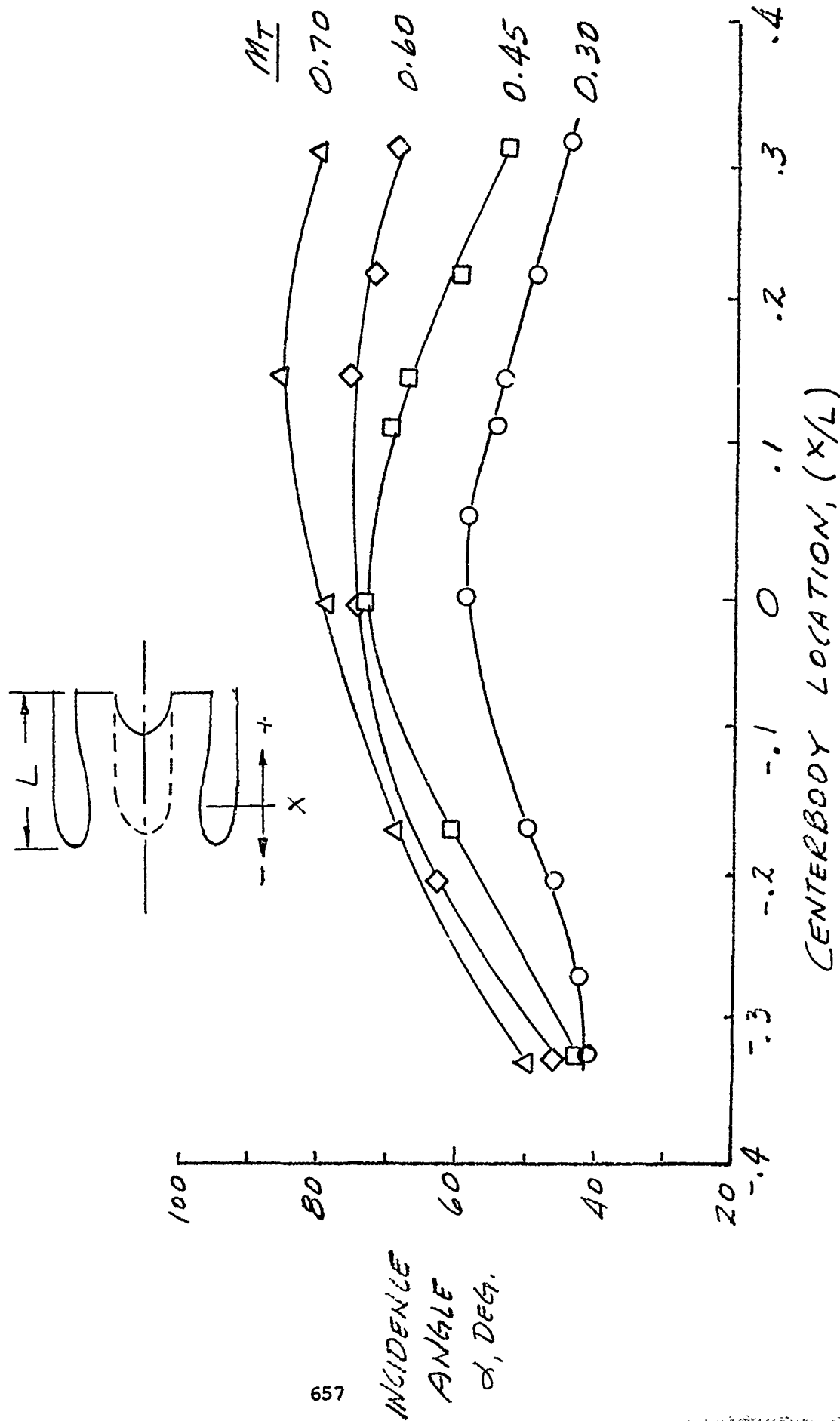
FIGURE 4.   SCARF INLET CHARACTERISTICS

$$(R_{HL}/R_T)^2 = 1.44$$

$L_1/D_E = .72$

$L_2/D_E = 1.3$

BASELINE $L/D_E = 1.3$

INCIDENCE ANGLE α, DEG.

VELOCITY RATIO, V_T/V_0
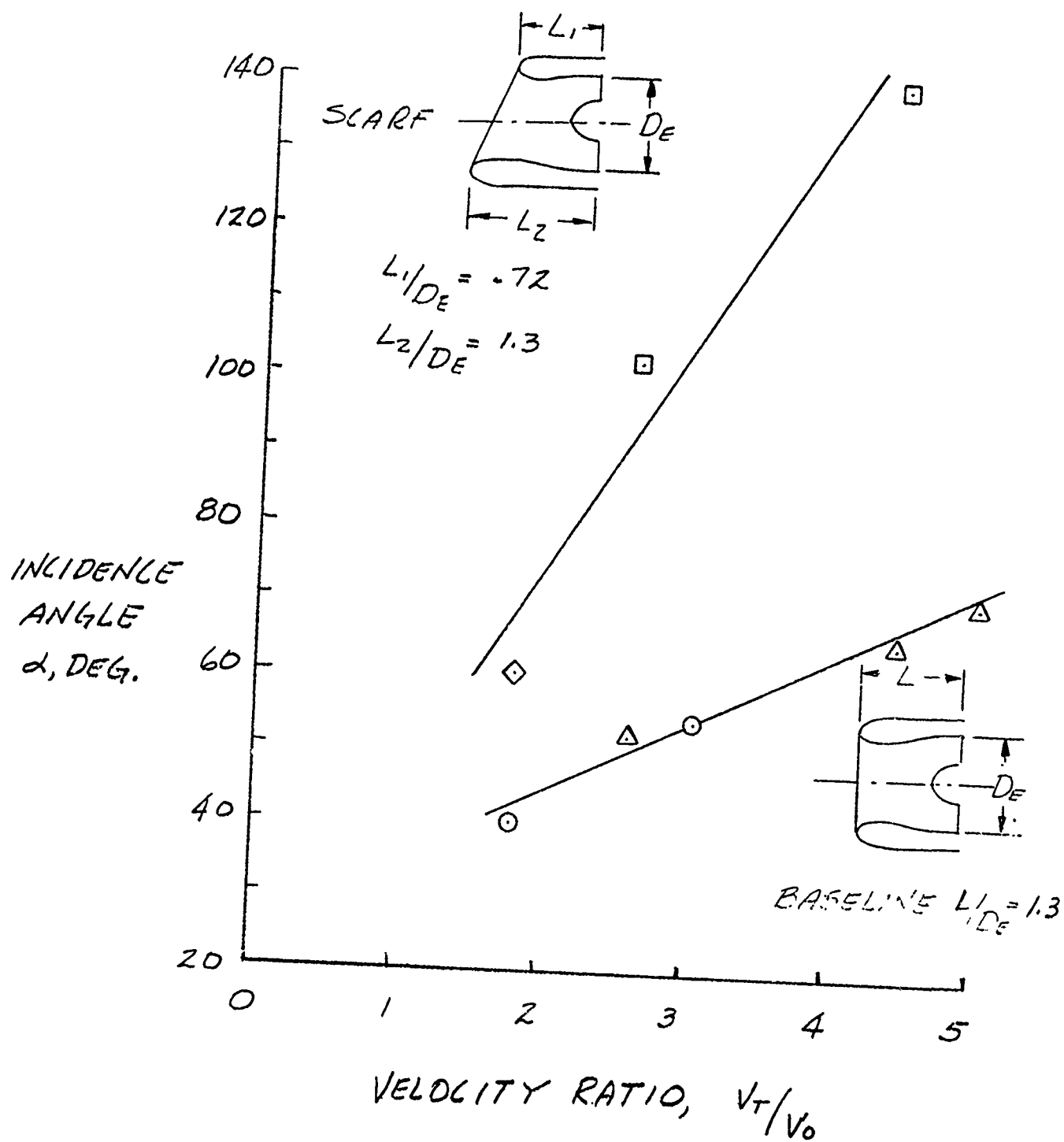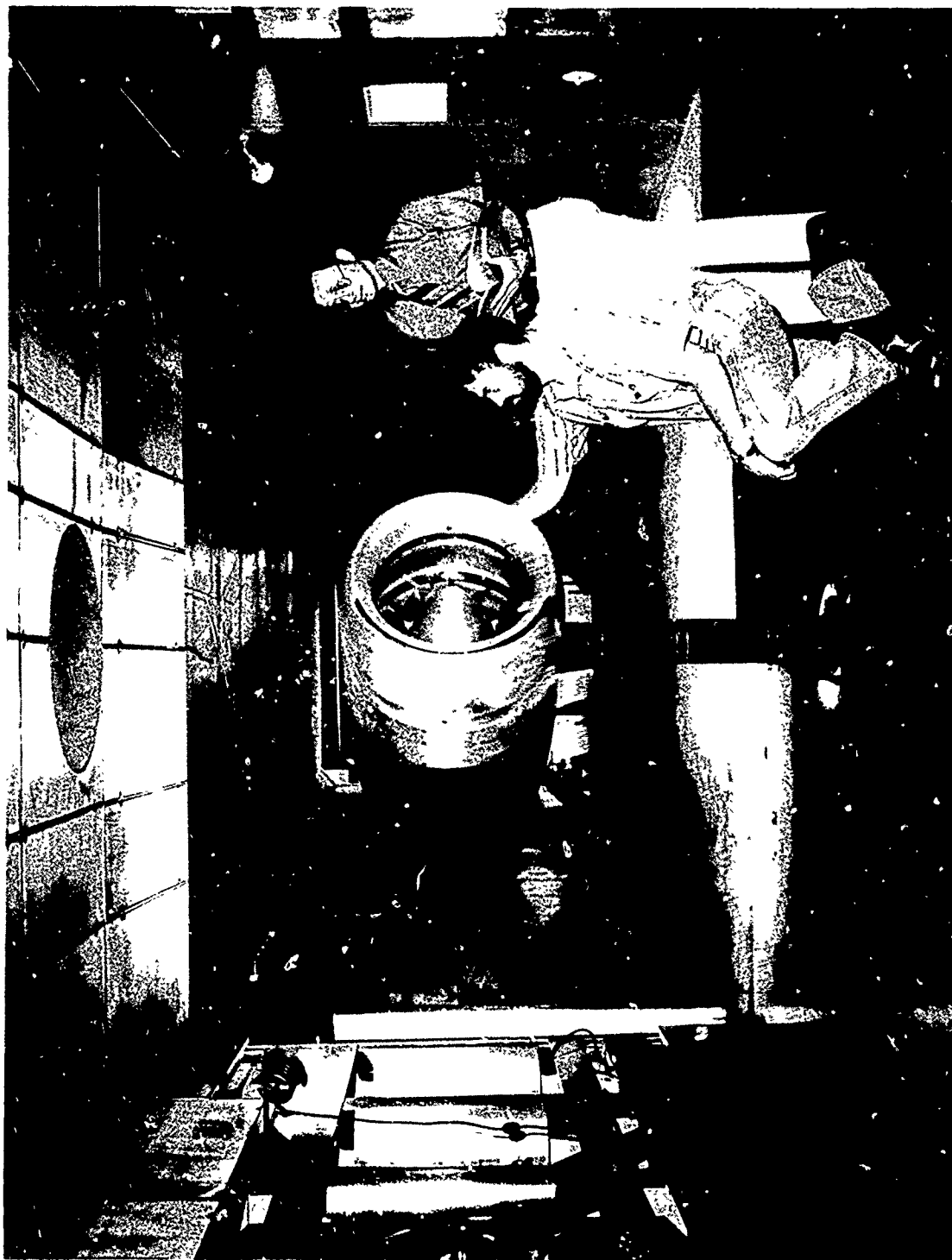
FIGURE 5.- 20 INCH DIAMETER MODEL FAN IN LEWIS 9X15 WIND TUNNEL

NASA
C-78-2491

659

FIGURE 6. EFFECT OF LIP BLOWING

$$\left(R_{HL}/R_T\right)^2 = 1.46$$

LIP BLOWING
$P_B/P_0 = 1.4$

BASELINE

INCIDENCE ANGLE, α, DEG

LIP BLOWING SLOT

VELOCITY RATIO, V_T/V_0
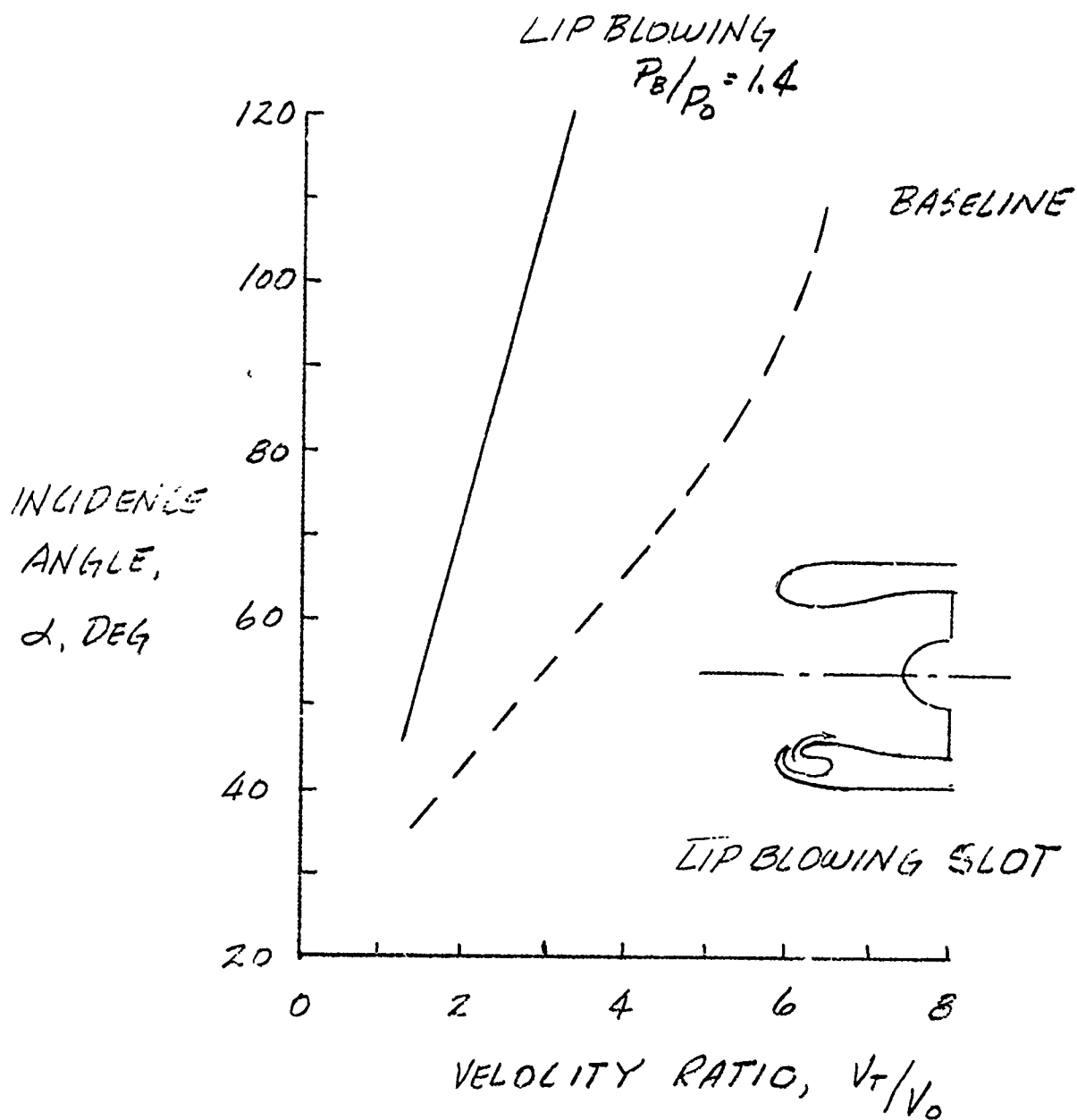
FIGURE 7.   EFFECT OF DIFFUSER BLOWING

$$\left(R_{HL}/R_T\right)^2 = 1.69 \text{ (WINDWARD)}$$

V_0

○ 30 M/SEC (60 KT.)
□ 41 M/SEC (80 KT.)

V_0

◇ 57 M/SEC (110 KT.)
△ 64 M/SEC (125 KT.)

$P_B/P_0 = 1.4$

BASELINE

INCIDENCE ANGLE α, DEG.

VELOCITY RATIO, V_T/V_0
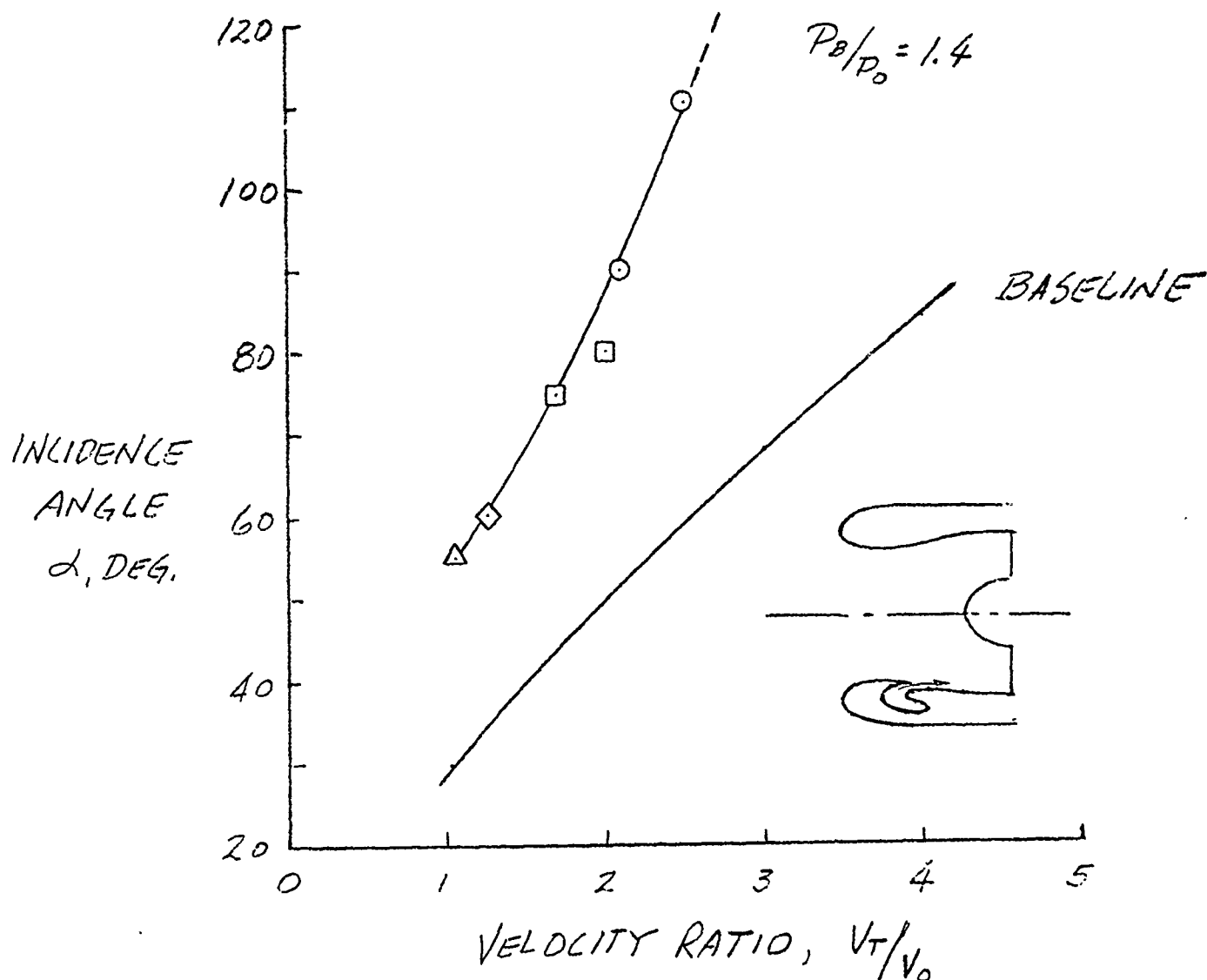
FIGURE 8 - COMPARISON OF INLETS

$V_0 = 41 \, M/SEC \, (80 \, KT.)$

$M_r = 0.45$
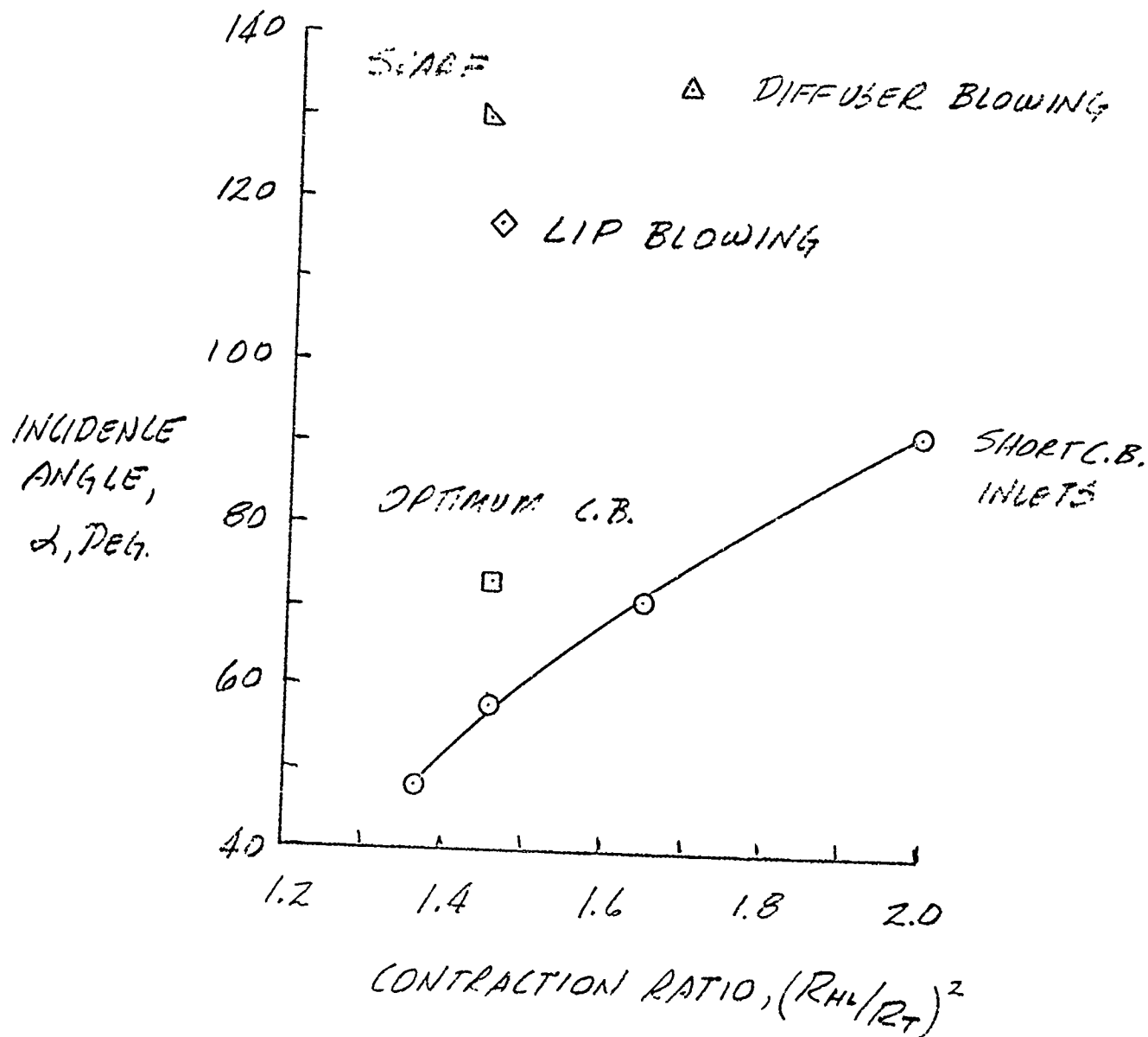
FIGURE 9.   FAN BLADE STRESS

$V_0 = 62$ m/sec (120 KT.)
$\alpha = 60°$

$(R_{HL}/R_T)^2$

1.46

1.76

BLADE STRESS % LIMIT

N/N_{DES}, %

INCREASING V_T/V_0 ⟶
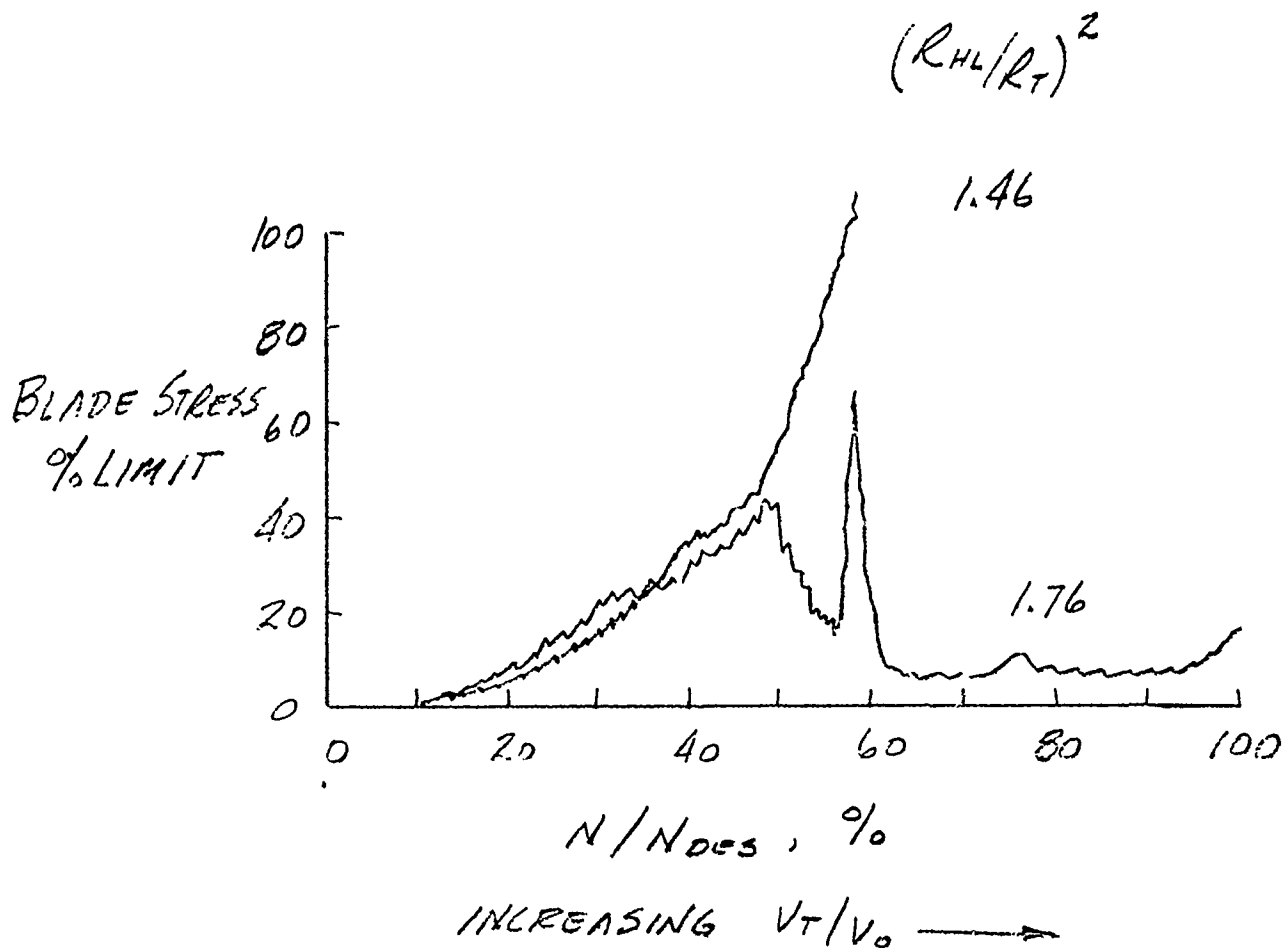
FIGURE 10. EFFECT OF BLOWING ON FAN BLADE STRE.

$$V_0 = 64 \text{ M/SEC (125 K.T.)}, \alpha = 55°$$

NO BLOWING· SMOOTH INLET
(SEPARATED FLOW)

BLADE STRESS
%oLIMIT

N/N_{DES}, %
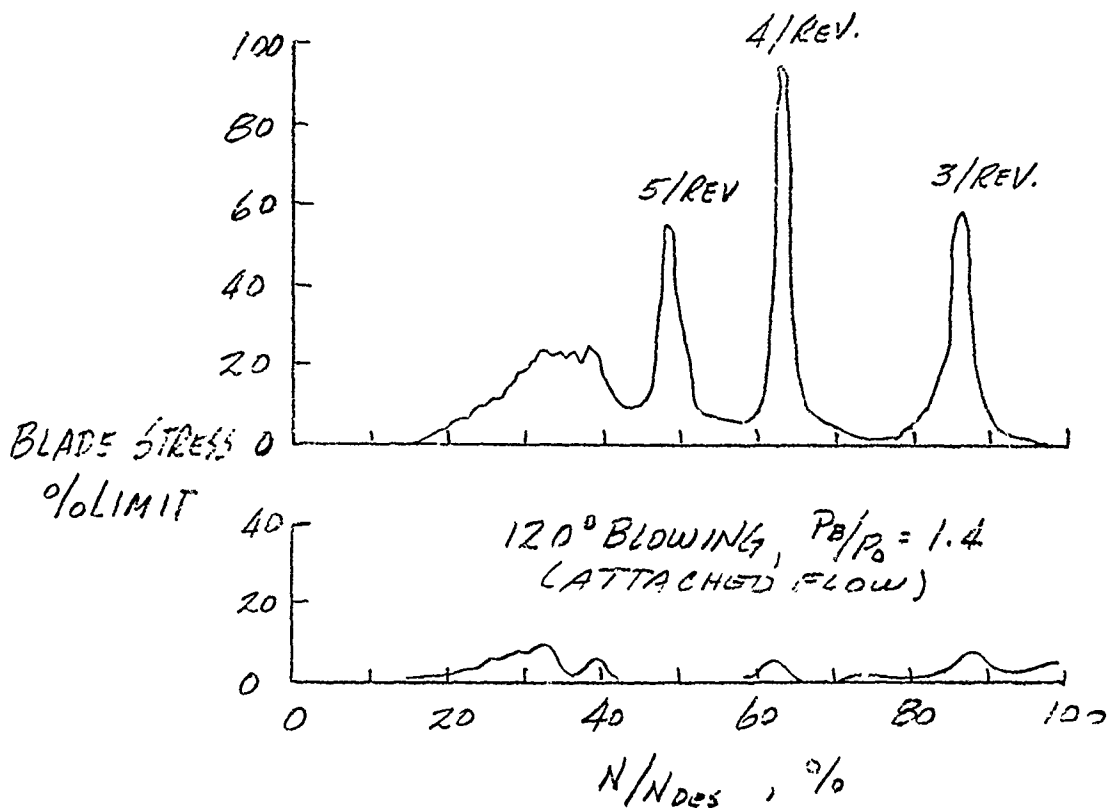
INLET RAM FORCES AND MOMENTS
FOR V/STOL AIRCRAFT

S. S. Kress
Vought Corporation

An approach to predicting inlet ram forces and moments has been developed at Vought. These inlet ram forces and moments can have a significant effect on the stability and control of V/STOL aircraft during transition and hover. The method incorporates four basic steps:

(1) For a given geometry, solve for the inlet surface pressure distribution and the streamwise velocity distribution at stations aft of the inlet throat.

(2) Define a control volume based on the computed stagnation points and a station where the streamwise velocity distribution is known.

(3) Write the conservation of momentum and moment of momentum equations for the control volume.

(4) Solve for the ram forces and moments using the predicted pressure and velocity data.

The inlet pressure and velocity distributions are predicted using the Stockman axisymmetric inlet routine. The following presentation shows the inlet forces and moments that affect V/STOL aircraft stability and control, when in the flight envelope they are important, and, briefly, the approach Vought has used to solve for these forces and moments. Also shown are some British test data for three fan/body configurations, and predicted data from the forces and moment program at three flight conditions for the NASA QCSEE inlet.

In summary, the approach is limited in that no test data has been found to verify the method. It is recommended that inlet force and moment test data should be obtained using a lip balance device where the forces and moments due to the inlet lip can be separated from nacelle or nacelle/body effects.

INLET RAM FORCES AND MOMENTS

FOR V/STOL AIRCRAFT

VOUGHT CORPORATION

TYPICAL V/STOL ENGINE INLET CONFIGURATIONS

(A) CTOL OR STOL ENGINE INLET

(B) VTOL ENGINE INLET

STAGNATION
POINT

INLET RAM FORCES AND MOMENTS

LIFT

DRAG

ENGINE LUG

M_y

A/C CG
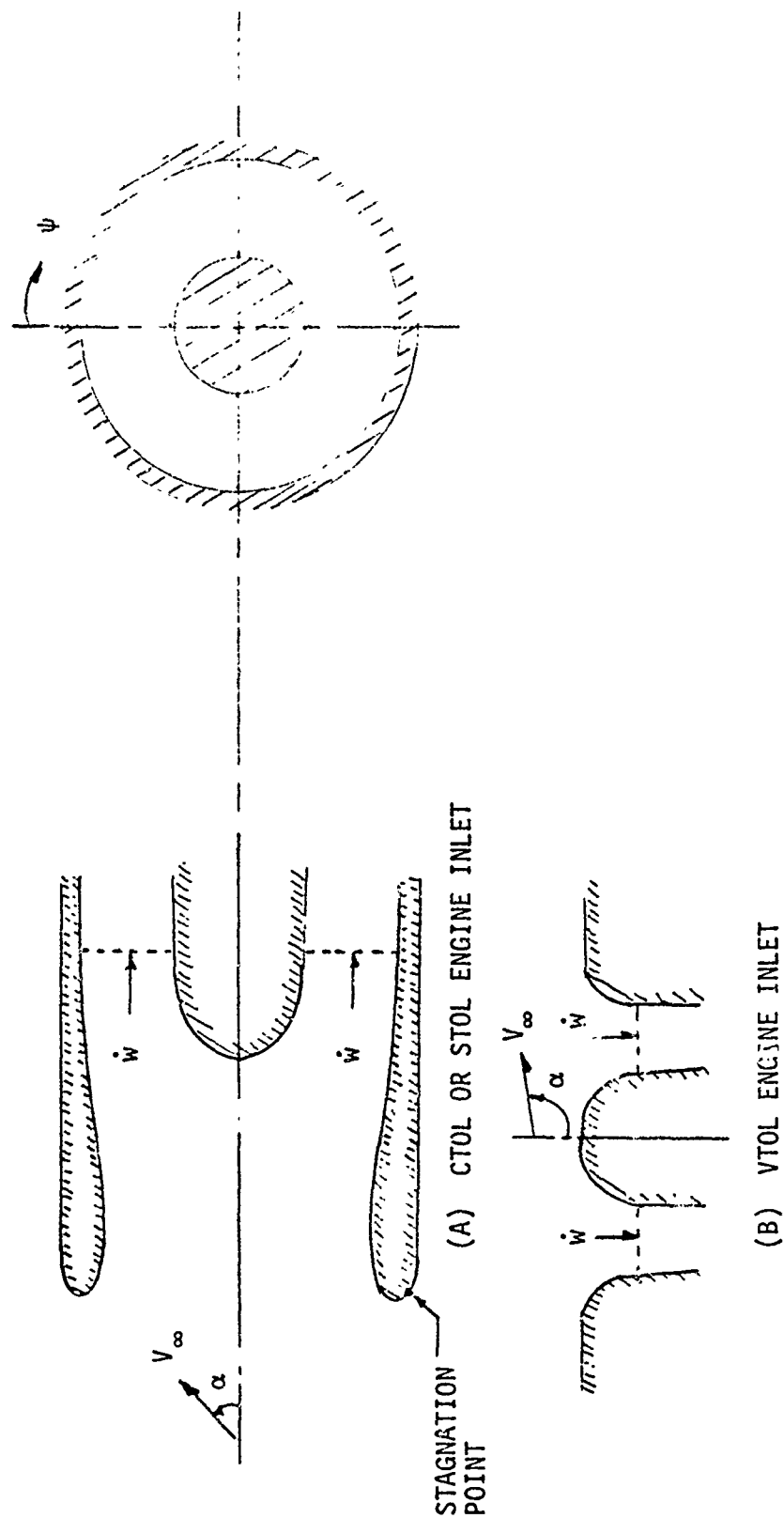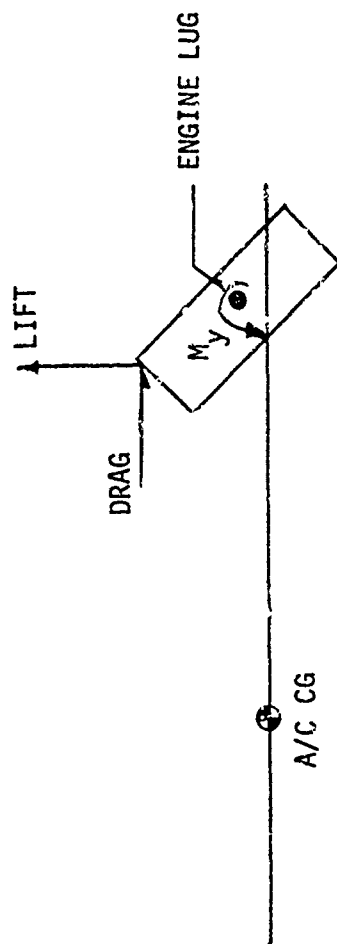
REPRESENTATIVE FLIGHT CONDITIONS FOR TILT-NACELLE VTOL AIRCRAFT
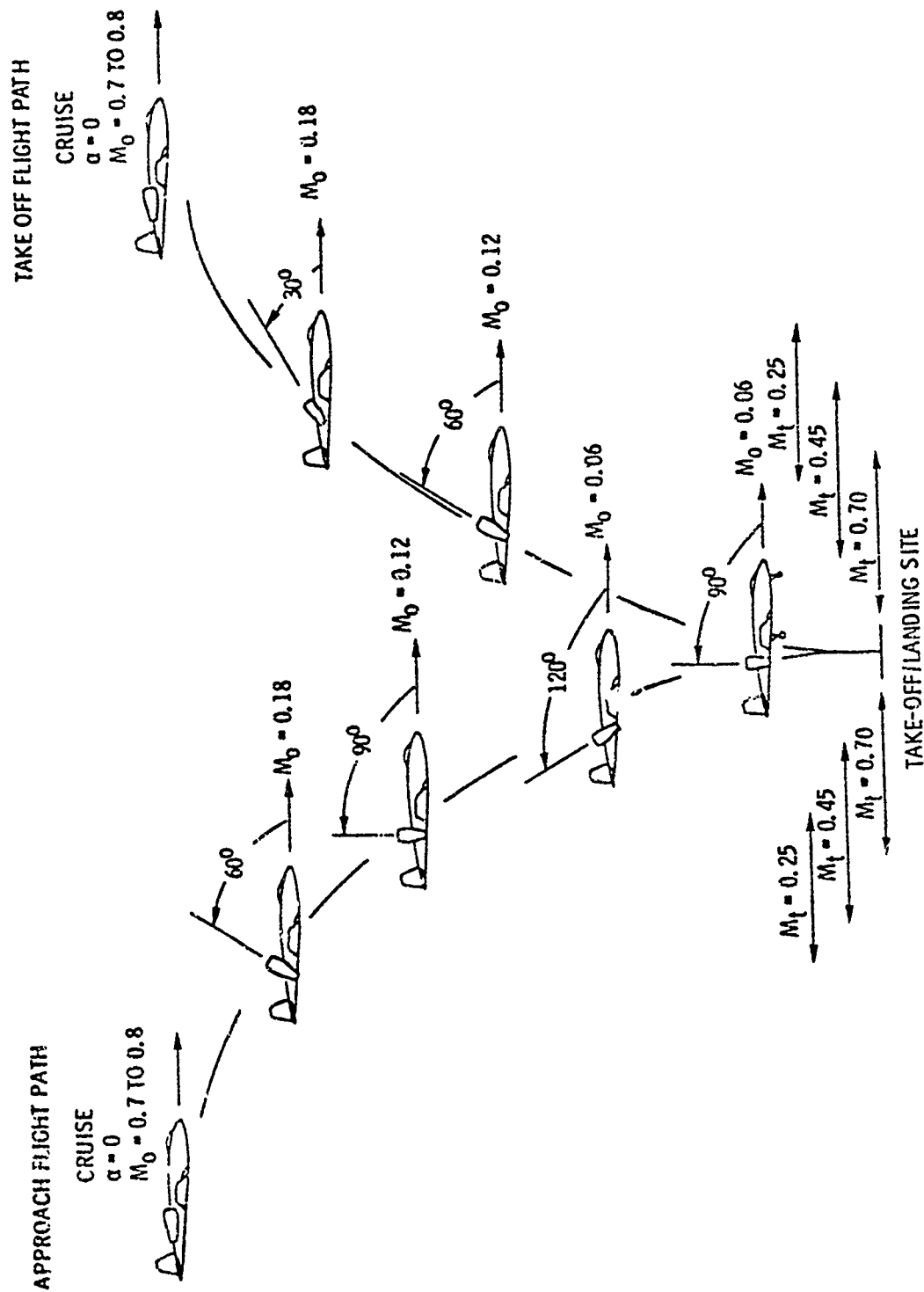
THREE FAN/BODY COMBINATIONS

AR-1 RECTANGULAR WING
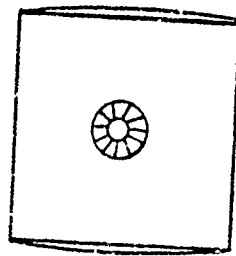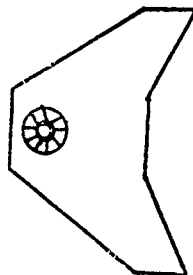
SWEPT WING

AR-2 RECTANGULAR WING
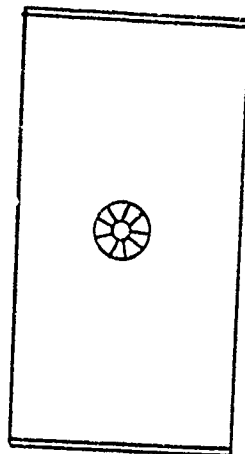
INLET FORCE AND MOMENT DATA FOR 3 FAN/WING CONFIGURATIONS

@ ZERO INCIDENCE

- ○ AR-1 RECTANGULAR WING
- △ SWEPT WING (APEX FORWARD)
- □ AR-2 RECTANGULAR WING

LIFT INCREMENT

$$\frac{\Delta L}{\rho A_F V_F^2}$$

DRAG INCREMENT

$$\frac{\Delta D}{\rho A_F V_F^2}$$

EFFECT ON X_{CP}

$$\frac{\Delta M}{d_F \Delta L}$$

V_∞ / V_F

671
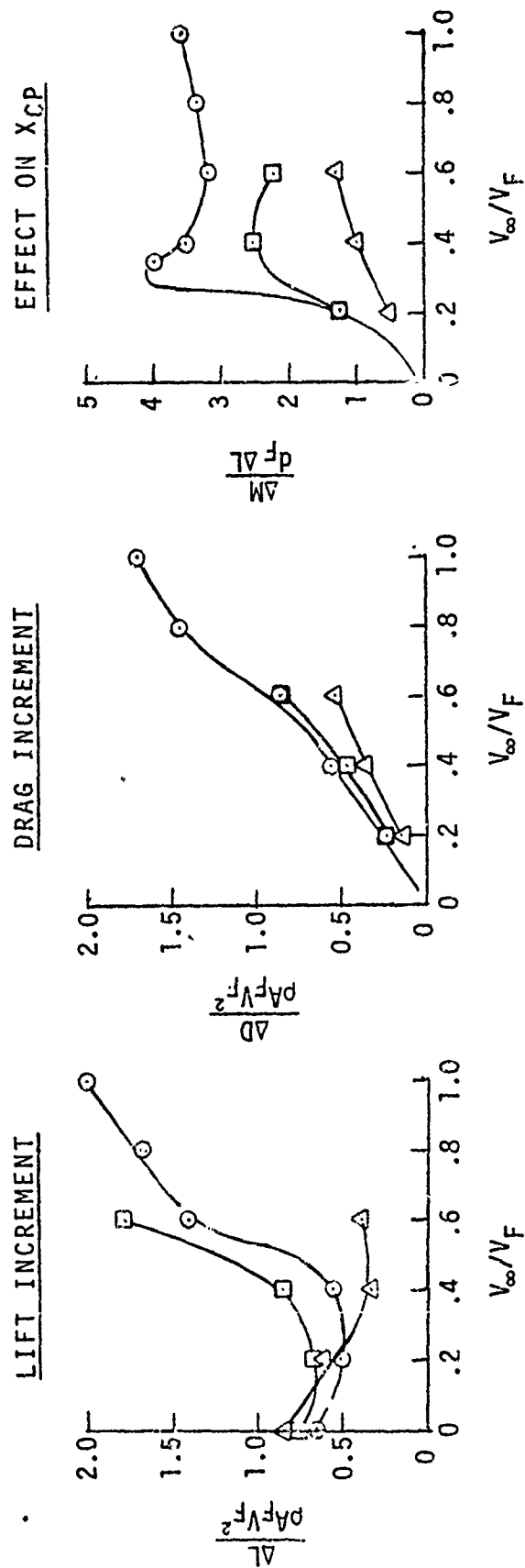
ANALYTICAL APPROACH TO SOLVING FOR V/STOL

INLET FORCES AND MOMENTS

(1) SOLVE FOR SURFACE PRESSURE AND STREAMWISE VELOCITY
DISTRIBUTIONS FOR AN INLET

(2) DEFINE AN INLET CONTROL VOLUME BASED ON THE COMPUTED
STAGNATION POINTS AND A STATION WHERE THE FLOW CONDITIONS
ARE KNOWN

(3) WRITE THE CONSERVATION OF MOMENTUM AND MOMENT MOMENTUM
EQUATIONS FOR THE CONTROL VOLUME

(4) EVALUATE THE INTEGRALS USING THE PREDICTED PRESSURE AND
VELOCITY DATA

CONTROL VOLUME FOR CALCULATING INLET

FORCE AND MOMENT INTEGRALS
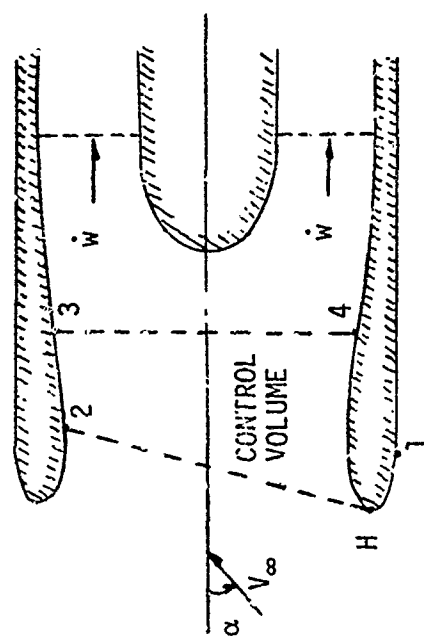
COMPUTER ROUTINES FOR CALCULATING

INLET FORCES AND MOMENTS

WOLFE PROGRAM → F_X F_Z M

$X, Y, dY/dX$

22

GEOMETRY DEFINITION PROGRAM (SCIRCL)

20

X_{ON}, Y_{ON}

DOUGLAS POT. FLOW INCOMPRESS. PROGRAM (EOD)

17

V_1, V_2, V_3

COMBINE WITH COMPRESS. PROGRAM (COMBYN)

23

V_X, V_Y, V_Z

P_S/P_T

INPUTS

GEOMETRY

IEOD = 20

$V_\infty, \dot{w}, \alpha$

674
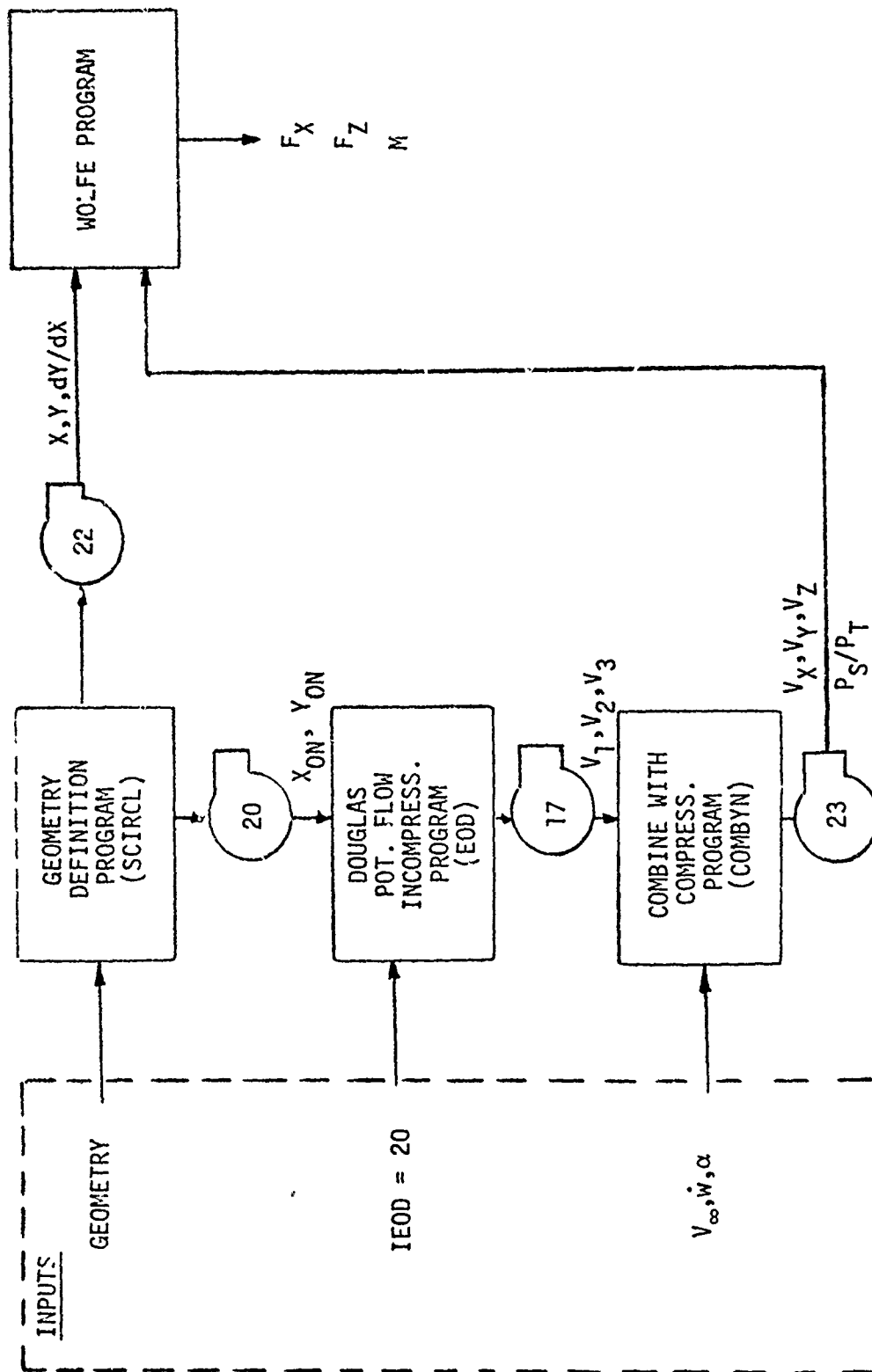
FORCE COMPONENTS ON NASA QCSEE INLET
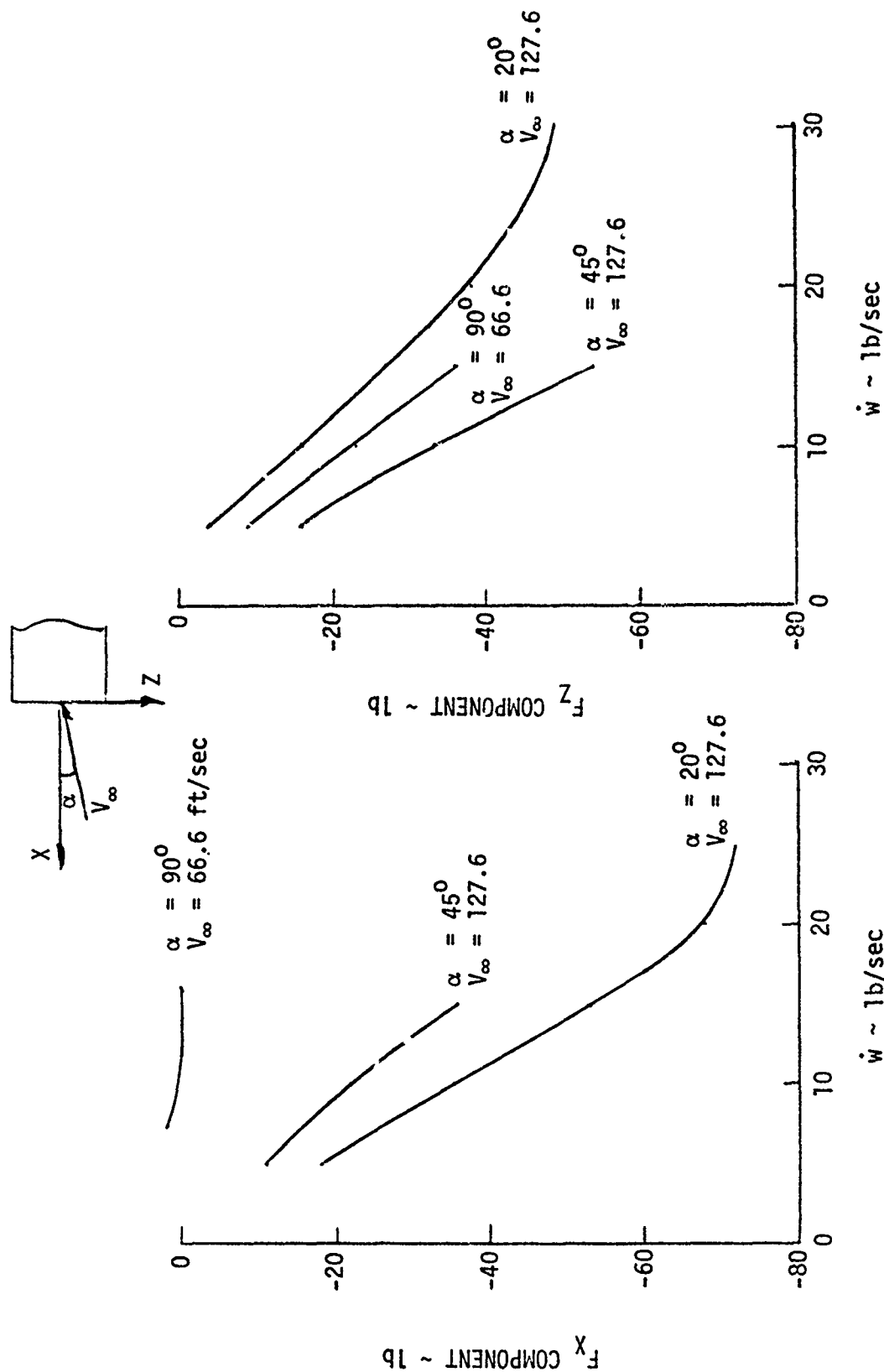
PITCHING MOMENT FOR NASA QCSEE INLET
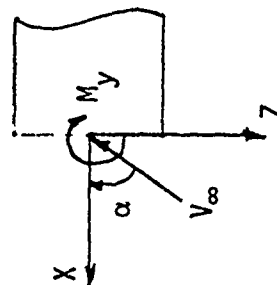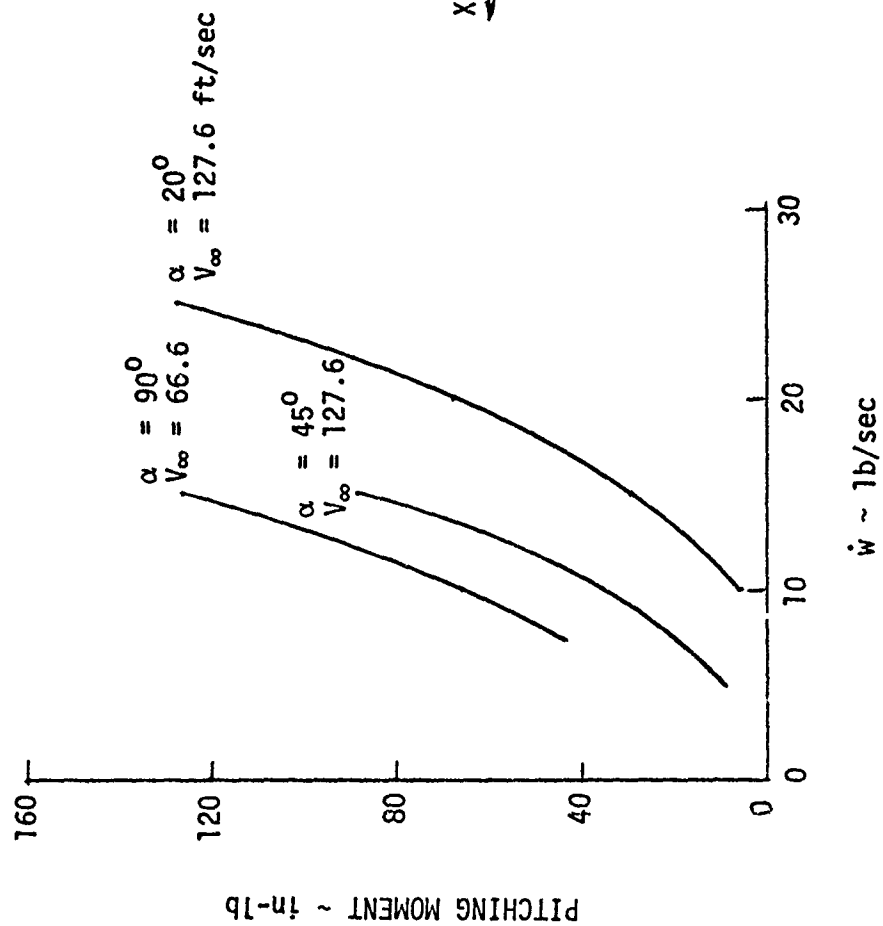
FUTURE WORK ON INLET FORCES AND MOMENTS

o VAPE: COMPUTER GENERATED PARAMETRIC CHARTS FOR RAM EFFECTS

o VERIFICATION

o IMPROVED DATA:

(A) 3-D STOCKMAN ROUTINE

(B) ISOLATE INLET LIP EFFECTS DURING WIND TUNNEL TESTING

677

THEORETICAL FAN VELOCITY DISTORTIONS
DUE TO INLETS AND NOZZLES

J. Dennis Hawk
Lewis Research Center
Cleveland, Ohio

THEORETICAL FAN VELOCITY DISTORTIONS DUE TO INLETS AND NOZZLES

by J. Dennis Hawk

NASA-Lewis Research Center
Cleveland, Ohio

ABSTRACT

Nonuniform velocity profiles imposed on the propulsion system fan can cause fan blade stresses and thrust losses. This paper presents a theoretical parametric study of the effects of inlets with 0° and 90° nozzle deflection on the velocity profile at a hypothetical fan. The parameters investigated are fan-to-nozzle spacing and inlet centerline offset. The interaction between the inlet and nozzle is also investigated. The study is made using a two-dimensional analysis.

E-006

INTRODUCTION

Deflected thrust nacelles (fig. 1) are being considered for several VTOL type aircraft. While these nacelles are not subjected to as severe external flow conditions as their tilt-nacelle counterparts, they can experience severe internal flow conditions when the nozzles are deflected 90°. This is especially true when the nozzles are placed close to the exit plane of the fan. Such close-coupled nozzles produce distortions which are propagated upstream to the fan and can be severe enough to induce high fan blade stresses and cause fan performance (airflow and efficiency) degradation. One solution is to place the nozzle far enough downstream to eliminate the distortion. Another approach is to design the inlet and deflecting nozzle to minimize flow distortion at the fan. However the design to reduce this fan velocity distortion for a 90° deflection must also yield low distortion for operation in the cruise mode (i.e., zero deflection).

It is the purpose of this paper to present the effects of pertinent nozzle and inlet geometric variables on the velocity profiles at the fan for configurations applicable to VTOL deflected thrust nacelles. The geometric parameters investigated were fan-nozzle spacing and inlet centerline offset for both cruise (zero deflection), and takeoff and landing (90° deflection).

Calculations were performed at zero free stream velocity using the two dimensional analysis procedure described in reference 1.

SYMBOLS

A   area

a   lip ellipse semi-major axis

b   lip ellipse semi-minor axis

D   diameter

L   length

r   radius

V   velocity

x   axial length

y   vertical height

Δy throat-to-fan centerline offset

Subscripts:

AVG   average

de   diffuser exit

f   fan

fe   fan exit

h_i highlight

i   inner

in   inlet

MAX   maximum

MIN   minimum

N   nozzle displacement

o   outer

t   throat

RESULTS AND DISCUSSION

The discussion starts with the distortion generated by an isolated nozzle, and then adds the distortion effects of the inlet. In the present calculations, the fan is idealized to a pressure ratio of unity so no distinction exists between distortions at the fan generated upstream or downstream of the fan.

Isolated 90° Nozzle

The isolated effects of a 90° deflected nozzle were obtained by using the configuration shown in figure 2. Straight ducts of constant area were extended a large distance upstream and downstream of the 90° turn to eliminate termination effects. The turn itself was a constant area turn. The inner wall was a circular arc section with a radius (r_i/D_f) of 0.25 and the outer wall was also circular with a radius (r_o/D_f) of 1.25. The hypothetical fan was placed at various locations upstream of the nozzle entrance. This fan-to-nozzle spacing (L_N/D_f) was varied between 0 and 0.83. Due to the straight sections upstream and downstream of the turn, any velocity distortions measured at the fan locations are due entirely to the proximity of the 90° turn.

Figure 3 shows the effects of the fan-nozzle spacing on the duct velocity profile at the fan. The most severe distortion occurred at a L_N/D_f of 0 with the maximum and minimum velocities occurring on the inner and outer walls, respectively. This kind of distortion (i.e., asymmetric about inlet centerline) would appear as a circumferential distortion to a rotating fan and will be referred to subsequently as circumferential distortion. As the fan-nozzle spacing was increased, the velocity distortion decreased.

In an attempt to characterize the effect of fan-nozzle displacement by a single quantity, a velocity distortion parameter, defined as $(V_{max} - V_{min})/V_{avg}$, was used. The parameter is shown in figure 4 as a function of fan-nozzle spacing. As expected, the distortion is highest when the nozzle is

nearest the fan. This distortion decreases to approximately 0.05 for the last nozzle location shown ($L_N/D_f = 0.83$), and it would approach zero if the fan were moved far enough upstream.

Nozzle With Straight Inlet

The interaction of the inlet and nozzle in both the zero deflection and 90° deflection modes was studied next. Figure 5 shows typical nacelle configurations for both 0° and 90° nozzle deflection for inlets with straight centerlines.

Both nacelles shown had the same inlet. The inlet had an elliptical internal lip with an a/b ratio of 2.0, a two-dimensional contraction ratio (D_h/D_t) of 1.56 and a DAC-1 external forebody (ref. 2).

The diffuser had a conic section with a wall angle of 14°. The diffuser was mated to the lip with an elliptic section with $a/b = 3$ and to the fan with a circular arc. The diffuser-exit-to-throat area ratio was 1.25. This results in a one-dimensional design throat Mach number of 0.73 for a diffuser exit Mach number of 0.5. The inlet-length-to-fan exit diameter ratio was 1.0.

For the zero deflection configuration, a constant area was maintained downstream of the fan. For the 90° deflection configuration, the fan-nozzle spacing was varied from 0 to 0.83. The nozzle was also a constant area turn as described previously.

Figure 6 shows the velocity profile at the fan for the inlet with a 0° and a 90° nozzle deflection for an L_N/D_f of 0. The zero nozzle deflection velocity profile shows a small distortion symmetrical about the centerline. This kind of distortion (i.e., symmetric about the inlet centerline) would appear as a radial distortion to a rotating fan and will be referred to subsequently as radial distortion. This distortion is due to the internal geometry of the diffuser upstream of the fan. For $L_N/D_f = 0$, the deflected nozzle velocity profile is strongly affected by the nozzle. Although not shown, additional calculations were performed for other values of L_N/D_f. As would be expected when the fan nozzle spacing is increased, the profile for the inlet with a 90° deflection nozzle approaches that of the inlet with a 0° deflection nozzle.

Figure 7 shows the effect of fan-nozzle spacing on the velocity distortion parameter $(V_{max} - V_{min})/V_{avg}$ at the fan. The inlet with zero deflection is not a function of L_N/D_f since the passage downstream of the fan is a straight constant area passage. It is, however, shown as an asymptotic reference line. The velocity distortion for the inlet with a 90° deflection nozzle shows high distortion for small values of L_N/D_f. In this region of high distortion, the fan velocity profile is strongly influenced by the nozzle. While for larger values of L_N/D_f, the distortion

for the inlet with the deflecting nozzle approaches that of the inlet with 0° deflection. In this region, the inlet and diffuser are the dominating factors determining distortion values. In the range between the two limits, the distortion is influenced by both the inlet and deflecting nozzle.

Nozzle With Offset Inlet

Some of the velocity distortions shown (fig. 7) may be excessive for safe, efficient operation of the fan. One method to reduce fan velocity distortion caused by the nozzle is to design the inlet to produce a fan velocity profile which will cancel part of the nozzle distortion. This can be accomplished by shaping the inlet centerline. Figure 8 shows nacelles with inlets offset by Δ_y/L_D for both the 0° and 90° deflection nozzles. A cubic centerline was fit between the inlet throat and the fan face. The diffuser walls, both inner and outer, were then shifted according to the local passage centerline offset. The passage area distribution as a function of axial distance for the offset inlets is the same as it was for the corresponding straight centerline inlets. The nozzle was also spaced at various distances from the fan in the same manner as it was for the straight centerline inlets.

Figure 9 shows the effect of centerline offset on the fan velocity profile for a fan-nozzle spacing of 0.16. (The curve for the zero offset inlet and 90° deflection nozzle is, of course, the same as that shown previously for the straight centerline nacelle.) For the 90° deflecting nozzle the velocity distortion has been markedly reduced by offsetting the centerline by 0.25. However, for the zero deflection nozzle (cruise mode) configuration, the velocity distortion is now high. Therefore, a compromise offset is required so that the nacelle can operate safely and efficiently at both 0° and 90° nozzle deflection.

The resulting velocity distortion parameter as a function of throat-to-fan centerline offset for a fan-nozzle displacement of 0.16 is shown in figure 10. For the nacelle with zero deflection, the distortion is a minimum at zero offset when the distortion is radial in nature. The distortion then increases with increasing inlet centerline offset due to circumferential distortion. For the nacelle with 90° deflection the distortion reaches a minimum where the circumferential distortion due to the inlet centerline offset cancels most of the circumferential distortion due to nozzle deflection. The minimum, however, cannot be less than the inlet radial distortion.

If the distortion at cruise (0° deflection) and takeoff and landing (90° deflection) are of equal importance, then the minimum distortion, considering both 0° and 90° deflection, occurs at the intersection of the dashed and solid curves, point A. In general, combinations of inlet offset and fan-nozzle spacing can be used to achieve the most compact nacelle possible constrained by the allowable velocity distortion at the fan.

SUMMARY OF RESULTS

The effect of close coupled inlets and nozzles on fan velocity profiles and distortions was investigated using two-dimensional potential flow analysis. Some of the specific results are:

1. As the distance from the fan to the nozzle entrance increases, the velocity profile distortion at the fan for a deflecting nozzle decreases.

2. Offsetting the inlet centerline reduces the distortion due to a 90° deflected nozzle but the offset increases the distortion for the 0° nozzle deflection. A value of offset exists which minimizes the distortion for operation over the range of nozzle deflections from zero to 90°.

REFERENCES

1. Hawk, J Dennis; and Stockman, N. O.: Computer Programs for Calculating Two-Dimensional Potential Flow Through Deflected Nozzles. NASA TM (to be published).

2. Albers, James A.; Stockman, N. O.; and Hirn, John J.: Aerodynamic Analysis of Several High Throat Mach Number Inlets for the Quiet Clean Short-Haul Experimental Engine. NASA TM X-3183, 1975.
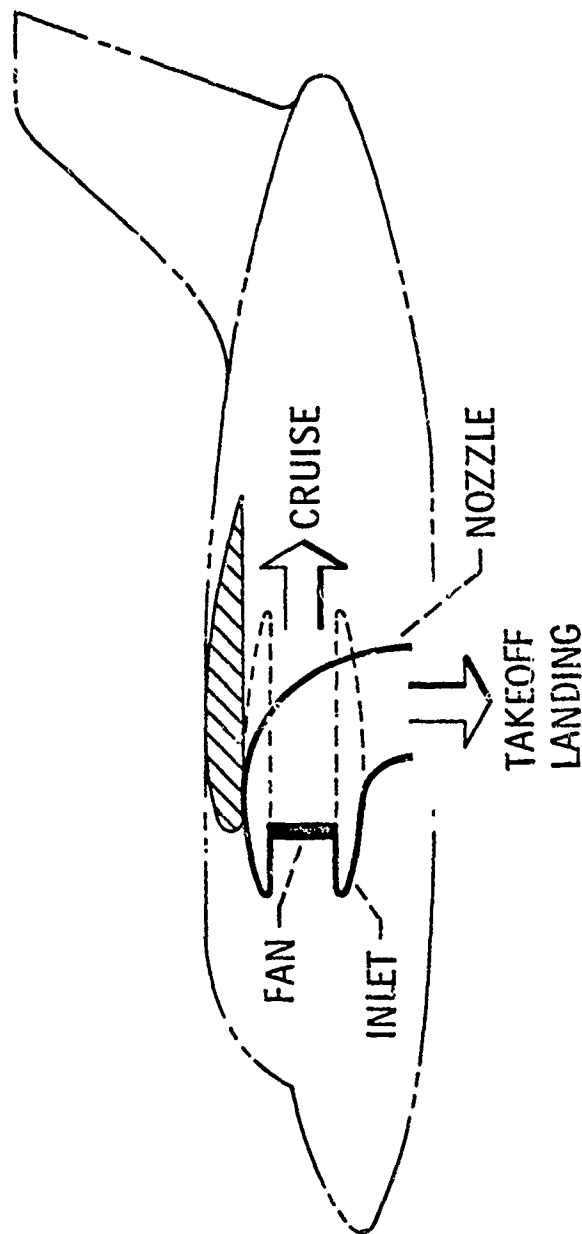
Figure 1. – Idealized VTOL aircraft with deflecting nozzle.
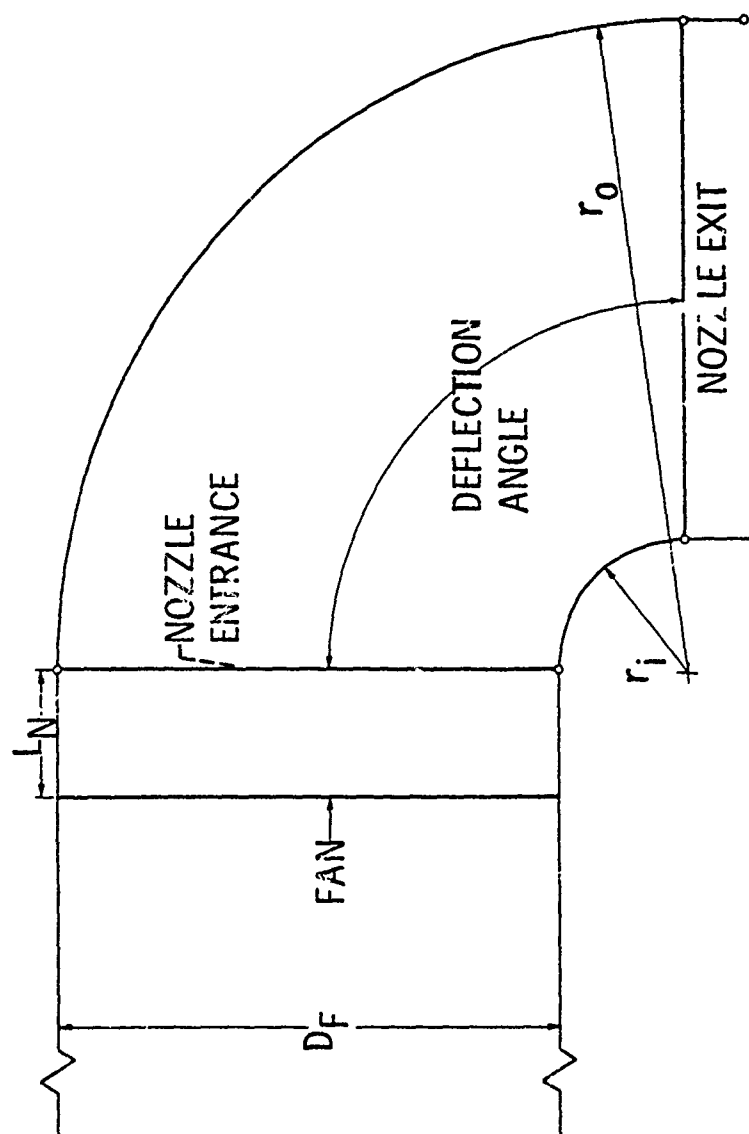
Figure 2. - Isolated nozzle: 90° deflection.
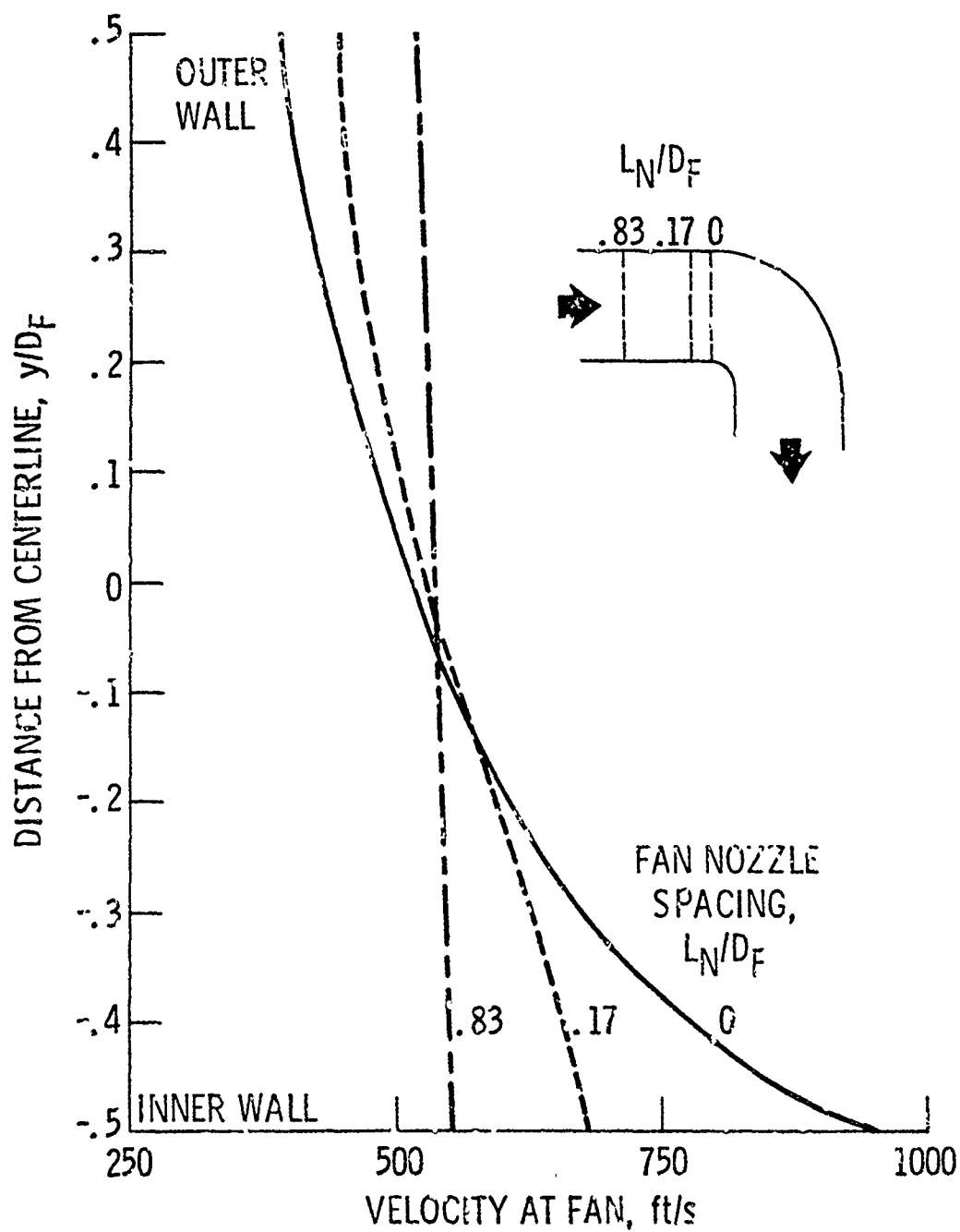
Figure 3. – Effect of fan-nozzle spacing on velocity profile at the fan: straight duct upstream of fan; 90° deflection.
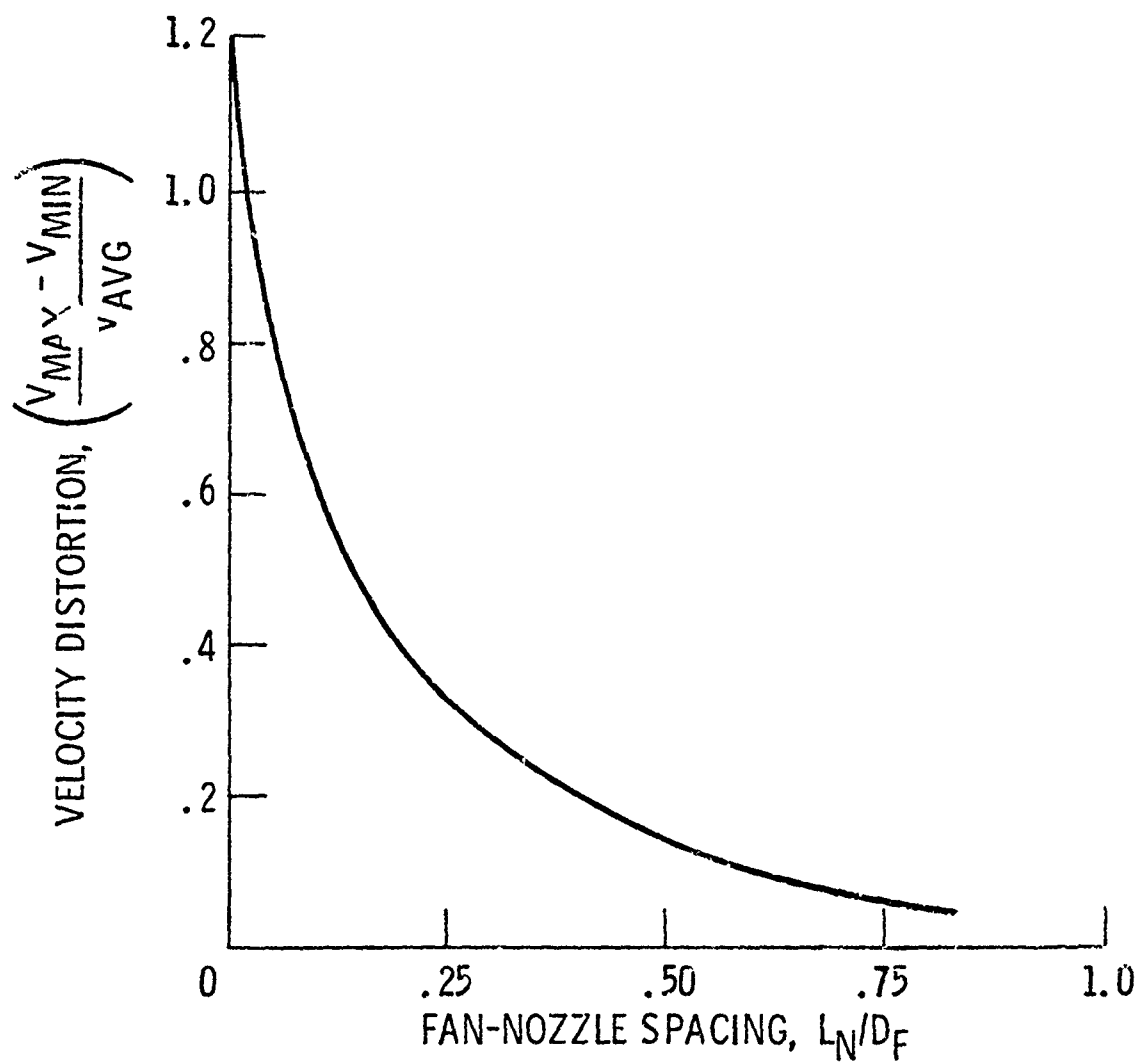
Figure 4. – Theoretical effect of fan-nozzle spacing on velocity distortion at the fan: 90^0 deflection.
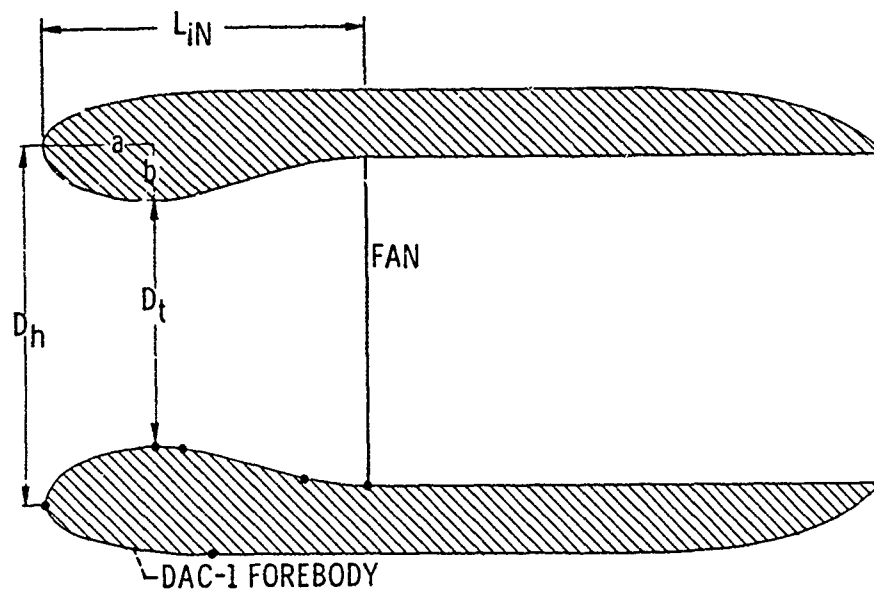
(a) 0^0 NOZZLE DEFLECTION.
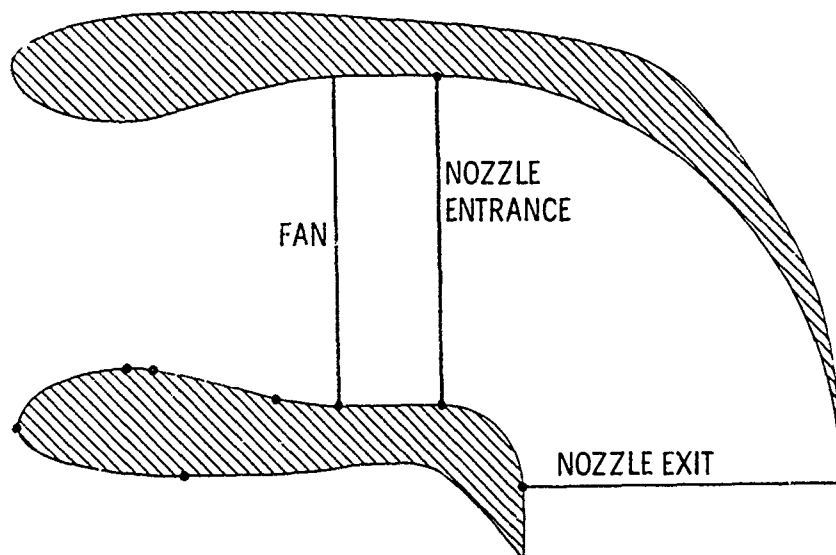
(b) 90^0 NOZZLE.

Figure 5. – Nacelles with straight inlets.
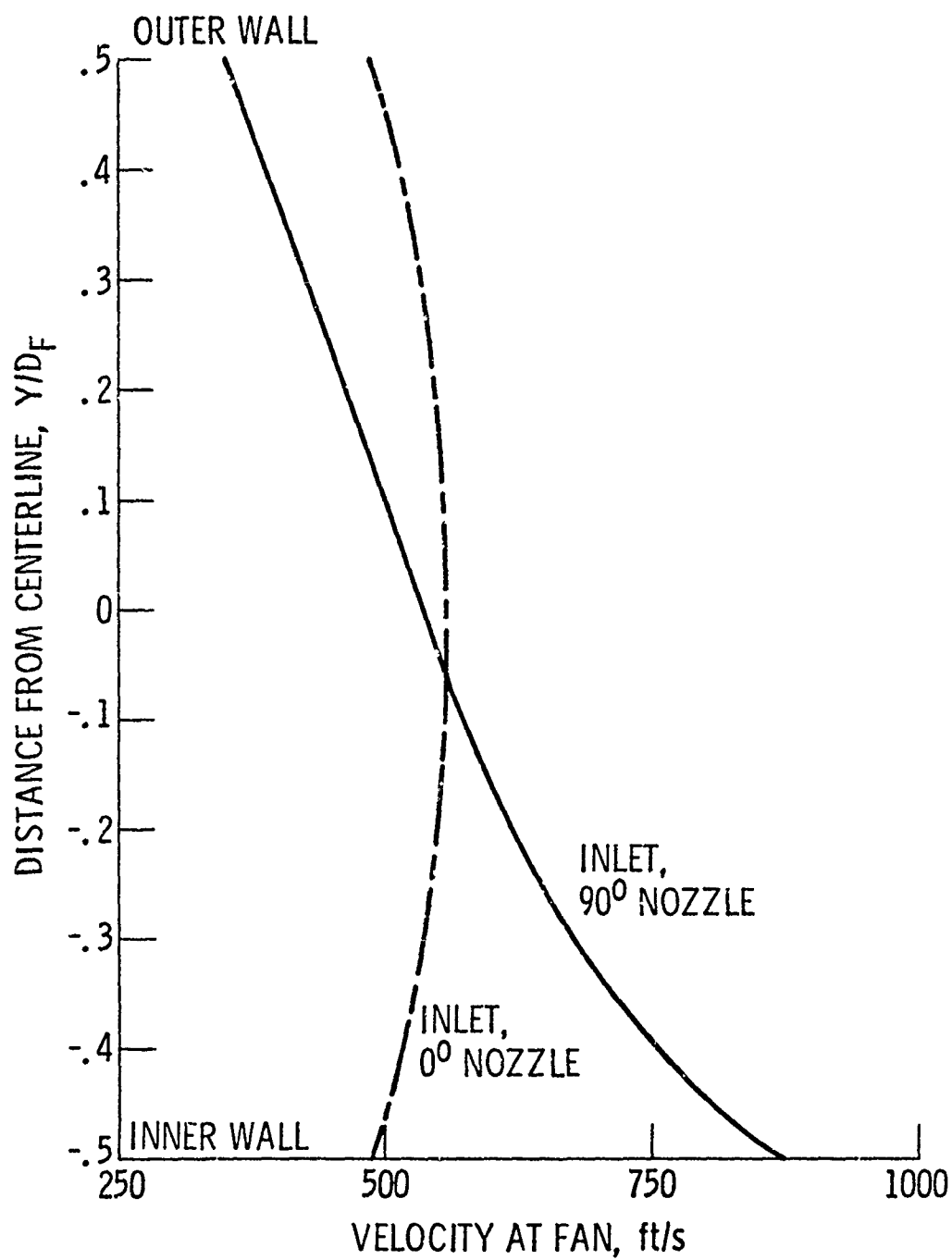
Figure 6. – Effect of nozzle deflection on velocity profile at the fan: straight inlet; $L_N/D_F = 0$.
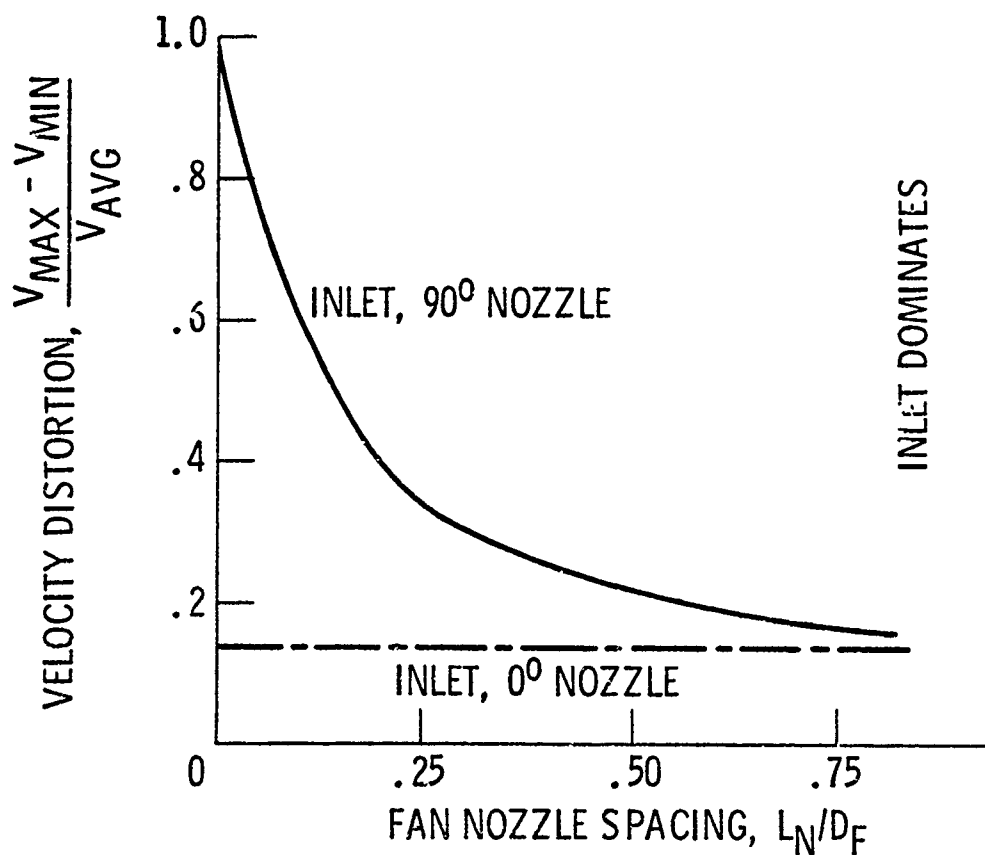
Figure 7. - Effect of fan-nozzle spacing on velocity distortion at the fan: straight inlet.
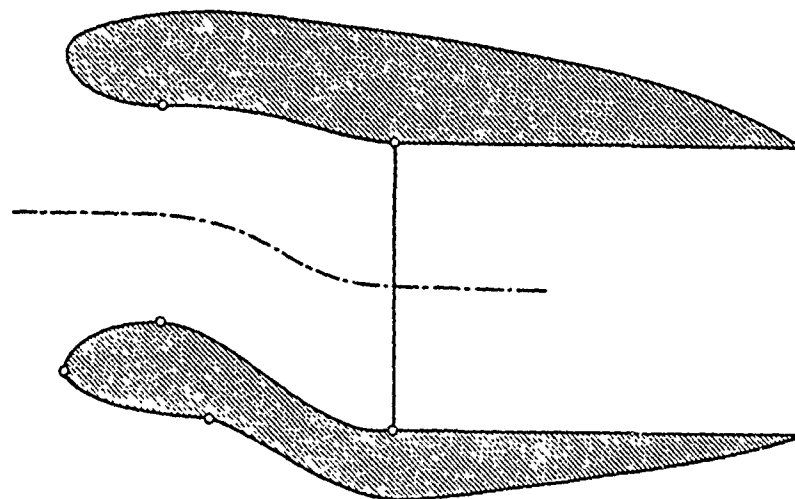
(a) 0° NOZZLE DEFLECTION.

$\Delta y/L_D$
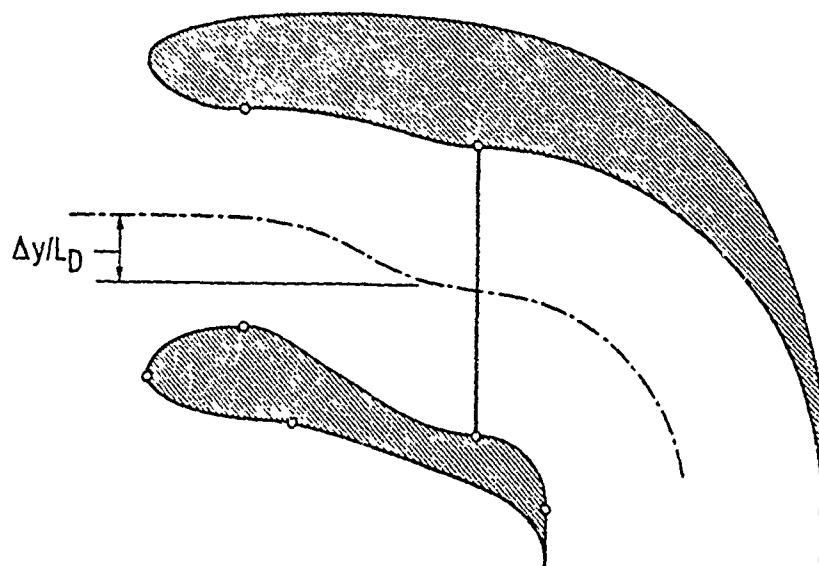
(b) 90° NOZZLE DEFLECTION.

Figure 8. – Nacelles with offset inlets.
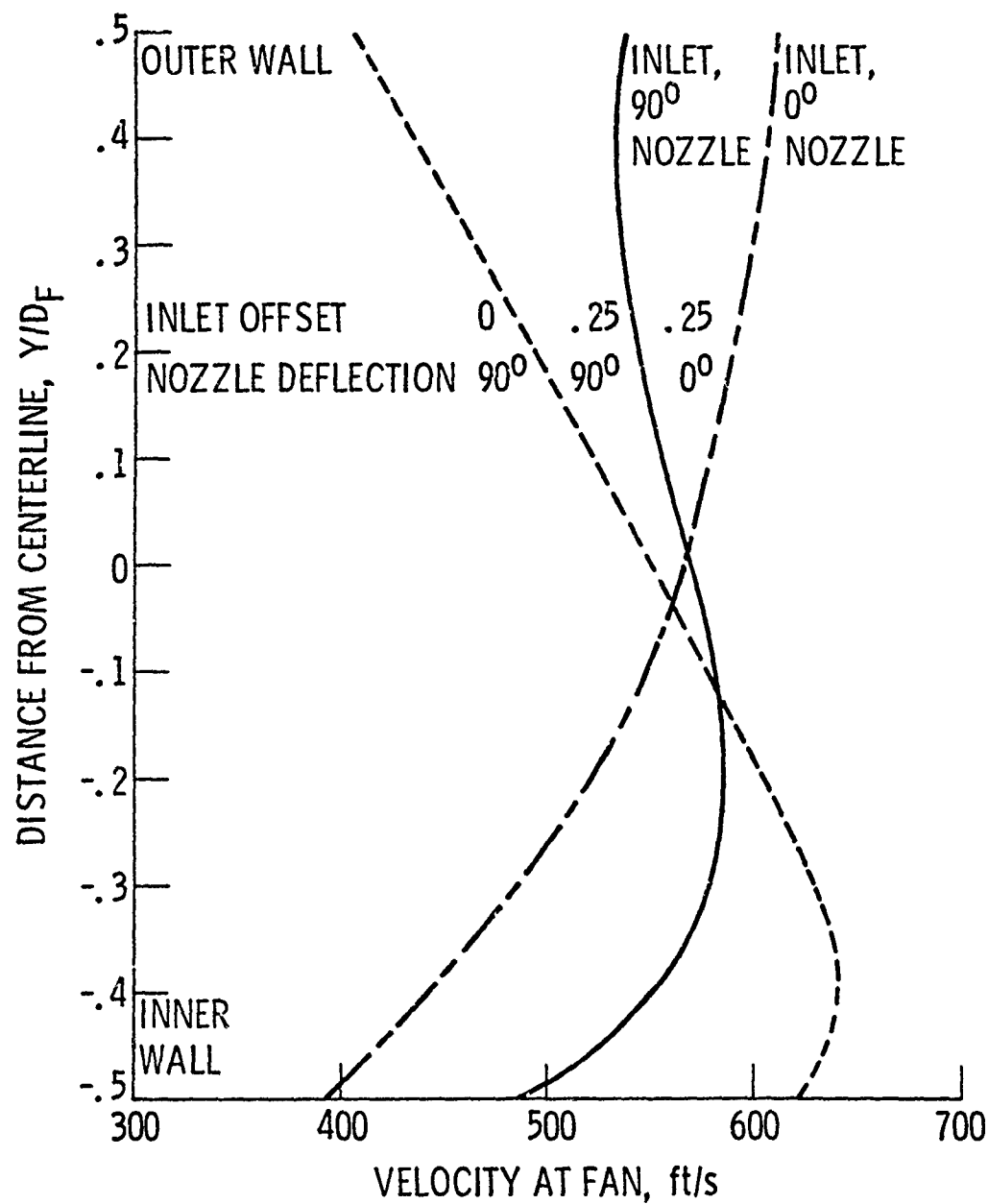
Figure 9. – Effect of inlet centerline offset and nozzle deflection on velocity profile at the fan: L_N/D_F = 0.16.
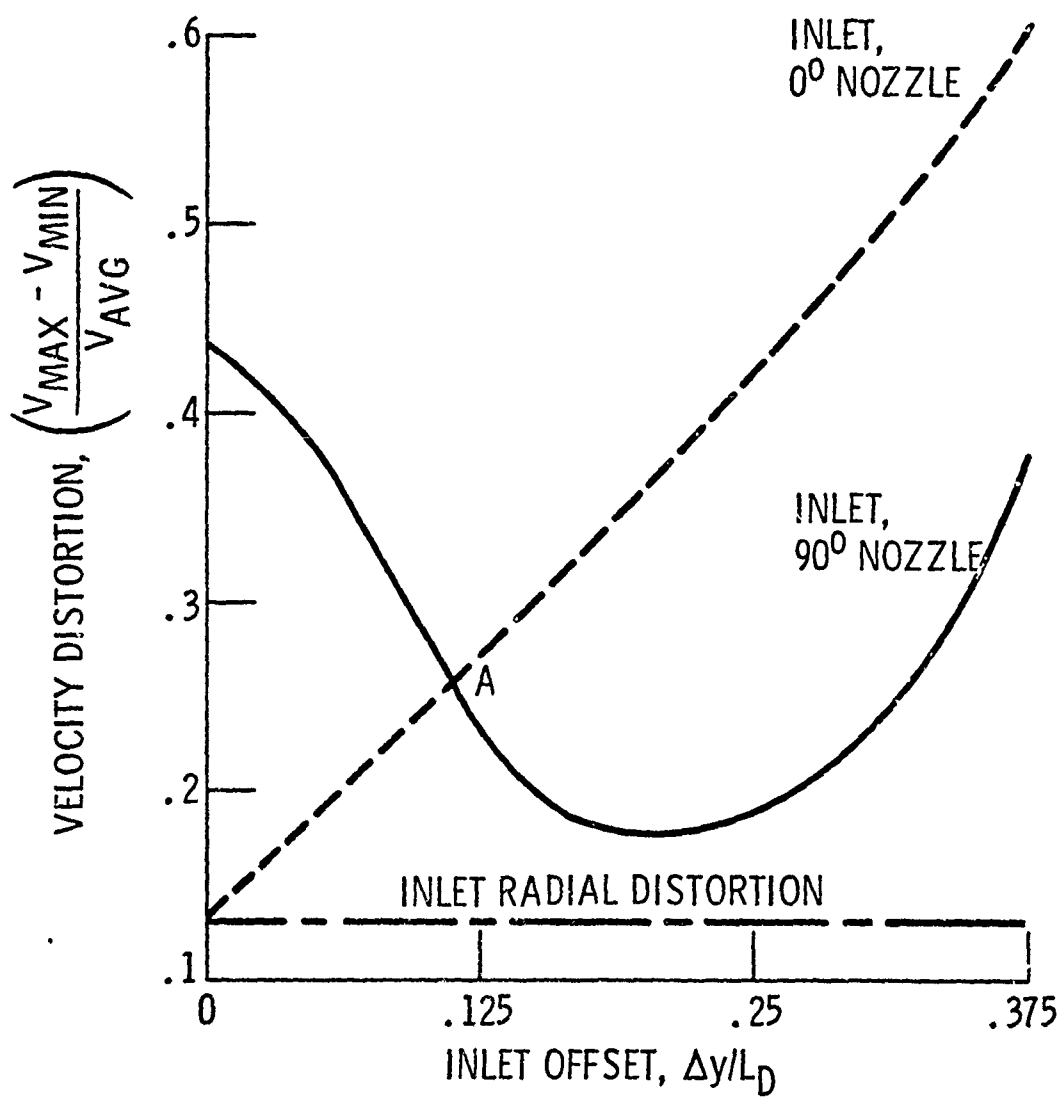
Figure 10. – Effect of inlet centerline offset and nozzle deflection on velocity distortion at the fan: $L_N/D_F = 0.16$.

1. Report No. NASA TM-79150	2. Government Accession No.	3 Recipient's Catalog No
4. Title and Subtitle THEORETICAL FAN VELOCITY DISTORTIONS DUE TO INLETS AND NOZZLES		5. Report Date April 1979
		6. Performing Organization Code
7. Author(s) J. Dennis Hawk		8. Performing Organization Report No E-006
		10. Work Unit No
9. Performing Organization Name and Address National Aeronautics and Space Administration Lewis Research Center Cleveland, Ohio 44135		
		11. Contract or Grant No.
12. Sponsoring Agency Name and Address National Aeronautics and Space Administration Washington, D.C. 20546		13. Type of Report and Period Covered Technical Memorandum
		14 Sponsoring Agency Code

15. Supplementary Notes

16. Abstract

Nonuniform velocity profiles imposed on the propulsion system fan can cause fan blade stresses and thrust losses. This paper presents a theoretical parametric study of the effects of inlets with 0° and 90° nozzle deflection on the velocity profile at a hypothetical fan. The parameters investigated are fan-to-nozzle spacing and inlet centerline offset. The interaction between the inlet and nozzle is also investigated. The study is made using a two-dimensional analysis.

17. Key Words (Suggested by Author(s)) Internal aerodynamics Fan distortions Nozzles	18. Distribution Statement Unclassified - unlimited STAR Category 02		
19. Security Classif. (of this report) Unclassified	20. Security Classif. (of this page) Unclassified	21. No of Pages	22 Price*

AERODYNAMICS OF A TILT-NACELLE

V/STOL PROPULSION SYSTEM

Mark D. Betzina and Michael D. Falarski
Ames Research Center, NASA
Moffett Field, California 94035

Presented at

Workshop of V/STOL Aerodynamics

May 1979

Naval Postgraduate School

Monterey, California

Aerodynamics of a Tilt-Nacelle

V/STOL Propulsion System

Mark D. Betzina and Michael D. Falarski

Ames Research Center, NASA, Moffett Field, California

Abstract

Wind tunnel tests were performed in the Ames 40- by 80-Foot Wind Tunnel on a large-scale, tilt-nacelle V/STOL propulsion system; the objective was to de ermine its aerodynamic characteristics. It is shown (1) that the characteristics of the unpowered nacelle can be estimated with annular airfoil data, (2) that the power-induced effects on the nacelle aerodynamics are significant, and (3) that pitching moment can be correlated with lift and thrust.

Introduction

A tilt-nacelle propulsion system, such as might be used on a V/STOL airplane, can be subjected to angles of attack greater than 90° during takeoff and landing maneuvers. These nacelles, which are large relative to the aircraft, have a significant effect on the aerodynamic characteristics of the aircraft. It is necessary, therefore, to be able to predict the aerodynamic characteristics of the nacelle so that the aerodynamics of the aircraft can be accurately represented.

Wind tunnel tests were performed in the Ames 40- by 80-Foot Wind Tunnel on a large-scale, tilt-nacelle V/STOL propulsion system, with the objective of determining its aerodynamic characteristics. Force and moment data were acquired from the wind tunnel balance system for various combinations of thrust and velocity at angles of attack from 0° to 120°. Results are separated into terms of unpowered nacelle aerodynamics and power-induced effects on nacelle aerodynamics. The unpowered nacelle characteristics are compared with those of an annular airfoil, the power-induced aerodynamics are discussed, and finally, in an attempt to establish a method for estimating the pitching moment produced by such a propulsion system, a relationship is determined between the total lift and the total pitching moment.

Nomenclature

A_F fan area, 1.206 m² (12.98 ft²)

C_D wind axis drag coefficient, $\dfrac{D}{qA_F}$

$C_{D_{AERO}}$ aerodynamic drag coefficient, $C_D - C_{D_T}$

C_{D_R} ram-drag coefficient, $\dfrac{D_R}{qA_F}$

C_{D_T} drag coefficient due to thrust and ram drag, $C_{D_R} - C_J \cos \alpha$

C_J thrust coefficient, $\dfrac{T}{qA_F}$

C_L wind axis lift coefficient, $\dfrac{L}{qA_F}$

$C_{L_{AERO}}$ aerodynamic lift coefficient, $C_L - C_{L_T}$

C_{L_T} lift coefficient due to thrust, $C_J \sin \alpha$

C_m pitching-moment coefficient about the nacelle pivot axis, $\dfrac{M}{qA_F d}$

d fan diameter, 1.397 m (4.583 ft)

D total measured wind axis drag, N

D_R ram drag, N

L   total measured wind axis lift, N

M   total measured pitching moment about the nacelle pivot axis, m – N

q   free-stream dynamic pressure, N/m^2

T   total gross thrust, N

α nacelle angle of attack, deg

Propulsion System Description

Figure 1 shows the propulsion system in the Ames 40- by 80-Foot Wind Tunnel. The system consisted of a 1.4-m (55-in.), 13-bladed, variable-pitch fan driven by a Lycoming T55-L-11A, 2800 kW (3750 hp) gas turbine core engine. The fan was driven through a 4.75:1 gear reduction to a maximum speed of 3365 rpm; it had a bypass ratio of 17:1. Additional information on the fan and core engine is available in reference 1. The asymmetric inlet, designed for a tilt-nacelle lift/cruise fan propulsion system, had a higher contraction ratio on the windward side than on the leeward side; as a result, testing was possible at high angles of attack without stalling the fan. The cowling was designed to provide a nacelle suitable for wind-tunnel testing. The components of the propulsion system and its major dimensions are shown in figure 2. A more detailed description is available in reference 2. The nacelle was mounted about 4 m above the wind-tunnel floor on a single strut which was shielded from the wind by a fairing. The nacelle was rotated in a horizontal plane about the strut centerline for angle-of-attack variation.

Test Procedure and Data Reduction

Most of the data were acquired by varying thrust at constant nacelle angles of attack and at constant tunnel velocities. The operating limits of the propulsion system were determined and are discussed in reference 3. Tunnel velocity varied from 0-82 m/sec (0-160 knots) and angle of attack varied from 0°-120°. Thrust coefficients were computed from gross thrust, which was determined from total and static pressure and total temperature measurements in the inlet, fan duct, and core engine inlet. Gross thrust was varied up to a maximum of 30,700 N (6900 lb) by changing engine speed and fan blade angle. Ram drag was computed from inlet airflow, determined from static and total pressure measurements in the inlet, and from free-stream velocity. The unpowered-nacelle data were obtained with the fan blades feathered to minimize drag through the nacelle.

Force and moment data, obtained from the wind-tunnel balance system, were used to compute coefficients for the total nacelle forces and moments in the wind axis system. The fan area, 1.206 m^2, and the fan diameter, 1.597 m, were used for the reference area and length, respectively. The moment center was located on the engine centerline, at the axis of rotation, 1.928 m aft of the inlet hilite.

Results

Basic Aerodynamics

Figure 3 shows the lift and drag characteristics of the propulsion system for thrust coefficient of 0, 10, and 20. The dashed lines represent the thrust and ram drag forces resolved into the lift and drag directions. Most of the resultant force on the nacelle is due to the thrust and ram drag forces; however, significant aerodynamic forces also are present, as shown by the difference between the solid and dashed lines in figure 3. At an angle of attack of 80° and a thrust coefficient of 10, 25% of the total lift is due to the nacelle aerodynamics.

Induced Aerodynamics

In order to determine what part of the aerodynamic forces was induced by power, the aerodynamic lift and drag coefficients were plotted versus angle of attack (fig. 4). The coefficients were obtained by subtracting the thrust and ram drag components from the total lift and drag coefficients. There is a substantial difference between the powered and unpowered curves which represents the power-induced effect on the aerodynamic coefficients. The maximum aerodynamic lift in the powered case is about the same magnitude as the unpowered maximum lift, but it occurs at a much higher angle of attack. This indicates that, in the powered case, flow separation on the nacelle is delayed until the angle of attack is about 80°. The power-induced effect on the aerodynamic drag is very small at angles of attack less than 55°. The difference shown is probably due to the greater drag resulting from the fan blades and core engine in the unpowered case. At angles of attack greater than 55°, however, there is a large power-induced effect on the aerodynamic drag, which increases as power is increased. The maximum aerodynamic drag occurs at an angle of attack of 60° for the unpowered case, and at 75° to 90° for the powered case. Also shown in figure 4 are data for an annular airfoil with an aspect ratio of 1/3 (see ref. 4). The coefficients for the annular airfoil were converted to the same basis as those for the propulsion system, that is, inside area and diameter. Considering the difference in configurations, the annular airfoil portrays the nacelle quite accurately. The greater lift for the propulsion system may be due to the large fairing around the support strut, and the greater drag at low angles of attack may be a result of the fan blades and core engine. It is reasonable, therefore, to use annular airfoil data to estimate unpowered nacelle characteristics.

The aerodynamic lift to drag ratio is shown in figure 5. A comparison between the powered and unpowered data indicates a very small power-induced effect on this ratio. The data indicate a maximum lift-to-drag ratio of about 1.8, which occurs at an angle of attack of about 20°. Not enough data were acquired to define these curves at low angles of attack; however, it appears that there is a maximum lift-to-drag ratio at some low angle of attack that should be considered. The annular airfoil data, also shown in figure 5, are greater at low angles of attack because of the lower drag of the annular airfoil. The accuracy of the lift-to-drag ratio is questionable at low angles of attack, since the aerodynamic forces are small.

Pitching-Moment Characteristics

The total pitching moment produced by the propulsion system is very large; it is shown as a function of angle of attack in figure 6. The maximum pitching moment occurs at angles of attack between 75° and 90° in the powered case, which is the same as the angle at which the maximum aerodynamic lift and drag occur. The total pitching moment consists of three parts: (1) aerodynamic pitching moment resulting from the aerodynamic forces on the nacelle, including power-induced effects; (2) moment produced by the flow turning into the inlet, which can be represented by the ram drag acting at an effective moment arm, and (3) moment caused by asymmetric fan thrust. Some asymmetry in the fan exhaust was present at high angles of attack, but the pitching moment resulting from it is a small percentage of the total and can be neglected. Therefore, the total pitching moment is primarily a result of both the ram drag and the nacelle aerodynamics. To assist in predicting pitching moments, it would be desirable to determine an effective ram drag moment arm. This requires separating the aerodynamic pitching moment from the pitching moment due to ram drag, however, because both contribute significantly. But this cannot be done quantitatively because the aerodynamic pitching moment is not known. Although the unpowered pitching moment, which agrees well with the annular airfoil data, is known, it does not include the power-induced effects. The power-induced effects on the aerodynamic forces were shown to be significant (fig. 4). But, since the location of these forces is unknown, their effect on pitching moment, although significant, cannot be determined. Therefore, the difference between the powered and unpowered data in figure 6 represents the sum of the ram-drag contribution and the power-induced effects on the nacelle aerodynamics.

In figure 7, the total nacelle pitching-moment coefficient is plotted versus the total lift coefficient. A good correlation between total lift and total pitching moment is indicated by the fact that for a given thrust coefficient, the data before and after maximum lift are near the same line. This correlation is shown in figure 8, where the ratio of total pitching-moment coefficient to total lift coefficient is shown as a function of thrust coefficient. This ratio changes only slightly with angle of attack at any given thrust coefficient. It is reasonable, therefore, to estimate the pitching moment of a tilt-nacelle V/STOL propulsion system for a given thrust coefficient as a percentage of the total lift, regardless of the angle of attack. Figure 8 indicates that this approximation results in a pitching-moment accuracy of about ±5%.

Conclusions

Although more testing is required to determine if the results presented in this paper are applicable to other configurations, the following conclusions can be made about a tilt-nacelle V/STOL propulsion system:

1. Unpowered-nacelle aerodynamics can be approximated by annular airfoil data for a similar aspect ratio.

2. Aerodynamic forces, including substantial power-induced effects, are a significant part of the total forces.

3. Very large pitching moments are produced and are a result of both ram drag and nacelle aerodynamics.

4. The maximum aerodynamic forces, as well as the maximum pitching moment, occur at angles of attack between 75° and 90°.

5. In order to determine an effective ram-drag moment arm, the aerodynamic pitching moment must be separated from the pitching moment due to ram drag.

6. Total pitching moment correlates well with total lift.

References

1. Demers, W. J.; Metzger, F. B.; Smith, L. W.; and Wainauski, H. S.: Testing of the Hamilton Standard Q-Fan Demonstrator (Lycoming T55-L-11A Core Engine). NASA CR-121265, March 1973.

2. Shain, W. M.: Test Data Report — Low Speed Wind Tunnel Tests of a Full Scale Lift/Cruise — Fan Inlet, With Engine at High Angles of Attack. NASA CR-152055, January 1978.

3. Syberg, J.: Low Speed Test of a High-Bypass-Ratio Propulsion System with an Asymmetric Inlet Designed for a Tilt-Nacelle V/STOL Airplane. NASA CR-152072, January 1978.

4. Fletcher, Herman S.: Experimental Investigation of Lift, Drag, and Pitching Moment of Five Annular Airfoils. NACA TN 4117, October 1957.

(a) 3/4 front view.

Figure 1.- Tilt-nacelle V/STOL propulsion system in the Ames 40- by 80-Foot
Wind Tunnel.

703

(b) 3/4 rear view.

Figure 1.- Concluded.

2.90m
1.928m
1.304m
1.00m

MOMENT CENTER
AND ROTATION AXIS

FAN

WINDWARD SIDE LIP

LYCOMING T-55L-11A
CORE ENGINE
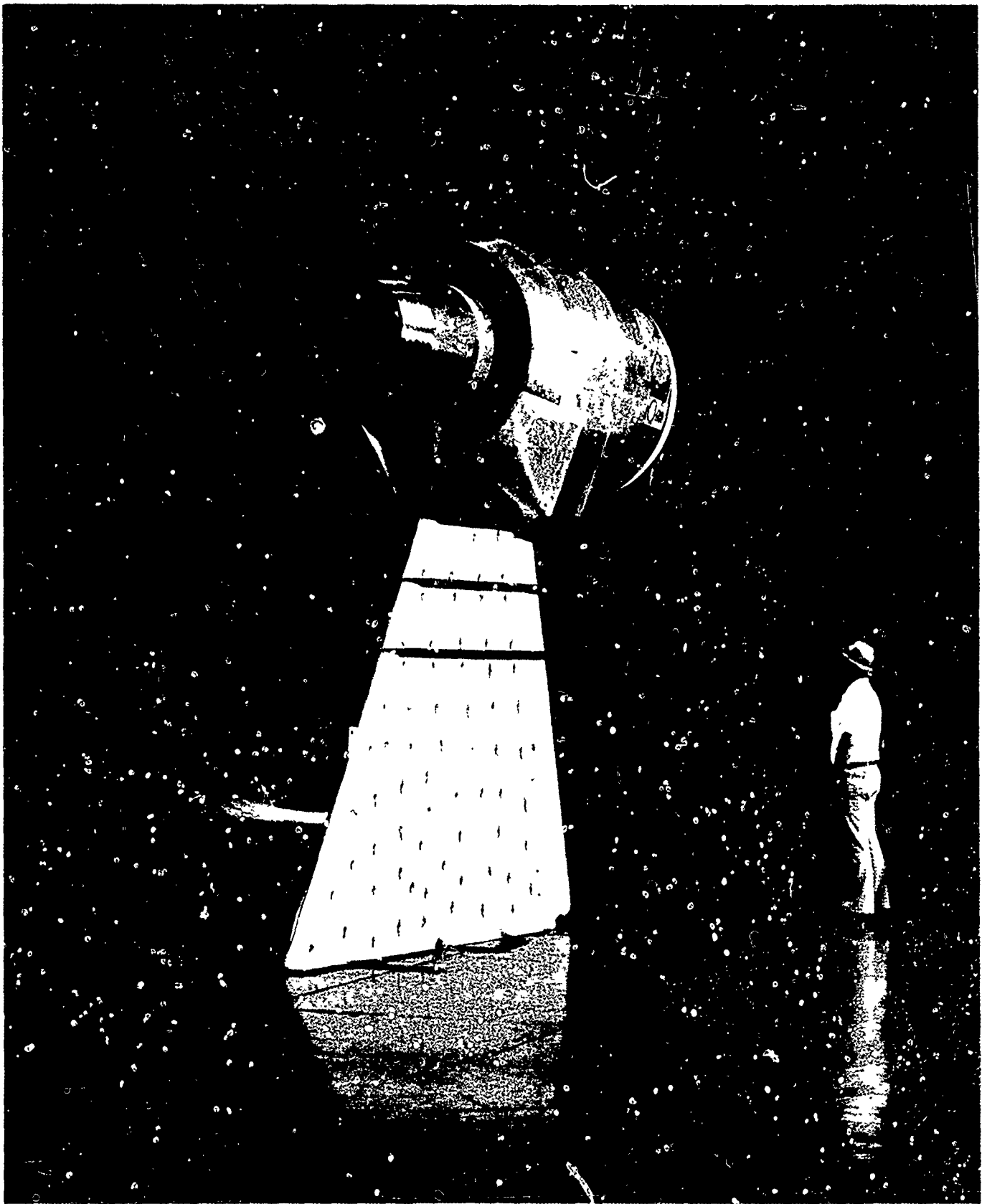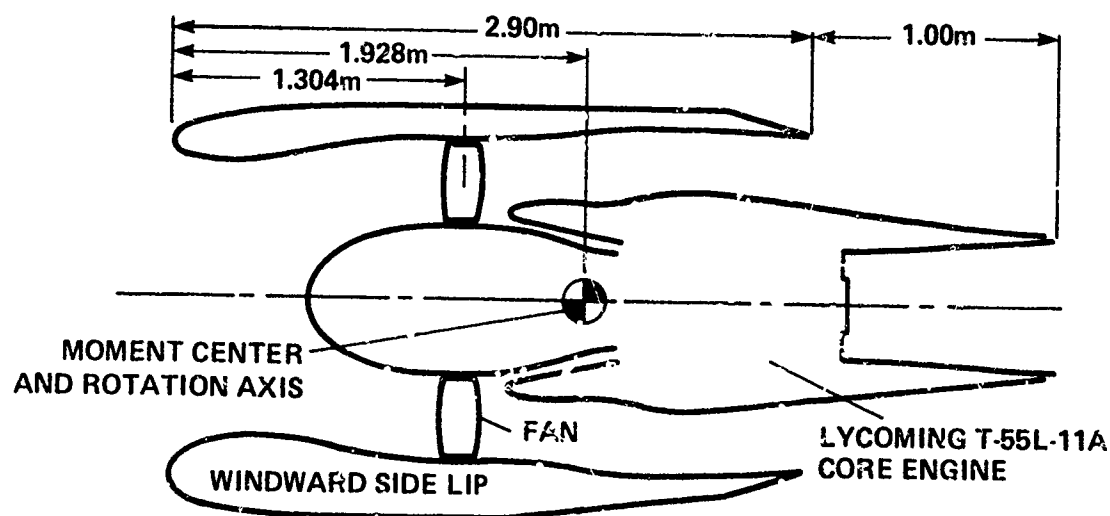
BYPASS RATIO:	17:1
MAX. FAN SPEED:	3365 rpm
FAN AREA:	1.206m^2
FAN DIAMETER:	1.397m
FAN EXIT AREA:	1.064m^2
CORE EXIT AREA:	0.25m^2

Figure 2.- Nacelle schematic.

$$C_{L_T} = C_J \sin \alpha$$

$$C_{D_T} = C_{D_R} - C_J \cos \alpha$$
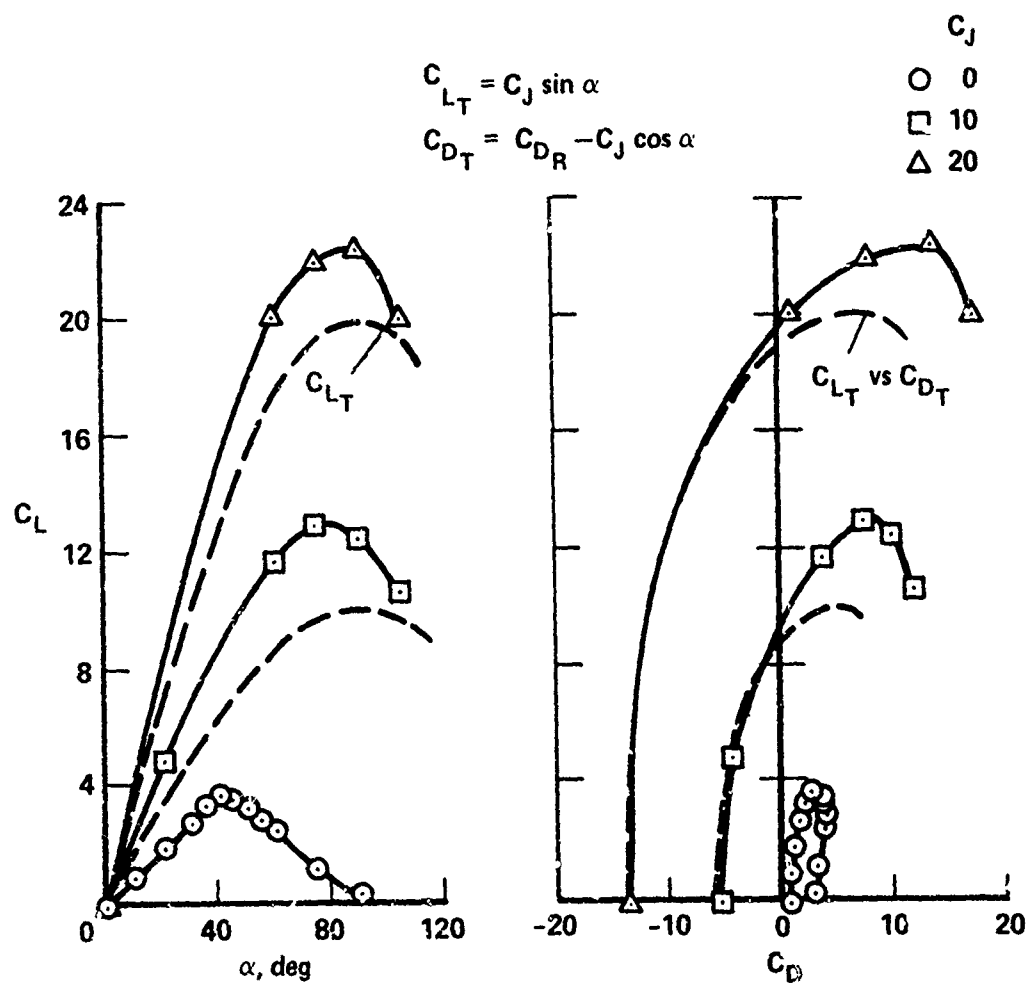
Figure 3.- Lift and drag characteristics.

706
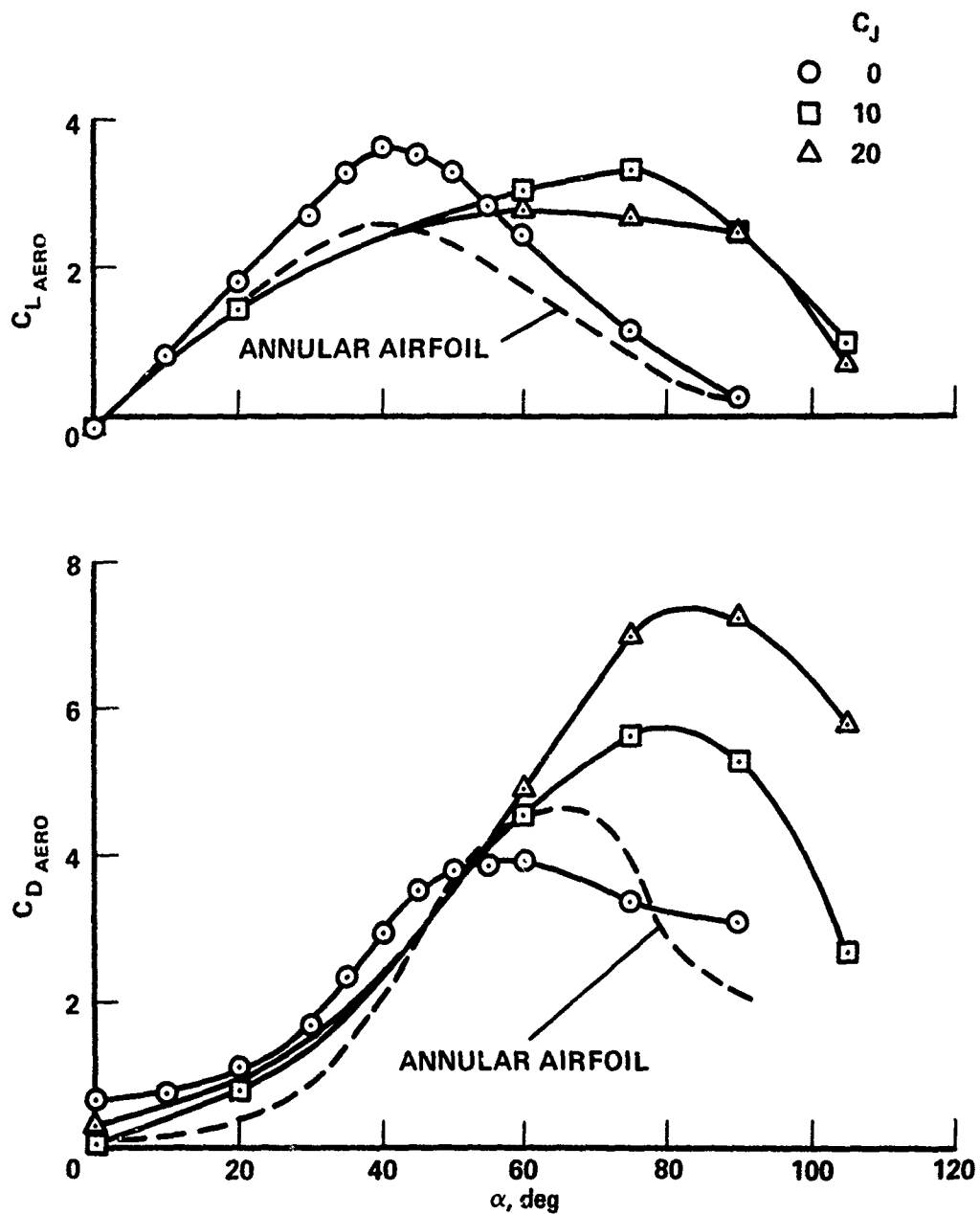
Figure 4.- Power-induced effect on aerodynamic lift and drag.
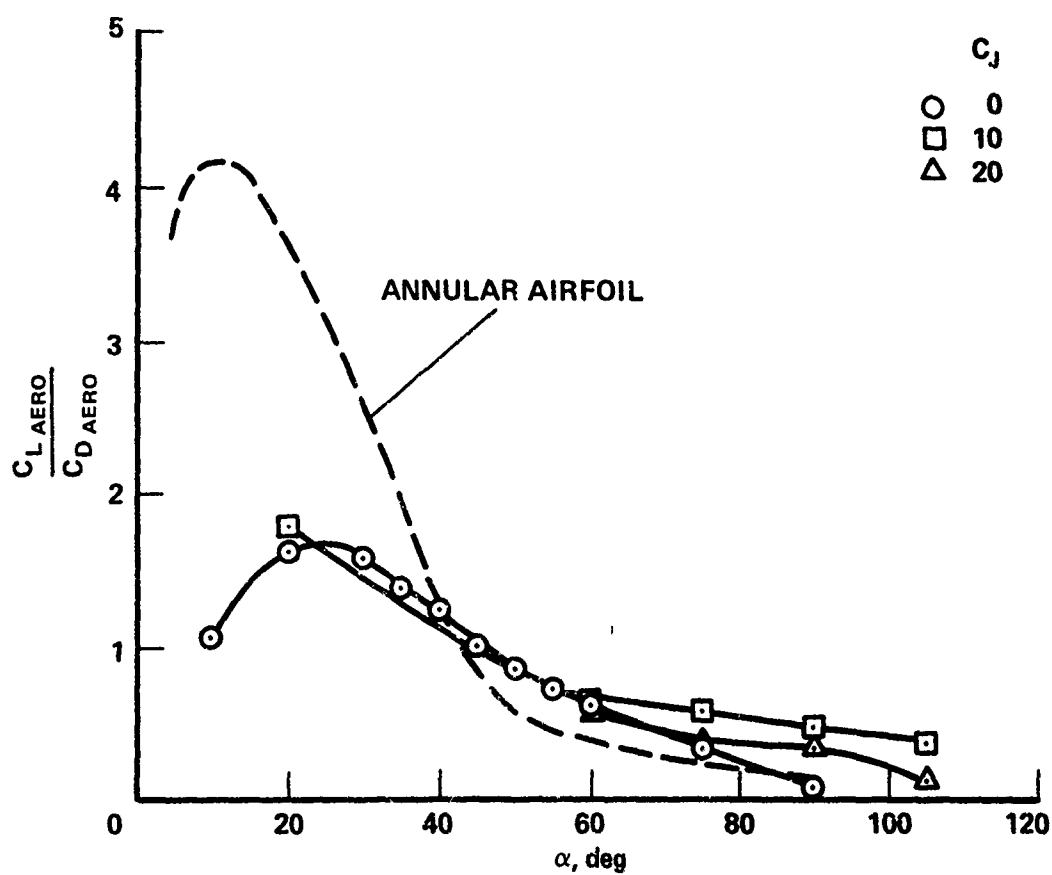
Figure 5.- Aerodynamic lift-to-drag ratio.
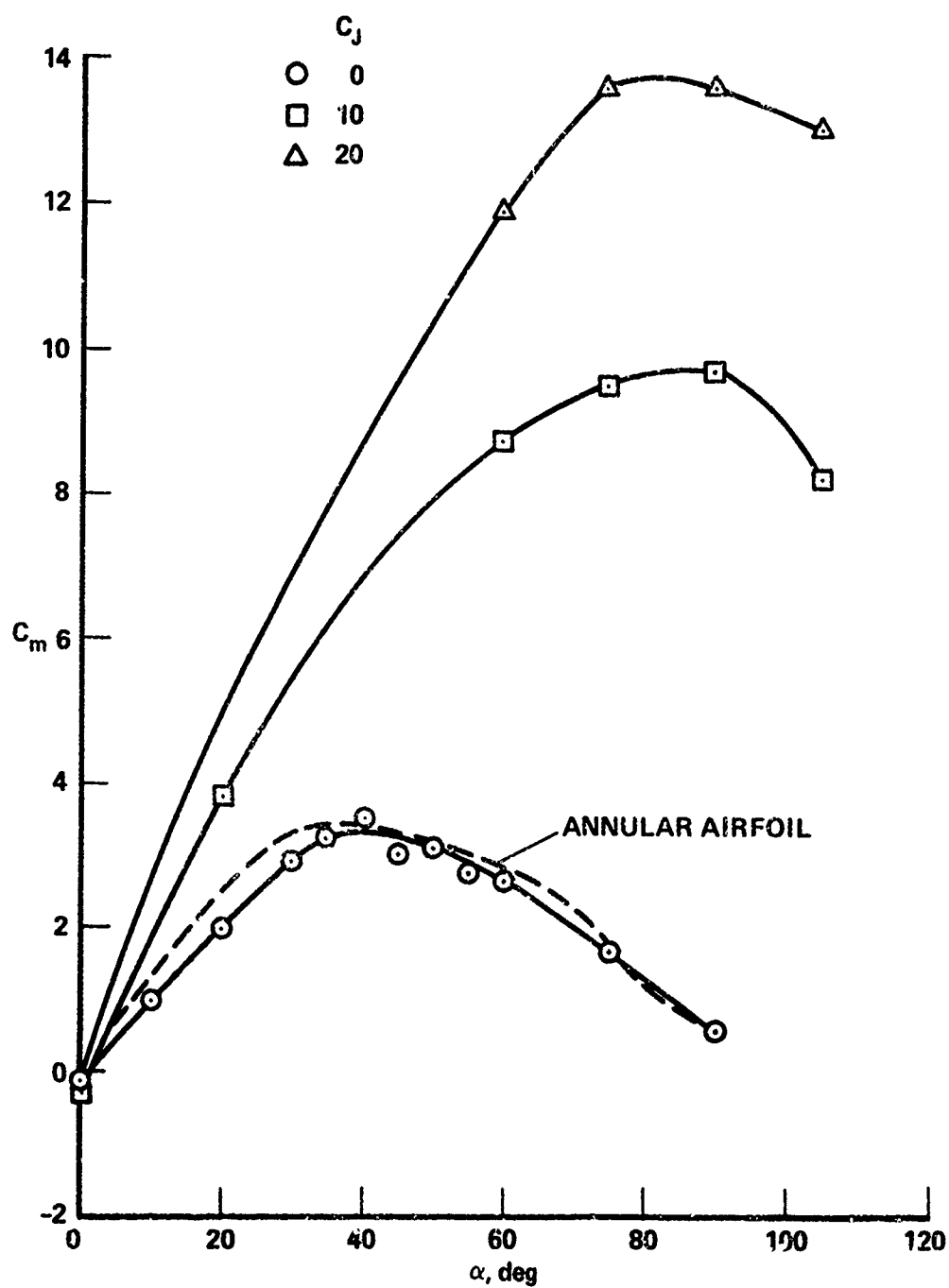
Figure 6.- Pitching moment vs angle of attack.
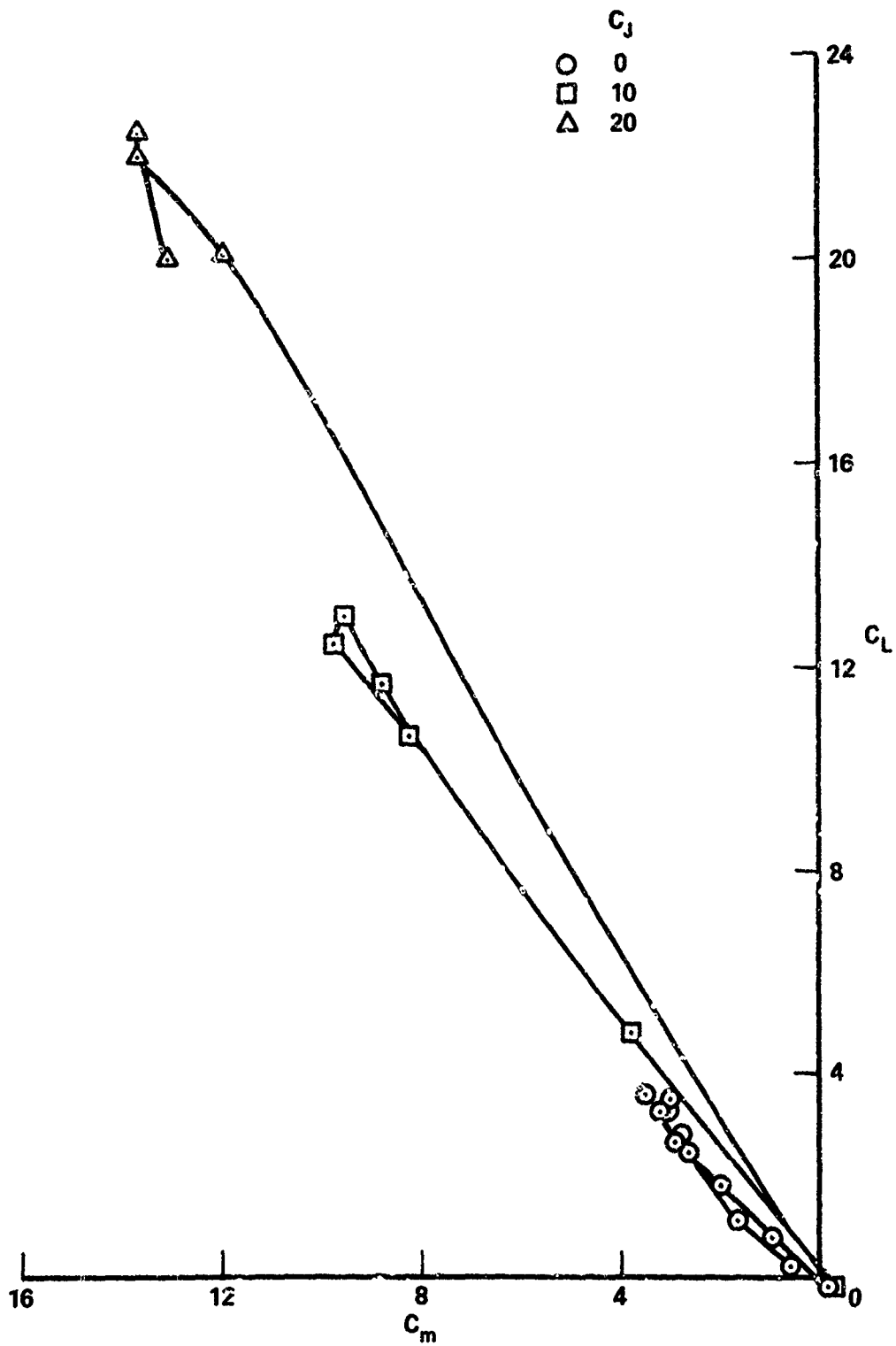
Figure 7.- Lift vs pitching moment.
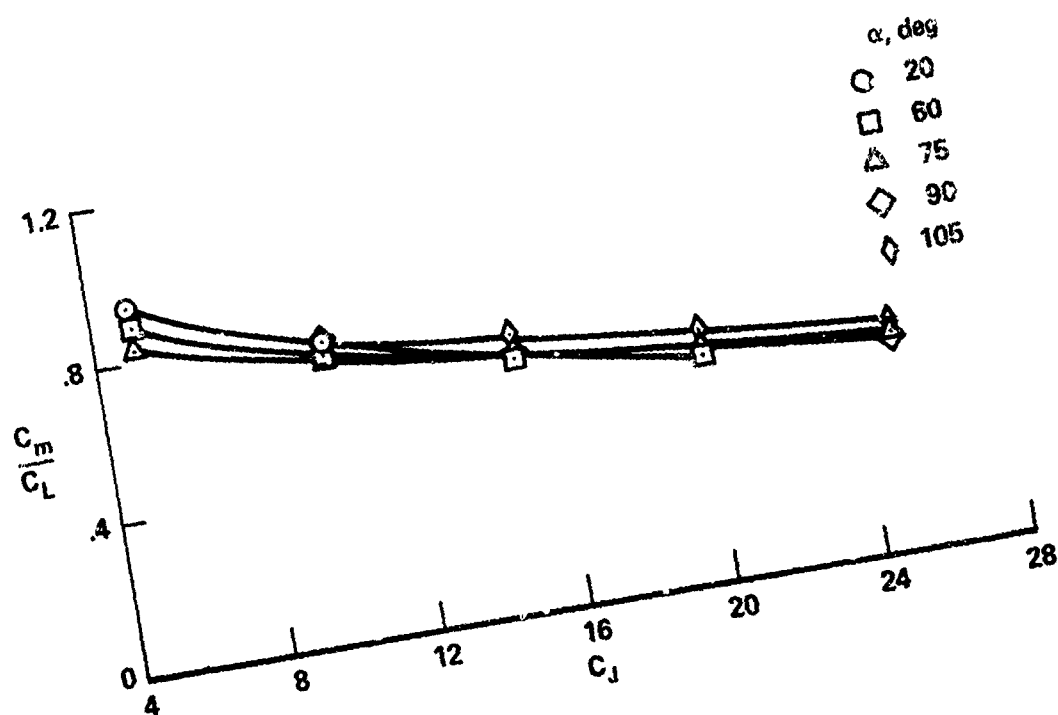
Figure 8.- Pitching moment to lift ratio.

ISOLATED DEFLECTOR

NOZZLE STATIC TESTS

FOR V/STOL AIRCRAFT

L. D. Miller
Propulsion Department
Lockheed-California Company
Burbank, California   91520

SUMMARY

A parametric deflector-nozzle test program was conducted to provide a
technical data-base for designing vented-type nozzles for V/STOL aircraft.
The isolated nozzle test program included static testing of circular-hood
and double-flap type deflector nozzles. The circular-hood nozzles had
either a "D" shaped or rectangular (aspect ratio of 0.5, 2.0, and 5.0)
cross-section. The deflector angles, throat area ratios, and flow
turning radius ratios, respectively, were varied from 0 to 135 degrees,
0.6 to 1.0, and 0.5 to 1.5. The nozzle pressure ratios varied from 1.1
to 1.8. Basic measurements included nozzle gross thrust (magnitude and
direction), mass flow, and nozzle entrance total and static pressure
and total temperature. Nozzle test data were correlated in terms of the
total pressure loss coefficient, thrust vector angle, throat area ratio,
and nozzle type. The rectangular nozzle with aspect ratio 5 was the
most efficient, followed by the aspect ratio 2 and double-flap nozzles,
the aspect ratio 0.5 nozzle, and the "D" nozzle. The nozzle efficiency,
in general, decreased with increase in thrust vector angle, reduction in
throat area ratio, and decrease in nozzle turning radius ratio.

NOMENCLATURE

A_D Total Duct Area at Rake Station, 38.484 in.^{2}

A_E Aerodynamic Nozzle Exit Area

A_{TH} Nozzle Minimum Area

b Height of Duct at Rake Station

C_d Discharge coefficient

C_T Thrust Coefficient, F_R/F_I

F_R Resultant Force Measured From Gross Thrust Balance

F_I Ideal Thrust Obtained From Mass Flow and Ideal Velocity

M_D Mach Number at Rake Station Based on Mass-Momentum Method (See Reference 5)

P_{T_D}/P_∞ Nozzle Pressure Ratio

P_{T_D} Total Pressure at Rake Station

P_∞ Ambient Pressure

q Dynamic Pressure at Rake Station

$\bar{R}/b$ Nozzles Average Turning Radius Ratio, $(R_1 + R_2)/(2b)$

R_1 Nozzle Inner Turning Radius

R_2 Nozzle Outer Turning Radius

α Nozzle Control Flap Angle

Θ_D Nozzle Deflector Angle at Trailing Edge

ϕ Thrust Vector Angle

ΔP_T Total Pressure Loss Between Nozzle Entrance Duct Flow and Nozzle Exit Flow

INTRODUCTION

V/STOL aircraft powered by high bypass turbofan engines installed in fixed horizontal nacelles require complex deflector nozzles which must be capable of vectoring the flow from the downward direction at takeoff to the horizontal direction at cruise. The nozzles should be efficient, light weight, compact, and provide high response thrust vector control. However, since these nozzle characteristics can not be achieved simultaneously, the selection of a nozzle for a particular type of V/STOL aircraft will involve compromises and design tradeoffs.

Several flow deflection schemes have been demonstrated such as those reported in References 1 through 4. One of the more promising concepts was the vented nozzles reported in References 1 and 2. These vented nozzles, discussed in more detail in the following section, have an open region at the inner elbow corner to allow the external flow to be entrained by the internal nozzle flow at the corner. Similar performance was obtained for both rectangular and "D" shaped vented nozzles with circular deflectors, as reported in References 1 and 2. The thrust coefficient of these vented nozzles was 0.96 for 90 degrees thrust vectoring and nozzle pressure ratios from 1.1 to 1.4.

Because of the limited amount of parametric data available for deflector nozzles, and particularly for vented deflector nozzles, a test nozzle program was conducted to determine the effects of design parameters such as nozzle pressure ratio, nozzle shape, deflector angle, throat area, and entrance Mach number on nozzle thrust coefficient, thrust vector angle, and discharge coefficient.

TEST HARDWARE

The tests were conducted using the test rig shown in the photograph of Figure 1 and in the schematic of Figure 2. A high pressure line with a control valve supplies air flow to a $1\frac{1}{2}$ inch choked Venturi meter. The flow passes through the outer shell of the gross thrust balance and enters normal to the balance axis so as to cancel the incoming momentum of the flow. The flow tube, including the flow conditioners and instrumentation, and the nozzle are attached to the metric portion of the balance as shown in Figure 2. Three flow tubes are available, two rectangular tubes with aspect ratio of 0.5 (or 2.0) and 5, and one "D" shaped tube. The flow tubes match the corresponding nozzle shape so that there is no transition section within the nozzle.

The isolated nozzles consist of circular and double-flap type deflectors as shown in Figures 3 and 4, respectively. Circular-deflector nozzles with average turning radius ratios of 0.5 to 1.5 are available for the configurations shown in Figure 3. Deflector trailing edge angles of 0 to 135 degrees are provided for the aspect ratio 2 and the "D" nozzles, and of 105 degrees for the aspect ratios of 0.5 and 5.0 nozzles. The aspect ratio 5.0 nozzle also has a 0 degree deflector. Nozzle minimum to rake station flow tube area ratios, A_{TH}/A_D, (throat area ratio) of 0.6 to 1.0 are obtained by translating inner flaps. The duct area at the rake station is 38.484 square inches for all three flow tubes. Reference nozzles with zero degree deflector are provided for the three different flow tubes. These nozzles have area ratios of 0.6 and 1.0 and were used to check the balance calibration.

The double-flap deflector nozzle, shown in Figure 4, has an aspect ratio of 2.0 with trailing edge flap angles varying from 45 to 135 degrees. The translating flap provides nozzle throat area ratios of 0.6, 0.8, and 1.0.

All of the nozzles are vented. This design concept, which is illustrated in Figure 5, does not employ an inner flow corner so as to allow the external

0.5 ASPECT RATIO 105° DEFLECTOR NOZZLE

GROSS THRUST BALANCE

VENTURI METER

Figure 1. Photograph of Static Test Rig
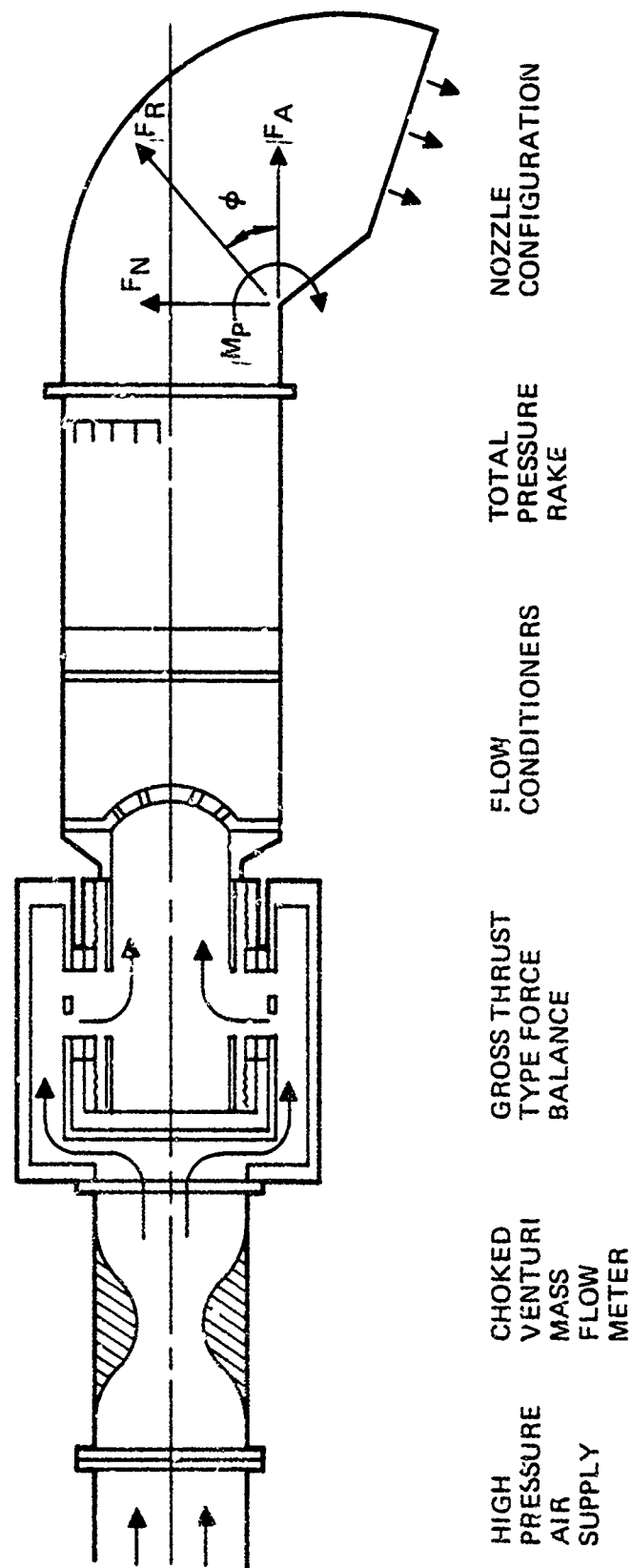
Figure 2. Static Test Rig for Propulsion Component Tests

HIGH
PRESSURE
AIR
SUPPLY

CHOKED
VENTURI
MASS
FLOW
METER

GROSS THRUST
TYPE FORCE
BALANCE

FLOW
CONDITIONERS

TOTAL
PRESSURE
RAKE

NOZZLE
CONFIGURATION

F_R

F_A

F_N

M_P

ϕ

RAKE STATION

SIDE VIEW

θ_D

R_1
R_2
4.76 in.
hi
bi
b

RECTANGULAR

"D"

END VIEW

a
b
b
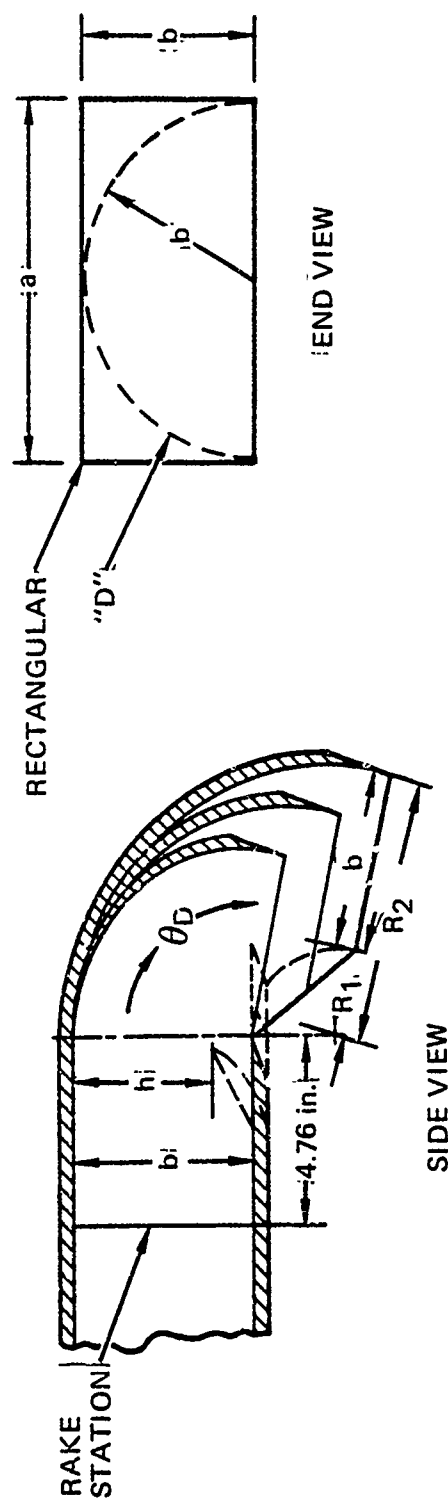
FLOW TUBE	DUCT WIDTH a in.	DUCT HEIGHT OR RADIUS b - in.	ASPECT RATIO a/b	THROAT AREA RATIO A_{TH}/A_D	AVE. RADIUS RATIO $(R_1 + R_2)/2$	DEFLECTOR ANGLE θ_D DEGREES	THROAT AREA VARIATION	
							TRANSLATING PLATE	ROTATING PLATE
1	4.387	8.773	0.5	0.6,0.8,1.0	0.75	105	X	
1	8.773	4.387	2.0	1.0	0.5	105	X	
				0.6,1.0	–	0		
				0.8	–	32		X
2	13.872	2.774	5.0	0.6,0.8,1.0	0.75	75, 105, 135	X	
				0.6,0.8,1.0	1.50	105	X	
				0.6,1.0	–	0	X	
				0.6,0.8,1.0	0.75	105	X	
				0.6,0.8,1.0	1.00	105	X	
				0.6,0.8,1.0	1.50	105	X	
D	9.900	4.950	–	0.64,1.0	–	0		
				0.83	–	32		
				0.64,0.83,1.0	0.75	75, 105, 135		

Figure 3. Circular – Deflector Nozzle Geometry

Figure 4. Double-Flap Deflector Nozzle Geometry
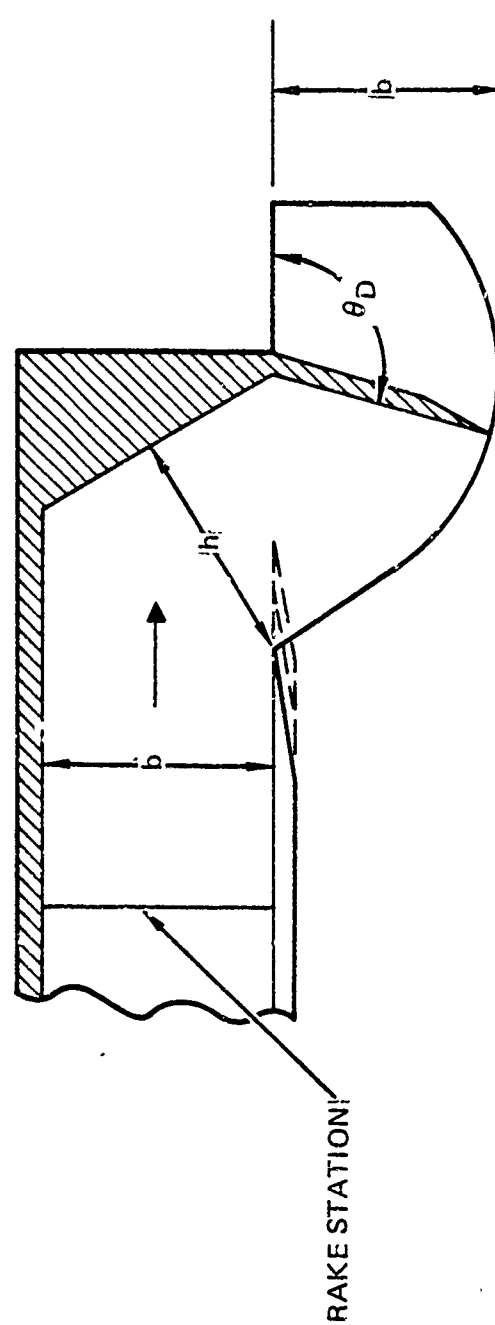
FLOW TUBE	WIDTH a - IN.	HEIGHT b - IN.	ASPECT RATIO a/b	THROAT AREA RATIO h/b	SECOND FLAP ANGLE θ_D - DEGREES
1	8.773	4.387	2.0	0.6, 0.8, 1.0	45, 75, 105, 135

AVERAGE RADIUS RATIO
$\bar{R}/b = (R_1 + R_2)/(2\,b)$

90 DEGREES TURN WITH
FIXED WALL NOZZLE
(FOUR WALLS)
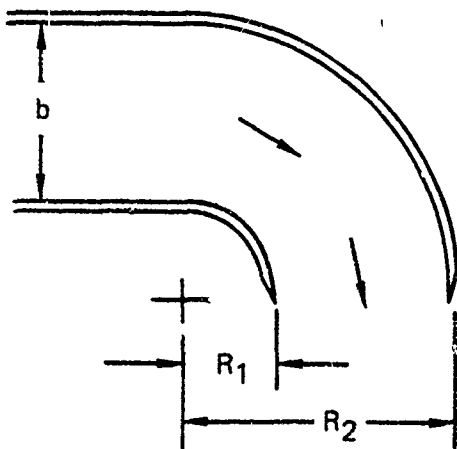
90 DEGREES TURN WITH
VENTED NOZZLE
(THREE WALLS)

b

R_1

R_2

b

R_2

AERODYNAMIC
INNER TURNING
RADIUS
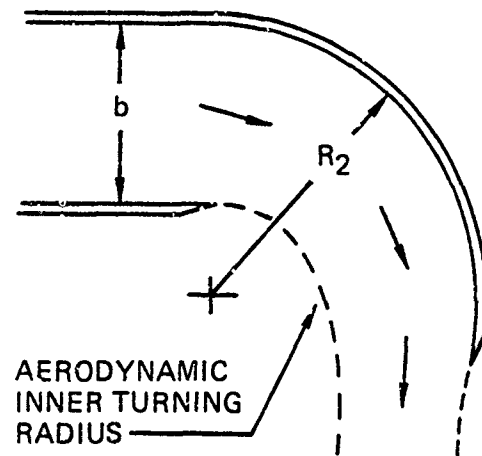
Figure 5.   Vented Nozzle Concept

flow to be entrained by the internal flow at the corner. Vented, rather than nonvented, nozzles were chosen because of the improved thrust coefficients, see Reference 1, easier nacelle installation, and because of the limited amount of parametric data for these nozzles. Vented nozzles, however, require larger deflector angles than the nonvented nozzles for a given thrust vector angle and thus may have a weight disadvantage.

Components of the aspect ratio 2 and "D" nozzles are shown in Figures 6 and 7, respectively. Shown are the reference nozzles, the flow tubes, the deflectors with angles of 32, 75, 105, and 135 degrees, the area control plates, and the survey rakes.

Figure 6. Photograph of Aspect Ratio 2 Deflector Nozzle Components

139 863R

Figure 7. Photograph of "D" Deflector Nozzle Components

TEST RESULTS AND DATA CORRELATIONS

The nozzle performance for the five types of deflector nozzles tested
is shown in Figure 8. The nozzle performance parameters consist of
thrust coefficient, C_T, thrust vector angle, ϕ, duct Mach number, M_D,
and discharge coefficient, C_d, as functions of nozzle pressure ratio, P_{T_D}/P_∞. Results are presented for deflector angles of 105 degrees and a throat
area ratio of 0.8. The 0.8 throat area ratio was obtained with a translating
plate.

The results show that the aspect ratio 5 nozzle is the best in terms of
thrust coefficient and deflector angle (except for the double-flap deflector).
The thrust coefficients of the aspect ratio 0.5 and 2.0 nozzles are similar
and are slightly below those of aspect ratio 5 nozzle. The thrust coef-
ficients of the double-flap deflector nozzle are similar to those of aspect
ratio of 0.5 and 2.0, however, the thrust vector angles for the double-flap
deflector are about 10 degrees greater than the vector angles of the other
nozzles. The thrust coefficients of the "D" nozzle are below those of the
other nozzles. The duct Mach number distributions as a function of nozzle
pressure ratio are similar for all of the nozzles. The duct Mach number
increases with increase in nozzle pressure ratio as expected; the dis-
charge coefficients are approximately 0.6 for all nozzles for the range
of nozzle pressure range from 1.1 to 1.8.

In an attempt to eliminate the duct Mach number and nozzle pressure ratio as
variables, the loss coefficients, $\Delta P_T/q$, were computed for the five nozzle
types and three throat area ratios and are shown in Figure 9. These results
are all for 105 degrees nozzle deflector angles. This loss coefficient is
defined as the total pressure loss of the internal flow divided by the
dynamic pressure at the rake station. The total pressure loss, which is
directly related to nozzle performance, was calculated using the nozzle
entrance flow properties and measured thrust. The lower the loss coeffi-
cient, the higher the thrust coefficient for a given duct Mach number and
nozzle pressure ratio. The loss coefficients are dependent on throat area
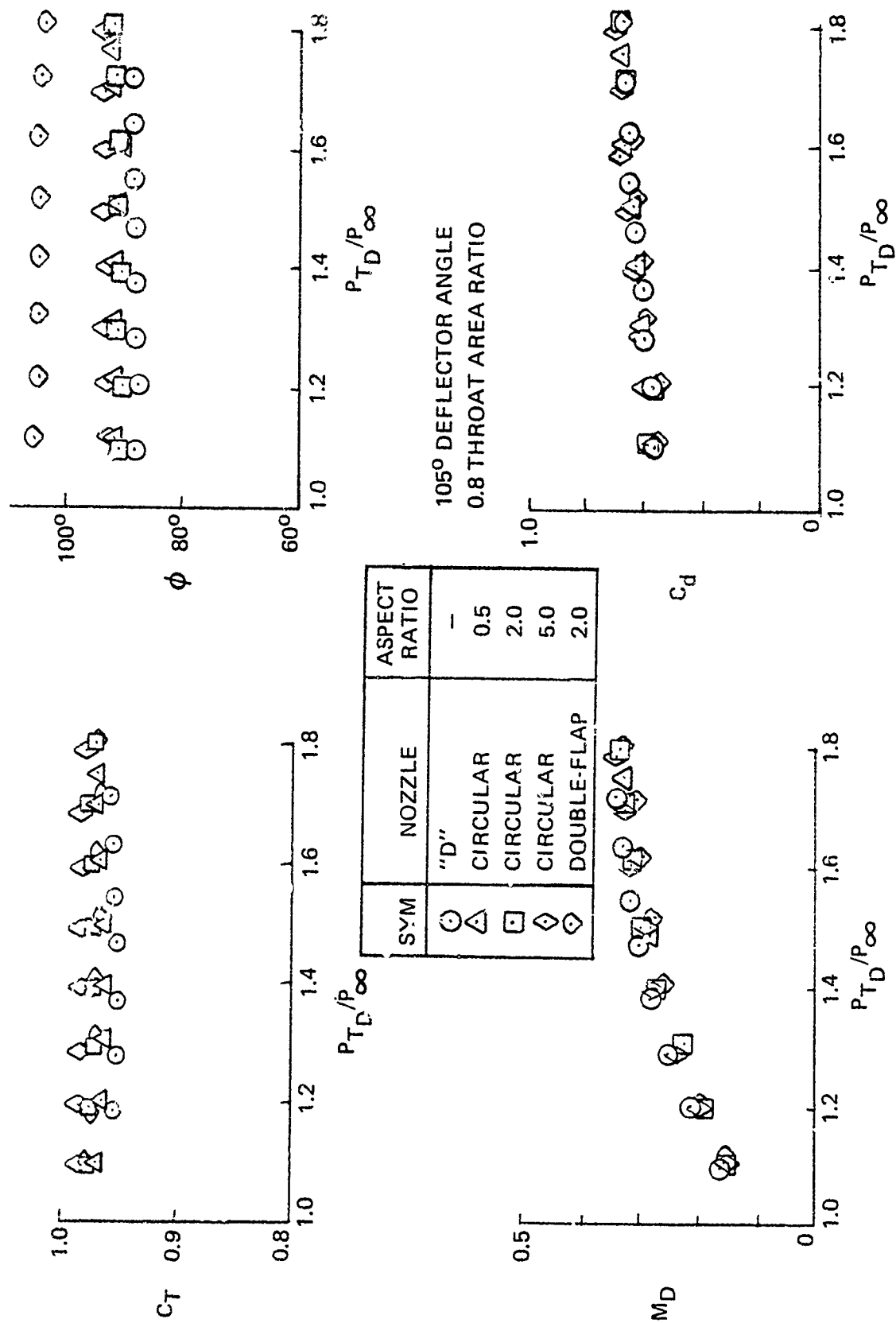
Figure 8. Effect of Nozzle Type on Nozzle Performance
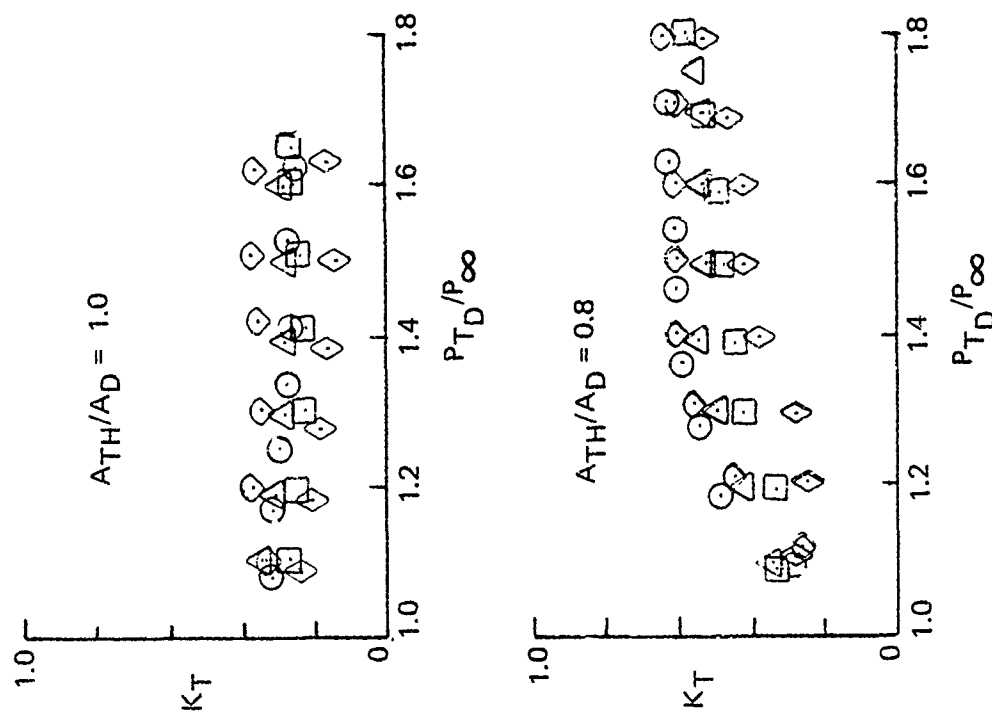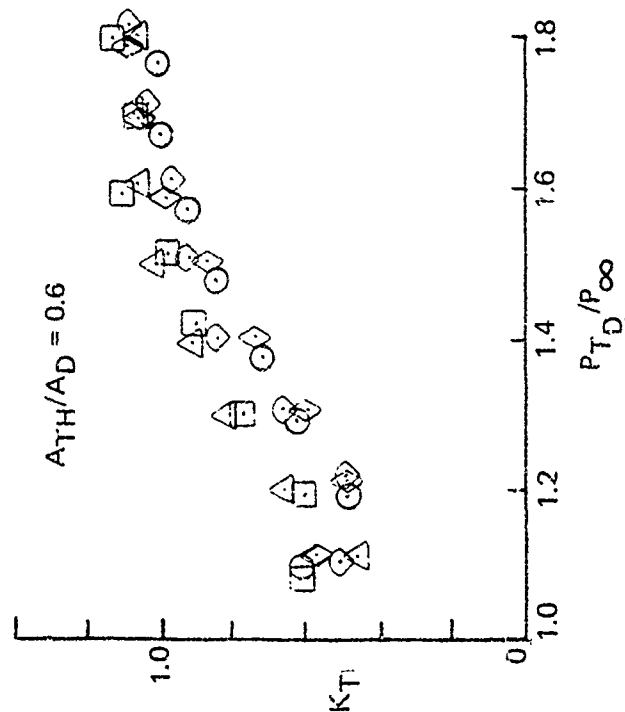
Figure 9. Effect of Nozzle Type on Loss Coefficient

ratio and nozzle type but are independent of duct Mach number and approximately independent of nozzle pressure ratio for throat area ratios of 0.8 and 1.0. The loss coefficient for the 0.6 throat area ratio varies significantly with nozzle pressure ratio, particularly for the low nozzle pressure ratios from 1.1 to 1.4. The loss coefficients in Figure 9 also illustrate that the aspect ratio 5 nozzle is, in general, the most efficient.

The effects of deflector angle on nozzle loss coefficient for the aspect ratio 2 nozzles, with 0.8 throat area ratio, are given in Figure 10. The expected trend of increasing loss coefficient with increasing deflector angle, in general, occurs except for the 135 degrees deflector. These results show that the 135 degrees deflector is as efficient or more efficient (lower loss coefficient) than deflector nozzles with lower angles. One possible explanation for this trend is as follows. The outer deflector hood of these nozzles does the basic turning of the flow, and the inner vented lip region causes the flow losses. As the deflector angle increases from 32 degrees to 105 degrees, see Figure 11, the nozzle becomes longer from the reference rake station to the nozzle exit and the inner flow turning radius decreases. This decrease in inner flow turning radius causes the performance to decrease. Increasing the deflector angle from 105 degrees to 135 degrees, however, results in about the same inner flow turning radius and an increase in nozzle length. This increase in nozzle length for the 135 degrees deflector provides more space for the flow from the inner lip to adjust to the exit, even though the flow is deflected more, and results in less losses.

The effects of deflector angle on loss coefficients for the double-flap nozzle with throat area ratios 0.6, 0.8, and 1.0, given in Figure 12, show the expected trend of decreasing nozzle efficiency with increasing deflector angle. Because the nozzle length does not change with change in deflector angle for the double-flap nozzle, the argument given above for explaining the high performance of the 135 degrees circular deflectors does not apply.
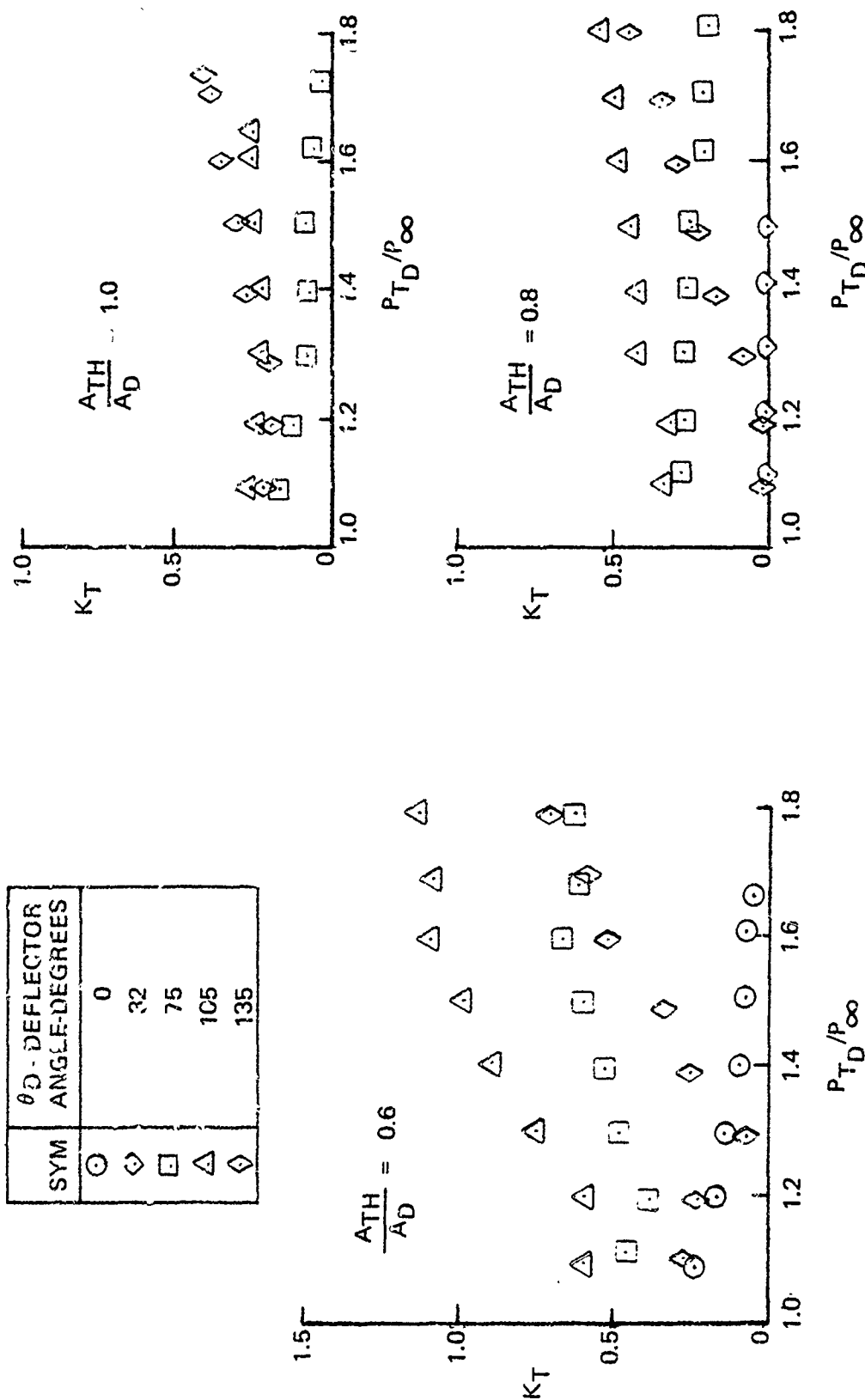
Figure 10. Effect of Deflector Angle on Loss Coefficient for Aspect Ratio 2 Nozzle
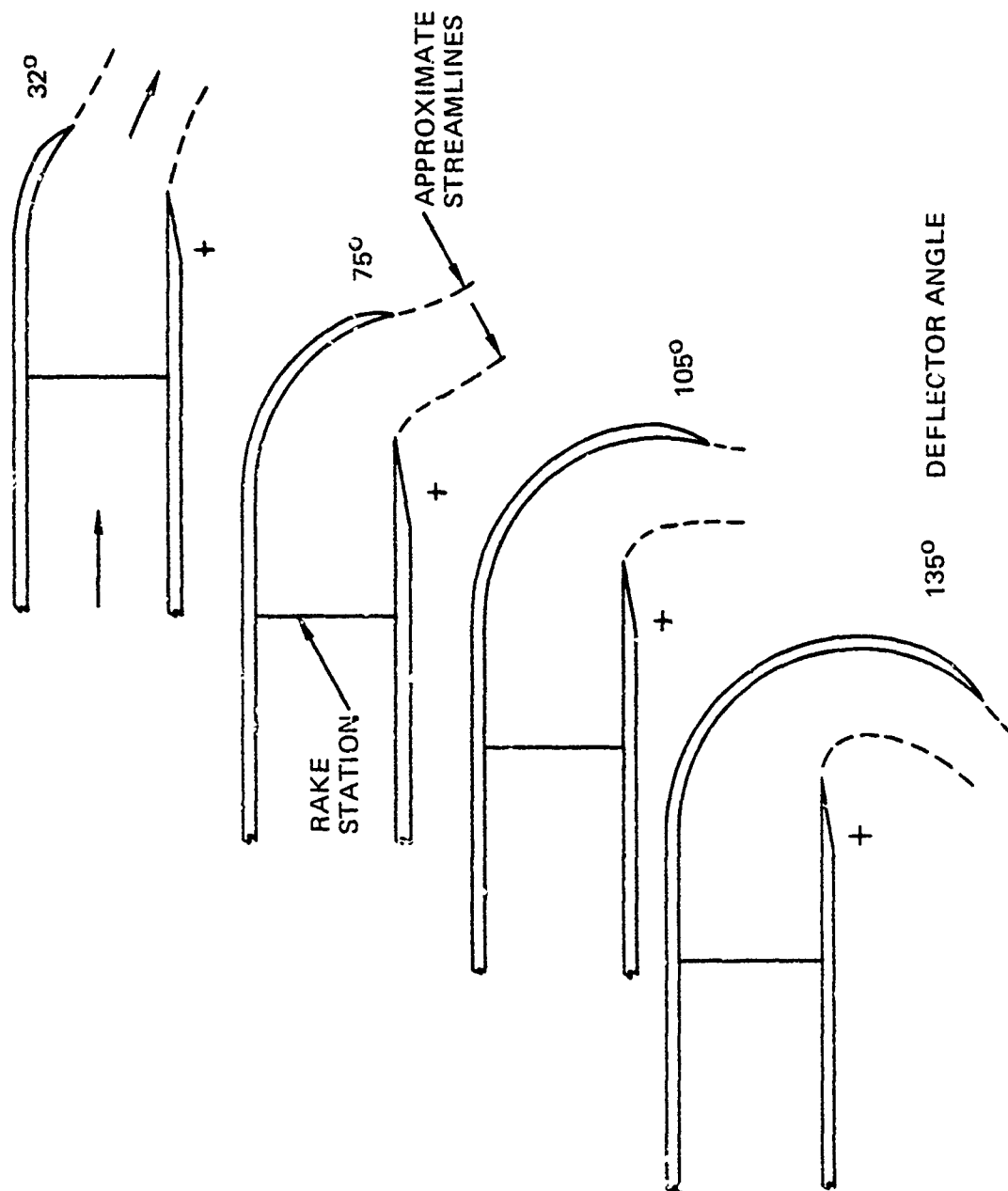
Figure 11. *Nozzle with Different Deflector Angles*
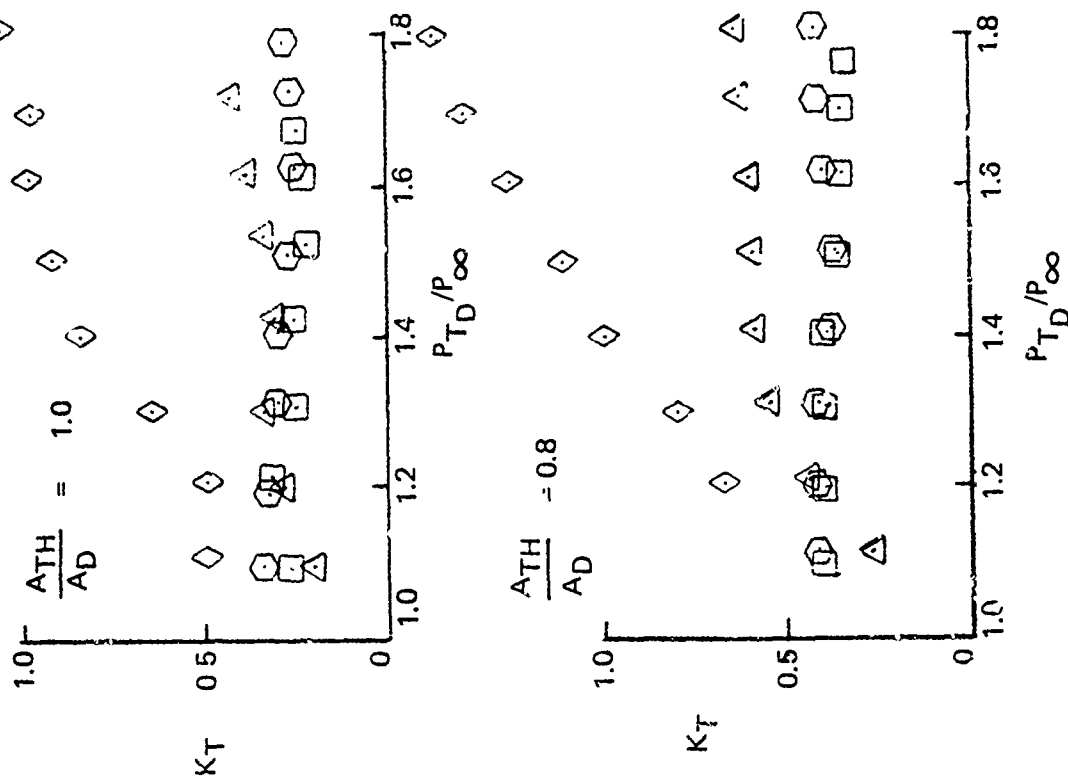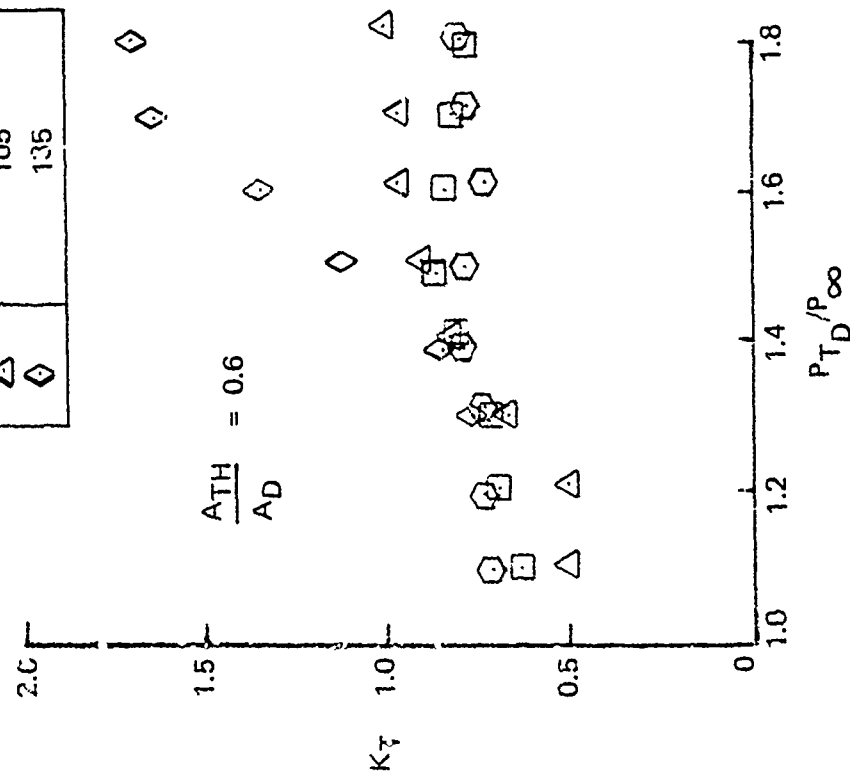
Figure 12.   Effect of Deflector Angle θ_D on Loss Coefficient K_T for Double Flap Nozzle

The effects of control flap angle on loss coefficient for 0.6 and 0.8 throat area ratios, given in Figure 13, show tnat the nozzle with the -41 degrees flap angle (negative flap angles downward away from the center main duct) is the most efficient. Results are given for flap angles 0, ± 19, and ± 41 degrees for the aspect ratio 2 deflector nozzles set at 105 degrees deflector angle. The 0 degree flap angle is the least efficient for 0.6 throat area ratio, and the nozzle efficiencies are insensitive to flap angles for 0.8 throat area ratio.

The effect of the nozzle turning radius ratio on nozzle loss coefficient, given in Figure 14, show the expected trend that, in general, the nozzle efficiency improves with increase in nozzle radius ratio. These results are for aspect ratio 5 deflector nozzle with 105 degrees deflector angle and throat area ratios of 0.6, 0.8, and 1.0.

The data for the five deflector nozzles have been correlated in terms of loss coefficient and thrust vector angle for 0.8 threat area ratio as presented in Figure 15. This correlation is possible because the loss coefficients and thrust vector angles are essentially independent of nozzle pressure ratio. These results enable the performance to be obtained for the different nozzles and thrust vector angles. Given the loss coefficient, the thrust coefficients can be computed for different duct Mach numbers and nozzle pressure ratios.

The derived performance characteristics for the aspect ratio 0.5, 2.0, 5.0, double-flap, and "D" nozzles for 0.8 throat area ratio, all for 90 degrees thrust vectoring, are given in Figures 16, 17, and 18. Thrust coefficients are given as functions of duct Mach numbers from 0 to 0.6 and nozzle pressure ratios from 1.1 to 1.8. Also, lines of constant aerodynamic exit to nozzle entrance duct area ratios, A_E/A_D, from 0.2 to 1.0 are given. Note the general trend that by decreasing nozzle pressure ratio for a given duct Mach number
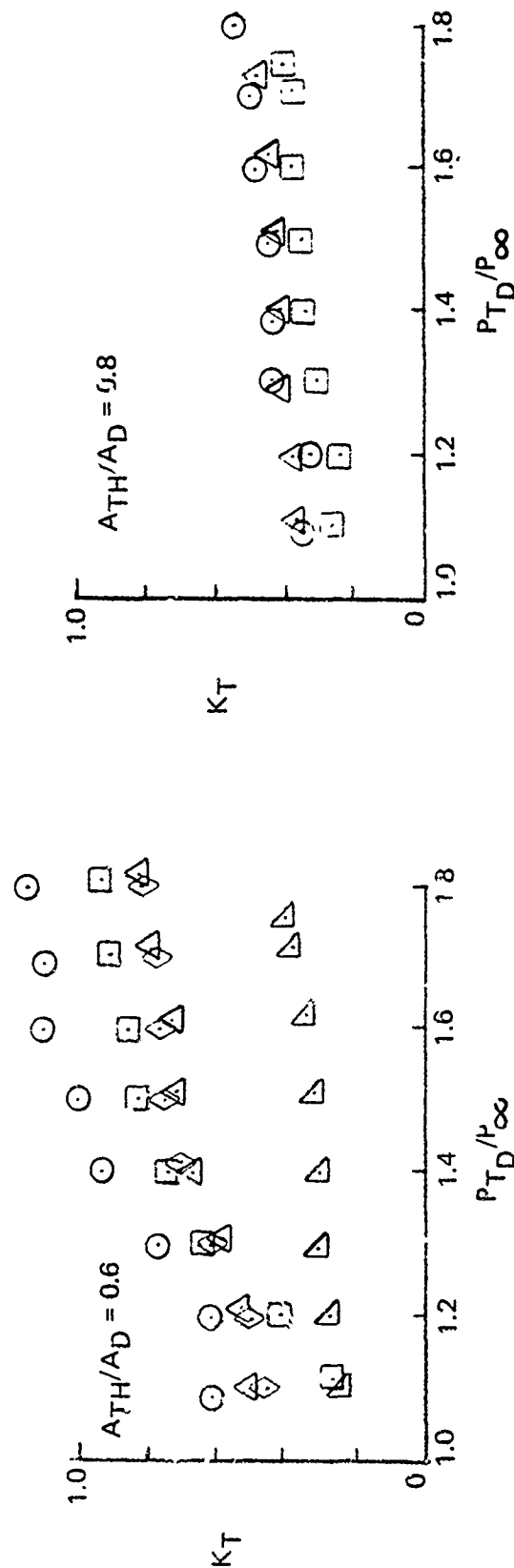
Figure 13. Effect of Flap Angle on Loss Coefficient for Aspect Ratio 2 Nozzle Performance
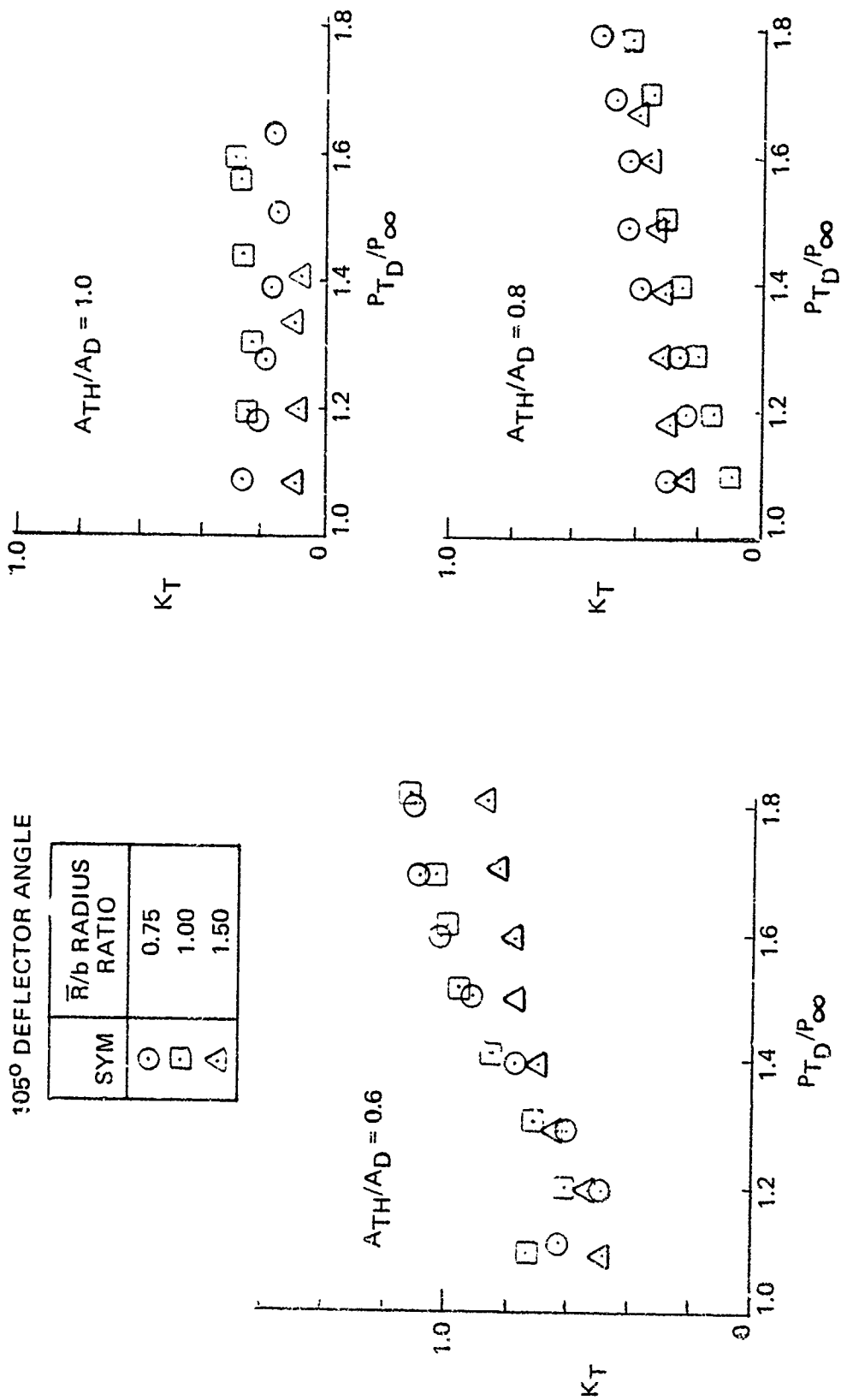
Figure 14. Effect of Turning Radius Ratio on Loss Coefficient K_T for Aspect Ratio 5 Nozzle

Figure 15. Loss Coefficient as Function of Thrust Vector Angle for Five Nozzle Types

SYM	NOZZLE	A.R.
⊙	"D"	–
△	CIRCULAR	0.5
⊡	CIRCULAR	2.0
◇	CIRCULAR	5.0
◈	DOUBLE FLAP	2.0

0.8 THROAT AREA RATIO

ϕ THRUST VECTOR ANGLE - DEGREES

K_T
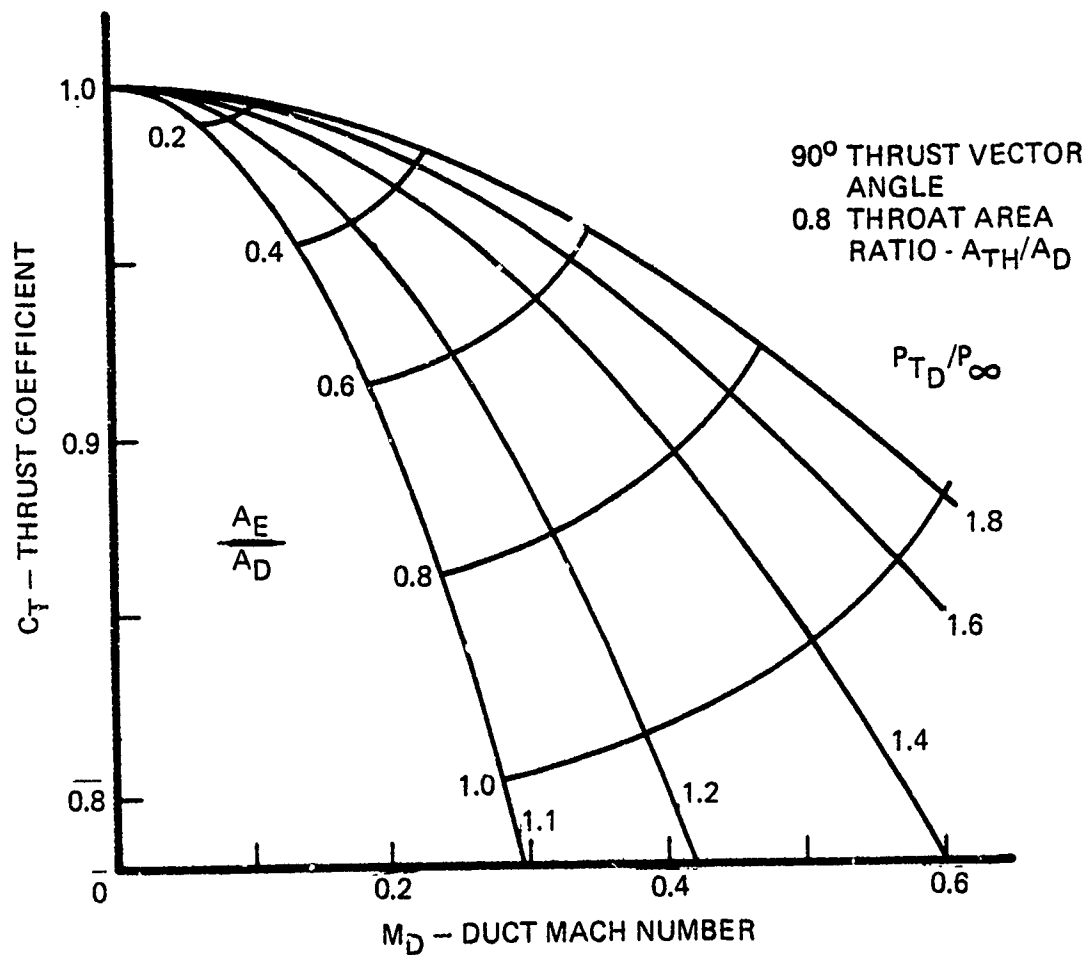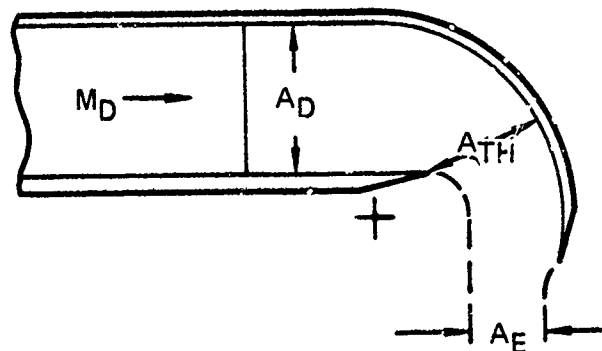
Figure 16. Derived Performance Characteristics for "D" Nozzle
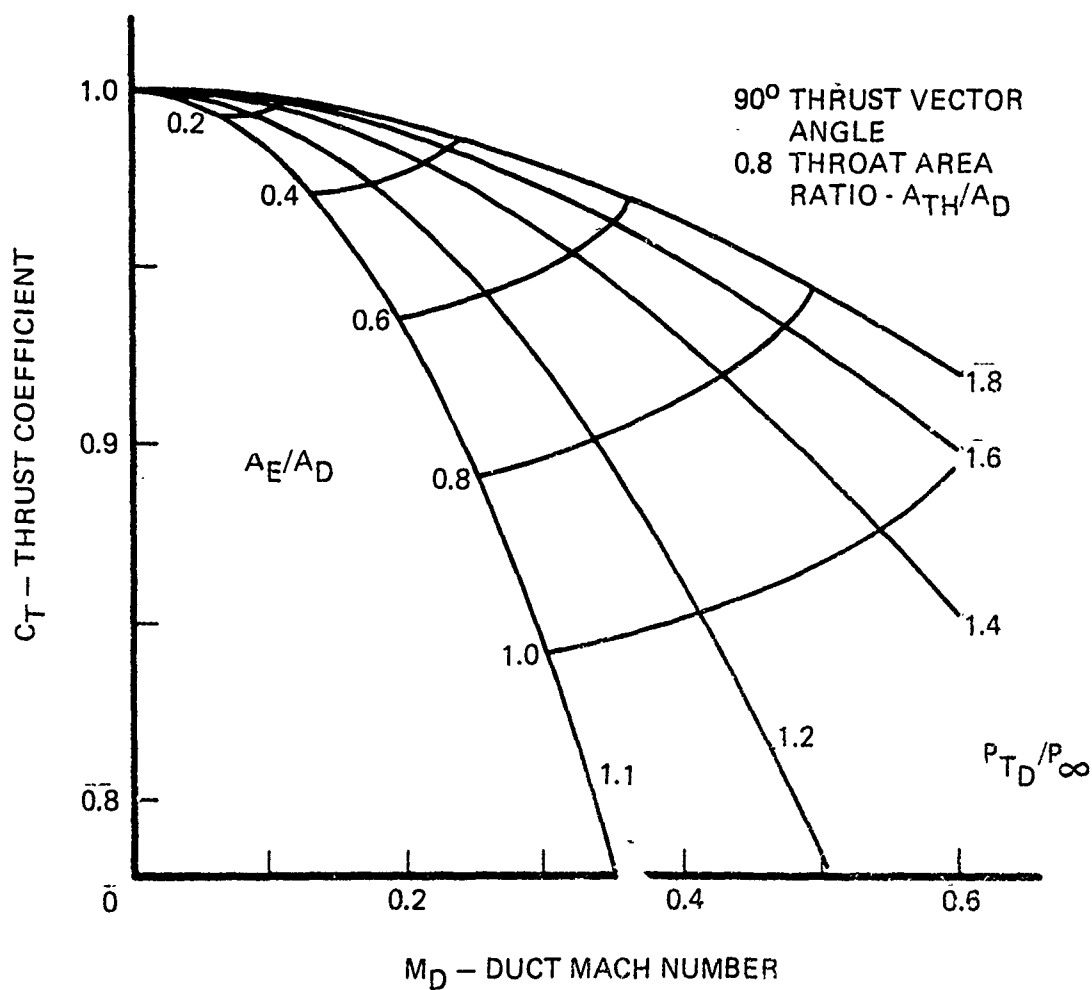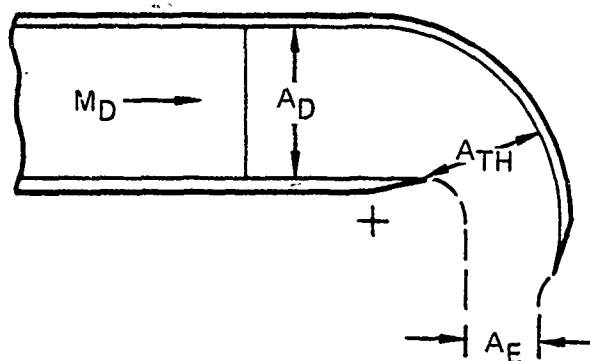
Figure 17. Derived Performance Characteristics for Aspect Ratio 2 and Double-Flap Nozzles
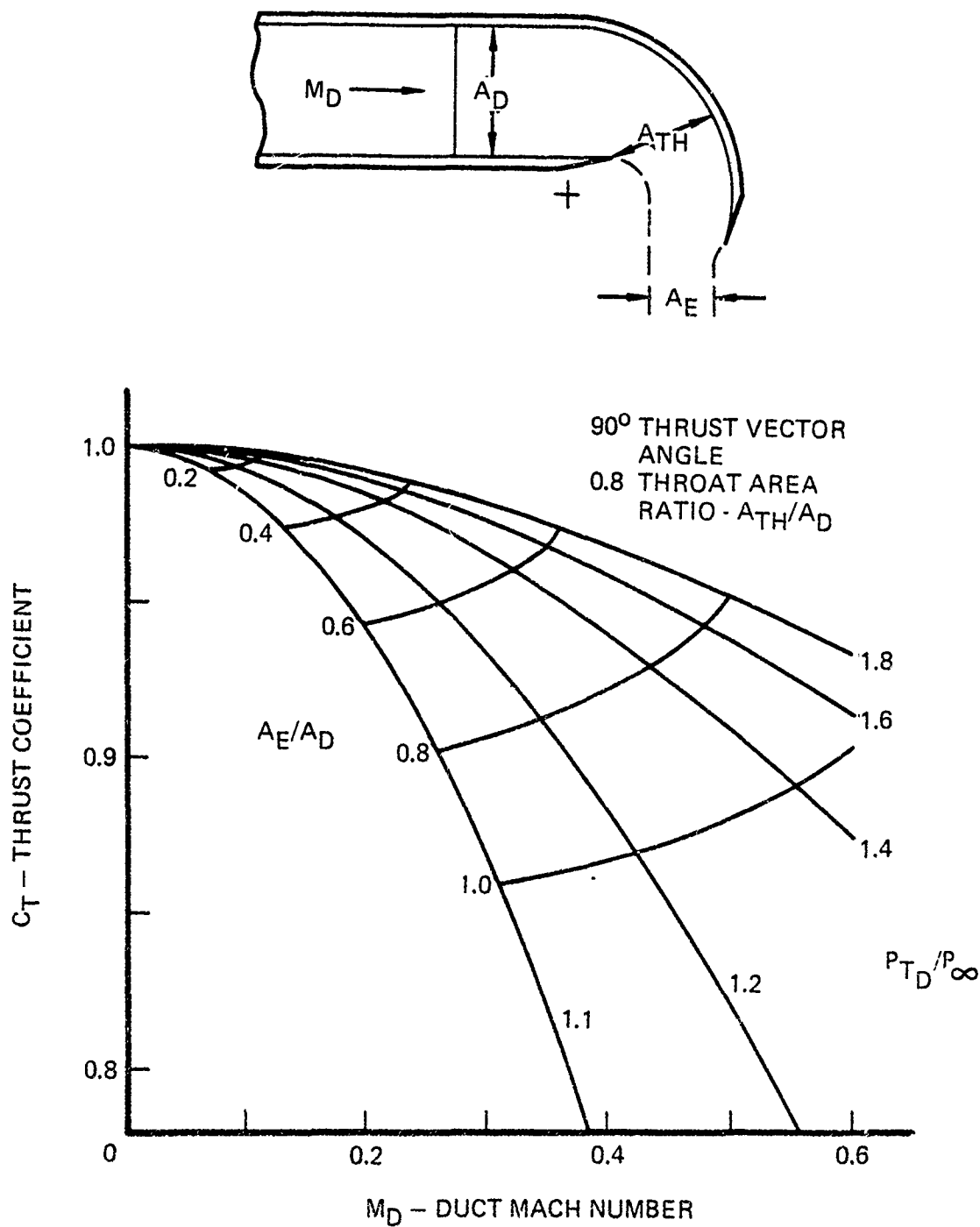
Figure 18. Derived Performance Characteristics for Aspect Ratio 5 Nozzle

or by increasing duct Mach number for a given nozzle pressure ratio both
result in lower thrust coefficients. This trend is expected since in
both cases the exit to duct area ratio increases and the exit to duct
Mach number ratio decreases, resulting in more adverse pressure gradients.
Correlations such as those in Figures 16, 17, and 18 will permit design
tradeoff studies to be made for V/STOL aircraft in selecting nozzle
types, nozzle pressure ratios, and nozzle entrance duct Mach numbers.

CONCLUSIONS

A data-base has been formulated for vented deflector nozzles for V/STOL application. This data-base includes "D", rectangular, and double-flap nozzle with deflector angles from 0 to 135 degrees and throat area ratios from 0.6 to 1.0. The rectangular nozzles had aspect ratios of 0.5, 2.0, and 5.0. The data was correlated in terms of loss coefficient, $\Delta P_T/q$, deflector angle up to approximately 90 degrees, and throat area ratios of 0.8 and 1.0 for the different nozzle types. These correlations enable nozzle thrust coefficients to be computed as functions of nozzle entrance Mach numbers and nozzle pressure ratios for a given nozzle type and thrust vector angle. The following results were found from the test program.

o The rectangular nozzle with aspect ratio 5 was the most efficient of the nozzles tested. This nozzle had a thrust coefficient of 0.96 for 90 degrees thrust vectoring for 0.3 entrance Mach number and 1.4 nozzle pressure ratio. The nozzle throat area ratio is 0.8.

o The nozzle efficiency in general decreased with increase in thrust vectoring angle for a given throat area ratio, and the efficiency decreased with decrease in nozzle throat area ratio for a given thrust vector angle.

o Control flap angles were more important for throat area ratios 0.6 than 0.8. The -41 degrees flap angle (flap downward away from the the center main duct) of the flap angles 0, ± 19, and ± 41 degrees tested resulted in the most efficient nozzle for throat area ratio of 0.6.

o The nozzle efficiency increased with increase in turning radius ratio. The largest effect was found for the aspect ratio 5 nozzle with turning radius ratios from 0.75 to 1.5.

o The nozzle efficiency increased with increase in throat area ratios.
  As the throat area ratio increased, the nozzle loss coefficients
  decreased.

REFERENCES

1. Rolls, L. S. and Aoyagi, K., "Experimental Investigations of Thrust Vectoring Systems for VTOL Aircraft," AIAA Paper No. 33-865, July 1977.

2. Anon., "Design of a Thrust Vectoring Nozzle for V/STOL Transport Lift Cruise Fans," NASA CR-114754, March 1974.

3. Limage, C. R., "Development of Low Pressure Ratio Vectoring Nozzles for V/STOL Aircraft," SAE Paper No. 770988, November 1977.

4. Lonthan, J. D., "Impact of Engine Cycle Parameters on V/STOL Type A Configuration and Commonality," SAE Paper No. 770980, November 1977.

5. Wyatt, D. D., "Analysis of Errors Introduced by Several Methods of Nonuniform Duct Flows," NACA TN 3400, March 1955.

SESSION V

V/STOL AIRCRAFT

CONFIGURATIONAL CONSIDERATIONS AND DEVELOPMENTS

Chairman:

Richard Kuhn
NASA-Langley Research Center (Retired)

HIGH ANGLE OF ATTACK AERODYNAMICS AT

DAVID W. TAYLOR NAVAL SHIP RESEARCH AND DEVELOPMENT CENTER

by

David W. Lacey

and

John F. Talbot

David W. Taylor Naval Ship Research and Development Center

ABSTRACT

Work on high angle of attack aerodynamics at DTNSRDC has been
ongoing since 1970. This paper summarizes the results of two projects.
These projects are the Close-Coupled Canard experimental program
conducted between 1970 and 1974.

The second project is the recently completed simulation study
on the use of reaction controls to augment existing control systems
in the post-stall regions.

Significant experimental results from the close-coupled canard
work are presented in the form of the effect of canard shape size,
position and deflection on the lift, drag and pitching moment of two
research models and the F-4 Phantom II.

Results from the simulation study include the improved roll
response at high angles of attack, control system implementation and
the manned simulation employing both tracking tasks and one-on-one combat.

INTRODUCTION

The topic of this paper as stated in the title is high angle of attack work conducted at DTNSRDC. This work has been primarily in two areas listed in their order of occurrance. The first area to be discussed is the Close-Coupled Canard research project. This project was primarily experimental in nature and was conducted between the years of 1970 and 1974. The second area to be covered is primarily analytical in nature. This area is the effect of reaction control on the manuevering performance of fighter aircraft at high angles of attack. This study took the form of a digital simulation at DTNSRDC and a manned simulation utilizing the Langley Research Center Differential Manuevering Simulation (DMS) in both one on one combat and tracking tasks.

Too do complete justice to either of the above mentioned subjects would require far more time and space than is available. Thus only the significant highlights of each program will be discussed.

CLOSE - COUPLED CANARDS

The close-coupled canard as opposed to the long-coupled canard Figure (1) has a beneficial effect on the wing flow by favorable interference. This interference can take the form of a strong vortex interaction as is the case for the two highly swept delta surfaces of the SAAB Viggen (Figure (2)) or the downwash from the canard can delay separation on the wing in a manner akin to a leading edge slat.

Strong vortex interaction requires highly swept planforms, however, very few carrier aircraft have been built with large leading edge sweep angles. Because of this reason the work on canards at DTNSRDC has been limited to aircraft of low to moderate wing sweep angles.

The goals f this project were: first to develop a strong aerodynamic base which would determine the effects of many variables such as position size, deflection and shape at speeds from subsonic to suppersonic and secondly improve the high alpha capability of fighter type aircraft without sacrificing high speed performance.

In order to attain proper favorable interference the canard must be properly positioned and in the first wind tunnel program (Figure 3) the effect of position and canard size was emphasized.

Figure 4 shows the model used in this and subsequent wind tunnel programs. The model has two separate wings one of a 50 degree sweep and one of 25-degrees. Seven canard positions were tested and deflection of the canard could be varied from -10 to +25 degrees. Various canard shapes and sizes have been evaluated with the majority of the work being done with the canard designated C_0 (Figure 5). Four different sizes of this canard have been evaluated, having projected area ratio of 0.10 to 0.25 of the wing area.

As mentioned earlier, position was to extreme importance and the first question to be answered was "did the canard have to be above or below the wing or would either position work?" The answer is that the canard must be at least in the plane of the wing or above it in order for favorable interference   is shown in Figure 6. Where it can be seen that a canard located below the   .g

can actually cause a lift loss. Examination of the incremental moment
characteristics of the configurations indicates an early stall of the canard
located below the wing where as no stall for the high mounted canard is evident
up to a canard angle of attack $(\alpha + \delta_c)$ of 30 degrees. The next question asked
was how large or small must the canard be to be effective and could the effect
of size be correlated. The effect of canard size on lift and moments is shown
in Figure 7. As shown reasonably linear lifts of the data occur when the various
coefficients are plotted against canard exposed area ratio and that the gains
in lift increase linearly with canard size. Similarly the neutral point shift
in proportional to exposed canard volume coefficient.

As mentioned previously seven positions were available for evaluation of
the canard, where then is the position which optimizes the effect of the canard
i.e. increase in lift and decreases in drag. This position is where the canard
exposed root trailing edge is slightly in front of the exposed wing leading
edge as shown in Figure 8. It was also found that lowering the canard tends to
reduce the gains in performance. Further work has shown that the canard should
be located between $0.15\bar{c}$ and $0.25\bar{c}$ above the wing for maximum performance.

A further area in which extensive data were taken was the effect of deflection.
Positive canard deflection reduced performance significantly at low angles of
attack whereas small negative deflections can have a beneficial effect as
indicated in Figure 10, where (L/D) vs δ is presented. As showned $(L/D)_{max}$
is dramatically reduced by positive deflection. Deflections wheather positive
or negative have only a small effect at high angles of attack as shown in
Figure 11.

The afore mentioned trends occurred for both the 25 and 50 degree swept
wings and occurred at Mach numbers up to 1.1 although there is a reduction
in the beneficial effect of the canard as Mach number is increased as shown
in Figure 12.

At transonic speeds the canard can have a beneficial effect of both buffet
onset and intensity as shown in Figure 13. Buffet onset lift coefficient is
increased and buffet intensity is decreased.

At supersonic speeds the drag penalty for carrying the canard is small as
shown in Figure 14. Also neutral point shift with Mach number is approximately
the same as for both canard/wing alone as shown in Figure 15.

The above discussion has been solely concerned with research models.
A full scale vehicle however, must be trimmed in pitch. The effectiveness
of the canard as a trimming device will be answered in the following section.
The aircraft designer has a number of options for trimming devices. There
options are horizontal tail, canard, combinations of both or wing elevons in
the case of the Viggen. A measure of the effectiveness of a trimming device
is the ratio of C_{M_δ} divided by C_{D_δ} this is shown in Figure 16 for both canard
and horizontal tail. As shown the horizontal tail is the better trimming device
for a stable aircraft assuming the canard is close enough for favorable inter-
ference.

The tail however, causes a lift loss which can be substantial at high α. A possible solution to this problem first evaluated at DTNSRDC in 1970 is the Tri-surface aircraft consisting of close-coupled canard either fixed or free floating at its optimum deflection angle, wing, and horizontal tail for trim. This configuration has been shown to have better lift and drag characteristics than either canard or horizontal tail alone configurations and is shown in Figure 17.

The tri-surface configuration brings us to the concluding section on canard work at DTNSRDC which was the aerodynamic evaluation and optimization of a canard for the F-4 Phantom II aircraft. The results of this study will be briefly touched on here.

The canard placement was fixed primarily by the inlet geometry and was mounted approximately mid way on the inlet. In order not to change the stability of the aircraft a free floating technique was used where the canard was allowed to float at approximately 5 degrees angle of attack. Installation of the canard is shown in Figure 18.

The canard on the F-4 demonstrated the same gains in performance as indicated for the research models. This is shown in Figure 19 where lift and drag are presented at Mach numbers of 0.9. These gains in lift and drag result in significant increases in turn rate and "g" capability as shown in Figure 20. In addition it was found that lift on approach was increased to the point that the BLC might not be necessary as shown in Figure 21.

It was stated in the beginning of the discussion that one of the goals at DTNSRDC in studying canards was to maximize high alpha performance while at the same time minimizing loses at low angles of attack. That this has been done in evidenced by the improved performance of the F-4 aircraft at high alpha without significantly decreasing $(L/D)_{max}$. The primary goal of the canard work has also been accomplished in that the effect of the parameters which affect the performance of the close-coupled canard have been determined and have been documented.

REACTION CONTROLS FOR HIGH ALPHA MANUEVERING

The second area to be discussed in this paper is the effect of Reaction Controls on high alpha manueverability. This project was recently completed at NASA Langley utilizing the Differential Manuevering Simulator (DMS).

The primary assumption of this study was that in the future, VSTOL aircraft will be in the fleet and that reaction controls will be used for control during the terminal flight phases. A penalty in engine size will be paid for these controls and if the controls could be used in other flight phases the penalty associated with the controls might not be so severe.

The flight phase choosen for investigation was the high alpha manuevering region. A region where normal aerodynamic controls are not powerful enough or have adverse effects on the aircraft stability.

The method of the study was to size a system based on the VSTOL criteria presented in AGARD 577 (Figure 22) and use these values as the maximum control

power available. The aircraft chosen for the study was the typical Navy fighter that has been completely programmed in the Langley DMS. A control system was then developed for the roll and yaw axes and is shown in Figure 23. No changes were made to the basic pitch system. The control system as shown, phases in roll jets between 15 and 20 degrees and incorporates a low gain roll damper which is operable between 20 and 35 degrees.

The yaw axes is augmented by a yaw jet which is propostional to rudder deflection thus augmenting both pilot input and yaw sas.

The aircraft is characterized by a high dihedral effect thus roll is accomplished primarily by the rudder at high angles of attack.

The roll response of the basic aircraft and augmented aircraft is shown in Figure 24 following a full step rudder input. As expected the time to roll increases as angle of attack is increased however, the reaction jet aircraft exhibits nearly constant time to roll throughout the angle of attack range.

Having determined that the system was workable, it was programmed at the Langley DMS a sketch of which is shown in Figure 25. The DMS consists of two spheres incorporating typical fighter cockpits and is fixed base.

Normal procedure is to evaluate a configuration against canned tracking tasks as well as one on one combat.

Typical results of a tracking task for the reaction controlled and basic aircraft are shown in Figure 26. The task is a wind up turn with bank to bank reversals and is considered extremely difficult for precise tracking. As shown the reaction jet aircraft exhibits a smaller boresight error than the basic aircraft throughout the task.

The real proof however, is in the one on one environment. Two pilots from NATC and two pilots from VF-101 participated in the one on one study. Each pilot flew against the others 4 times in the reaction aircraft and 4 times in the basic aircraft. Initial conditions were M = 0.7 at 25,000 feet, starting from a head to head pass with 15,000 foot separation. The scoring parameter was Time on Advantage (TOA). TOA is defined by the following, if aircraft "A" has aircraft "B" in "A"'s forward hemisphere and aircraft "A" is in aircraft "B"'s aft hemisphere than aircraft "A" has the advantage. If the roles are reversed "B" has the advantage. Nose to nose and tail to tail encounters are neutral.

TOA is continually changing and was integrated with respect to time. Engagements were limited to 150 seconds. Results of these engagements are shown in Figure 27. As shown the reaction controlled aircraft has an average TOA of 32.5% verses the basic aircrafts 8.2% giving the reaction aircraft a 4 to 1 advantage ratio. The distribution of TOA for all flights is shown in Figure 28. As indicated in over 70 percent of the flights the basic aircraft had a TOA of less than 10 percent as compared to only six percent for the augmented aircraft.

Twelve runs were also made with an aircraft at a disadvantage. This disadvantage was to put one aircraft 5000 feet in front of the other aircraft.

Eight runs were made with the augmented aircraft having the disadvantage and 4 runs were made with the basic aircraft having the disadvantage. Results of this are shown in Figure 29. Even with the disadvantage the reaction jet aircraft had a higher average TOA. However, in no case could the basic aircraft when it was given the disadvantage, gain a significant advantage as indicated in Figure 30. The pilots commented that having the basic aircraft at a disadvantage was akin to a tracking task.

A summary of the overall average TOA for the three different encounters is shown in Figure 31 and clearly demonstrates the usefullness of reaction controls for high alpha manuevering.

FUTURE PLANS

The previous discussion has focused on work already completed at DTNSRDC. Plans for the future include a continuation of the work to even higher angles of attack. Canards and Lex's have been shown to imporve the longitudinal characteristics of fighter type aircraft but little generic data exists on the influence of such devices on the Lateral - directional characteristics. A project is now in progress to determine these characteristics on such a generic model. The goal of this project is to obtain smooth aerodynamic characteristics on all axes by combinations of various canards Lex's, and changes to the basic wing. These smooth characteristics in conjunction with reaction controls would make a aircraft sutiable for post stall manuevering without fear of departuer. A sketch of the proposed future aircraft is shown in Figure 32.
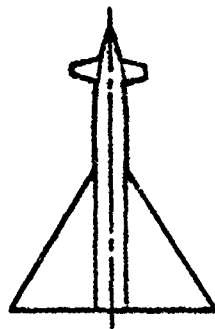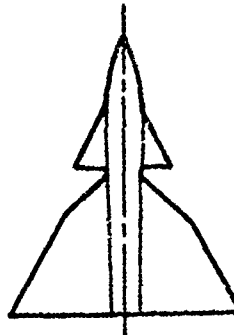
Figure 1 – Long verses Close-Coupled Canard
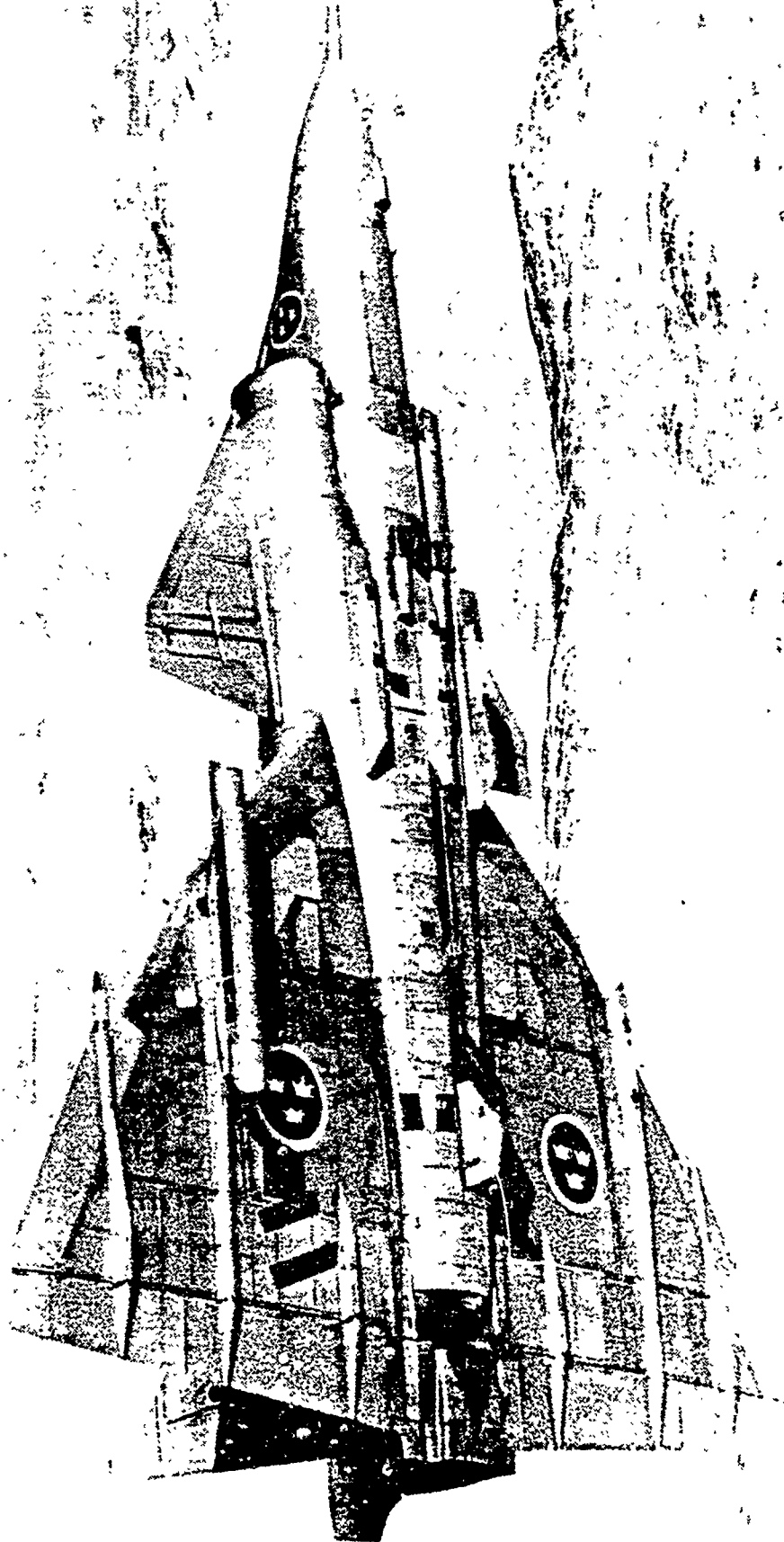
Figure 2 — SAAB Viggen
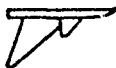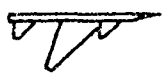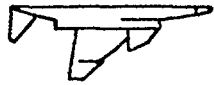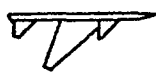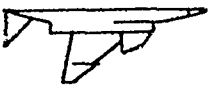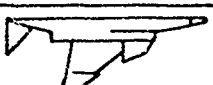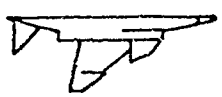
	Date	Tunnel	DTNSRDC ASED Report	Main Variable
	Jun 1970	Subsonic	AL 199	Canard size, position, deflection
	Dec 1970	Subsonic	--	Wing L.E. and droop, comparison with horizontal tail
	Dec 1970	Transonic	AL 81	Canard position, deflection, comparison with horizontal tail
	May 1971	Subsonic	AL 253	Canard position, deflection
	Jul 1971	Supersonic	--	Canard position, deflection, buffet
	Aug 1971	Subsonic	--	Build-up data, canard interference
	Sep 1971	Subsonic	AL 91	Canard shapes, flow visualization studies
	Sep 1971	Transonic	AL 87	Canard position, deflection, comparison with tail, buffet
	Nov 1971	Transonic	AL 88	Canard shape, position, deflection, buffet
	Mar 1972	Transonic	AL 293	Canard size, position, deflection, aileron efficiency
	Jan 1973	Subsonic	ASED 304	Double delta canard, flaps and slats
	Mar 1973	Transonic	AL 303	Double delta canard, simulated free-float, slats

Figure 3 - Wind Tunnel Program

50-DEGREE SWEPT WING

25-DEGREE SWEPT WING
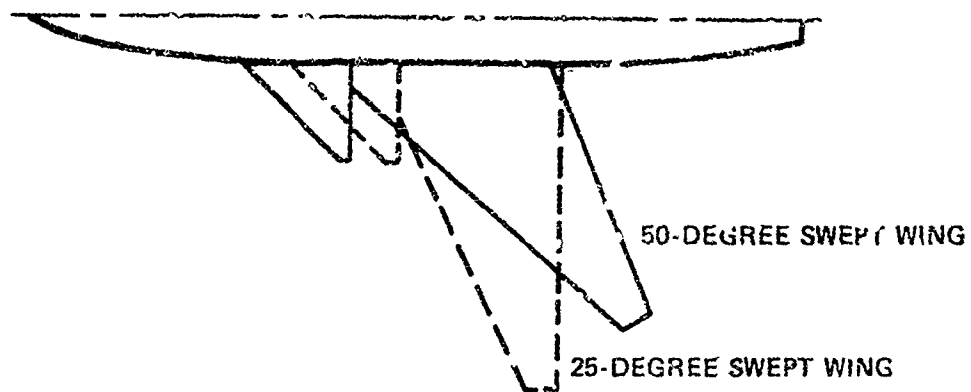
Figure 4 – Wind Tunnel Model

C_0 C_1 C_2 C_3
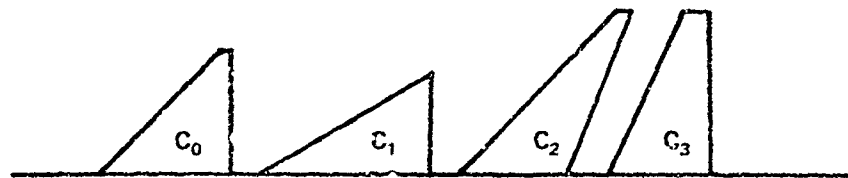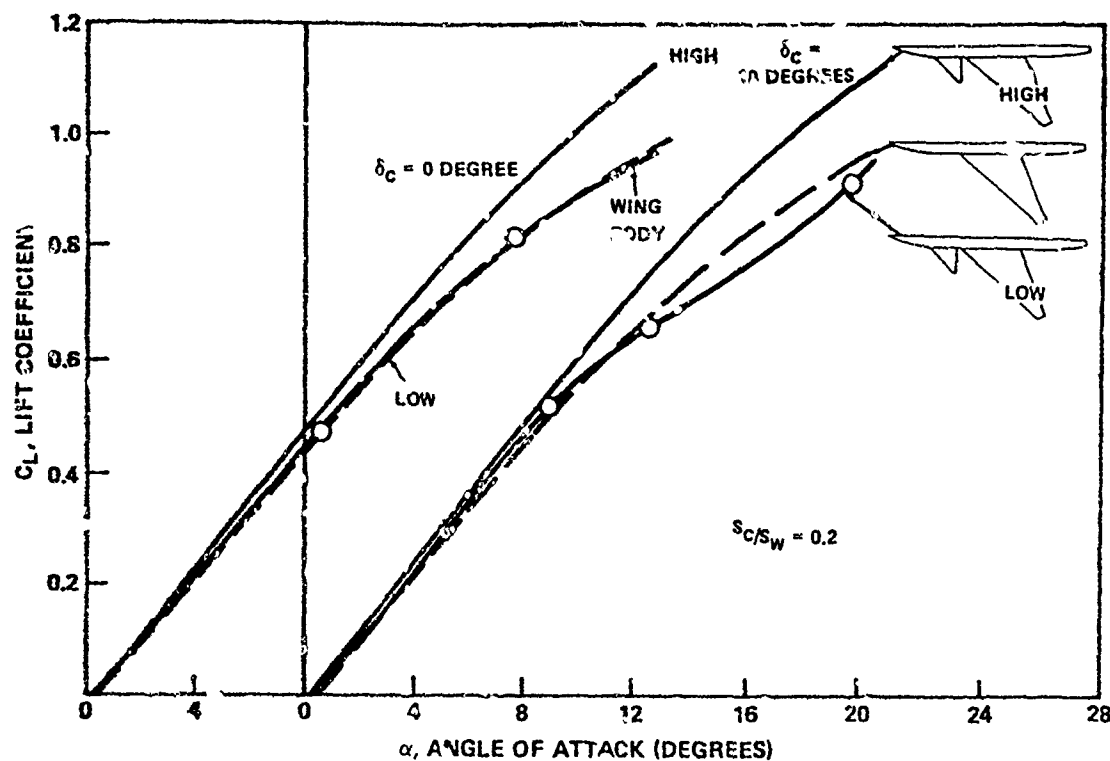
Figure 5 – Canards

Figure 6 - High verses Low Canard

LIFT COEFFICIENT AT 20 DEGREES ANGLE OF ATTACK
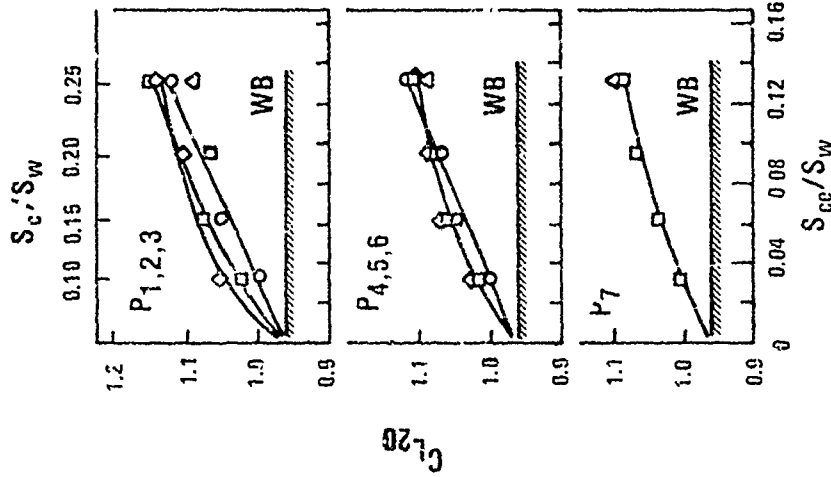
NEUTRAL POINT VARIATION
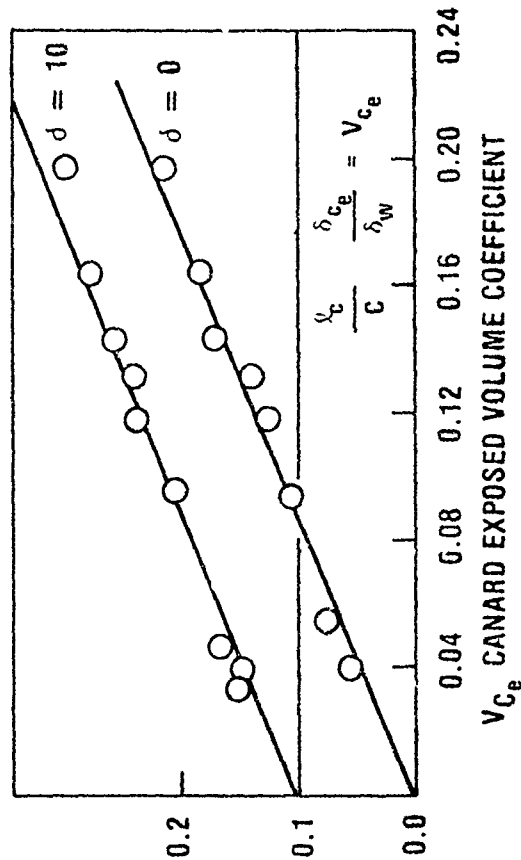
Figure 7 - Effect of Canard Size

MAXIMUM LIFT-TO-DRAG RATIO
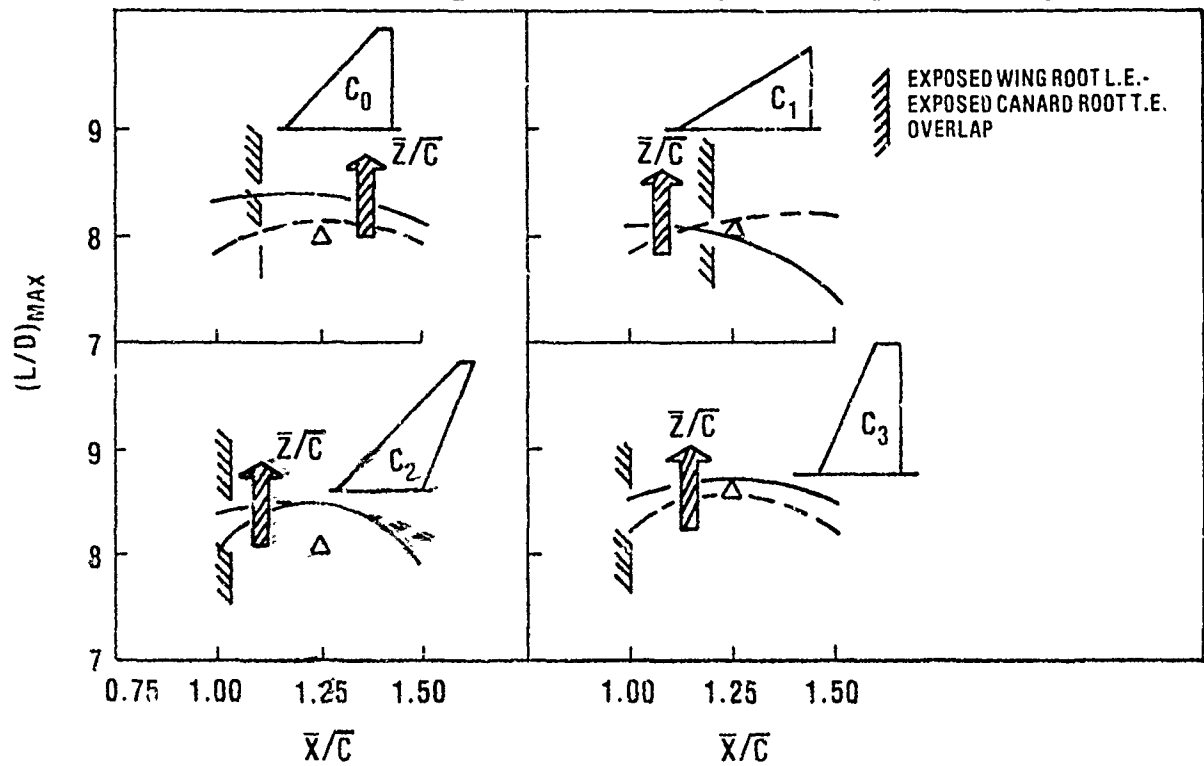
MAXIMUM LIFT
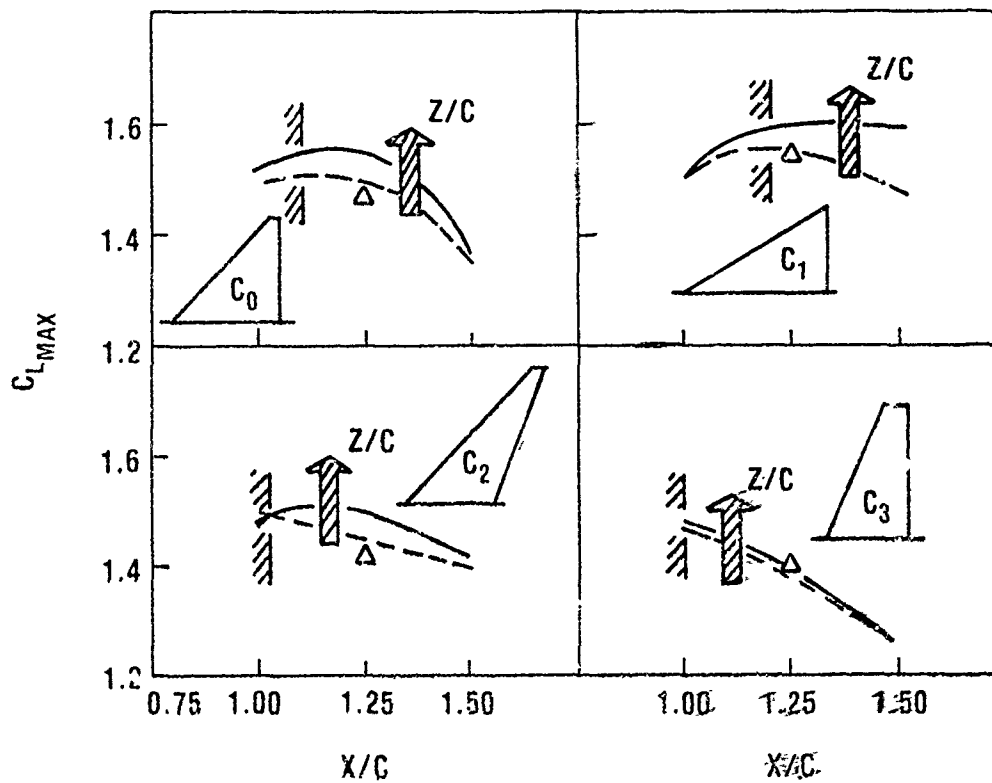
Figure 8 - Effect of Canard Location

Figure 9 - Effect of Canard Shape
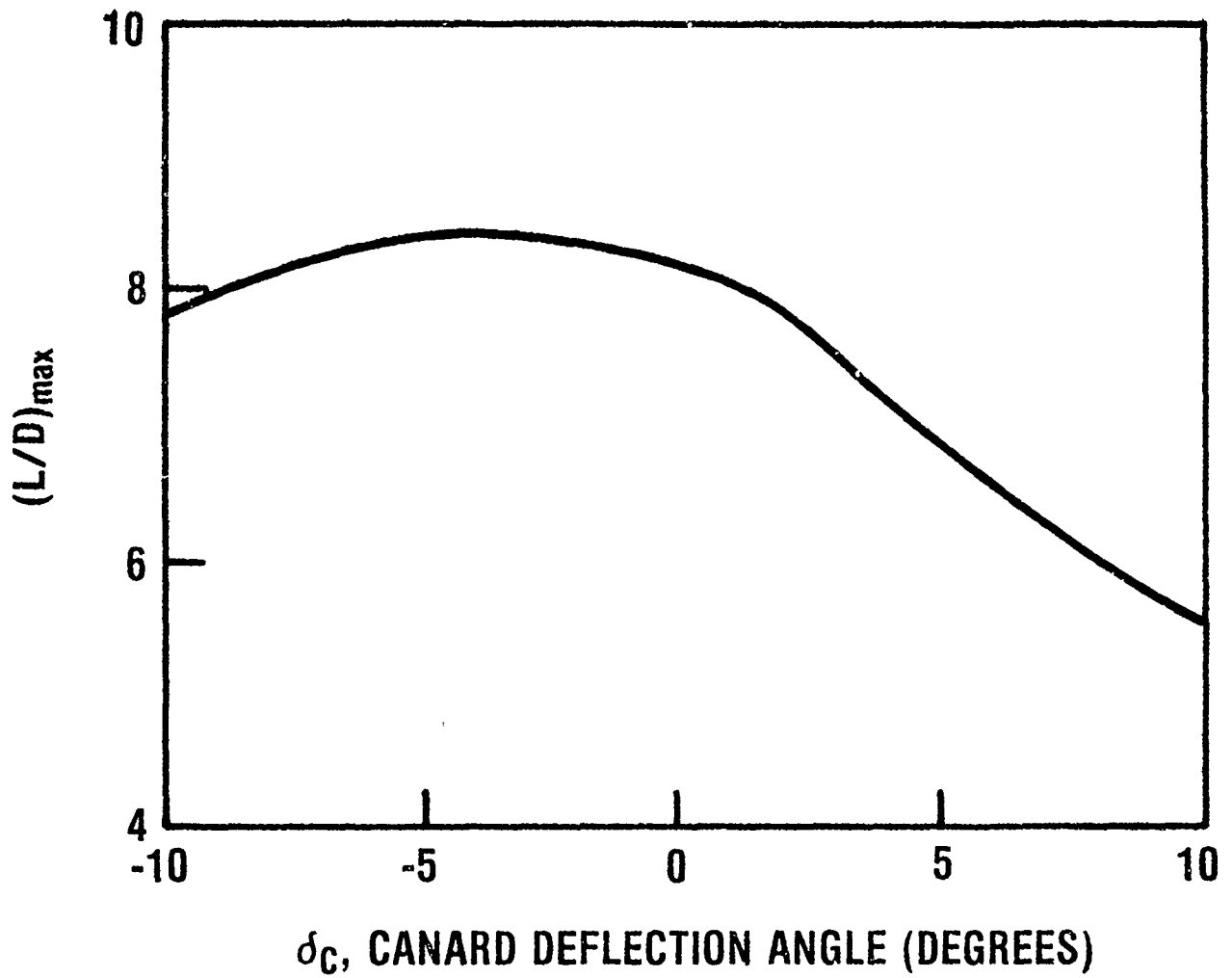
Figure 10 – Effect of Deflection on $(L/D)_{max}$
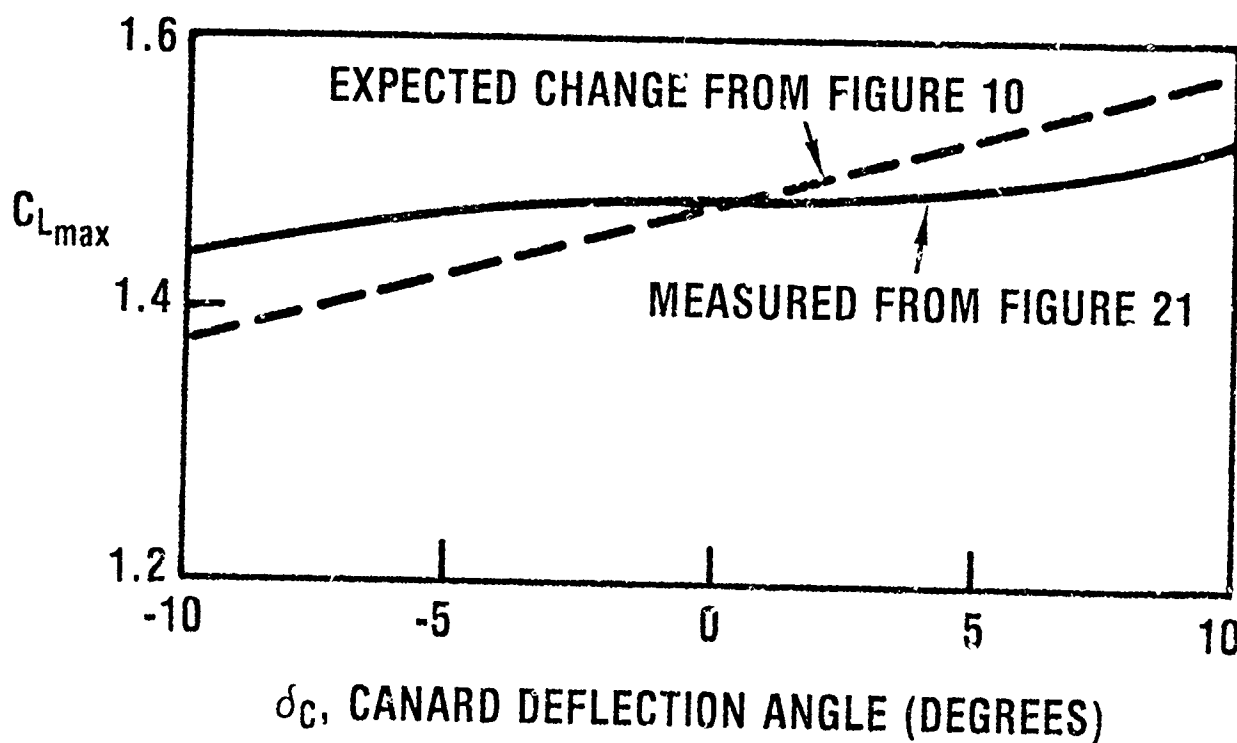
Figure 11 - Effect of Deflection on $C_{L_{max}}$
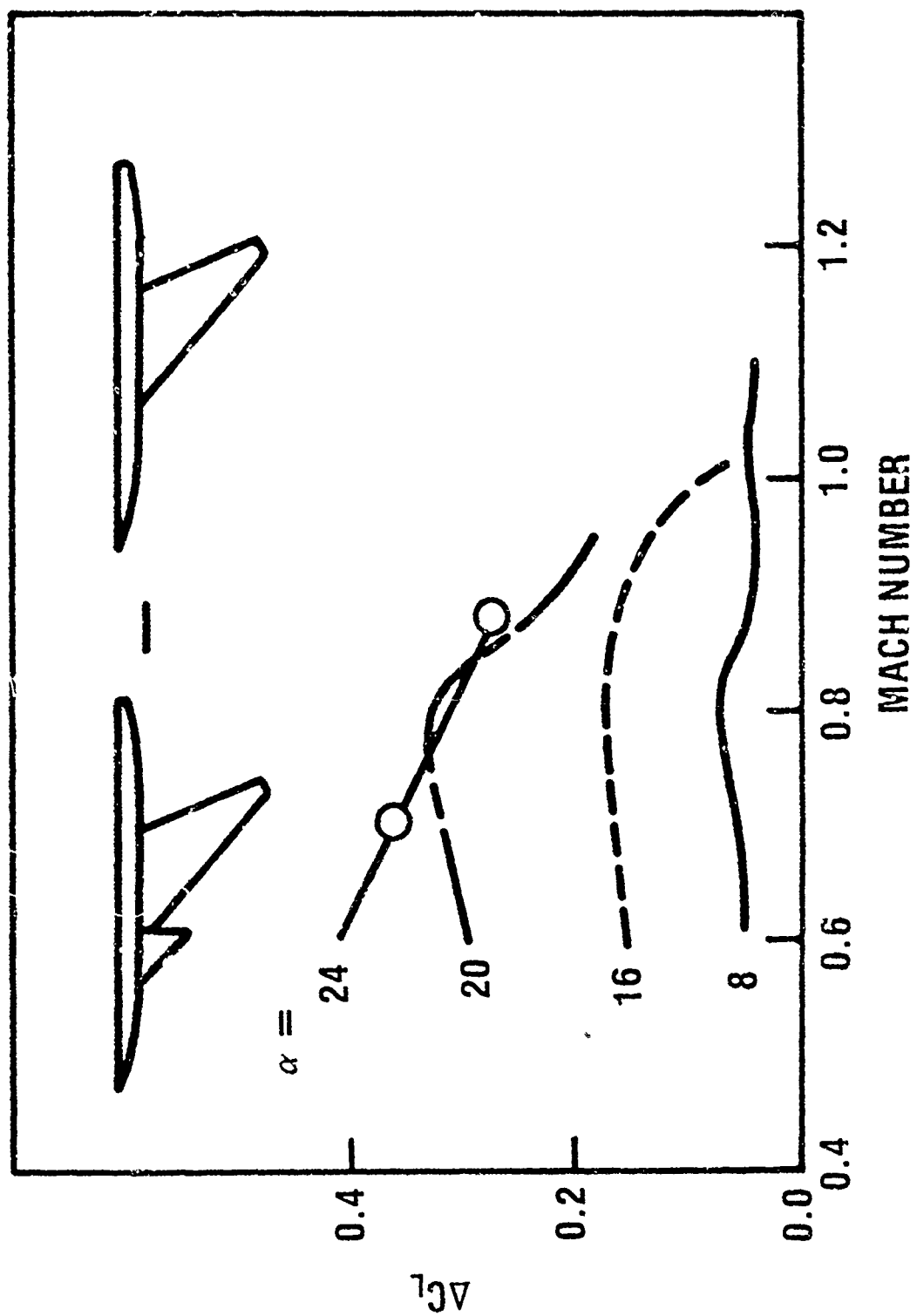
Figure 12 – Effect of Mach Number

MACH NUMBER

ΔC_L

$\alpha =$

24

20

16

8

Figure 13b – Effect of Canard on Buffet Intensity
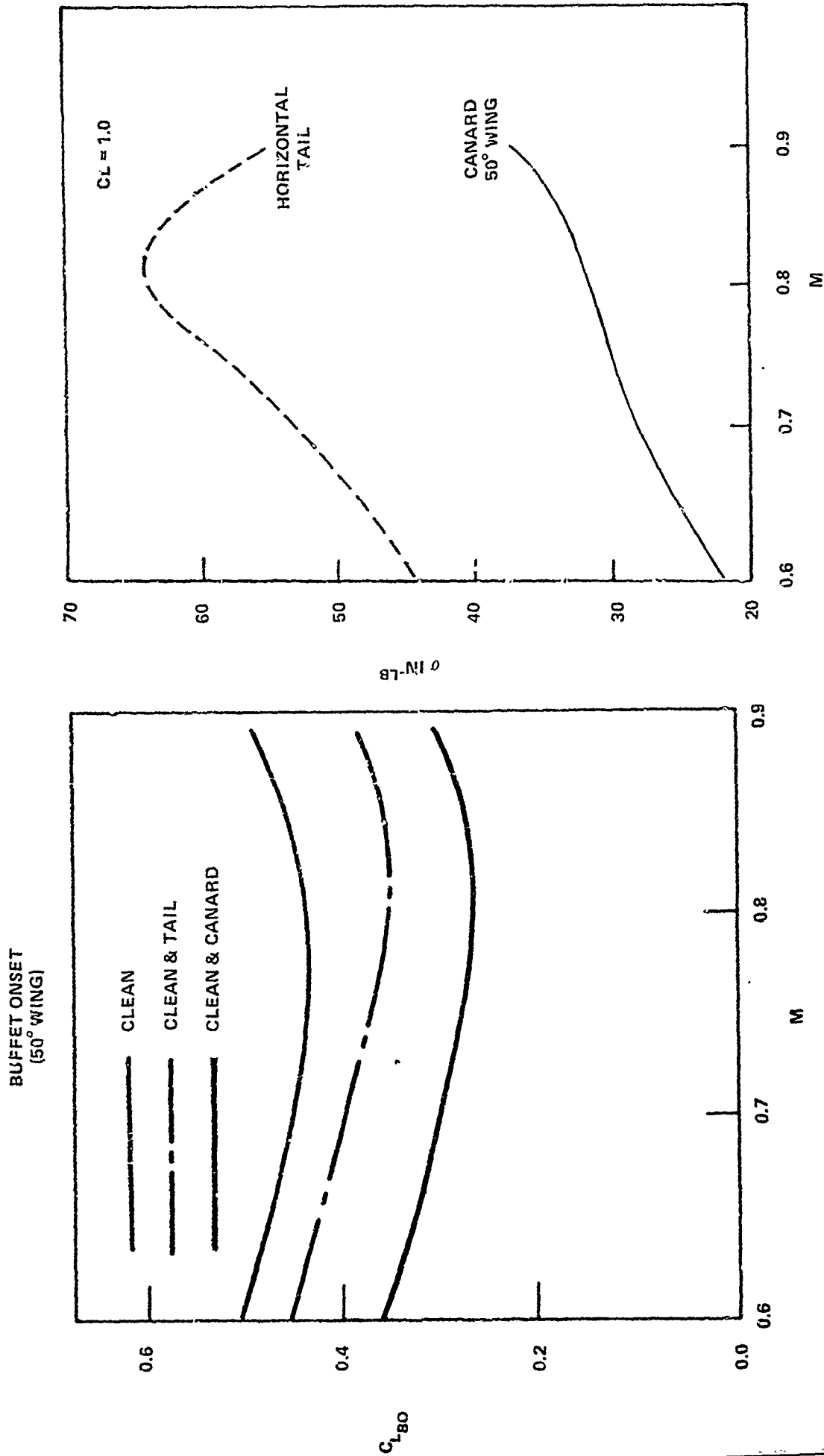
Figure 13a – Effect of Canard on Buffet Onset Lift Coefficient
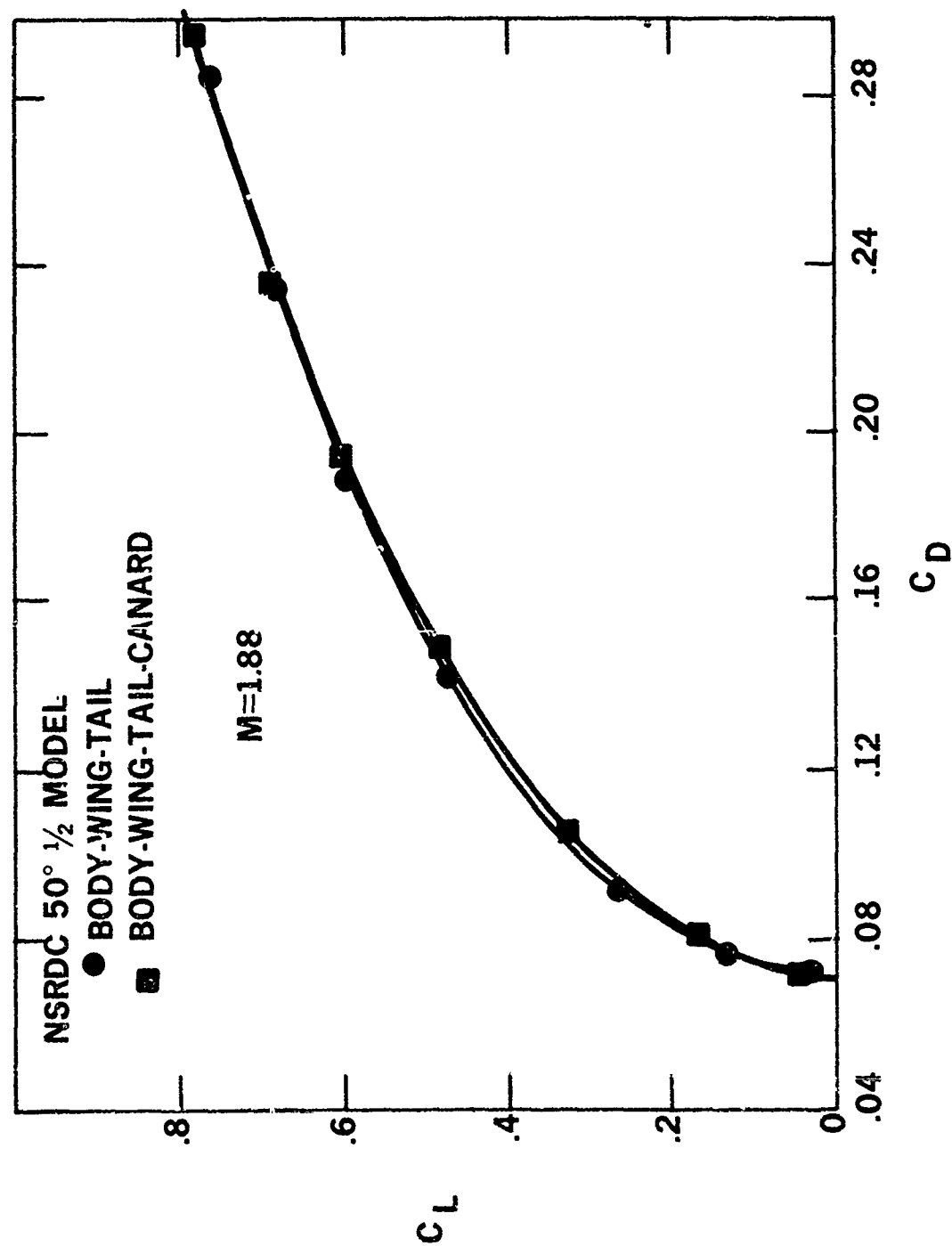
Figure 14 – Supersonic Drag
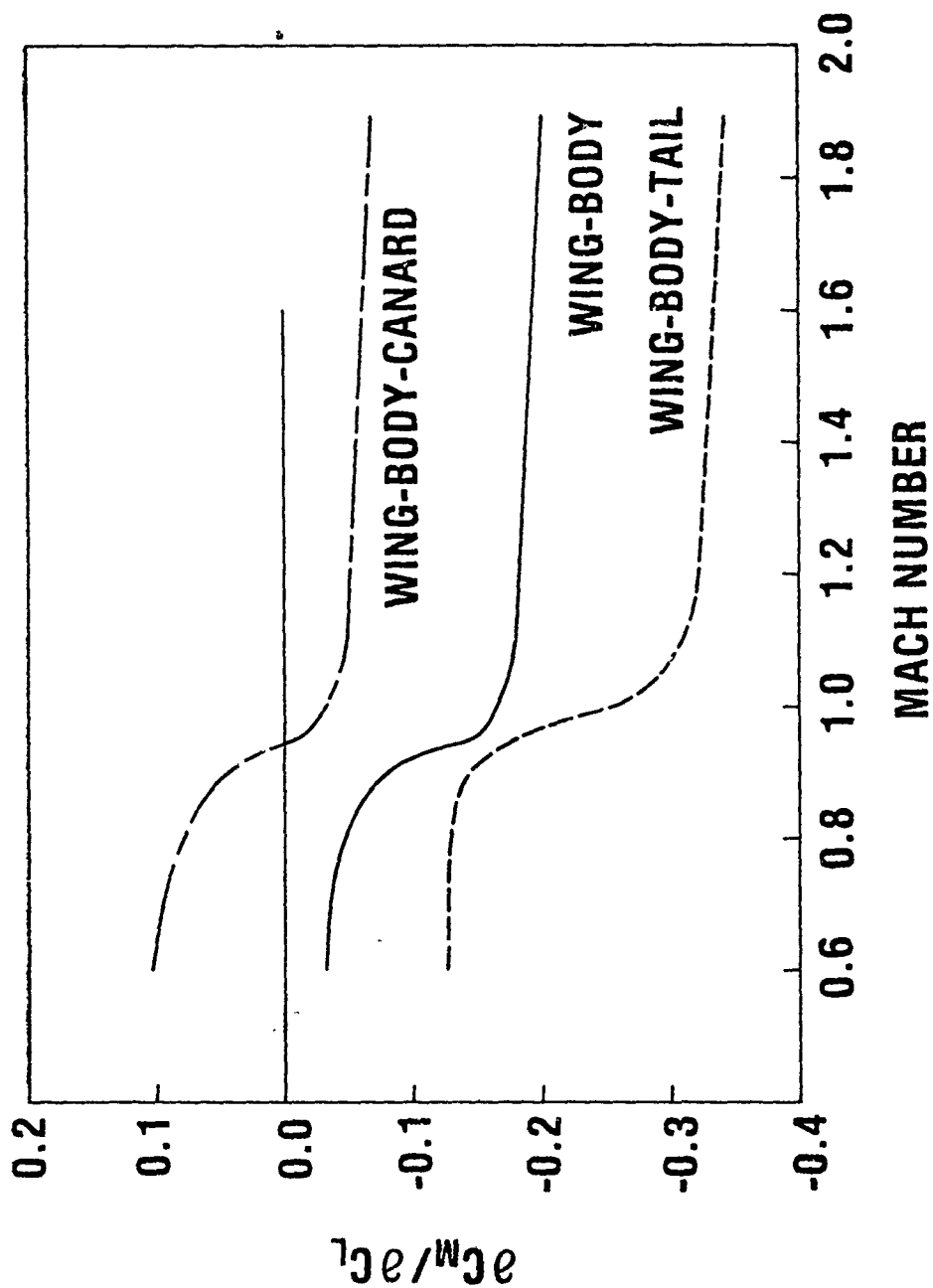
Figure 15 – Neutral Point Variation with Mach Number
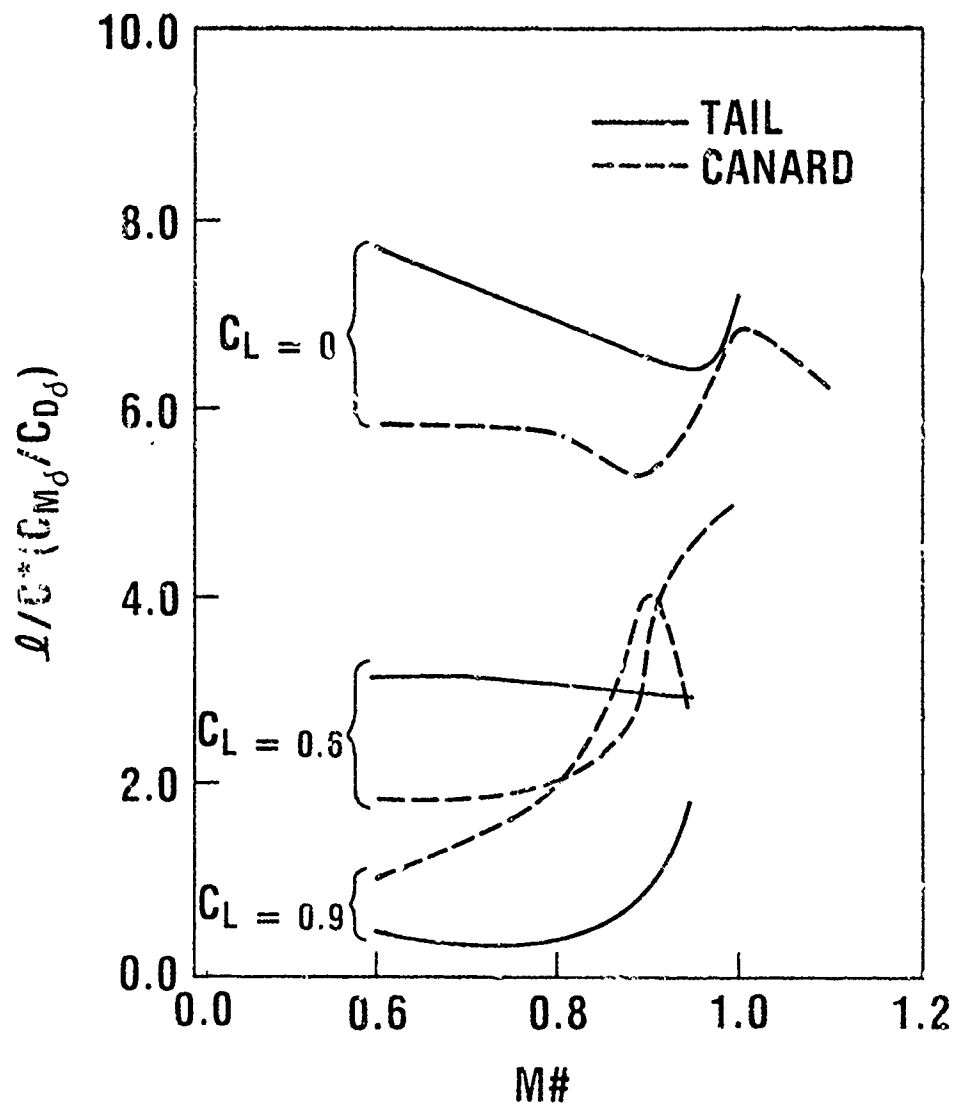
Figure 16 - Control Efficiency
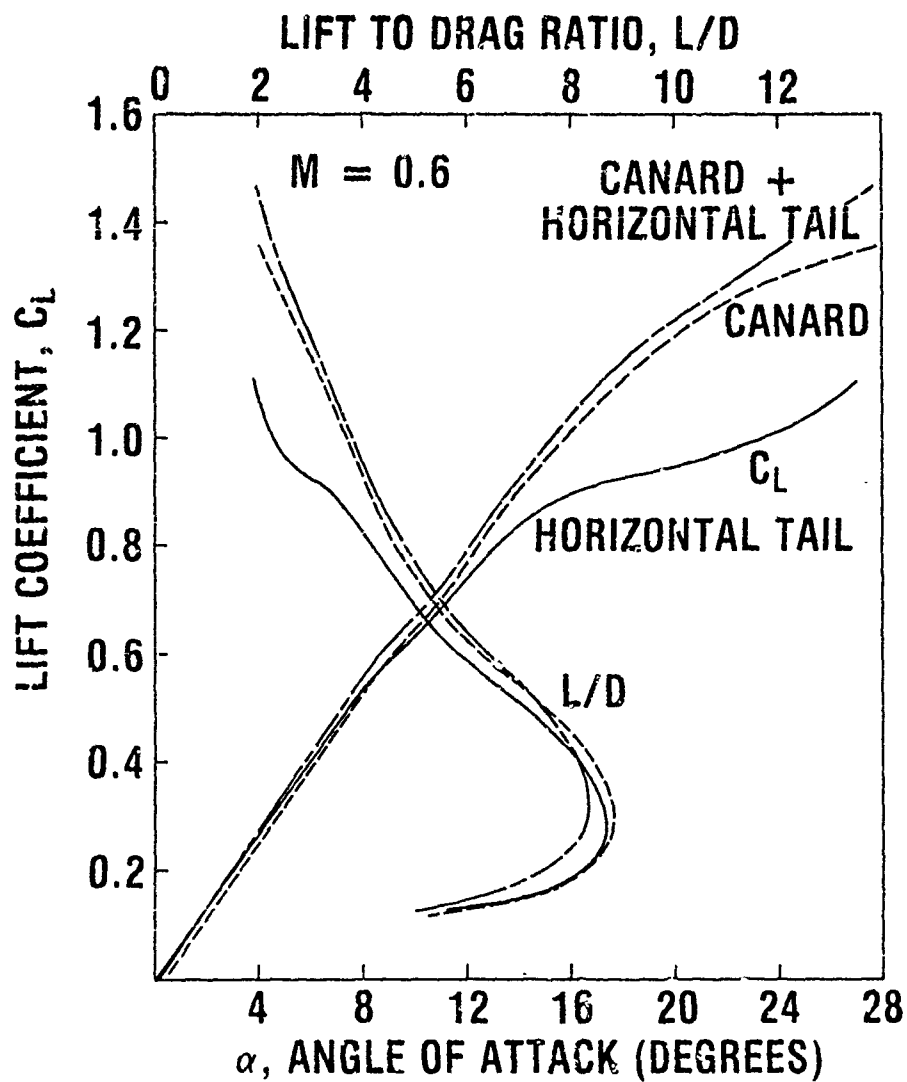
Figure 17 - Tri-Surface Characteristics
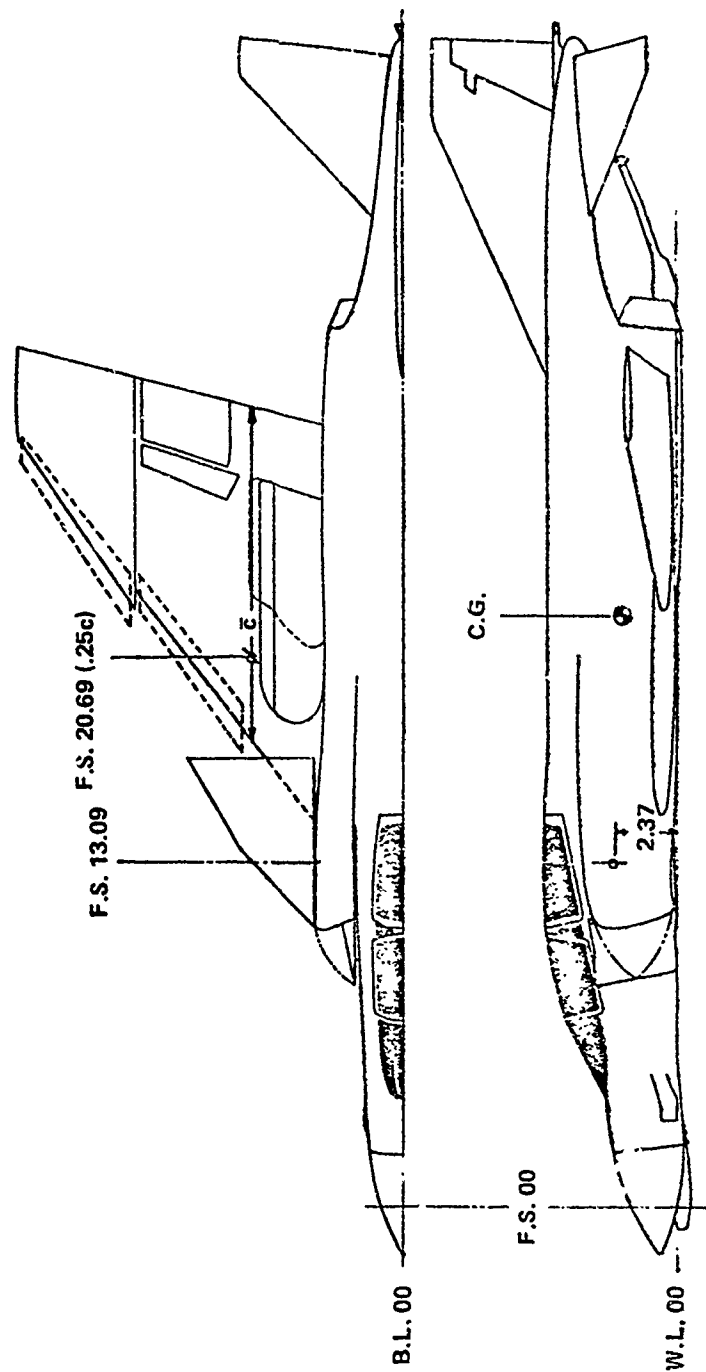
Figure 18 – F-4 Canard Installation
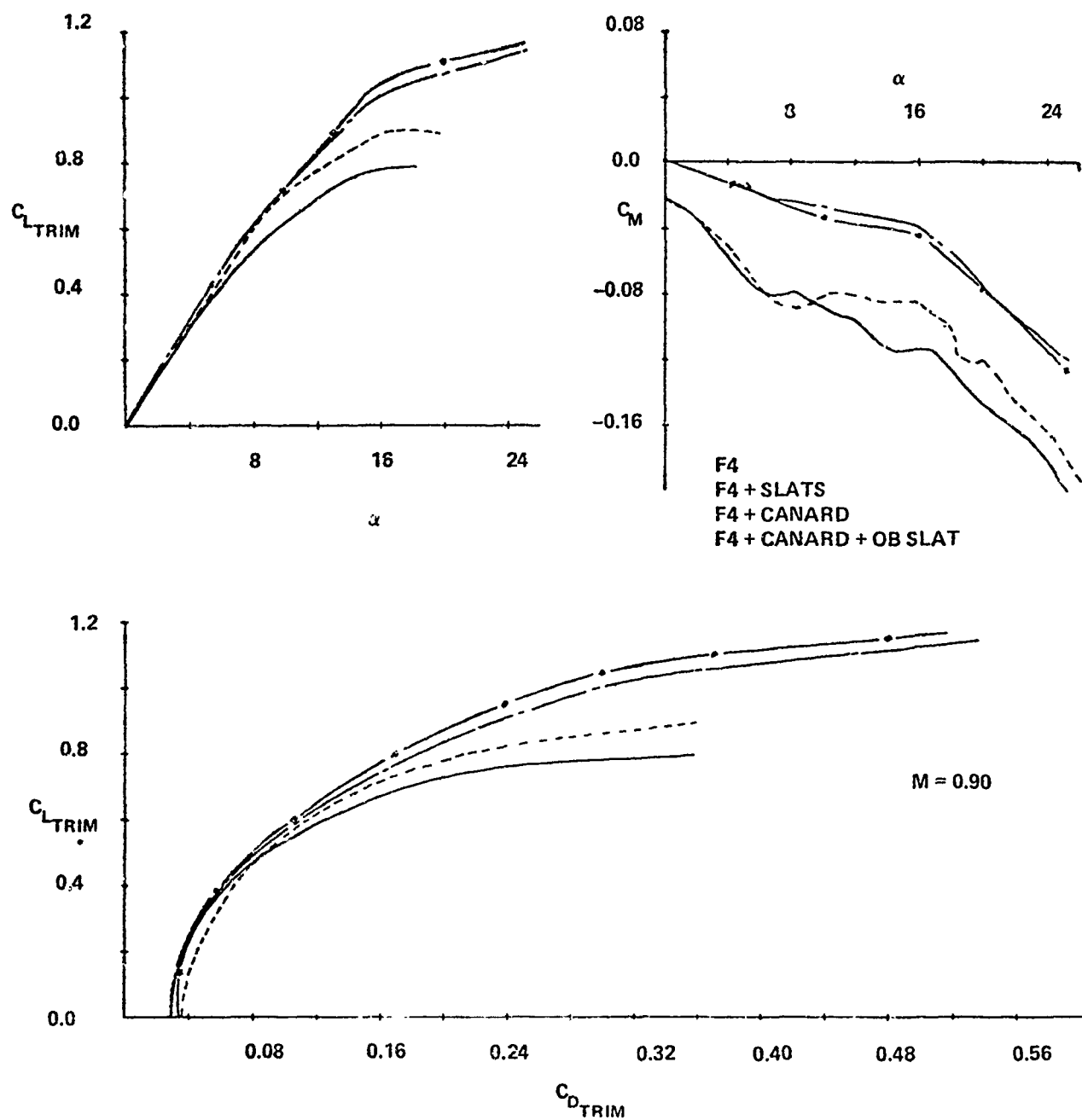
Figure 19 - F-4 Canard Characteristics
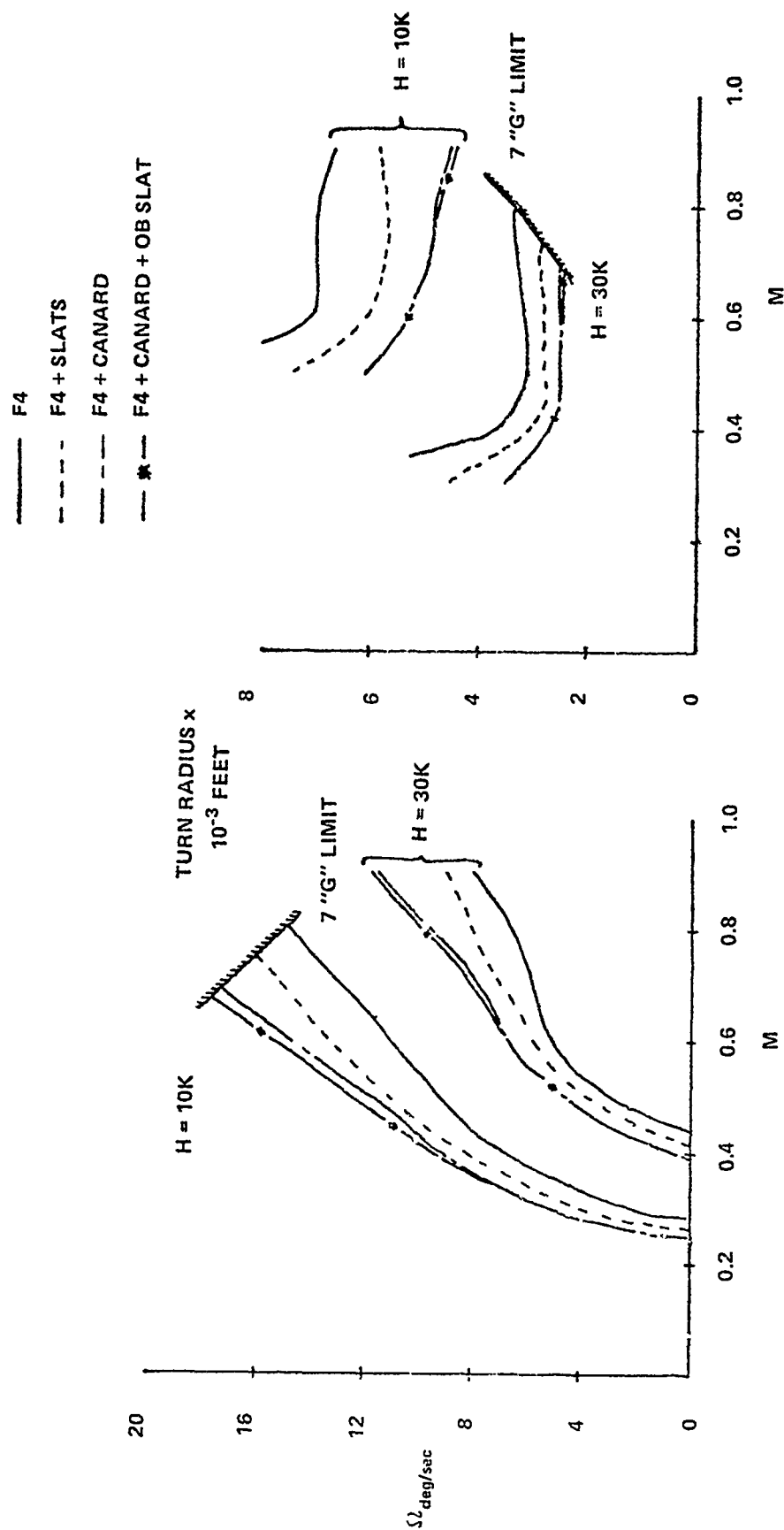
Figure 20 – F-4 Turn Performance

Figure 21 - F-4 Landing Configuration Characteristics

$\delta_{HOR.TAIL}$	δ_{CANARD}	T.E. FLAPS/ AILERON	L.E. FLAPS INB./OUTB.
VAR.	OFF	60/16	60/60
VAR.	+5,FREE FL.	60/16	60/SLAT
VAR.	+5,FREE FL.	60/16	60/60

● FLIGHT TEST (REF. 12)

$$\text{ROLL} - \frac{L_\delta \, \delta_{max}}{I_{XX}} = 1.2 \longrightarrow 2.0$$

$$\text{YAW} - \frac{N_\delta \, \delta_{max}}{I_{ZZ}} = 0.35 \longrightarrow 0.8$$

$$(\text{RAD/SEC}^2)$$

AGARD 577 +
NASA TND-6900

Figure 22 - VSTOL Criteria
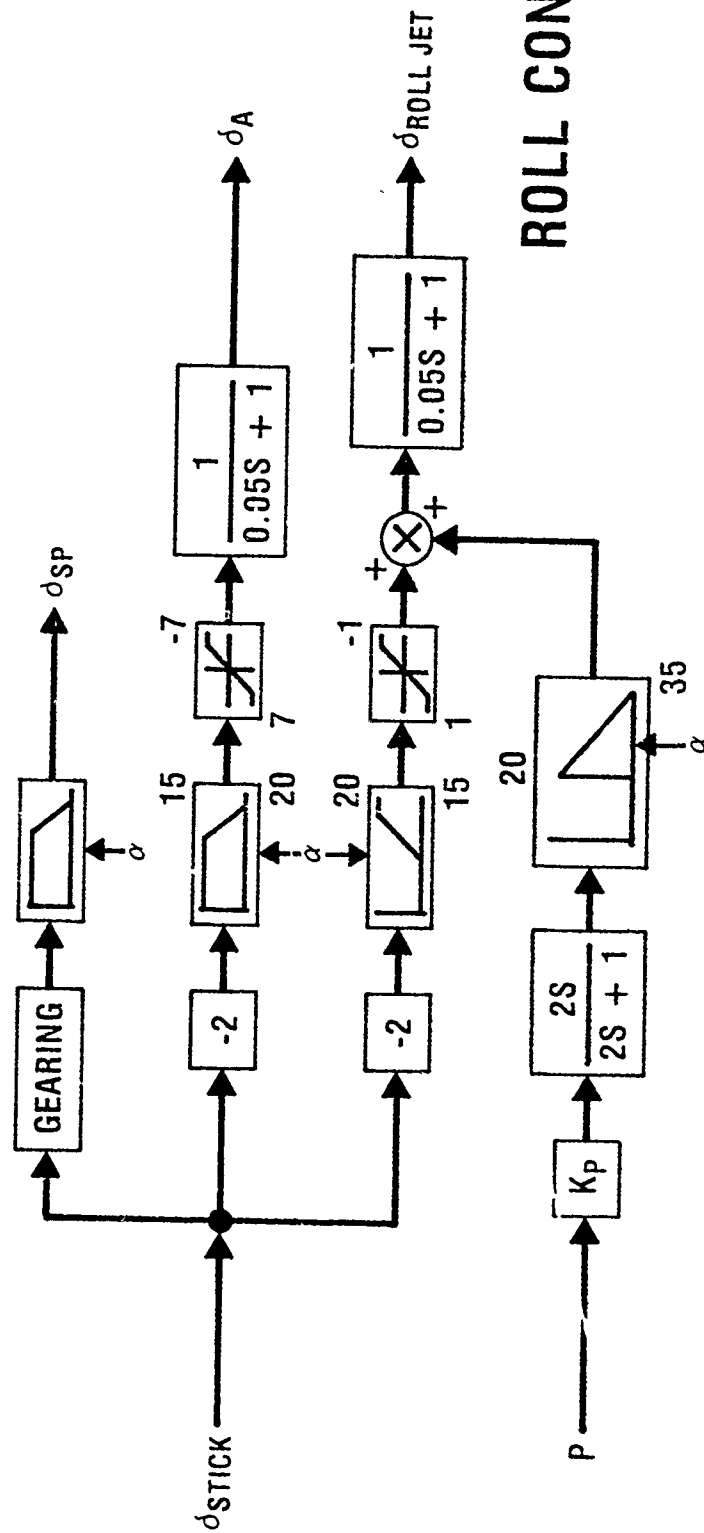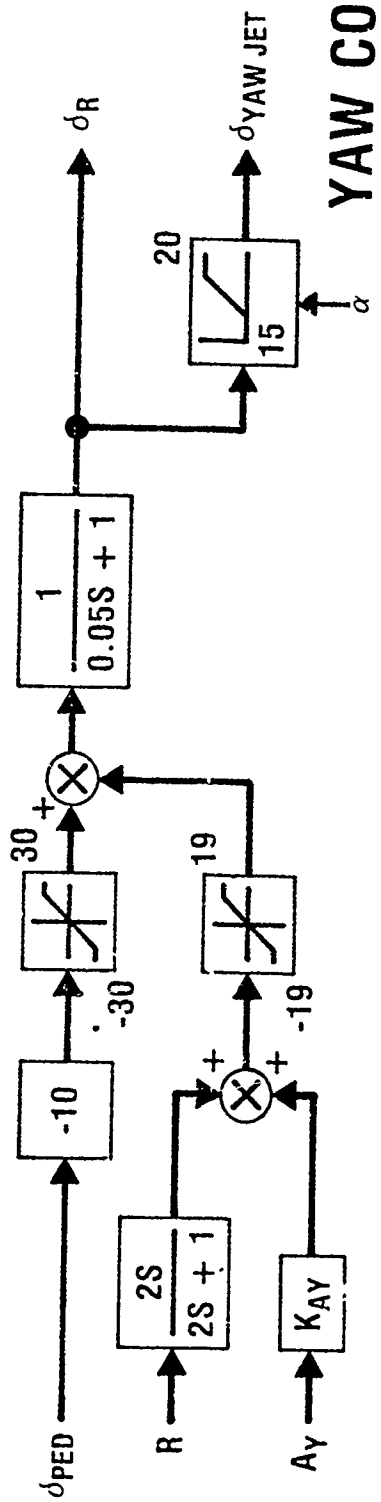
Figure 23 - Roll and YAW Control Systems

TIME TO BANK
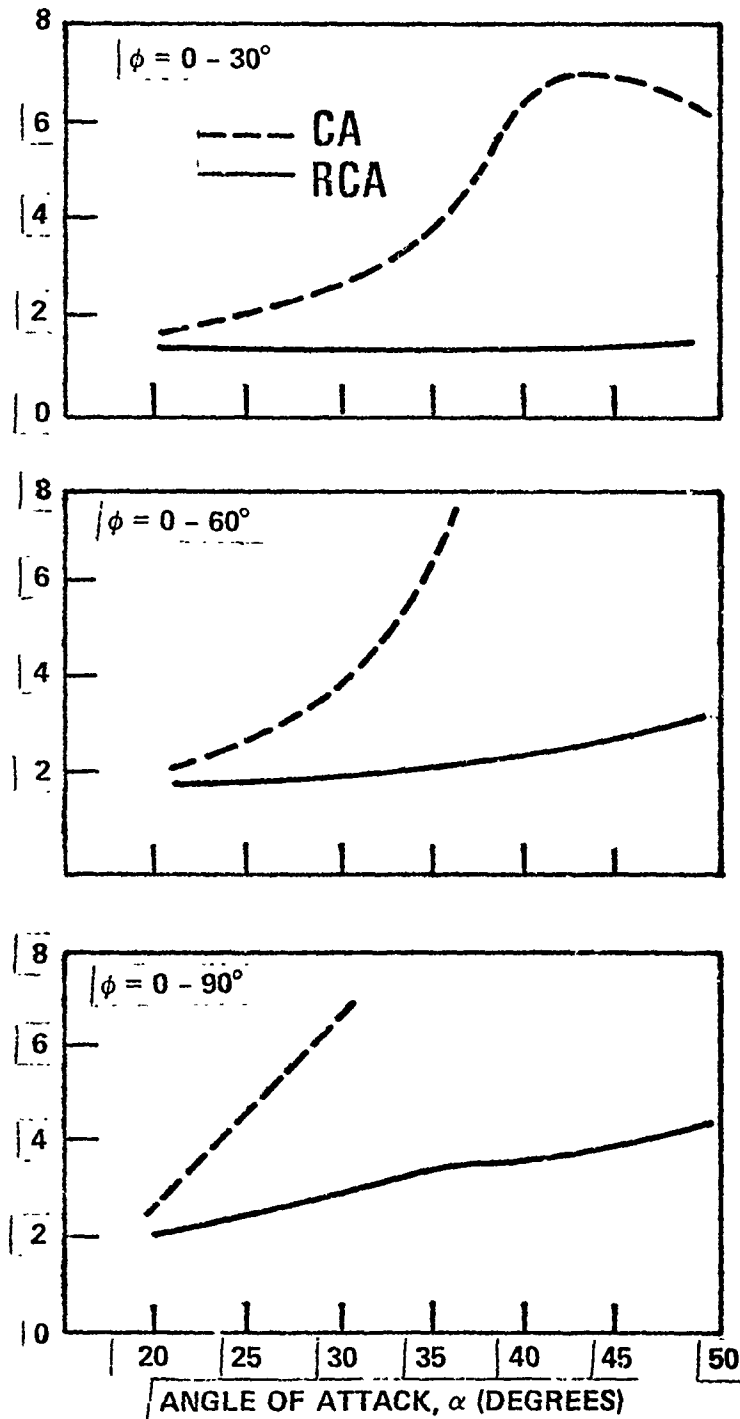
Figure 24 – Roll Response

771
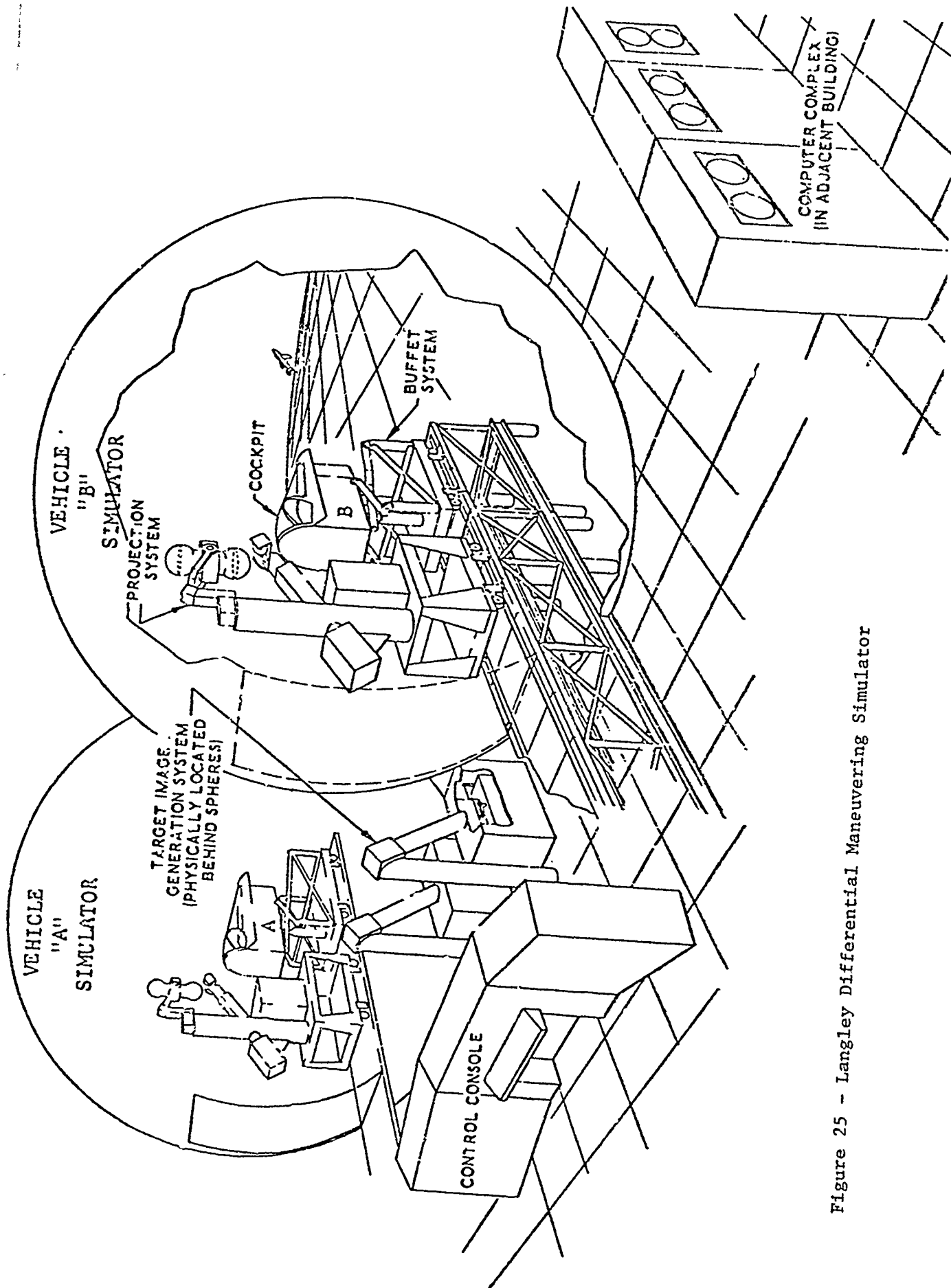
Figure 25 - Langley Differential Maneuvering Simulator
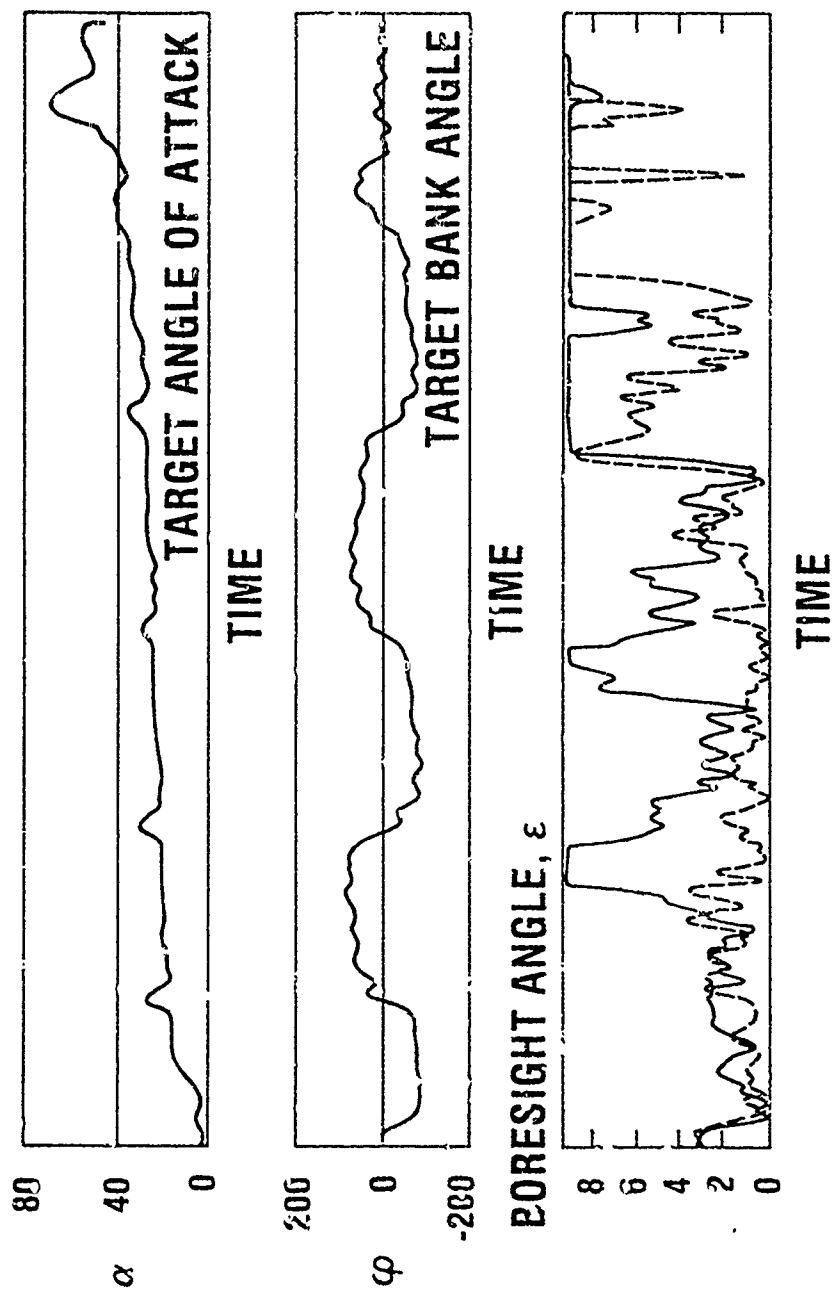
Figure 26 – Tracking Results
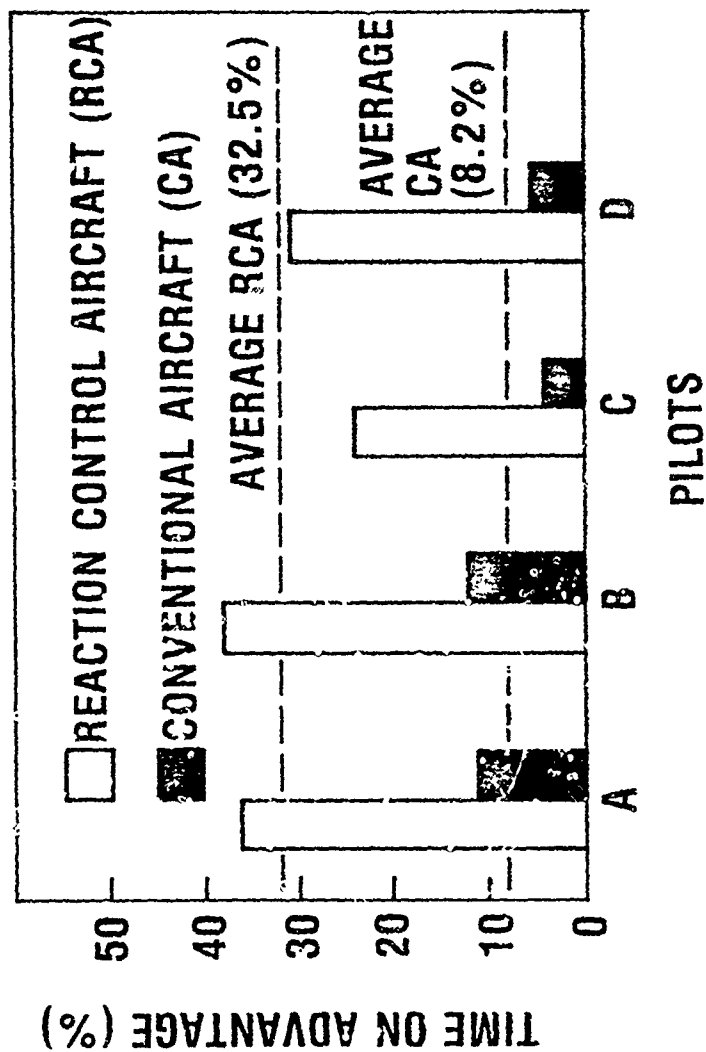
Figure 27 – Neutral Engagement Results
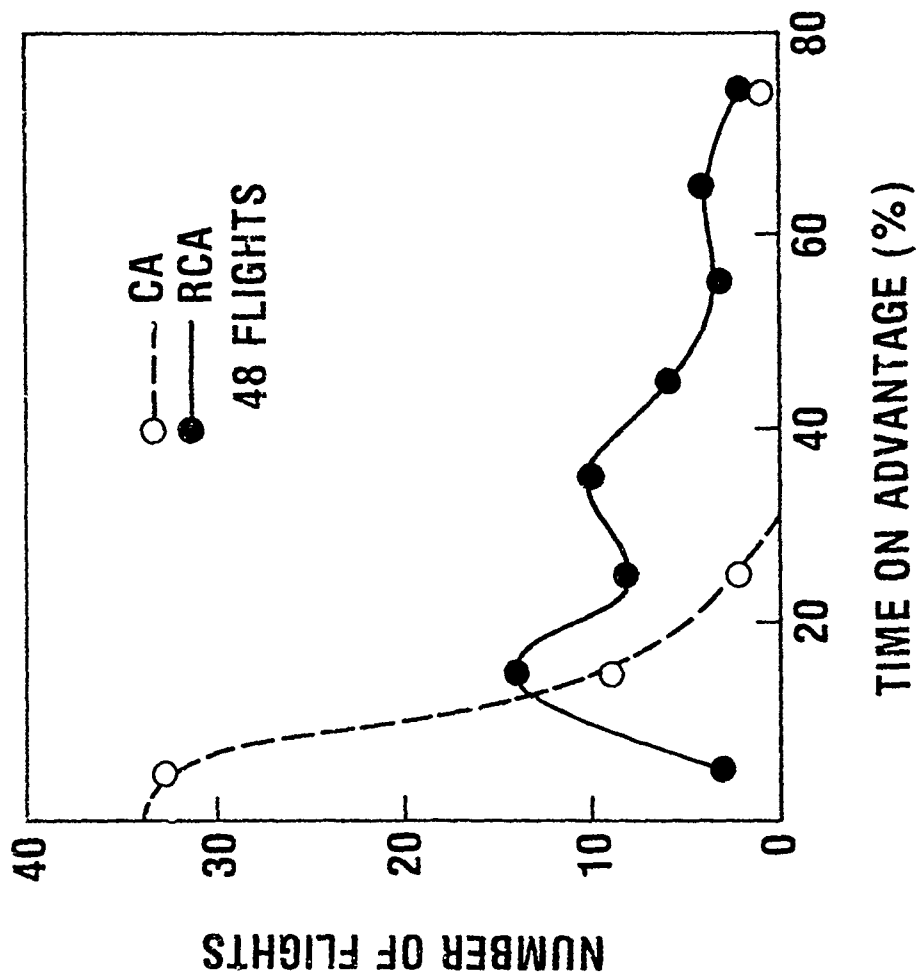
Figure 28 – Distribution of Time on Advantage
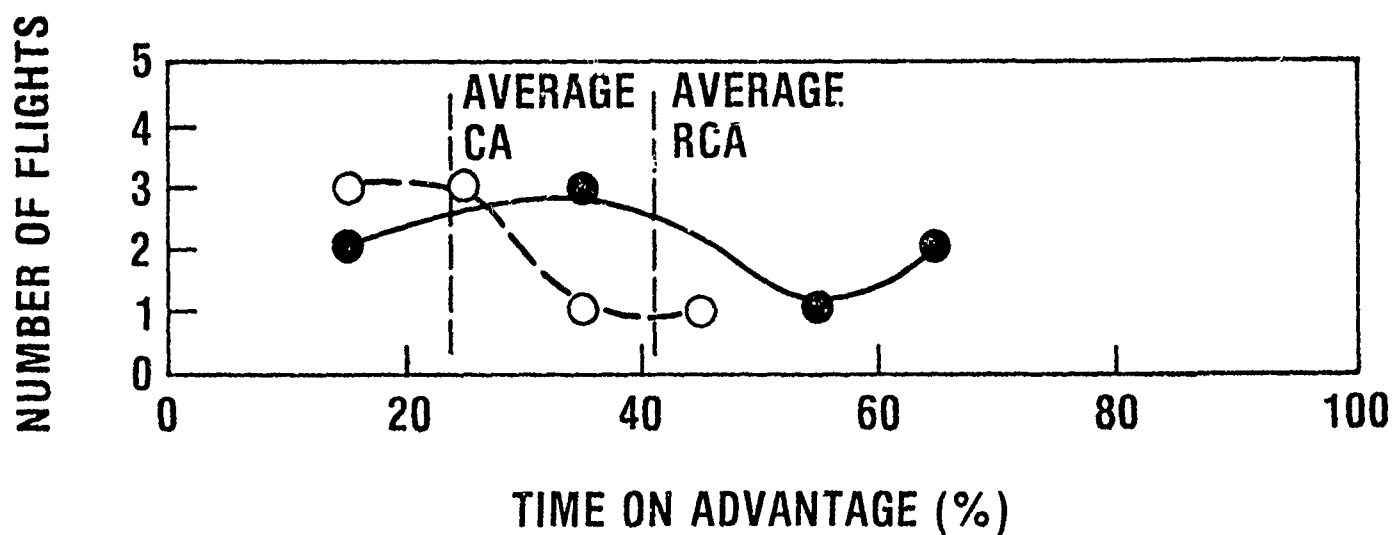
Figure 29 - Reaction Control Aircraft at Disadvantage
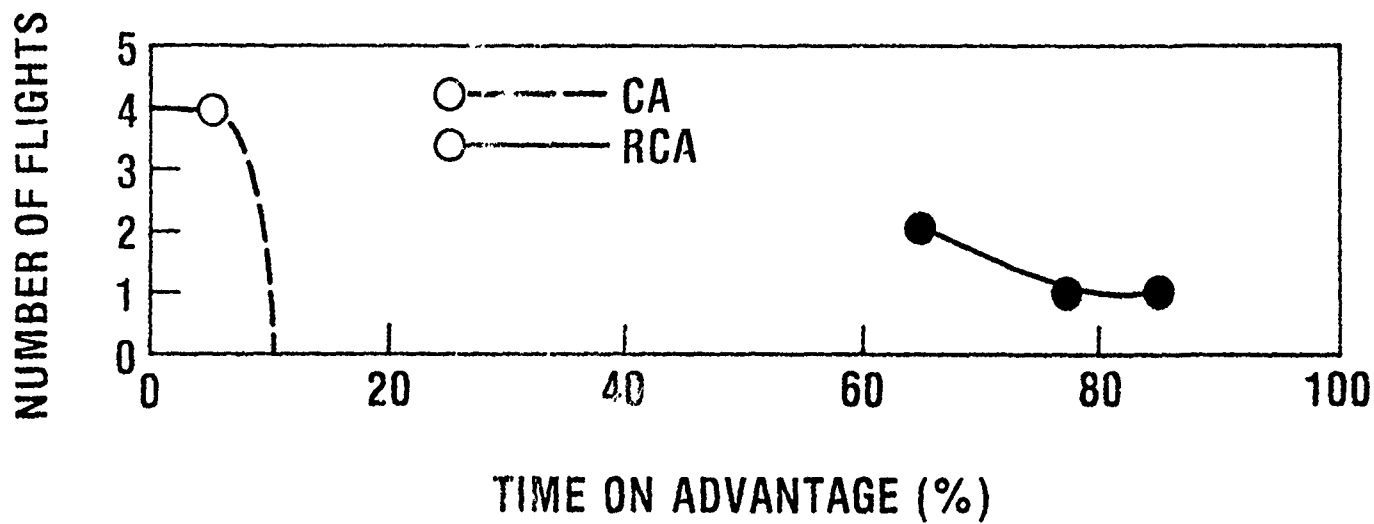
Figure 30 - Basic Aircraft at Disadvantage

DEVELOPMENT OF HIGH LIFT DEVICES FOR

APPLICATION TO ADVANCED NAVY AIRCRAFT

by

James H. Nichols, Jr.

David W. Taylor Naval Ship Research and Development Center

A number of methods for generating high lift to provide a STOL capability
for advanced Navy aircraft are evaluated, with emphasis on low aspect ratio
wings. Upper Surface Blowing, Circulation Control Wing, and Wing Tip Sails are
given the most attention. Experimental data are being obtained in the DTNSRDC
wind tunnels on these concepts as specifically applied to wings of aspect ratio
3 to 5. Flight demonstrations by Grumman/DTNSRDC of a CCW application to the
A-6 aircraft have shown the ability to more than double the lifting capability
which resulted in landing speed reductions of more than 30 percent, landing
ground roll reductions of more than 50 percent, and take off distance reductions
of at least 25 percent. The experimental high lift system data have been applied
to a conceptualized STOL baseline aircraft in order to estimate the impact on
mission performance and identify their various merits as applicable to the
particular restrictions of small ship operations.

INTRODUCTION

Operating fixed wing aircraft from ships imposes a number of unique size constraints and performance requirements on the aircraft. This is particularly true for aircraft wing span and take-off and landing performance. For V/STOL or STOL aircraft to be effective, they must be able to operate from small deck areas that preclude conventional aircraft operations. A strong implication of these requirements to aircraft design is the need for improved propulsion and high lift systems. However, the size constraints and speed requirements tend to force reductions in both wing span and aspect ratio.

A number of methods are under development for generating high lift, however this work has been directed at applications to higher aspect ratio wings. The objective of the effort at the David W. Taylor Naval Ship Research and Development Center (DTNSRDC) is to maximize the effectiveness of powered high lift systems for low aspect ratio wings. A significant part of the effort is directed at better understanding the phenomena occurring between the regions of high energy strong circulation air and low energy or free-stream air. In particular, it is felt that mechanical devices with or without supplementary blowing must be incorporated with a powered high lift system to make it useful, at least for wings of lower aspect ratios. Furthermore, these same high lift enhancement devices may also serve to increase the effective aspect ratio and thereby improve cruise performance if appropriately designed.

The high lift systems being developed appear to fall into three categories based on the amount of energy required to operate the system:

Category A - High lift produced by high propulsive energy input

Category B - High lift produced by low propulsive energy input

Cateogry C - High lift produced by no propulsive energy input (mechanical systems)

Category A systems can be currently characterized by significant thrust-lift coupling while Category B and C systems are relatively thrust-lift independent. Category A systems examined were Externally Blown Flap (EBF), Upper Surface Blowing (USB), Combined Surface Blowing (CSB), and Augmenter Jet Flap (AJF). The Category B system considered was the Circulation Control Wing (CCW). The Double Slotted Flap (DSF) was selected from Cateogry C devices to serve as a state-of-the-art baseline for conventional unpowered high lift systems in order to compare lift and performance benefits of the powered systems.

A conceptualized Short Take-Off and Landing (STOL) baseline aircraft was developed to allow an assessment of the ability to perform a typical S-3 ASW type of mission with each of the high lift devices. A STOL aircraft was chosen since the impact of the high lift devices would have more visibility. It was this assessment that highlighted mission performance deficiencies for the required limited wing spans thereby substantiating a need for additional help for the high lift device operation. Furthermore, in addition to presenting a challenge for useful high lift devices, low aspect ratio wings typically suffer in cruise performance. However, if the devices that can help high lift performance are designed properly, they may also improve cruise performance. Anticipated methods of such high lift/cruise enhancement are winglets (unblown

or blown), wing tip sails (fixed or adjustable), fences, wing tip blowing, and leading edge devices. Each of these approaches has been shown to provide improvements in either lift or cruise.

The specific effort at this time involves aspect ratios from 3 to 5 and has been narrowed down to the Double Slotted Flap (Category C), the Circulation Control Wing (Category B) and Upper Surface Blowing (representing Category A) for evaluating high lift/cruise enhancement devices.

ASSESSMENT OF CURRENT HIGH LIFT TECHNOLOGY

Several approaches to generating high lift are currently under development (Figure 1). Of the several systems looked at in the initial stages of this work, data were most readily available for the following systems:

o Augmented Jet Flap (AJF)

o Externally Blown Flap (EBF)

o Combined Surface Blowing (CSB)

o Upper Surface Blowing (USB)

o Circulation Control Wing (CCW)

The focus of the preliminary evaluation was on these systems, however, it became readily apparent that all data available were for wings of relatively high aspect ratio. Therefore, an experimental program would certainly be required for any further effort for low aspect ratio wings. For this reason, part of the initial assessment was conducted with the intent of narrowing down the number of concepts to keep such an experimental program within manageable bounds.

In order to compare each of these high lift systems, a conceptual STOL aircraft was developed using a 14 percent thick supercritical wing (Figure 2). An analysis was performed comparing the effects of the different high lift systems on the wing span requirements of aircraft with low aspect ratio ($3.5 \leq R \leq 5.0$) wings for an ASW type mission and a required take-off distance of 400 feet. Rather than sizing the aircraft to meet a certain mission radius, internal fuel was fixed and the aircraft was allowed to perform its maximum radius for the selected performance characteristics. Results were developed in terms of ranges of thrust-to-weight ratio (T/W) required to achieve the above constraints for a range of fixed internal fuel that would keep the aircraft gross weight below 55,000 pounds. Results of this analysis are summarized below, however, a major conclusion was reached:

o The ineffective high-lift capability of low-aspect ratio wings is difficult to overcome by powered high-lift systems alone.

Therefore, an additional emphasis was placed on the experimental program to not only improve the efficiency of the high lift system but also increase the effective aspect ratio with the same high lift enhancement devices.

Augmented Jet Flap

The Augmented Jet Flap (AJF) operates on the ejector principle by taking a primary jet of engine fan bypass air and exhausting it downward through an adjustable flap system which further entrains secondary flow from the wing upper surface (Figure 1). This concept has the advantage of a reasonably effective engine-out capability. Experimental data were obtained for wings of aspect ratio 8.0 which achieved maximum lift coefficients ($C_{L_{max}}$) on the order of 7-1/2 (Figure 3). This sytem has been installed and flown successfully on a modified C-8 Buffalo research aircraft in a Boeing/NASA effort.

A performance analysis indicated that the AJF configured baseline aircraft would have a mission radius capability slightly better than but similar to that of the USB configured baseline aircraft. In addition, the AJF system mechanism is fairly complex, this complexity extending over much of the wing span, thereby rendering it difficult and expensive to produce in model scale. Although the performance warrants further work and the high lift/cruise enhancement devices could very well be unique for this system, the decision was made to eliminate this system from the experimental program in deference to a system more readily modeled.

Externally Blown Flap

The Externally Blown Flap involves locating the engine ahead of and beneath the wing so that the engine exhaust creates a high velocity flow of air from near the leading edge and under the wing which then blows over a multi-element flap (Figure 1). Very high values of $C_{L_{max}}$ on the order of 10 have been achieved experimentally (Figure 4). This system has been installed and successfully flown on the 4-engine McDonnell-Douglas YC-15 aircraft. However, the system does not lend itself to having an engine-out capability for a two-engine installation and for this reason has been eliminated from further consideration for this program.

Combined Surface Blowing

Combined Surface Blowing (CSB) places the flap within the engine fan exhaust adding high energy air to both the upper and lower surface of the wing and flap (Figure 1). The fans can be cross-shafted which provides a potential engine-out capability. NASA/Boeing Vertol experimental data has shown very high $C_{L_{max}}$ achievable (on the order of 12) and for aspect ratios getting close to the low range (Figure 5). Furthermore, the flow can be turned beyond 90 degrees (to around 105 degrees) which implies that a VTOL capability is conceivable with a high enough thrust to weight ratio. At least a good STOL capability should be achievable with this kind of thrust deflection.

This system shows high potential for contributing to the objectives of this work; it is planned to include this concept in the experimental program at some future time.

Upper Surface Blowing

The Upper Surface Blowing (USB) system involves Coanda turning of the engine exhaust over the upper surface of a smoothly curved flap. The resulting powered lift is due both to a component of the thrust vector and to increased circulation around the wing as a result of flow being entrained by the jet over the upper surface of the wing. This system has been installed and flown successfully on the Boeing YC-14 aircraft which incorporates a double-slotted flap system on the outboard portion of the wing. An effective engine out procedure has been established for this two engine aircraft.

A substantial amount of wind-tunnel data has been generated for USB on high aspect ratio wings, a sampling of which is shown in Figure 6. These data show the importance of exit nozzle shape to generating high lift, although the effect of nozzle shape on cruise performance is not shown. The curved surface "D" nozzle is easily out-performed in lift generation by the "rectangular" nozzle. However, the "D" nozzle offers superior cruise performance and may in fact offer the best overall design. Also not shown in Figure 6 is the effect of nozzle aspect ratio for the rectangular nozzle, although values near 3 seem to offer the best lift performance.

The high aspect ratio experimental data was extrapolated to the low aspect ratios in order to conduct the performance analysis on the baseline aircraft. The wing loadings (W/S) required for a 400 foot deck run takeoff were determined for a range of thrust-to-weight ratios (T/W). This range of parameters used with selected internal fuel weights was used to generate aircraft configurations having aspect ratios of 5.0, 4.25, and 3.5. Mission radii were then determined for these designs and are shown versus takeoff weight for the aspect ratio - T/W carpet as shown in Figure 7. The wing span required is then superimposed on the figure.

Of considerable significance is the fact that the STOL USB aircraft configuration could achieve a 300 nautical mile radius mission within the desired range of parameters of T/W, aspect ratio and takeoff gross weight. However, the configuration studied could not achieve a wing span within the 45 foot requirement for an LPH type ship. The USB system potentially offers considerable high lift performance - particularly with an appropriate engine/airframe match for both takeoff and cruise. Furthermore, integrating USB into a wind tunnel model is relatively straightforward. Therefore, USB was selected for the low aspect ratio experiments for high lift/cruise performance enhancement, thus representing the Category A high propulsive energy class of high lift devices.

Circulation Control Wing

The Circulation Control Wing (CCW) concept involves controlling the stagnation points on the airfoil by means of a thin jet of air which remains attached to a rounded trailing edge (Coanda principle). By moving the stagnation points toward the center of the airfoil undersurface, the circulation around the airfoil is considerably increased, producing an effective camber much greater than the airfoil geometry dictates. An extensive amount of experimental data has been generated by DTNSRDC for both fixed wing and rotary wing applications. Several papers on the subject of fixed wing applications have been written by Mr. Robert J. Englar and others (DTNSRDC).

The fixed wing effort was recently culminated in the highly successful flight demonstration of a CCW installation on an A-6 aircraft by Grumman/DTNSRDC[1] (Figure 8). Details of the installation for the flight demonstration are shown in Figure 9. The objective of the flight program was a full-scale technology demonstration and as such the installation was designed as an add-on system using the A-6 aircraft. The A-6 was chosen for this role because of highly desirable airframe and propulsion system characteristics. The modification to the aircraft were conservative to provide adequate safety and keep program costs to a minimum.

Lift performance demonstrated in the flight program is summarized in Figure 10. The best lift coefficient achieved was $C_L = 3.34$ at an angle of attack of only 16 degrees and an altitude of 5,000 feet, enabling the A-6 to fly at a speed of 67 knots. However, $C_{L_{max}}$ was never achieved in flight although an angle of attack of almost 30 degrees was flown at 15,000 feet. Therefore, all "maximum" values of C_L from the flight program are the maximum values of lift actually flown. These data are shown in Figures 10 and 11. Wind tunnel results for the A-6/CCW are shown as solid lines in Figure 11. The maximum value of trimmed $C_{L_{max}}$ is shown as about 3.9 at a blowing coefficient (C_μ) of 0.30. Calculated values of trimmed C_L based on flight data are shown as the dashed lines and fall somewhat below the wind tunnel data. However, during the flight program, the vehicle performance was such that a significant amount of spoiler (flaperon) action was required for maintaining a zero bank angle. An adjustment made to the data at 5,000 feet to correct for this lift loss yields a C_L of 3.60 generated by the CCW. This adjustment brings the wind tunnel and flight data into agreement. This $C_L = 3.60$ is shown in Figure 10 and is also the value used in calculating the percent increase over the standard A-6 performance. On this basis, the value of $C_{L_{max}}$ at $C_\mu = 0.20$ is likely to be about 3.7 which compares to a $C_{L_{max}}$ of about 2.1 for the standard A-6 with a 30 degree flap setting. Further, this $C_{L_{max}}$ is accomplished at an angle of attack of about 17 degrees, whereas the A-6/30 degree flap $C_{L_{max}}$ occurs at an angle of attack of about 22 degrees. As will be shown, the high lift capability of the CCW translates into significant takeoff and landing performance benefits.

For the flight demonstration, the CCW was powered by bleed air from the J52 engine. Engine tests conducted by DTNSRDC at the Naval Air Propulsion Center demonstrated the capability to bleed these engines as much as 16 percent of total airflow, however, the CCW system was designed to use a maximum of 11 percent (37 psig). When bleed air is diverted from the engine, there is a consequent loss in thrust. Also, as this bleed air is used to produce lift in the CCW, it also produces induced drag. Therefore, using 100 percent of the maximum pressure available does not provide the best takeoff performance. A careful examination of the use of bleed air showed that the best overall takeoff performance is achieved somewhere between 50 to 70 percent of the maximum bleed available for a takeoff procedure where the blowing is turned on at the point of rotation (see Figure 12). Furthermore, if blowing is employed from the beginning of the takeoff roll, the thrust loss and induced drag increase serve to significantly penalize performance, and only about 20 percent of the maximum bleed available can be usefully employed for CCW. This was substantiated during the flight demonstration as both procedures were used. Calculations for an A-6

gross weight of 45,000 pounds are presented in Figure 12, however, the trends shown are quite representative for the range of gross weights for the A-6.

Takeoff and landing performance is summarized in Figure 13. In evaluating these performance gains for the A-6/CCW, it is important to consider that neither the flight nor the flight operations were optimized to the extent of demonstrating the full potential of the CCW system. This is particularly true in the area of minimum takeoff and landing performance. The detrimental effect of using spoilers has already been discussed.

A takeoff distance of 700 feet was measured for 60 percent maximum pressure takeoff (Figure 13). However, this distance was enhanced by a head wind and a non-standard day. When adjusted to a standard day with no head wind for comparison purposes, this distance extends to 865 feet. Examining takeoff performance in further detail, a comparison of the A-6 and the A-6/CCW is made in Figure 14. The solid curve shows the standard A-6 takeoff characteristics at a gross weight of 35,700 pounds and is extended below the minimum takeoff distance to indicate performance potential with higher $C_{L_{max}}$ than is now available. Only three measured takeoffs were accomplished in this flight program, therefore the CCW demonstration points shown are not a good representation of CCW performance that could be achieved as standard procedure. That is, the best combination of angle of attack, point of rotation, etc. for a particular amount of blowing has not been established since more flight experience is necessary. These "unoptimized" takeoff procedures result in the CCW demonstration points falling above the 35,700 pound gross weight curve. Flight experience will result in further improvements in takeoff distances at any given takeoff speed. For example, taking off at 60 percent of maximum pressure for blowing can probably be accomplished in a ground roll distance of about 700 feet at 84 knots. This is less than half the distance required for the A-6 normal takeoff.

As anticipated, landing performance showed even greater improvements (Figure 13), this being due in no small part to the increase in drag at the high lift/high power settings experienced. Two landing distances are used in making a performance comparison: (1) a normal landing which is accomplished at a speed 30 percent higher than the aircraft stall speed; and (2) a minimum distance landing where the landing speed is only 20 percent higher than the stall speed. The solid curve in Figure 15 represents the A-6 landing characteristics. The gross weights shown along this curve are based on which landing method is used. The flight test data shown does not fall on the standard A-6 curve probably as a result of the higher power settings and different glide slopes possible for CCW. During the flight program, only one minimum distance landing was accomplished, this being flown at a relatively high approach speed of about 85 knots. Although an 1110 foot distance was achieved, the best approach speed flown was 76 knots (at 75 percent maximum pressure), but with no attempt to control groundroll. This approach speed would probably yield a minimum distance landing of about 900 feet.

A summary of actual STOL performance achieved by the A-6/CCW relative to the standard A-6 is shown in Figure 16. A significant STOL performance has been demonstrated by the CCW system, even when considering the additional degree of attention required for improving the system hardware and increasing flight experience in order to achieve the best performance. In particular, the takeoff

and landing performance can put the A-6 in a near--STOL category (if STO still means 400 feet). And the potential for providing some degree of STOL performance to other conventional takeoff and landing (CTOL) aircraft is clearly indicated. The full benefits of CCW will, of course, be achievable through any new aircraft specifically designed at the outset to incorporate the CCW system.

Experimental values of $C_{L_{max}}$ for the A-6/CCW with an aspect ratio of 5.3 are shown in Figure 17. Extrapolating these values to the 3.5 to 5.0 aspect ratio range and applying them to the conceptualized STOL aircraft yields conclusions similar to those obtained in the USB assessment. Operationally feasible CCW designs were generated for DTNSRDC by the Lockheed California Company, thereby providing credible weights and other useful design information. The mission performance analysis (Figure 18a) shows that the aspect ratio 5 STOL CCW aircraft can barely achieve the 300 nautical mile mission radius within the specified gross weight range, and then only with a wing span greater than about 53 feet. If the aspect ratio is lower (Figure 18b), the 300 nautical mile radius cannot be achieved within the desired specified parameters. A better engine airframe match can be achieved by duct burning and better T/W performance of CCW can be shown (Figures 18c and d) for a lower range of aspect ratios. However, the wing span requirements are still too large for compatibility with an LPH size ship which imposes a limit of 45 feet, although spans on the order of 52 feet are indicated for an aspect ratio 4.25 STOL CCW aircraft.

Overall Assessment Findings

A comparison of circulation lift produced by both CCW and USB is shown in Figure 17. The USB system operates best in a range of C_μ of around 3 and can achieve a circulation lift of about 6, whereas the CCW system operates best in a range of C_μ around 0.3 and can achieve a circulation lift of about 4-1/2.

Either of these high lift devices, as well as CSB and AJF systems, could provide the lift required for a 400 foot takeoff within a desirable range of wing loadings and achieve a 300 nautical mile mission. However, the resulting aircraft wingspans required consistently exceed a 45 foot LPH ship requirement. Therefore, if aircraft are indeed going to be operated from small ships, a better propulsion match and an aerodynamic breakthrough in high lift/cruise enhancement will be in order.

An experimental program has been designed to push for such a breakthrough by evaluating the various combinations of powered lift systems with cruise enhancement devices. The potential result could be the development of a synergistic combination that provides the maximum efficiency needed for the high lift system as well as provides the means for increasing the effective aspect ratio for improved cruise thereby further reducing the weight and wingspan.

POTENTIAL HIGH LIFT/CRUISE ENHANCEMENT DEVICES

The technology for improving cruise performance by devices to increase effective aspect ratio has had considerable attention over the years. The recent development of winglets and wing tip sails by NASA and the Cranfield Institute in England, respectively, have successfully shown attractive benefits in reducing induced drag, and both devices will offer significant cruise performance benefits when fully perfected and applied. The winglets go a step

beyond what an end plate can do by providing a force component in the forward direction. The tip sails have an effect of unwinding the tip vortex, increasing the lift contributed by the outer portion of the wing, thereby making the wing more "2-dimensional". An extension of the tip sail technology has been hypothesized by DTNSRDC by applying the knowledge gained during the considerable effort put into close-coupled canard technology development. The favorable interference generated between the canard and wing can possibly be duplicated in a "close-coupled-cascade" arrangement. The tip sail and close-coupled-cascade devices are shown in Figure 20 as they have been arranged for wind tunnel experiments.

Preliminary work using tip blowing was done at DTNSRDC in conjunction with the X-Wing program. Blowing from the rounded tip shifted the tip vortex core outward and upward which showed the potential for improving cruise performance (Figure 21). This approach has shown enough promise to warrant further pursuit. In addition, the use of blowing on the winglet is of interest. For example, a winglet design that will enhance the high lift performance may very well be different from the winglet designed to enhance cruise performance. The use of blowing potentially offers to bridge the resulting tradeoff gap.

Although the potential improvements in cruise performance have been amply demonstrated, the hypothetical improvements in high lift enhancement have yet to be arranged. The most important challenge will then be to orchestrate the designs resulting from cruise and high lift enhancement into a single device or system that will aerodynamically accomplish both objectives.

EXPERIMENTAL PROGRAM

The experimental program is built around a NASA supercritical wing design which incorporates a double-slotted flap (Figure 22) thereby representing a reasonable baseline of the state-of-the-art in unpowered high lift technology. The wind tunnel model is presently designed for three aspect ratios (3.1, 4.0, 5.2) in order to make a unique evaluation of aspect ratio effects. The model presently accommodates both USB (Figure 23) and CCW systems as well as various tip devices (for example those shown in Figure 20).

Experimental results have thus far focused on the basic high lift performance of the DSF, USB, and CCW systems. Initial wing tip work has been done with an end plate which is shown in Figure 23.

Double-Slotted Flap

Typical DSF performance on aspect ratio 3 and 4 wings is shown in Figure 24. A $C_{L_{max}}$ of nearly 2.4 at a flap setting of 60 degrees is achieved at about 26 degrees angle of attack on the aspect ratio 4 wing. Reducing the wing aspect ratio to 3 reduces the achievable $C_{L_{max}}$ to about 2.2. A 40 degree flap setting could only produce a $C_{L_{max}}$ of 2.1 and 1.9 for aspect ratio 4 and 3 wings, respectively (not shown).

Upper Surface Blowing

The USB model accommodates nozzle aspect ratios of 2, 4 and 6. Not surprisingly, the aspect ratio 6 nozzle has given the best lift performance

since the exhaust jet encompasses most of the flap system. However, the practicality of such an arrangement for a low aspect ratio wing is questionable. At this point in time, our limited air supply has precluded the USB model from being operated beyond a C_μ of about 1.5. The Tech Development fan being used will operate at a much higher capacity and arrangements are being made to increase C_μ to at least 3.0, which will be adequate for this evaluation. At this moderate value of C_μ, USB produced a C_L of 2.8 for the aspect ratio 3 wing/aspect ratio 6 nozzle and did somewhat better with a C_L of 3.3 for the aspect ratio 4 wing/aspect ratio 6 nozzle (Figure 25). The data shown in this figure are for the USB model with a tip fence installed (Figure 23) since it appeared that considerable flow separation was occurring over the outboard portion of the wing. There was some indication that this tip fence arrangement may offer improved high lift capability at higher values of C_μ than were used, however the lift gains were insignificant at C_μ up to 1.5. Furthermore, there will be some exhaust jet impingement on the tip fence at the high nozzle aspect ratio/low wing aspect ratio combination which may serve to counteract any gains achieved. It is certain that flow improvements are necessary, however, it is anticipated that these flow improvements will be better accomplished with some of the other tip devices. The experiments conducted so far have not simulated a double-slotted flap outboard of the exhaust jet (the configuration employed by the YC-14). This is easily accomplished and will be done in the near future. This arrangement promises to show some lift gains, particularly for the lower aspect ratio nozzles.

Circulation Control Wing

The CCW configuration represents a first attempt at a low aspect ratio (below 5) application in an otherwise extensive technology development program involving both rotary and fixed wing aircraft. Where a $C_{L_{max}}$ of 3.9 at a C_μ of 0.3 was achieved experimentally with an installation on the aspect ratio 5.3 A-6 wing, the effect of reducing aspect ratio is significant (see Figure 26). A $C_{L_{max}}$ of only 3.0 was initially reached on the aspect ratio 4 wing which is only a moderate increase over the $C_{L_{max}}$ of 2.4 of the 60 degree DSF. A further reduction in aspect ratio to 3 resulted in a further reduction in $C_{L_{max}}$ to barely over 2.6 which approaches the 60 degree DSF value of 2.2. Furthermore, where increased C_μ tended to increase $C_{L_{max}}$ at least up to $C_\mu = 0.3$ for the aspect ratio 5.3 wing, best $C_{L_{max}}$ was reached at a C_μ near 0.18 for the lower aspect ratio wings.

In examining the flow around the wing, it was found that considerable flow separation was being induced over the outboard portion of the wing caused by the effective flow discontinuity occurring between the region of strong circulation over the wing and the flow at the tip. The installation of an end plate ("tip fence") offered to resolve most of this problem and an increment of 0.4 was restored to $C_{L_{max}}$ generating more competitive values of 3.4 and 3.0 for respective aspect ratios of 4 and 3. It is evident that further work is still required to fully restore the flow and, as in the case of USB, various tip devices will be used to accomplish this purpose.

CONCLUDING REMARKS

The desire to operate fixed wing aircraft from small ships poses many delemmas. A real challenge lies in trying to create an aircraft for such shipboard operations and yet still perform meaningful missions. The requirements for a small wing span for physical fit and for high speed flight conflicts directly with the requirements for adequate (if not excellent) short takeoff and landing ability and for efficient cruise flight -- whether the aircraft is VSTOL, STOVAL, or STOL (or even CTOL).

This effort addresses a critical need to fully exploit both high lift and improved cruise technology for use on low aspect ratio wing aircraft that can fulfill the above requirements. Although the new technology powered high lift systems offer excellent short takeoff and landing capability, they all are seen to lose their effectiveness when applied to a short wing span. However, the employment of appropriately designed tip devices offers the potential of not only improving cruise performance but also restoring much of the high lift capability. The experimental program is being enthusiastically pursued to this end.

In the mean time, a new technology has been developed that offers another option in producing high lift. The Circulation Control Wing concept is now a reality. An extensive technology program has been pursued by DTNSRDC and proven in flight by Grumman on their A-6 aircraft. CCW offers a finesse approach rather than a brute force approach and can be accomplished with the same level of complexity (or simplicity) as state-of-the-art systems in use, as evaluations by Grumman and Lockheed have shown. CCW is certainly not a panacea, but it has earned an important and permanent place on the high lift aerodynamics shelf for serious consideration in achieving a short takeoff and landing performance capability. The potential for CCW as a maneuvering device has yet to be developed but the potential as such is becoming recognized.

The high lift business can best be put in perspective by viewing Figure 27. At the aspect ratios under consideration, some current aircraft can operate in the $C_{L_{max}}$ range of 1.0 to 1.5. Some advanced aircraft concepts show the potential for operating in a much higher range around 2.0, although this is still far short of what is theoretically attainable. However, based on the experimental data generated so far, powered lift systems seem to overcome that which the conventional systems cannot. And there is no good reason they cannot be encouraged to exceed even the limits imposed for theory for conventional systems as long as they get a little help.

REFERENCES

1. Englar, R.J., "STOL – The Potential of the Circulation Control Wing Concept,"
Naval Engineer's Journal, April 1979

MECHANICAL

SLOTTED

ROTATING CYLINDER

CALDERON FLAP

INTERNALLY BLOWN

BLOWN FLAP

CIRCULATION CONTROL

JET FLAP

AUGMENTED JET FLAP

EXTERNALLY BLOWN

UPPER SURFACE BLOWING

EXTERNALLY BLOWN FLAP

COMBINED SURFACE BLOWING
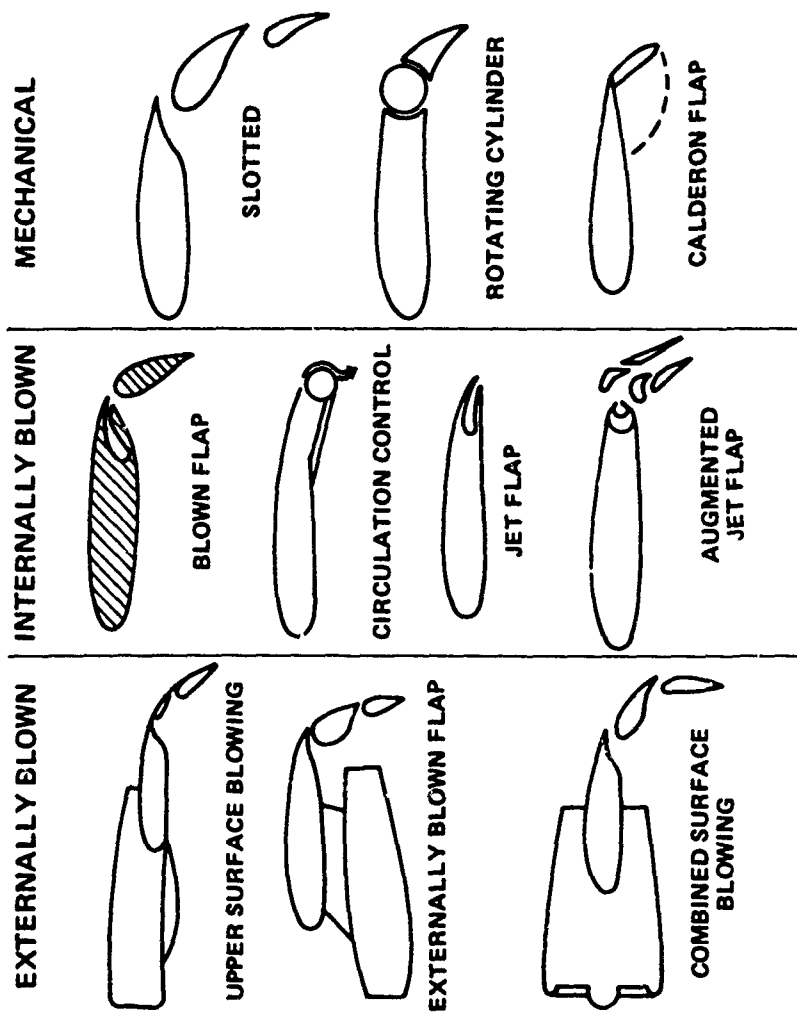
Figure 1 – HIGH LIFT AERODYNAMICS
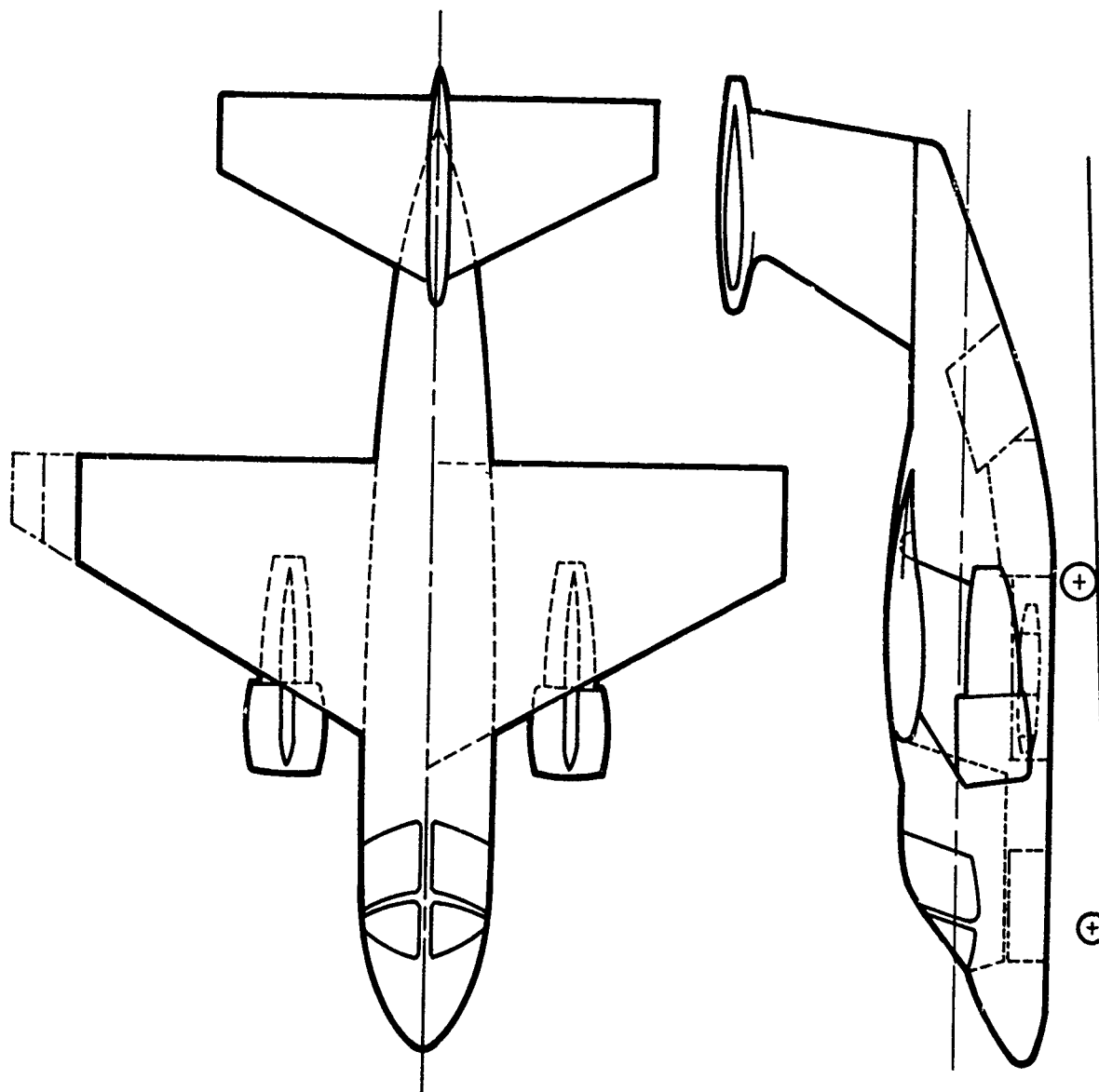
FUSELAGE:
LENGTH = 47.1 FT
MAX WIDTH = 6.80 FT
MAX HEIGHT = 8.55 FT
WING:
$\mathcal{R}$ = 3.5, 4.25, 5.0
C_t/C_r = 0.35
$A_c/4$ = 22°
AIRFOIL—14% SUPERCRITICAL
PROPULSION:
2-SCALED BPR = 6.2 TURBOFANS

FIGURE 2 - Conceptual baseline STOL aircraft
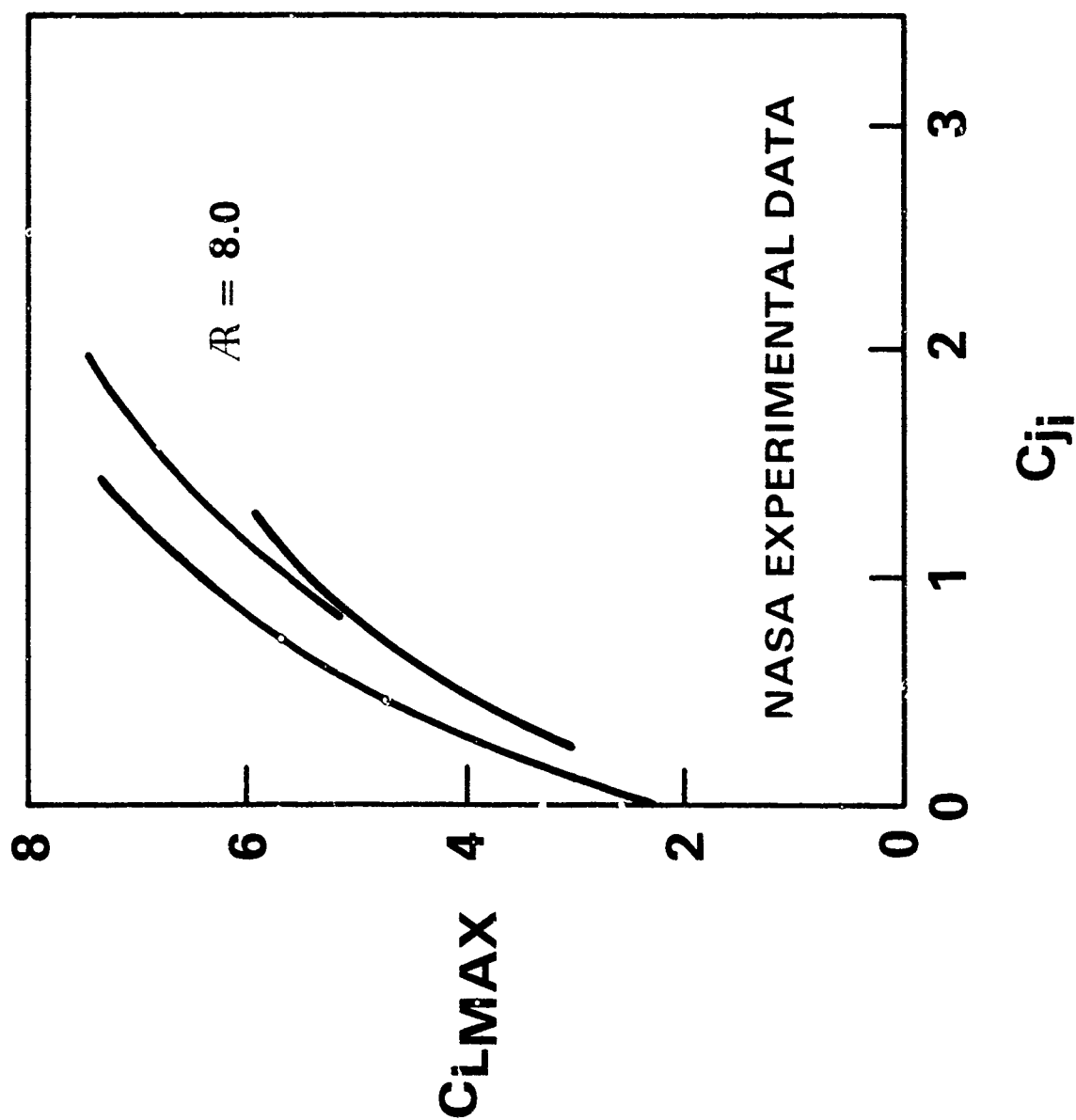
FIGURE 3 – Maximum lift of augmented jet flap
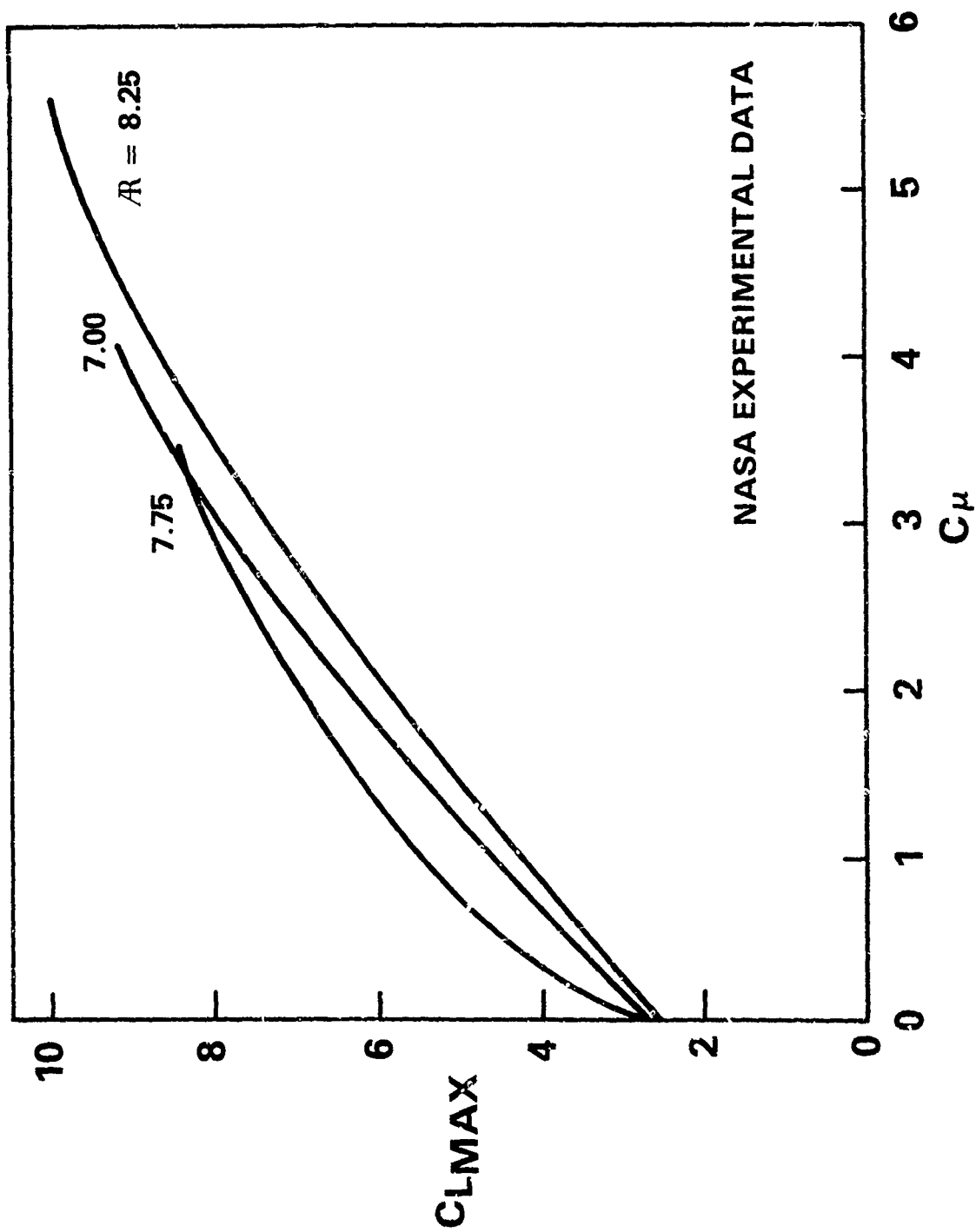
FIGURE 4 - Maximum lift of externally blown flap
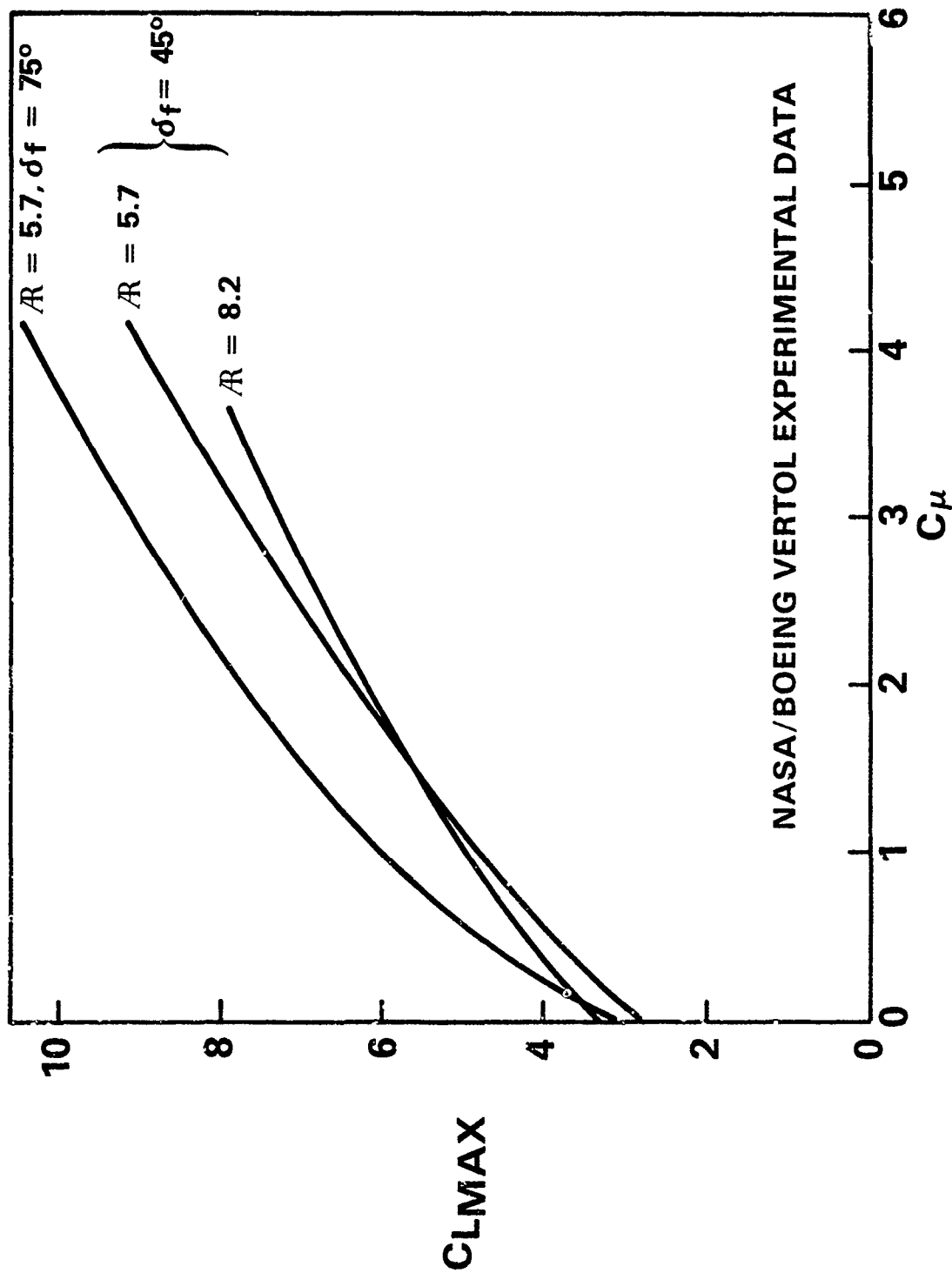
FIGURE 5 – Maximum lift of combined surface blowing
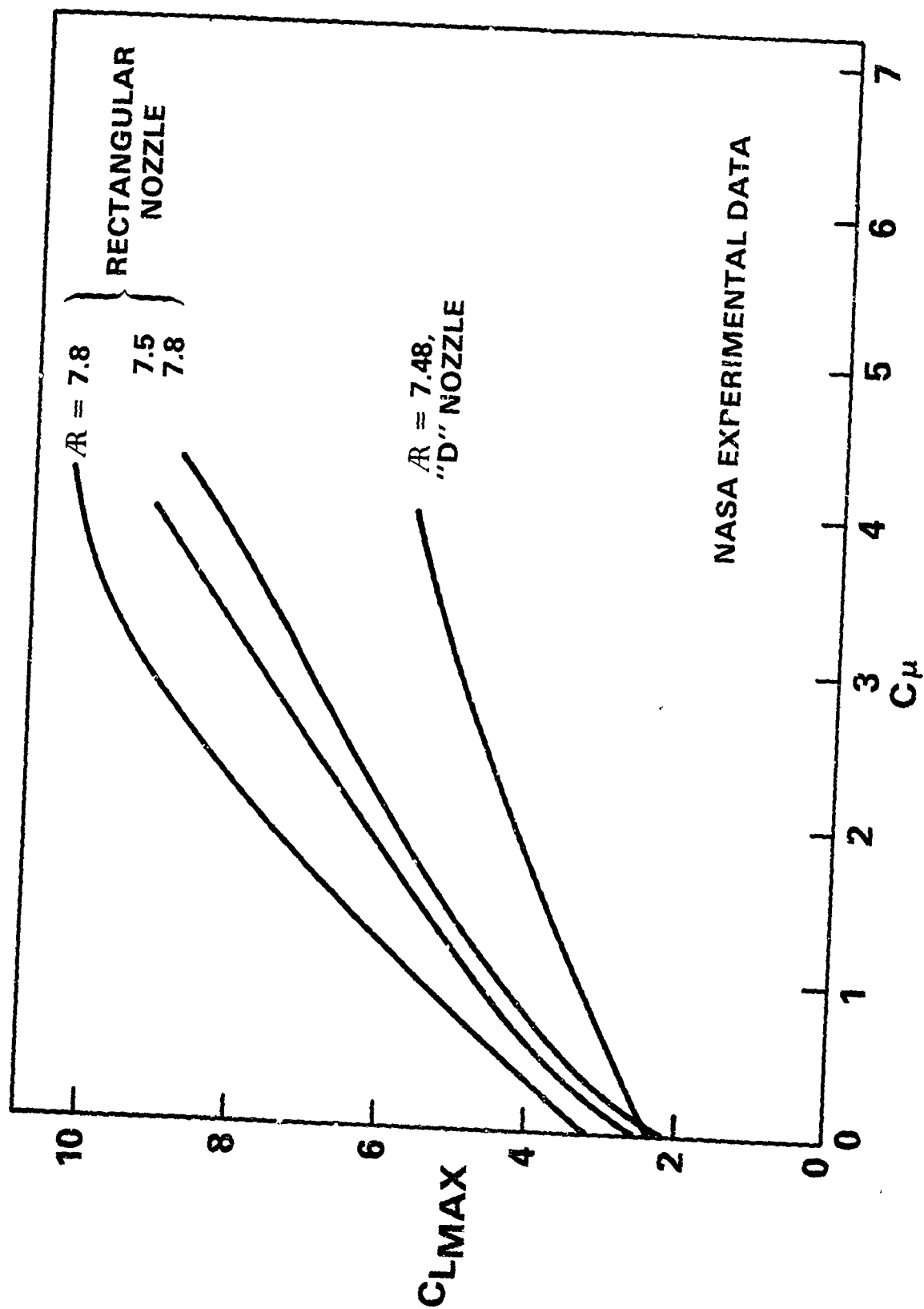
FIGURE 6 – Maximum lift of upper surface blowing
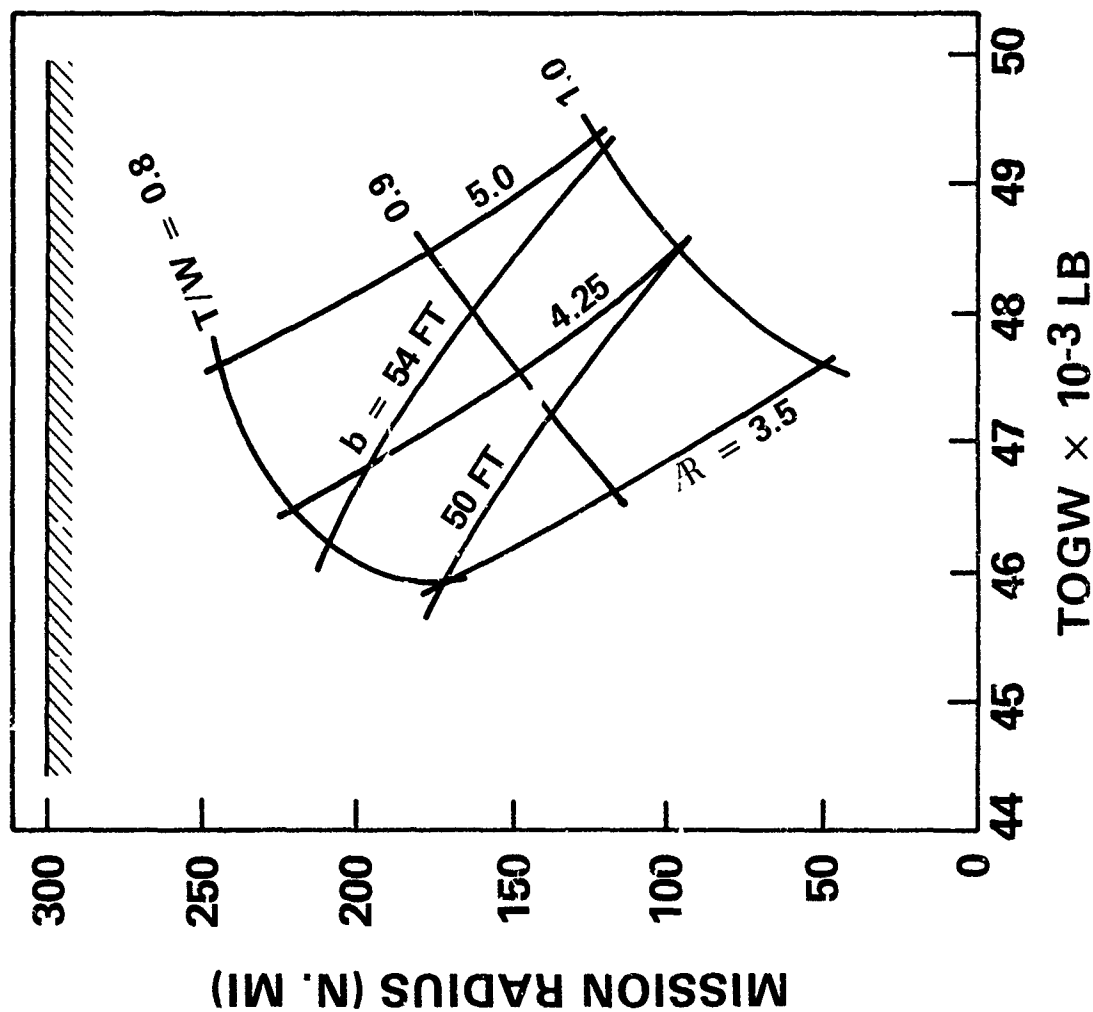
FIGURE 7 – Mission performance parameters for low aspect ratio wing STOL USB aircraft
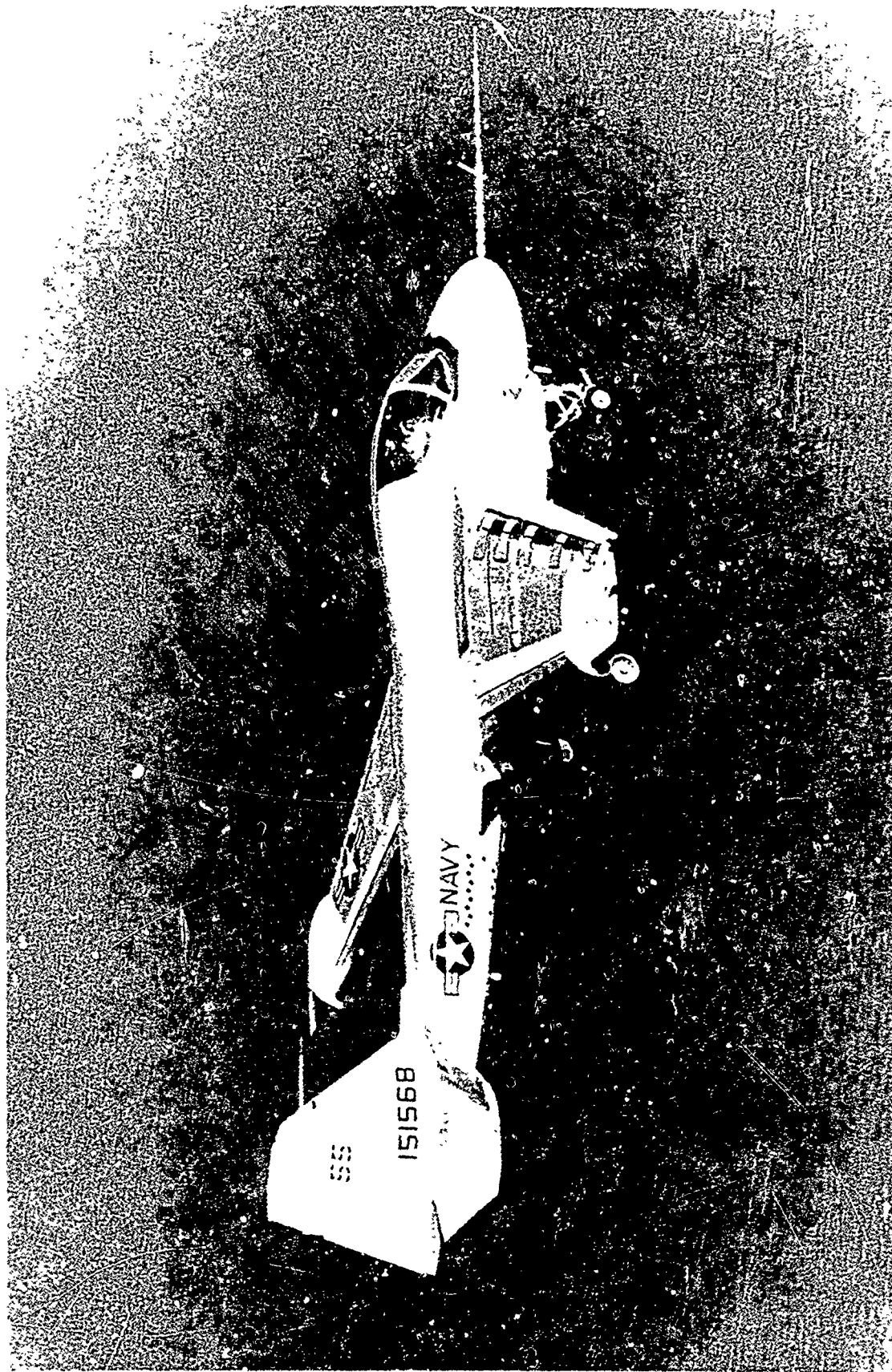
Figure 8 - A-6/CCW flight demonstration aircraft

FIGURE 9 - **CCW AIRFRAME CHANGES**

STABILIZER

ADD 40% CHORD

REINDEXING OF STABILIZER

ADD FIXED L.E.

ADD FLOW FENCE

BLEED AIR SYSTEM

ADD BLEED AIR SYSTEM CONTROLS

ADD FIXED KRUEGER L.E. FLAP

ADD BLEED AIR SYSTEM

ADD COANDA T.E.

SLAT FIXED AT 25°

INCR. RADIUS

WING
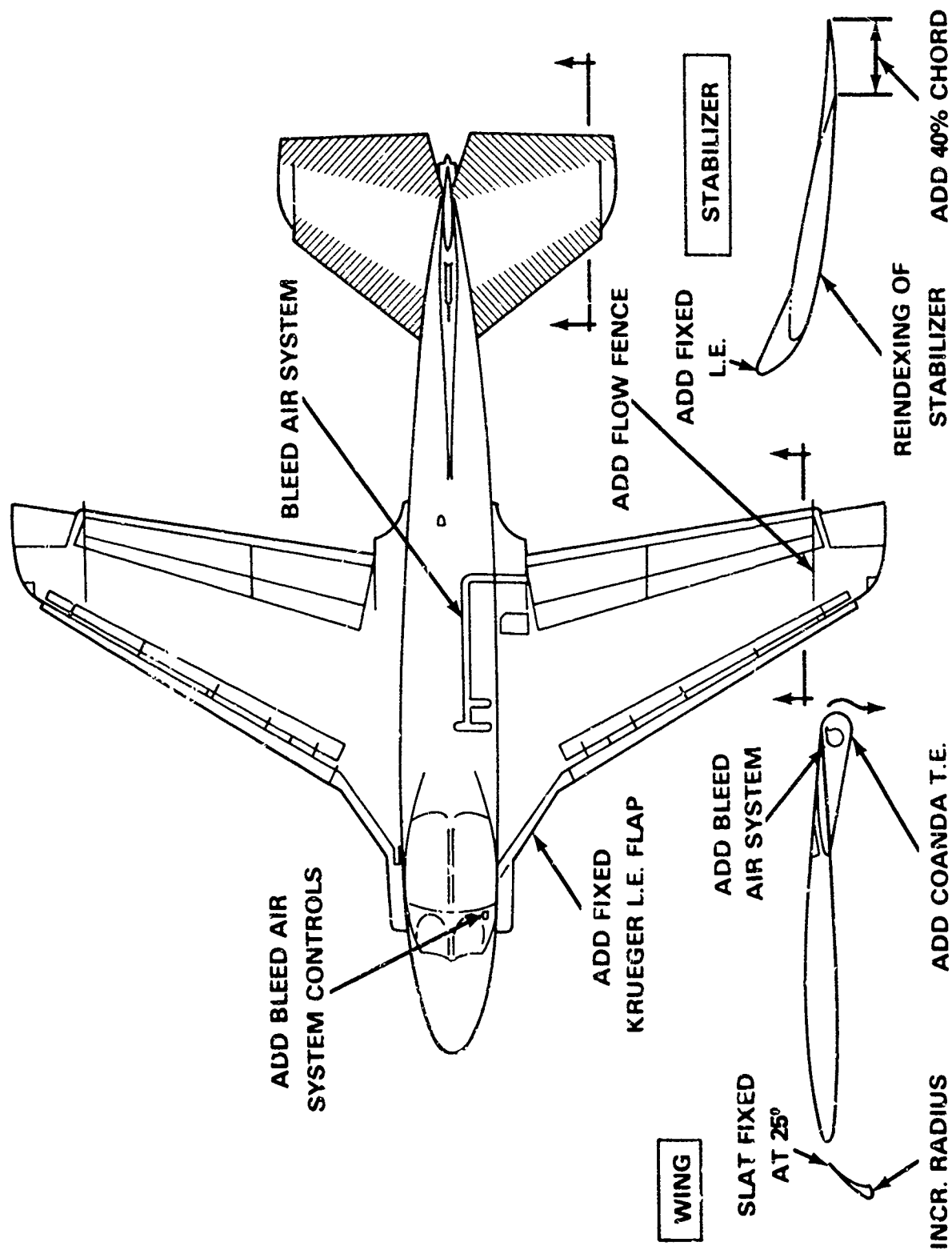
FIGURE 10- A-6/CCW

DEMONSTRATED LIFT PERFORMANCE

ALTITUDE	POWER* SETTING	PRESSURE RATIO	ANGLE OF ATTACK	C_μ	$C_{L_{AERO}}$	INDICATED V, KTS.
15000	PLF	1.0	29.4°	0	1.92	99
15000	MT	4.4	8.9°	.093	2.23	101
12000	MT	4.6	16.0°	.145	2.92	85
10000	PLF	4.5	16.9°	.15	2.91	76
5000	MT	3.7	16.0°	.20	3.34	67
					(3.60**)	

* MT = Military Thrust

  PLF = Power For Level Flight

** Corrected for Flaperon Input

79:3

FIGURE 11 -   A-6/CCW TRIMMED LIFT CURVES
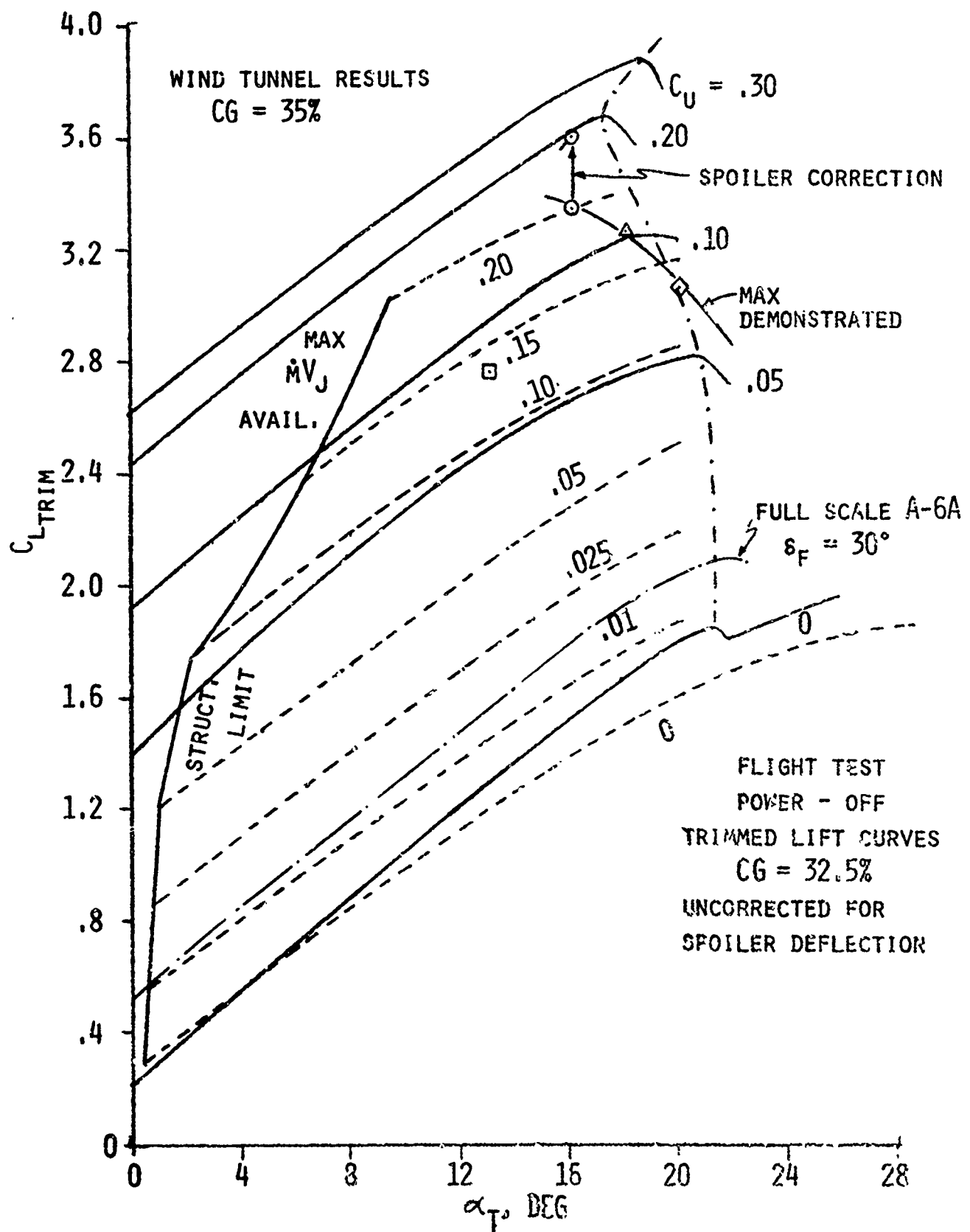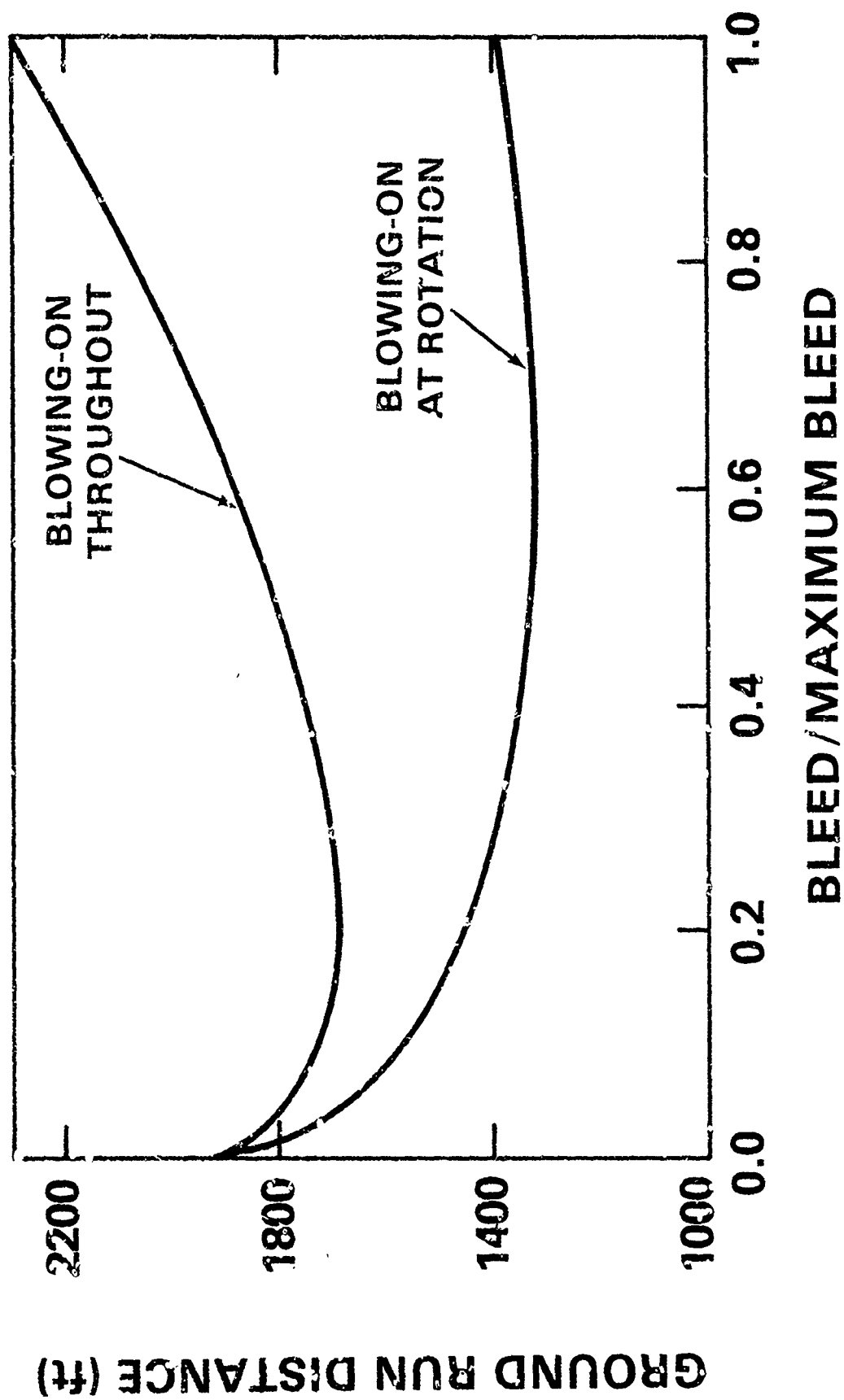
FIGURE 12 – Effect of engine bleed on takeoff performance

FIGURE 13 - A-6/CCW

DEMONSTRATED LANDING & TAKEOFF PERFORMANCE

APPROACH, 3° GLIDE SLOPE, W = 33000 LB.

STANDARD A-6 :   V = 118 KTS.

CCW :   V = 76 KTS. AT 75% MAX. PRESSURE $(C_L = 2.78)$

LANDINGS

STANDARD A-6:   MIN. LANDING DIST. = 2250', V_{APP} = 111 KTS.

CCW, 76% MAX. PRESSURE,   DIST. = 1110', V_{APP} = 85 KTS. $(C_L = 2.58)$

TAKEOFF, W = 35700 LB.

STANDARD A-6, δ_F = 30° : NORMAL TAKEOFF DIST. = 1500', $V_{LIFTOFF}$ = 120 KT.

MIN.   TAKEOFF DIST. = 1160', $V_{LIFTOFF}$ = 105 KT.

CCW :	% MAX. PRESSURE	TAKEOFF DISTANCE, FT.	$V_{LIFTOFF}$, KT.
	20	1090	102
	40	900	88
	60,	700 (865)	84

FIGURE 14 - A-6/CCW TAKEOFF DISTANCE AND SPEED

GW = 35,700 LB.

SEA LEVEL, STD. DAY
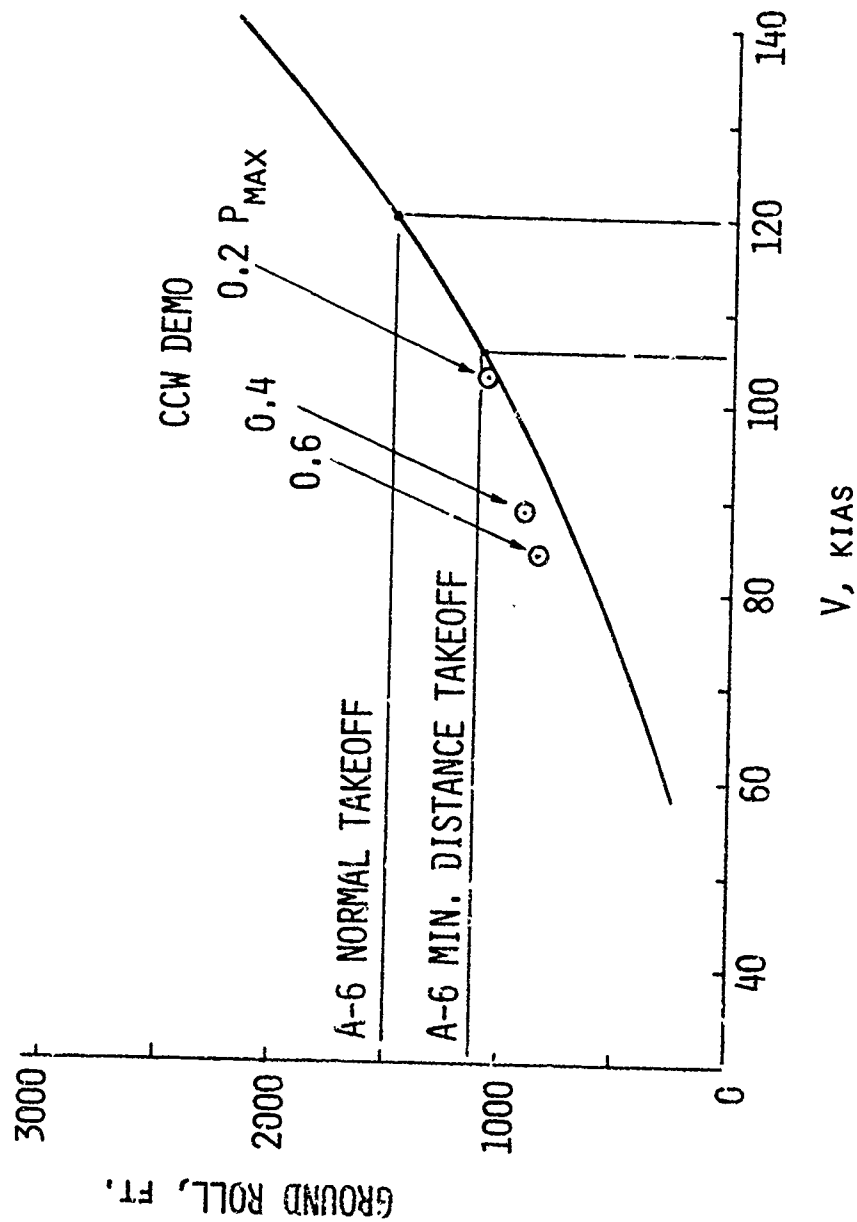
FIGURE 15 - A-6/CCW LANDING DISTANCE AND SPEED

SEA LEVEL
STANDARD DAY
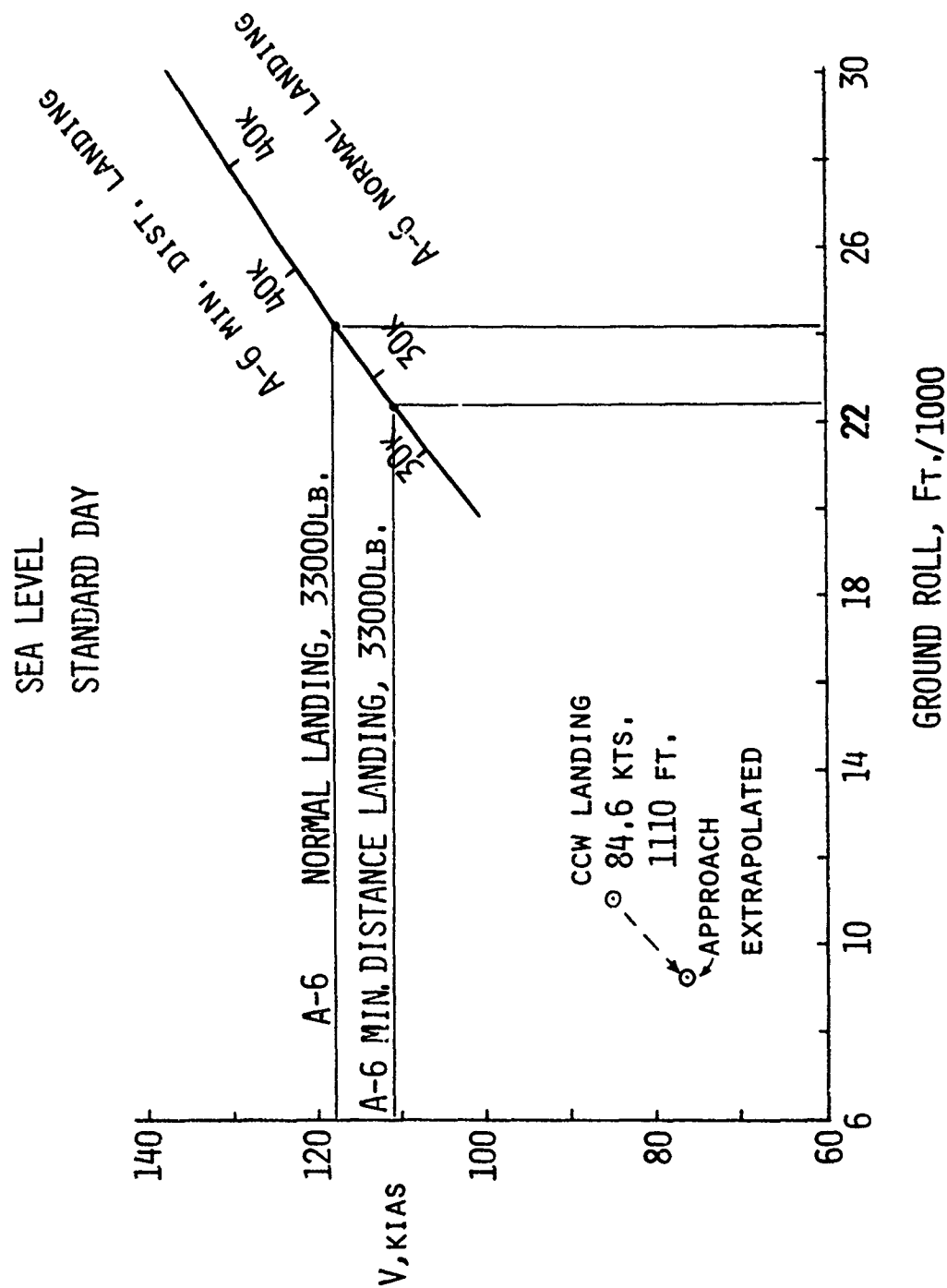
FIGURE 16 - A-6/CCW

STOL PERFORMANCE SUMMARY

	GOAL	DEMONSTRATED
INCREASE IN CONVENTIONAL A-6 $C_{L_{MAX}}$	81% (C_L = 3.8 AT C_μ = .27)	71% (C_L = 3.6 AT C_μ = .20)
REDUCTION IN POWER - ON APPROACH SPEED	30%	32%/36% *
REDUCTION IN LIFTOFF SPEED	14%	20%/30%
REDUCTION IN LANDING GROUND ROLL	50%	51%/54%
REDUCTION IN TAKEOFF GROUND ROLL	22%	25%/42%

*MIN. DISTANCE EFFORT/NORMAL EFFORT
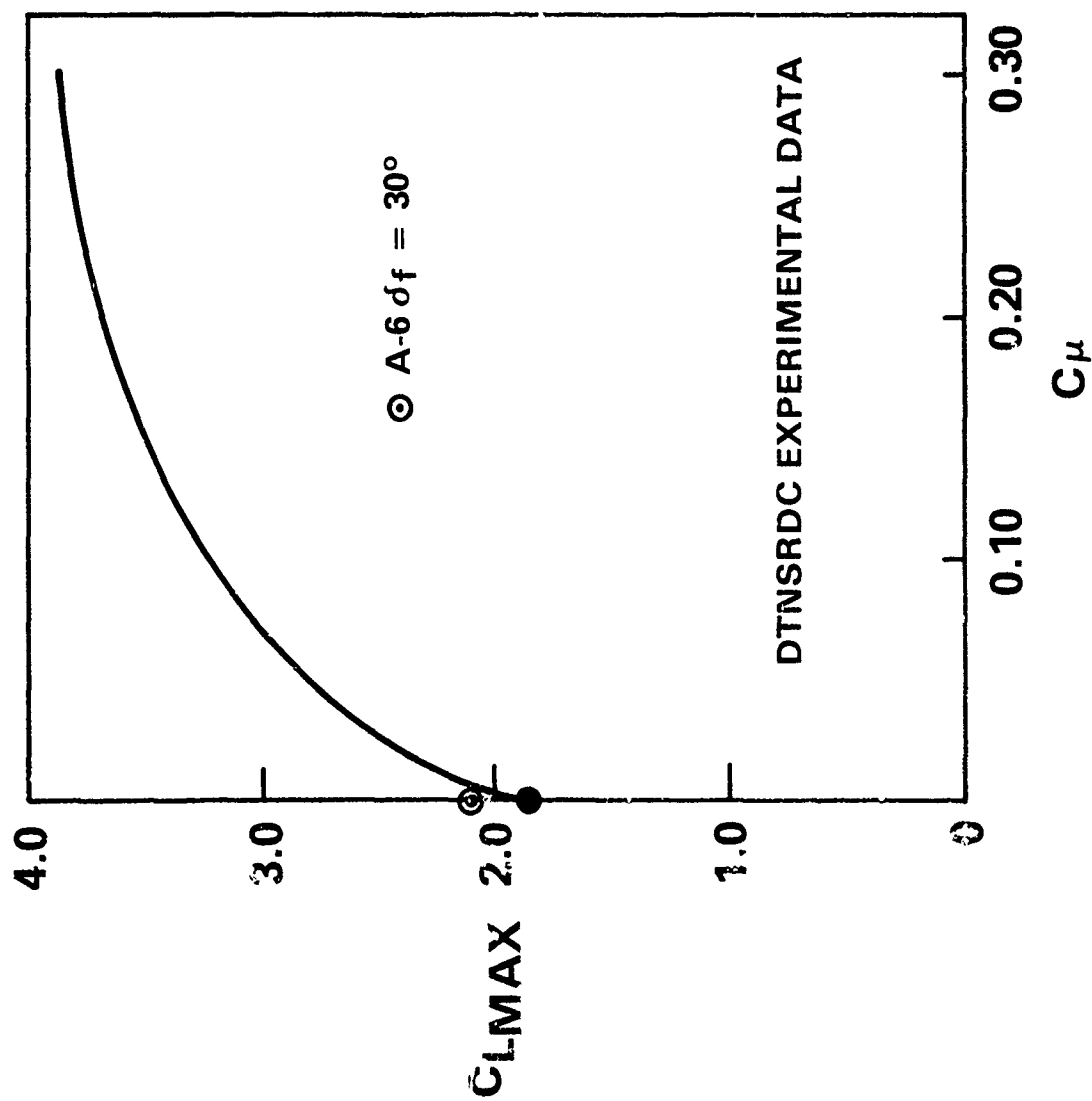
FIGURE 17 – Maximum lift of circulation control wing on A-6
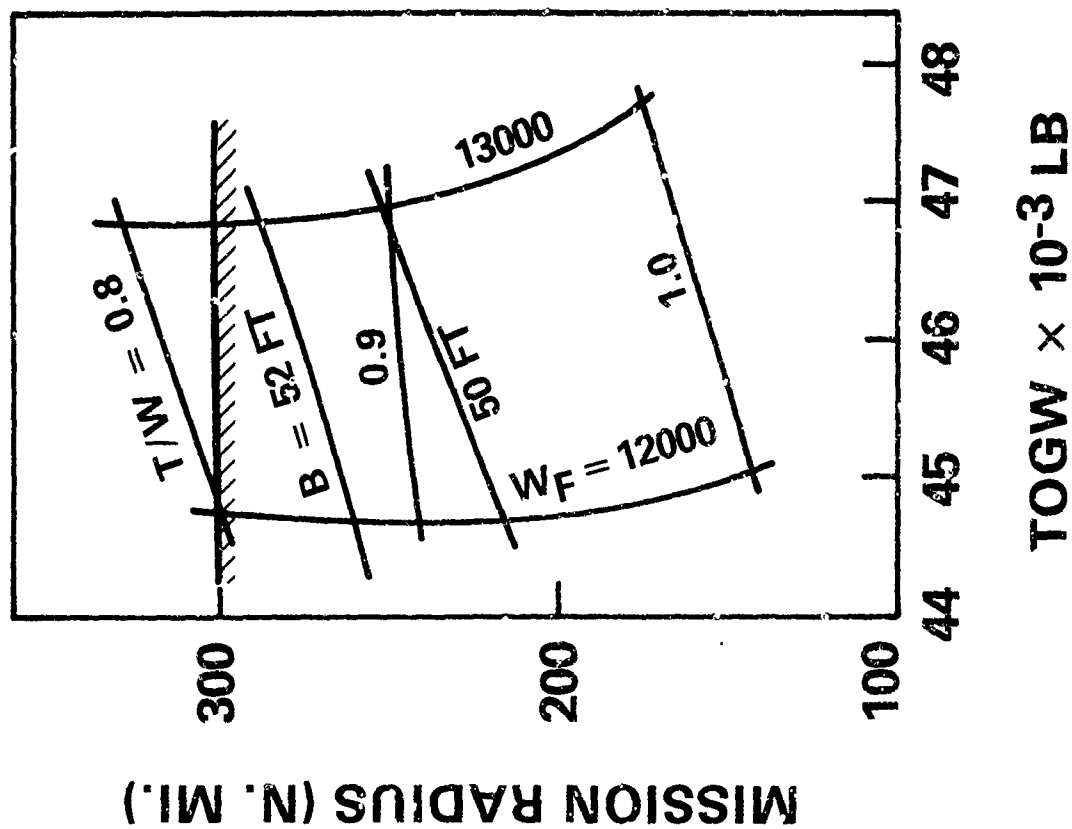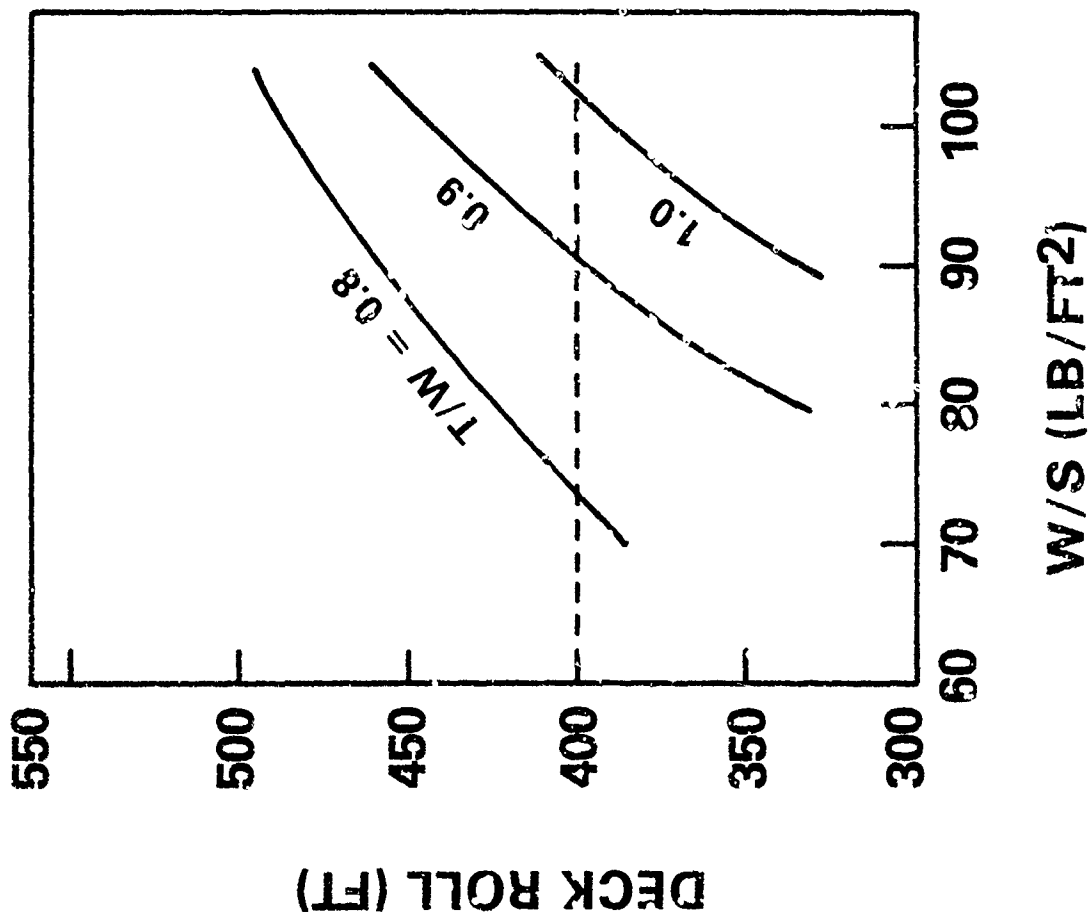
FIGURE. 18a – W/S, T/W, and wing span requirements for $R = 5.0$ STOL CCW

FIGURE 18B — W/S, T/W, and wing span requirements for
$\mathcal{R} = 4.25$ STOL CCW

807
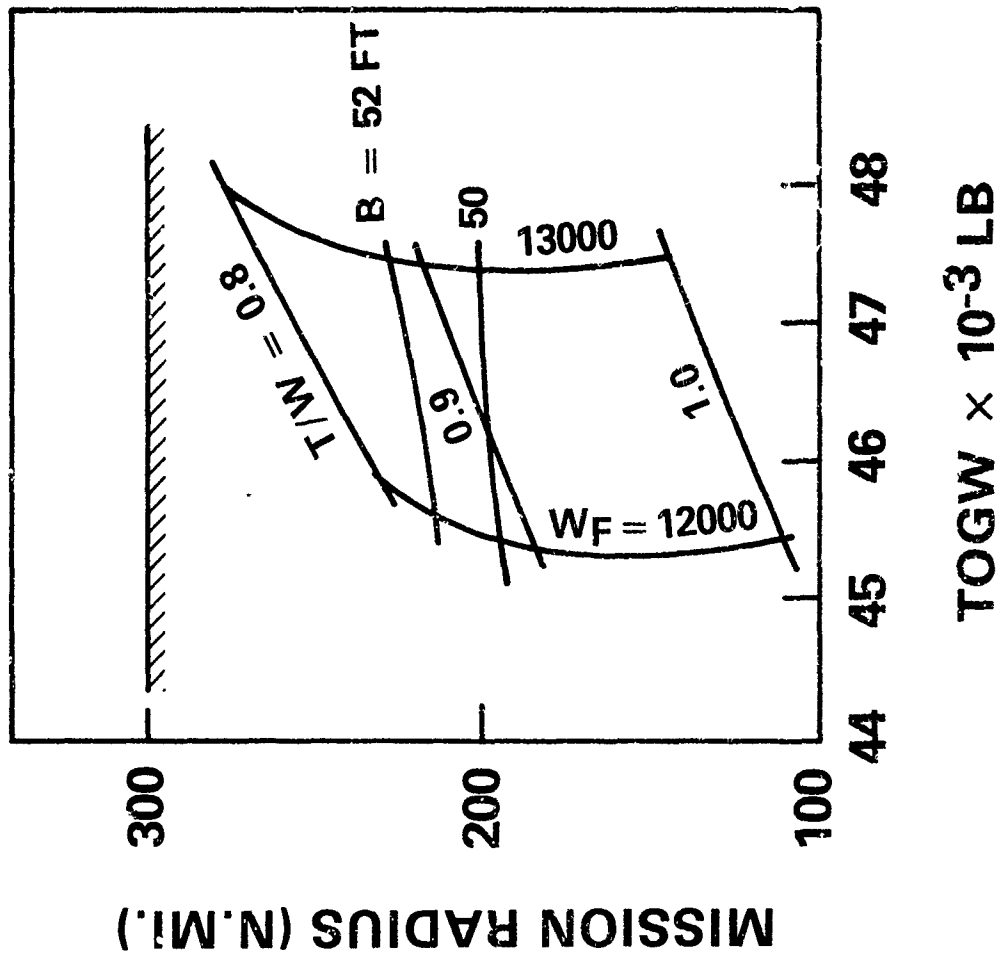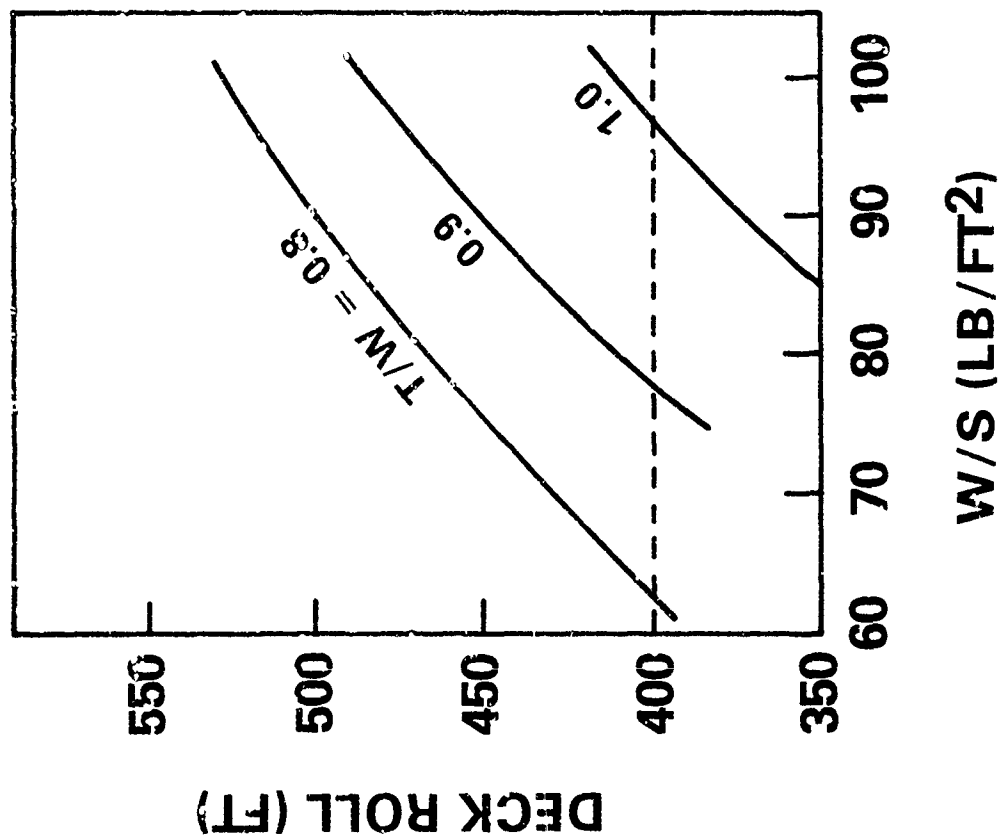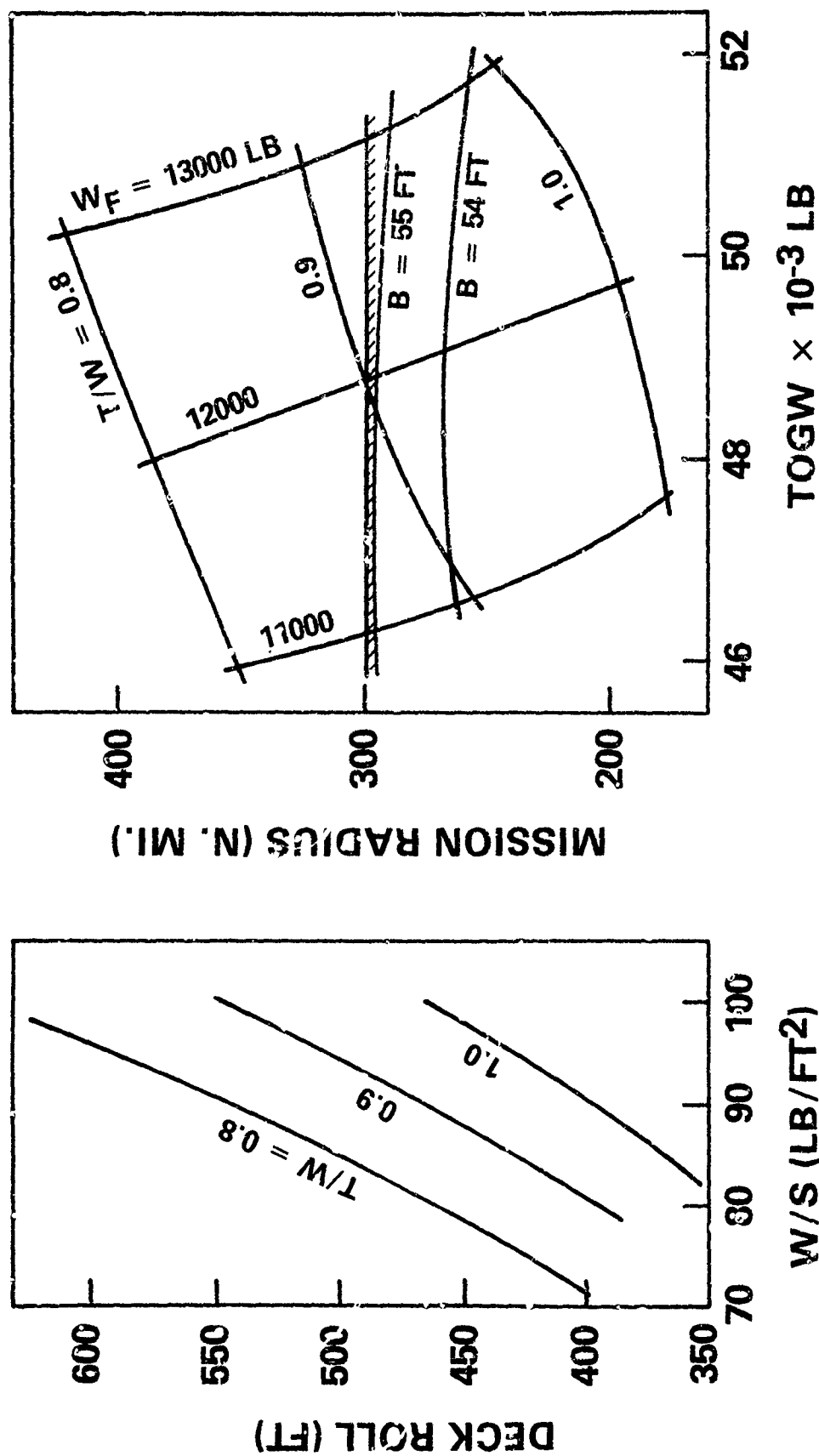
FIGURE 18c - W/S, T/W, and wing span requirements for
ÆR = 5.0 STOL CCW 50% duct burning
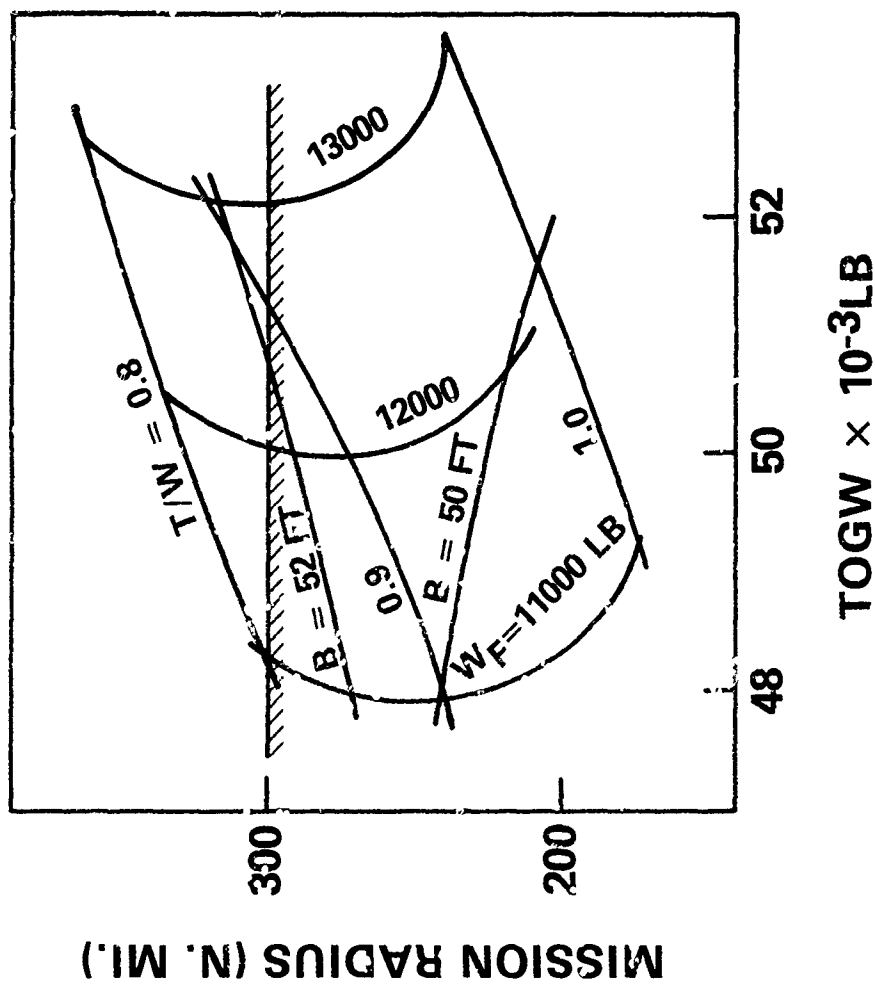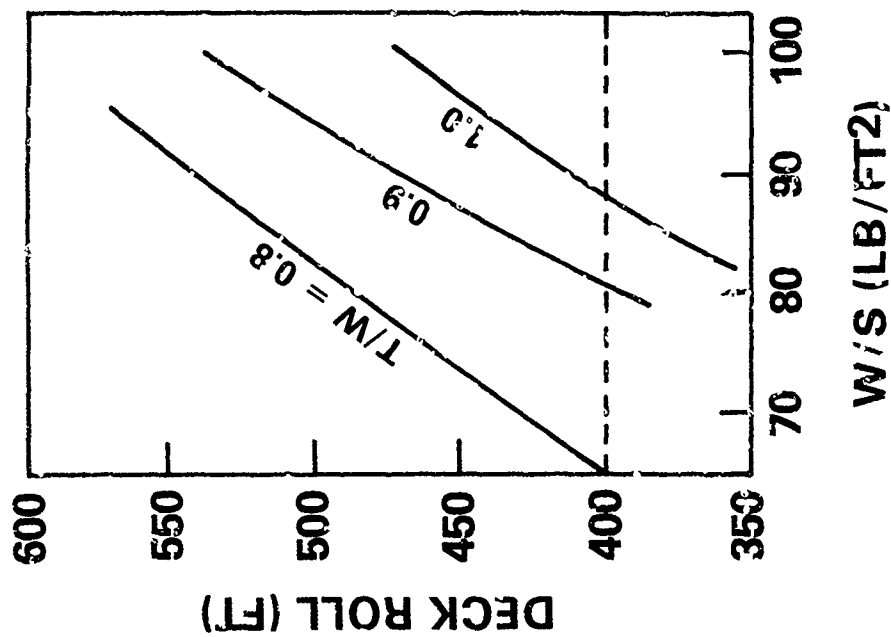
FIGURE 18b – W/S, T/W, and wing span requirements for
$R = 4.25$ STOL CCW 50% duct burning
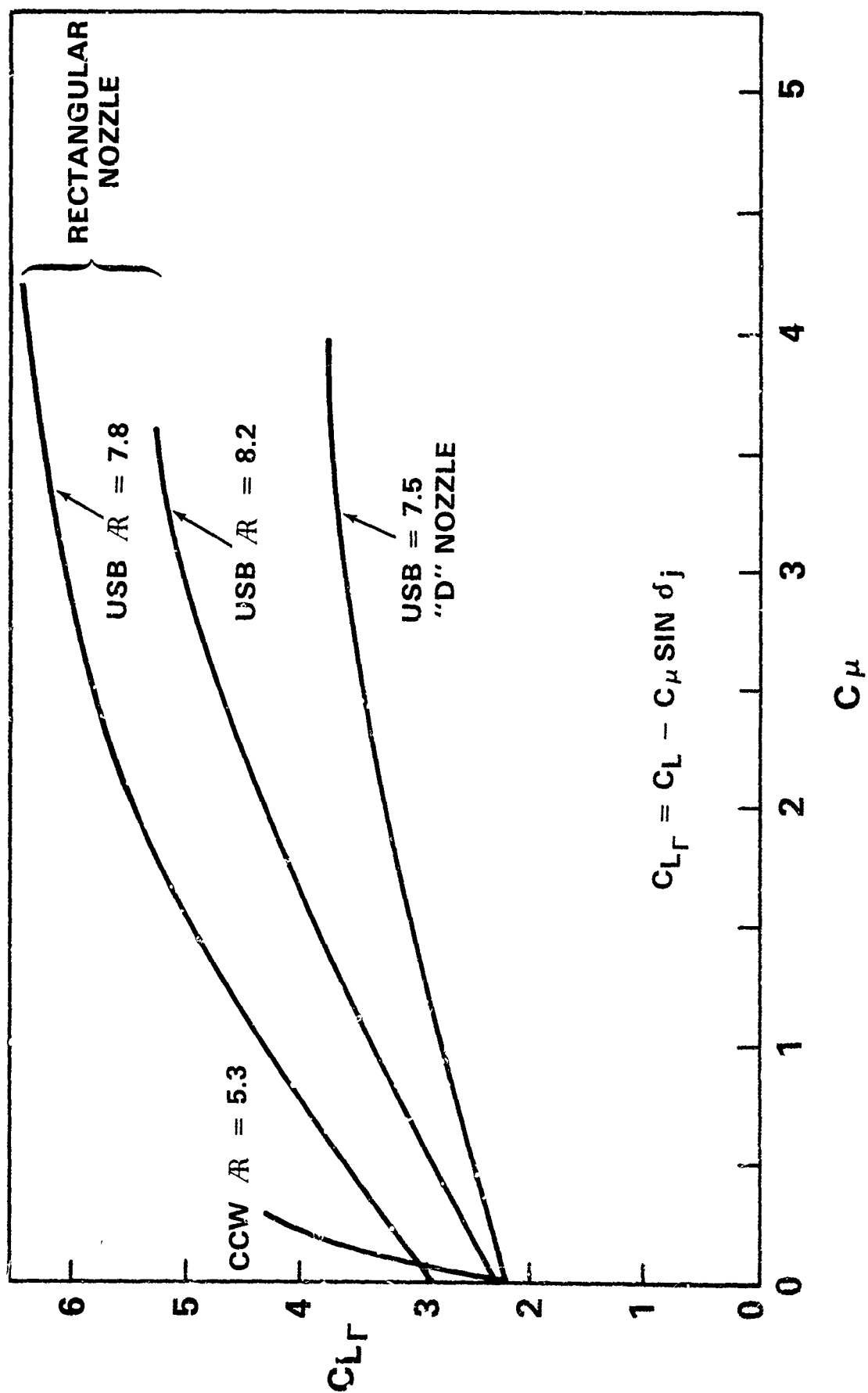
FIGURE 19 – Circulation lift comparison USB and CCW
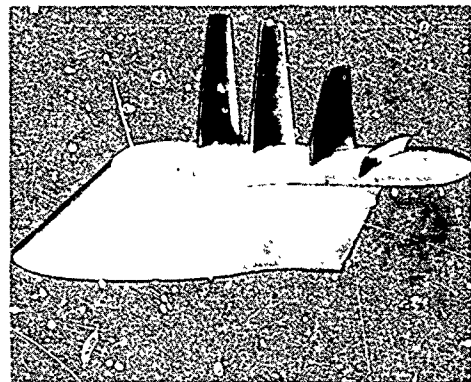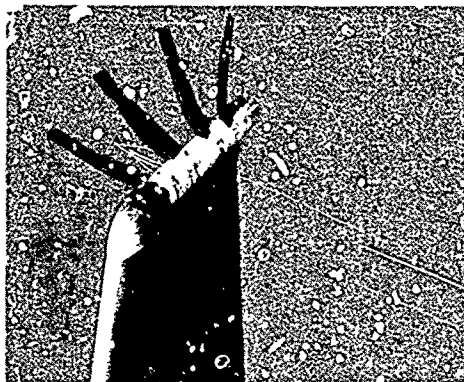
TIP SAILS
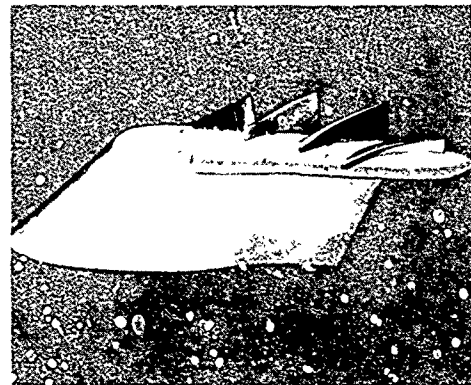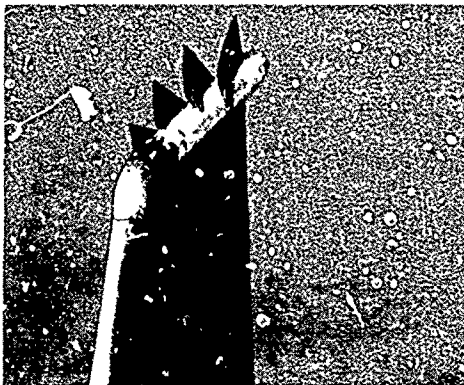
CLOSE-COUPLED CASCADE

Figure 20 — WING TIP HIGH LIFT/CRUISE ENHANCEMENT DEVICES
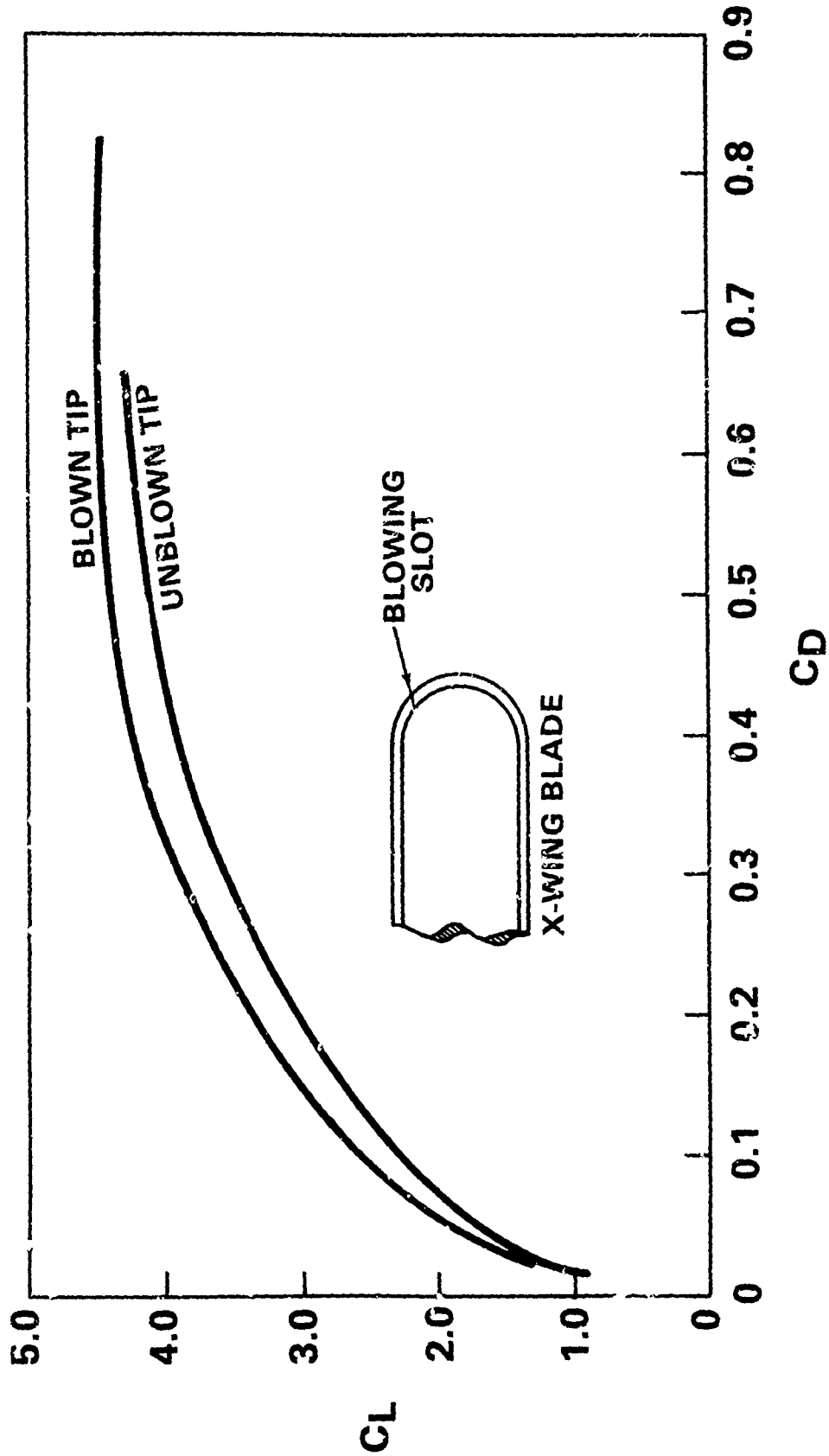
FIGURE 21 – Cruise performance improvement potential from tip blowing

δ_{f_2} (deg)	δ_{f_1} (deg)	GAP$_1$	GAP$_2$	OVERLAP$_1$	OVERLAP$_2$
40	9.8	0.012C	0.012C	0.021C	0.042C
60	10.4	0.020C	0.020C	0	0
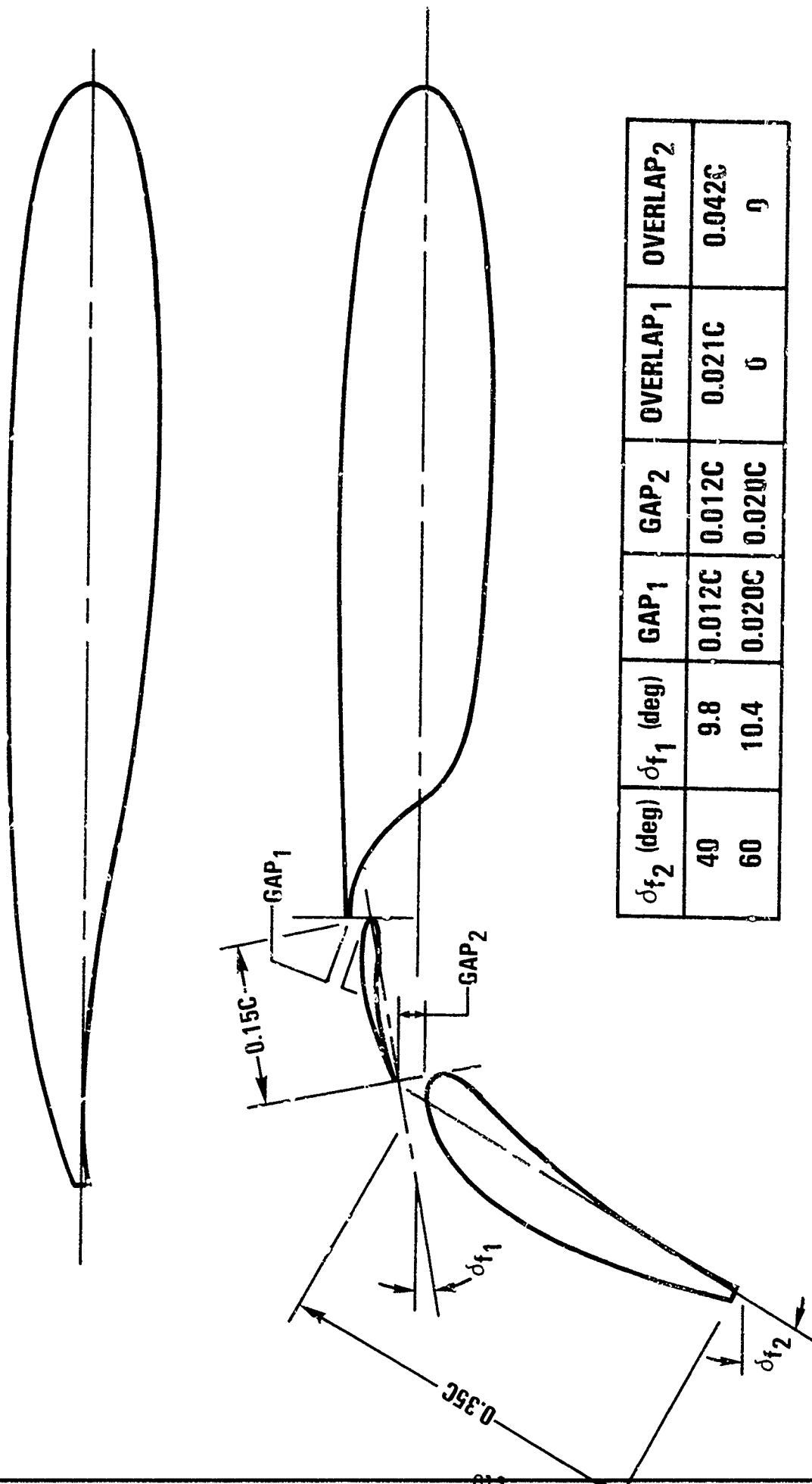
FIGURE 22 – Double slotted flap assembly
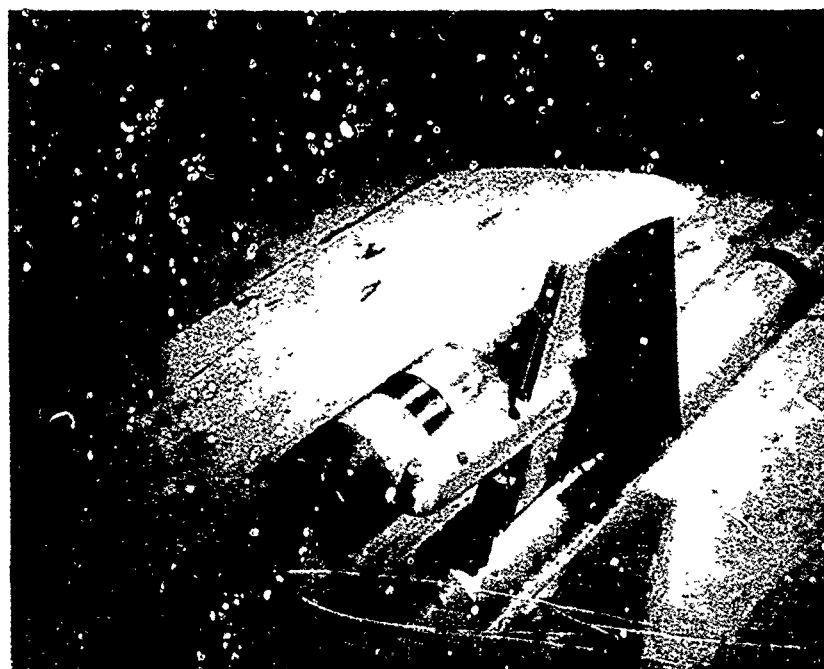
Figure 23 – TIP FENCE INSTALLATION
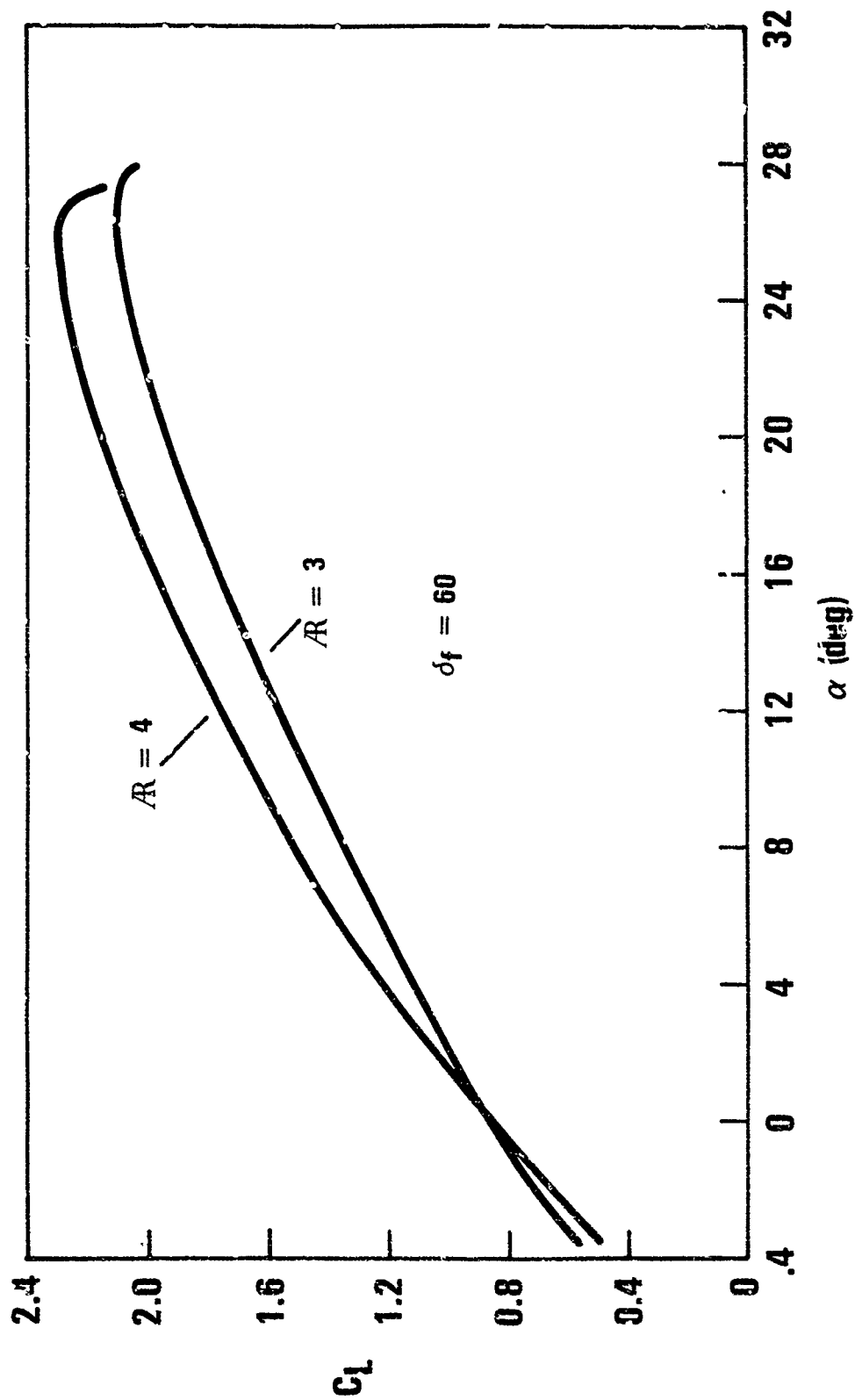
FIGURE 24 - Double slotted flaps
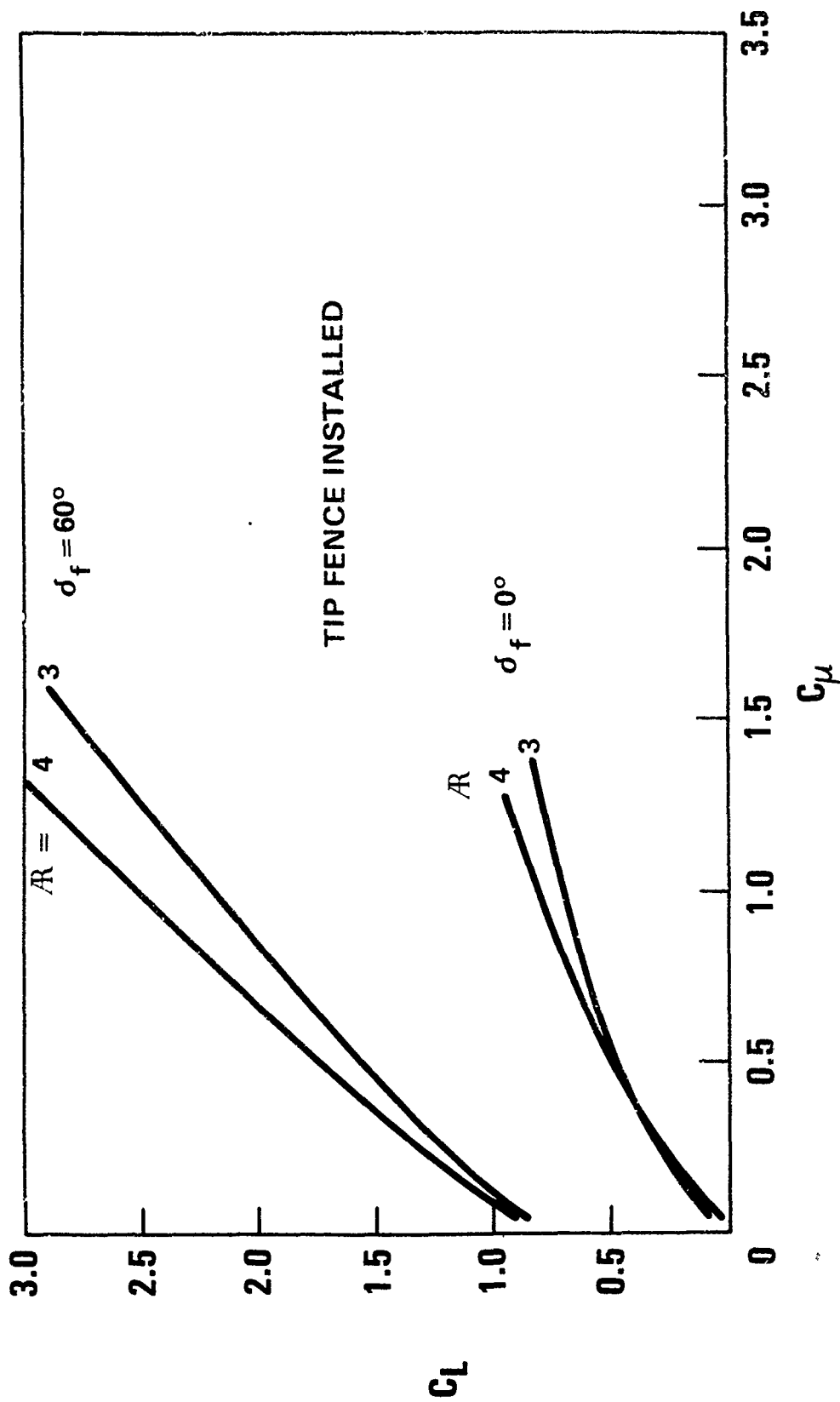
FIGURE 25 – Lift curve for upper surface blowing model
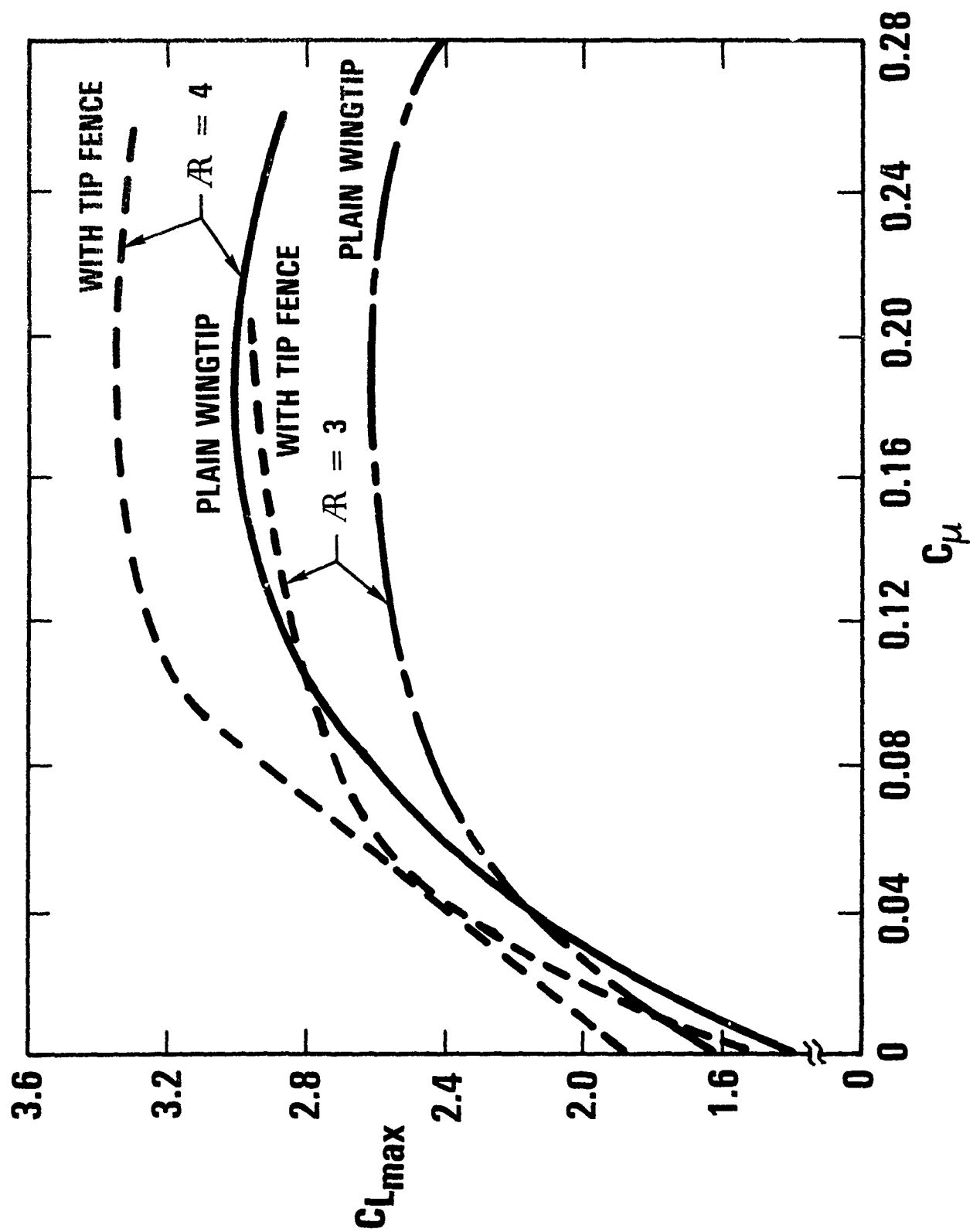
FIGURE 26 – Tip fence effect on circulation control wings
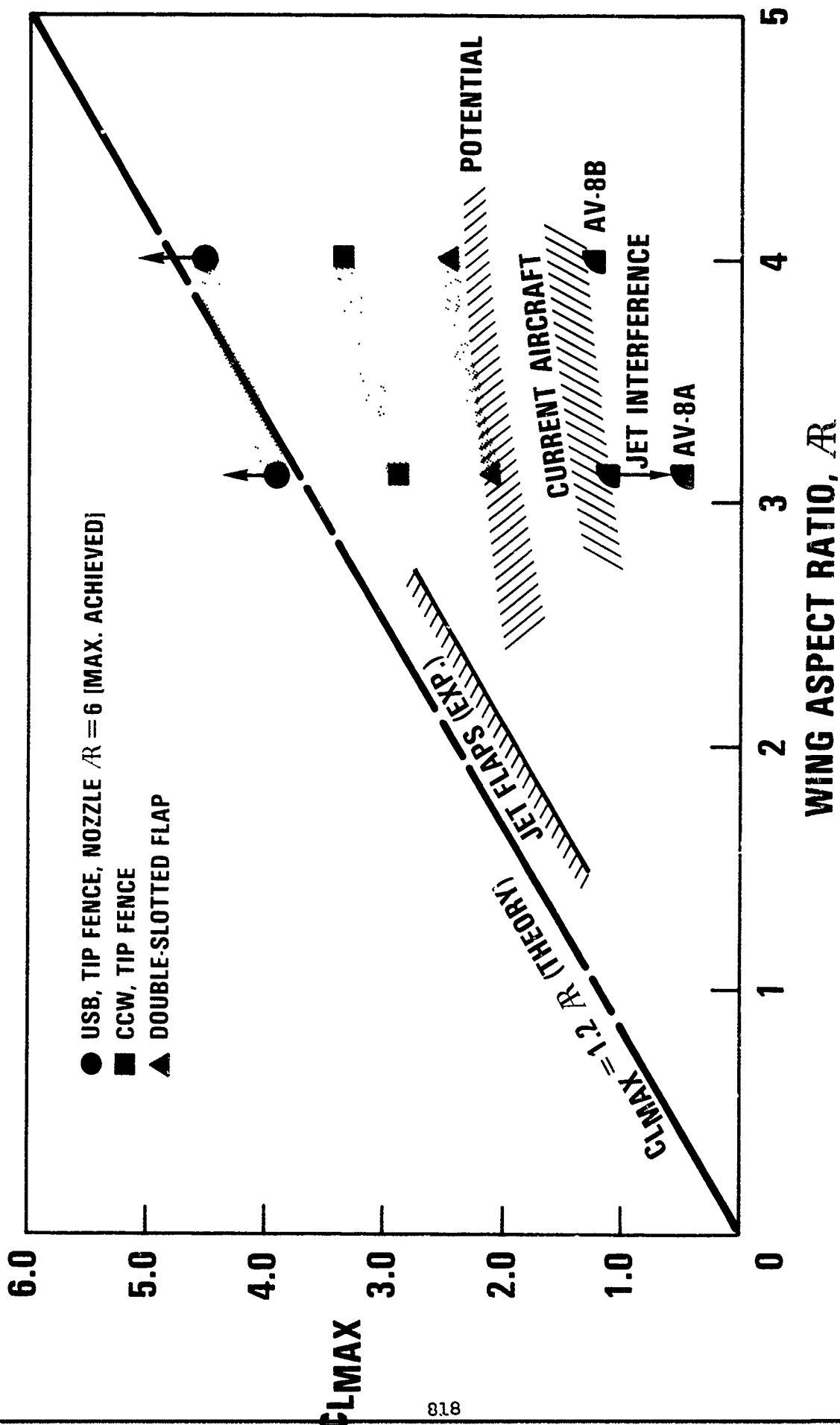
FIGURE 27 – Maximum lift achievable for low aspect ratio wings

YC-14

LOW SPEED TESTING TECHNIQUES

TED NARK

BOEING AEROSPACE COMPANY

WORKSHOP ON V/STOL AERODYNAMICS

MONTEREY, CALIFORNIA

MAY 16, 17, & 18, 1979

YC-14 POWERED LIFT SYSTEM

o ENGINE NOZZLE

o VORTEX GENERATORS

o USB FLAP

o CURVED LEADING EDGE KRUGER FLAPS

o DOUBLE SLOTTED OUTBOARD FLAPS

o LEADING EDGE B.L.C.

820
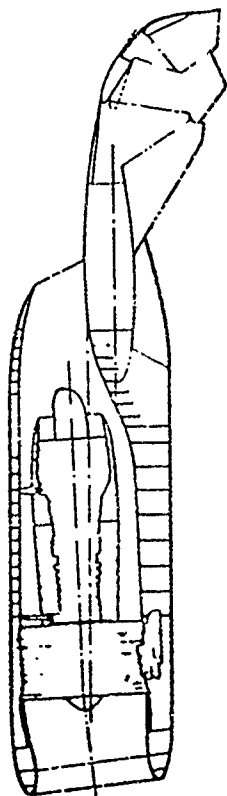
YC-14 USB INSTALLATION

REFERENCE 6

NOZZLE

NOZZLE DOOR

VORTEX GENERATORS

USB FLAP
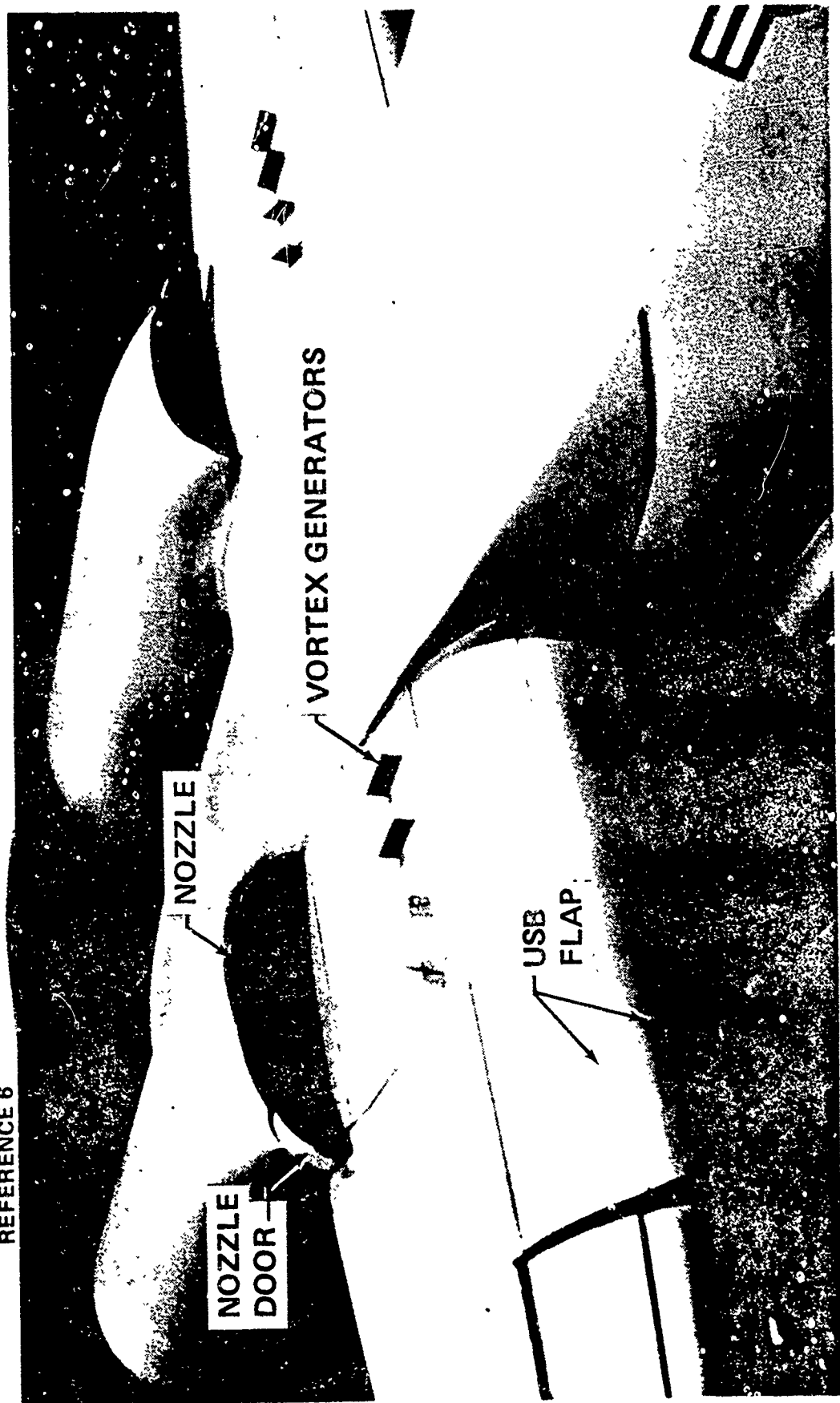
DEVELOPMENTAL TESTING

FACILITY	MODEL
3'x8' RESEARCH TUNNEL	PARTIAL HALF-MODEL
9'x9' PROPULSION TUNNEL	TRUE HALF-MODEL
STATIC THRUST STAND	COMPLETE MODEL OR HALF-MODEL
FLIGHT SIMULATION CHAMBER	TURBO-POWERED NACELLES
THRUST VECTORING RIG	NACELLES
BOEING-VERTOL WIND TUNNEL	COMPLETE MODEL

DEVELOPMENTAL TESTING

3' x 8' RESEARCH TUNNEL

PARTIAL HALF-MODEL

o NOZZLE DESIGN FOR COANDA TURNING

o VORTEX GENERATOR CONCEPT DEVELOPED

o INITIAL USB FLAP DESIGN

REF. SAE PRE-PRINT 740469 SKAVDAHL, HIRT, WANG

TWO-DIMENSIONAL WING

o LEADING EDGE BOUNDARY LAYER CONTROL

NOZZLE GEOMETRY DEVELOPED

REF. AIAA PRE-PRINT 79-0116

EFFECT OF NOZZLE DESIGN PHILOSOPHY

LIFT COEFFICIENT

HIGH-TURNING NOZZLE DESIGN

CRUISE NOZZLE DESIGN

$\Delta c_L = 1.3$

$\Delta c_D = 3$

$C_J = 1.0/1.0$

$\delta_f = 36/68$

ANGLE OF ATTACK

DRAG COEFFICIENT

DRAG-COEFFICIENT

HIGH-TURNING NOZZLE DESIGN

CRUISE NOZZLE DESIGN

6% A/P DRAG

$\Delta M = .01$

MACH NUMBER
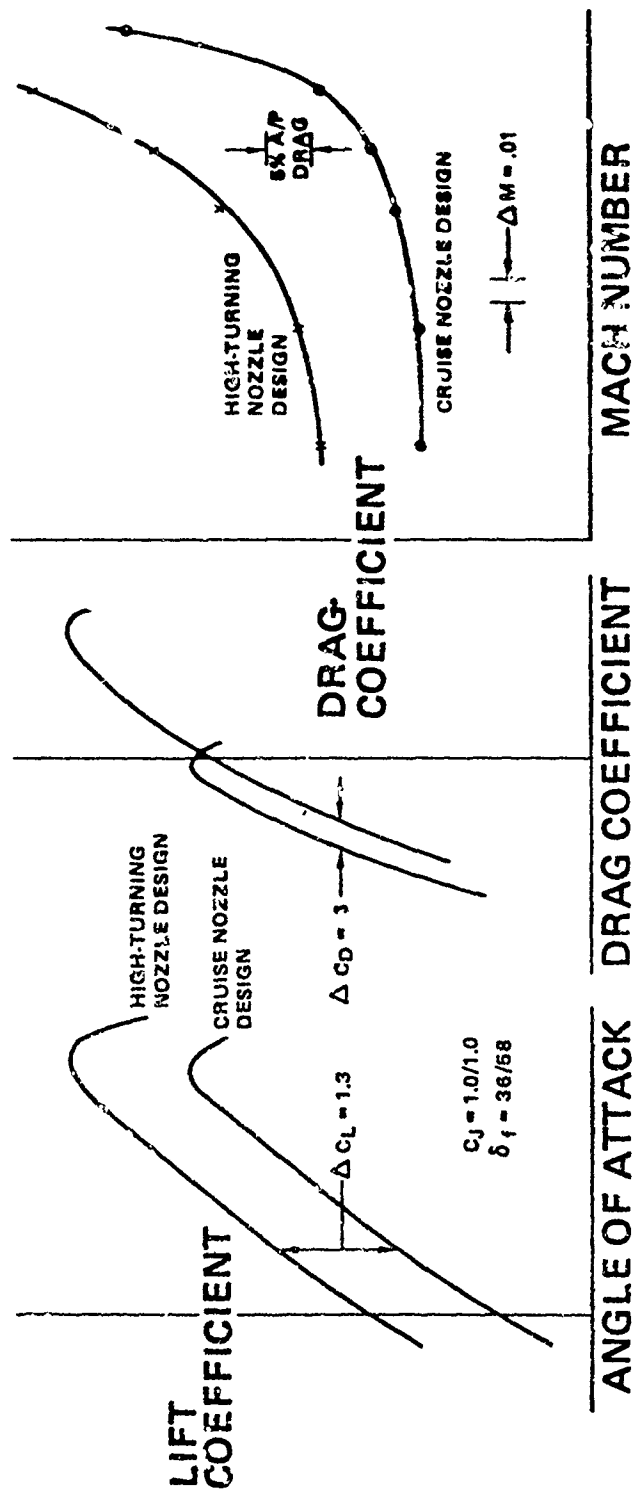
SCHEMATIC OF TEST ARRANGEMENT AT BOEING RESEARCH WIND TUNNEL (BRWT)

TRAVERSING BOUNDARY LAYER PROBE

FIXED BOUNDARY LAYER RAKE

MODEL

3-ft-DIAMETER TURNTABLE

TURNTABLE BLC SLOTS

WALL BLC BLOWING SLOT

FLOW

AUXILIARY AIR SUPPLY LINE

BALANCE

SIDE VIEW

3 ft

8 ft

TURNTABLE

MODEL

MODEL SUPPORT YOLK

BALANCE

FRONT VIEW
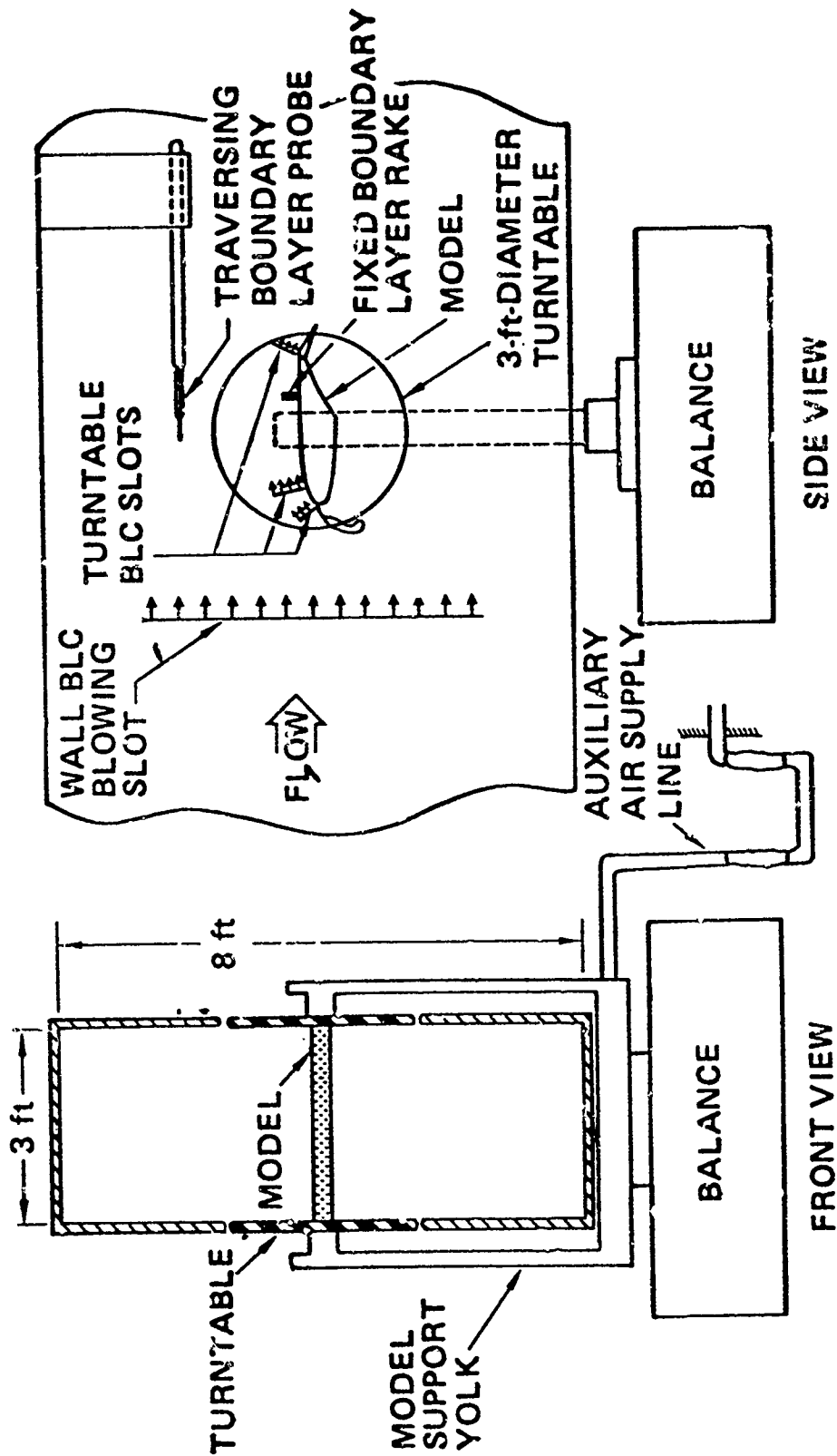
DEVELOPMENTAL TESTING

9' x 9' PROPULSION TUNNEL

TRUE HALF-MODEL

o NOZZLE EFFECTS WIND-ON   DOMED BLOWING NACELLES

o HOT FLOW NOZZLE

o DUAL FLOW NOZZLE

o TURBO-POWERED SIMULATORS   PARTIAL INLET FLOW

REF. AIAA PRE-PRINT 77-888

SINGLE-FLOW BLOWN NACELLE

LOW-PRESSURE CHOKEPLATE

HIGH-PRESSURE CHOKEPLATE

SCREEN

TOTAL PRESSURE RAKE

TOTAL TEMPERATURE PROBE

FLOW

PLENUM STATIC PRESSURE PROBE

COMPRESSED AIR SUPPLY

TURBO NACELLE

FAN TOTAL PRESSURE
AND TEMPERATURE RAKES (7)

PRIMARY TOTAL PRESSURE
AND TEMPERATURE RAKES (4)

CRITICAL FLOW VENTURI
IN WING DUCT

COMPRESSED AIR SUPPLY

3-STAGE TURBINE

SUPPLY AIR
TOTAL PRESSURE
AND TEMPERATURE PICK'JP

STATICS
THROAT
INLET

2-STAGE FAN

FLOW

DUAL-FLOW BLOWN NACELLE

THERMOCOUPLES

PRIMARY
CHOKEPLATES

FAN CHOKEPLATES

FAN PLENUM STATIC
PRESSURE PROBE

FAN TOTAL
PRESSURE RAKES (4)

PRIMARY TOTAL
PRESSURE RAKES (4)

FAN COMPRESSED
AIR SUPPLY (2)

PRIMARY COMPRESSED
AIR SUPPLY

PRIMARY PLENUM
STATIC PRESSURE PROBE

THERMOCOUPLES

B

C

B

C

B-B

C-C

DEVELOPMENTAL TESTING

STATIC THRUST STAND

   o INITIAL USB STATIC TURNING EFFICIENCY STUDIES

   o THRUST CALIBRATION FOR DOMED BLOWING MODELS & T.P.S.

FLIGHT SIMULATION CHAMBER

   o CALIBRATE FLOW-THROUGH NACELLES

   o CALIBRATE T.P.S. AT TUNNEL PRESSURE RATIOS

THRUST VECTORING RIG (PROPULSION STUDIES)

   o NOZZLE C_V FOR FINAL PERFORMANCE

   o DEVELOP INTERNAL NOZZLE LINES

MODEL INSTALLATION ON STATIC THRUST STAND

Ref: AIAA preprint 79-0335
D. N. Hunt, Boeing

SIDE VIEW

FRONT VIEW
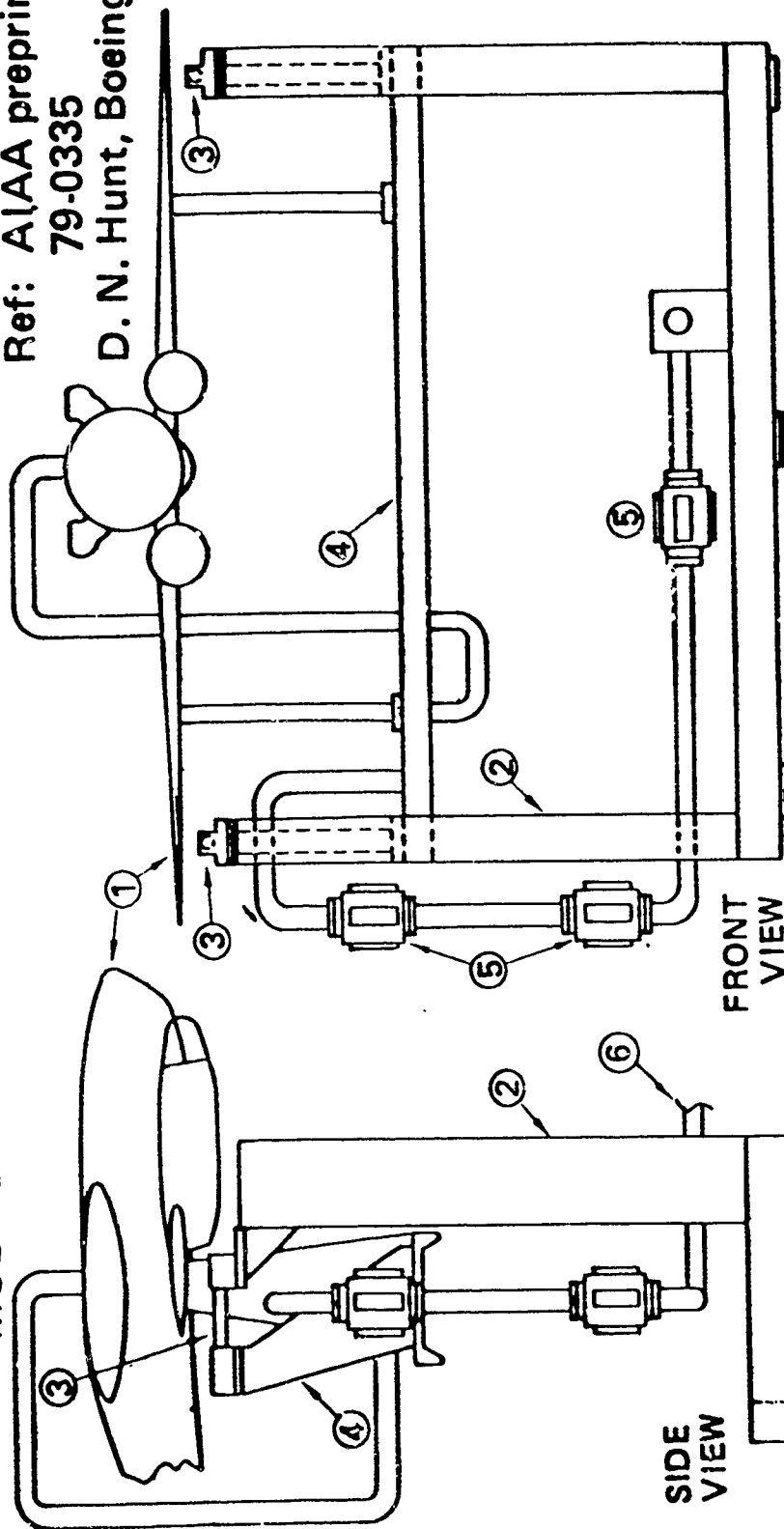
① YC-14 wind tunnel model (inverted)
② Dual-pedestal stand (nonmetric)
③ Six-component strain-gage balances (2)
④ Model support frame (metric)
⑤ Bellows airline fixtures (3)
⑥ High-pressure air supply line

STATIC THRUST DEFLECTION
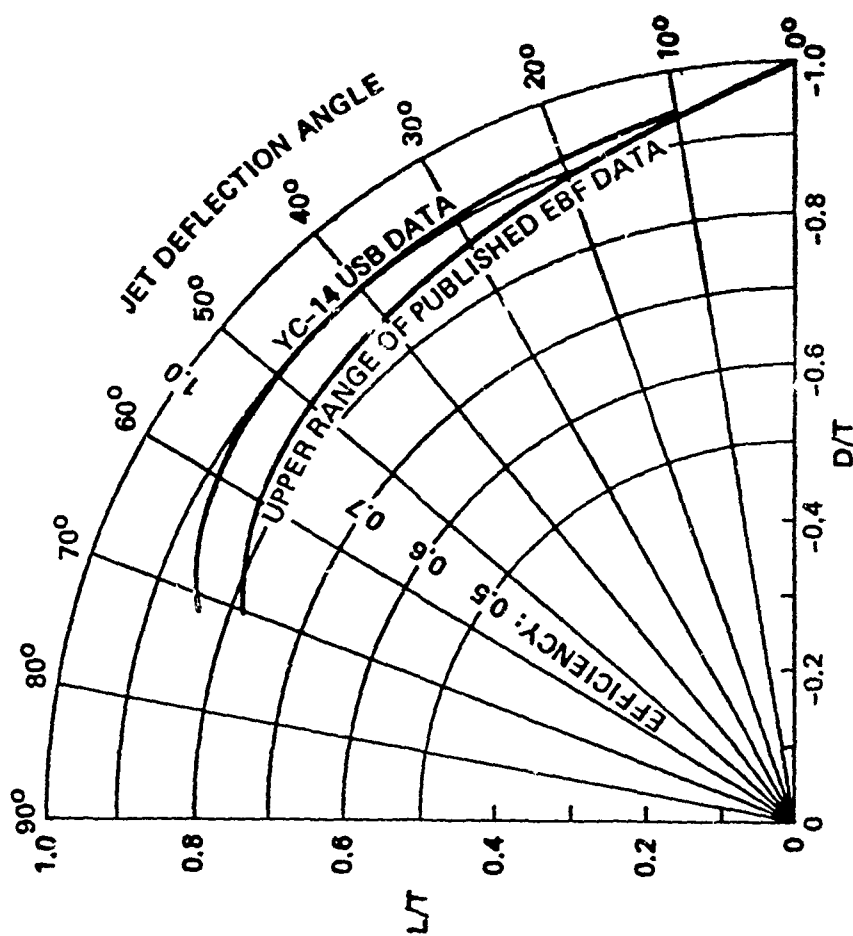
INLET INSTALLATION IN FLIGHT SIMULATION CHAMBER CALIBRATION FACILITY

NACELLE SIMULATION
- Flow through
- Blown
- TPS

VACUUM CHAMBER (4 ft IN DIAMETER X 10 ft LONG)

FLOW STRAIGHTENING SCREEN (6 LOCATIONS)

EJECTOR PRIMARY NOZZLE

NOZZLE (2 LOCATIONS)

EJECTOR PRIMARY AIR SUPPLY

CRITICAL FLOW VENTURI METER

PLEXIGLAS WINDOW

Ref:
AIAA preprint 79-0335,
D. N. Hunt, Boeing

833
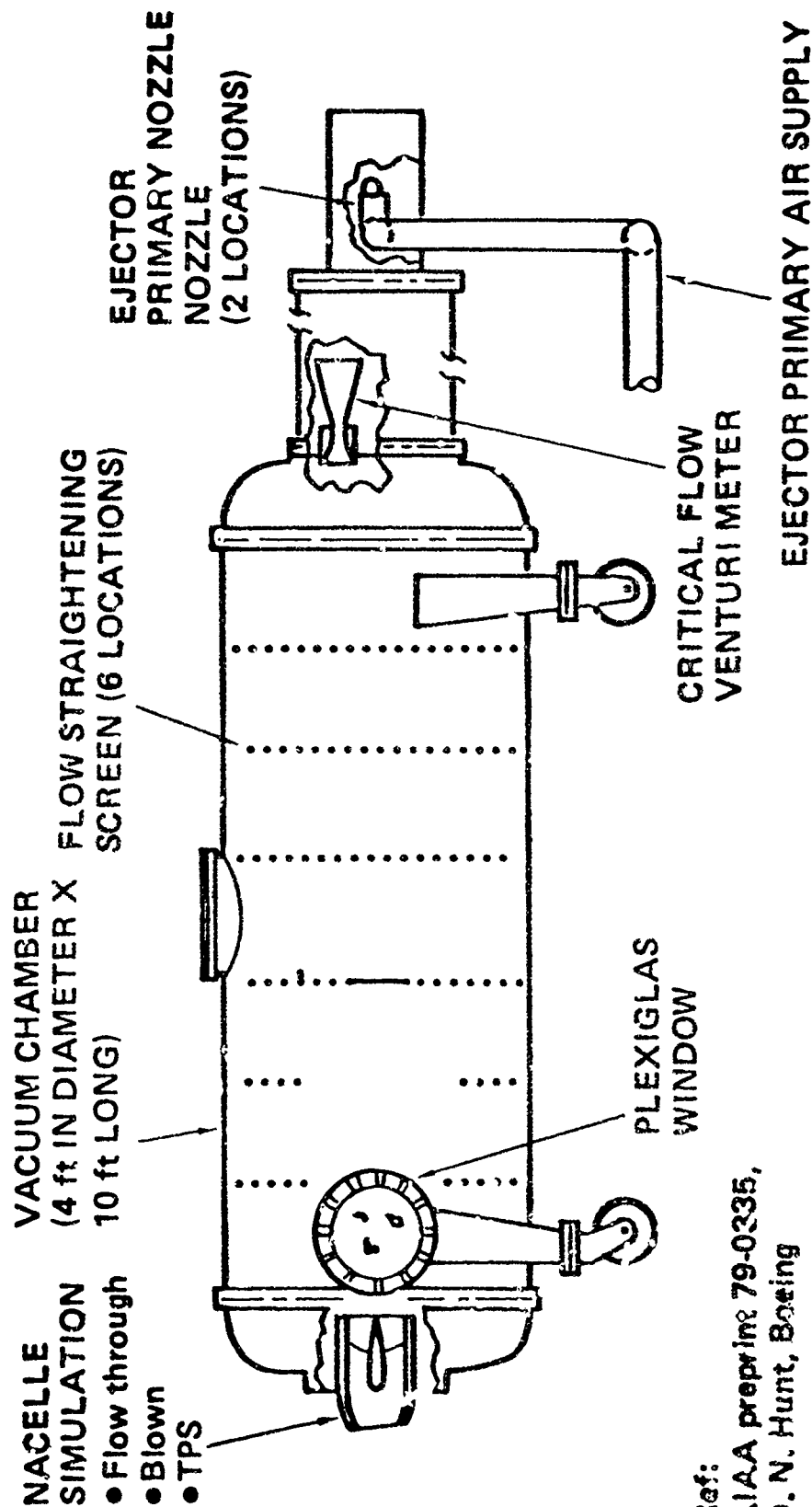
NACELLE INSTALLATION IN CALIBRATION FACILITY
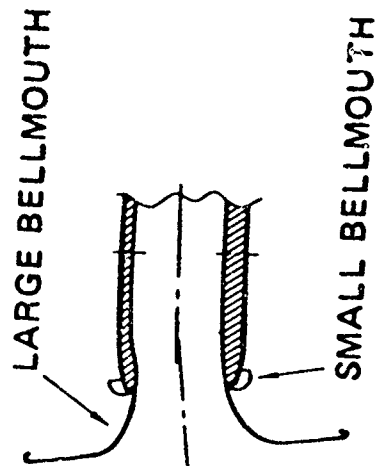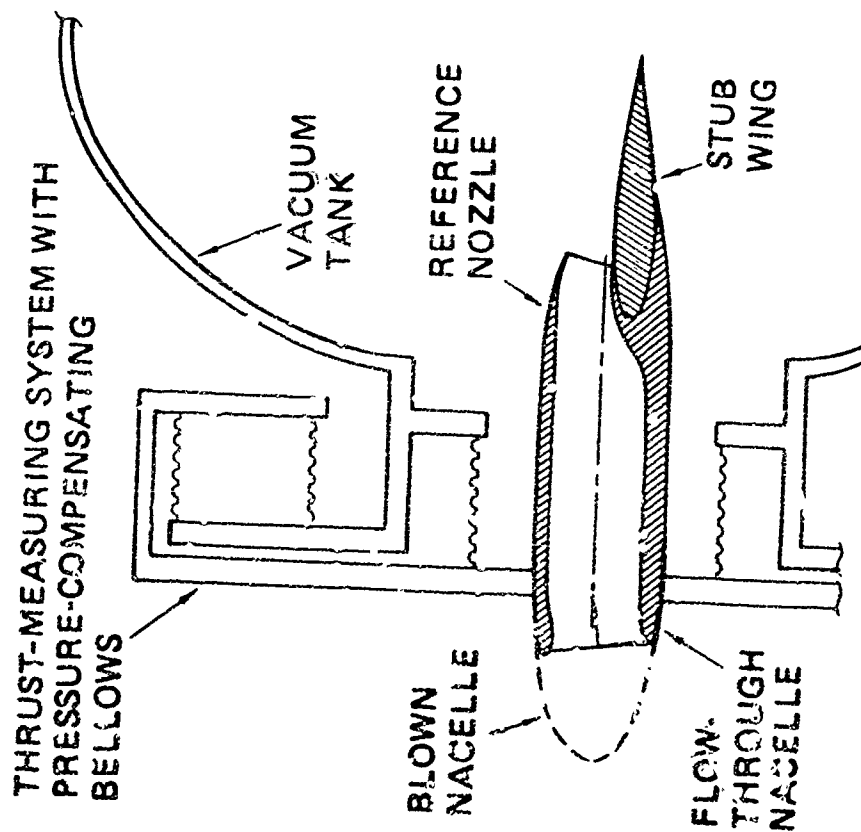
LARGE BELLMOUTH

SMALL BELLMOUTH

BELLMOUTH COMPARISON

THRUST-MEASURING SYSTEM WITH PRESSURE-COMPENSATING BELLOWS

VACUUM TANK

REFERENCE NOZZLE

STUB WING

BLOWN NACELLE

FLOW-THROUGH NACELLE

INSTALLATION DETAILS

Ref: AIAA preprint 79-0335, D. N. Hunt, Boeing

834

DEVELOPMENTAL TESTING

20' x 20' VERTOL V/STOL TUNNEL

COMPLETE MODEL

o SPAN WISE DISTRIBUTION OF LEADING EDGE BLOWING

o LEADING & TRAILING EDGE FLAP POSITIONING

o AIR DATA SYSTEM – STOL

o ENGINE OUT APPROACH CONFIGURATION

o TAKE-OFF CONFIGURATION

YC-14 POWERED LIFT TESTING

o .06 SCALE MODEL

o THRUST ON BALANCE

o BOEING DEVELOPED INTERNAL BALANCE

o BOTH SWEPT STRUT & CONVENTIONAL STING ARRANGEMENT

o DOMED BLOWING NACELLES

o ALL GROUND PLANE TESTING WITH MOVING GROUND BELT

STING-MOUNTED BLOWING BALANCE SCHEMATIC

☐ High-pressure air
■ Atmospheric vent
☐ Metric
☐ Nonmetric

STING

MASS FLOW DISTRIBUTOR

AIRFLOW

BALANCE FLEXURES

OPPOSING BELLOWS SEALS

MODEL MOUNT

MODEL PLENUM (METRIC)
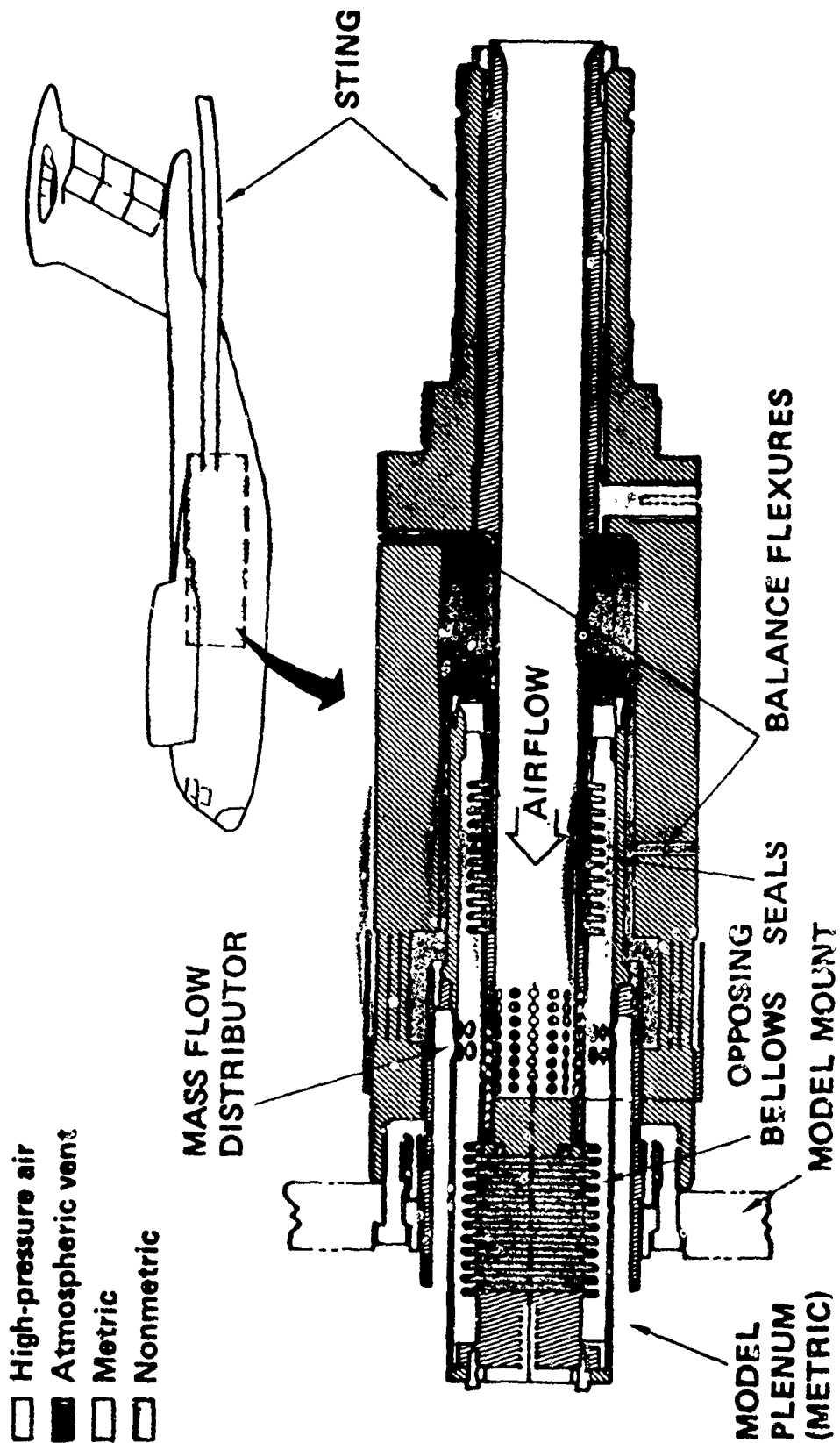
DATA BASE ACQUISITION:

20' x 20' VERTOL V/STOL TUNNEL

COMPLETE MODEL — HIGH FIDELITY REPRESENTATION OF FLIGHT VEHICLE

  o ENGINE OUT PERFORMANCE & CONTROL

  o GROUND EFFECT, TAKE-OFF & LANDING CONFIGURATION
     (MOVING GROUND BELT, $V_{BELT} = V_{FREE\ STREAM}$)

  o THRUST REVERSER EFFECTIVENESS & IMPACT ON CONTROLS

  o FAILURE EFFECTS, HYDRAULIC SYSTEM, JAMS

  o BASIC LONGITUDINAL & LATERAL/DIRECTIONAL DATA

TYPICAL TEST CYCLE

o CALIBRATE BLOWING SYSTEM STATICALLY ON THRUST STAND

o CALIBRATE "WIND-OFF" IN TUNNEL (QUALITY CHECK)

o ACQUIRE DATA "WIND-ON"

- MANY VARIABLES TO CONSIDER

- LOTS OF DATA TO ACQUIRE BY CONVENTIONAL LOW SPEED TESTING STANDARDS

- CHECK "HEALTH" OF BLOWING SYSTEM OFTEN DURING TEST

- UPRIGHT & INVERTED MODEL TESTS

- MORE INTERESTED IN POWERED LIFT THAN DRAG

- COLLECT UNTRIMMED DATA & TRIM EFFECTS

TEST VARIABLES

TYPE OF TEST	THRUST-DEPENDANT VARIABLES	ENGINE-OUT TESTING	BLOWING MOMENTUM	BLOWING CALIBRATIONS & DIAGNOSTICS
DEVELOPMENT	$\delta_{LE\ DEV'}$, $\delta_{TE\ FLAP'}$ $\alpha_{W'}$, h/b	ASYM DEFL ASYM BLC BLC DISTRIBUTION USB CONFIG VORTEX GEN NOZZLE DOOR	C_J (3 OR 4) $C_{\mu_{LE}}$ (2 OR 3)	$W \sim f\ (P_T/P)$ $C_V \sim f\ (P_T/P)$ $C_d \sim f\ (P_T/P)$

THRUST-DEPENDENT CONTROLS

- ENGINE OUT T.O. DIRECTIONAL CONTROL, LDG LATERAL CONTROL
- INFLUENCE OF POWER-LIFT ON CONTROL SYSTEM CHARACTERISTICS
- SPANWISE BLOWING DISTRIBUTION

CONTROLS $\delta_{TE\ FLAP'}$, $\alpha_{W'}$, $\delta_{AIL'}$, $\delta_{SP'}$, $\delta_{ELEV'}$, $\delta_{RUD'}$, ψ

DATA BASE $\delta_{LE\ DEV'}$, $\delta_{TE\ FLAP'}$, $\alpha_{W'}$, h/b, $\delta_{AIL'}$, $\delta_{SP'}$, $\delta_{ELEV'}$, $\delta_{RUD'}$

- AEO AND CEI VARIATIONS WITH POWER SETTING
- ACCEL AND DECEL ON GROUND ($\alpha = 0$) WITH CONSTANT THRUST AT VARIABLE q

FAILURE CONDITIONS

- HYDRAULIC SYSTEMS
- ELECTRICAL SYSTEMS
- L.E. & TRAILING EDGE FLAPS
- ENGINE OUT
- THRUST-DEPENDENT
- BLC
- NOZZLE DOORS
- USB FLAP

DATA REDUCTION

CORRECT UNTRIMMED DATA FOR

o DIFFERENCES BETWEEN MODEL & AIRPLANE

o WIND TUNNEL CORRECTIONS

o SCALE EFFECTS ON DRAG (NONE MADE FOR LIFT)

o DIFFERENCE BETWEEN TEST C_J AND NOMINAL C_J USING WIND TUNNEL
  DEVELOPED INFLUENCE COEFFICIENTS

MODEL TO WIND TUNNEL TEST SECTION – GEOMETRIC RELATIONSHIPS
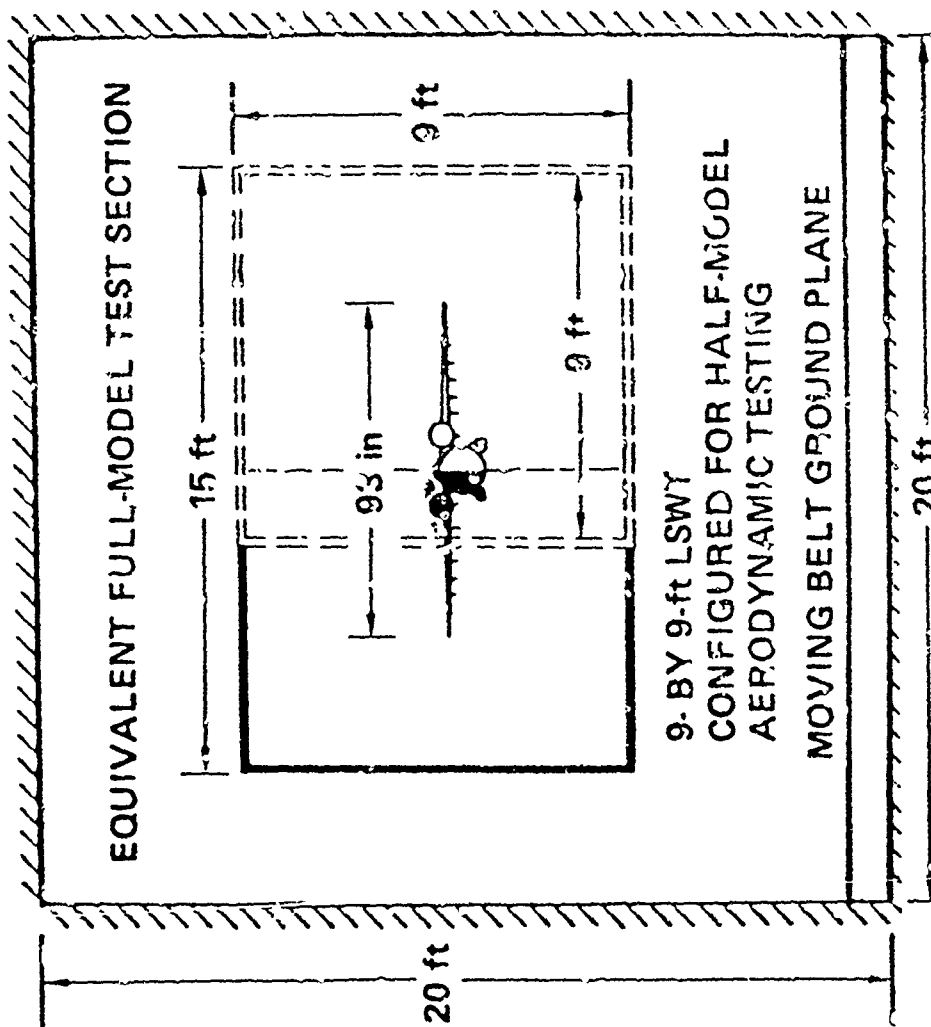
SCHEMATIC OF C-14
LOW-SPEED MODEL
IN THE BVWT 20- BY 20-ft
WIND TUNNEL

EQUIVALENT FULL-MODEL TEST SECTION

9 ft

15 ft

93 in

9 ft

20 ft

20 ft

9- BY 9-ft LSWT
CONFIGURED FOR HALF-MODEL
AERODYNAMIC TESTING

MOVING BELT GROUND PLANE

Ref: AIAA preprint 77-888
        Zierten and Rettie, Boeing

242

ALPHA CORRECTION FOR WALL EFFECTS
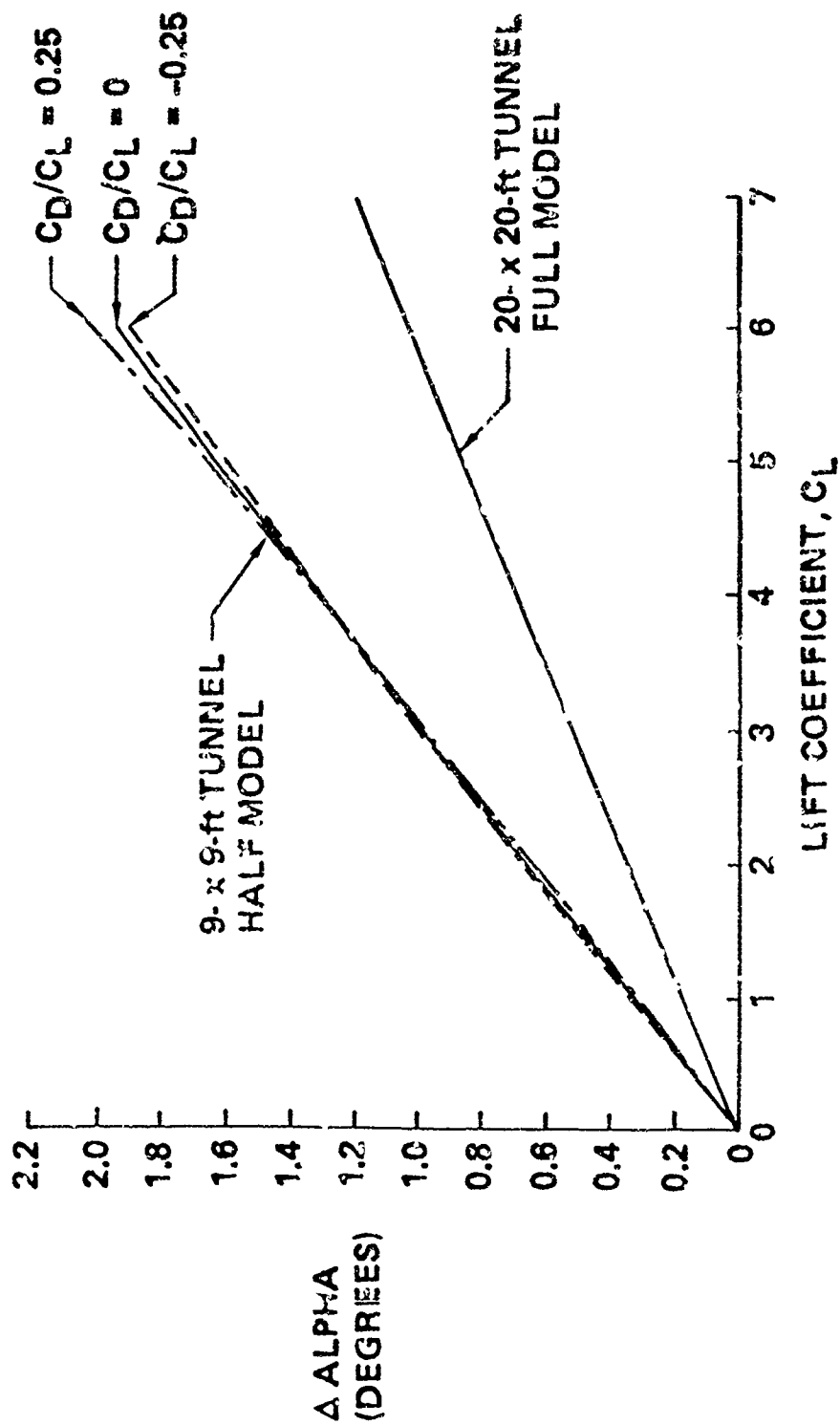
DIFFERENCES BETWEEN
MODEL & AIRPLANE

- DOMED INLET

- NOZZLE DISTORTION UNDER LOAD

- DIFFERENCE IN LOCATION OF CHARGING STATION

- EFFECTS OF TWO STREAM FLOW

- BOUNDARY LAYER CONTROL
  SLOT VS DRILLED HOLES

TRIMMED DATA

o START WITH UNTRIMMED DATA & SIX COMPONENT CONTROL SYSTEM DATA

o ADD ENGINE DECK AND CONTROL SYSTEM DESCRIPTION

o SUM & TRIM ANALYTICALLY (BASICALLY YC-14 SIMULATOR PROGRAM IN BATCH.MODE)

o OUTPUT γ vs V PLOTS & TRIMMED C_L vs α & C_J

VARIABLES C.G. LOCATION   OUTBOARD FLAP POSITION

           V.G.'S UP OR DOWN   HOT/STD. DAY

           USB FLAP POSITION   ALL ENGINE/ENGINE OUT

           WEIGHT   ALTITUDE

           THRUST   BLC CONDITION

FLIGHT PATH
ANGLE, δ
(DEGREES)

20

16

12

8

4

0

60   70   80   90   100   110   120   130   140   150   160

EQUIVALENT AIRSPEED (KNOTS)

THRUST$_{GROSS}$
(T_G)

85000
80000
75000

LT OUTBD FLAP (DEG) = 58
RT OUTBD FLAP (DEG) = 58
LT USB FLAP (DEG)   = UP
RT USB FLAP (DEG)   = UP
BLC BLEED
  8TH STAGE (PCT)   = 5
  14TH STAGE (PCT)   = 0

YC-14 USAF S/N 72-01873
CF6-50D ENGINES
SEA LEVEL STANDARD DAY

TWIN ENGINE
GROSS WEIGHT
160,000 LB

$V_{CLIMBOUT}$

$V_{TAKEOFF}$

REFERENCE FLAP = 30°
LANDING GEAR = UP

SYM	CCND	T_G (LB)
⊙	.001	75000
△	.002	80000
⊡	.003	85000

—— PREDICTED

Velocity vs Flight Path Angle Performance — Twin Engine

REF. R.L. MCPHERSON   AIAA -77-1259

846

YC-14 USAF S/N 72-01873
CF6-50D ENGINES
SEA LEVEL STANDARD DAY

SINGLE ENGINE
GROSS WEIGHT
160,000 lb

SYM	COND	T_G (LB)
◯	0.004.1	42500
△	0.005	42500
⬡	0.006	42500
●	0.004.3	37500
■	0.004.2	37500
◯	0.003	37500
♂	0.003.3	42500

—— PREDICTED

REFERENCE FLAPS = 30°
LANDING GEAR = UP
OPERATING ENGINE = NO. 1

LT. OUTBD FLAP (deg) = 58
RT. OUTBD FLAP (deg) = 58
LT. USB FLAP (deg) = 0
RT. USB FLAP (deg) = 6(I)
BLC BLEED
  8TH STAGE (PCT) = 5
  14TH STAGE (PCT) = 0

THRUST GROSS
(T_G)
42,500
37,500

$V_{CLIMBOUT}$
$V_{TAKEOFF}$
3% CLIMB

FLIGHT PATH ANGLE, δ (DEGREES)
847

EQUIVALENT AIRPSEED, (kn)

Velocity vs Flight Path Angle Performance – Single Engine

TAKEOFF/GO AROUND
GW = 160,000 lb
FLAPS 30
SEA LEVEL STANDARD DAY

BOTH ENGINES,
TAKEOFF THRUST

ONE ENGINE, TAKEOFF THRUST

$V_{APPROACH}$

$V_{CLIMBOUT}$

RATE OF CLIMB (ft/min)

3,500
3,000
2,500
2,000
500

EQUIVALENT AIRSPEED (kn)

70 80 90 100 110 120 130 140 150
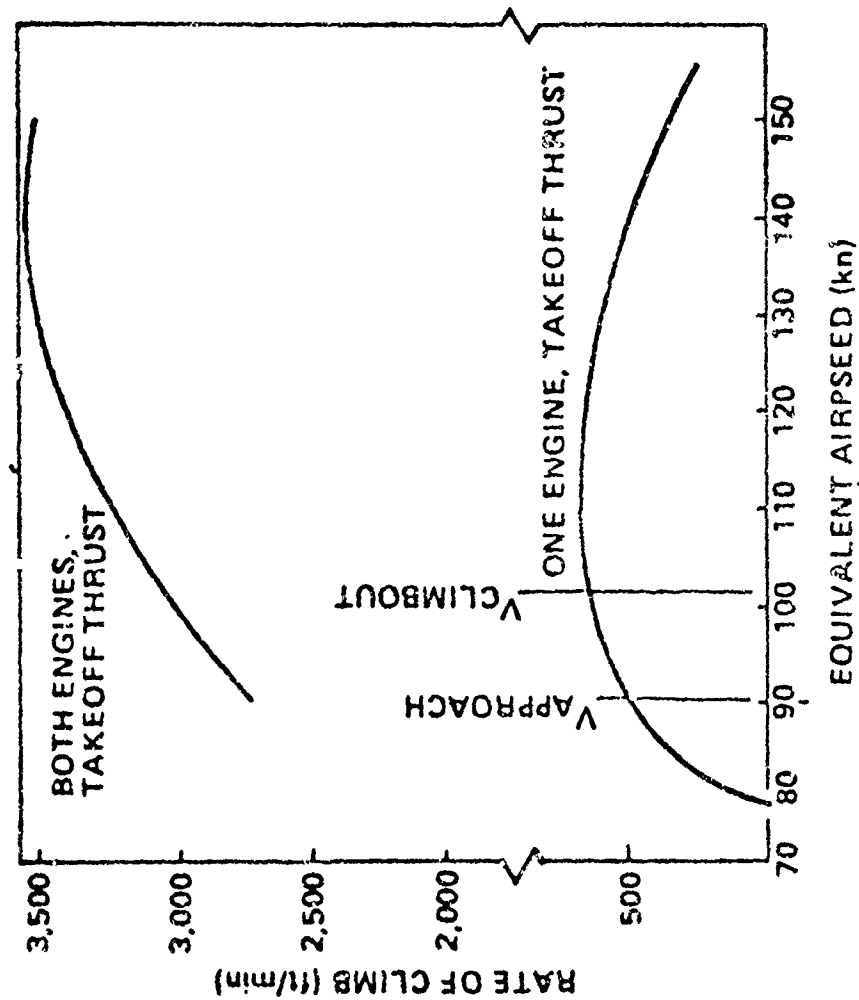
Demonstrated Climb Performance

REF: R.L. MCPHERSON   AIAA -77-1259

848

ALL ENGINES OPERATING
GW = 157,400 LB
T/W = 0.60
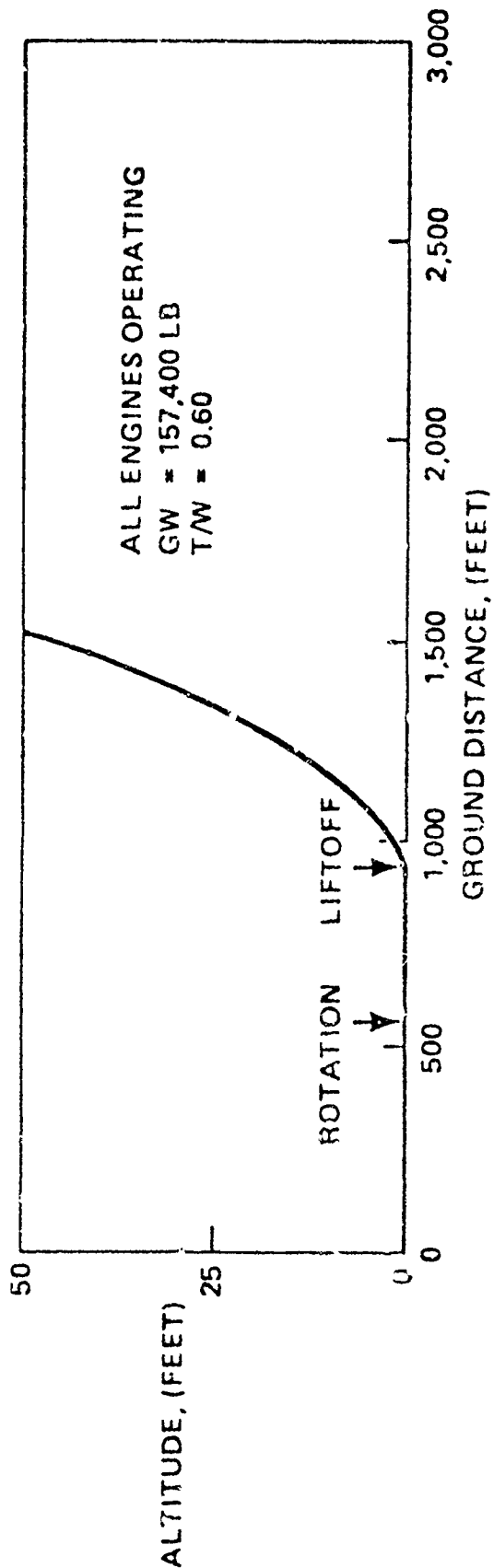
FLAPS 30
ALTITUDE = 2300 FT
TEMPERATURE = 8°C

ROTATION   LIFTOFF

GROUND DISTANCE, (FEET)

ALTITUDE, (FEET)

ENGINE FAILURE DEMONSTRATION
(CUT TO GROUND IDLE)

GW = 156,600 LB
T/W = 0.60/0.30

ENGINE CUT ROTATION LIFTOFF

GROUND DISTANCE, (FEET)

ALTITUDE, (FEET)
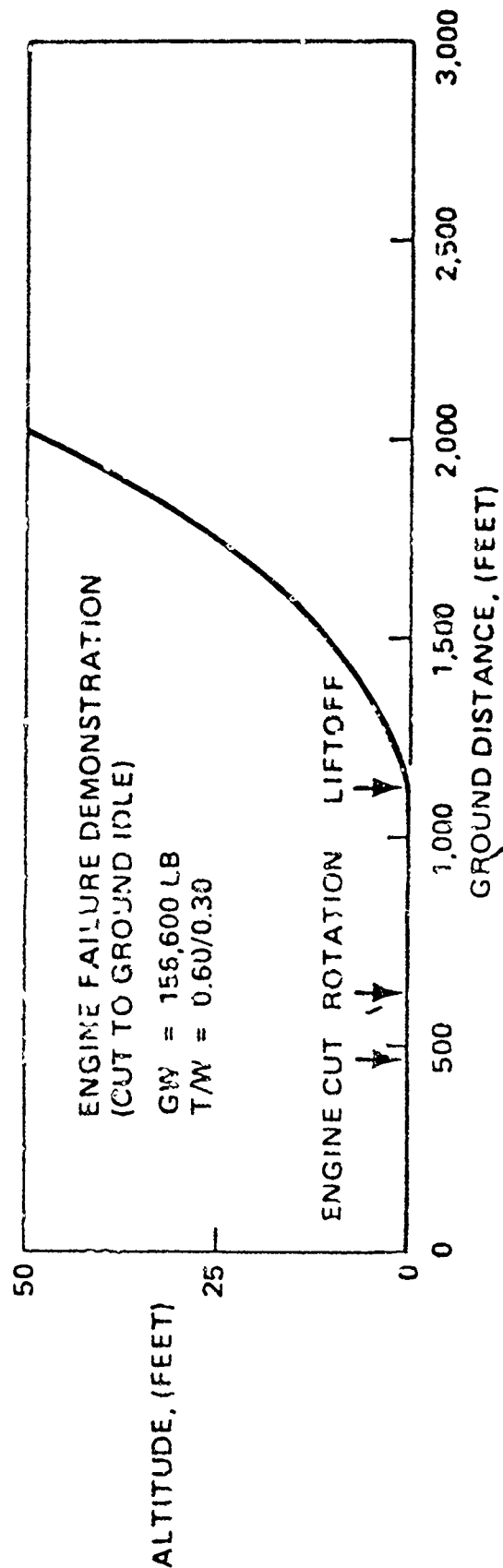
Takeoff Performance

REF, R.L. MCPHERSON   AIAA-77-1259

VECTORED ENGINE-OVER-WING CONCEPT DEVELOPMENT

STEPHEN C. STUMPFL

U.S. AIR FORCE FLIGHT DYNAMICS LABORATORY
WRIGHT-PATTERSON AIR FORCE BASE, OHIO

ABSTRACT

Vectored Engine-Over-Wing (VEO-Wing) is a STOL, propulsive-aerodynamic
design concept for advanced tactical aircraft applications. Development
of the concept has proceeded from experimental investigations through design
evaluations. Extensive experimental data have been obtained for parametric
variations of geometric and propulsion system characteristics at low subsonic,
transonic and supersonic speeds. A discussion of the test results is
presented, highlighting nozzle investigations and research model and con-
figuration model testing. The aerodynamic/propulsive data base has been
used in the evaluation of advanced tactical aircraft configurations utilizing
the VEO-Wing design concept. Results of air-to-air and air-to-ground design
investigations are presented to show the maneuver performance potential and
the STOL capability of the VEO-Wing concept.

NOMENCLATURE

AEDC	Arnold Engineering Development Center
ALPHA, α	Angle-of-attack
C_{D-T}	Drag minus thrust coefficient
ΔC_D	Incremental drag coefficient
C_L	Lift coefficient
ΔC_{L_B}	Incremental lift coefficient due to blowing
ΔC_{L_Γ}	Circulation lift coefficient due to flap deflection and blowing
$C_{M_{\bar{c}}/4}$	Pitching moment coefficient about quarter chord mac
C_T	Thrust coefficient
C_μ	Jet momentum coefficient
G'	Adjusted lift-gain factor
LaRC	NASA/Langley Research Center
M	Mach number
mac	Mean aerodynamic chord
S'	Area of wing affected by blowing
S_G	Takeoff and landing ground distance
S_{REF}	Reference area
TOGW	Takeoff gross weight
T/W	Thrust to weight ratio
V_{SINK}	Sink rate
W/S	Wing loading
$\overline{X}_{cp_\Gamma}$	Action point of circulation lift
δ_{CAN}	Canard deflection
δ_F	Trailing-edge flap deflection
Θ_j	Jet static turning angle
Λ_{LE}	Leading-edge sweep angle

INTRODUCTION

Changing military requirements put continuous demands upon the designers of advanced tactical aircraft. A design goal today seems to be the development of low cost supersonic fighter aircraft with long range capability, superior transonic maneuverability and the ability to operate out of extremely short air strips. Over the past several years, the major mission emphasis for advanced fighters has shifted between air superiority and air-to-surface. Growing concern in the Air Force for being able to carry out flight operations from bomb damaged air fields has prompted designers to rethink STOL, VTOL or V/STOL. The challenge is to provide an affordable short-field capability without compromising transonic and supersonic performance. Over the years, numerous propulsive-aerodynamic schemes have been investigated with varying degrees of success.

Propulsive-aerodynamics or powered-lift can be defined as the attempt to use an aircraft's high energy, propulsive exhaust to enhance the basic vehicle aerodynamics. Improvements result from boundary layer control, induced circulation or supercirculation, and from the direct thrust components. The goal of most powered-lift schemes is to maximize the supercirculation. Supercirculation is obtained when a propulsive jet induces a flowfield around an aerodynamic surface, resulting in higher lift and/or reduced drag for equiva-

lent lift. The resultant aerodynamic improvements are available for enhanced maneuverability and shorter takeoff and landing distances. The measure of the effectiveness of a particular powered-lift system is the amount of complexity required to achieve the aerodynamic improvements.

Many powered-lift concepts have integrated the propulsive-jet with the wing trailing edge or trailing-edge flaps. Both thick and thin jet-flaps have been investigated. The thin jet-flap is one in which high energy flow obtained from the engine is ducted to the wing trailing edge and exhausted as a thin jet sheet. This approach has been experimentally investigated[1-3] and shown to produce significant improvements in subsonic and transonic aerodynamics. These improvements can be obtained for reasonable values of the jet momentum coefficient, however, the use of compressor bleed from current technology engines can result in large thrust losses. Employing auxiliary power units for the air supply as well as the required wing ducting adds weight. Also, the wing ducting requirements can drive wing thickness, thus compromising the supersonic performance of an advanced fighter configuration.

In an effort to avoid the design compromises of the thin jet-flap, some powered-lift concepts have employed the full engine exhaust to augment the aerodynamics. The difference between each concept is basically the location of the engine exhaust exit plane and the wing trailing edge. For example, Vectored Thrust/Supercirculation, developed by the NASA/Langley Research Center, locates the vectorable engine nozzle(s) within the fuselage and in line with the wing trailing edge. The Externally Blown Flap, on the other hand, utilizes slotted trailing-edge flaps which are located in the engine exhaust flow. Upper Surface Blowing concepts exhaust the engine efflux over the top surface of the wing and turn the flow with the trailing-edge flap. Each of these concepts has been shown, experimentally, to have potential for advanced tactical aircraft application. However, aircraft balance, engine bleed and integration of the concept into low cost/light weight designs have been the major obstacles confronting powered-lift concept development.

Another concept more recently investigated is wing leading-edge vortex augmentation by spanwise blowing. A high pressure stream of air is vectored along the axial direction of the wing leading-edge vortex core. The spanwise blowing augments the leading-edge vortex strength and delays vortex burst to higher angles of attack. This enhancement of the leading-edge vortex can result in higher maximum lift coefficients and improvements in drag polar shape and lateral stability. The major design problem for spanwise blowing is obtaining the high pressure air supply without excessive thrust penalties.

Development of a powered-lift concept which is practical for advanced tactical fighter application has proved to be a formidable task for the aircraft designer. As mentioned above, cost, weight, aircraft balance, engine bleed and complexity of integration have been major development obstacles. These considerations have led to the Vectored Engine-Over-Wing (VEO-Wing) powered-lift concept which combines the best features of the thick jet-flap with leading-edge vortex augmentation

This paper will summarize the exploratory development of the Vectored Engine-Over-Wing concept. Results from the numerous VEO-Wing experimental

investigations will be reviewed and conclusions from STOL design studies will be presented for advanced tactical aircraft missions.

THE VEO-WING CONCEPT

The Vectored Engine-Over-Wing concept, shown in Figure 1, vectors the engine exhaust over the wing trailing-edge flaps to produce a jet-flap effect. This upper surface blowing arrangement is combined with spanwise blowing to achieve aerodynamic improvements over the full angle-of-attack range. Vectoring the engine exhaust over the wing trailing-edge flaps improves the flow over the flap and produces supercirculation. Leading-edge vortex augmentation is obtained by diverting a portion of the engine exhaust flow in a spanwise direction.

The concept was originally conceived as a "near-term" transonic fighter application. It is near-term since existing engines may be used without advanced engine cycle development. Use of the full engine exhaust instead of engine bleed eliminates the requirement for thick, heavy wing ducting which permits thin wing design for supersonic application. At transonic speeds, the main feature of the concept is its ability to turn the thick, high nozzle pressure ratio (NPR) exhaust jet over the trailing-edge flap. Early attempts[4] to accomplish this by "Coanda turning" with convergent nozzles were shown to be ineffective above an NPR of about 2.5. The VEO-Wing concept obtains flow turning through use of a non-axisymmetric convergent-divergent (C-D) half-wedge nozzle in conjunction with a simple trailing-edge flap.

Spanwise blowing enhances the configuration aerodynamics primarily at high angles-of-attack. At transonic speeds, these advantages are predominately at instantaneous maneuver conditions. However, at takeoff and landing speeds spanwise blowing is seen to significantly increase maximum useable lift, and in conjunction with vectored thrust, provides a potential for short takeoff and landing (STOL). As the mission requirements within the Air Force have changed over the past several years, the technology focus of the VEO-Wing concept development has shifted from transonic maneuver improvements to short field operations.

Extensive testing has been conducted under joint Air Force, NASA and General Dynamics Sponsorship to evaluate the VEO-Wing potential. The propulsive/aerodynamic characteristics have been defined for variations in propulsion system and configuration geometry. The powered-lift characteristics were evaluated at low speed through transonic Mach numbers and considerable data have been obtained for evaluation of the VEO-Wing STOL capability. Test results have been used in the development of advanced fighter designs. Maneuver capability, STOL, and supersonic performance have been estimated for representative Air Force missions.

EXPERIMENTAL INVESTIGATIONS

Promising results from various powered-lift wind tunnel investigations documented the potential of using upper surface blowing or spanwise blowing

for advanced tactical aircraft application. General Dynamics conducted several concept feasibility wind tunnel tests to gain insight into the mechanism and potential of combining upper surface blowing and spanwise blowing in the same configuration. Early conceptual tests verified the potential of the VEO-Wing powered-lift scheme. Smoke flow studies qualitatively showed the supercirculation effects on the flow streamlines. Investigations of leading edge vortex augmentation[5,6] verified that spanwise blowing improves the high angle-of-attack aerodynamic characteristics. Of particular importance was the development of the VEO-Wing nozzle/flap arrangement which was designed to achieve high nozzle pressure ratio flow turning at transonic speeds. Results from the conceptual testing led to research model and configuration model experimental investigations. A summary of the VEO-Wing wind tunnel test programs is shown in Figure 2.

Nozzle Tests

As mentioned earlier, use of the "Coanda effect" with two-dimensional (2-D) convergent nozzles was found to be ineffective in turning high NPR exhaust flows over the trailing-edge flap at transonic speeds. A series of conceptual, small-scale tests was conducted, in-house at General Dynamics, to gain some insight into the flow phenomena of nozzle-wing configurations. Results from these studies are presented in Reference 7. Figures 3 and 4 show some of the nozzle and flap geometry variations investigated during these tests. Both convergent and convergent-divergent half-wedge nozzle concepts were integrated with contoured and segmented plain flaps. Variations in nozzle cowl lengths, shown in Figure 5, were also evaluated to determine the effects of internal and external expansion on flow turning.

The conceptual, small-scale tests revealed that turning of a high NPR jet at transonic speeds is best accomplished internal to the nozzle. A half-wedge C-D nozzle with an intermediate length cowl was found to be superior to a convergent nozzle. Figure 6 presents a comparison of transonic lift augmentation obtained from force tests of several nozzle/flap configurations. These results show the half-wedge C-D nozzle as the superior approach in achieving transonic lift enhancement.

Research Model Tests

Results from the VEO-Wing concept feasibility and nozzle tests indicated significant potential for transonic maneuver improvements as well as a fall-out STOL capability. The Air Force Flight Dynamics Laboratory and the NASA/Langley Research Center entered into a joint program with General Dynamics to verify the aerodynamic/propulsion benefits of the VEO-Wing concept and to develop a technology data base from which vehicle applications could evolve.

A 1/10-scale, powered research model was fabricated for testing at NASA and Air Force test facilities. The model, shown in Figure 7, has been extensively investigated in a series of low speed and transonic tests, as previously shown in Figure 2. Complete documentation of the results of the low speed and transonic tests may be found in References 8, 9 and 10. High angle of attack and STOL testing is documented in References 11, 12 and 13.

Additional testing of the research model modified with outboard nacelles, is currently being conducted. These tests are identified in Figure 2 by the unshaded symbols. The results of these tests will be documented in a future technical report.

The powered research model has a cylindrical centerbody sized to accommodata a six-component flow-through balance. Twin, over-wing engine nacelles/ nozzles with faired-over inlets are attached to the model centerbody. The design of the canard and wing is representative of current high-performance aircraft. Additional model parts and the versatility of the model permitted testing of a wide range of propulsion system and configuration variables. Some of the parameters investigated were canard size and deflection, leading-edge and trailing-edge flap deflection, and engine and spanwise nozzle configuration. The test results have provided parametric data for VEO-Wing configuration development.

Considerable static calibration testing was conducted to define the static thrust and jet-turning characteristics of the various nozzle/flap combinations. Figure 8 shows static turning angle as a function of NPR and flap deflection for a representative nozzle (aspect ratio 4). The data show that flow turning is achieved since the turning angle approximates the value of the flap upper surface angle which is nominally 6 degrees greater than the flap deflection. The flap-off case shows a steady decrease in turning from a value approximating the wedge angle at NPR's greater than 3.0. This indicates the significance of the flap in achieving jet turning at the high NPR's of afterburning engines.

Good jet turning can result in significant lift augmentation. In Figure 9, lift augmentation resulting from jet turning and circulation is shown as a function of Mach number and NPR. In this plot, the lift augmentation, ΔC_{LB}, is defined as the difference between the power-on C_L and the power-off C_L at zero angle-of-attack. For this representative nozzle (aspect ratio 6) and a moderate flap deflection of 15 degrees, significant lift augmentation is obtained at all Mach numbers.

Lift gain factors have been used to assess the lift effectiveness of powered-lift concepts. Figure 10 is a plot of lift gain factor (G'), adjusted for the fraction of the reference wing area affected by blowing, versus momentum coefficient. The definition of G' is shown on the figure. The VEO-Wing lift effectiveness is compared to a correlation of blown-flap and jet-flap data from other sources[14]. The figure shows that the VEO-Wing concept has considerable potential as a powered-lift application as indicated by the lift effectiveness improvement over the existing state-of-the-art.

The canard is seen to be one of the most important geometry variables on a VEO-Wing configuration. At takeoff and landing speeds, the canard is the primary trimming device, and at transonic speeds the canard presence helps reduce the vehicle static stability. The inherent nose-down moments produced by the deflected engine jet are opposed by the nose-up moment of the canard and by the negative static stability which the canard helps create. Figure 11 shows the strong effect of the canard on the lift, drag and pitching moment of the research model at .9 Mach. Addition of the canard relieves the wing flow separation which is seen to start at about 6 degrees angle-of-attack. The result is a linearization of both the lift and pitching moment curves with a

corresponding improvement in the drag polar. These improvements to the aerodynamics are seen at all Mach numbers and are somewhat enhanced with the addition of power.

Major emphasis was given during the research model tests to the investigation of the high-lift aerodynamic benefits of spanwise blowing. Transonic testing indicated that significant aerodynamic improvements were obtainable with spanwise blowing, however, the benefits exist primarily at the high lift coefficients corresponding to instantaneous maneuver conditions. On the other hand, spanwise blowing was seen to be extremely effective in generating high useable lift coefficients at low speeds. Figure 12 illustrates this lift effectiveness. Figure 13 shows the spanwise blowing effects on lift augmentation as a function of thrust coefficient and angle-of-attack. At the same engine operating conditions, spanwise blowing generates more than twice the lift augmentation of the deflected engine thrust alone. Figure 14 shows a favorable effect of spanwise blowing on the center of pressure location. Spanwise blowing produces a forward movement of the center of pressure which is beneficial in reducing the trim requirement. Aircraft balance during STOL operation is one of the most serious problems confronting powered-lift systems. Spanwise blowing offers an effective means of producing high lift without an adverse effect on the aircraft balance. Figure 15 presents photographs of some of the spanwise nozzles investigated during the low speed tests.

Configuration - Model Tests

Effectiveness of propulsive-aerodynamic concepts is highly configuration dependent. Preliminary design studies at General Dynamics defined a VEO-Wing air superiority configuration arrangement to exploit the concept's powered-lift benefits. In an effort to assess this configuration concept the Air Force Flight Dynamics Laboratory contracted for fabrication of a 1/15-scale, unpowered, flow-through model of the General Dynamics design. Although the model was unpowered, it did permit assessment of the power-off aerodynamics as well as supersonic characteristics. In addition, nacelle/wing/body interference could be investigated over the Mach number range.

The model was investigated[15,16] during two entries in the AEDC four foot Transonic Wind Tunnel. The first entry employed a vertical tail, blade support strut and evaluated the longitudinal characteristics. The second entry permitted both longitudinal and lateral/directional testing while employing a straight aft sting. Figure 16 shows a photograph of the VEO-Wing configuration model installed in the AEDC wind tunnel facility on the vertical tail blade support strut.

Considerable data were obtained during the 150 hours of testing. Effects of configuration geometry variations, such as canard, leading-edge and trailing-edge flap, beavertail, and vertical tail/rudder were investigated over the Mach number range of .2 and 2.0. Configuration interference and component interaction were evaluated through a "build-up" series of runs. The aerodynamic results were complemented with fluorescent oil flow photographs. Analysis of the data has indicated that the longitudinal and lateral/directional aerodynamic characteristics are generally well behaved. The results,

however, did indicate a higher than predicted minimum drag level (C_{DMIN}) at Mach numbers less than 1.6 and an unexpected nose-down (negative) zero-lift pitching moment (C_{M0}) at subsonic speeds.

In Figure 17, the minimum drag characteristics of the 1/15-scale model, corrected to a full scale flight conditions, are compared to prediction and to a current technology fighter configuration. The higher than predicted drag level was found to be the result of fuselage and nacelle camber and interference. An estimate of the minimum drag characteristics of a refined configuration is also shown in Figure 17.

The fuselage of the model was cambered in an effort to achieve a positive C_{M0} of .04. The unexpected zero-lift pitching moment was found to be primarily the result of nacelle/fuselage interference. Figure 18 shows the configuration build-up of C_{M0} for the 1/15 scale model. It can be seen that the fuselage does achieve a C_{M0} equal to the design level of .04. Addition of the nacelle, however, negates this effect and causes the complete configuration to experience a nose-down zero-lift pitching moment.

During the second test entry, an attempt was made to isolate some of the nacelle/fuselage interference effects. Various fairings were added forward and aft in the channel between the nacelle and fuselage. The forebody strake was also removed. Typical incremental results obtained for some of the fairings are shown in Figure 19. These studies indicated that significant drag reductions may be possible with detailed refinement and area ruling of the nacelle/wing/fuselage junction. The "refined configuration" drag characteristics, shown previously in Figure 17, were developed by removing interference and camber drag increments deduced from the "build-up" and fairing studies. Further refinements to the configuration model are subjects for possible future investigation.

STOL DESIGN INVESTIGATIONS

Recent concern for being able to conduct air operations from bomb damaged air fields has prompted a renewed interest in STOL and V/STOL. As mentioned earlier, the VEO-Wing concept was originally developed for transonic maneuver enhancement. With the recent interest in STOL, however, emphasis was shifted to the short field capability. Design analyses have been conducted by General Dynamics both in-house and under contract for the AFFDL. Advanced STOL fighter configurations have been designed for air-to-air and air-to-ground missions. Results from these investigations indicate that the VEO-Wing concept can be integrated into practical designs with impressive maneuver and take-off and landing performance. Results from these STOL design investigations are documented in Reference 17.

Air-to-Air

Figure 20 presents a sketch of the VEO-Wing air-to-air (ATA) fighter configuration designed to accomplish the 500 n. mi. air superiority mission profile shown in Figure 21. This configuration was used as the basis for

design of the 1/15-scale configuration model discussed above. The performance capability of the ATA design is summarized in Figure 22. This level of performance is seen to be very impressive when compared to current and advanced technology fighters. Most impressive, however, is the short takeoff and landing capability of this configuration.

STOL performance was estimated using the takeoff and landing ground rules summarized in Figure 23. The takeoff performance determined for the VEO-Wing ATA configuration is shown in Figure 24. The liftoff speeds, corresponding to the spanwise blowing on and off curves are 84 and 110 knots, respectively. When spanwise blowing is applied near the rotation speed it is seen to be effective in reducing both the liftoff speed and takeoff ground roll. Use of spanwise blowing results in a takeoff ground roll of 315 feet as compared to 475 feet without it. The landing performance is shown in Figure 25. In the landing case, spanwise blowing is used throughout the landing approach until touchdown. A 15 degree pitch attitude is maintained with a glideslope angle of about 7 degrees. The angle of attack is reduced to 15 degrees (tailbump angle) at touchdown. The landing results in Figure 25 show that a minimum landing ground roll of 260 feet occurs for an approach speed of 69 knots. For conservatism a ten percent margin was assumed giving a ground distance of 305 feet at 76 knots approach speed.

It should be mentioned that these short distances were predicted under the ground rules identified above. Pilot response time and control system limitations may increase these distances, however, they do indicate the potential STOL performance limits for powered lift systems with aerodynamic controls.

Air-to-Ground

Conceptual and point design studies were conducted to compare VEO-Wing and conventional advanced fighter concepts for an air-to-ground (ATG) mission application. The selected mission, shown in Figure 26, is battlefield interdiction of second-echelon targets and close air support. The aircraft were to have a Mach 1.6 supersonic capability for alternate mission applications and be able to takeoff and land in less than 1000 feet of ground roll. The purpose of the study was to determine the benefits of VEO-Wing concept application as compared to an advanced conventional design. The selected advanced conventional configuration employed an advanced blown-flap design concept. Point designs were developed following the conceptual design and sizing studies.

Sketches of the VEO-Wing and conventional blown-flap point designs are shown in Figures 27 and 28, respectively. For the VEO-Wing configuration, the critical sizing parameter was the transonic maneuver requirement while for the conventional blown-flap concept it was the 1000-foot STOL requirement. A summary comparison of the mission and STOL performance results for the two point designs is presented in Figure 29. The results indicate that the STOL requirement puts greater demands upon the conventional design than the maneuver requirement put upon the VEO-Wing. As seen in Figure 29, the VEO-Wing point design misses the required sustained 3.0 g requirement at .9M/30000

feet by only .15 g's. The conventional blown flap point design, however, exceeds the 1000 foot takeoff and landing ground roll requirement by 285 and 45 feet, respectively. Reoptimization of the point designs was beyond the scope of this study, however, sensitivity analyses conducted during the conceptual design and sizing studies indicated the trends on vehicle gross weight.

The sensitivity analyses indicated that for the design mission, equal weight vehicles of 48,000 pounds would result for the VEO-Wing and conventional blown-flap vehicles at a STOL distance requirement of approximately 1225 feet. At distances less than 1225 feet the gross weight of the conventional vehicle increases rapidly as wing area and engine size grow. The VEO-Wing is capable of satisfying all mission requirements for STOL distances of less than 900 feet. These effects are summarized in Figure 30.

CONCLUDING REMARKS

The Vectored Engine-Over-Wing propulsive-aerodynamic concept provides a reasonable design alternative for advanced STOL tactical aircraft applications. The concept has been extensively tested in the wind tunnel and integrated into advanced supersonic fighter designs. Results from testing and design investigations have indicated that the VEO-Wing concept has the potential to provide superior transonic maneuver performance together with an impressive STOL capability. This potential will best be realized through advanced development and flight demonstration. Continuing development in several parallel technology areas is required to exploit the VEO-Wing. Non-axisymmetric nozzle development, flight propulsion/control coupling, and thermal/acoustic protection are important technologies for effective VEO-Wing design integration.

This paper has summarized the historical development of the VEO-Wing concept and those experimental and design investigations which the Air Force had cognizance over. General Dynamics has conducted additional VEO-Wing design investigations in support of NASA and Navy V/STOL activities. NASA-Ames Research Center has constructed a large-scale, highly maneuverable supersonic V/STOL fighter model for testing in the 40 x 80 foot wind tunnel. The model is powered by two J-97 non-afterburning engines and employs the VEO-Wing design concept. Results from the 40 x 80 tests should provide valuable insight into the low speed effectiveness of the Vectored Engine-Over-Wing propulsive-lift concept.

REFERENCES

1. Yoshihara, H., Zonars, D., and Carter, W., High Reynolds Number Transonic Performance of Advanced Planar Airfoils with Jet Flaps, AFFDL-TR-71-61, June 1971.

2. Yoshihara, H., Benepe, D. B., and Whitten, P. D., Transonic Performance of Jet Flaps on an Advanced Fighter Configuration, AFFDL-TR-73-97, September 1973.

3. Ely, W. L., and Berrier, B. L., Performance of Steady and Intermittent Blowing Jet Flaps, and Spanwise Upper Surface Slots, AFFDL-TR-75-128, November 1975.

4. Ishimitsu, K. K., Investigation of Upper Surface Blowing Applied to High Speed Aircraft, AFFDL-TR-74-89, July 1974.

5. Cornish, J. J., III, "High Lift Applications of Spanwise Blowing," ICAS Paper No. 70-09, September 1970.

6. Bradley, R. G., Smith, C. W., and Wray, W. O., An Experimental Investigation of Leading-Edge Vortex Augmentation by Blowing, NASA CR-132415, April 1974.

7. Whitten, P. D., Kennon, I. G., and Stumpfl, S. C., "Experimental Investigation of a Nozzle/Wing Propulsive Lift Concept," AIAA Paper No. 76-625, July 1976.

8. Woodrey, R. W., Whitten, P. D., Smith, C. W., and Bradley, R. G., An Experimental Investigation of a Vectored-Engine-Over-Wing Powered-Lift Concept, Volume I - Low Speed and Transonic Tests, AFFDL-TR-76-92, Vol. I, September 1976.

9. Huffman, Jarrett K., and Fox, Charles H., Jr., Subsonic Longitudinal Aerodynamic Characteristics of a Vectored-Engine-Over-Wing Configuration Having Spanwise Leading-Edge Vortex Enhancement, TM X-73955, 1977, NASA.

10. Bradley, R. D., Jeffries, R. R., and Capone, F. J., "A Vectored-Engine-Over-Wing Propulsive Lift Concept," AIAA Paper No. 76-917, Sept 1976.

11. Whitten, P.D., An Experimental Investigation of a Vectored-Engine-Over Wing Powered-Lift Concept Volume II - High Angle of Attack and STOL Tests, AFFDL TR-76-92, Vol. II, March 1978.

12. Leavitt, L. D., Whitten, P.D., Stumpfl, S.C., "Low Speed Aerodynamic Characteristics of a Vectored Engine-Over-Wing Configuration," AIAA Paper No. 78-108, July 1978.

13. Leavitt, L. D., Yip, L. P., Effects of Spanwise Nozzle Geometry and Location on the Longitudinal Aerodynamic Characteristics of a Vectored-Engine-Over-Wing Configuration at Subsonic Speeds, NASA Technical Paper 1215, May 1978.

14. Sedwick, T. A., Investigation of Augmented Deflected Exhaust Nozzles Installed in Tactical Aircraft, AFFDL-TR-75-42, 1 May 1975.

15. Heim, E. R., Basic Aerodynamic Data for a Vectored-Engine-Over-Wing Configuration, AEDC TR-78-1, February 1978.

16. Heim, E. R., Wind Tunnel Tests of a Vectored Engine-Over-Wing Model, AEDC-TSR-78-P38, October 1978.

17. Whitten, P. D., Howell, G. A., Investigations of the VEO-Wing Concept in An Air-to-Ground Role, AFFDL-TR-79-3031, March 1979.
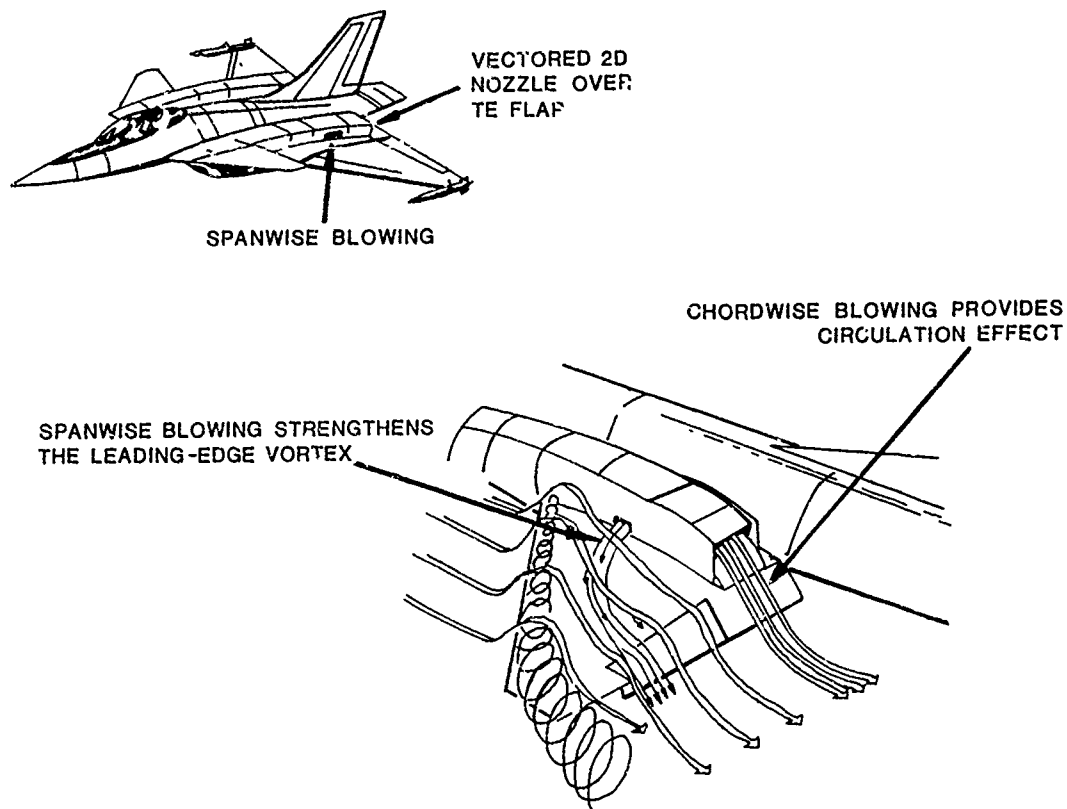
FIGURE 1. VEO-WING CONCEPT

☩ CONCEPTUAL SPANWISE BLOWING TESTS

☐ VEO-WING CONCEPTUAL TESTS – HALF SPAN

▽ PARAMETRIC NOZZLE TESTS

◇ 1/10 – SCALE POWERED RESEARCH MODEL TESTS

◯ 1/15 – SCALE UNPOWERED CONFIGURATION MODEL TESTS
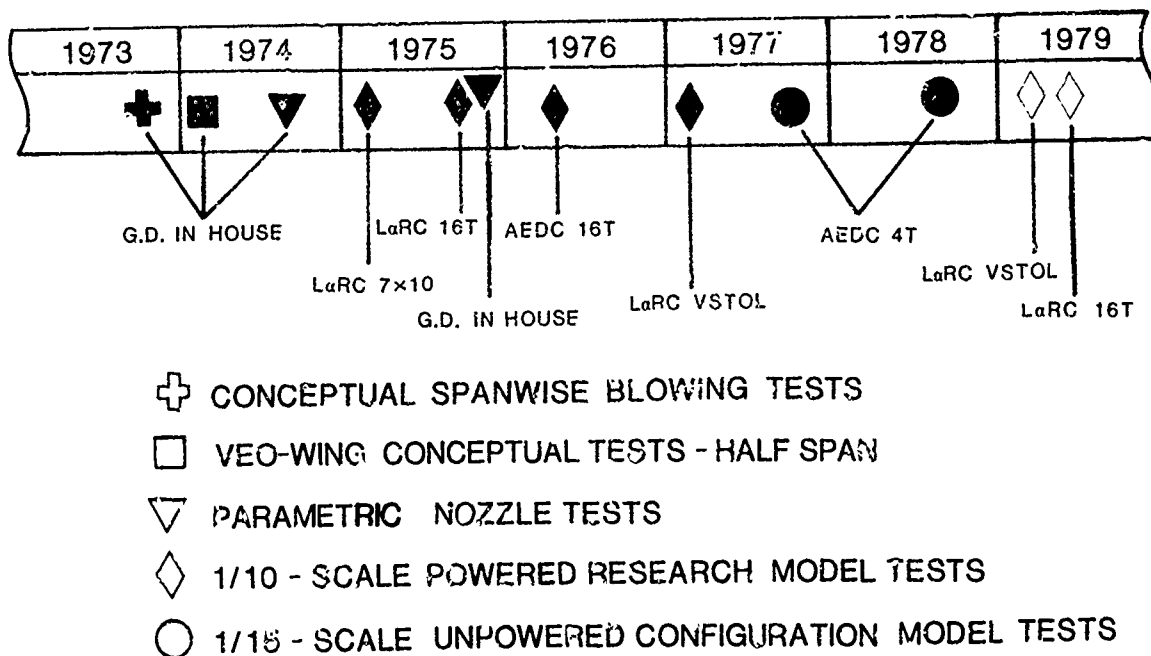
FIGURE 2. SUMMARY OF VEO-WING TEST PROGRAMS

CONVERGENT   CONVERGENT-DIVERGENT
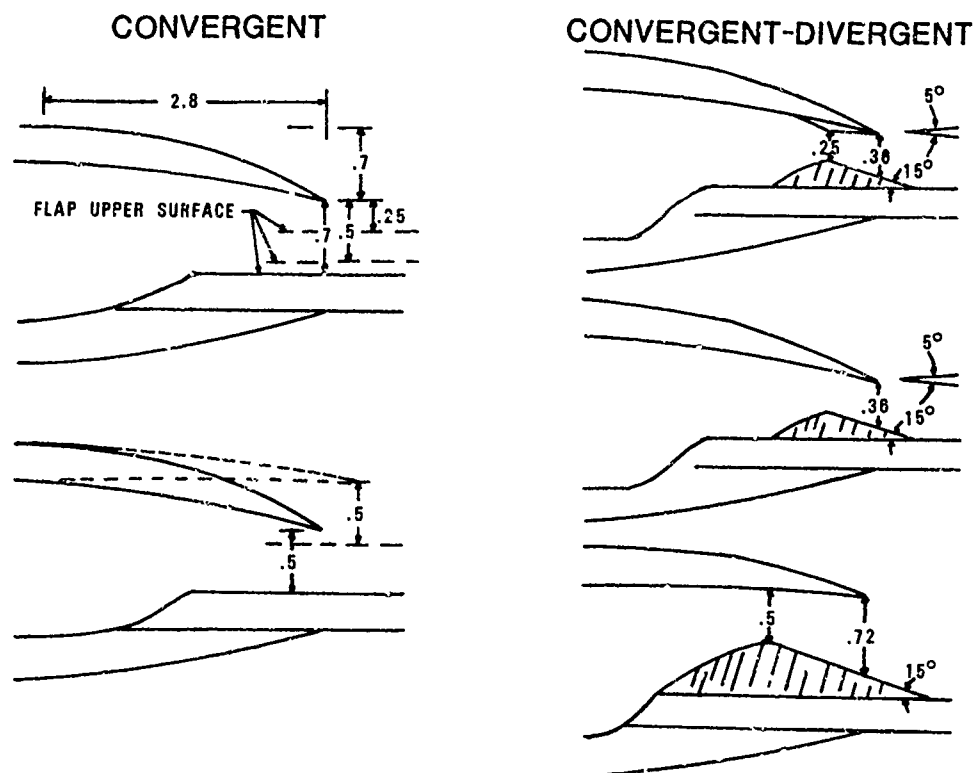
FIGURE 3. NOZZLE GEOMETRY VARIATIONS

CONTOURED FLAP

SEGMENTED PLAIN FLAPS

$\delta_1 = 0^\circ, 5^\circ, 10^\circ, 15^\circ, 20^\circ, 25^\circ$

$\delta_2 = 0^\circ, 5^\circ, 10^\circ, 15^\circ, 30^\circ$
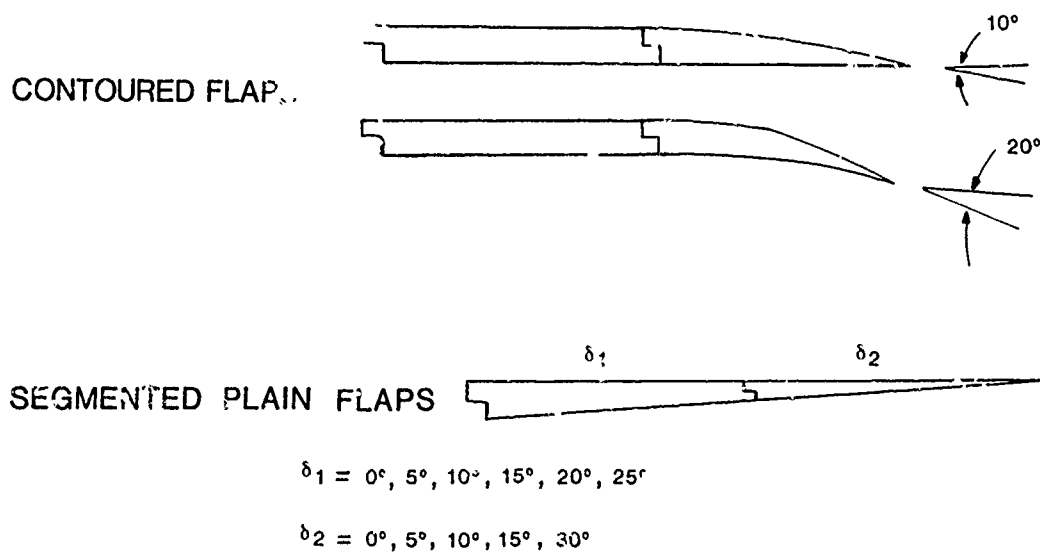
FIGURE 4. FLAP GEOMETRY VARIATIONS
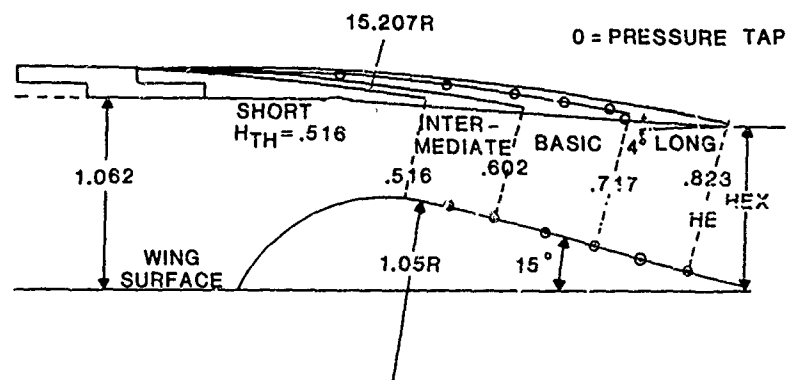
NOZZLE	HE/H_{TH}	HEX/H_{TH}	$(NPR)_{DES}$
BASIC	1.390	1.841	5.35
SHORT	1.595	1.764	7.04
INTERMEDIATE	1.166	1.919	3.59
LONG	1.000	2.002	1.89

FIGURE 5. NOZZLE COWL GEOMETRY VARIATIONS
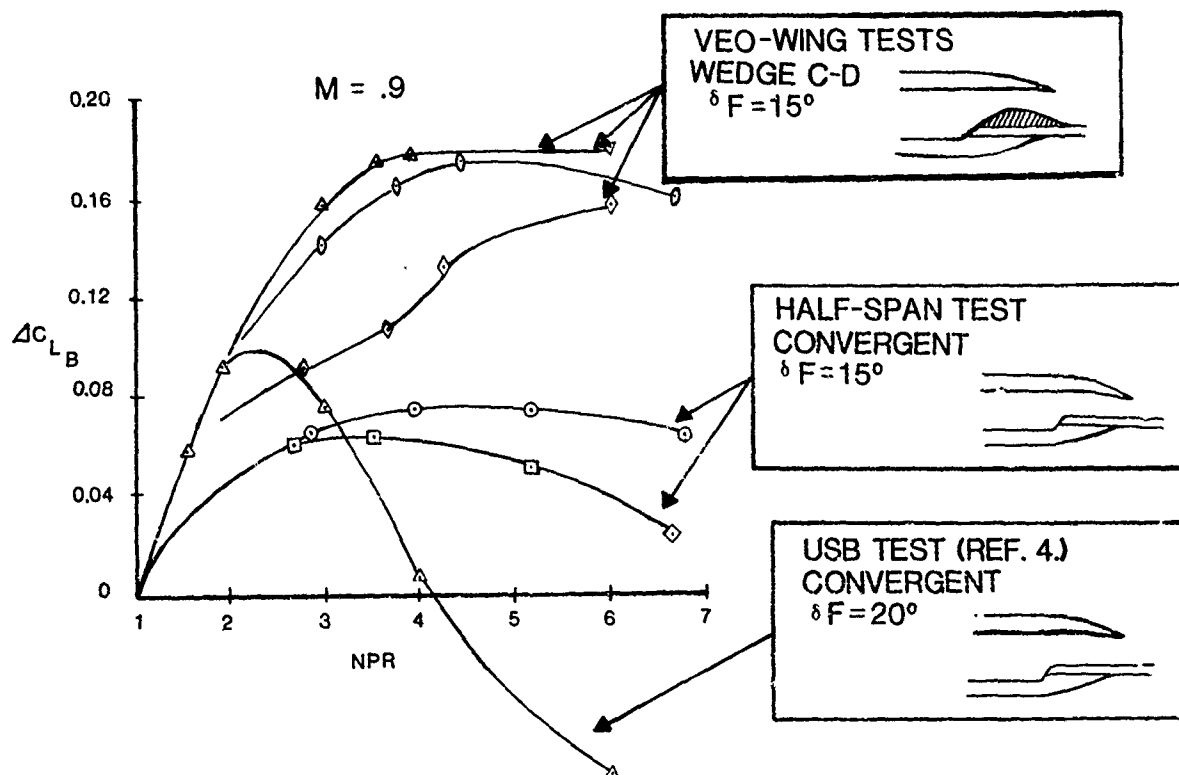
FIGURE 6.   COMPARISON OF TRANSONIC LIFT AUGMENTATION

FIGURE 7. VEO-WING 1/10-SCALE POWERED RESEARCH MODEL

1/10-SCALE POWERED RESEARCH MODEL

ASPECT RATIO 4 NOZZLE
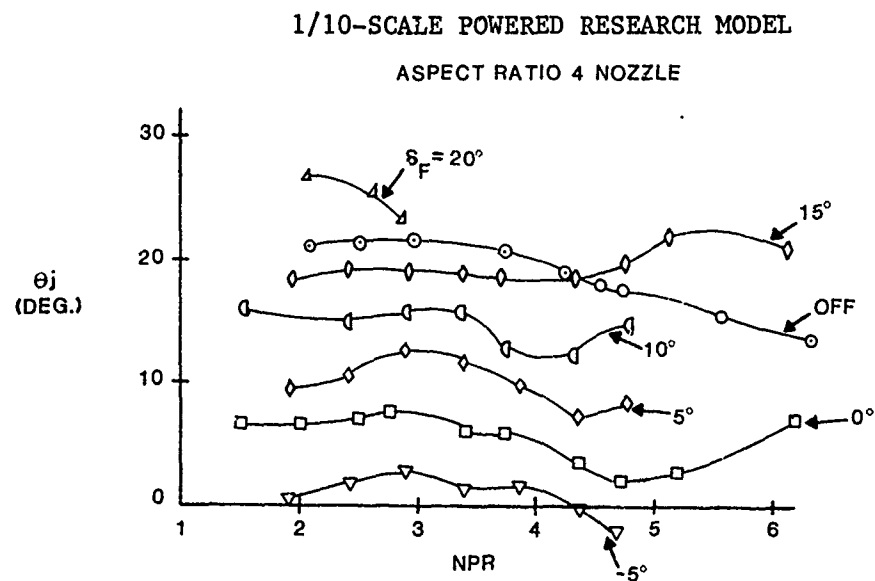
FIGURE 8. STATIC TURNING ANGLE
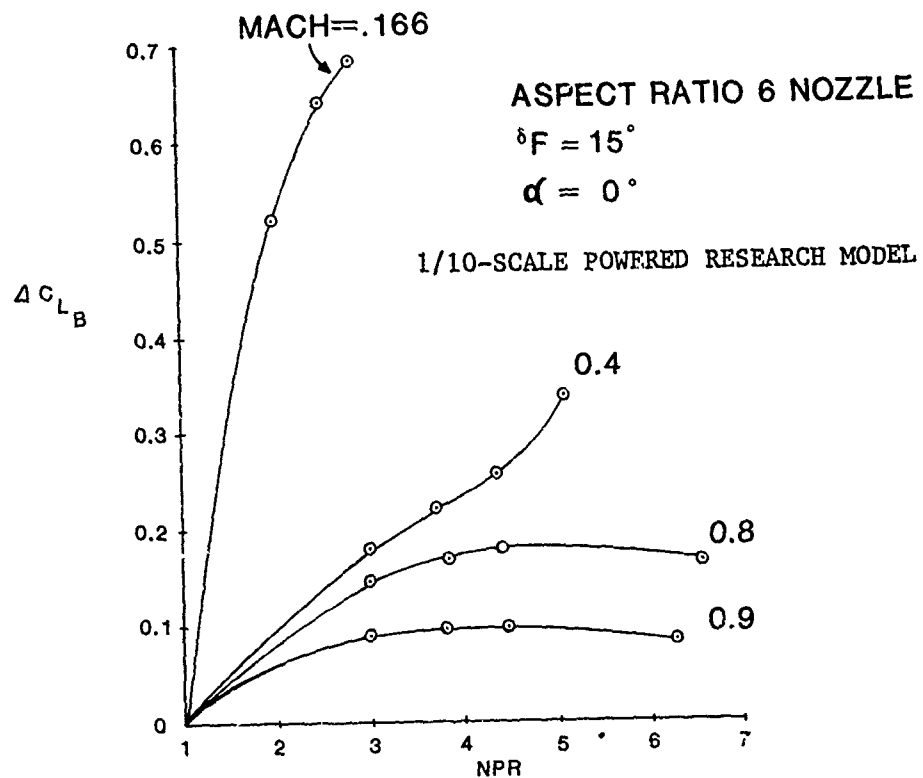
FIGURE 9. LIFT AUGMENTATION COMPARISON

$$G' = \frac{\Delta C_{L_B}}{C_\mu \dfrac{S'}{S_{REF}} \, SIN \, (\theta_j + \alpha)}$$
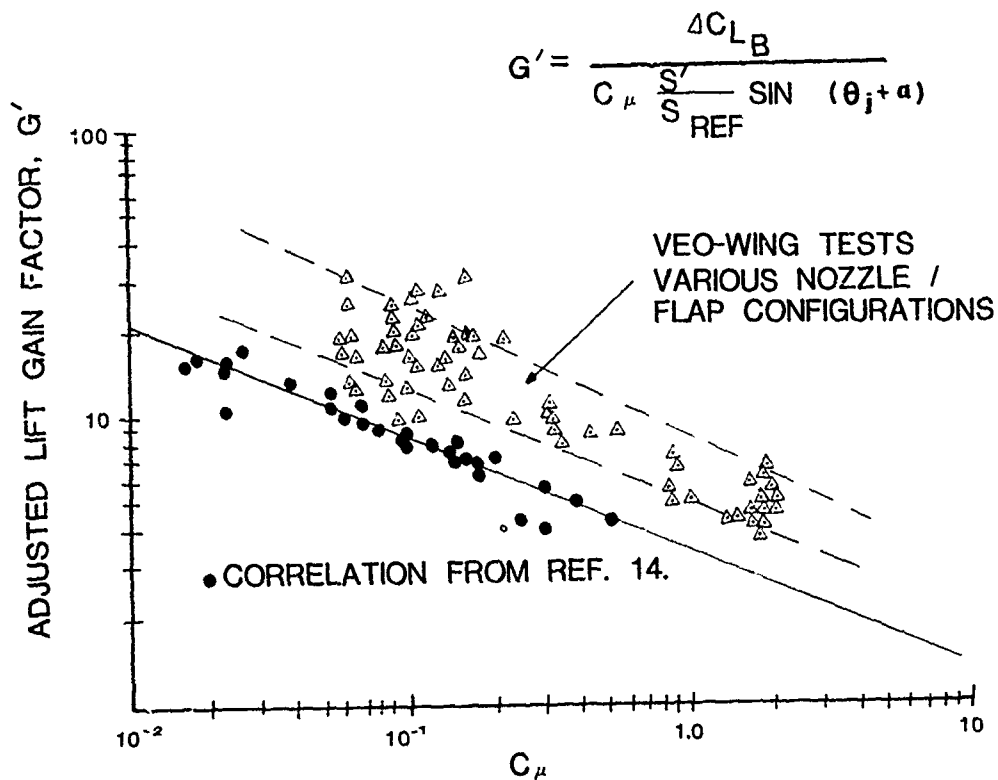
FIGURE 10. COMPARISON OF LIFT GAIN FACTORS
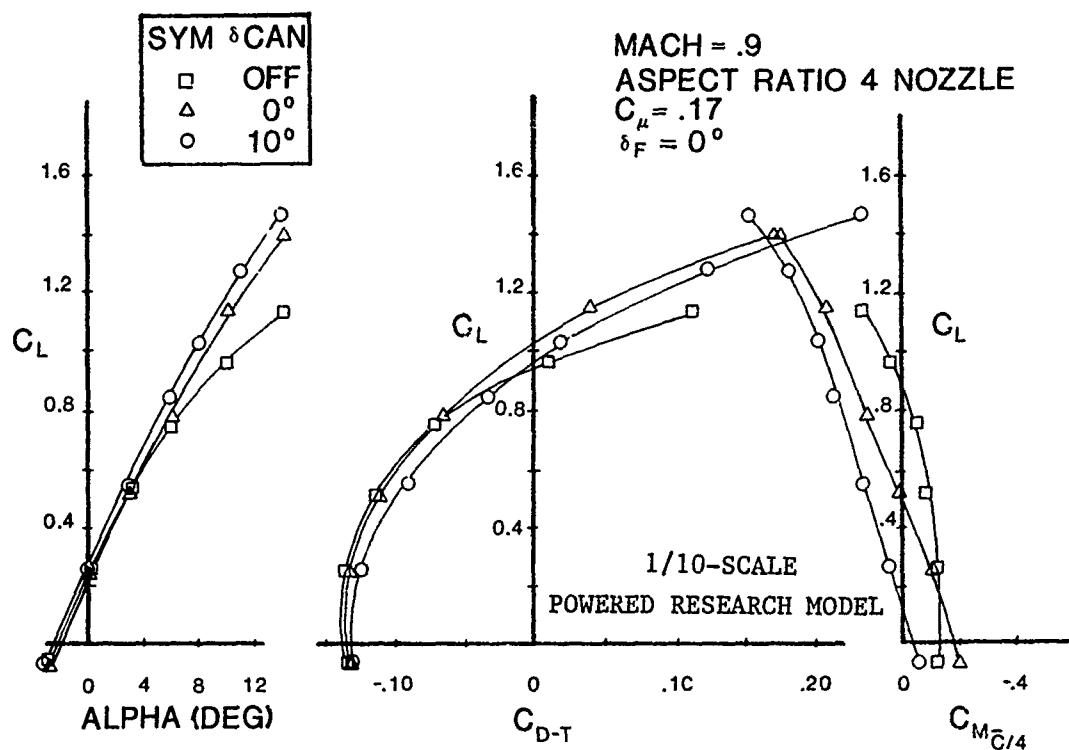
FIGURE 11. CANARD EFFECTS
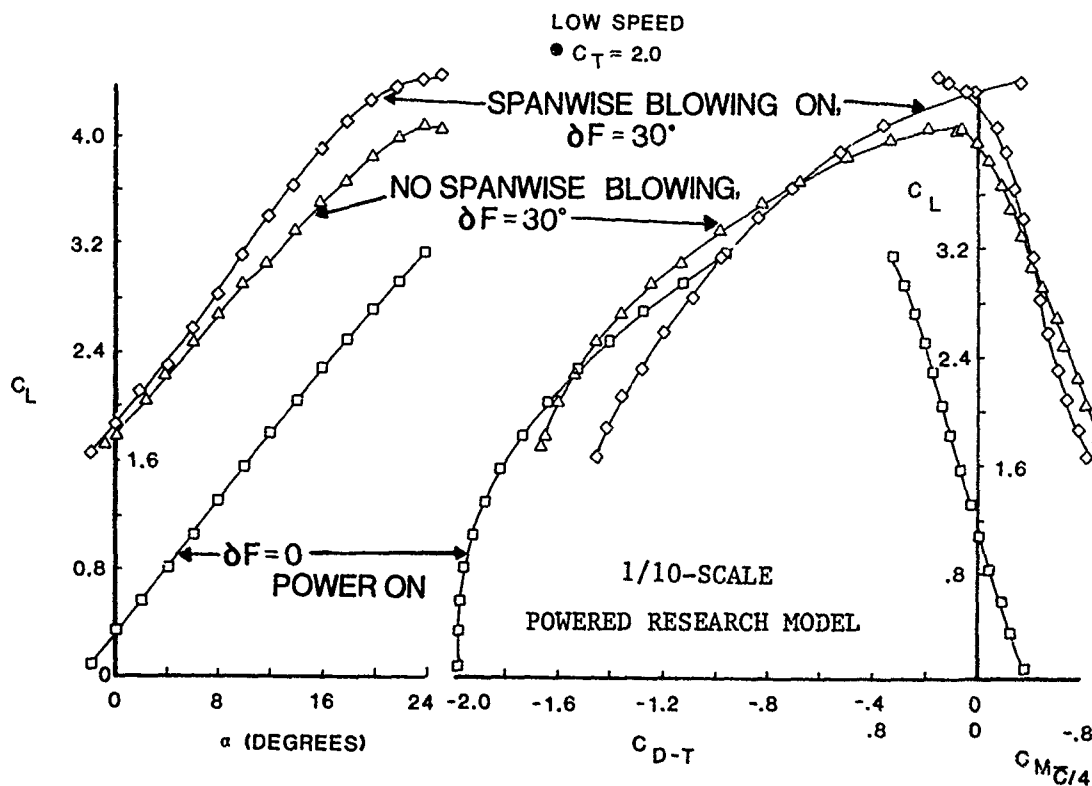
FIGURE 12. SPANWISE BLOWING EFFECTIVENESS
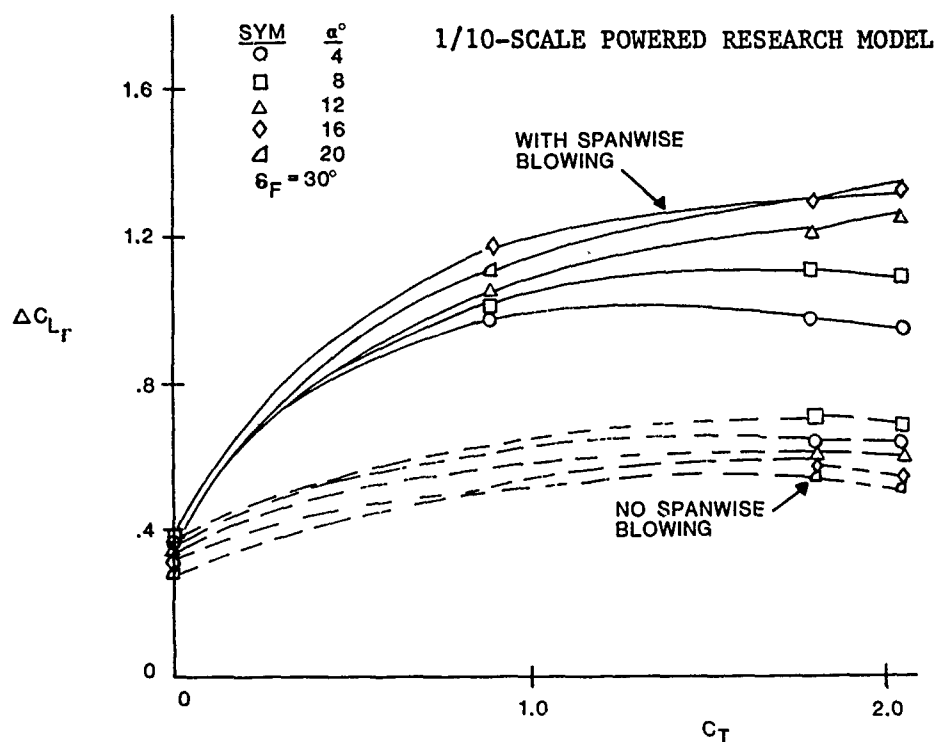
FIGURE 13. LIFT AUGMENTATION
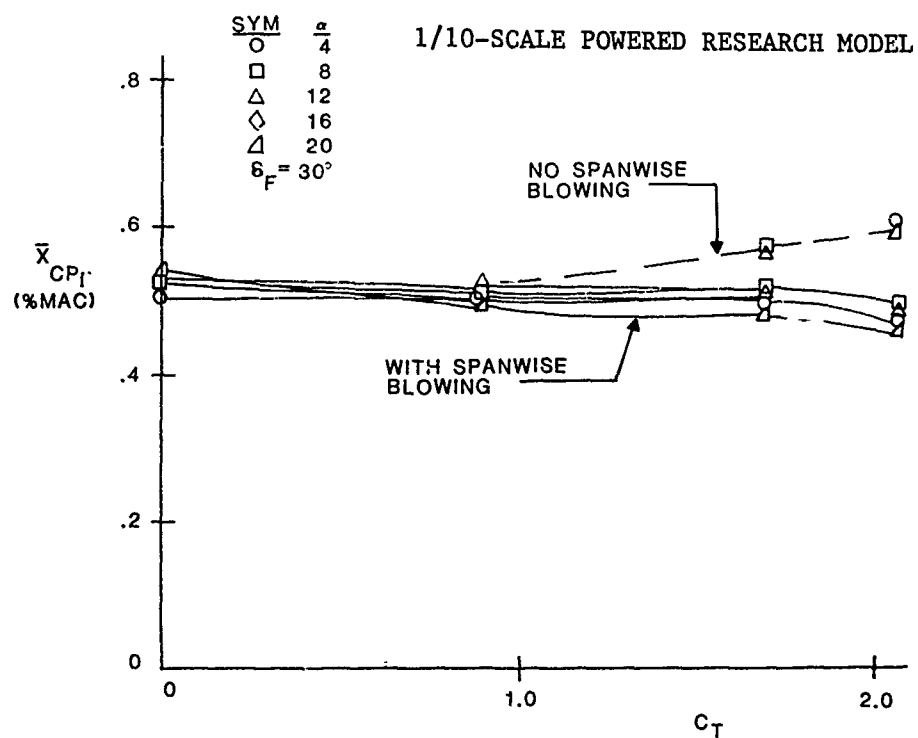
FIGURE 14. CENTER OF PRESSURE EFFECTS
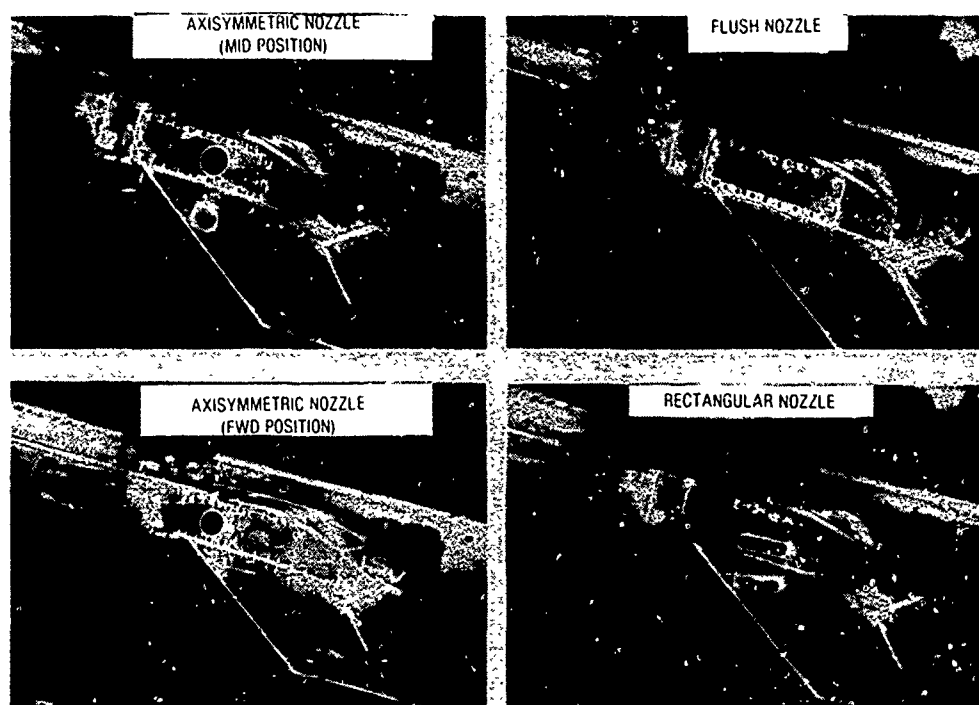
FIGURE 15. SPANWISE NOZZLE PHOTOGRAPHS
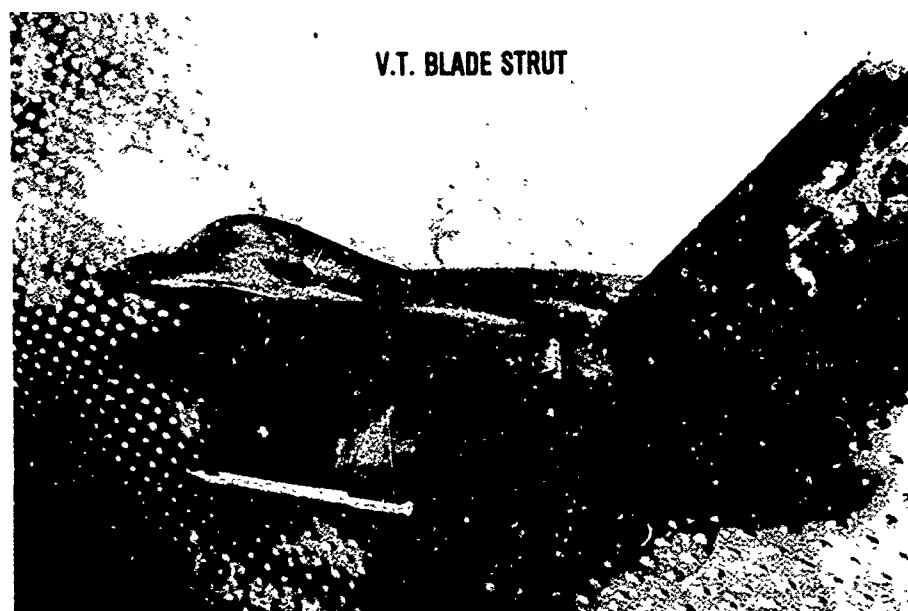
FIGURE 16. VEO-WING 1/15-SCALE CONFIGURATION MODEL
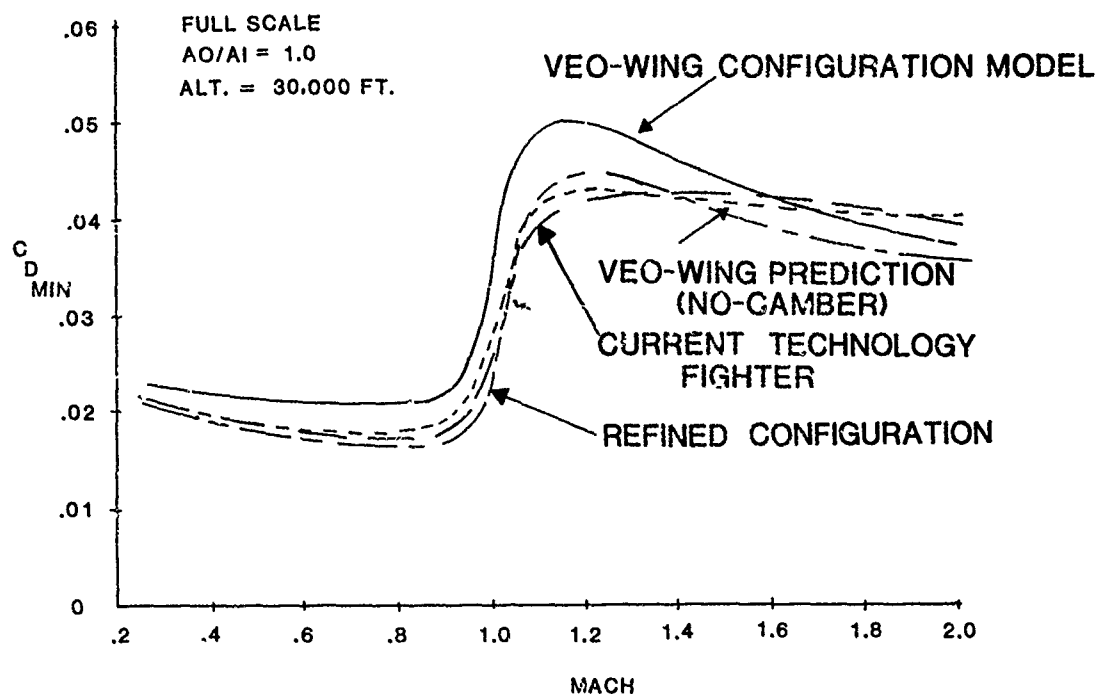
FIGURE 17. MINIMUM DRAG CHARACTERISTICS
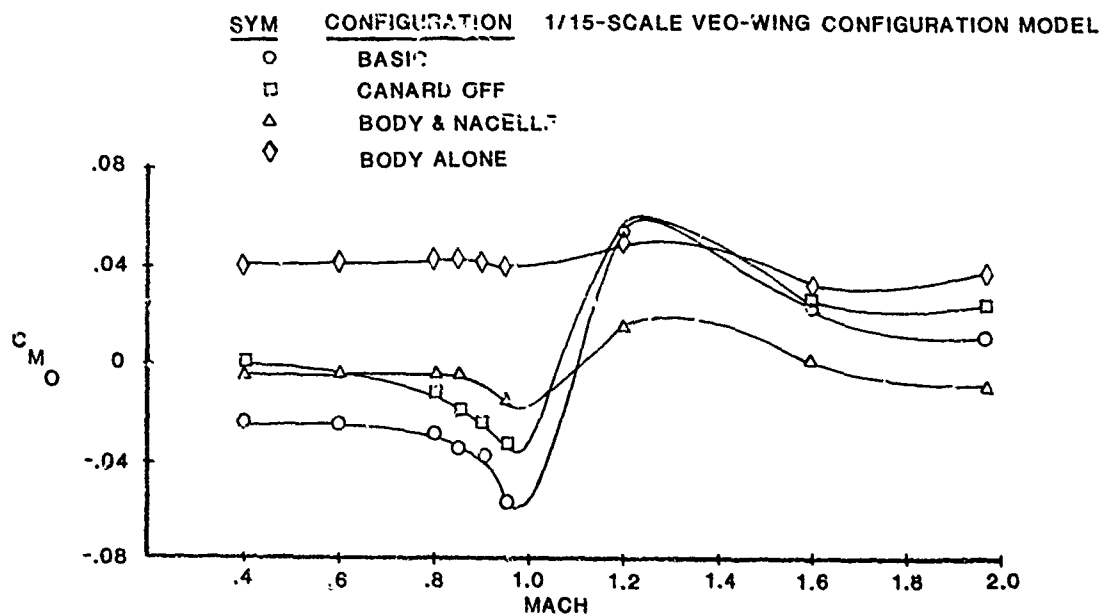
FIGURE 18. ZERO LIFT PITCHING MOMENT BUILDUP

Legend: O STRAKE OFF, △ FWD UPPER, ◻ FWD LOWER, ◊ AFT

$\Delta C_{D_{MIN}} = C_{D_{ON}} - C_{D_{OFF}}$

1/15-SCALE VEO-WING CONFIGURATION MODEL
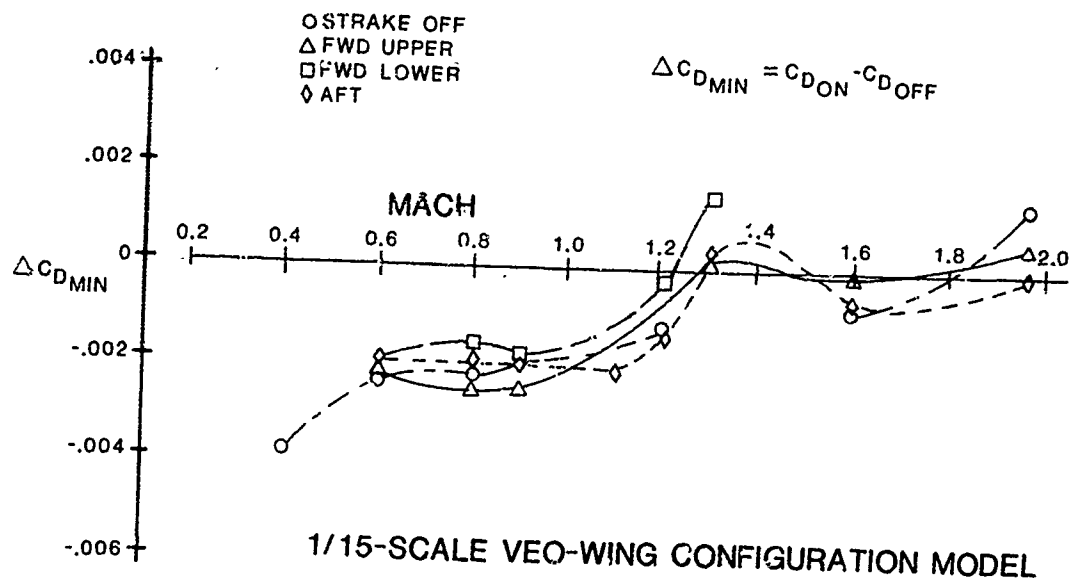
FIGURE 19. EFFECT OF FAIRINGS

WING
  AREA   300 FT^2
  ASPECT RATIO   3.6
  TAPER RATIO   .20
  AIRFOIL   64A204 MOD

CANARD
  EXPOSED AREA   66 FT^2
  ASPECT RATIO   2.16
  TAPER RATIO   .37
  AIRFOIL   64A004

VERTICAL TAIL
  AREA   43 FT^2
  ASPECT RATIO   1.72
  TAPER RATIO   .42
  AIRFOIL   ROOT 5 3X BICON, TIP 4% BICON

PROPULSION
  2 GE F404 ENGINES

ARMAMENT
  GAU-9 30MM GUN
  (2) AIM-9J
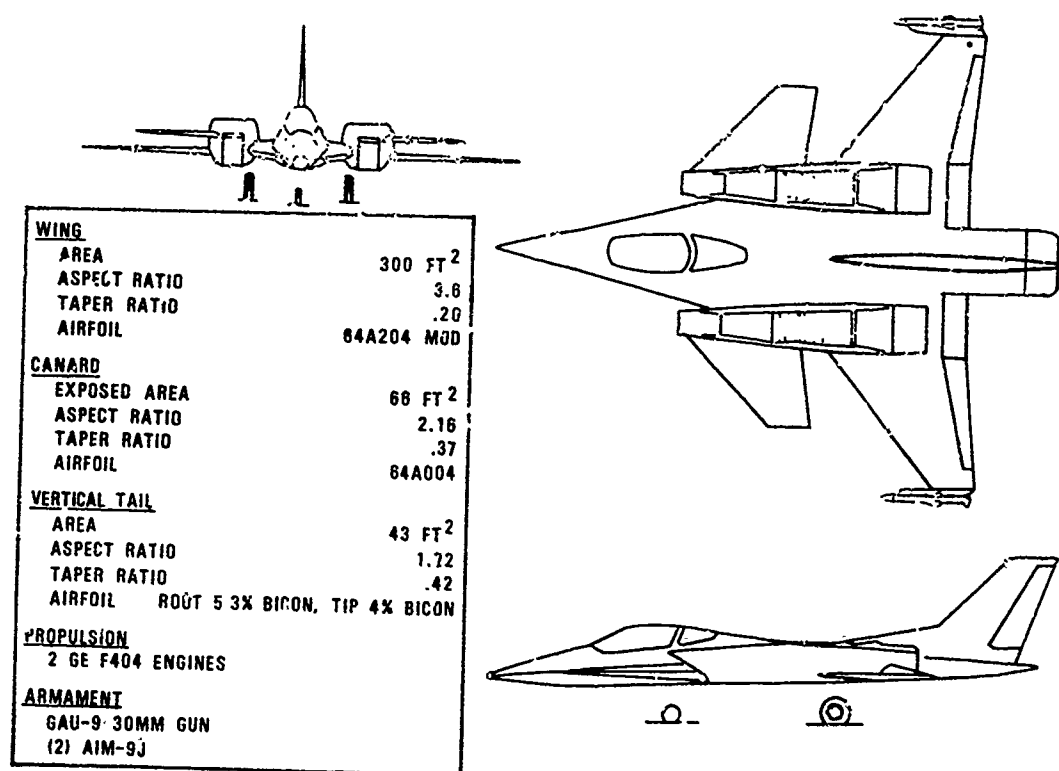
FIGURE 20. VEO-WING ATA FIGHTER
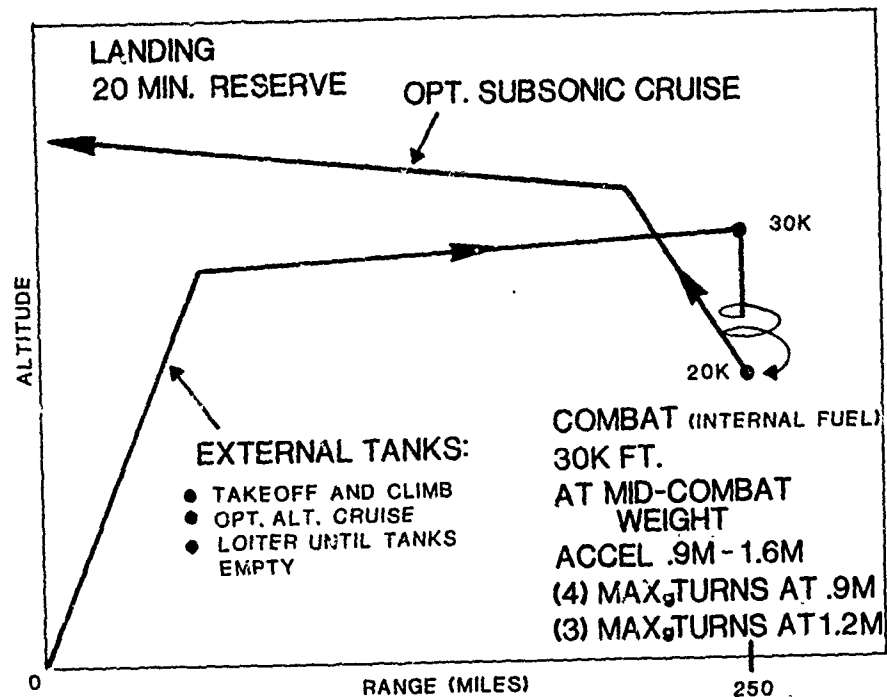
FIGURE 21. AIR SUPERIORITY MISSION PROFILE

MANEUVER PERFORMANCE

● START COMBAT WT	22,718 LB
● MID COMBAT WT	21,197 LB
● COMBAT T/W (.9M/30K FT)	.77
● COMBAT W/S	70.66 LB/FT^2
● SUSTAINED TURN RATE (°/SEC)	
.9 M/30K FT	11.49
1.2 M/30K FT	9.8
.4 M/10K FT	16.84
● ACCEL TIME (SEC)	
.9 M TO 1.6 M/30K FT	34.9

STOL PERFORMANCE

● TAKEOFF GROSS WT	24,016 LB
● LANDING WT	17,077 LB
● TAKEOFF GROUND ROLL	315 FT
● LANDING GROUND ROLL	305 FT

FIGURE 22. VEO-WING ATA FIGHTER PERFORMANCE CAPABILITIES

TAKEOFF

- 3-DOF SIMULATION
- GEAR REACTIONS INCLUDED
- NO ENGINE SPIN-UP
- INSTANTANEOUS PILOT INPUT
- NO WIND
- TAIL BUMP ANGLE 15°
- SPANWISE BLOWING APPLIED NEAR ROTATION

LANDING

- STABILIZED APPROACH (CONSTANT VELOCITY)
- NO FLARE
- MAX SINK RATE 15 FT/SEC
- 1 SEC REVERSE THRUST / BRAKING TIME DELAY
- 50% MIL POWER REVERSE THRUST
- BRAKING COEFFICIENT .45

FIGURE 23. STOL GROUND RULES

TOGW = 24016 LB.
SEA LEVEL STANDARD DAY

SPANWISE BLOWING
ON
OFF

⊙ CONTROLS ACTUATED FOR ROTATION
□ LIFT-OFF
△ 50- FT ALTITUDE

ALTITUDE (FT)

GROUND DISTANCE (FT)
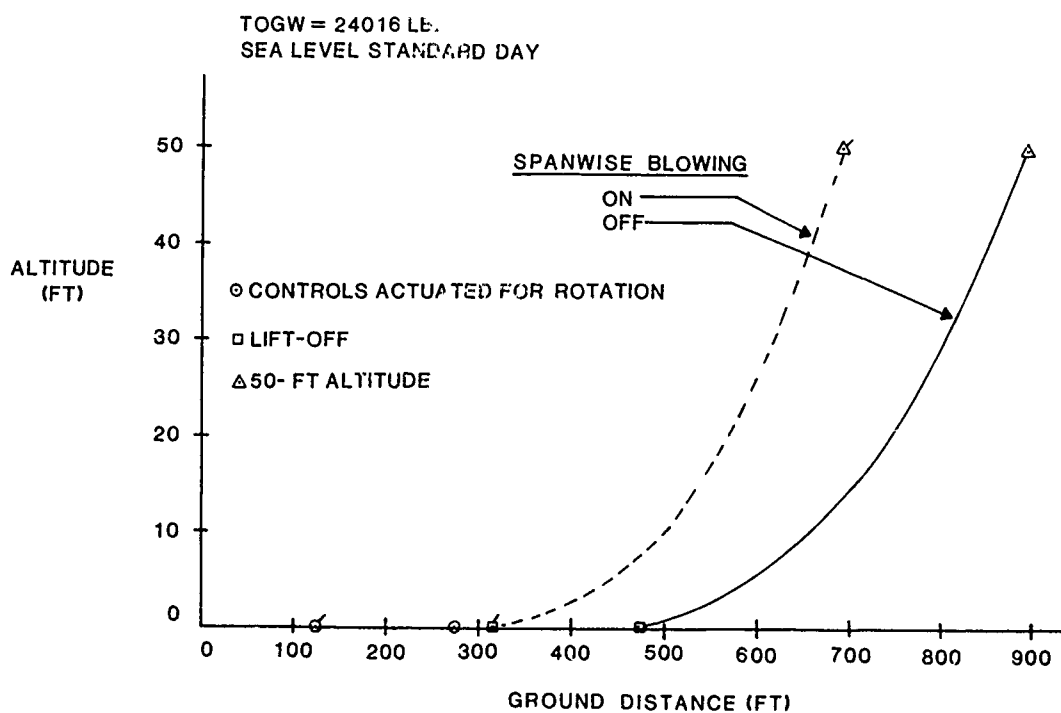
FIGURE 24. VEO-WING ATA FIGHTER TAKEOFF PROFILE

SEA LEVEL STAND. DAY
LAND WT. = 17077 LB
VSINK = 15 FPS
PITCH ATTITUDE = 15"
50% MIL PWR REV. THRUST
1 SEC TIME DELAY FOR THRUST REV/BRAKING
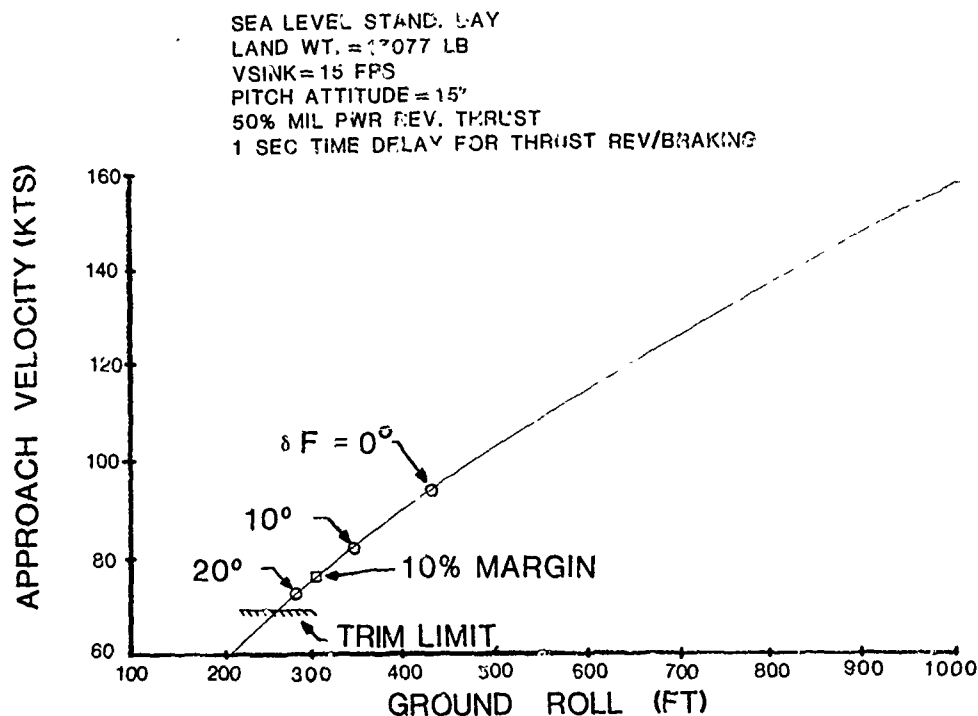
FIGURE 25. VEO-WING ATA FIGHTER LANDING PERFORMANCE

- PAYLOAD-5000LB. ADVANCED WEAPONS & 30 MM GUN

- STOL-SG ≤ 1000 FT. (TROPICAL DAY)

- ALTERNATIVE MISSION CAPABILITY:
  2g'S @ M = 1.6/30 KFT

  3.0g'S @ M = .9/30 KFT 80% FUEL & WEAPONS

① PRE PENETRATION: M = .9/200' AGL
② PENETRATION: M = .9/200' AGL
③ INTERCEPTOR AVOIDANCE:
   • (2) 4.5g TURNS
   • ACCEL M= .9 TO M=.95
④ SAM AVOIDANCE: (6) -8g 45° BREAKS
⑤, ⑥, ⑦ "TANK BUST": CLIMB TO 1000' AGL.

- DECEL TO M=.8,270° 7g TURNS
- EXPEND AMMO,
- LAUNCH WEAPONS,
- REACCEL TO M= .9. DESCEND TO 200' AGL

⑧ EGRESS: ACCEL TO M = 1.15,200' AGL
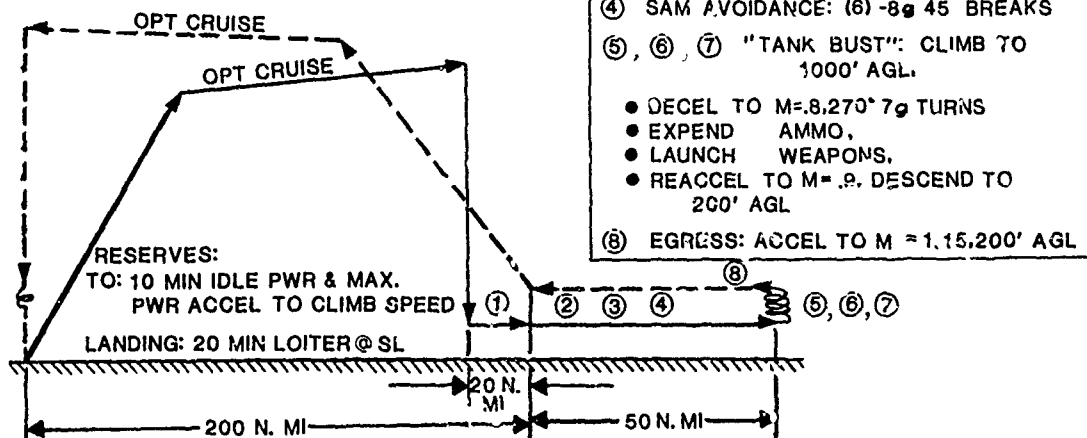
FIGURE 26. AIR-TO-GROUND MISSION PROFILE

WING

AREA	395 FT^2
ASPECT RATIO	2.84
TAPER RATIO	0.1728
AIRFOIL	NACA 64A003.5

CANARD

EXPOSED AREA	70 FT^2
ASPECT RATIO	2 18
TAPER RATIO	0.3701
AIRFOIL ROOT 64A006, TIP 64A003	

VERTICAL TAIL

AREA (THEO)	41.39 FT^2
ASPECT RATIO	1.07
TAPER RATIO	0.4752
AIRFOIL ROOT 6% BICON, TIP 3.0% BICON	

PROPULSION

2 P&W PARAMETRIC ENG.
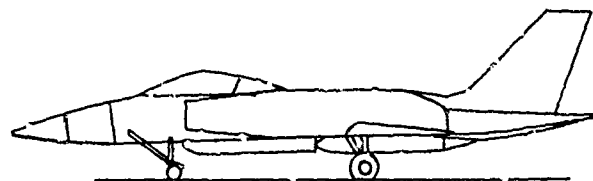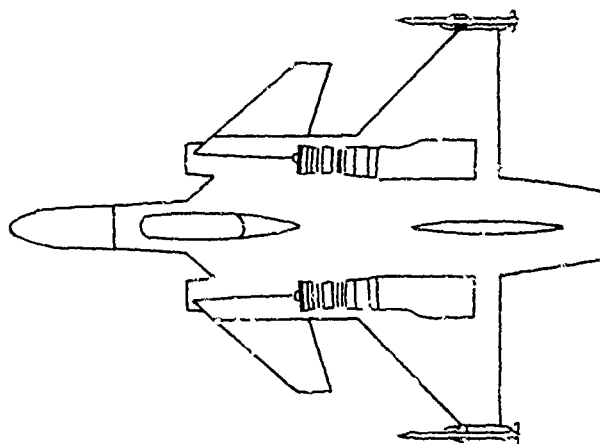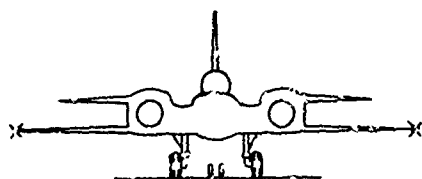
FIGURE 27. VEO-WING ATG FIGHTER POINT DESIGN

WING

AREA	475 FT^2
ASPECT RATIO	3.12
TAPER RATIO	0.1980
b/2	230.931 IN.
AIRFOIL NACA 64A004	

HORIZONTAL TAIL

EXPOSED AREA	85 FT^3
ASPECT RATIO	2.82
TAPER RATIO	.252
AIRFOIL ROOT 6% BICON, TIP 3.5% BICON	

VERTICAL TAIL

AREA (THEO)	78.55 FT^2
ASPECT RATIO	1.17
TAPER RATIO	0.2701
AIRFOIL ROOT 6% BICON, TIP 3C% BICON	

PROPULSION

2 P&W PARAMETRIC ENG.
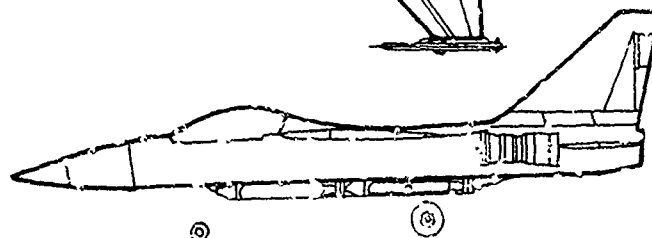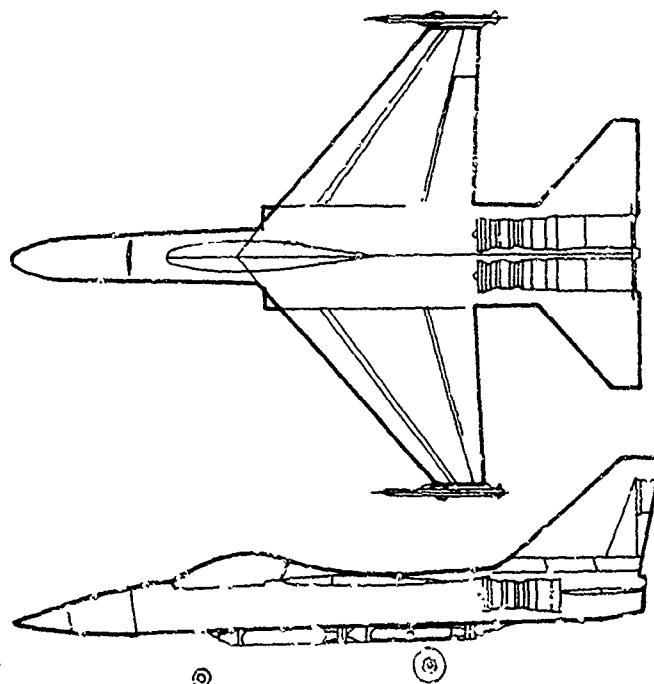
FIGURE 28. CONVENTIONAL ATG POINT DESIGN

	CONVENTIONAL	VEO-WING
SIZE		
TOGW (LB)	47040	47326
T/W	.939	.893
W/S (LB/FT^2)	99	119.8
S$_{REF}$ (FT^2)	475	395
MISSION PERFORMANCE		
SUST g @ .9M/30K FT.	3.17	2.85
.9M/200 FT.	9.0	9.0
1.6M/30K FT.	3.82	3.33
ACCEL TIME (SEC)		
.9M TO 1.6M/30K FT.	64	56.7
FERRY RANGE (N. MI)	2371	2112
STOL PERFORMANCE		
LIFTOFF SPEED (KT)	140	117
TAKEOFF GROUND ROLL (FT)	1285	940
TOTAL TAKEOFF TO 50 FT.	1748	1280
APPROACH SPEED (KT)	108	100
LANDING GROUND ROLL (FT)	1045	885
TOTAL LANDING DISTANCE FROM 50 FT	2149	1600

FIGURE 29. PERFORMANCE COMPARISON
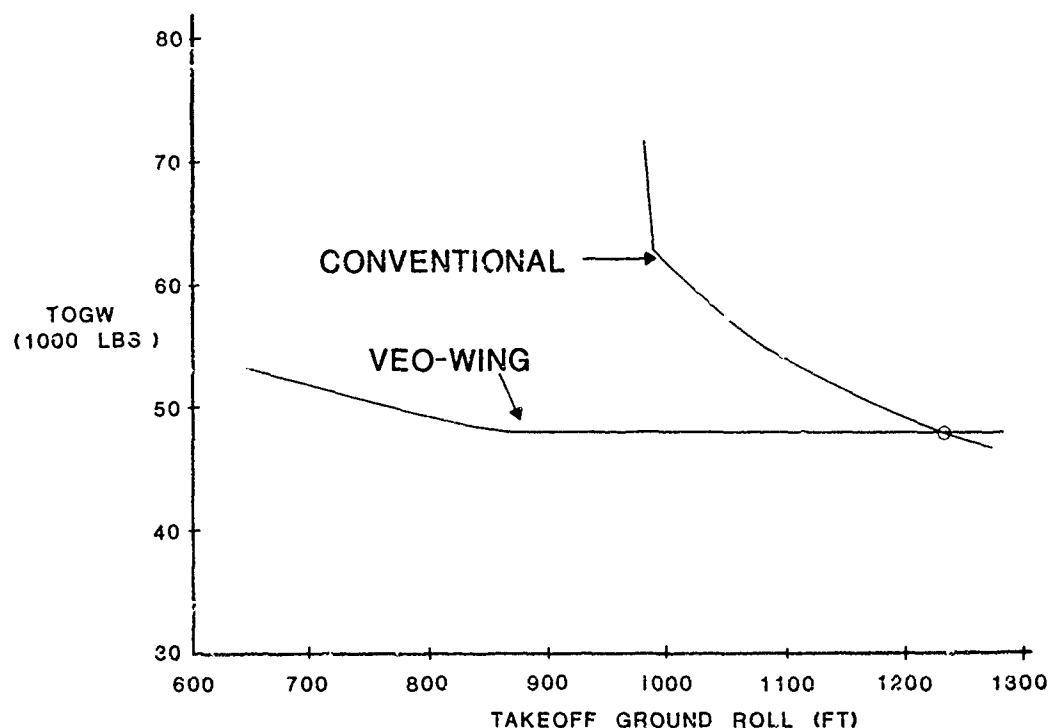
FIGURE 30. ATG POINT DESIGN SENSITIVITY

ERRATA

for

Wind-Tunnel Investigation of Highly-Maneuverable

Supersonic V/STOL Fighter

by

Michael Falarski

The pitching moment data in the paper are incorrect because of an error in the length of the mean aerodynamic chord (mac). The actual mac is 2.61 m (8.56 ft.) not 2.33 m (7.66 ft.) as reported, which makes an 11.7 percent error in the calculation of pitching moment coefficient. The moments reference is at 12% of the mac, not the leading edge as stated in the text. The pitching moment data has been corrected and is presented in AIAA Paper 80-0234 along with the data from other model configurations.

WIND-TUNNEL INVESTIGATION OF HIGHLY MANEUVERABLE

SUPERSONIC V/STOL FIGHTER

Michael Falarski

Ames Research Center, NASA
Moffett Field, California 94035

Presented at

V/STOL Aerodynamics Workshop

May 1979

U.S. Naval Postgraduate School, Monterey, California

WIND-TUNNEL INVESTIGATION OF HIGHLY MANEUVERABLE

SUPERSONIC V/STOL FIGHTER

Michael Falarski

Ames Research Center, NASA
Moffett Field, California 94035

ABSTRACT

This paper presents a brief summary of the results from the initial wind-tunnel test of a large-scale, highly maneuverable supersonic V/STOL fighter model in the Ames 40- by 80-Foot Wind Tunnel. The STOL configuration which was tested combines upper surface blowing and spanwise blowing to improve the lift characteristics over a wide angle-of-attack range. A close-coupled canard was added to this configuration to create a highly maneuverable STOL aircraft. The 7.28 m (24 ft) span model is powered by two J-97 turbojet engines, each producing 9340 N (2200 lb) thrust at a pressure ratio of 2.

With the nozzle flap and aileron set at 30°, the model produced lift coefficients greater than 4. The model was longitudinally unstable because of the forward canard position and because of the large body area of fuselage, strake, and nacelles forward of the center of gravity. The canard had a positive interference effect on both lift and drag but was limited in its control effectiveness by stall. Spanwise blowing delayed wing stall and increased the linear portion of the lift curve. It did not significantly increase maximum lift, however, because of body stall.

INTRODUCTION

In recent years, interest in military application of V/STOL technology has revived, especially regarding the development of a highly maneuverable, supersonic fighter aircraft. Recent aircraft design studies (ref. 1) have detailed areas where technological uncertainties still exist which will impede the development of a V/STOL aircraft. Because the takeoff and approach performance is one of these areas of uncertainty, Ames has designed and fabricated a large-scale wind-tunnel model of a V/STOL fighter to study low-speed aircraft characteristics. This model can be adapted to different V/STOL propulsion concepts.

This paper presents a brief summary of the results from the initial wind-tunnel test of this model adapted to the upper surface blowing propulsion concept. This is combined with spanwise blowing (SWB) and closed-coupled canards to augment the lift over a wide angle-of-attack range. Results of wind-tunnel tests of a similar small-scale model (refs. 2-3) have shown that this combination produces a highly maneuverable STOL concept.

The complete model description and analysis of all the wind-tunnel results will be published at a later date in a NASA Technical Memorandum.

SYMBOLS

b wing span, m (ft)

C_d drag coefficient, $\dfrac{\text{drag}}{qs}$

C_L lift coefficient, $\dfrac{\text{lift}}{qs}$

C_{L_Γ} circulation lift coefficient, $\dfrac{\text{circulation lift}}{qs}$

C_l roll moment coefficient, $\dfrac{\text{roll moment}}{qs\,b}$

C_{l_β} rate of change of C_l with β

$C_{m_{LE}}$ pitching-moment coefficient, $\dfrac{\text{pitching moment}}{qS\bar{c}}$

C_n yawing-moment coefficient, $\dfrac{\text{yawing moment}}{qs\,b}$

C_{n_β} rate of change of C_n with β

C_T thrust coefficient, $\dfrac{\text{total axial gross thrust}}{qs}$

C_Y side-force coefficient, $\dfrac{\text{side force}}{qs}$

C_{Y_β} rate of changes of C_Y with β

c   local wind chord, m (ft)

$\bar{c}$ mean aerodynamic chord, m (ft)

q   wind-tunnel free-stream dynamic pressure, n/m (lb/ft)

S   wing reference area, m (ft)

α wing angle of attack, deg

β sideslip angle, deg

δ_a aileron deflection angle ref. to aileron centerline, deg

δ_c canard deflection angle, deg

δ_f nozzle flap deflection angle ref. to flap centerline, deg

Note: All moments referenced to leading edge of $\bar{c}$. Forces are wind axes and
        moments are stability axes.

MODEL AND TEST DESCRIPTION

The V/STOL fighter model is shown installed in the test section of the
Ames 40- by 80-Foot Wind Tunnel in figure 1. A sketch of the overall model
and propulsion system geometries are presented in figure 2. The model is
approximately 0.7 scale incorporating a 40° swept wing with pitching moment
control provided by a close-coupled canard and beaver tail. For this investi-
gation the canard was mounted in the forward position of the three available
longitudinal canard positions. Limited test time did not allow for the inves-
tigation of the canard leading- and trailing-edge flaps nor the beaver tail.

The model is powered by two J-97 turbojet engines mounted in nacelles at
0.33 b/2 to provide a strake between the fuselage and nacelles for future
integration of a VTOL ejector propulsion system. The engine exhaust is pre-
turned to 25° by the aspect ratio = 8, two-dimensional wedge nozzle. It is
blown over the upper surface of the nozzle flap. The nozzle flap is capable
of vectoring the exhaust from -10° to +30°. When tests were made with SWB,
the flap nozzle area is reduced 17% and the SWB nozzle uncovered. The SWB
nozzle is mounted flush with the outboard nacelle wall at 23% of the wing root
chord. Both a circular and an aspect ratio = 4 rectangular nozzle have been
designed for the model. The rectangular nozzle was used for this
investigation.

The model has been instrumented to measure: canard, strake, wing, and beaver-tail surface pressures; wing- and beaver-tail surface temperatures; exhaust total pressure distribution at nozzle exit and flap trailing edge; and engine duct flow properties before and after the SWB nozzle station. The surface instrumentation is located on the model's left side and can be seen in figure 1 as the unpainted strips.

The model was investigated through angle of attack and sideslip ranges of -8° to +40° and -10° to +30°, respectively, and thrust coefficients of approximately 0 to 2.0. The engines were operated at exhaust total pressure ratios of 1.8 and 2.0. Most of the data were taken at 2.0 which produces a thrust per engine of 9341 N (2200 lb) and an exhaust temperature of 1100° F. The model is now undergoing a static thrust calibration to determine exact thrust coefficients.

RESULTS AND DISCUSSION

The principal objective of this first wind-tunnel test was to investigate the longitudinal aerodynamics of the basic V/STOL fighter configuration, and to briefly sample the canard and SWB effects and lateral-directional characteristics. The longitudinal results will be discussed first in detail followed by a brief discussion of the lateral-directional data. The model data matrix will be completed with two additional wind-tunnel entries in 1979.

Basic Model Longitudinal Characteristics

The longitudinal characteristics of the model with the nozzle flap and aileron set at 30° and the canard at 0° is presented in figure 3. The lift curve slope is linear up to $\alpha = 15°$ where the wing stalls. The lift continues to increase after the wing stalls because of the lift generated by the body consisting of the strake, fuselage, and nacelles. Power increased $C_{L_{MAX}}$ and α_{STALL} but had little effect on the lift curve slope. The $C_{L_{MAX}} > 4$ were achieved with $C_T = 2$.

The model pitching moment has been referenced to the leading edge of the mean aerodynamic chord, $\bar{c}$, which design studies have shown to be a reasonable location of the aircraft center of gravity. With this moment reference the model is longitudinally unstable with a negative static margin of >0.40. Power does not change the margin but does produce large negative moment shifts. This large instability results from the lift generated by the canard, strake, nacelle, and fuselage forward of the reference. Moving the canard to the aft position will relieve this instability but may not reduce it to the -0.15 to -0.20 static margin desirable for modern aircraft control systems.

Canard Effects

The effect of canard presence and its deflection are presented in figures 4 and 5, respectively. The canard has a favorable effect on both lift

and drag. Wing stall is delayed and $C_{L_{MAX}}$ increased by approximately 0.3. Drag is reduced over the entire lift range with the effect larger at the high lifts. The principal adverse effect is the increased longitudinal instability. Moving the canard aft would reduce this instability. This configuration will be investigated during the next wind-tunnel test.

The canard was effective in controlling pitching moment up to a combined canard deflection and angle of attack of 24°. Above 24° the canard stalled and the pitching moment returned to the undeflected valve. The use of the canard leading edge to delay stall and extend the canard usefulness will be investigated during the next test.

Nozzle Flap Effects

The data discussed up to now have been for a nozzle flap deflection of 30°. A limited amount of data was also recorded at a deflection of 0°. In both cases the aileron were deflected to the same angle as the nozzle flap. A comparison of the two flap deflections with the canard removed is presented in figure 6. Reducing the flap deflection reduced the lift at a constant angle of attack and delayed stall allowing almost the same maximum lift to be achieved. Drag was reduced at low lifts and increased at the high lift. This flap change also produced a large positive shift in the zero-lift pitching moment.

Spanwise Blowing (SWB) Effects

The upper surface blowing concept is designed to enhance aircraft lift over a wide range of α by combining the jet flap effect to induce circulation lift, and vortex augmentation to delay wing stall. The jet flap effect is created by the two-dimensional nozzle/flap, while the vortex augmentation is provided by the SWB. The SWB delays wing leading-edge vortex breakdown delaying wing stall (ref. 4). The SWB for the fighter model is provided by diverting 17% of the J-97 exhaust to a rectangular nozzle mounted flush with the outboard nacelle wall at 23% of the wing root chord. As can be seen in figure 7, SWB did delay stall and increased lift at the high α. The maximum lift and model stall were not significantly altered because they are controlled by body stall. SWB also reduced drag and pitching moment at the high lifts. All of these effects were much more pronounced at the high thrust coefficients.

To assist in understanding of the SWB effects, the wing surface pressures and temperatures are being analyzed. A typical example of these data is presented in figures 8 and 9. These data show SWB to significantly increase both the aerodynamic load and temperature at the wing tip. The temperature data were severely limited by premature failure of the thermocouple probes resulting from the adverse flow environment. These probes will be modified for future tests, and several dynamic transducers will be installed in the wing to measure pressure fluctuations. The SWB data are still being analyzed, but initial results indicate that incorporation of SWB into an aircraft will necessitate change in the wing structure to cope with the pressure and temperature environment.

Circulation Lift

As previously indicated the model is designed to provide flow circulation to enhance the aircraft lift. The model circulation lift, C_{L_Γ}, at $\alpha = 0$ with and without SWB is presented in figure 10. The upper surface blowing does benefit from circulation lift and SWB increases it even further. The C_{L_Γ} can amount to 15 to 30% of the total lift depending on the thrust coefficient and the SWB. Without SWB the C_{L_Γ} increases very slowly above $C_T = 0.8$, while with SWB operation C_L continues to increase as a result of increased circulation around the wing.

Lateral-Direction Characteristics

The limited lateral-directional data recorded during this first test indicate no unusual characteristics (figs. 11-12). The basic model, with the flaps and aileron deflected to 30°, and the canard at 0°, shows positive side force and lateral stability. It also shows neutral to slightly unstable directional stability at low α and β. Power has a small effect on the lateral and directional stability. Angle of attack has a destabilizing effect on the lateral stability while increasing directional stability. SWB had only small effects on the lateral-directional characteristics.

CONCLUSIONS

The following general conclusions can be drawn from the results of the initial investigation of the fighter model:

1. An upper surface blowing concept applied to a V/STOL fighter configuration can produce maximum lift coefficients greater than 4.

2. Lift generated by the canards, strake, and fuselage area forward of the c.g. contributes to static instability, and for the configuration tested, resulted in a large unstable static margin.

3. Canards delay wing stall and reduce drag, but their control effectiveness is limited by stall.

4. The spanwise blowing delayed wing stall but did not significantly increase maximum lift because maximum lift is controlled by body stall.

5. At $\alpha = 0°$, the upper surface blowing induces circulation lift that is about 15 to 20% of the total lift.

REFERENCES

1. Lummus, J. R.: Study of Aerodynamic Technology for a V/STOL Fighter/ Attack Aircraft. NASA CR-152128, 1978.

2. Whitten, Perry D.: An Experimental Investigation of a Vectored-Engine-Over-Wing Powered-Lift Concept. AFFDL-TR-76-92, 1978.

3. Bradley, R. G.; Jeffries, R. R.; and Capone. F. J.: A Vectored-Engine-Over-Wing Propulsive-Lift Concept. AIAA Paper 97-917, Sept. 1976.

4. Bradley, R. G.; and Wray, W. O.: A Conceptual Study of Leading-Edge Vortex Enhancement by Blowing. AIAA J. of Aircraft, vol. II, Jan. 1974.
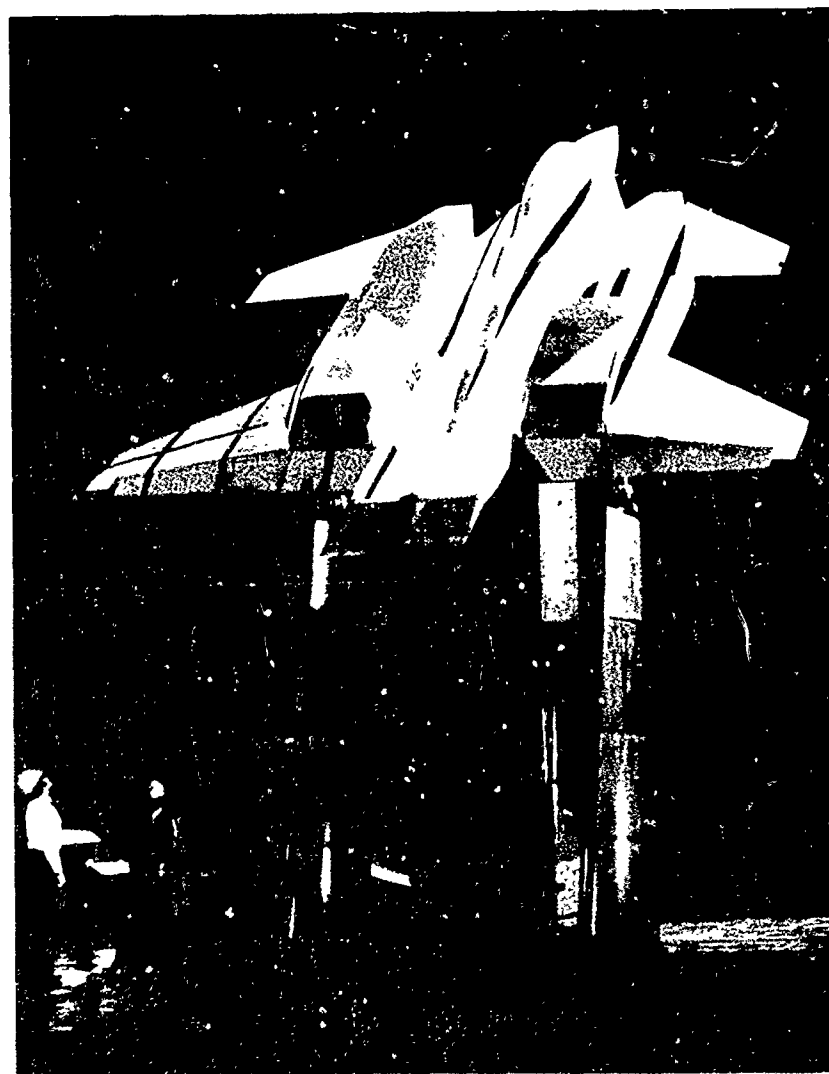
(a) 3/4 rear view.

Figure 1.- V/STOL fighter model installed in wind tunnel.
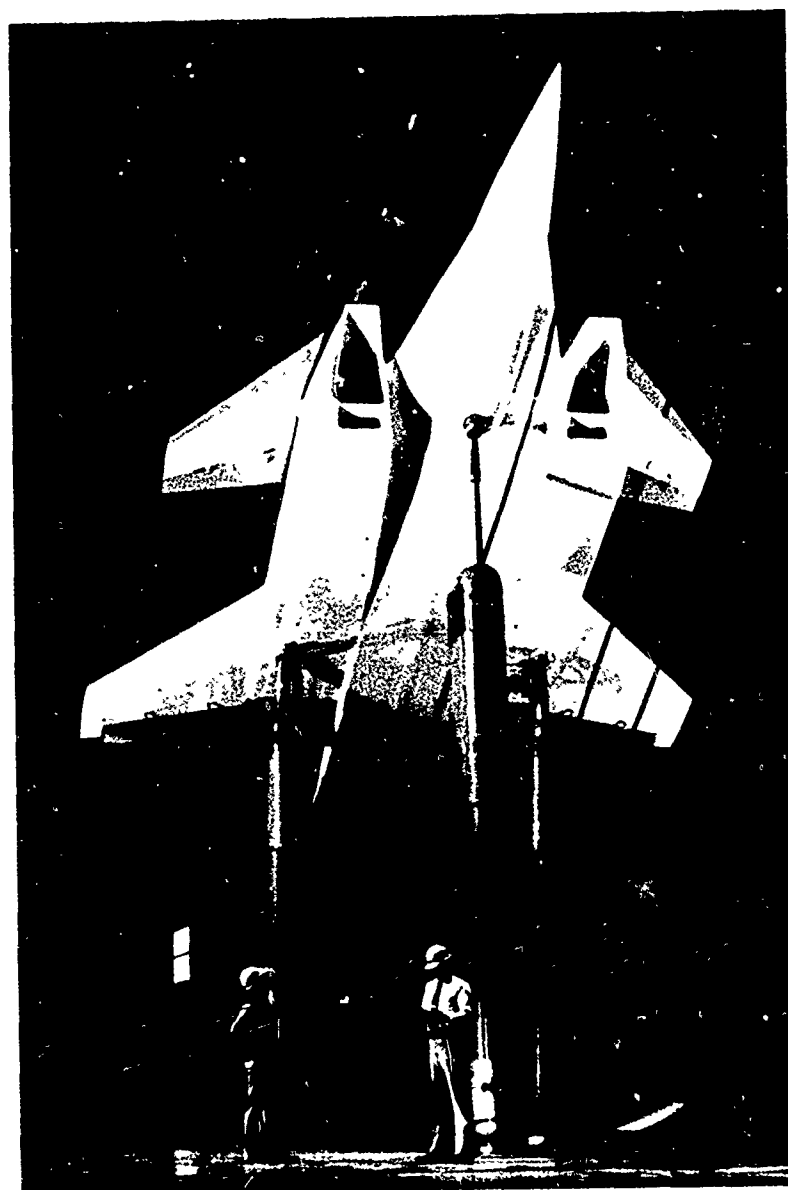
(b) 3/4 front view.

Figure 1.- Concluded.
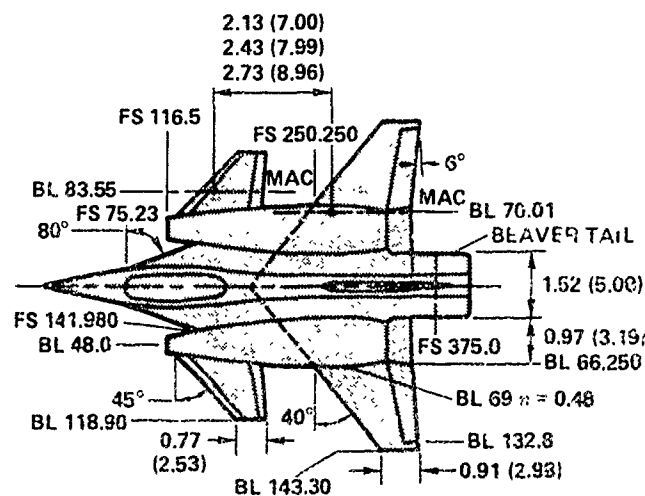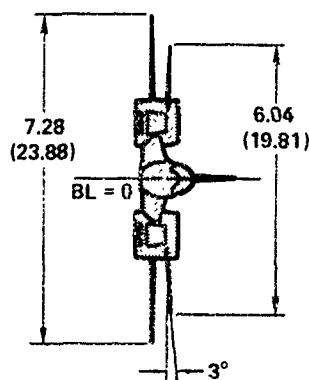
WING:

REFERENCE AREA, m² (ft²)	17.00 (183.0)
ASPECT RATIO	3.12
TAPER RATIO	0.238
AIRFOIL SECTION	64A204
GEOMETRIC TWIST	-4°
MEAN AERO CHORD, m (ft)	2.33 (7.66)

CANARD:

AREA, m² (ft²)	5.43 (58.5)
CANARD AREA/WING AREA	0.32
ASPECT RATIO	2.4
TAPER RATIO	0.345
AIRFOIL SECTION	64A004
MEAN AERO CHORD, m (ft)	1.51 (4.94)
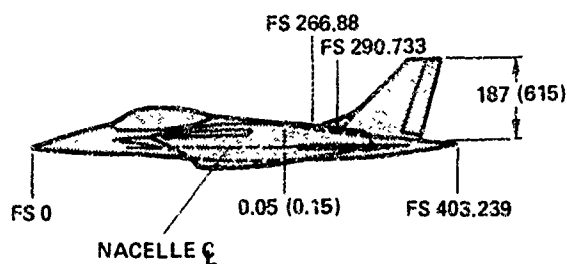
ALL DIMENSIONS IN m (ft)

(a) V/STOL fighter model overall geometry.

Figure 2.- V/STOL fighter model geometry.
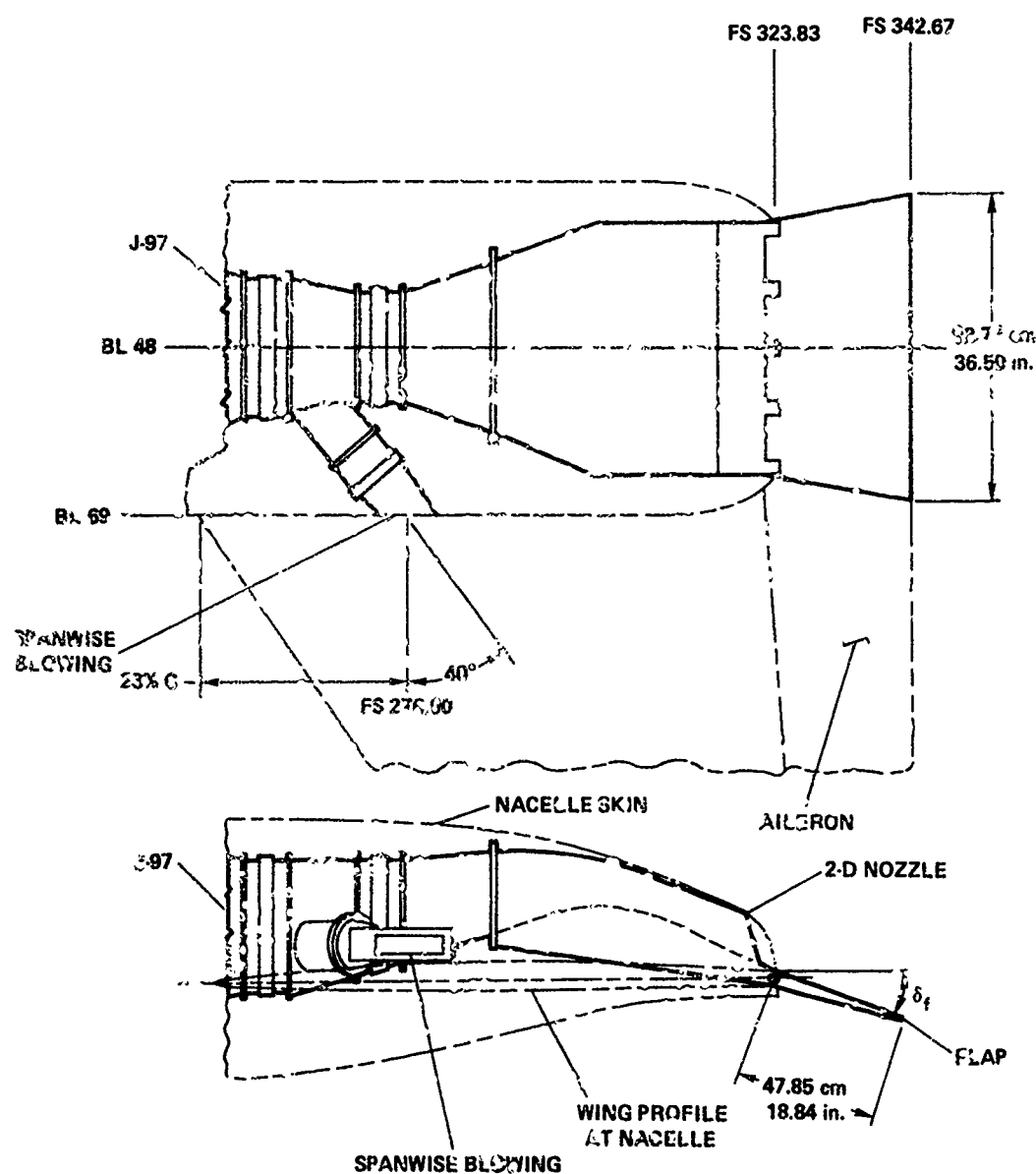
(b) Nozzle geometry.

Figure 2.- Concluded.
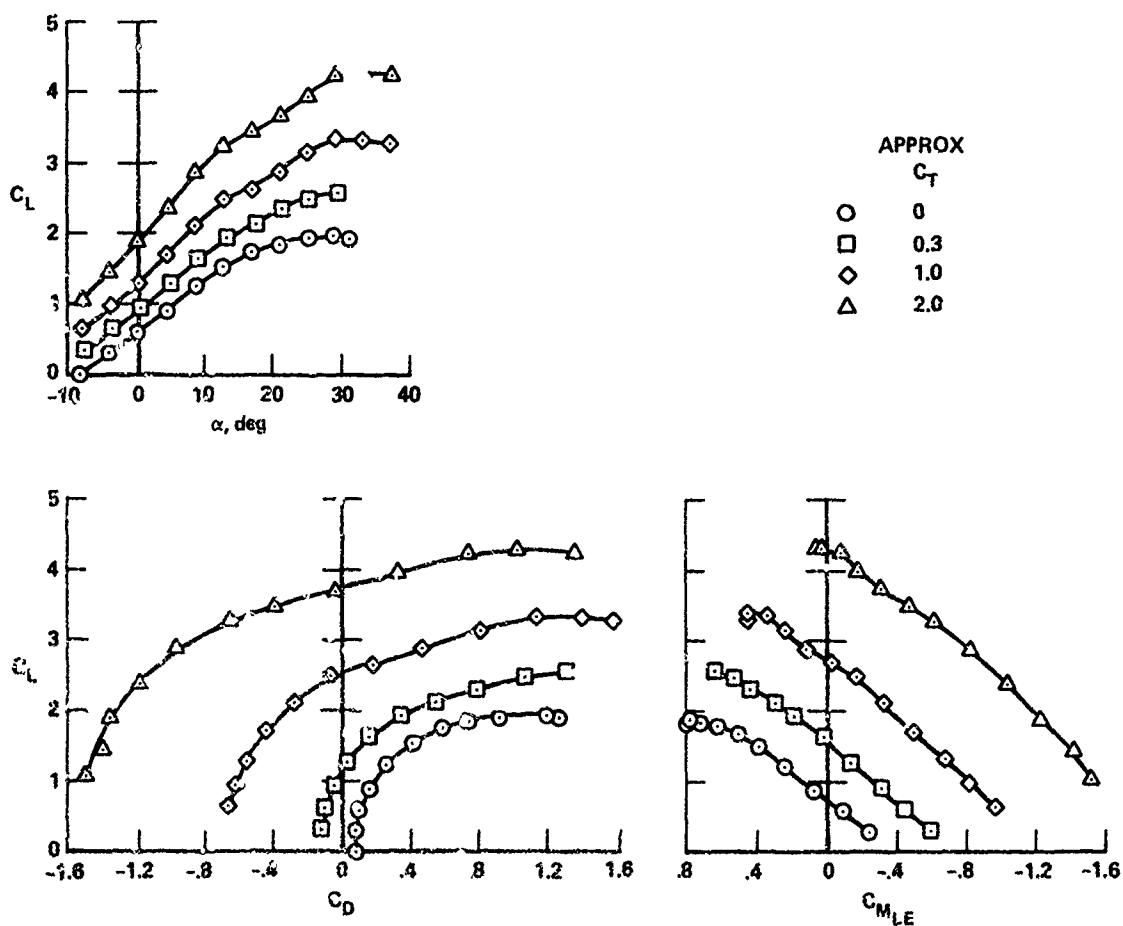
Figure 3.- Basic model longitudinal characteristics; $\delta_f = \delta_a = 30°$, $\delta_c = 0°$, SWB off.

	APPROX C_T	CANARD
□	2.0	ON
◇	↓	OFF
○	0	ON
△	↓	OFF
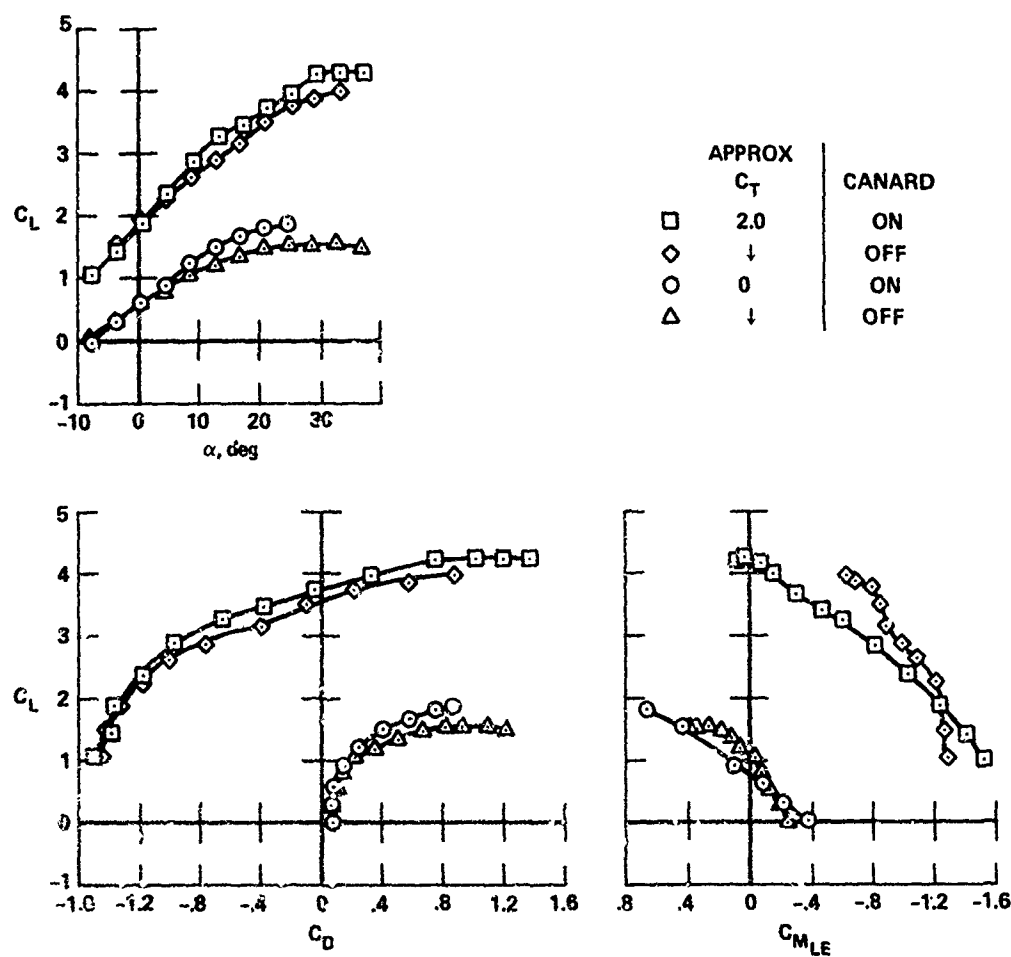
Figure 4.— Effect of canard on longitudinal characteristics; $\delta_f = \delta_a = 30°$, $\delta_c = 0°$, SWB off.
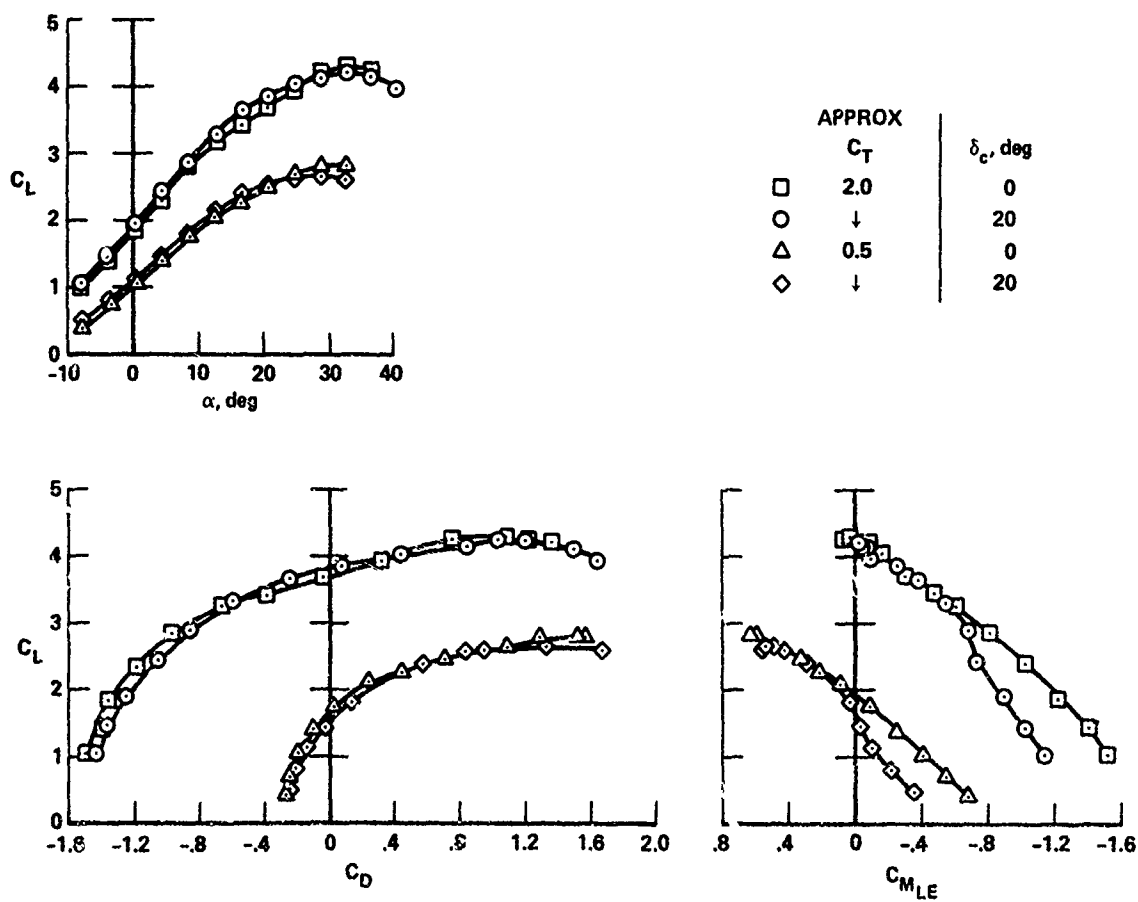
Figure 5.- Effect of canard deflection on longitudinal characteristics; $\delta_f = \delta_a = 30°$, SWB off.
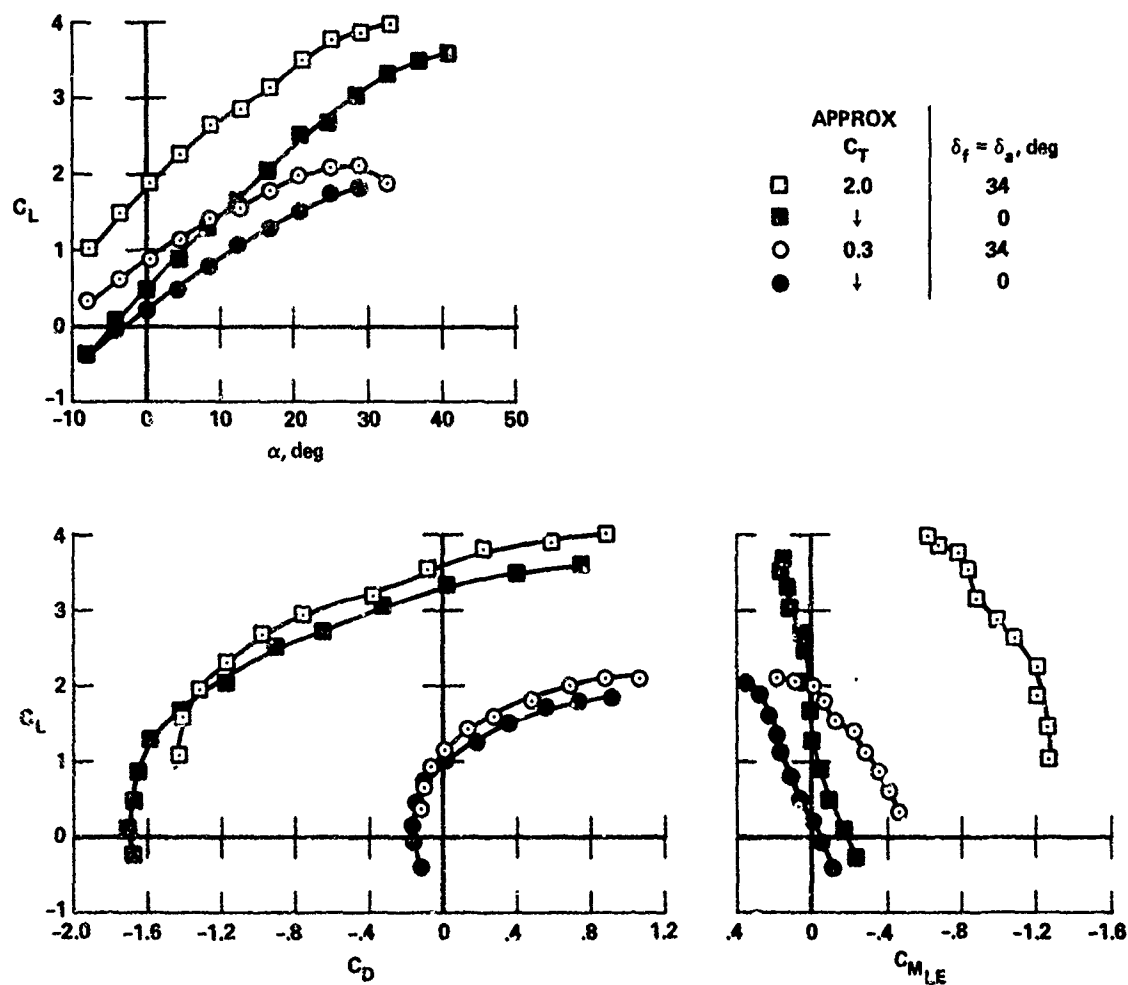
Figure 6.- Effect of flap/aileron deflection on longitudinal characteristics; canard and SWB off.
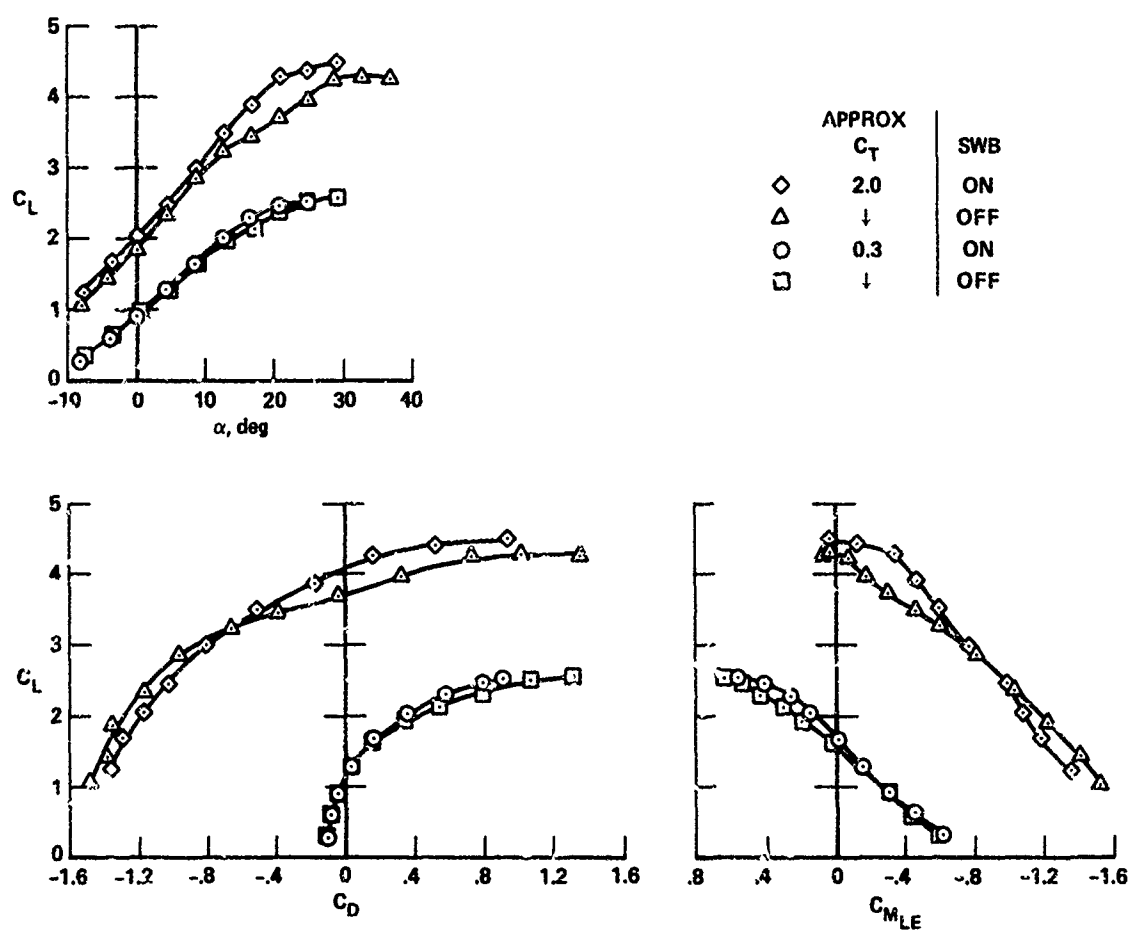
Figure 7.- Effect of spanwise blowing on longitudinal characteristics;
$\delta_f = \delta_f = 30°$, $\delta_c = 0°$.
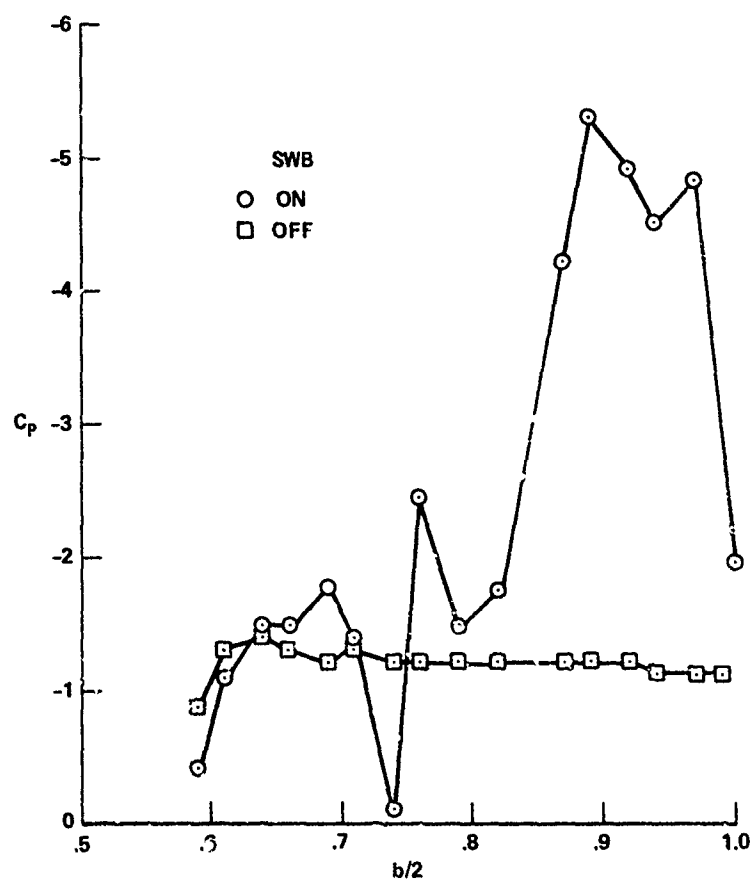
Figure 8.- Spanwise wing pressure distribution with and without SWB;
$\delta_f = \delta_a = 30°$, $\delta_c = 0°$, $\alpha = 20°$, 0.50c.
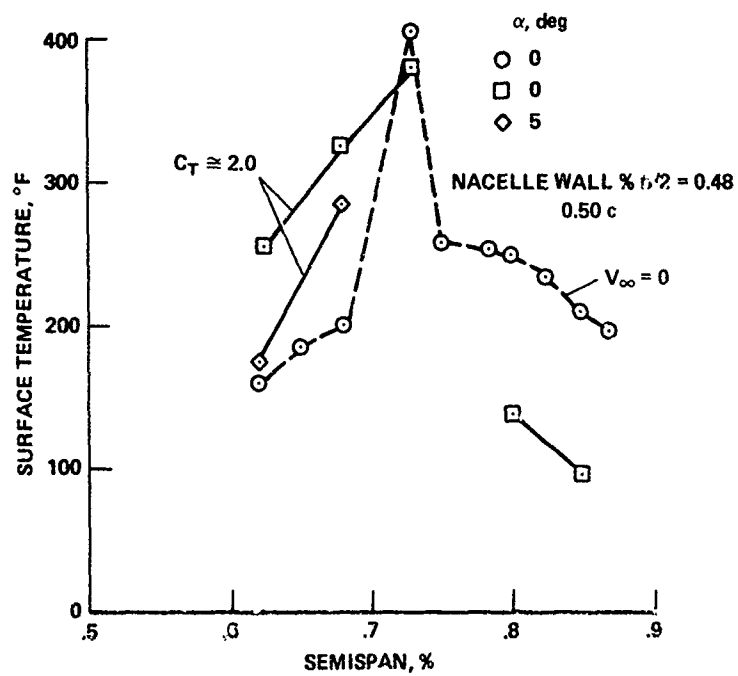
Figure 9.- Wing surface temperatures with SWB; $\delta_f = \delta_a = 30°$, $\delta_c = 0°$, $\alpha = 0°$.
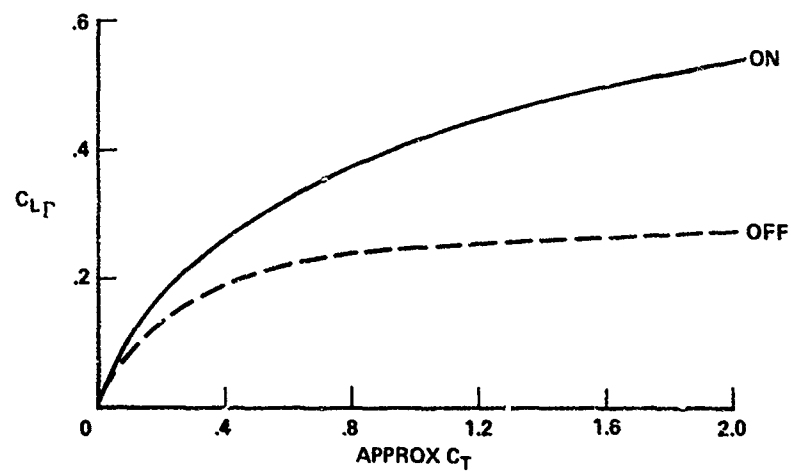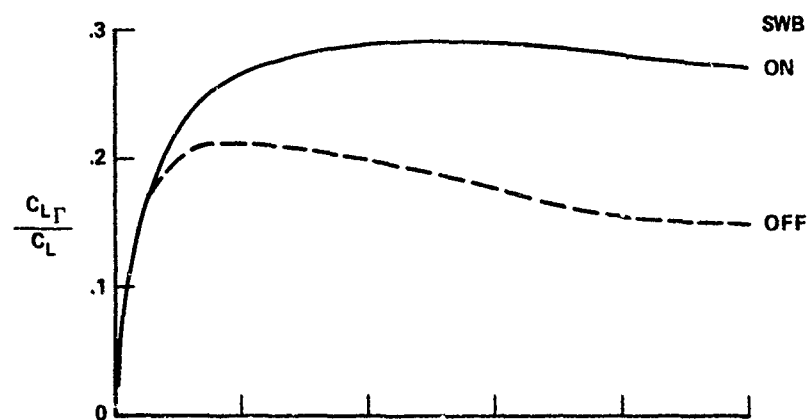
Figure 10.- Fighter model circulation lift; $\delta_f = \delta_a = 30°$, $\delta_c = 0°$, $\alpha = 0°$.
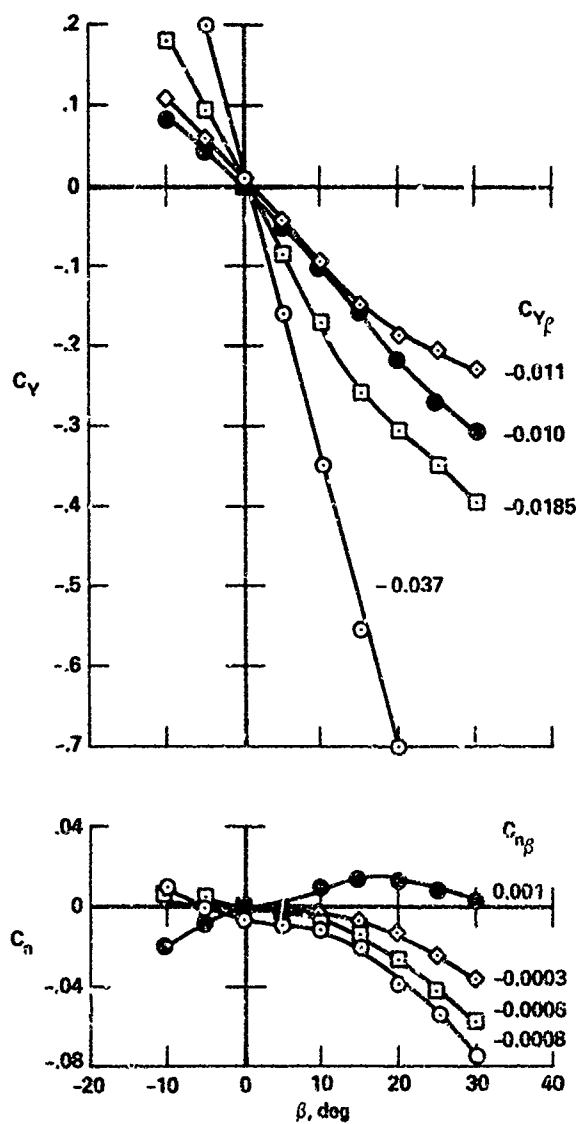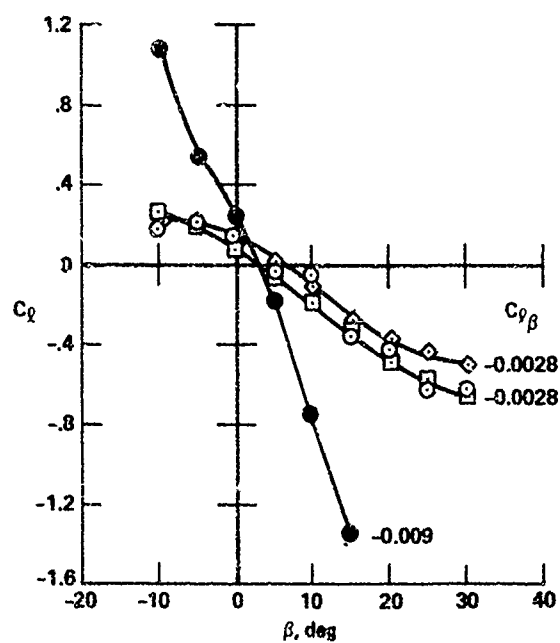
Figure 11.- Basic model lateral-direction characteristics; $\delta_f = \delta_a = 30°$, $\delta_c = 0$, SWB off.
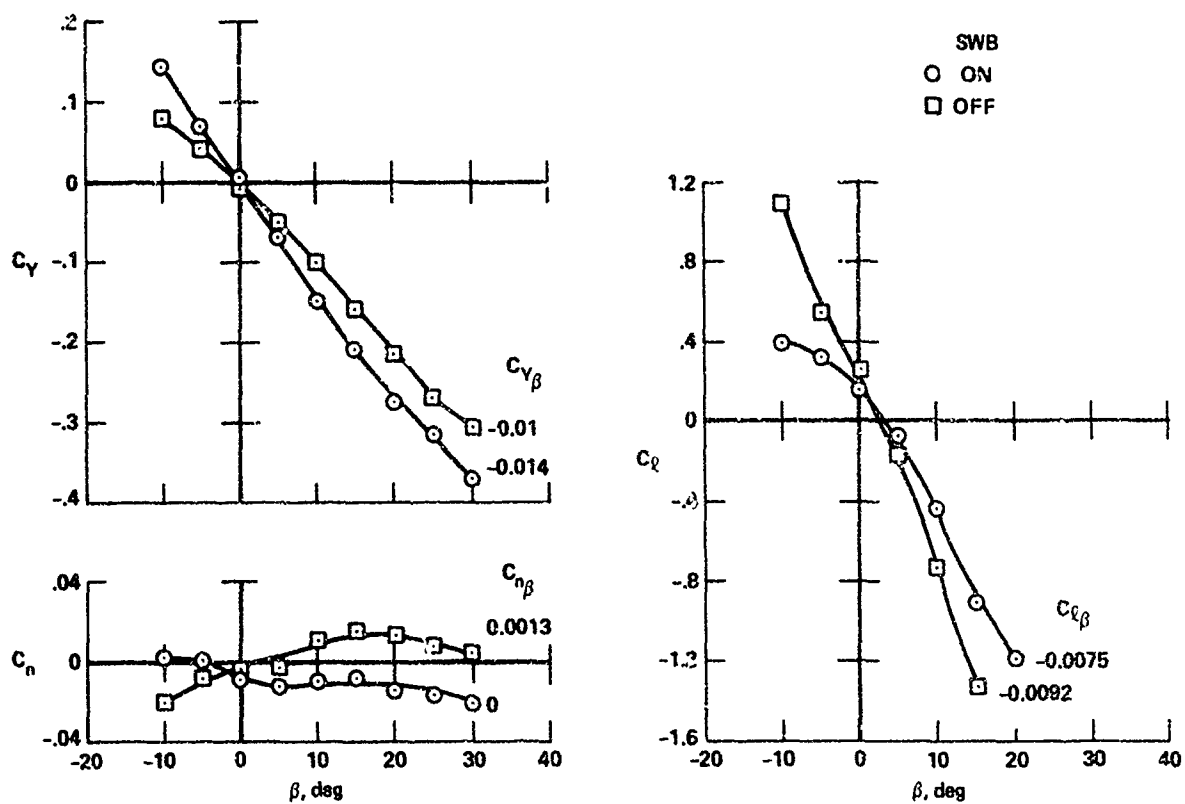
Figure 12.- Effect of SWB on lateral-directional characteristics; $\delta_f = \delta_a = 30°$, $\delta_c = 0°$, $\alpha = 0°$.

TRANSITION CHARACTERISTICS OF THE EXTERNAL-AUGMENTOR V/STOL AIRCRAFT CONCEPT

D.B. Garland
Senior Research Engineer
The De Havilland Aircraft of Canada, Limited
Downsview, Ontario.

Abstract

The particular ejector-powered, V/STOL aircraft concept being developed by DHC is described, with special attention paid to features which affect the transition maneuver.   From an analysis of large-scale wind tunnel test data, the approximate magnitudes of the components of the longitudinal forces and moments involved in transition were determined.   The design parameters applicable to the concept are discussed and a computer program to calculate transition accelerations described.   Typical results are presented and comparisons made with specific data from wind tunnel tests.

INTRODUCTION

The beneficial aspects of ejector-powered VSTOL aircraft have been recognized as follows:

a) Compared with direct jet lift engine designs

    (i) Reduction in powerplant size and weight due to thrust augmentation.

    (ii) Reduction in fuel consumption during hover and transition due to augmentation.

    (iii) Reduction in jet efflux temperature and velocity in hover due to distribution of the primary nozzle thrust and associated jet mixing, which lessens the severity of ground erosion and makes handling of the aircraft easier, especially on a flight deck.

    (iv) Reduction in jet noise during hover and transition due to confining the severe jet mixing region within the augmentor shrouds.

b) Compared with lift fans or rotors

    (i) Relatively simple thrust augmenting hardware.

Although these advantages are well recognized there remains the challenge of incorporating an ejector system in a high performance VSTOL aircraft and of overcoming the problems peculiar to the ejector concept as well as those generally associated with a VSTOL design of any kind.

The "external augmentor" (Ref. 1) is a de Havilland concept which utilizes twin chordwise ejector slots located adjacent to and on either side of the fuselage (Figure 1). The volume of the ejector mixing/diffusing region is "external" to the basic fuselage cross-section (Figure 2) and disappears as the augmentor doors are folded into the sides of the fuselage. An appropriately small frontal area is achieved for high speed flight and, as well, the valuable internal payload space near the aircraft c.g. is preserved.

The twin parallel augmentors provide a large positive ground effect near ground and suffer a small lift loss in free-air (see Figure 3) as the base pressure changes from positive to negative.

In addition to the fuselage mounted ejectors an augmentor-flap or wing ejector is also a fundamental part of the concept. (See Figure 1.) It is used for lift generation, for thrust deflection and for generating a nose-down pitching moment during transition to help off-set the nose-up moment of the fuselage augmentor inlet flow. The percentage of thrust used by the wing augmentor nozzles is typically about 25% of the total installed thrust but will vary with the actual layout chosen for any particular design.

The general layout of the concept, using the double-delta type of planform, achieves approximate coincidence of the centre of gravity with the aerodynamic centre and the centre of static thrust (with the wing augmentor flap deflected to 90°). In some design studies additional powerplants were considered as well as other wing planforms.

Transition from 'jet-borne' to 'wing-borne' flight is accomplished by the use of flap deflection and thrust transfer from the fuselage augmentor to a variable area propulsion nozzle in the rear fuselage. After-burning to augment the rear nozzle thrust is considered very likely. The fuselage augmentor is eventually shut down and folded away. Inlet doors close off the intakes in the upper surface of the wing. The wing augmentor flap with a small deflection is used to minimize the transition speed to wing-borne flight and to reduce the angle of attack required at transition. It is expected that the wing augmentor flap will remain operative throughout the speed range, in the manner of the cruise-augmentor multi-foil wing.

Control at low-speed would be assisted by 'puff-pipes' - the primary controls might very well be differential flap angle and augmentor throttling. A tailplane or canard surface would likely be used to trim flap deflection moments, particularly at the higher transition speeds.

DESIGN PARAMETERS

Some of the design parameters which influence the transition characteristics are:-

(1)   Installed Thrust and Thrust Augmentation Ratio

For steady hovering flight out of ground effect, the augmented thrust of fuselage and wing ejectors approximately equals the aircraft weight. Extra thrust is required for vertical acceleration and control during early phases of the transition maneuver before aerodynamic lift becomes significant. This extra thrust is defined by the ratio, Maximum thrust/Hovering thrust.

A large thrust augmentation ratio is important in reducing installed thrust but it does imply a relatively large secondary/ primary mass flow ratio and a corresponding inlet flow momentum drag and nose-up moment.

(2)   Wing/Fuselage Thrust Split

The percentage of installed thrust employed in the wing augmentor is variable within certain limits. Factors such as maximum available duct size and aircraft balance (both statically and at forward speed) affect these limits.

(3)   Fuselage Augmentor Thrust Deflection

Variable thrust deflection of the fuselage augmentor efflux would be ideal if it could be done in a practical and simple manner.

One alternative is to use a fixed nozzle deflection and accept a
small nose-up attitude in hover.

This built-in nozzle angle reduces the amount of nose-down
angle of the fuselage during accelerating transition and is a power-
ful parameter in transition dynamics.

(4) Thrust Transfer

To accomplish transition from jet-borne to wing-borne flight
(and the reverse) it is necessary to transfer the fuselage augmen-
tor thrust to a rear propulsion nozzle. The mechanical details of
doing this do not concern us at the moment but the timing and method
of doing so affect the transition maneuver.

(5) Augmentor Throttling

Reduction in augmentor diffuser area ratio is a means of re-
ducing the secondary/primary mass flow ratio and the resulting inlet
momentum drag and nose-up moment. It also reduces the augmentor
thrust of course, but at the higher transition speeds wing lift
takes the place of jet lift.

EXPERIMENTAL DATA BASE

A relatively low level research program to study the concept
has been underway since 1966, funded by DHC, the Canadian Depart-
ment of National Defence and Ames Research Center, NASA.

Augmentor development has been in parallel with that for the
Augmentor-Wing and cruise-augmentor programs, References 2 and 3.
It was originally pursued with cold, compressed air tests in the
DHC laboratory. Hot gas tests were first done with a J-85 powered
model which was mounted on a variable height rig to measure ground
effect (Figure 4). Early insight into forward speed character-
istics was provided by small scale models (Figure 5).

In the last two years a large scale model powered by a J-97
engine (Figure 6) was built and tested statically, out of ground
effect, at DHC (Figure 7). It provided an excellent opportunity
to compare the performance of a full-scale augmentor operating on
hot gas with a laboratory model operating on cold air. The design
of the augmentor in this model is the result of studies into high
aspect ratio lobe nozzles operating at high pressure ratio (NPR
up to 3.5, the J-97 upper limit). A cross-section through the
fuselage augmentor is shown in Figure 8. The wing augmentor,
using similar technology, is shown in Figure 9. In this model,
the shrouds are attached to the duct/nozzle assembly and all rotate
together for flap deflection.

Following a successful static program, the model was tested
twice in the 40 x 80 foot wind tunnel at Ames (Figures 10 and 11).
The longitudinal test program included effects of:

(a) Flap angle
(b) Thrust transfer
(c) Augmentor throttling
(d) Tailplane and canard surfaces
(e) Fuselage augmentor nozzle angle
(f) Wing L/E slats

Further test programs are planned to expand the range and combination of variables tested so far.

SUMMARY OF TEST RESULTS

A systematic study of segmented lobe nozzles over a wide range of nozzle aspect ratio and spacing ratio has resulted in a relatively simple thrust augmentor with a very good performance. Large scale cold flow tests showed gross thrust augmentation ratio about 1.7 at high pressure ratios and the augmentor powered by the J-97 engine gave a measured $\emptyset_G$ of 1.60 at a nozzle pressure ratio of 3.0 and an exhaust gas temperature of about $700^{\circ}C$, (Figure 12). (The definition of gross thrust augmentation ratio is measured thrust/nozzle thrust at the same pressure and mass flow.) This was accomplished within a mixing length ratio of $L/_t$ = 75 and with a secondary/primary area ratio of 22. The diffuser and end-wall boundary layer control is provided only by proximity of the primary nozzle jet flows - no separate BLC ducting or nozzles are employed. With this arrangement a diffuser area ratio of 1.6 is found to be optimum at high NPR and about 2.0 at low NPR.

The secondary/primary mass flow ratio has been determined to be about 10, based on exit rake pressure surveys. This technique, although very simple, is not particularly accurate due to the high level of turbulence in the augmentor efflux, which causes total pressure probes to read high by as much as 20%. Correction factors can be determined from balance readings versus rake thrust integrations.

The packaging of such an augmentor within the envelope of a high speed aircraft can be achieved quite well with the 'external augmentor' concept as can be seen in Figure 6.

The wing augmentor, using high aspect ratio lobe nozzles similar to the fuselage augmentor, gave a similar augmentation ratio.

Ground effect in hover, determined with the J-85 powered model, showed a base thrust increment of about 30% of the free air augmented thrust with a ground clearance typical of a normal undercarriage height. (Figure 13). The wing is mounted at shoulder height to minimize adverse ground effect and maximize augmentor length. Augmentor efflux temperatures and velocities reflect the high mass flow ratio of an ejector system.

In the wind tunnel, the most notable characteristic of the J-97 powered model (and previous small-scale models) is the almost total absence of adverse lift interference at forward speed (see Figure 14). The reasons for this are not yet fully explored but are probably related to jet efflux patterns and increase of gross thrust at forward speed.

The low aspect ratio augmentor-flap wing produced lift at zero angle of attack as shown in Figure 15 with the flap angles indicated.

The fuselage augmentor intake flow produces a nose-up pitching moment (Figure 16) which is largely off-set by the nose-down moment of the deflected augmentor-flap, (Figure 17). At higher speeds, where flap deflection is reduced, a horizontal tail (or canard) provides pitch trim. In hover, the model layout has presently been designed to be in balance with about 22% of the thrust in the wing augmentor.

The drag of the model is the net result of many components, both "reactive" and "aerodynamic". Wind tunnel data for two configurations are shown in Figure 18, illustrating the change in drag with fuselage augmentor nozzle angle.

ANALYSIS OF TEST DATA

The absence of strong, adverse interference effects on lift and drag, particularly, has enabled analysis of wind-tunnel test data to be made in a relatively straightforward manner. From the J-97 model tests, these data have been broken down into the components given below.

Lift Components

(i)   Reactive lift component of the fuselage augmentor (based on static augmented thrust measurement).

(ii)   Reactive lift component of the wing augmentor (based on static augmented thrust measurement).

(iii)   Reactive lift component of rear nozzle thrust.

(iv)   "Aerodynamic lift" = the difference between the measured total lift and the sum of the "reactive" components above. Hence $C_{L_{aero}}$ includes lift interference effects on the wing of the fuselage augmentor. These effects appear to be very small.

Drag Components

(i)   Profile drag, a function of flap angle.

(ii)   Induced drag, a function of $C_{L_{aero}}$ squared.

(iii)   Reactive drag component of the fuselage augmentor efflux, based on static augmented thrust measurement.

(iv)   Net thrust of the wing augmentor, assuming typical thrust lapse rate and full thrust recovery.

(v)   Reactive drag component of the rear nozzle thrust.

(vi)   Inlet momentum drag of the J-97 engine.

(vii)   Inlet momentum drag of the fuselage augmentor, based on exit rake estimates of secondary mass flow, and on force data.

Pitching Moment Components

(i)   Power-off C_{m_0} at $\alpha = 0^\circ$, $\delta_F = 0^\circ$.

(ii)   Due to angle of attack, a function of $C_{J_{Nw}}$

(iii)   Due to wing flap angle (at $\alpha = 0^\circ$), a function of $C_{J_{Nw}}$

(iv)   Reactive moment of the fuselage augmentor, based on static augmented thrust measurement.

(v)   Moment due to inlet flow of the J-97 engine.

(vi)   Moment due to inlet flow of the fuselage augmentor, from test data at $\alpha = 0^\circ$, $\delta_F = 0^\circ$.

MATHEMATICAL MODEL

Since wind tunnel tests can cover only a limited combination of the many variables and parameters involved in a VSTOL aircraft development program, it is instructive and cost effective to synthesize the components of the longitudinal forces and moments into a mathematical model to examine the effects of variables one at a time. For configurations not too different from the wind tunnel model extended ranges of variables can also be studied. The elements of the present mathematical formulation are based on the analysis of a limited number of test configurations and, at this time, represent only a first attempt at a full synthesis. The computer program which has been set up determines the angle of attack for vertical equilibrium and calculates the corresponding longitudinal acceleration for any given configuration over the speed range 40 knots to 200 knots.

THE TRANSITION MANEUVER

The hovering configuration, having the wing augmentor flap deflected 90° and the fuselage augmentor efflux deflected aft by 10° or so, defines a nose-up hovering attitude. The respective thrust augmentation ratios define the nozzle thrust/weight ratio required for hover out of ground effect.

Initial motion is obtained by a combination of rearward rotation of the wing augmentor-flap, an increase in engine thrust and application of pitch control to give a nose-down attitude. The details of this action are not discussed in this note. Rather, the motion above about 40 knots is examined. Figure 19, for example, shows the effect of flap angle on the acceleration available

in level flight and the associated angle of attack. With this 'basic' configuration of the model (the fuselage augmentor unchanged from its hovering configuration) a nose-down attitude of about -10° is optimum and gives essentially maximum acceleration throughout the speed range. This varies from about 1/3g at low speed to zero at about 130 knots. The corresponding optimum flap angle diminishes from about 40° to about 25°. An augmented thrust/weight ratio of 1.10 is assumed in this calculation. This part of the transition maneuver is very much affected by the degree of deflection built-in to the fuselage augmentor thrust vector, as indicated in Figure 20. The ratio of wing thrust/fuselage thrust has a smaller influence (Figure 21).

At the other end of the transition maneuver, the fuselage augmentor is fully closed, the fuselage thrust is transferred to the rear propulsion nozzle and the aircraft is wing-borne as a jet-flapped vehicle. This configuration has not yet been tested in the wind tunnel but predicted performance, based on the effectiveness of the wing augmentor in the combined flight mode, indicates an acceleration capability and corresponding angles of attack as shown in Figure 22. Increasing the percentage of thrust in the wing allows a reduction in flap angle and an improved performance (Figure 23).

The intermediate region, where transition has to be made between augmentor-open and augmentor-closed states, lies roughly between 80 and 120 knots for the present configuration. In this region the attitude of the aircraft changes from about -10° to about $+10^\circ$ and the flap angle either remains fixed, perhaps at about 30°, or reduces slightly.

Closing of the augmentor and transferring of thrust to the rear nozzle has been partially investigated in the wind tunnel. Test data plus predictions indicate that a progressive transfer of thrust, with the fuselage augmentor remaining at essentially DAR = 1.6, is a feasible operation. Some reduction in acceleration at intermediate augmentor settings may occur but a value in excess of 1/8g appears achievable as shown in Figure 24. With afterburning applied to the transferred thrust the minimum acceleration is improved (Figure 25) and the time required to achieve wing-borne flight (from hover to fuselage augmentor closed) is in the order of 20 seconds.

CONCLUSIONS

A mathematical model of the external-augmentor V/STOL aircraft concept, based on large-scale wind tunnel test data, has indicated the transition performance characteristics to be expected with a full-scale aircraft. The advantages of fuselage augmentor nozzle deflection and of a moderately high wing thrust/fuselage thrust ratio have been shown. Transfer of fuselage augmentor thrust to the rear propulsion nozzle is probably best accomplished before significantly reducing the augmentor exit area.

REFERENCES

1. Whittley, D.C. - "Ejector-Powered Lift Systems for V/STOL Aircraft."
   CASI Journal, May 1974.

2. Whittley, D.C. - "The Buffalo/Spey Jet-STOL Research Aircraft."
   AGARD Flight Mechanics Panel Symposium, Brussels, October 1972.

3. Farbridge, J.E., Smith, R.C. - "The Transonic Multi-Foil Augmentor-Wing."
   AIAA Paper No. 77-606, June 1977.

ACKNOWLEDGEMENTS

DHC EXTERNAL AUGMENTOR V/STOL CONCEPT
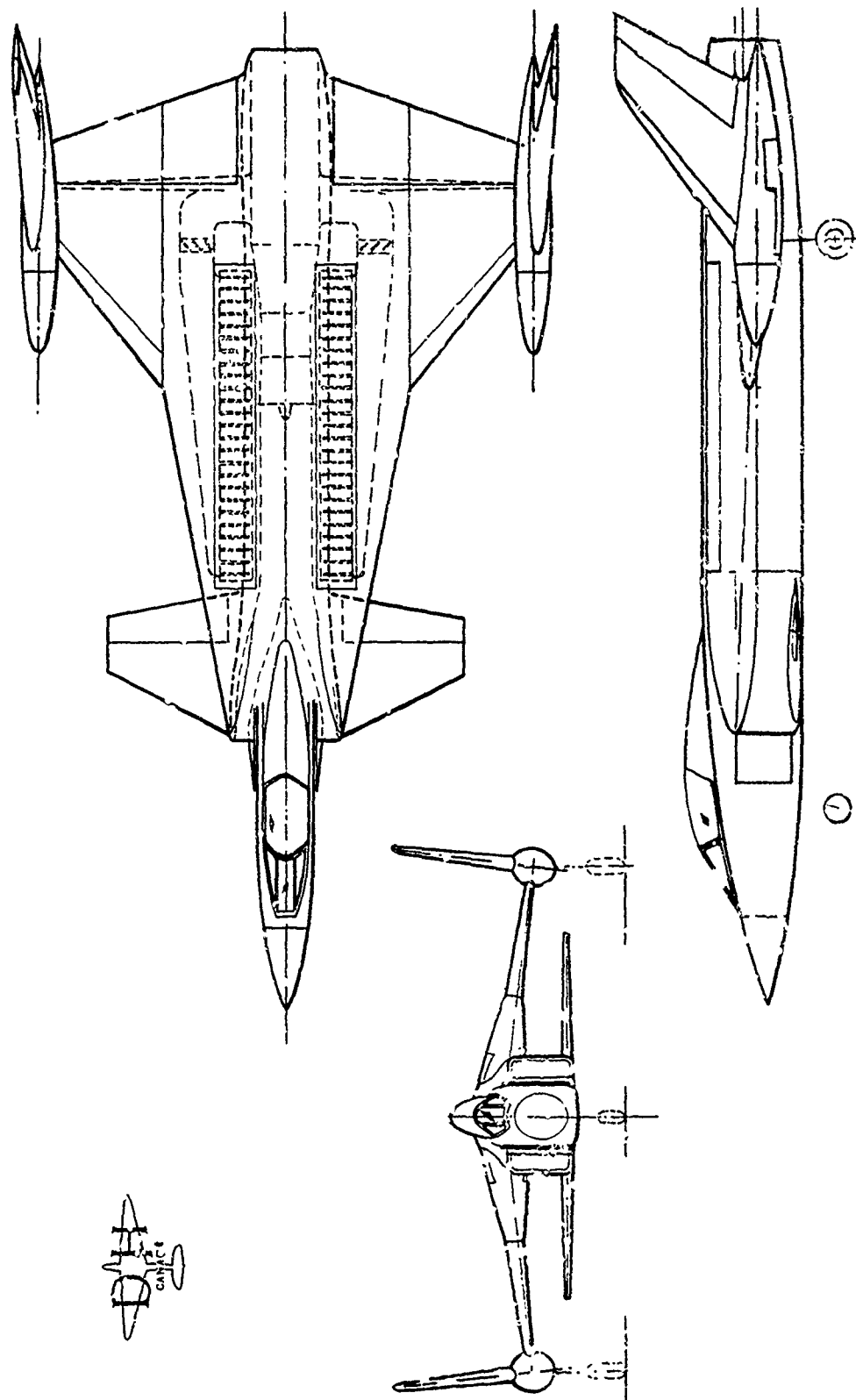
FIGURE 1
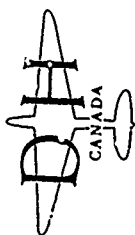
FUSELAGE CROSS-SECTIONS
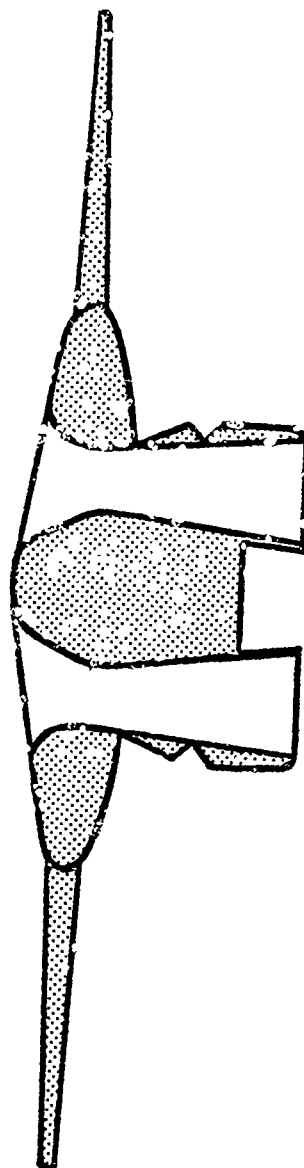
OPEN
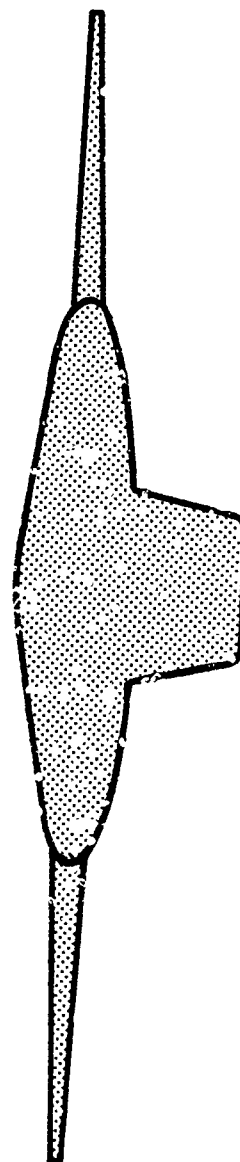
CLOSED

FIGURE 2

GROUND EFFECT WITH FUSELAGE AUGMENTORS
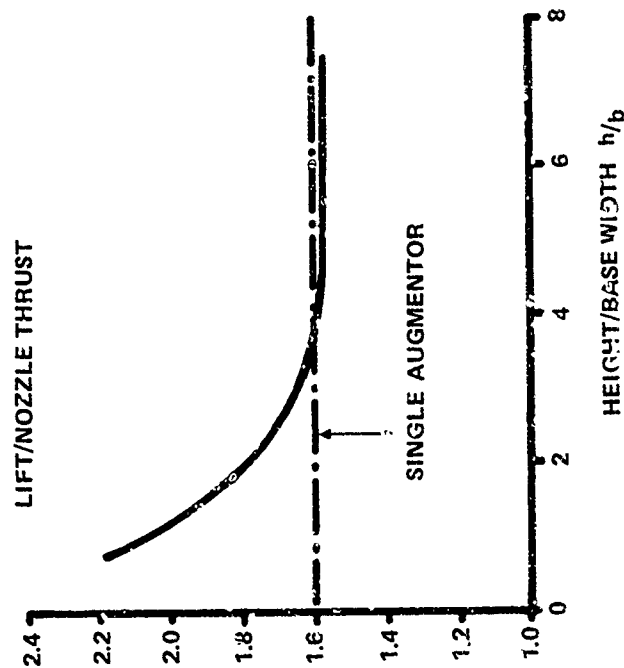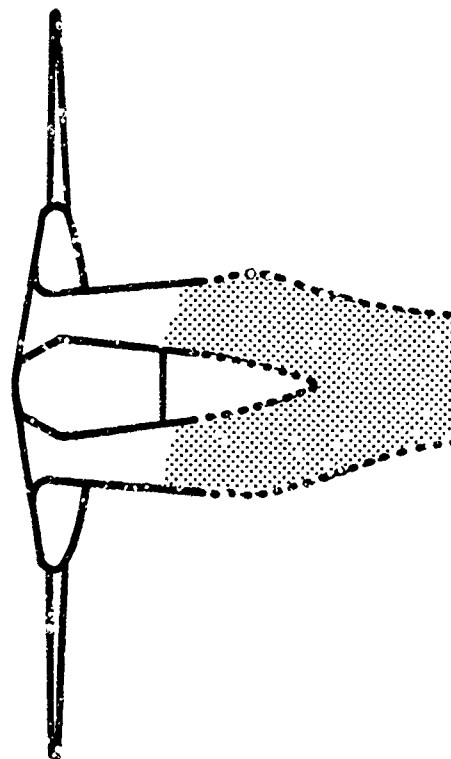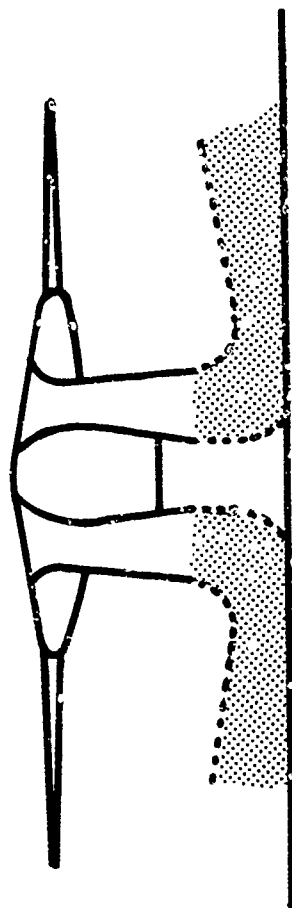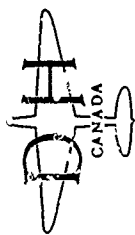
FIGURE 3

J-85 POWERED MODEL ON VARIABLE HEIGHT RIG
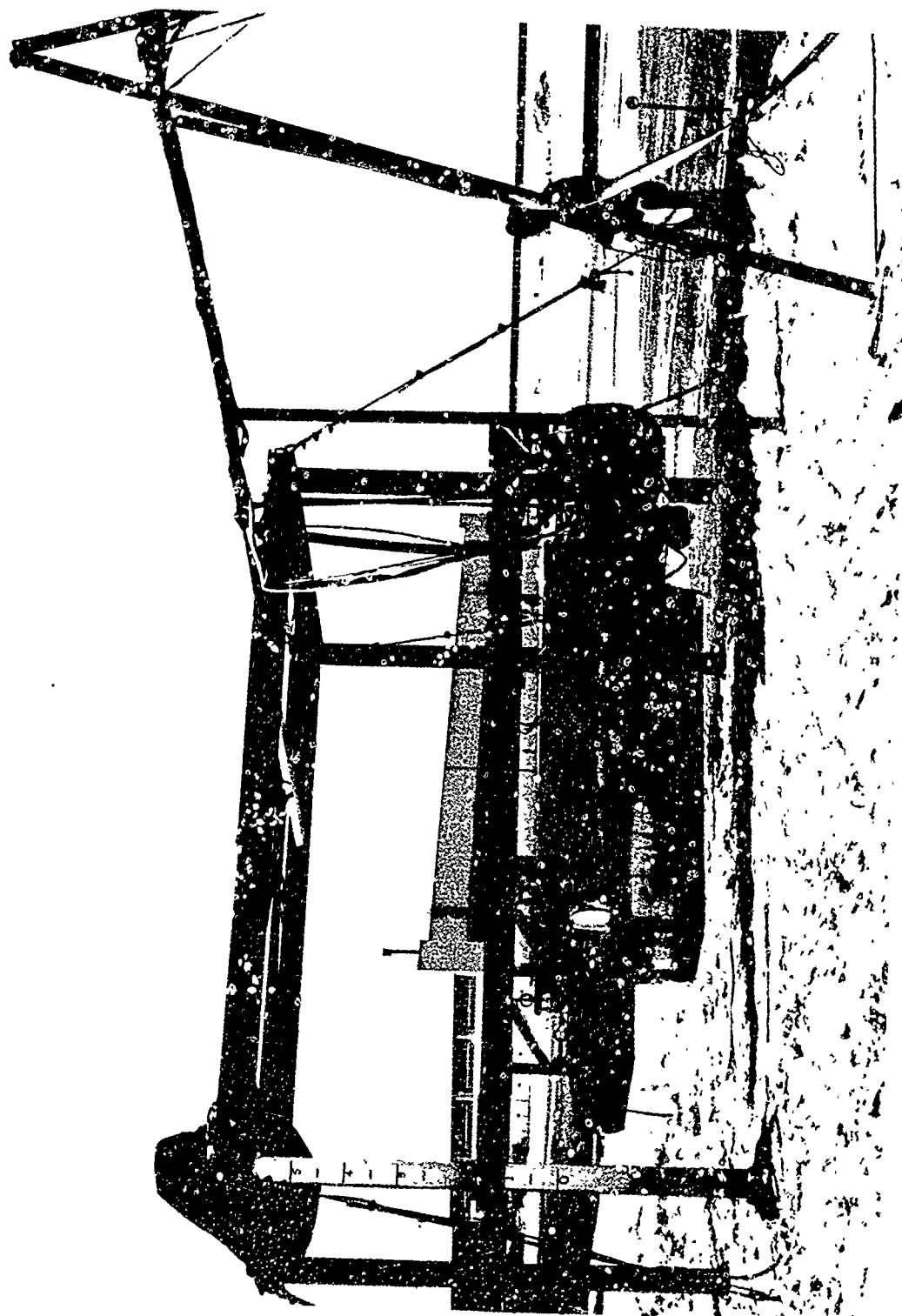
FIGURE 4
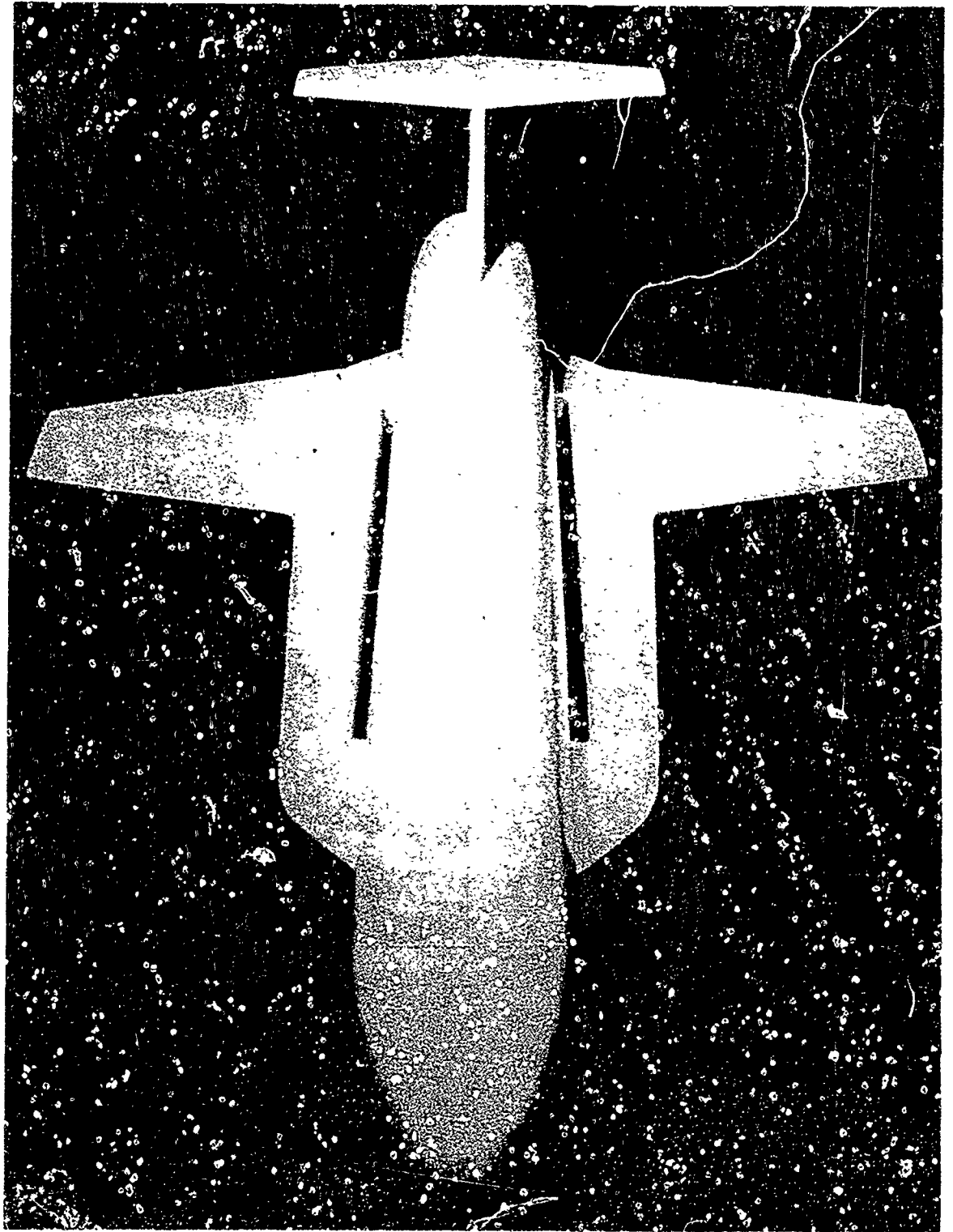
FIGURE 5

DHC EXTERNAL AUGMENTOR V/STOL CONCEPT
G.A. OF J-97 POWERED MODEL
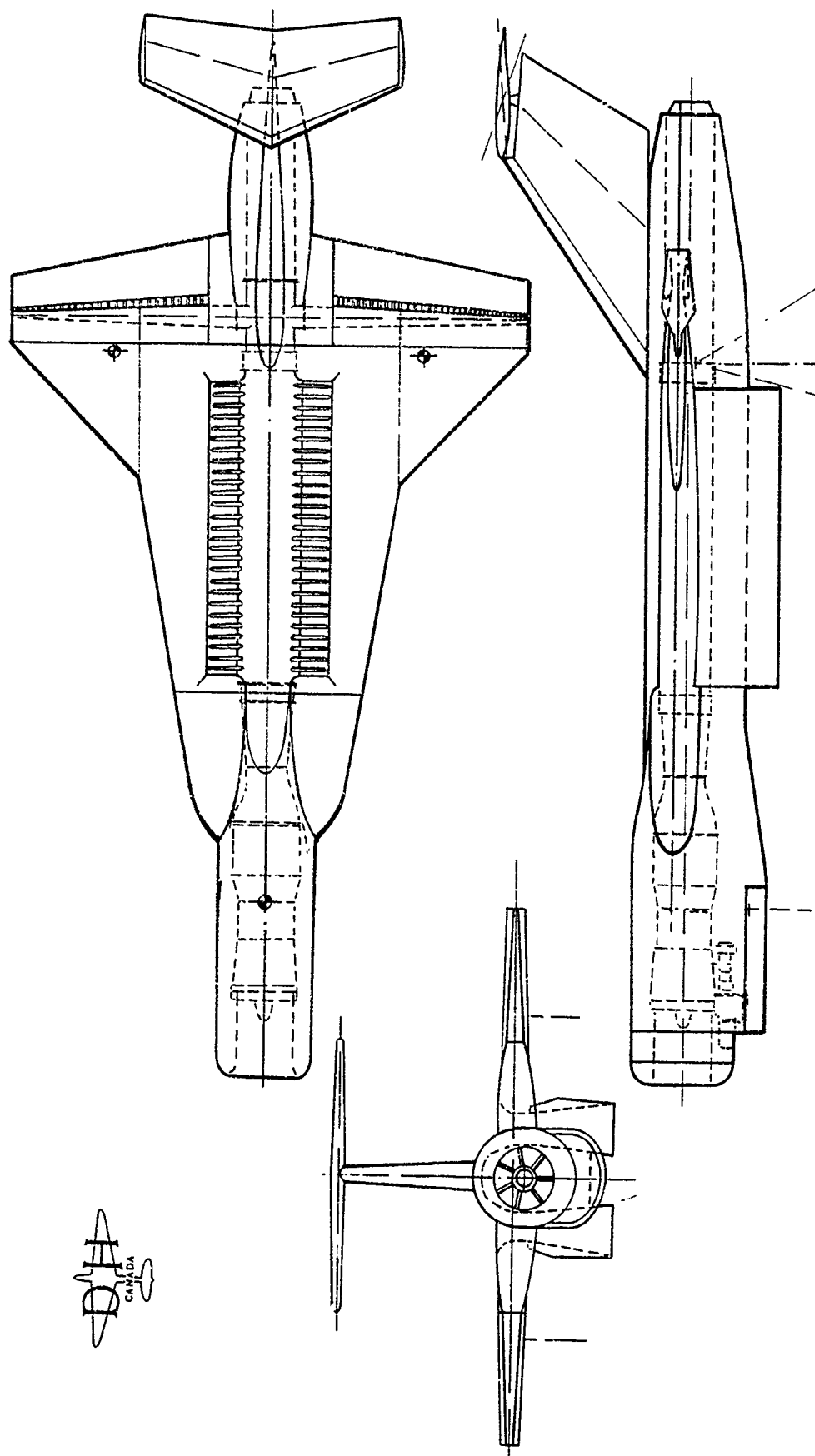
FIGURE 6
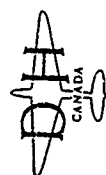
J-97 POWERED MODEL ON STATIC TEST RIG

FIGURE 7

913
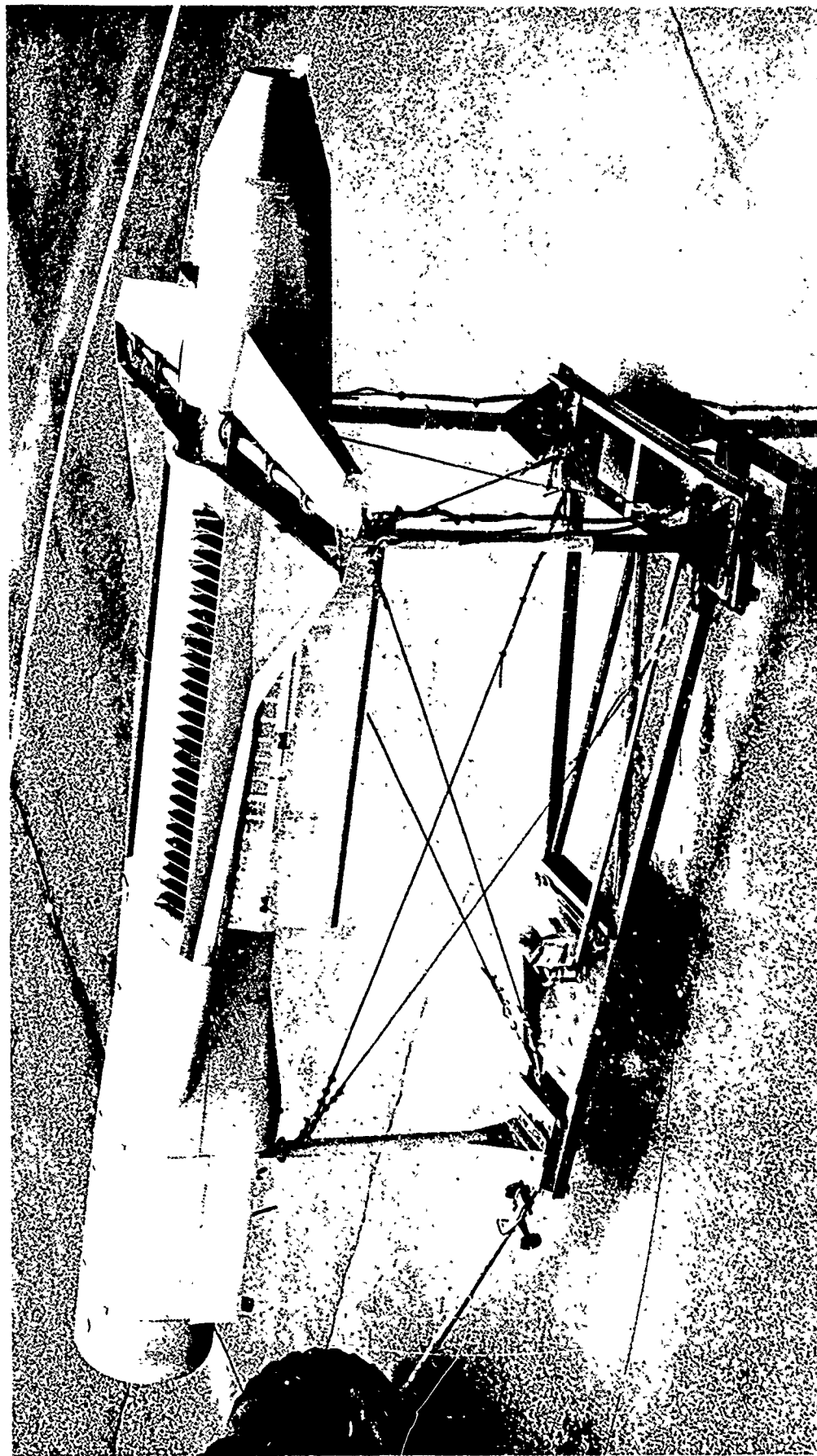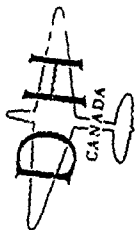
SECTION THROUGH FUSELAGE AUGMENTOR

HOT DUCT/NOZZLE ASSEMBLY

CLOSED AUGMENTOR CONTOUR
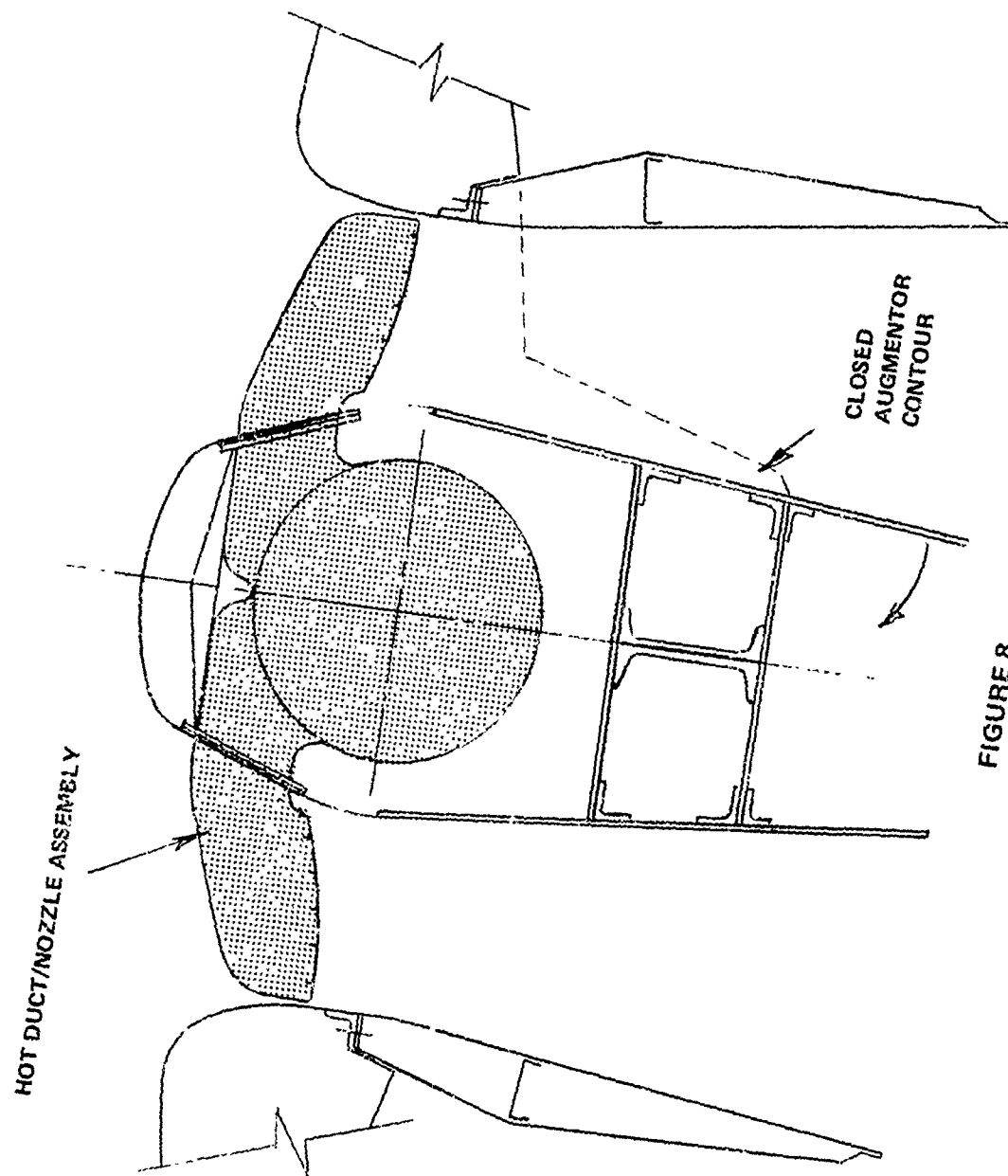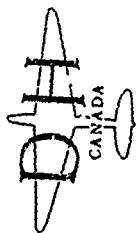
FIGURE 8

SECTION THROUGH WING AUGMENTOR FLAP
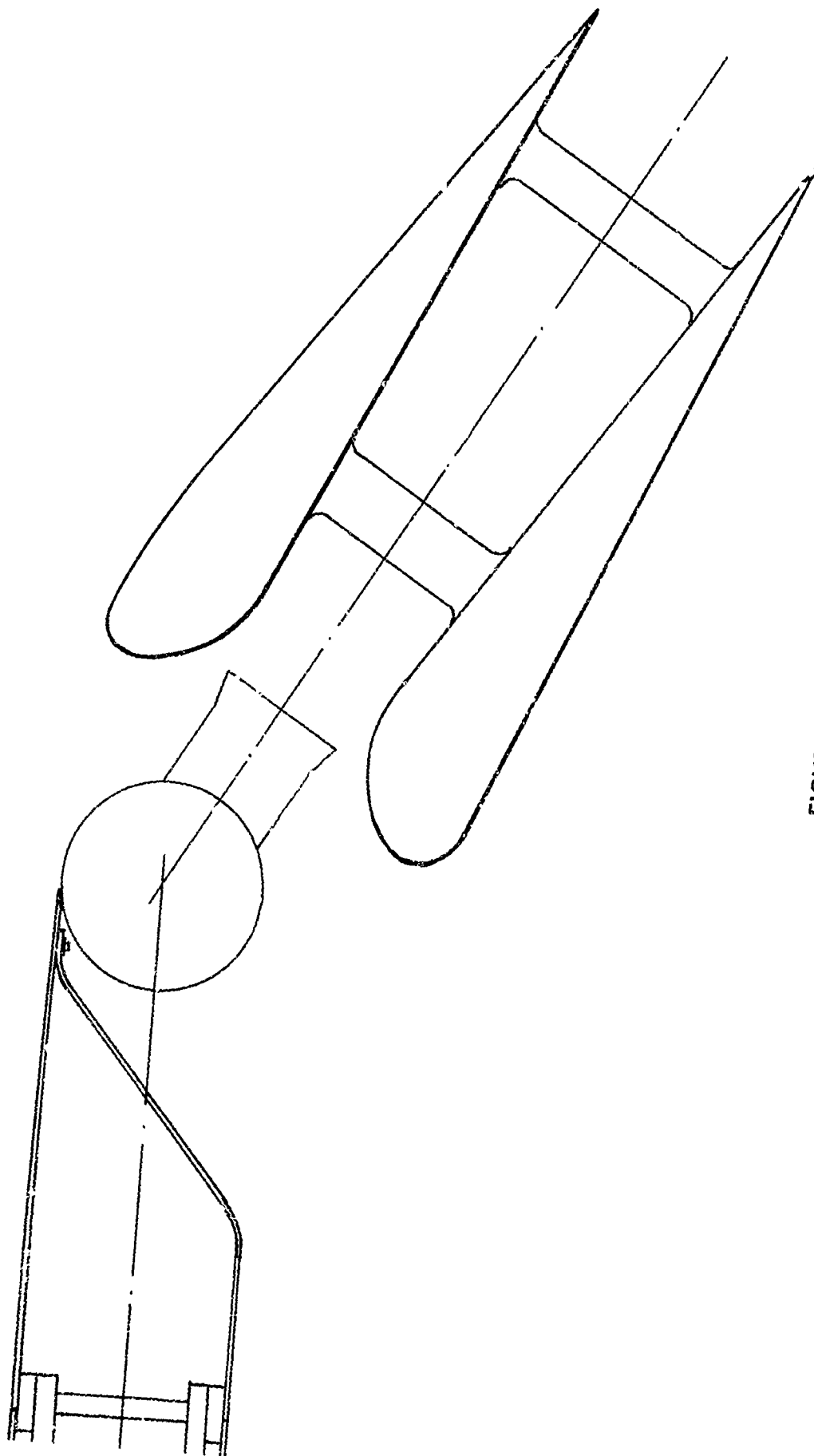
FIGURE 9
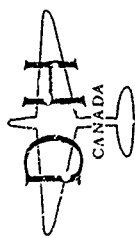
J-97 POWERED MODEL IN 40' x 80' WIND TUNNEL
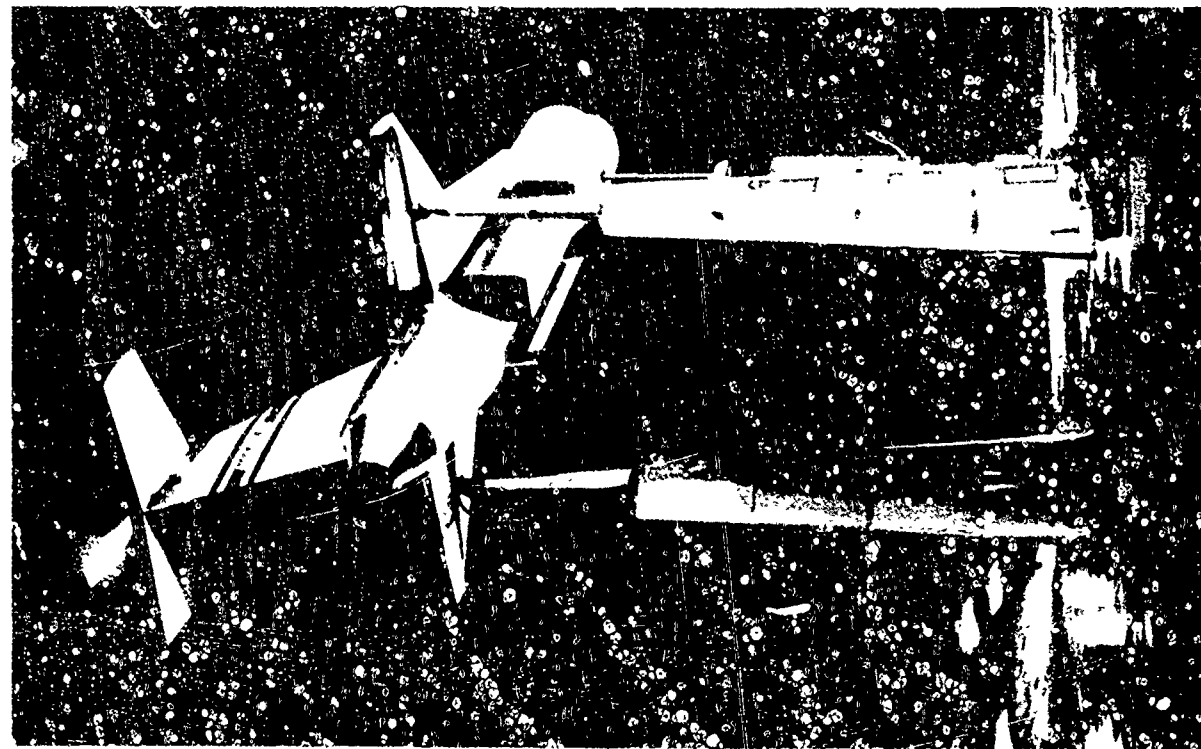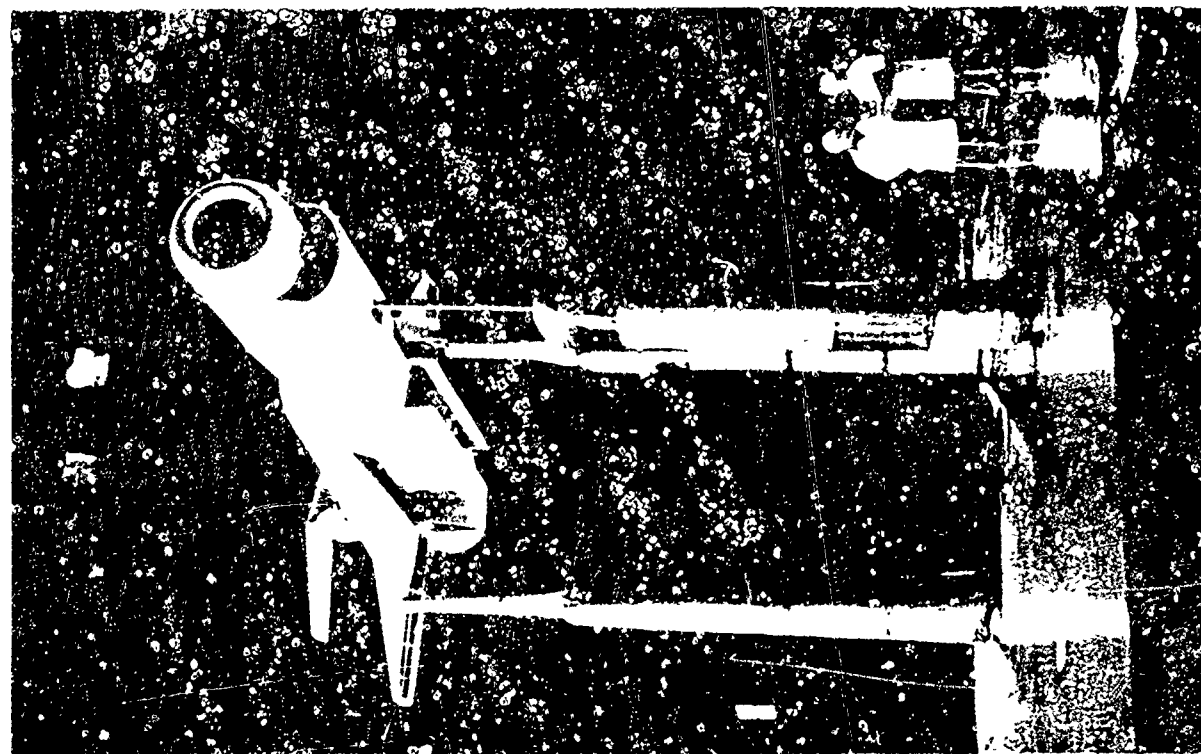
FIGURE 10

J-97 POWERED MODEL IN 40' x 80' WIND TUNNEL
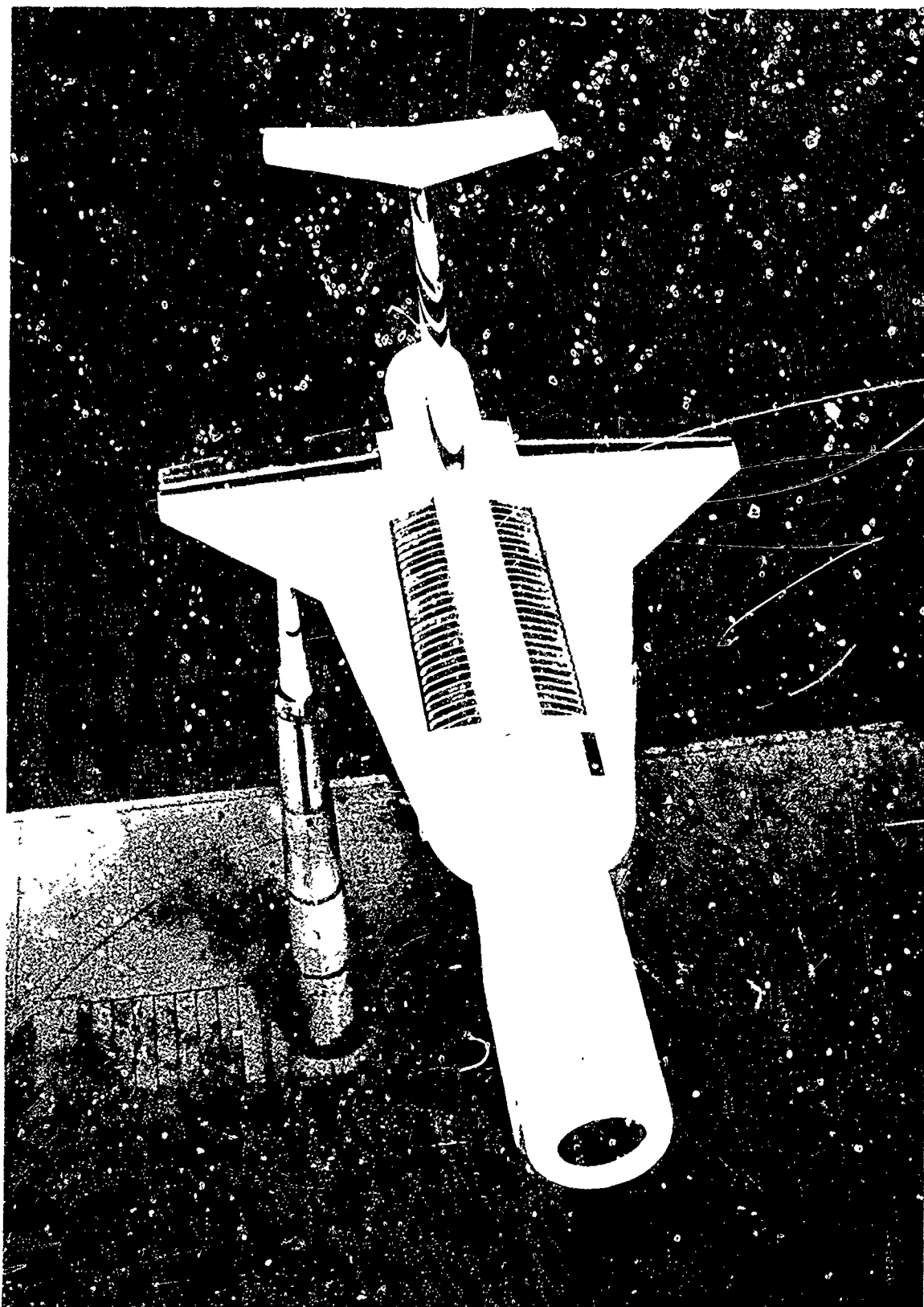
FIGURE 11
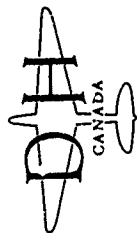
THRUST AUGMENTATION, COLD AIR AND HOT GAS COMPARISON
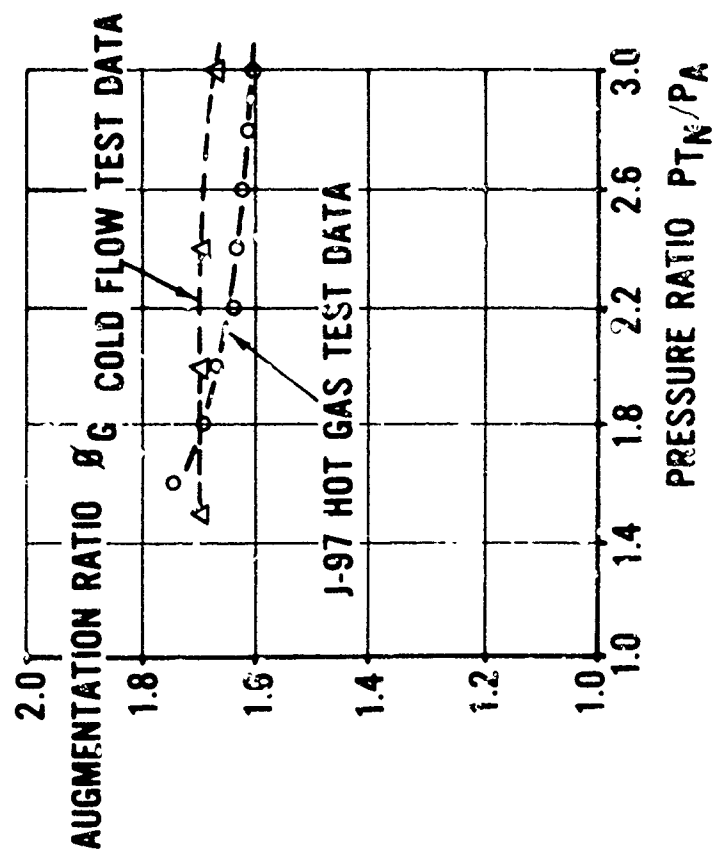
FIGURE 12

J-85 POWERED MODEL AND GROUND EFFECT
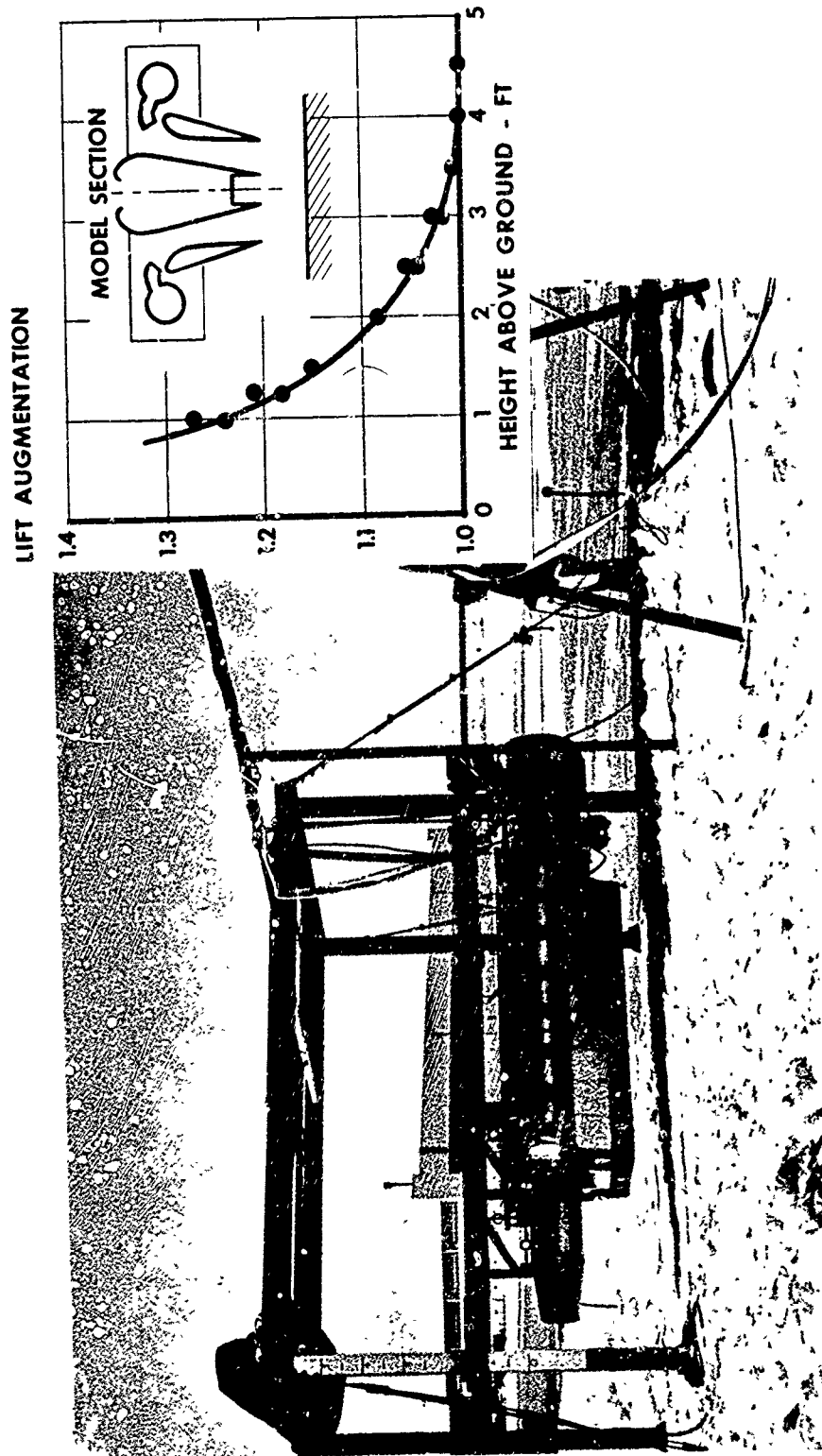
FIGURE 13

INTERFERENCE OF FUSELAGE AUGMENTOR
ON AERODYNAMIC LIFT COEFFICIENT

$\delta_F = 0^0$; DAR = 1.6; RPR = 2.3
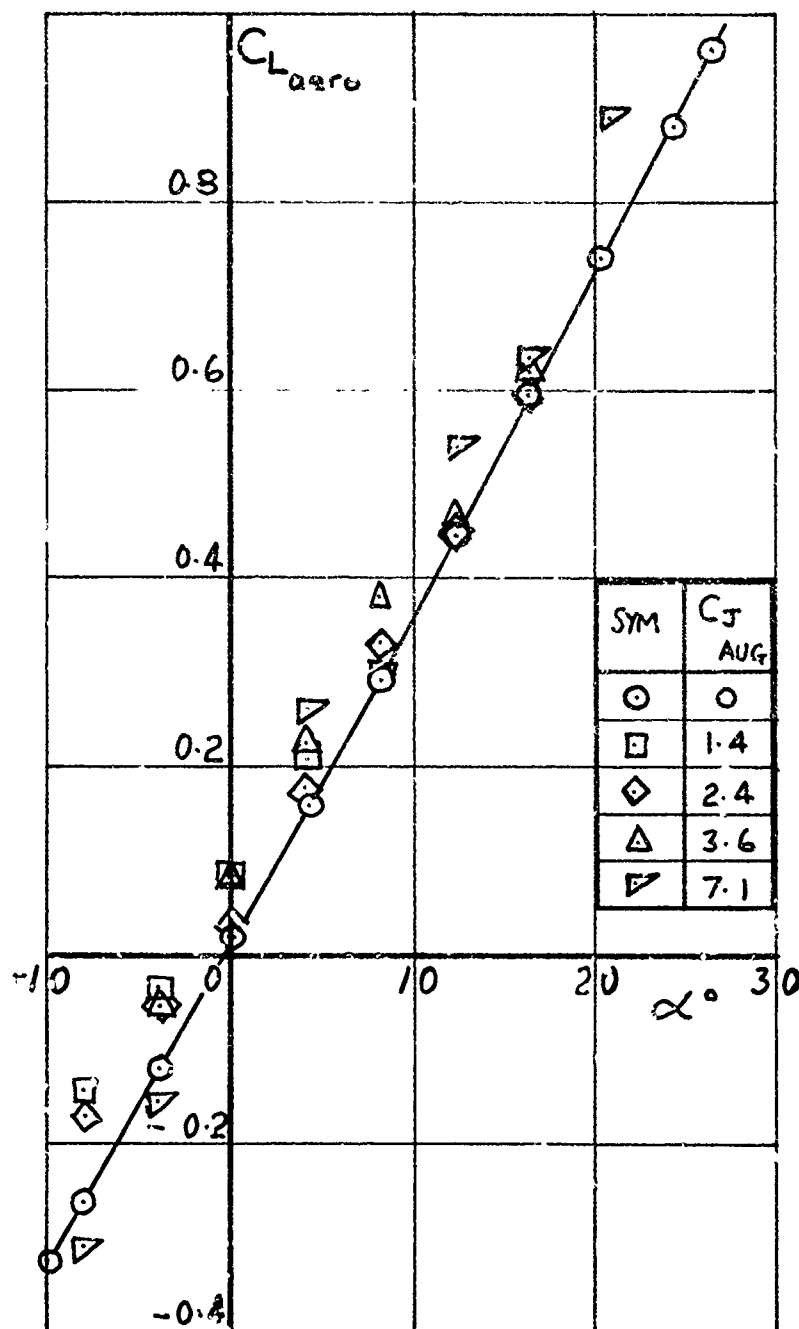
FIGURE 14

EFFECT OF FLAP ANGLE
ON AERODYNAMIC LIFT COEFFICIENT

DAR = 1.6

FIGURE 15

921
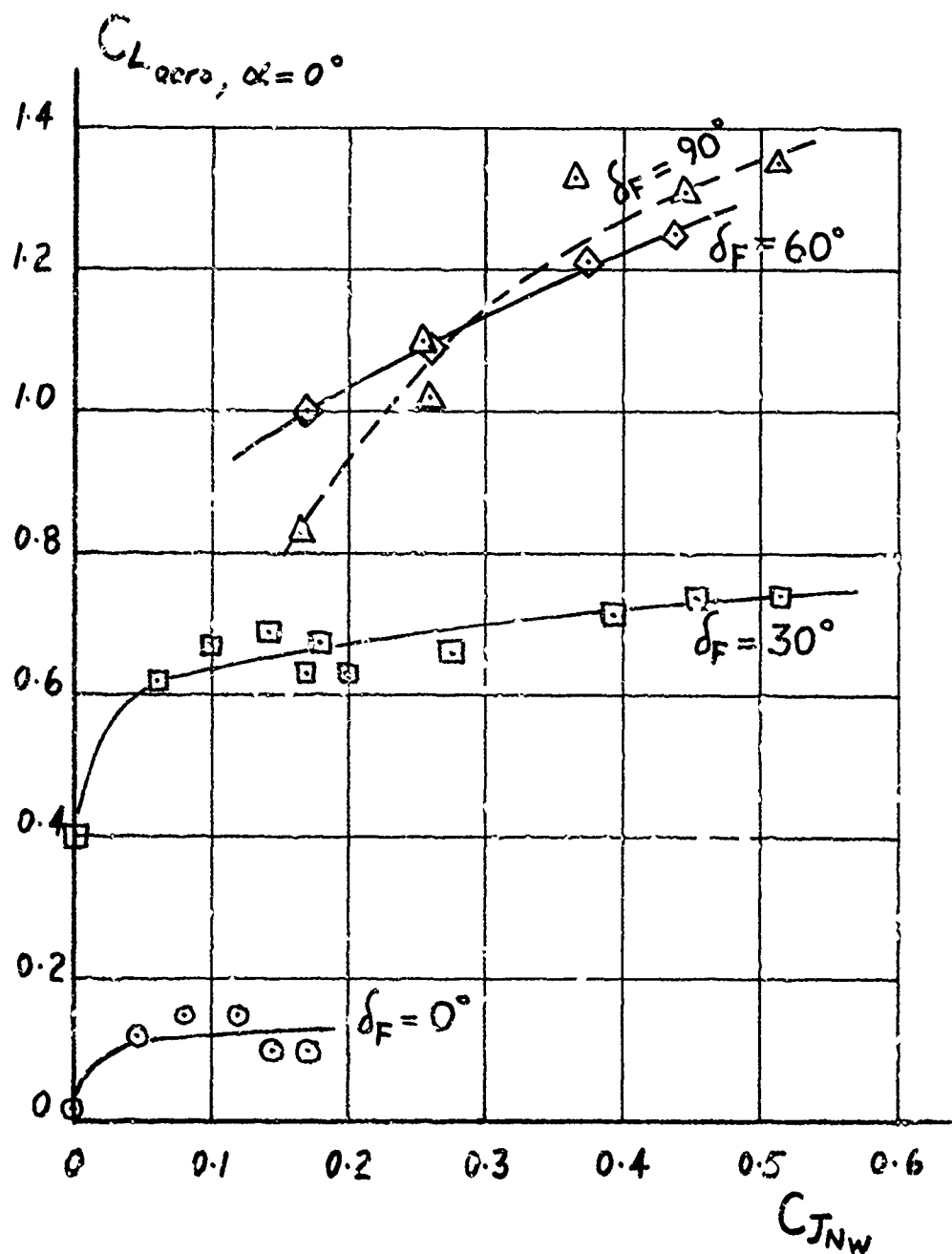
NOSE-UP MOMENT DUE TO FUSELAGE AUGMENTOR INFLOW

$\delta_F = 0^o; \alpha = 0^o$

SYM	‰
⊙	10
△	15
⊡	25

C_{M_i}

$C_{D_M} = 2C_Q$
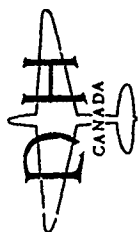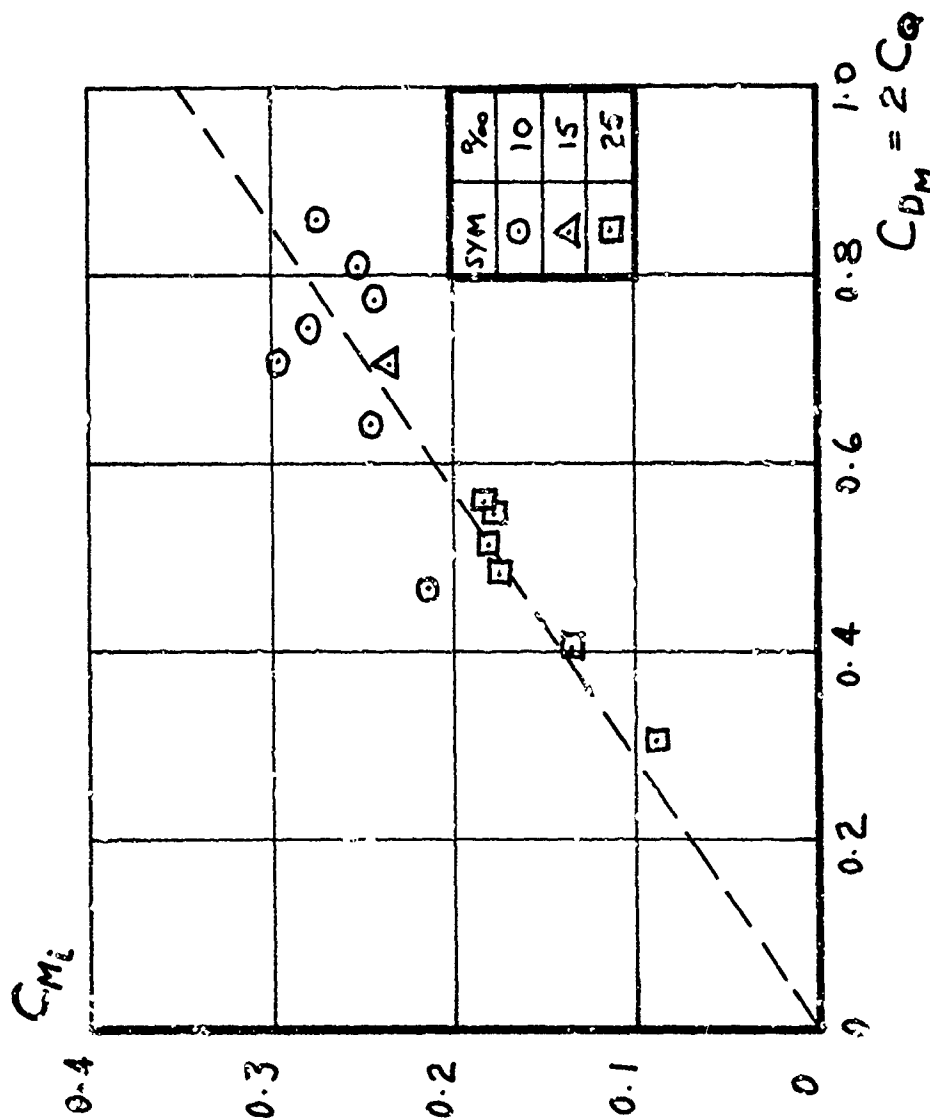
FIGURE 16

EFFECT OF FLAP ANGLE ON PITCHING MOMENT

DAR = 1.6; RPR = 2.3; $\alpha = 0^\circ$
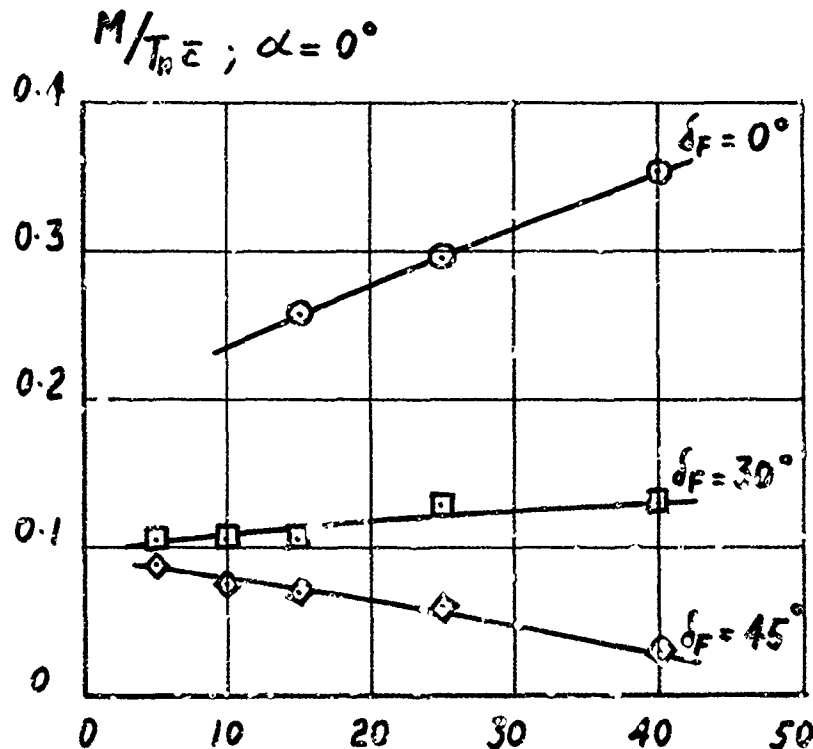
PHASE 2 DATA

NOZZLE ANGLE = 12.5°
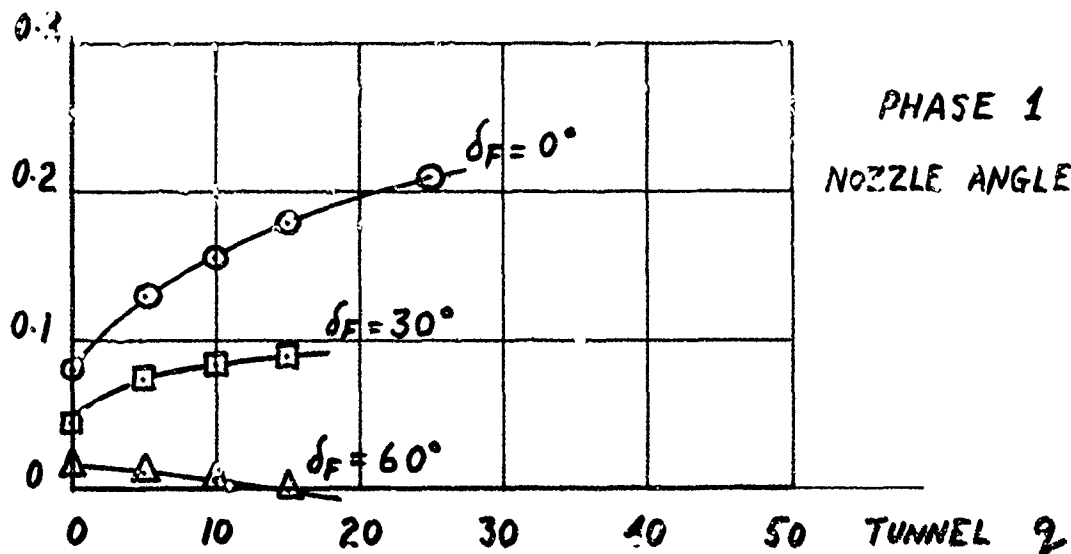
PHASE 1 DATA

NOZZLE ANGLE = 0°

FIGURE 17

EFFECT OF FUSELAGE AUGMENTOR NOZZLE ANGLE ON DRAG DATA
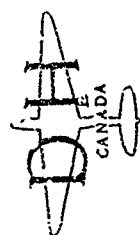
$\delta_F = 30°$; DAR = 1.6; T/W = 1.10
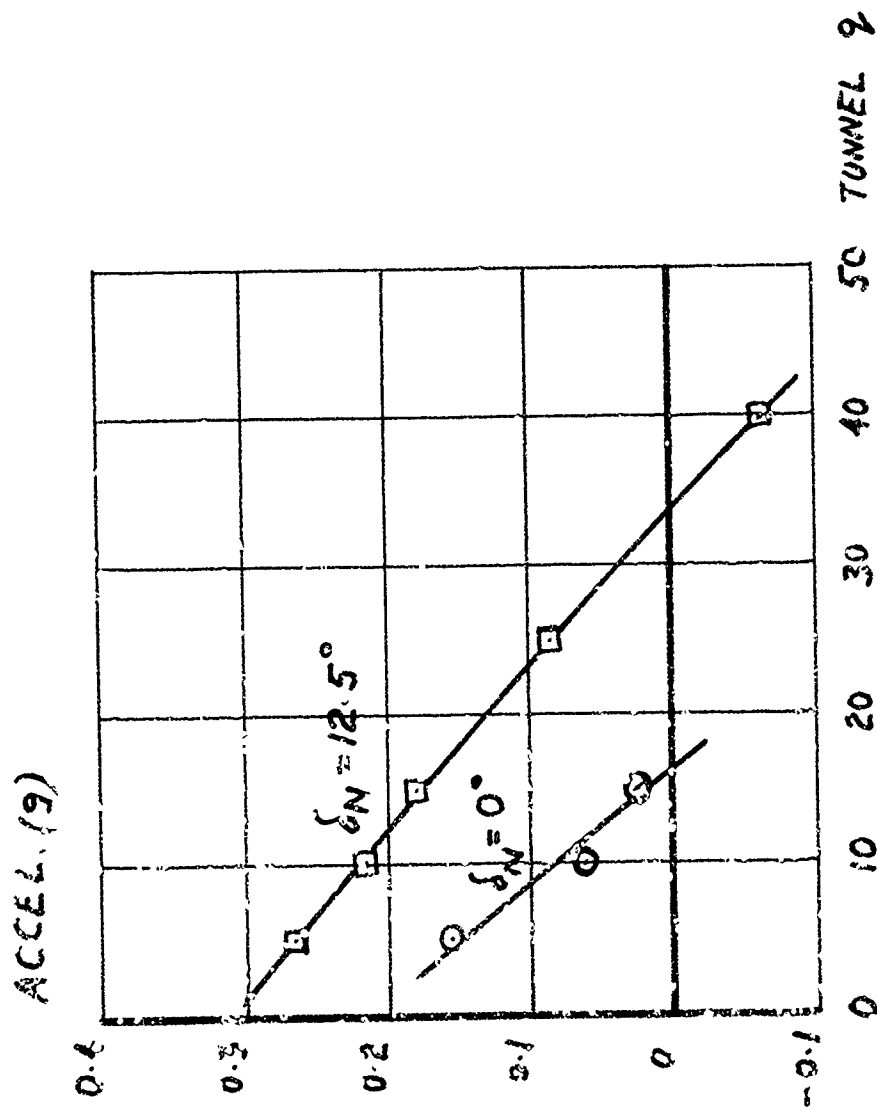
FIGURE 18

PREDICTED PERFORMANCE:

DAR = 1.6; Aw/A = 0.25; $\delta_N = 15°$

FIGURE 19

925
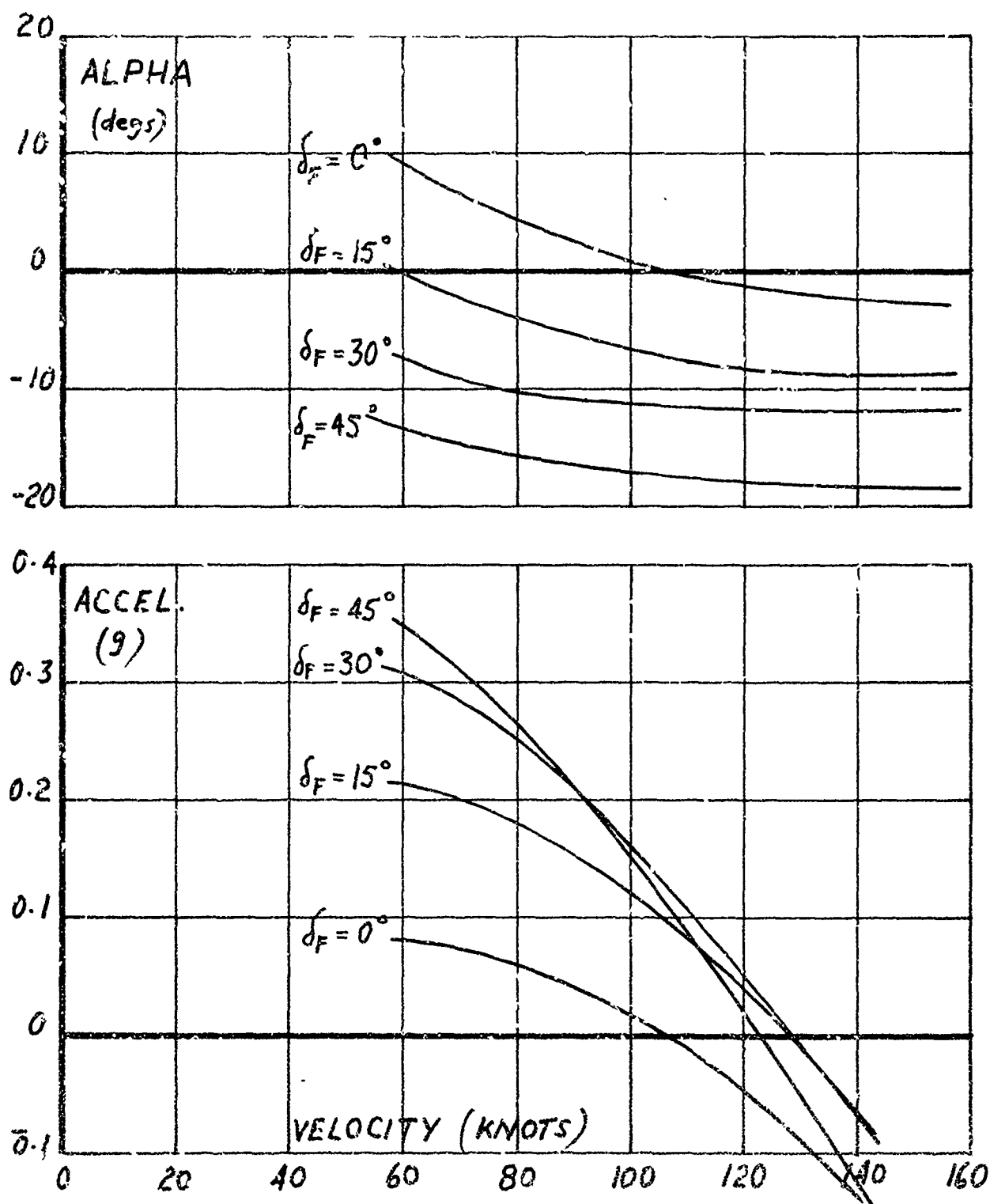
PREDICTED PERFORMANCE: EFFECT OF FUSELAGE AUGMENTOR NOZZLE ANGLE
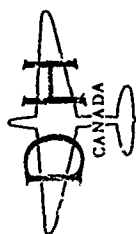
Aw/A = 0.25; DAR = 1.6; α = -10°
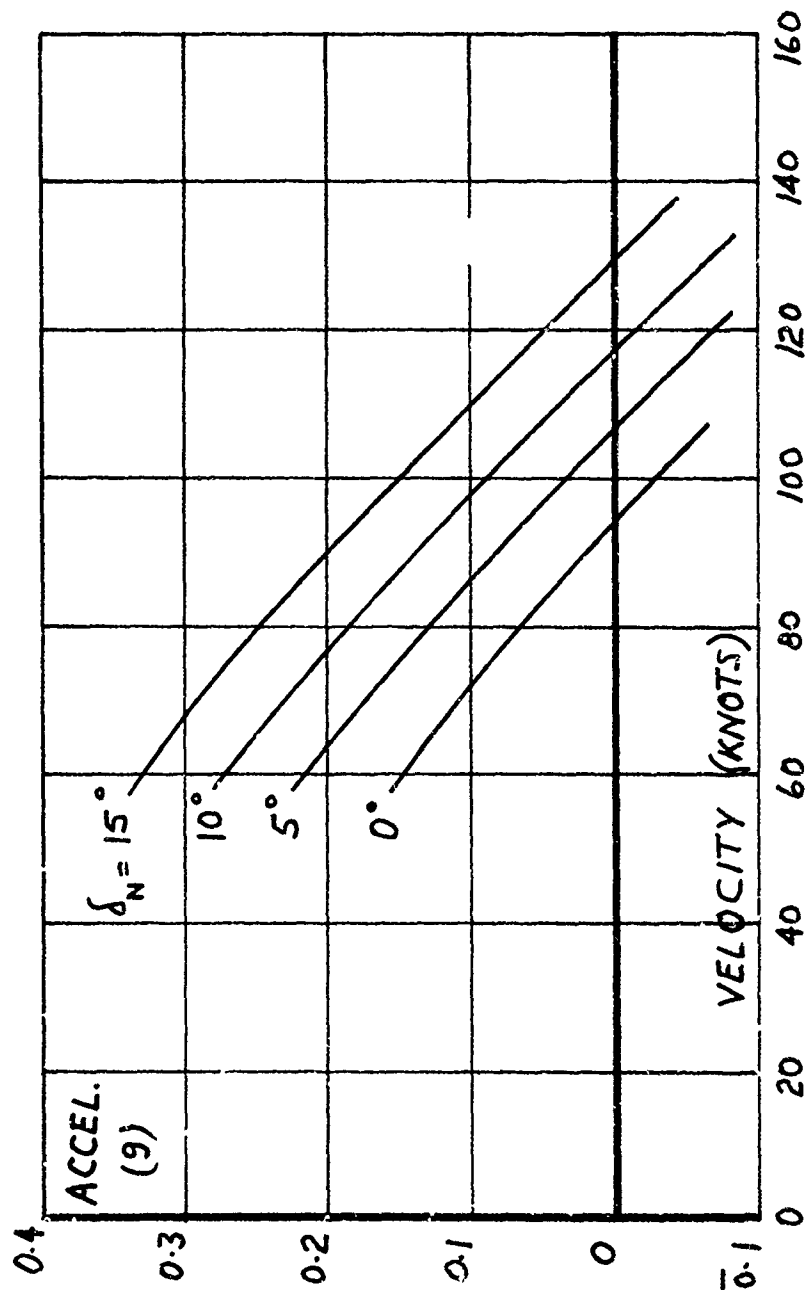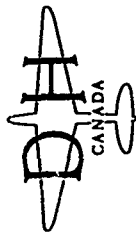
FIGURE 20

PREDICTED PERFORMANCE: EFFECT OF WING/FUSELAGE THRUST SPLIT

$\delta_N = 15°$; DAR = 1.6; $\alpha = -10°$
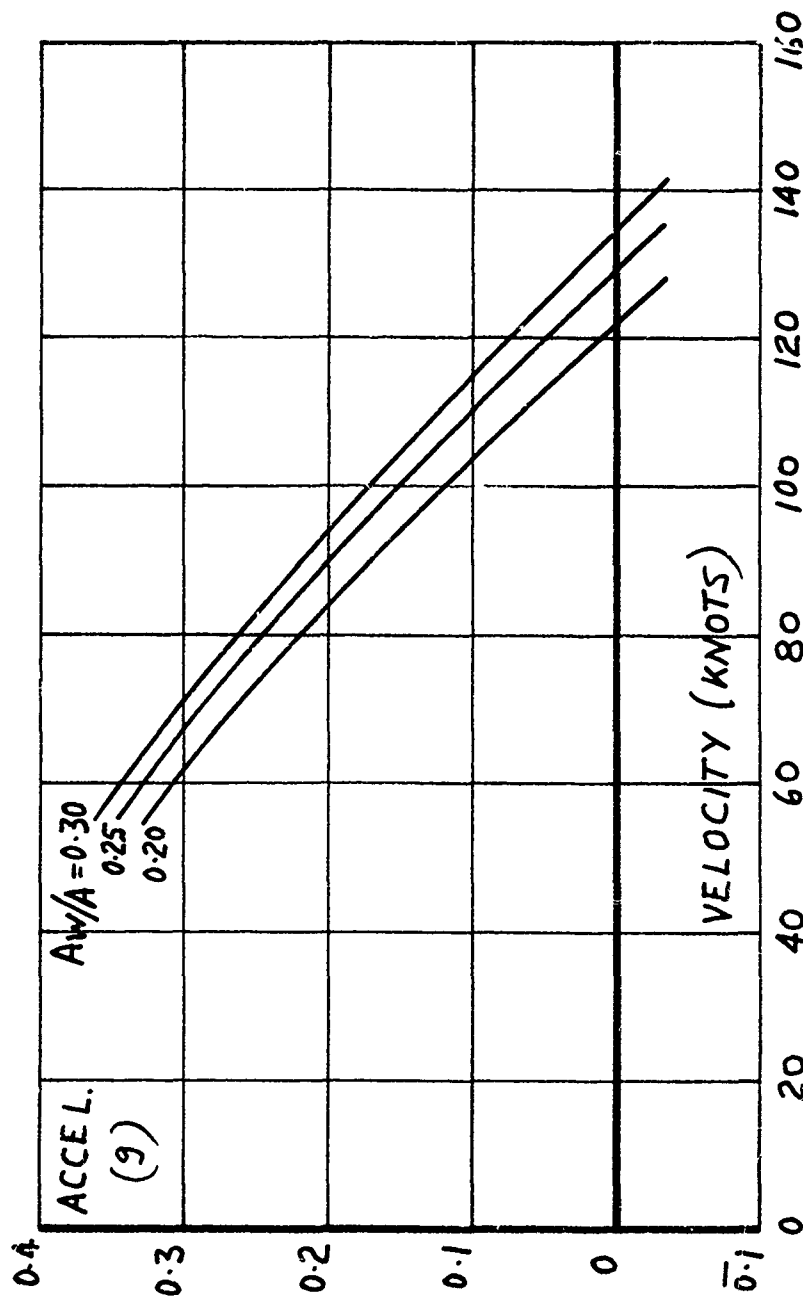
FIGURE 21

PREDICTED PERFORMANCE:

EFFECT OF FLAP ANGLE, WING-BORNE

Aw/A = 0.25
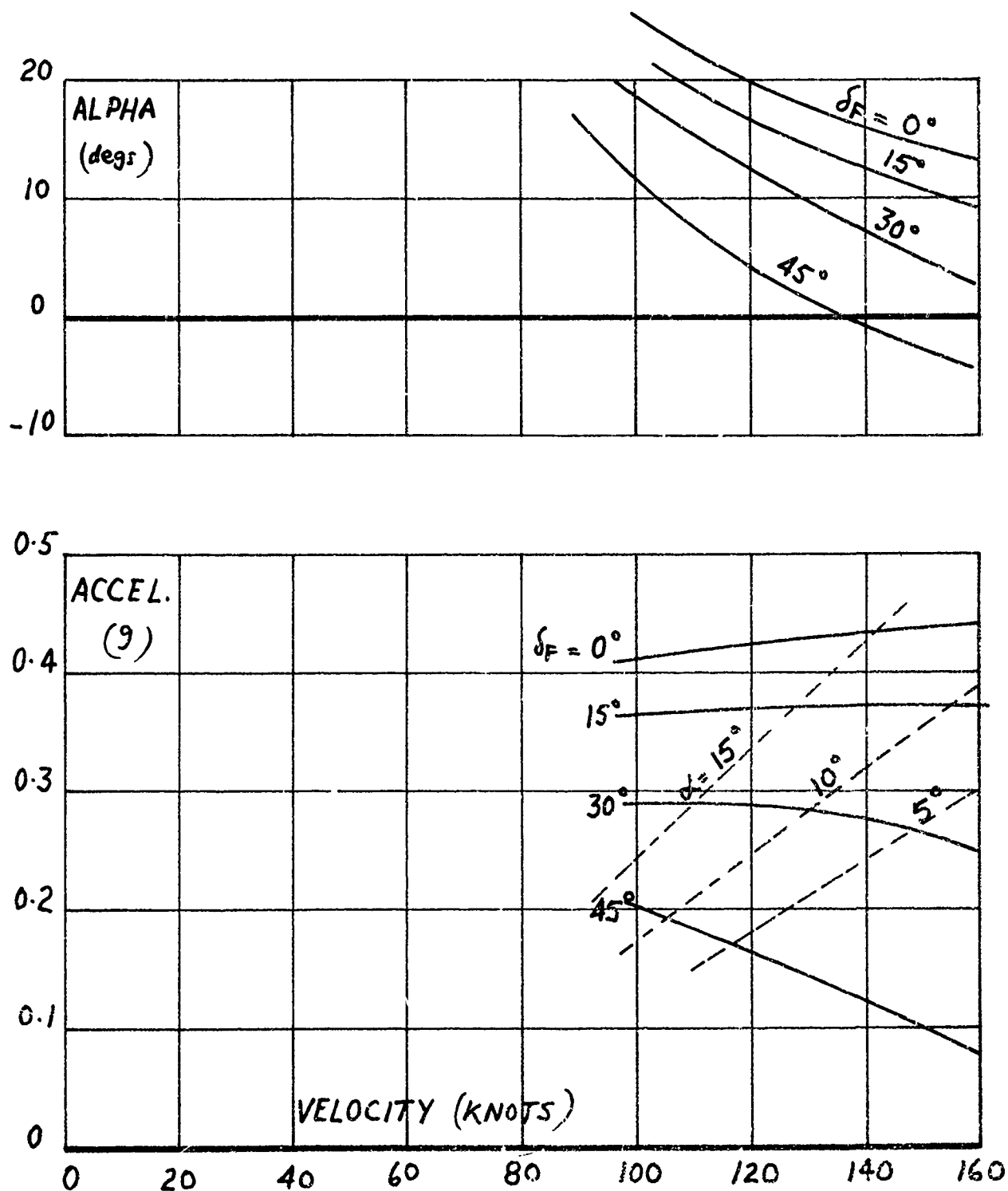
FIGURE 22

PREDICTED PERFORMANCE: EFFECT OF Aw/A, WING-BORNE

$\alpha = +10°$
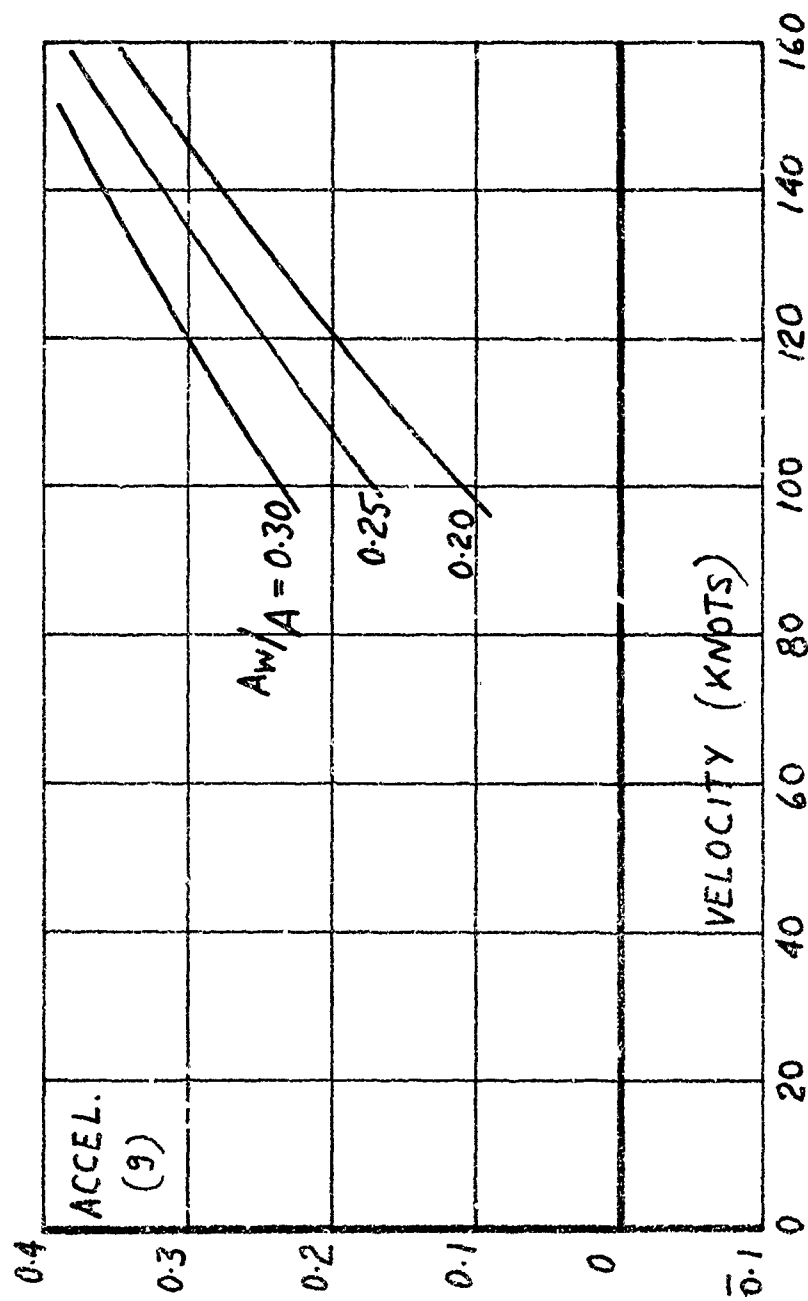
FIGURE 23

PREDICTED PERFORMANCE: EFFECT OF THRUST TRANSFER WITH DAR = 1.6

Aw/A = 0.25

FIGURE 24

930
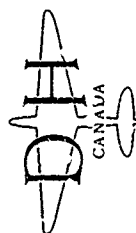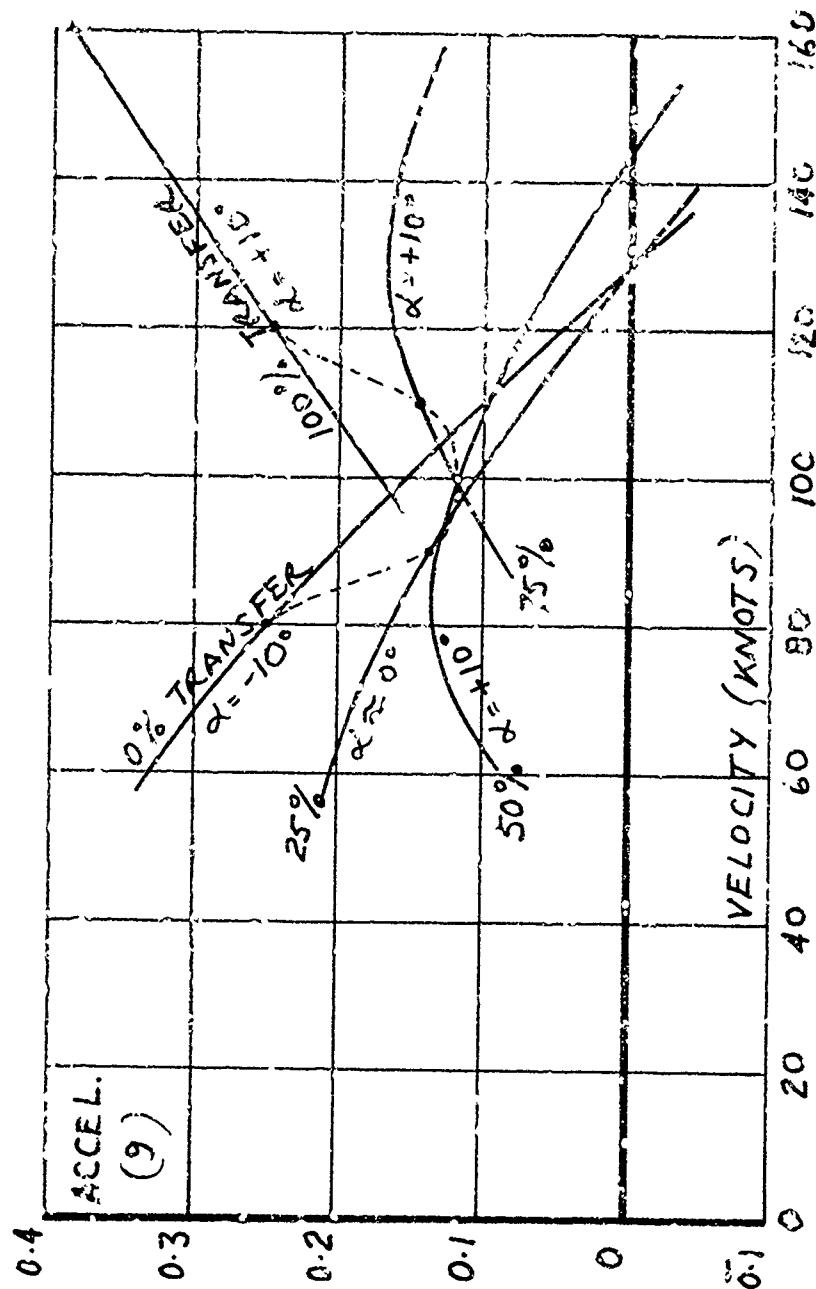
PREDICTED TRANSITION CHARACTERISTICS:

Aw/A = 0.30

VELOCITY (KNOTS)
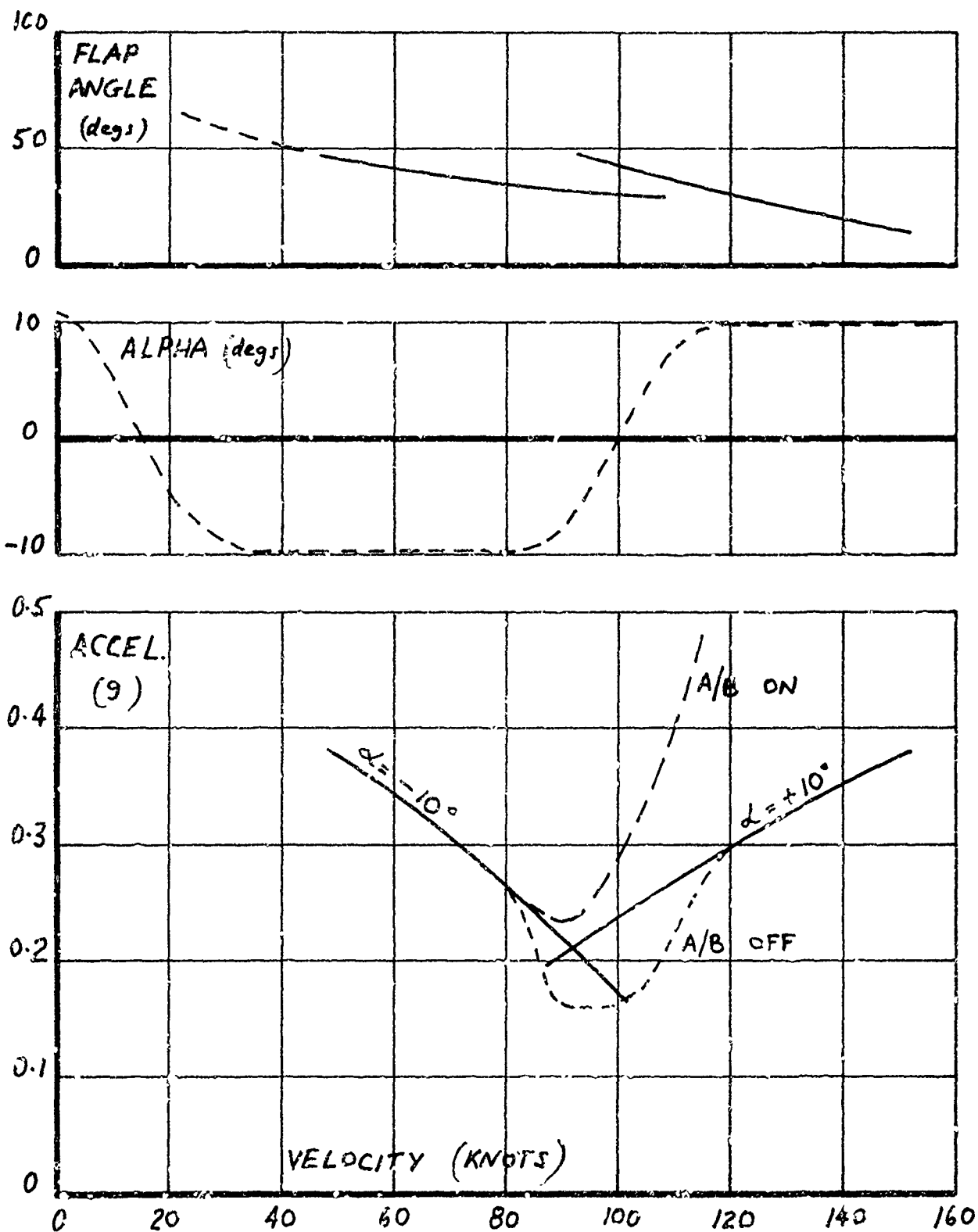
FIGURE 25

CALCULATION OF FORCES AND MOMENTS ACTING ON AN AUGMENTOR WING FOR A VTOL FIGHTER IN HOVER OR TRANSITION FLIGHT

Marnix F. E. Dillenius
Nielsen Engineering & Research, Inc.
Mountain View, California

ABSTRACT

A method based on potential flow theory has been developed for predicting forces and moments acting on augmentor wings for prescribed ejector jet characteristics. A three-dimensional nonplanar vortex lattice is laid out on the chordal planes of the augmentor wing components. Jet induced effects are included in the boundary condition from which the horseshoe vortex strengths are obtained. The jet within the diffusor is made to expand from the primary nozzles to the diffusor exit and is represented by a distribution of vorticity on the jet boundary to provide proper entrainment. The jet wake downstream of the diffusor exit is modeled by a vorticity distribution and blockage panels and its centerline location and spreading rate are taken from experimental data. The vortex lattice and jet models are used in an iterative manner until the predicted diffusor exit velocity matches the specified one. Some comparisons with available data show good agreement at lower power settings.

1. INTRODUCTION

The objective of this paper is to describe an analytical method capable of predicting the external aerodynamic characteristics of an augmentor wing for specified jet velocities at the primary nozzles and diffusor exit. The augmentor wing of interest here consists of a fixed wing with a set of large flaps at the trailing edge. The flaps can be deflected at large angles to guide and control engine exhaust gas diverted to primary nozzles at the trailing edge of the center flap. This flap is positioned above the forward and aft flaps designed to form a diffusor or ejector system. The primary jet issues from the nozzles and entrains secondary air drawn into the diffusor thereby augmenting the mass flow. As a result, the overall thrust is larger than the primary thrust generated by the primary jet. Furthermore, additional lift is generated by the wing/flaps system due to interference effects induced by the augmented jet flow. Effects from secondary jets are not accounted for in the present analysis. Flow conditions include hover and forward flight.

In the past, several two-dimensional analytical methods based on jet flap theory have been developed to analyze wind-on performance of augmentor wings. The thin jet flap approach is not a realistic model for the "thick" augmentor wing jets. The present method is directed towards the three-dimensional case of a finite-aspect-ratio wing with sweep and taper and a highly deflected, thick augmentor jet. The approach consists of developing models for the wing-flap system and those aspects of the augmentor jet that are required to properly model the interference effects of the jet on the wing/flaps loadings. Potential flow methods are employed and no flow separation on the surfaces is assumed to occur. Details of the flow inside the augmentor and the mixing of the primary and secondary flows are not addressed; the augmentor jet characteristics are assumed to be prescribed in terms of parameters which yield the primary jet velocity and the mixed flow velocity at the augmentor exit. Very recently, Bevilaqua (ref. 1) has developed a viscous inner flow solution capable of accounting for hypermixing nozzles and predicting details of the flow inside the diffusor including average jet velocities at the diffusor exit.

During the past 2 years, a Navy fighter prototype designated XFV-12A and employing an augmentor canard and wing was built and tested. It is shown in figure 1. The prediction method was designed to handle such augmentor systems; however, test data is not readily available for this configuration. In order to evaluate the methods and to provide some comparisons with data, calculations were made on the rectangular, aspect ratio seven V/STOL transport augmentor wing associated with the wind tunnel model shown in figure 2 and described in reference 2. Note that unlike the fighter configuration, the transport wing, with cross section shown in figure 3, has a short chord and high thickness ratio and the flap segments also have high thickness ratios.

In the following, the method of solution is briefly discussed and some comparisons with the data taken with the transport model are described.

The work described herein forms the starting point for the prediction of the longitudinal aerodynamic forces and moments acting on a complete VTOL fighter type fighter aircraft with one or more augmentor wing systems. This initial effort was sponsored and funded jointly by NASA and NAVAIR with Mr. Dave

Koenig and Dr. Max Platzer as technical monitors, respectively. More detailed
descriptions of the methods and results are given in the final technical report,
reference 3.

2. METHOD OF SOLUTION

The basic objective of the analytical method is to represent the solid surfaces
of the augmentor wing by a distribution of lifting-type singularities for the
purpose of calculating aerodynamic loads including jet interference effects.
To this end, the jet must be represented by suitable singularities from its
origin to some distance downstream of the diffusor in order to model the jet
induced effects. A nonplanar vortex lattice is laid out on the augmentor
wing components. This lifting surface model is basically a modified form of
the vortex lattice approach described in reference 4. The vortex distribution
used to model the jet over its length is an adaptation of the jet model used
in the work described in references 4 and 5. In addition, the jet wake (jet
downstream of the diffusor exit) makes use of blockage panels on its boundary.
This part of the jet model is an extension of the blockage panel scheme
described in reference 6.

The lifting surface and jet models have been programmed and are used in sequence
to form an iterative approach to the calculation of the longitudinal aerodynamic
characteristics (lift, drag, pitching moment) of augmentor wing configurations.
In this process, the assumption is made that flow entrainment by the primary
jet is such that the flow at the diffusor exit is completely mixed. This con-
dition, to a first approximation, is approached in practice when hypermixing
primary nozzles are employed in conjunction with limited boundary layer blowing.

In the following, brief descriptions are given of the lifting surface and jet
flow models, and the iteration scheme will be discussed. Attention will be
focused on the special features developed to apply the flow models to augmentor
wings.

Vortex-Lattice Model for Augmentor Wing/Flaps System

In the present investigation, the chordal planes of each component of the
augmentor wing/flaps system are divided into trapezoidal area elements or panels.
A horseshoe vortex is placed in each panel such that the bound leg lies along
the panel quarter chord and the trailing legs lie along the side edges of the
panel. A few horseshoe vortices and the reference coordinate system are
indicated in figure 4. The trailing legs extend back to infinity in the plane
of the panel. However, the trailing legs of the horseshoe vortices on the
wing (or that surface of the augmentor wing ahead of the forward flap) are
bent at the wing trailing edge so that they lie in the plane of the forward
flap as illustrated in figure 4.

The wing/flaps geometric parameters and flow conditions taken account of in the
present methods are summarized below. The wing may have

- finite span
- breaks in sweep of the leading and trailing edges
- uniform dihedral over the span
- taper set by leading- and trailing-edge shapes
- twist and camber
- zero wing thickness only

Up to 10 flap surfaces can be accounted for. The description of the planform of the flaps is governed by the following geometric characteristics.

- partial span
- straight leading- and trailing-edge shapes over the span
- taper set by leading- and trailing-edge sweeps
- root chord in plane parallel to vertical or x-z plane, see figure 4
- tip chord must lie in a vertical plane parallel to the vertical plane containing the root chord
- twist and camber
- zero flap thickness only

Effects of angle of sideslip and compressibility are not included. Angle of attack, flap deflection angle, dihedral angle, twist and camber angles are accounted for in the flow tangency condition using trigonometric functions since some of these angles can be large.

The flow tangency boundary condition is applied at control points located at the midspan of the three-quarter chord line of each area element or panel. Some control points are shown in figure 4. Designating the resultant velocity vector at one control point as $\vec{q}$ and the normal to the panel in question as $\vec{n}$, the boundary condition states

$$\vec{q} \cdot \vec{n} = 0 \tag{1}$$

for a finite set of control points. With no jet present, velocity $\vec{q}$ includes contributions from all the horseshoe vortices laid out over the augmentor wing surfaces and the free stream component. The velocity components induced by the horseshoe vortices are related to the unknown vortex strengths through the use of influence functions given in reference 4. The functions associated with horseshoe vortices on the wing account for the effects of the angle of deflection of the trailing legs. In the application to augmentor wings, velocity contributions induced by the jet singularities are included in equation (1) for the purpose of accounting for jet interference. A later section concerned with the jet model describes the method used to generate the jet induced velocity contributions. Note that the free stream component represents the flight condition: hover (zero velocity), transition or forward flight (nonzero).

The application of the flow tangency condition, equation (1), at the control points distributed over the chordal planes of the augmentor wing surfaces results in a set of simultaneous equations from which the unknown vortex strengths are obtained. Once the strengths are known, the aerodynamic forces and moments acting on the augmentor wing components are calculated using the method described next. At this stage it is also possible to compute, at any field point, the flow field induced by the horseshoe vortices representing the surfaces of the augmentor wing.

The aerodynamic forces acting on one elemental area or panel can be determined from the application of the Kutta-Joukowski law for forces acting on a vortex filament. For a vortex filament, the aerodynamic force acting on it per unit length is expressed as the vector product of the flow velocity $\vec{q}$ past the vortex of strength $\vec{\Gamma}$ as follows.

$$\vec{F} = \vec{q} \times \vec{\Gamma} \qquad (2)$$

Contributions from all horseshoe vortices laid out over the augmenter wing components, free stream and jet induced contributions are included in the calculation of $\vec{q}$. The elemental panel force calculated with equation (2) can be used to compute spanwise load distributions by summing over a row of panels in the chordwise direction. Overall forces are determined by summing over all the panels and overall pitching moments are determined by using the panel forces times the appropriate moment arms. The results include normal force, axial force and pitching moment coefficients. The directions of the normal and axial force coefficients, C_N and C_A, respectively, are shown in figure 4.

Jet Model Including Jet Wake

The objective of the jet model is to represent the induced external flow effects of the entire jet, ignoring the details of the mixing flow inside the diffusor. The basic flow model used as a starting point for the required jet model is that of an actuator disk which can be used to represent a jet of fluid with higher velocity and higher total head than the surrounding fluid. The equivalent singularity distribution for an actuator disk is a semi-infinite length cylinder with a uniform distribution of vorticity on its surface. Two characteristics of this model are a uniform velocity profile inside the jet and an increasing mass flow within the boundary over the initial few diameters of length.

This flow model has been used to represent the external flow field induced by the wake from a turbojet or turbofan engine (refs. 4 and 5). In reference 4, the development of the flow model for circular and elliptic cross section jets is described, and in reference 5, the extension of this model to a rectangular cross section jet is presented. During the course of the modifications, the analytical singularity model of a uniform vorticity distribution on a semi-infinite cylinder was changed to a finite length distribution of vortex rings. This change was necessitated by numerical difficulties in calculating the induced velocity field associated with the singularity distribution for curved jets, and more details of this change are presented in reference 5.

The jet, exhausting from the trailing edge of the center flap (fig. 4), is divided into two distinct regions for modeling. Secondary jets are not included in the present analysis. The first region is that portion of the jet from the exhaust nozzles to the exit of the diffusor. The second region is the remainder of the jet from the diffusor exit to its chosen end point at a finite distance downstream of the exit. The following is a short description of this jet model.

The upstream region of the jet model, in the diffusor region, is quite different from previous jet models. For the case at hand, the jet exhausts from a very high aspect ratio slot nozzle at the trailing edge of the center flap and expands very rapidly to fill the diffusor. The assumption is made that the jet and entrained air are completely mixed and fill the diffusor exit. (This is not a restriction of the jet model in that it can also be laid out to fill the exit in part only.) The rates of expansion and entrainment of secondary fluid by the jet are much larger than typical free jet rates because of the

enhanced mixing over the relatively short length of the diffusor. Therefore, a special flow model is required in this region. This is described next.

The boundaries of the jet in the diffusor region are shown dashed in figure 4. Since the present model is not concerned with the details of the internal flow, the idealized boundaries are prescribed by straight line segments as shown. As a consequence of the fully mixed flow assumption, the jet model is made to fill the exit at the end of the diffusor. The initial portion of the jet is sized to match the actual cross sectional area of the jet nozzle at the center flap. The short length of nonexpanding boundaries near the trailing edge of the center flap, shown in figure 4, is included to give the analytical jet model an initial run length to build up to the correct jet velocity. This length is typically four to five times the minimum cross section dimension, in this case, the width of the jet. Since details of the actual jet in the diffusor are unknown, the jet boundary is specified to expand linearly to the exit of the diffusor after the initial run length, and the centerline of the jet is positioned approximately midway between the forward and aft flaps. The spanwise dimension of the jet is assumed constant; therefore, the width of the jet is the only changing dimension. A schematic of the jet model, to be used later, is shown in figure 5(a).

The distribution of vorticity, γ, along the length of the jet boundary is determined in the following manner. The initial vorticity strength at the primary jet nozzle is specified from the known value of primary nozzle mass flow velocity v_{j_I} to be

$$\gamma_I = v_{j_I} \tag{3}$$

This vorticity strength per unit length remains constant in the initial region to give the centerline velocity an opportunity to stabilize at the correct value. Since the jet model does not attempt to model the distribution of velocity inside the diffusor, the next point at which jet mass flow is known is at the diffusor exit. At this station the vorticity strength per unit length is specified to be

$$\gamma_E = v_{j_E} \tag{4}$$

where v_{j_E} is the flow velocity associated with the total mass flow at the end of the diffusor. The distribution of vorticity between the initial and exit values was found to be best represented by a ninth-order polynomial distribution. The first three derivatives are set equal to zero at the initial station, S_I, and the first six derivatives are set equal to zero at the exit station, S_E. In this way, the vorticity is concentrated towards the primary jet exhaust allowing for high jet-flow velocity at the exhaust nozzle and high entrainment rate over the length of the diffusor. As a result, the vorticity distribution is given by

$$\left.\begin{array}{l} \dfrac{\gamma - \gamma_E}{\gamma_I - \gamma_E} = \quad 9 - 63\xi^8 + 36\xi^7 \\[2em] \xi = \dfrac{S_E - S}{S_E - S_I} \end{array}\right\} \tag{5}$$

where

which produces smooth centerline velocity distributions between S_I and S_E for any values of γ_I and γ_E as shown in figure 5(b).

The portion of the jet model in the region downstream of the diffusor exit is treated as a free jet wake. The vorticity distribution on the wake boundary is held constant at the value γ_E specified at the end of the diffusor, which is the requirement for a free jet model (ref. 5).

The wake cross section is rectangular over the entire length of the wake, but the boundary is allowed to expand according to available empirical information. Holding the span of the wake constant, the spreading information contained in reference 6 is applied to the wake width.

The path taken by the jet after it leaves the end of the diffusor must be specified with respect to the location of the diffusor exit. This is done using empirical information on the path of a rectangular jet in a crossflow (ref. 7). Small differences in the centerline path do not create large differences in the induced loading on the lifting surfaces; therefore, based on the success of a similar approach in reference 6, the empirical data of reference 7 are used for all calculations included in this report. The jet wake boundaries are shown in figure 6(a) for the case $v_{j_E}/V_\infty = 4$ and in figure 6(b) for $v_{j_E}/V_\infty = 1.4$.

The final component of the jet wake model in the downstream region is the blockage model. It is well known that a jet exhausting into a crossflow behaves as if the jet boundary is nearly a solid surface. To approximate this effect, the surface of the wake is represented by a finite number of vortex quadrilateral panels with a control point at the panel centroid as shown in figure 6. The boundary condition of no flow through the control point on each panel results in a set of simultaneous equations. The velocity to be canceled at the blockage panel control points consists of a contribution of the free stream to which are added the perturbation velocity components induced by the vortex lattice on the wing/flaps system with power off. This has the effect of allowing the blockage panels to be porous to the fluid entrained by the distribution of vorticity modeling the wake (as well as the jet). It also takes account in the first approximation, of the effects caused by the augmentor wing on the jet wake. The blockage panel or quadrilateral vortex strengths are then determined from the simultaneous equations. Velocities induced by the blockage panels will be included in the calculation of the power-on horseshoe vortex strengths of the wing/flaps system at a later stage.

Iteration Scheme

The flow models discussed above are implemented in computer programs to be used in a sequential manner. This arrangement was found to be convenient in the iteration scheme used to generate a solution. In a series of steps, the vortex lattice and jet analysis are applied as follows:

Step 1. The vortex lattice analysis is applied to the augmentor wing
         surfaces <u>without</u> jet induced effects in the boundary condition.
         The power-off horseshoe vortex strengths are determined.
         Velocities induced by the horseshoe vortices at the control
         points of the blockage panels are computed.

Step 2. The jet wake centerline and boundaries are located. Blockage
         panel strengths are calculated using velocities induced by the
         power-off horseshoe vortex lattice with strengths determined
         in step 1. At this point the blockage portion of the jet wake
         model has been modeled. The blockage-induced effects at the
         control points on the wing/flaps surfaces are calculated and
         will be used in step 4.

Step 3. The jet model is now applied to the augmentor jet and the dis-
         tribution of vorticity within the augmentor and downstream of
         the augmentor exit is calculated. As noted previously, the
         vorticity distribution is determined by the jet velocity at
         the exhaust nozzle of the center flap and at the diffusor exit.
         These are specified from the augmentor performance prescribed
         initially. In this step, the assumption is made that these
         velocities are produced only by the distribution of vorticity
         representing the jet, and the vorticity distribution is calcu-
         lated. The jet-induced velocities at the wing/flaps control
         points are calculated.

Step 4. The vortex lattice analysis is applied again to the augmentor
         wing surfaces. This time, the boundary condition includes
         velocity components induced by the distribution of vorticity
         and the blockage panels modeling the jet and its wake. The
         horseshoe vortex strengths are recalculated. Next, the flow
         field at the diffusor exit is computed including contributions
         generated by the vortex lattice on the wing/flaps system, the
         distribution of vorticity and the blockage panels modeling
         the jet, and the component of the free stream (zero for the
         hover case). The area averaged flow velocity is determined
         and compared with the specified diffusor exit average velocity.

At this stage, the predicted value is usually larger in magnitude than the
specified value. A lower diffusor exit velocity is selected and fed back to the
jet analysis, step 3. All other input is kept the same including jet exhaust
velocity, centerline location, and spreading rates inside and downstream of the
diffusor region. For the same horseshoe vortex lattice and blockage panel lay-
out, step 3 is repeated with the adjusted diffusor exit velocity for the jet
analysis. A new vorticity distribution is computed for the jet and the induced
velocity components at the wing/flaps control points are updated. Step 4 is
repeated and the average flow velocity at the diffusor exit recomputed. If
the updated value matches the specified one within a selected error bound, the
iteration is stopped. The forces and moments calculated by the horseshoe vortex
analysis now reflect the effects of the mutual interference between the jet and
the augmentor wing surfaces and the effect of the free stream. The overall

forces and moments are calculated as the sum of the contribution from the jet itself (thrust at the exhaust nozzle) and the contribution from forces acting on the horseshoe vortex lattice representing the wing/flaps system.

It should be noted that the specified velocities at the exhaust nozzle (at the trailing edge of the center flap) and the diffusor exit should be for the actual flow conditions at hand. As such, the specified diffusor exit velocity deduced from experimental data (or directly measured) is already representative of the presence of the augmentor wing surfaces and especially the effects of the actual jet wake. Therefore, as long as the iteration scheme described above results in a predicted flow velocity at the diffusor exit that matches the specified value, the location and shape of the jet wake is not of primary importance in the calculation of the forces and moments. In other words, under these conditions the jet wake has a small effect on loads. The region of the jet inside the diffusor, through its large entrainment effect, is mainly responsible for the interference effects of the jet on the aerodynamic loads acting on the augmentor wing surfaces. Finally, it is noted that this procedure not only produces the correct mass flow at the center flap nozzle exit and the diffusor exit, but the correct secondary flow entering the diffusor.

3. THEORETICAL RESULTS AND COMPARISONS

Partially due to the newness of the augmentor wing concept and partially for proprietary reasons, very limited experimental data involving augmentor wing configurations are in the public domain. In particular, component loading and pressure distribution data on a VTOL fighter-type configuration such as shown in figure 1 are practically unavailable.

The only data made available to test the augmentor wing analysis described herein involves the wind tunnel transport model of reference 2. This model is shown in figure 2. A cross section of its rectangular augmentor wing system is indicated in figure 3 for a set of flap deflection angles representative of transition conditions. Inherently, this model does not resemble a VTOL fighter type, figure 1, in that the augmentor wing system is unswept and thick in section. Compared to the streamwise flap lengths, the forward or wing part is extremely short. In addition, the model employs a fuselage with considerable cross section area atypical of a VTOL fighter. Furthermore, figure 3 shows secondary jet nozzles on the forward and aft flap components. In VTOL fighter configurations, these jets serve to control the boundary layers on the diffusor walls formed by the forward and aft flap surfaces. The amount of engine exhaust diverted to the secondary nozzles may vary. For the transport model under consideration, all the engine exhaust is assumed to issue from the primary nozzles at the trailing edge of the center flap. Reference 2 does not contain information about the division in flow between the primary and secondary nozzles.

In spite of the somewhat unsuitable geometric characteristics of the wind tunnel model described above and the uncertainty in the division of flow between the primary and secondary jet nozzles, the theoretical methods were applied to this configuration for preliminary verification and to point out the usefulness of the methods for indicating areas of improvement in the

preliminary design stages of augmentor wings. As far as the model components
are concerned, the augmentor wing system and horizontal tail will be handled
by the present methods including an approximation for the lift carried over
on to the fuselage. Flow conditions include zero angle of attack and two
forward flight speeds.

In what follows, the layout of the horseshoe vortices on the surfaces of the
augmentor wing will be specified. The jet wake and the blockage panel layout
are shown for two power settings. Some of the calculated flow fields induced
by the vortex lattice alone and jet alone will be shown. As a result of the
iteration, the final velocity distributions calculated by the present method
at the exit are indicated. Finally, comparisons are made between the predicted
and measured overall forces and moments. The wing, forward flap, center flap,
and aft flap components of the augmentor wing system, shown in figure 3, are
idealized to the chordal plane representation shown in figure 6 The wing/
flaps components are extended through to the fuselage centerline to account
for body lift carryover. However, the jet is made to span only over the
exposed wing/flaps region and the effects of the jet are felt by the surfaces
in that region only (i.e., no jet effects are included on the part of the
augmentor wing surfaces inside the fuselage). In this way, the lift carry-
over onto the fuselage is accounted for to first order for both power-on and
power-off conditions. At the present time, the methods cannot account for
the effects of the fuselage (Beskin upwash) on the augmentor wing surfaces.
Therefore, flow conditions including nonzero angle of attack introduce
uncertainty with the present method when a fuselage is part of the config-
uration under consideration.

Because of geometrical and flow symmetry about the vertical plane through the
fuselage centerline, only one-half of the configuration need be covered with
a vortex lattice. In the chordal plane of the wing shown in figure 6, 11
horseshoe vortices are laid out along the span and three along the chord. On
the forward flap, the spanwise number is the same but four horseshoe vortices
are laid out on the chord because of the longer length involved. On the
center flap, the spanwise number is also 11, and three are placed along the
chord. The aft flap, with the longest chord length, is covered by 11 spanwise
and five chordwise horseshoe vortices. As a consequence, there are 33 horse-
shoe vortices on the wing, 44 on the forward flap, 33 on the center flap and
55 on the aft flap. Note that the trailing legs of the horseshoe vortices on
the wing are bent at the wing trailing edge to lie in the chordal plane of
the forward flap. This construction is also indicated for the one horseshoe
vortex on the wing of the general augmentor wing system of figure 4. Finally,
the horizontal tail is covered by an additional horseshoe vortex lattice
consisting of five vortices along the span and three along the chord. Thus,
a total of 180 horseshoe vortices represent the augmentor wing/flaps and
horizontal tail. Their strengths are determined from one set of simultaneous
equations as described earlier.

For the case at hand, the jet and its wake are modeled for two power settings
using the methods described in this paper. Due to symmetry, the effects of
the jet on the opposite side of the vertical plane of symmetry must be accounted
for At the present time, the mutual interference between the left and right

jets is not included in the analysis. For the power or thrust settings C_μ = 7.31 and C_μ = 1.5, the jet centerline and boundaries deduced from the information based on experimental data of references 6 and 7 are shown in figures 6(a) and 6(b), respectively. The length of the jet wake is taken approximately as three times the chord length of the forward flap. In connection with the externally blown flaps work (ref. 4), it was found that greater jet lengths produce very small changes in aerodynamic loadings at the expense of additional computer time. The blockage of the jet boundaries is modeled by quadrilateral vortex panels with ten in the spanwise direction and seven along the direction of the jet. The sides of the jet wake are covered by four blockage panels in the direction normal to the centerline and seven along the lengthwise direction. Thus, the boundaries of the jet wake on the left hand side of the plane of symmetry are covered by 196 panels. To preserve symmetry, the same jet wake and its singularity layout is positioned on the right hand side of the symmetry plane. Mutual interaction is not accounted for, however.

The velocity field to be counteracted by the jet wake blockage panels is shown in figure 7 in a vertical plane for part of the jet length. In accordance with step 1 of the iteration scheme, the flow velocities are generated by the vortex lattice laid out on the surfaces of the augmentor wing and include the free stream velocity. The flow vectors indicated in figure 7 are calculated by the vortex lattice (180 horseshoe vortices) on the lifting surfaces. Flow conditions are zero degrees angle of attack and zero power setting. Note that the flow velocities at the blockage panel control points are directed downwards. Since the vortex lattice and blockage panel strengths are solved for separately, the flow field seen by the jet wake should be generated by the horseshoe vortices as influenced by the jet. As a first approximation, the power-off horseshoe vortex strengths are used and in the succeeding steps of the iterative approach the blockage panel strenths are kept constant. This constraint can be relaxed and the flow field impressed on the jet wake recalculated once the jet singularities are known. At this time, for the sake of economy the former approach is adopted.

In order to provide some insight into the entrainment properties of the jet model, the flow field induced by the jet model at the control points of the augmentor wing are shown in figure 8 for the jet and jet wake layout of figure 6(a). The directions of the flow vectors at the control points on the forward and aft flaps and the diffusor entrance indicate strong inflow or entrainment towards the initial or narrow part of the jet near the trailing edge of the center flap. In addition, the flow inside the jet at the diffusor exit is fairly uniform and the average velocity ratio (v_{j_E}/V_∞) at the diffusor exit is about 3.8. Note that at this stage the effects of the horseshoe vortices are not included in the diffusor exit velocities.

At the end of the first pass through the iteration procedure, the flow velocities across the diffusor exit are computed as the sum of the vortex lattice and jet-singularities-induced velocities added to the free stream. For both power settings, the predicted velocities at the exit were higher than the specified average flow velocity. In accordance with step 4 of the solution procedure, the diffusor exit velocity, serving as one of the velocity inputs to the jet model, is reduced and the jet model rerun (step 3). The adjusted jet induced velocities, such as shown in figure 8, are then used in step 4. At the end of step 4, the diffusor exit velocities are calculated again and

compared with the specified average flow velocity. When the predicted average diffusor exit velocity matches (to within a few percent) the specified one, the solution is considered to be converged.

For the C_μ = 1.5 and 7.31 power settings, the following table contains the final input velocities for the jet model and the average of the predicted and specified diffusor exit velocities.

C_μ	specified and used as initial input to jet model		used as final input to jet model		vortex lattice + jet model
	$\left.\frac{v_{j_I}}{V_\infty}\right\|_{initial}$	$\left.\frac{v_{j_E}}{V_\infty}\right\|_{initial}$	$\left.\frac{v_{j_I}}{V_\infty}\right\|_{final}$	$\left.\frac{v_{j_E}}{V_\infty}\right\|_{final}$	$\left.\frac{v_{j_E}}{V_\infty}\right\|_{calc.}$
1.50	8.33	1.40	8.33	0.70	1.46
7.31	16.94	3.89	16.94	3.40	3.83

The calculated flow velocity at the diffusor exit, v_{j_E}/V_∞, is obtained from the area-averaged distribution of flow velocities shown in figure 9(a) for C_μ = 1.5 and in figure 9(b) for C_μ = 7.31, respectively. Note that these velocities are generated by the vortex lattice, the jet vorticity and jet wake blockage panels and include a component of the free stream. The velocity vector associated with the free stream is also shown. The distribution of flow velocities across the diffusor exit is seen to be fairly uniform in accordance with the assumption made to that effect in the description and specification of the jet model. Reference 2 contains some total pressure data obtained with a rake located at the diffusor exit for one spanwise station. The distributions of flow velocities deduced from that data are not uniform and in fact show peaks near the diffusor walls formed by the inner surfaces of the forward and aft flaps. In the tests of reference 3, additional jets issue from the leading edges and are directed along the inner walls of the diffusor for boundary layer control. It is possible, therefore, that the rake measurements are influenced by these secondary jets which are not accounted for in the present method.

The agreement between the calculated diffusor exit flow velocity and the specified value shown in the table above is quite good. At this (final) stage, the forces and moments computed by the vortex lattice method should be representative of the augmentor wing loading including the effects of the jet.

Lift, drag and moment coefficients are shown as a function of thrust or jet momentum coefficient C_μ in figures 10(a), 10(b), and 10(c), respectively, for zero angle of attack. The open symbols are values measured on the complete

configuration shown in figure 2 for the set of flap deflection angles specified. The closed symbols represent calculated values for C_μ = 0.0, 1.5 and 7.31 obtained with the paneling layout and jet specification described above for the same flap deflection angles. Only the augmentor wing and horizontal tail surfaces are accounted for in the present method; therefore, any effects from the fuselage on the aerodynamic loads are not included in the calculated values. As far as the drag is concerned, the theory calculates the induced (due to lift) drag contribution only.

At the zero and lower (C_μ = 0.0, 1.5) power settings, the agreement between measurement and theory is good. At the highest moment coefficient (C_μ = 7.31) the lift and drag coefficients are overpredicted and the pitching moment is underpredicted. Overall, the predictions show similar trends as the experiment for increasing thrust coefficient.

Reference 2 contains a few chordwise pressure distributions for one spanwise location for the selected flap settings. Especially at the higher power setting, flow separation is indicated on the center and aft flap. The experimental pressure distribution along the upper surface of the wing and forward flap components (see fig. 3) indicate strong suction pressures aft of the secondary nozzle. Similar behavior is indicated at the leading edge of the aft flap on the surface ahead of the secondary nozzle. These observations and the nonuniform measured total pressure across the diffusor exit discussed earlier seem to indicate strong blowing out of the secondary nozzles. This behavior makes itself felt more strongly at the higher power setting since the total pressure distribution at the diffusor exit is shown to be more uniform for the C_μ = 1.5 case. Thus, the partial separation and the strong effects of the secondary nozzles at the higher power setting (C_μ = 7.31) may account for the discrepancy between theory and experiment for that condition.

4. CONCLUDING REMARKS

A method has been developed for determining the external aerodynamics of VTOL fighter-type augmentor wings in hover or transition flight for prescribed ejector jet characteristics. Specifically, the flow velocity at the primary nozzle and an average velocity at the diffusor exit must be prescribed for the flight condition at hand. The augmentor wing may have sweep and taper. The method is based on potential flow theory and attached flow is assumed. For given primary nozzle and diffusor exit jet velocities, the aerodynamic loadings acting on the augmentor wing are obtained as the result of an iteration scheme which produces a calculated average diffusor exit flow velocity to match the specified one in magnitude. The iteration scheme consists of a serial application of the vortex lattice and jet model methods.

Some comparisons with experimental data taken with a V/STOL transport model are shown. This configuration is not representative of a VTOL fighter in that the streamwise sections of the augmentor wing components are very thick. The division of exhaust gas flow between the primary nozzle and secondary is not readily available. At the present time, the method can only accommodate a primary jet issuing from the trailing edge of the center flap located above the diffusor. Consequently, the assumption was made that all the engine exhaust is

fed to the primary nozzle and the total entrainment by the single jet is made to be the same as in the case when the power is divided into primary and secondary nozzles. As a result, the calculated overall forces and moments should be representative but detailed information such as component loadings require more knowledge about the flow division.

With these simplifications, the present method calculates lift, drag and pitching moments which agree well with the experimental data at lower power settings. For the higher power setting, the lift and drag are overestimated and the pitching moment is underestimated; however, the predictions show the same trends as experiment for increasing thrust.

The usefulness of the present method includes the capability of indicating potential problem areas during preliminary design of an augmentor wing system. If the components are reasonably slender in section, the developed methods can be used to map the flow field in the vicinity of the augmentor wing for determining interference on other components of the aircraft. In addition, the flow field impressed on each of the flap surfaces of the augmentor wing system can be analyzed so that secondary nozzles for boundary control can be positioned and sized on the basis of that knowledge. Furthermore, the present method can be applied to an existing configuration for which component loads have been measured. By comparing the component load prediction with measurement, components suffering from flow separation and stall can be identified and remedies effected.

On the basis of the work performed so far, the following recommendations are offered.

1. To validate the present method further, additional comparisons should be made with available data for different flap settings and nonzero angle of attack. Component load comparisons should be made. The majority of the engine exhaust should be applied to the primary nozzles for comparison purposes.

2. Detailed data should be taken with a XFV-12A type augmentor wing and made available for testing the developed method.

3. Based on the outcome of 1 and 2, the single augmentor wing system model can be improved by studying effects of different jet boundary layouts and jet vorticity distributions (affecting entrainment) inside the diffusor. Also, the effects of the jet wake on overall and component loads should be determined.

4. It is possible to circumvent the specification of experimentally deduced jet velocities at the primary nozzle and the diffusor exit. Detailed internal flow analyses have been developed elsewhere (ref. 1) capable of generating the required quantities for the jet model of the present method.

5. The present method can be extended to account for more than one jet, i.e. to handle secondary jets and account for the associated Coanda effects on the aerodynamic loads acting on the augmentor wing components. The applicable technology has been developed in connection with USB (Upper Surface Blowing) work described in reference 5.

6. The present method can be extended to account for augmentor canard/
    augmentor wing systems attached to a fuselage, accounting for mutual
    interference between the canard, wing, and fuselage.

REFERENCES

1. Bevilaqua, P. M.: Optimization of Hypermixing Nozzles. Paper given at
    the ONR-NAVAIR Contractors Review. Nov. 28-29, 1978. Proceedings to
    be published.

2. White, E. R.: Experimental and Theoretical Analysis of Augmentor Diffusor
    Effectiveness on Transport Model (TPA 210, Task 0010). Rockwell Inter-
    national Internal Letter 511-38-75, March 1975.

3. Dillenius, M. F. E. and Mendenhall, M. R.: Theoretical Analysis of an
    Augmentor Wing for a VTOL Fighter. NEAR TR 183, Dec. 1978. Work per-
    formed under NASA contract NAS2-9605. To be published as NASA CR-152254.

4. Mendenhall, M. R., Spangler, S. B., Nielsen, J. N. and Goodwin, F. K.:
    Calculation of the Longitudinal Aerodynamic Characteristics of Wing-Flap
    Configurations with Externally Blown Flaps. NASA CR-2705, Sept. 1976.

5. Mendennall, M. R. and Spangler, S. B.: Calculation of the Longitudinal
    Aerodynamics Characteristics of Upper-Surface-Blown Wing-Flap Configura-
    tions. NASA CR-3004, 1978.

6. Perkins, S. C., Jr. and Mendenhall, M. E.: A Correlation Method to
    Predict the Surface Pressure Distribution on an Infinite Plate from
    which a Jet is Issuing. NASA CR-152,160, May 1978.

7. Thames, F. C. and Weston, R. P.: Properties of Aspect Ratio 4.0 Rectangular
    Jets in a Subsonic Crossflow. AIAA Paper No. 78-1508, Aug. 21, 1978.
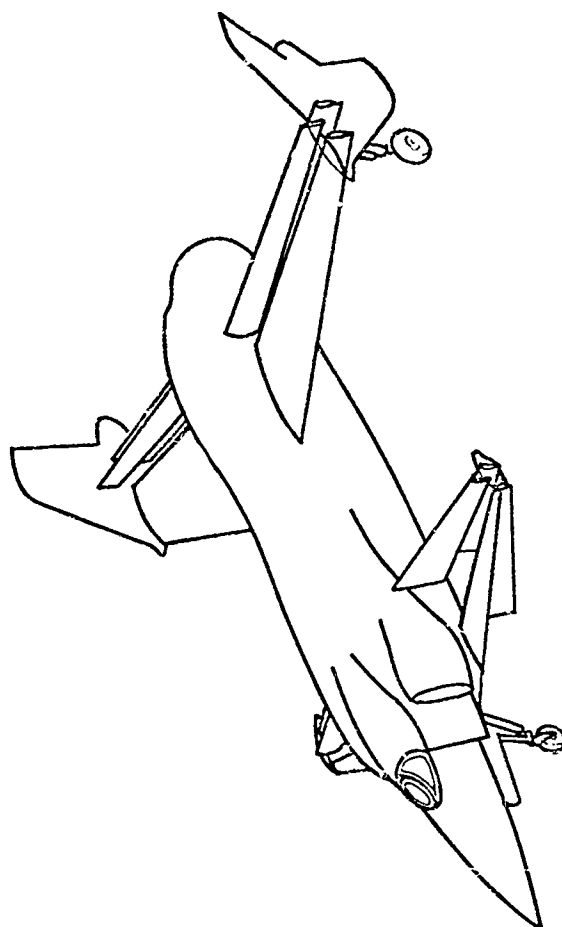
Figure 1.- VTOL fighter with augmentor canard and wing.

$$\text{AR} = 6.9$$

$$\tilde{c} = 50.8 \ (20.0)$$

$$S_{Ref} = 8903.21 \ cm^2 \ (1380 \ in.^2)$$

$$\frac{x_{CG}}{\tilde{c}} = -0.34$$

$$\frac{z_{CG}}{\tilde{c}} = -0.14$$
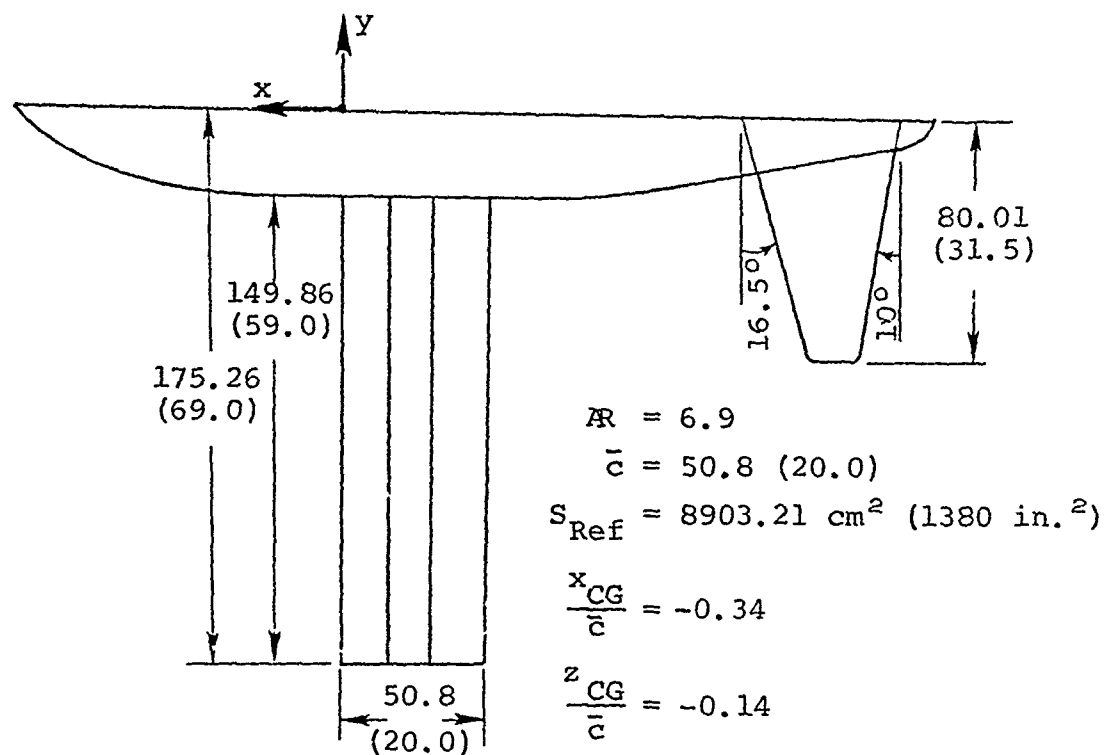
All dimensions in cm (in.)
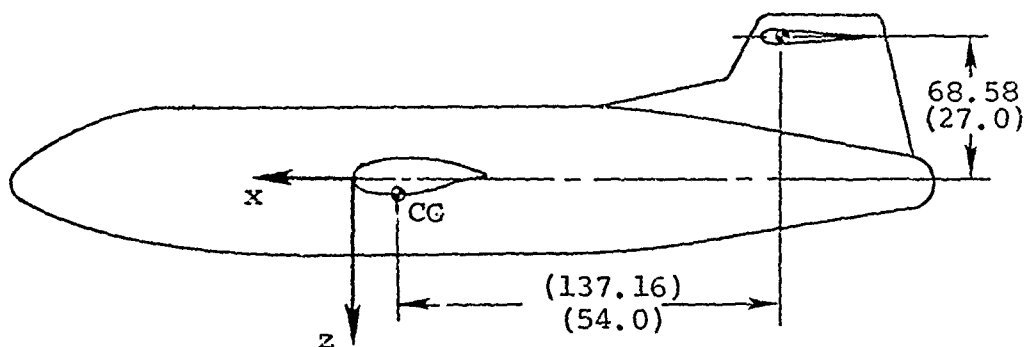
Figure 2.- Rockwell International NACAL 211
Transport Model, references 8 and 15.
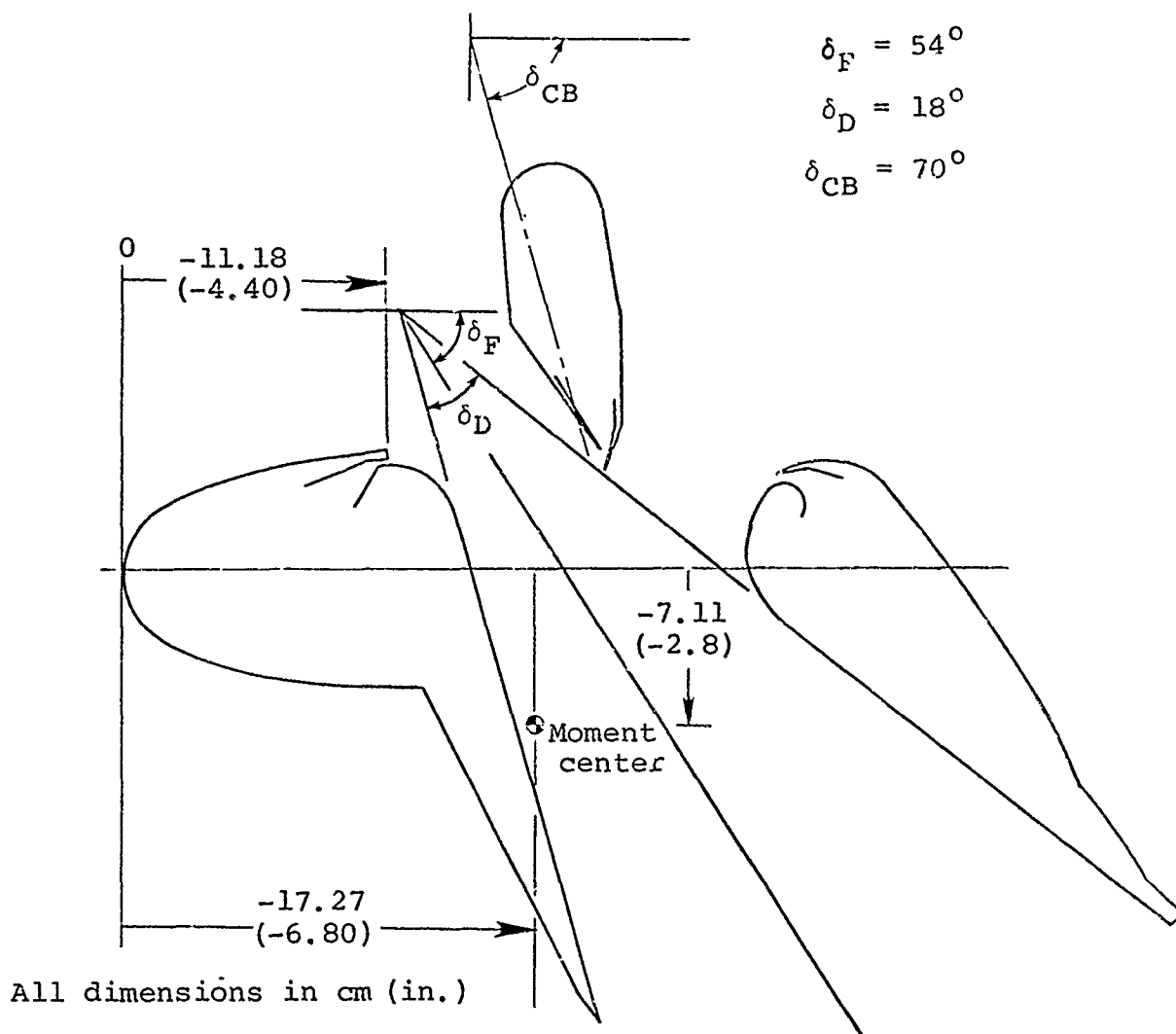
Figure 3.- Chordwise section of transport model augmentor wing of reference 8.

Figure 4.- Chordal planes of an augmentor wing with
one horseshoe vortex shown on each surface.
Idealized jet centerline and boundaries.
Reference coordinate system.
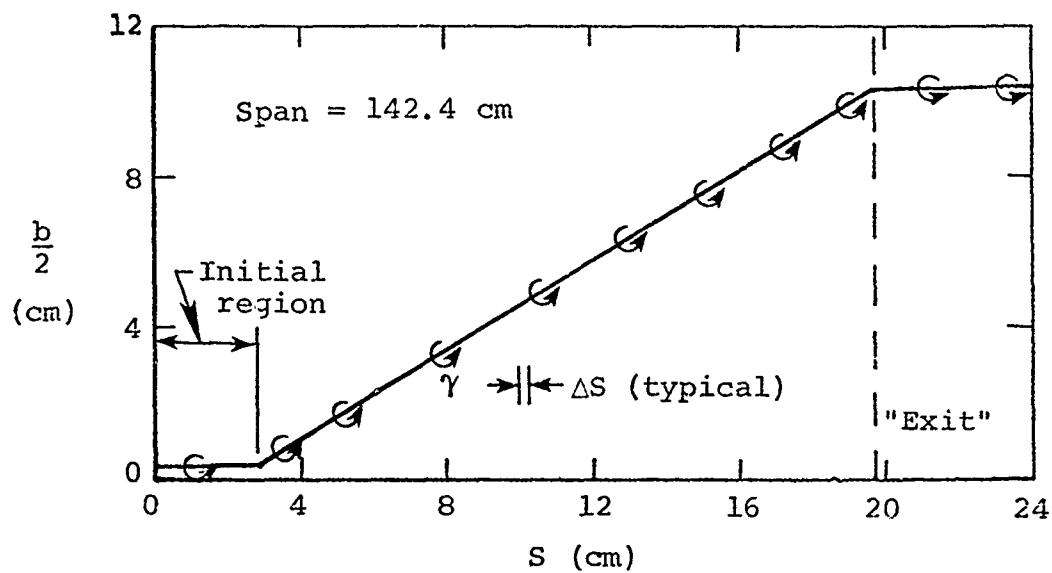
(a)   Jet boundary in diffuser region.
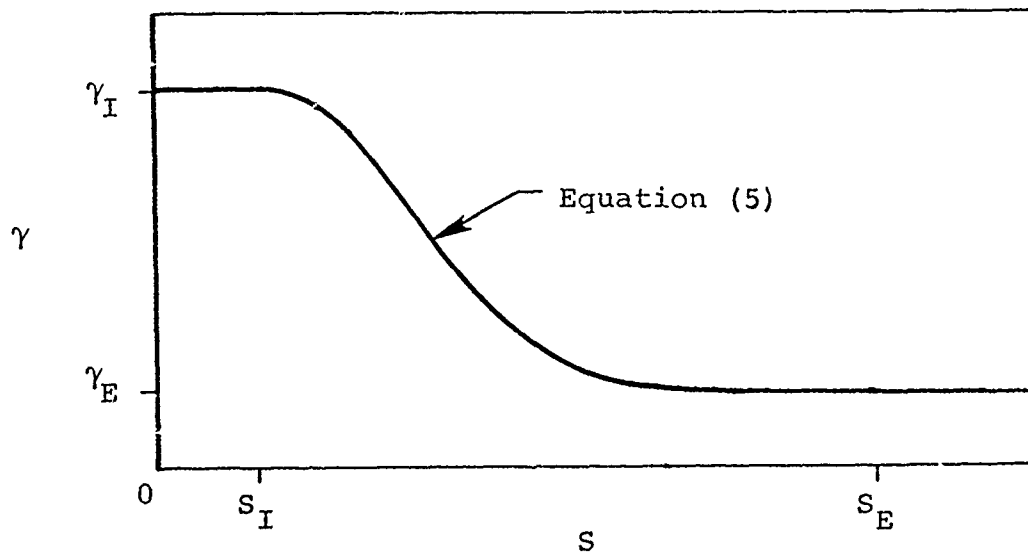
(b)   Vortex strength.

Figure 5.– Primary jet model.
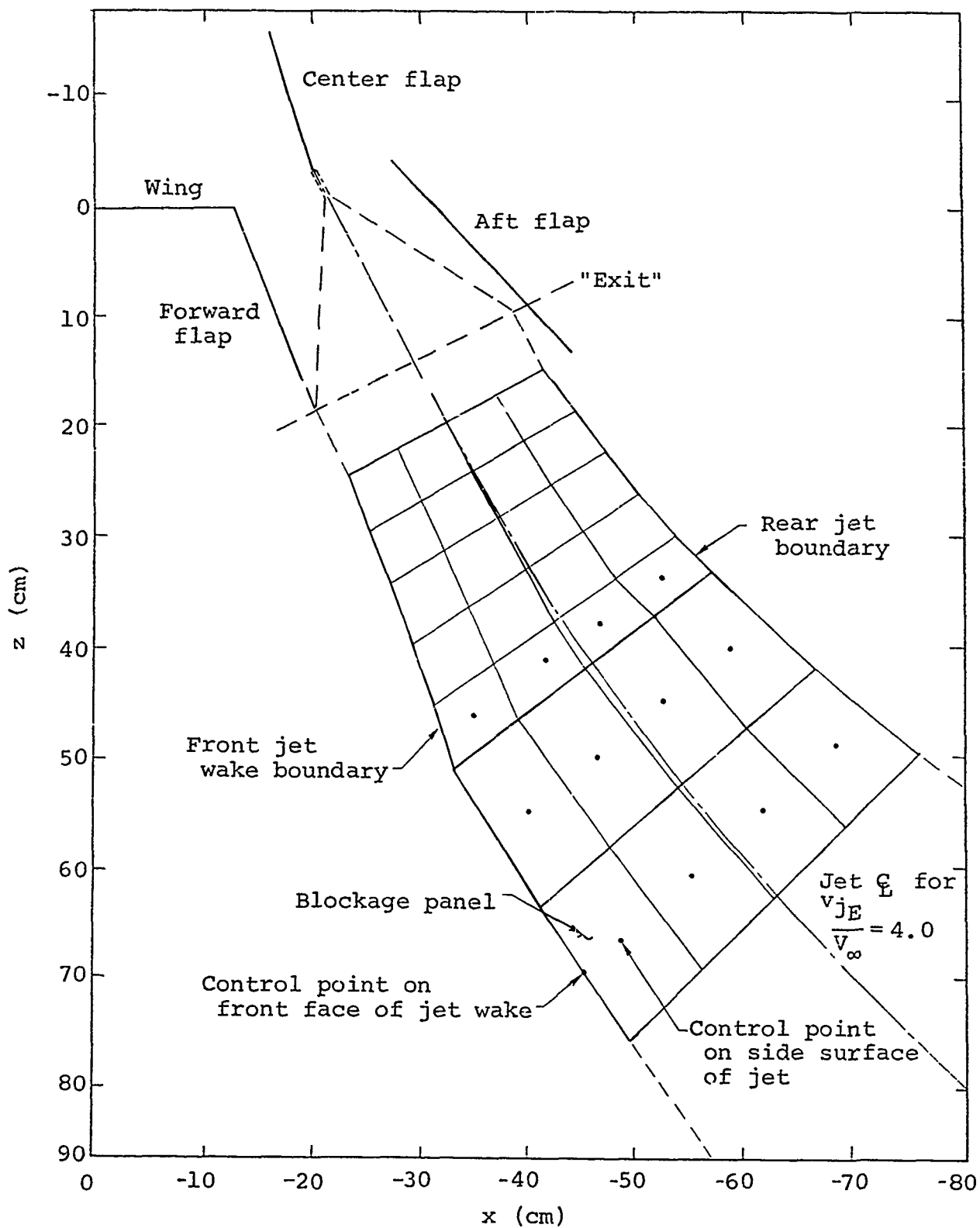
(a) $C_\mu = 7.31$, $\alpha = 0°$.

Figure 6.- Side view of idealized augmentor wing with jet model.
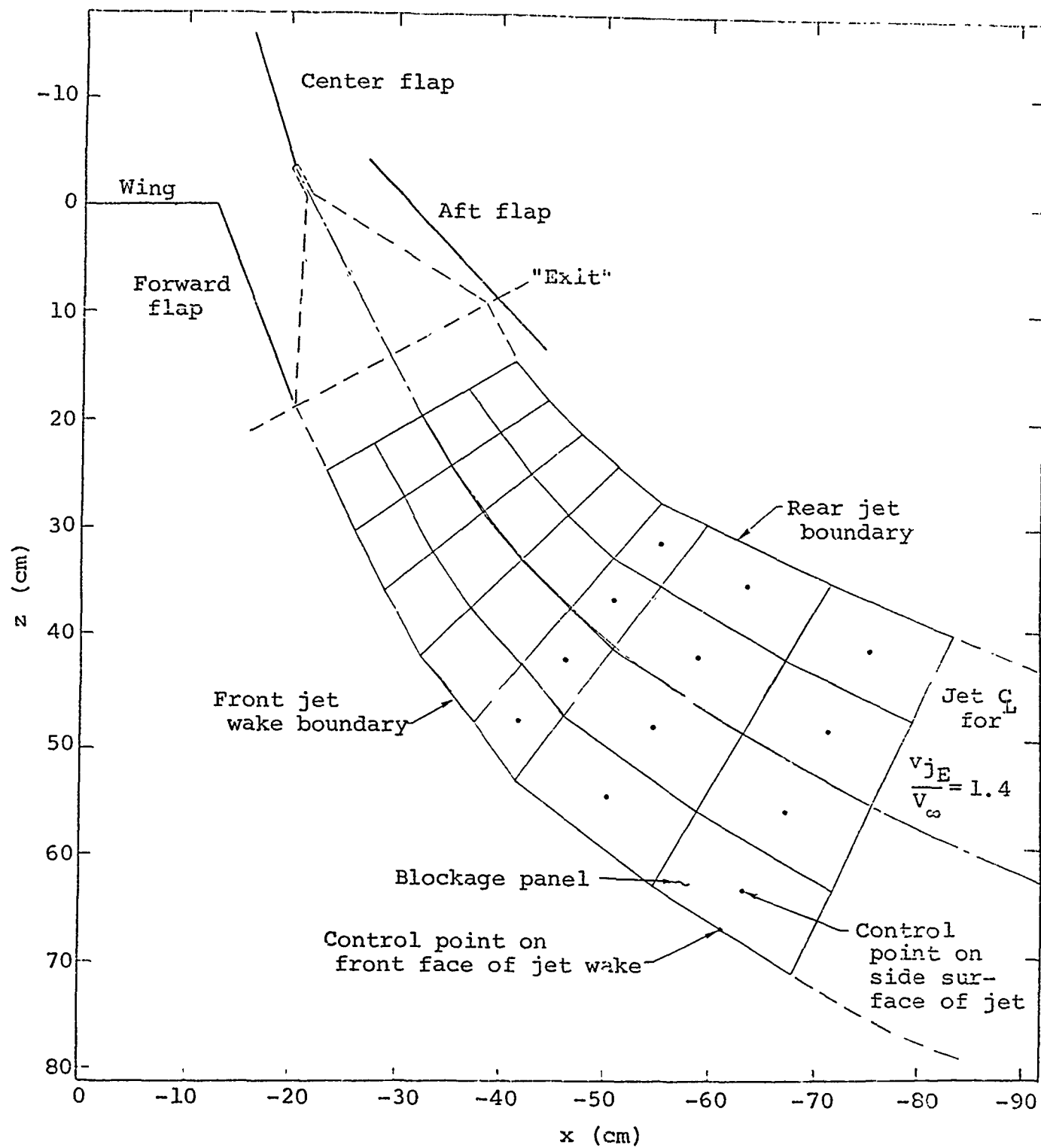
(b) $C_\mu = 1.5$, $\alpha = 0^\circ$.

Figure 6.- Concluded.
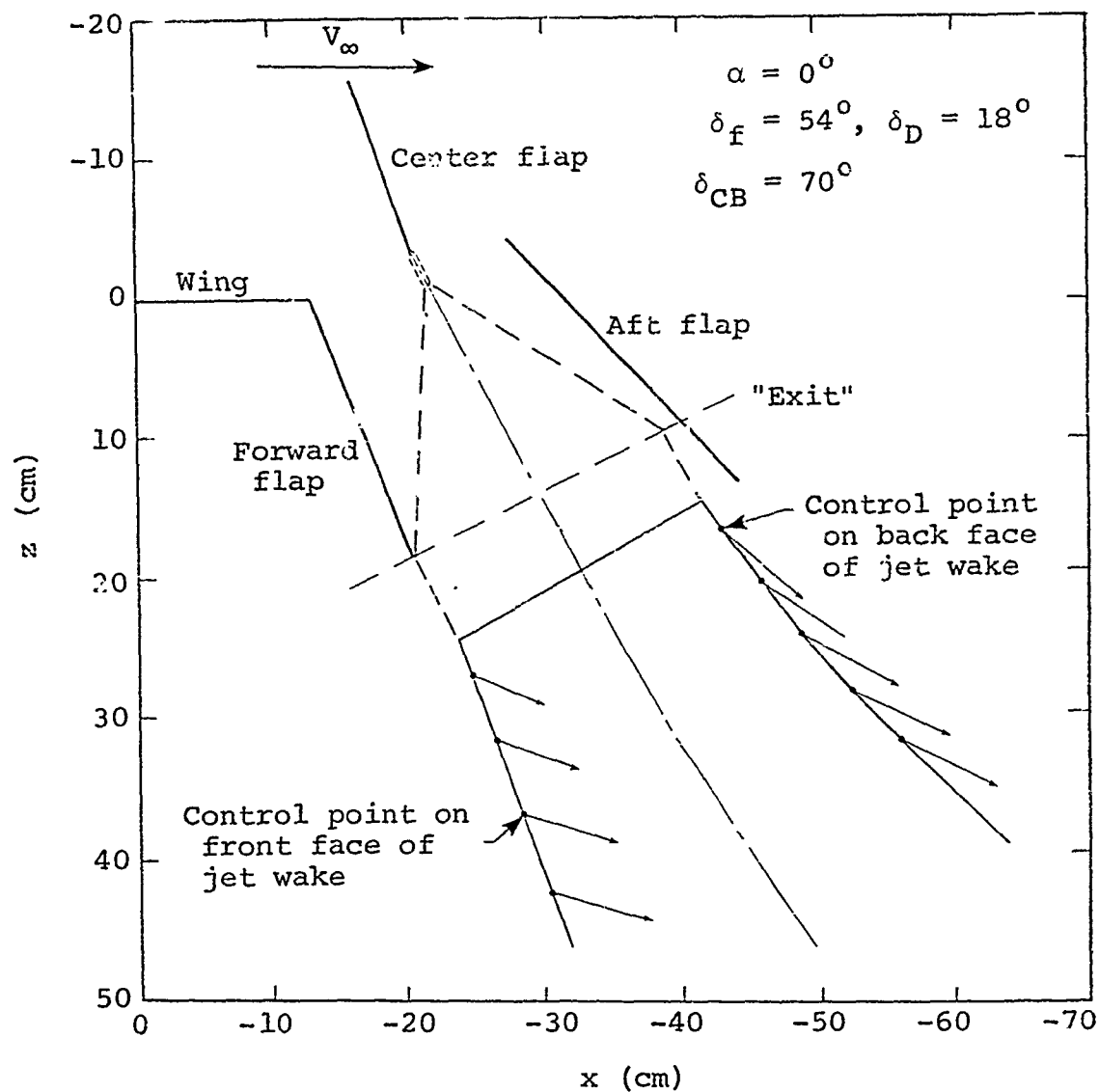
Figure 7.- Velocities induced by vortex lattice on
augmentor wing surfaces at control points of
blockage panels on upper part of jet wake at
y = -103.71 cm (-40.83 in.)
spanwise location.
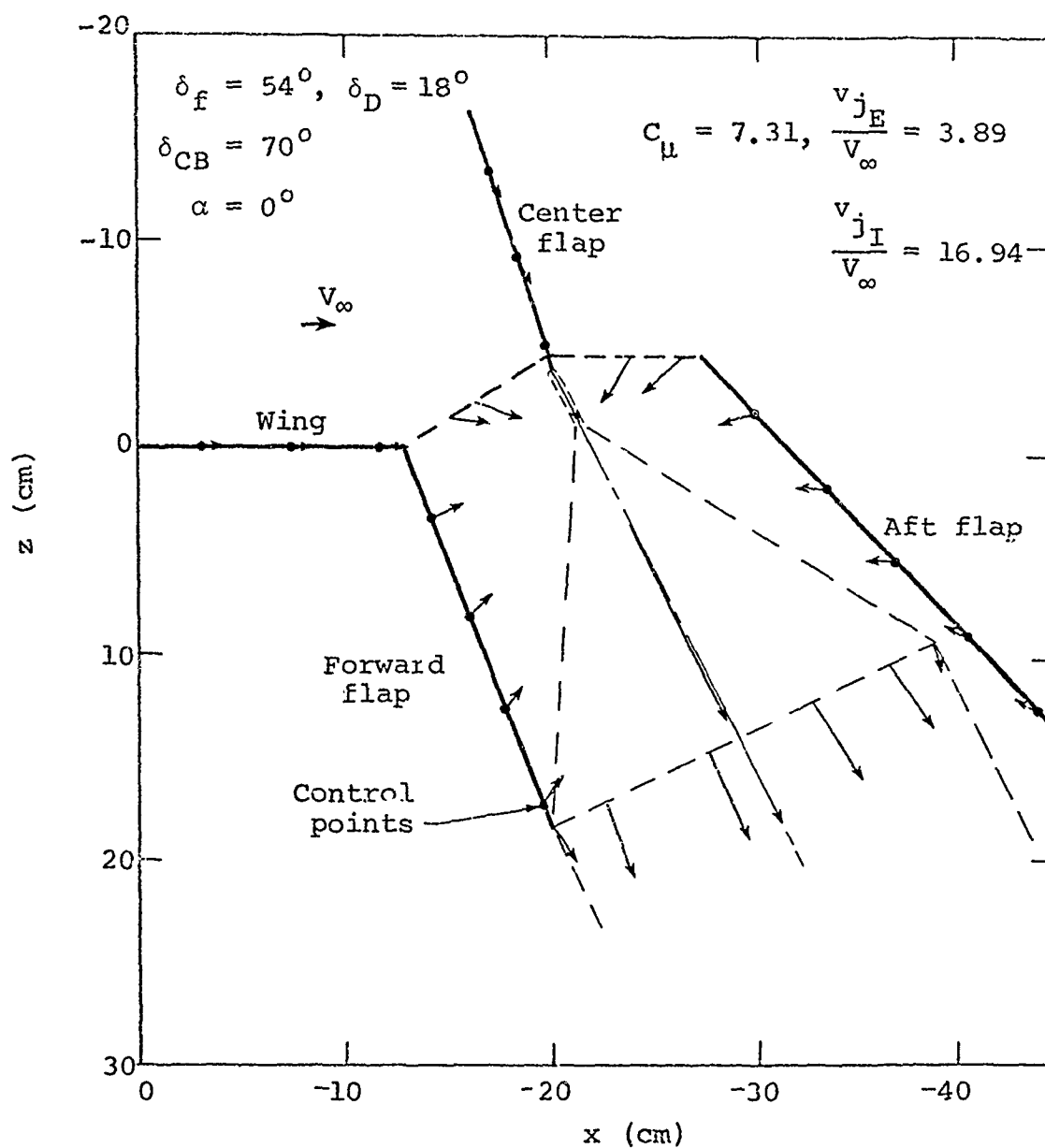
Figure 8.- Velocities induced by jet and jet wake at control points on surfaces of the transport augmentor wing at $y = -77.85$ cm (-30.65 in.) spanwise location.
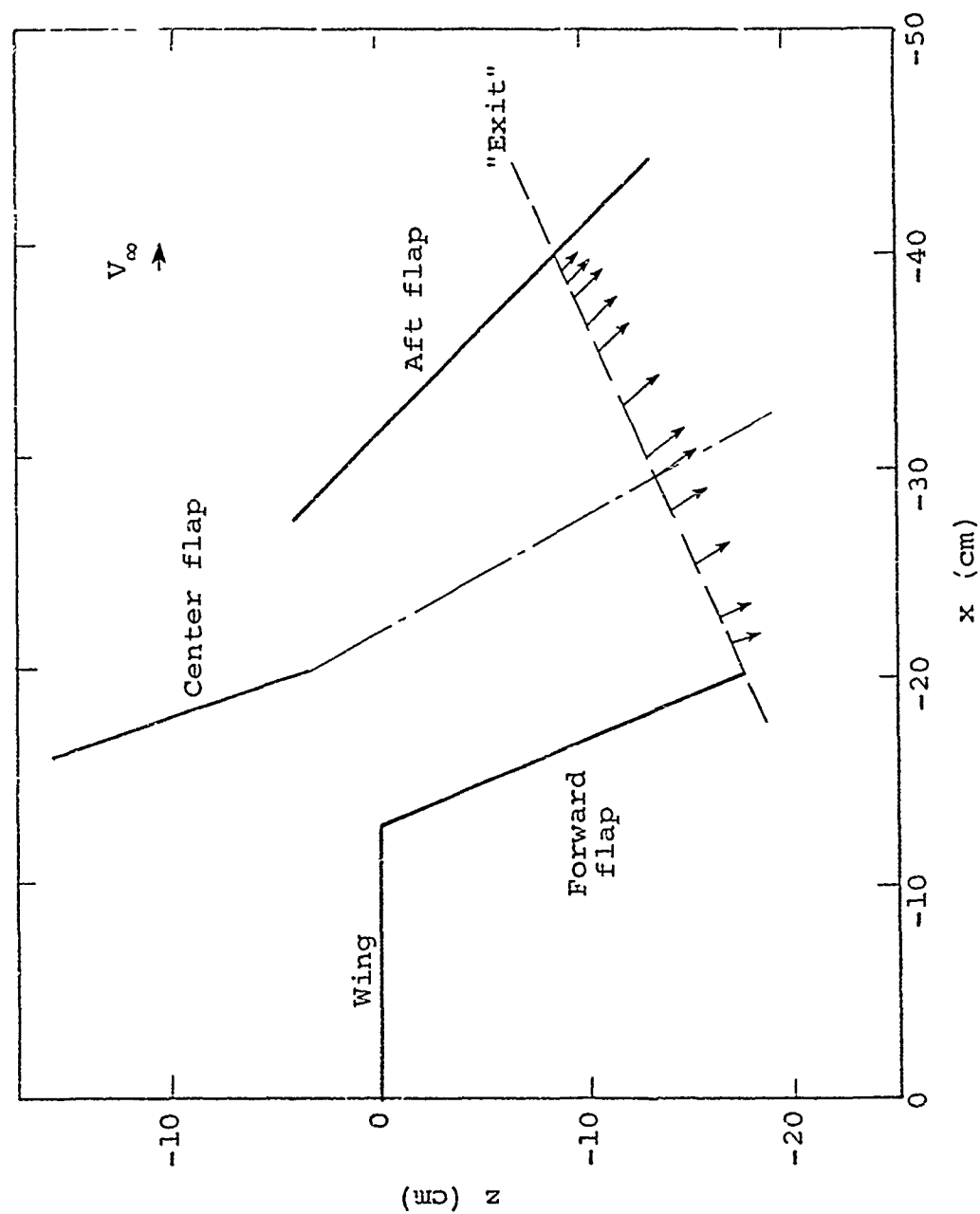
Figure 9.- Calculated flow velocities in the diffusor exit at spanwise location $y = -74.93$ cm (-29.50 in.), $\alpha = 0°$.
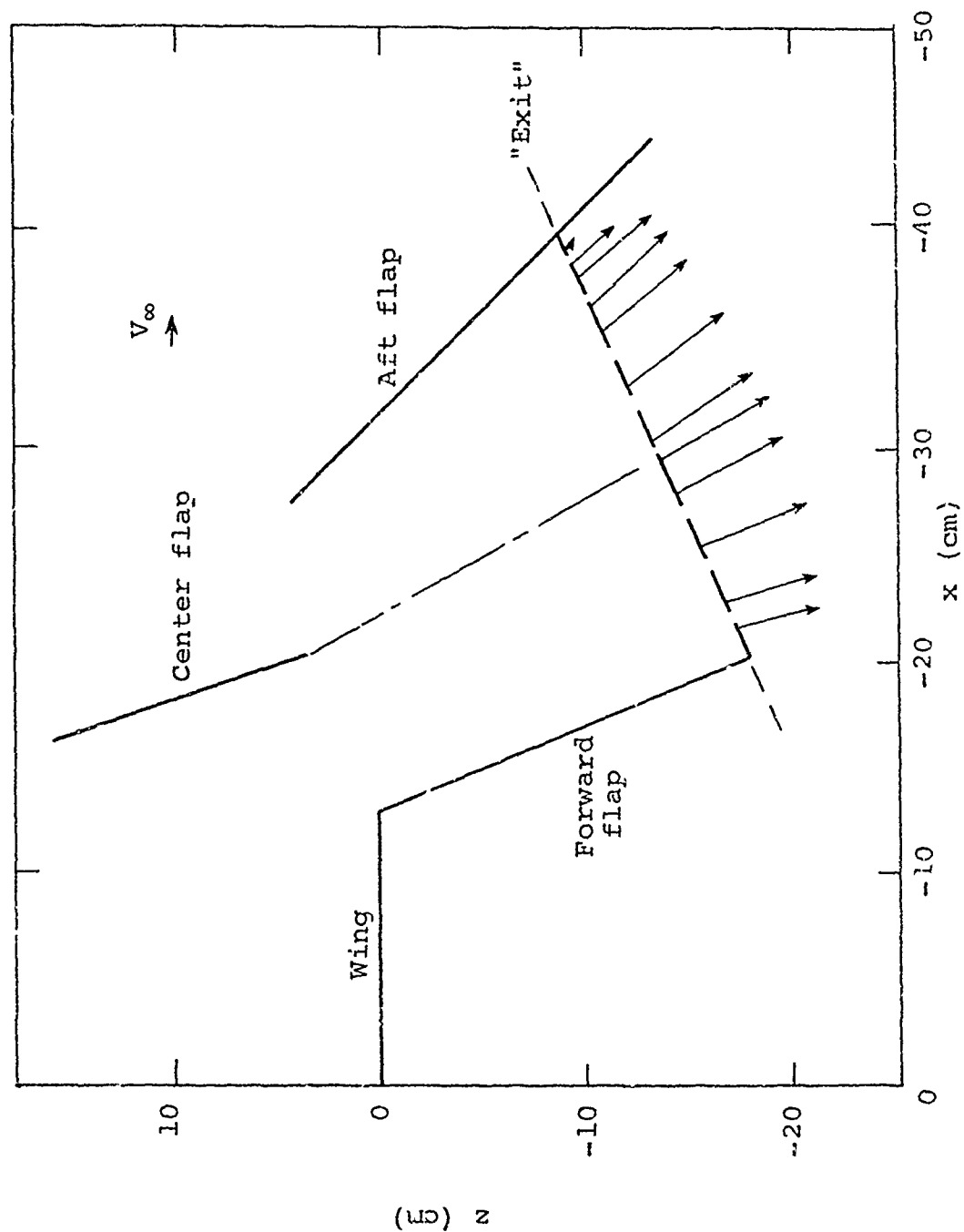
(b) $C_\mu = 7.31$.

Figure 9.- Concluded.
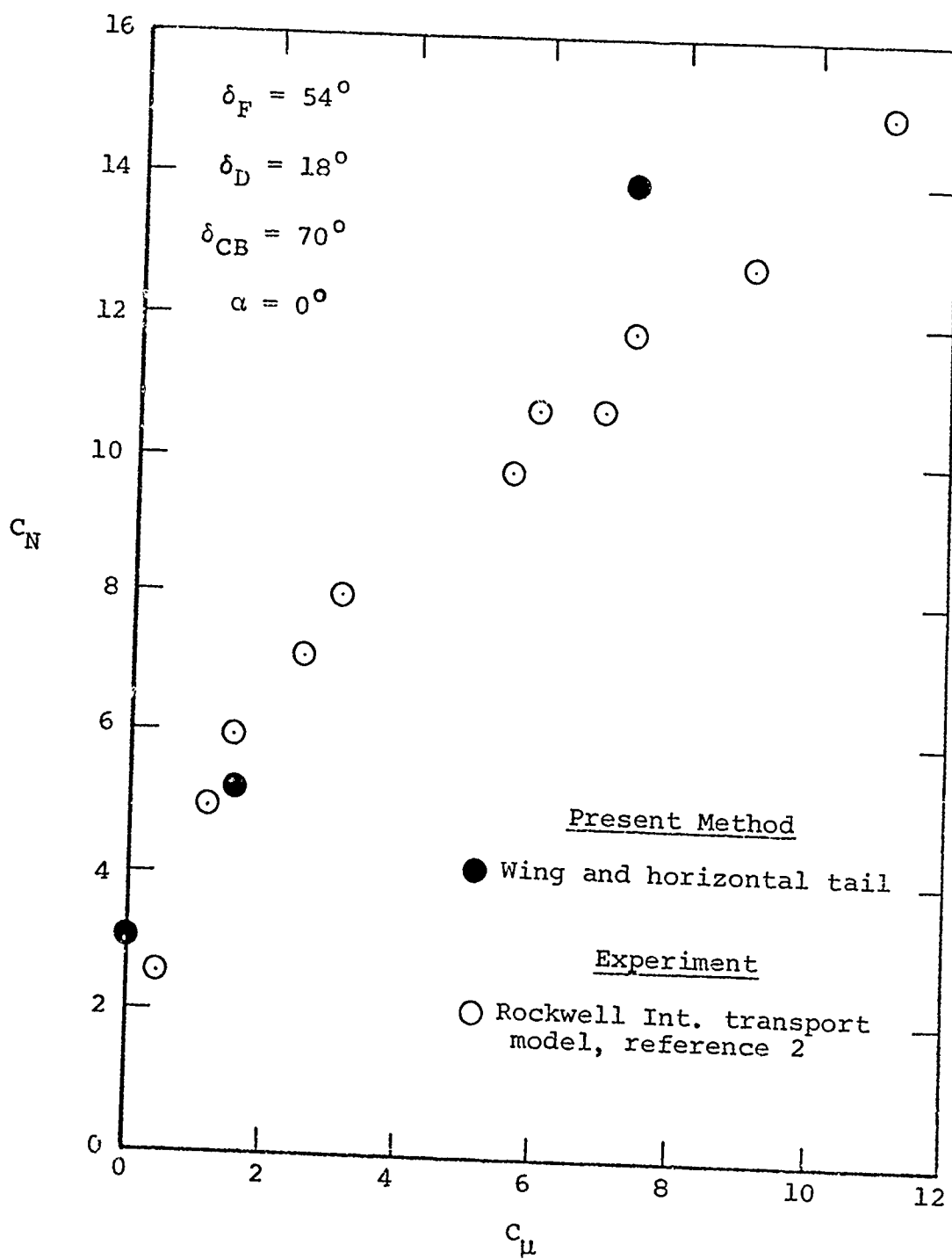
(a) Lift.

Figure 10.- Overall force and moment coefficients as a function of jet momentum coefficient for the NACAL 211 semispan transport model.
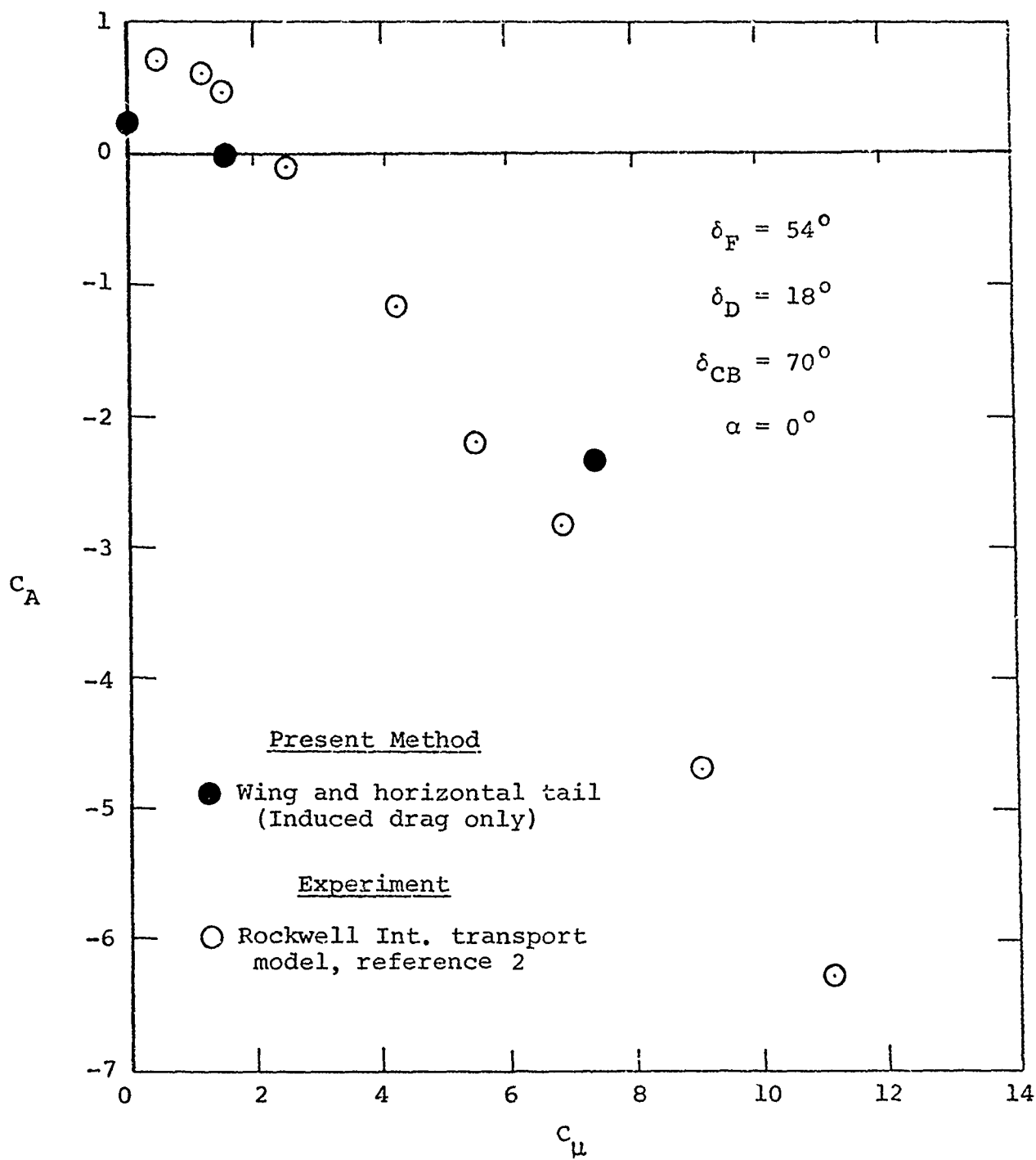
(b) Drag.

Figure 10.- Continued.
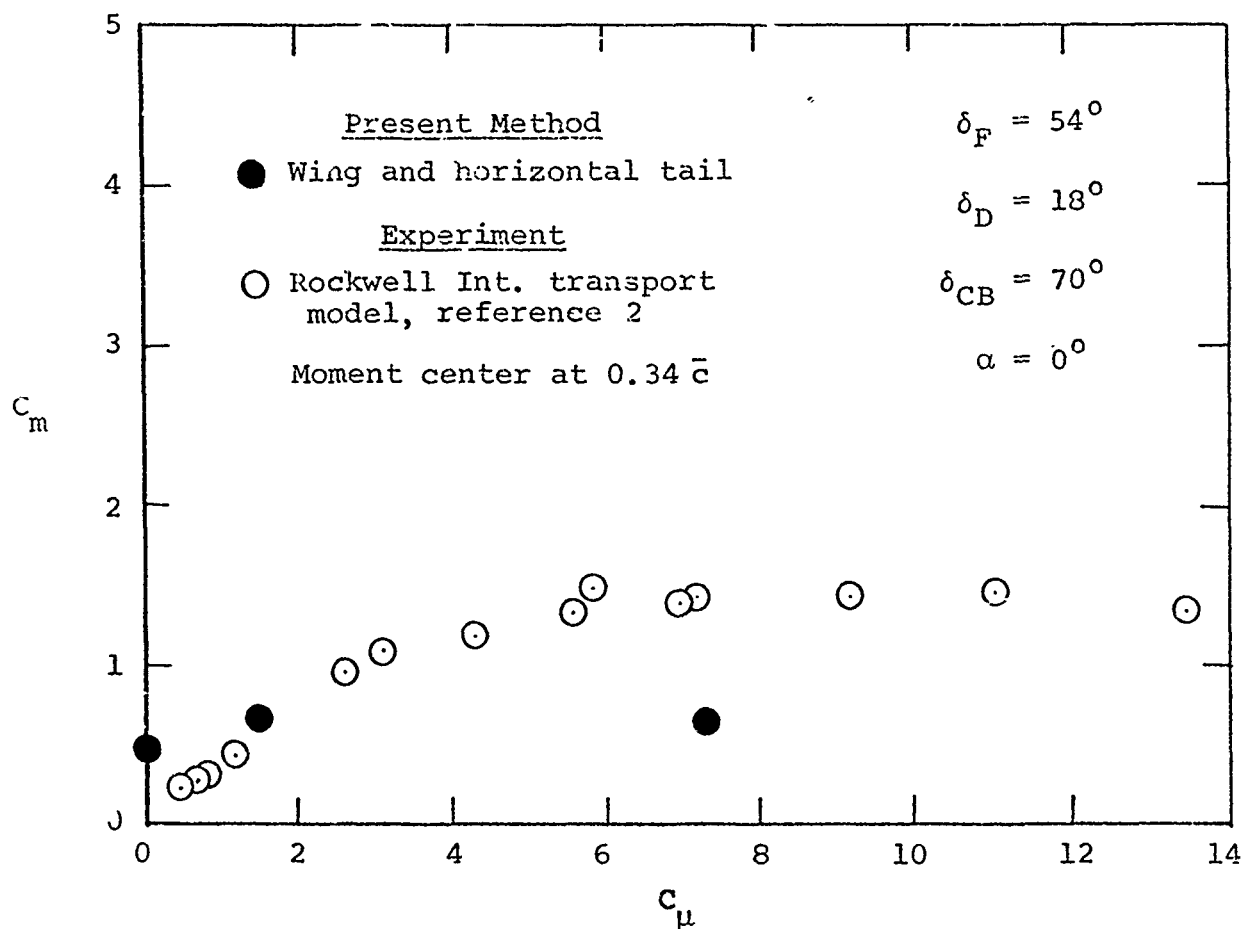
(c) Pitching moment.

Figure 10.- Concluded.

AERODYNAMICS OF AN ADVANCED JET FLAP
AND AN ULTRA-STOL APPLICATION

Ya-Tung Chin

Lockheed-California Company
Burbank, California 91520

ABSTRACT

A novel propulsive-lift system is a potential candidate for application to sea-based turbofan multi-purpose aircraft required to have ultra-STOL performance capability. This Lockheed-developed advanced internally blown jet flap (AIBF) system is a unique flap configuration which features: (1) a main flap with blowing BLC at the knee; (2) a lower-surface flap with trailing-edge blown jet flap; (3) a variable-geometry air duct formed between the main flap and the lower-surface flap when the flap system is deflected; and (4) a short-chord control flap with blowing BLC at the knee and located at the jet-flap exit. Some AIBF aerodynamic characteristics based on a large-scale three-dimensional model investigation conducted during 1972-73 in the NASA Ames 40-ft by 80-ft wind tunnel are discussed. The results of a parametric study of the deck takeoff and landing performance of a typical sea-based turbofan AIBF ultra-STOL aircraft are also discussed. The application study showed that the combined thrust-vectoring and control capabilities of the AIBF can provide outstanding deck performance and high overall performance.

NOMENCLATURE

AEO	all engines operating
C_D	drag coefficient
C_J	jet thrust coefficient, $C_J = J/qS$
C_ℓ	rolling-moment coefficient
C_L	lift coefficient
$C_{L_{MAX}}$	maximum lift coefficient
J	thrust of wing jets
OEI	one engine inoperative
q	dynamic pressure
S	wing area
T	installed engine thrust
V_{APP}	approach speed
V_{LO}	liftoff speed
V_{MC}	minimum control speed
V_S	stall speed
W	aircraft weight
WOD	wind over deck
α	angle-of-attack
δ_c	control-flap deflection relative to δ_f, positive down
δ_{cL}, δ_{cR}	left and right control-flap deflection
δ_f	main-flap deflection
δ_j	main-jet angle, $\delta_j \approx \delta_f + \delta_c$
Δ	incremental change
ϑ	engine residual thrust deflection

INTRODUCTION

In general, an aircraft which does not takeoff and land vertically is a short takeoff and landing (STOL) vehicle, if it requires ground rolls of 2000 feet or less. A STOL aircraft is arbitrarily called an ultra-STOL, if it has the performance potential of ground rolls of 400 feet and less. To achieve STOL performance it is necessary to integrate the wing and the engines to provide propulsive lift, or powered lift. Simply defined, propulsive lift is the use of all or a portion of the installed propulsive flow to augment the aerodynamic lift of an airplane. Jet propulsive-lift concepts which are based on the jet flap principle are classified as either internally blown or externally blown. The level of lift augmentation attainable with internally blown jet flap concepts is usually limited by the availability of adequate air ducting.

During the period 1968-1973, intensive research and development efforts were expended by the federal laboratories, primarily the NASA field centers, and by the aerospace companies, independently and under USAF or NASA contracts, to develop jet STOL technologies. As a result, an extensive data base exists for a number of competitive jet-flap concepts, e.g., IBF, AW, EBF, and USB. The particular interest of that time period was to provide design data for STOL tactical transport and quiet STOL commercial transport programs. Since the performance goal of these transport aircraft was a nominal field length of 2000 feet and landing critical, there was little emphasis on really minimizing takeoff run.

As far as is known, the Navy did not participate in earlier STOL activities because, at that time, it did not have defined near-term application of STOL technology. Recently, however, due to the Navy's uncertain V/STOL development plan, interest is emerging in sea-based STOL aircraft. One of these is a turbofan multi-purpose ultra-STOL aircraft capable of 400-ft takeoff distance, at sea level 90°F with 10-knot wind over deck, without catapult or ski jump. For a jet propulsive-lift concept to be applicable to this aircraft with moderate thrust-to-weight ratio, it must be capable of providing very high usable lift coefficient at liftoff, in order to meet the primary performance requirement. In addition, the engine-mounting arrangement associated with the concept must be compatible with folding wing designs.

Of the existing jet propulsive-lift concepts, the Advanced Internally Blown Jet Flap (AIBF) is a potential candidate for application to ultra-STOL because of its special features. This Lockheed-developed concept is relatively new, compared with the other well-known jet-flap concepts. During 1972-1973, a large-scale three-dimensional AIBF model was investigated in the NASA Ames 40-ft by 80-ft wind tunnel in a NASA/USAF/Lockheed joint research program (References 1 through 4). This paper will discuss the features and some aerodynamic characteristics of the AIBF pertaining to ultra-STOL application. It will also discuss the deck takeoff and landing performance potentialities of a typical sea-based turbofan AIBF ultra-STOL aircraft.

AIBF SPECIAL FEATURES

The basic AIBF concept is illustrated in Figure 1. This unique trailing-edge flap configuration consists of a main flap and a lower-surface flap elements hinged along longitudinally displaced lines which move apart during flap deflection to create an air duct. Availability of a large expandable spanwise flap duct makes it feasible to distribute large quantities of blowing air to produce very high lift augmentation without large fixed ducts. This feature makes the AIBF especially compatible with aircraft powered by high-bypass-ratio turbofan engines for cruise efficiency which use relatively low pressure-ratio bypass air for blowing.

Another feature is the simultaneous blowing from two primary spanwise slots: a small one at the knee of the main flap and a larger one near the trailing edge. The amount of discharge from the upper slot is relatively small and provides only enough boundary-layer energization to create flow attachment. The bulk of the blowing air is ejected through the lower slot in the manner of a pure jet flap. Aerodynamically, this mechanical flap/BLC/jet flap combination provides very efficient conversion of jet propulsive thrust to lift.

A third special feature of this concept is a short-chord, low-inertia, fast-acting control flap located near the jet-flap exit. Articulation of this powerful device can rapidly vary the jet-flap deflection angle and vector the jet-flap thrust axis. This permits the use of one moderate main-flap setting for both takeoff and landing. For sea-based ultra-STOL aircraft, vectoring jet-flap thrust can: (1) maximize deck acceleration and minimize liftoff speed for takeoff; (2) minimize landing approach speed and provide accurate approach flight path control for precision touchdown; (3) waveoff without changing the main-flap setting in case of landing abort; and (4) provide effective lateral control when the control-flap segments are asymmetrically or differentially deflected. To further increase the effect-iveness of the control flap at large downward deflections, it is provided with blowing BLC at the knee.

Figure 1 also shows a typical high-bypass-ratio turbofan/AIBF integration scheme for a multi-engine STOL aircraft. For this application, all the bypass air of each engine is ducted to the AIBF flap through a two-dimensional exhaust nozzle for powering the slots during low-speed operation of the air-craft. The main-flap deflection shown is for both the takeoff and landing modes. Additional deflection of the control flap is used, instead of increas-ing the main-flap angle, for landing to achieve the proper lift-to-drag ratio. Through ingenious mechanical design, the flap-duct size attained can be considerably larger than for the basic concept. More descriptions on this design integration scheme is given in Reference 3.

LARGE-SCALE MODEL AND TESTS

Figure 2 shows photographs of the NASA/USAF/Lockheed large-scale AIBF model mounted in the NASA Ames 40-ft by 80-ft wind tunnel. Details of this high-wing, T-tail model can be found in References 1 through 3.

The aspect-ratio 8 wing had a span of 42.9 feet, quarter-chord sweep of 27.5°, taper ratio of 0.3, root-thickness ratio of 0.125, tip-thickness ratio of 0.105, full-span leading-edge slats, and segmented trailing-edge flaps designed for the AIBF concept. The wing section and flap geometric details were identical to that shown in Figure 1a. Instrumentation included surface pressure taps and probes for measuring the flap-duct pressures and temperatures.

The model propulsion system consisted of two Pratt and Whitney JT15D-1 turbofan engines installed side-by-side in the fuselage with a bifurcated air inlet in the nose (the photographs show the model with a nose fairing installed). All the bypass air of the engines were supplied to the flaps via the wing spar box. The core jets of the engines were exhausted out the tail-pipes in the rear of the fuselage.

Two series of tests without and with the horizontal tail were conducted during 1972-1973. The basic configurations were main-flap deflections of 30 degrees and 60 degrees. Several symmetric and asymmetric control-flap deflections were tested in conjunction with each of the main-flap angles. Most of the tests were conducted with the outboard 30 percent span configured as a 30 degree blown aileron and the slats deflected 60 degrees. Six-component data were obtained for a Reynolds number range of 2 to 5.35 million, based on the wing mean aerodynamic chord of 5.88 feet. The jet thrust coefficient, C_J, range was from 0 to 2.31.

AERODYNAMIC CHARACTERISTICS

Figures 3 and 4 present the low-speed longitudinal aerodynamic characteristics of the AIBF model for a 30 degree flap with zero degree control-flap deflection and a 60 degree flap with 30 degree control-flap deflection, respectively. These data show the effect of jet thrust coefficient on the lift and drag coefficients. It can be seen that the AIBF produces very high lift augmentation, by virtue of the aerodynamically efficient flap system, for moderate amount of thrust. Pitching-moment data are not presented. It is typical of all jet flap propulsive-lift systems that the generation of very high lift is accompanied by large nose-down pitching moments, which can be satisfactorily trimmed with a properly sized horizontal tail.

Articulation of the control flap as a jet-flap thrust vectoring device provides effective modulation of lift and drag during low-speed operation of the aircraft. Figure 5 shows the lift and drag increments due to symmetric deflection of the control flap in combination with a main-flap deflection of 30 degrees. For constant jet thrust coefficients, the lift and drag increments increase nearly linearly with control-flap deflections. Actually, maximum lift increment is attained at a jet-flap deflection of approximately 90 degrees (the total of main-flap and control-flap deflections). Forward vectoring of the jet-flap thrust, say from 90 degrees to 110 degrees, provides steady drag increase but has little effect on lift. Thus, the control flap permits optimization of the jet-flap deflection for takeoff and landing without changing the main-flap setting, which is especially desirable in the ultra-STOL environment.

The possibility of a single main-flap setting for both takeoff and landing is further illustrated in Figure 6. Typically, a takeoff flap setting is 30 degrees to minimize flap drag during acceleration. This figure shows that a 30 degree flap with 30 degree control-flap deflection (total jet-flap deflection of 60 degrees) has identical drag polar for a given jet thrust coefficient as that for a 60 degree flap with zero degree control-flap deflection. A 30 degree flap with 50 degree control-flap deflection (total jet-flap deflection of 80 degrees) provides the same characteristics as that of a 60 degree flap with 20 degree control-flap deflection. Therefore, a simple two-position flap system can be designed to provide a main-flap deflection of 30 degrees for both the takeoff and landing configurations. Additional jet-flap deflections can be provided by vectoring the jet-flap thrust.

The maximum lift performance of several jet flap propulsive-lift systems are compared in Figure 7. For this comparison, data of similar sized models tested in the NASA Ames 40-ft by 80-ft wind tunnel are used. The AW, IBF, USB, and EBF data were obtained from References 5, 6, 7, and 8, respectively. Although the AIBF system tested was not optimized, for a 30 degree flap the AIBF effectiveness compares very favorably with the other systems. It should be pointed out that, because of the availability of very large flap duct, the AIBF can provide higher thrust coefficients required for ultra-STOL than the maximum value tested, to achieve even higher maximum lift.

While all jet flap propulsive-lift systems are capable of generating very high maximum lift coefficients, lifting capability at low speeds beyond the control capability of the aircraft is useless. In this regard, the fast-acting control flap of the AIBF can provide very effective lateral control for engine-out safety, if asymmetrically or differentially deflected, because it is jet augmented. Figure 8 shows the effect of asymmetric control-flap deflection on the longitudinal characteristics for a 30 degree flap configuration. It is seen that for a constant jet thrust coefficient, lift changes linearly with control-flap deflections. The roll effectiveness due to asymmetric control-flap deflections is shown in Figure 9. For a constant jet thrust coefficient, the rolling moment increments also increase linearly with control-flap deflections which are sufficient to produce good roll performance.

ULTRA-STOL PERFORMANCE

To assess the AIBF ultra-STOL performance potential, the experimental data
developed by the NASA/USAF/Lockheed large-scale tests for the AIBF concept
were used for analyzing the deck performance of a typical sea-based aircraft
configuration. Figure 10 depicts this conceptual AIBF ultra-STOL configura-
tion which had an aspect-ratio 7.73 wing of 68-ft span and a wing area of
598 sq.ft. The power plants were four TF34-GE-2 turbofans. It was assumed
that the TF34/AIBF installation was similar to the AIBF application scheme
shown in Figure 1b and that the flap setting for both takeoff and landing
configurations was 30 degrees.

For the performance computations, the engine performance data were based on
the sea level, 90°F conditions. It was assumed that all the fan bypass
airflow was supplied to the trailing-edge ducted flap for blowing and that
the bypass duct total pressure loss was ten percent. For these conditions,
the installed maximum static thrust was 6841 pounds per engine. The primary
parameters for the computations were the wing loadings, control-flap settings,
wind-over-deck values, and either four or three engines (all engines operating
or one engine inoperative).

The takeoff deck-roll computations for both the all-engines-operating and
engine-failure cases were based on an AEO acceleration to liftoff. A no-
catapult takeoff procedure was assumed: (1) begin the deck run with the
flap deflected but the fast-acting control flap retracted; (2) accelerate
the aircraft to the liftoff speed corresponding to a pre-selected thrust
vector/jet deflection angle; and (3) at the liftoff speed, the control
flap is instantaneously deflected to the pre-selected angle to obtain liftoff.
For the calculations, the liftoff speed was based on either the AEO stall
speed, or the OEI stall speed, as appropriate, but never below an input
minimum control speed of 50 knots. A rolling friction coefficient of 0.025
was assumed.

The landing deck-roll calculations were performed for a range of throttle
settings in conjunction with the main-flap/control-flap deflections. For
these calculations, it was assumed that the ship had no arresting-gear
capability; therefore, the brakes were assumed to be set before touch-down
in order to minimize deck roll. A braking friction coefficient of 0.3 was
also assumed.

Figures 11 through 16 present some of the results of this parametric perform-
ance study. The effect of control-flap deflection on liftoff speed is shown
in Figure 11. It is seen that large reduction in liftoff speeds accompanies
control-flap deflections. For example, this figure shows that for a wing
loading of 80 lb/ft^2 (thrust-to-weight ratio of 0.57), the AEO liftoff speed

can be reduced from 72 to 54 KTAS, when the control flap is deflected from zero degrees to 30 degrees at liftoff. Reduction in liftoff speed results in shortened takeoff deck roll, as shown in Figure 12 for takeoff with a wind-over-deck of ten knots. For the case of 80 lb/ft^2 wing loading, the AEO takeoff deck rolls are 420 and 200 feet, corresponding to control-flap deflections of zero degrees and 30 degrees, respectively. The takeoff deck roll is also influenced by the headwind. Figure 13 shows that for a 30 degree flap with 30 degree control-flap deflection, at a wing loading of 80 lb/ft^2 the AEO deck roll varies from 305 feet for zero WOD to 60 feet at a WOD of 30 knots. The one-engine-inoperative takeoff distances are greater than the AEO values.

Control-flap deflection is also effective in reducing the landing approach speed. Figure 14 shows that for a wing loading of 80 lb/ft^2 and a power setting of 50 percent, the AEO approach speed reduces from 68 to 65 KTAS by increasing the control-flap deflection from 30 degrees to 50 degrees. For this wing loading and a control-flap deflection of 50 degrees, Figure 15 shows that the deck roll decreases with increasing power setting and wind-over-deck. For a WOD of ten knots, this figure shows that the unarrested AEO landing distance is 440 feet at a power setting of 50 percent, and it is 380 feet when the power setting is increased to 60 percent. The effect of WOD on landing deck roll for a range of wing loading is shown in Figure 16 for a power setting of 50 percent and a control-flap deflection of 50 degrees. This figure shows that at a wing loading of 70 lb/ft^2, the AEO landing distance is only 380 feet with a WOD of 10 knots.

While the AIBF deck performance is impressive, it is interesting to compare it with the performance of other jet flap propulsive-lift concepts. Figure 17 provides a takeoff performance comparison for AIBF, USB, and EBF concepts as applied to the four-engine conceptual airplane, although the engine mounting arrangements associated with the USB and EBF concepts are not very compatible with folding wing design requirements. It is quite obvious from this comparison that AIBF provides superior performance, largely because of the availability of the fast-acting control-flap feature, which is unique to the AIBF concept.

CONCLUDING REMARKS

Based on the design considerations and the aerodynamic characteristics, it can be concluded that the AIBF concept, with its special design features, is very promising for providing superior overall performance to STOL and ultra-STOL aircraft. The results of a takeoff and landing performance study for a conceptual sea-based turbofan ultra-STOL aircraft indicate that this concept can provide outstanding deck performance because of the availability of combined thrust vectoring and control capabilities. Since this concept is especially compatible with high-bypass-ratio turbofan engines, it should provide good engine and airframe match for meeting cruise efficiency requirements. It is also obvious that AIBF allows many engine mounting arrangements and is not restricted to a specific number of engines.

REFERENCES

1. Aiken, T. N., Aoyagi, K., and Falarski, M. D., "Aerodynamic Characteristics of a Large-Scale Model with a Swept Wing and a Jet Flap Having an Expandable Duct," NASA TM X-62,281, September 1973.

2. Falarski, M. D., Aiken, T. N., and Aoyagi, K., "Acoustic Characteristics of a Large-Scale Wind Tunnel Model of a Jet Flap Aircraft," NASA TM X-3263, July 1975.

3. Chin, Y. T., Aiken, T. N., and Oates, G. S., Jr., "Evaluation of a New Jet Flap Propulsive-Lift System," Journal of Aircraft, Vol. 12, No. 7, July 1975, pp. 605-610.

4. Oates, G. S., Jr., "A Brief Review of Three Powered Lift STOL Concepts," AFFDL-TM-74-215-PTC, November 1974.

5. Falarski, M. D. and Koenig, D. G., "Aerodynamic Characteristics of a Large-Scale Model with a Swept Wing and Augmented Jet Flap," NASA TM X-62,029, July 1971.

6. Falarski, M. D. and Koenig, D. G., "Longitudinal and Lateral Stability and Control Characteristics of a Large-Scale Model with a Swept Wing and Augmented Jet Flap," NASA TM X-62,145, April 1972.

7. Aoyagi, K., Falarski, M. D., and Koenig, D. G., "Wind Tunnel Investigation of a Large-Scale Upper Surface Blown-Flap Transport Model Having Two Engines," NASA TM X-62,296, August 1973.

8. Aoyagi, K., Falarski, M. D., and Koenig, D. G., "Wind Tunnel Investigation of a Large-Scale 25° Swept-Wing Jet Transport Model with an External Blowing Triple-Slotted Flap," NASA TM X-62,197, November 1973.

BLC SLOT

VARIABLE CAVITY
FLAP DUCT

BLC SLOT

JET-FLAP
EXIT
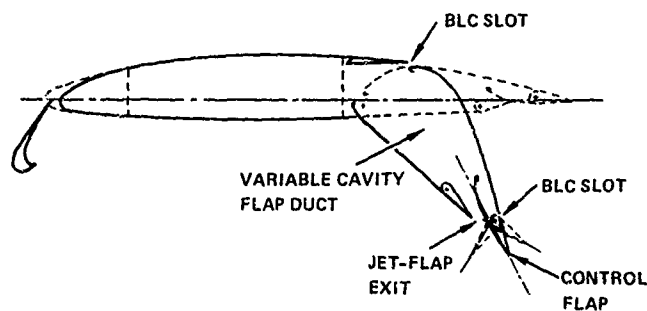
CONTROL
FLAP

- MECHANICAL FLAP + BLC + JET FLAP
  - HIGH OVERALL LIFT AUGMENTATION
- FAST-ACTING CONTROL FLAP
  - POWERFUL MEANS FOR FLIGHT-PATH AND LATERAL CONTROLS
  - ONE MAIN-FLAP DEFLECTION FOR TAKEOFF/LANDING A POSSIBILITY
- LARGE FLAP DUCT
  - NO FIXED INTERNAL FLOW DUCT
  - LOW DUCT LOSSES AND NOISE
- PROPULSION/LIFT SYSTEM INTEGRATION FLEXIBILITY
- APPLICABLE TO STOL AND ULTRA-STOL

a. BASIC CONCEPT

TAKEOFF &
LANDING MODE

CRUISE MODE

BLOW-IN
DOORS

δ_t

δ_c

θ
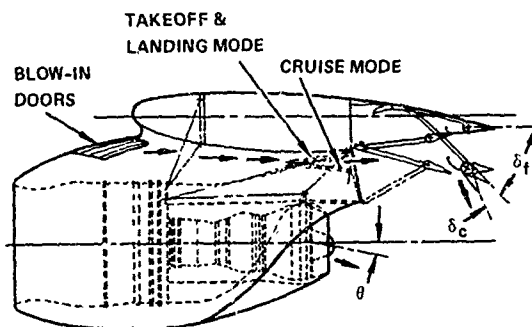
b. TYPICAL APPLICATION

Figure 1. Advanced Internally Blown Jet Flap (AIBF)
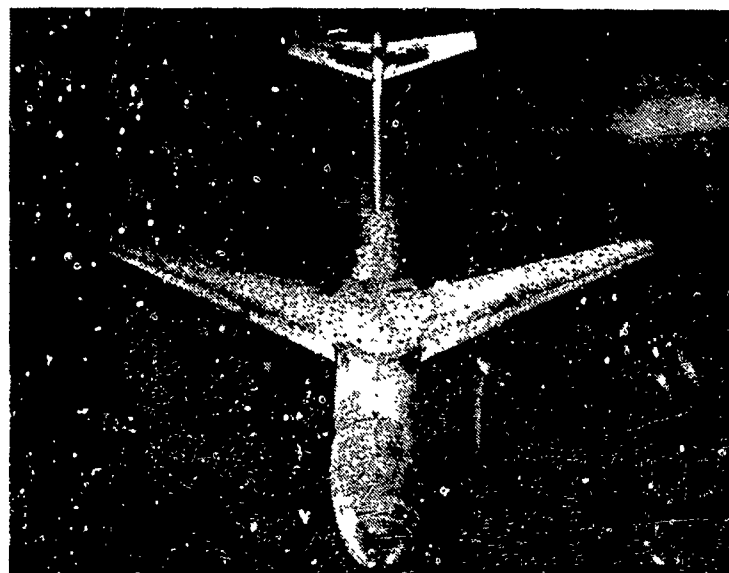
*Figure 2. NASA/USAF/Lockheed AIBF Model, NASA
Ames 40 x 80-ft Wind Tunnel*
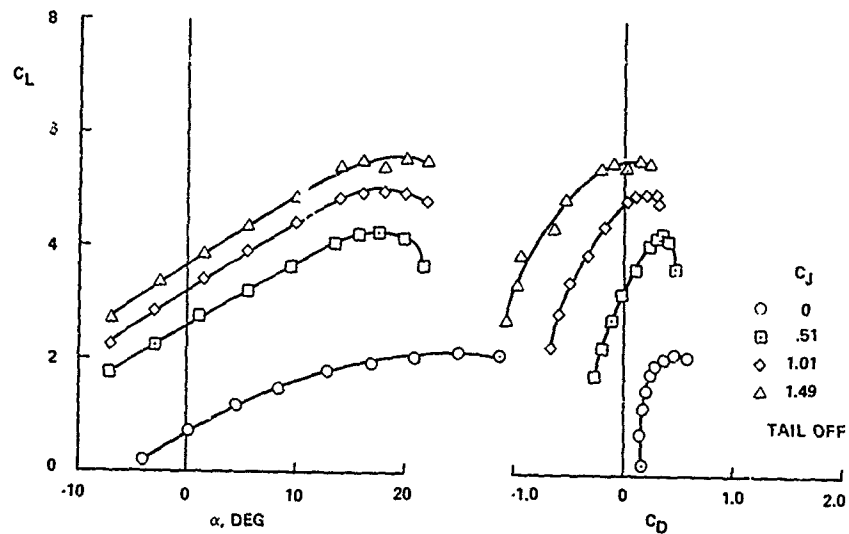
Figure 3. Longitudinal Characteristics, $\delta_f = 30^o$, $\delta_c = 0^o$
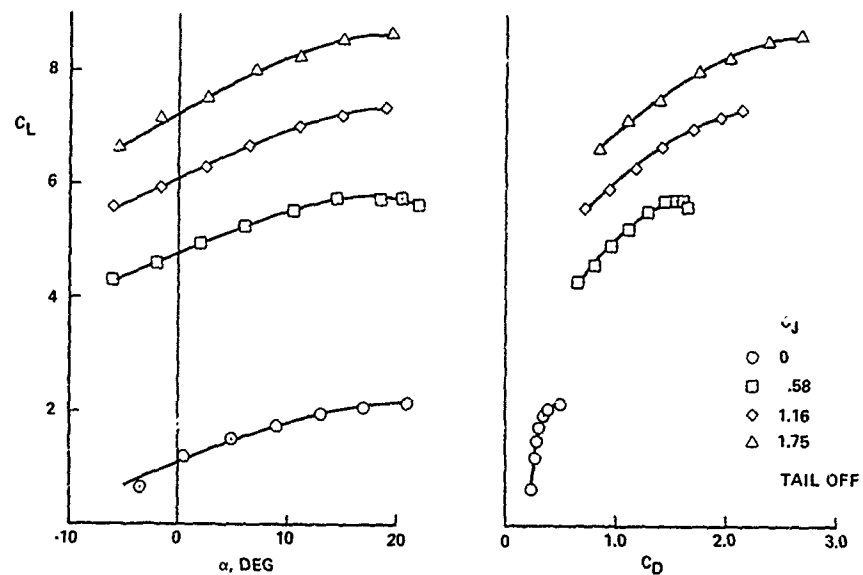
Figure 4. Longitudinal Characteristics, $\delta_f = 60^o$, $\delta_c = 30^o$
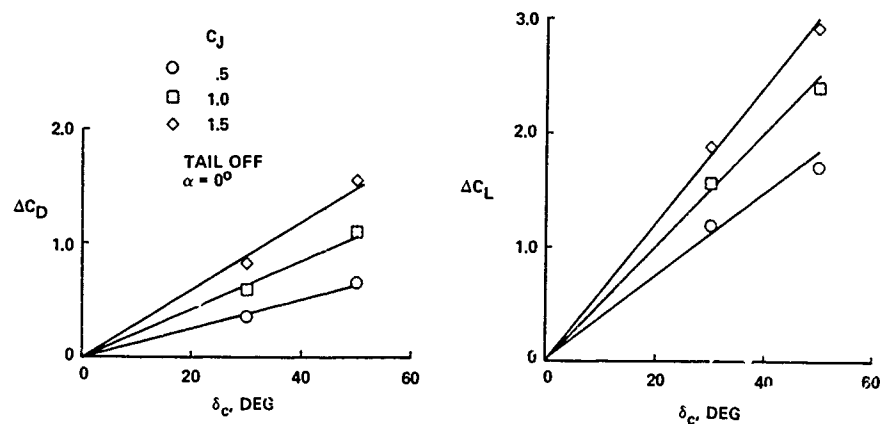
Figure 5. Effect of Symmetric Control-Flap Deflection on Lift and Drag, $\delta_f = 30^0$
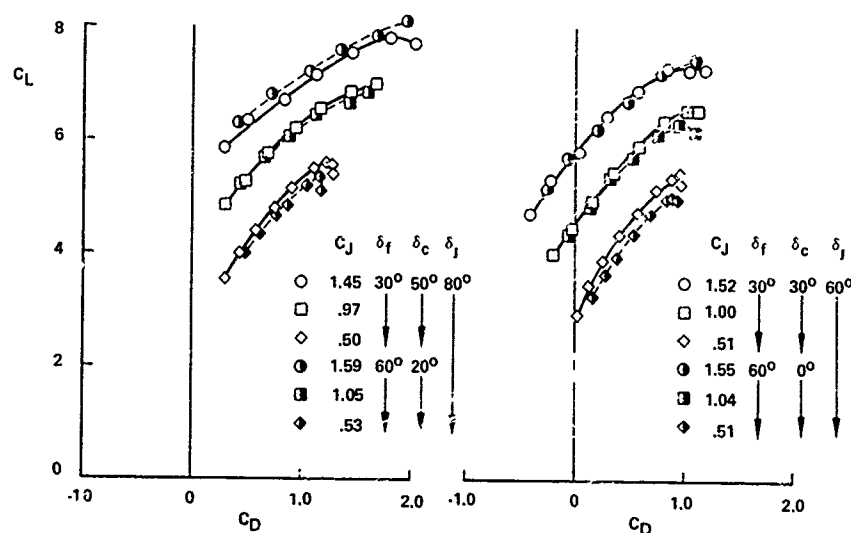
Figure 6. Effect of Jet Angle on Drag Polar
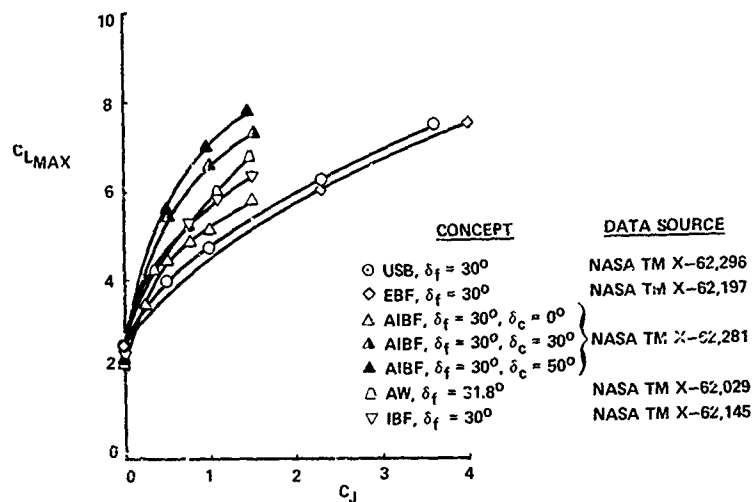
Figure 7. *Jet-Flap Maximum Lift Comparison, $\delta_f = 30^o$, NASA Ames Large-Scale Tests*
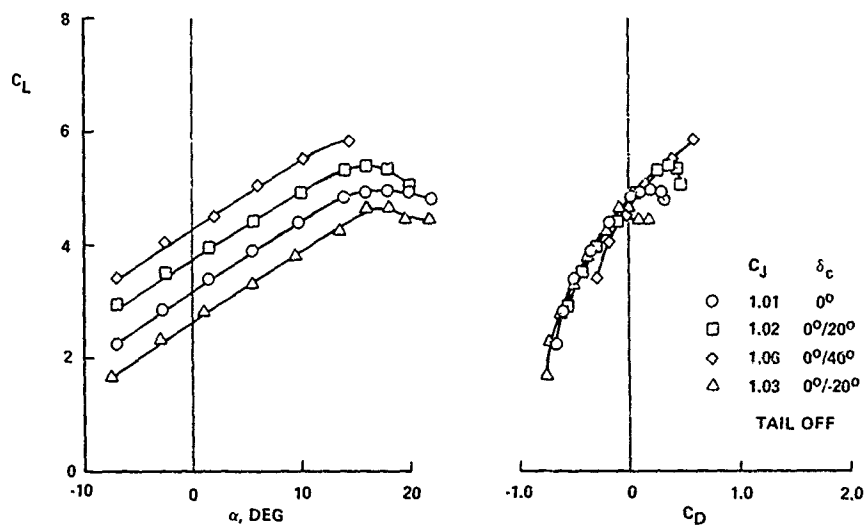
Figure 8. *Effect of Asymmetric Control-Flap Deflection on Lift and Drag, $\delta_f = 30^o$*
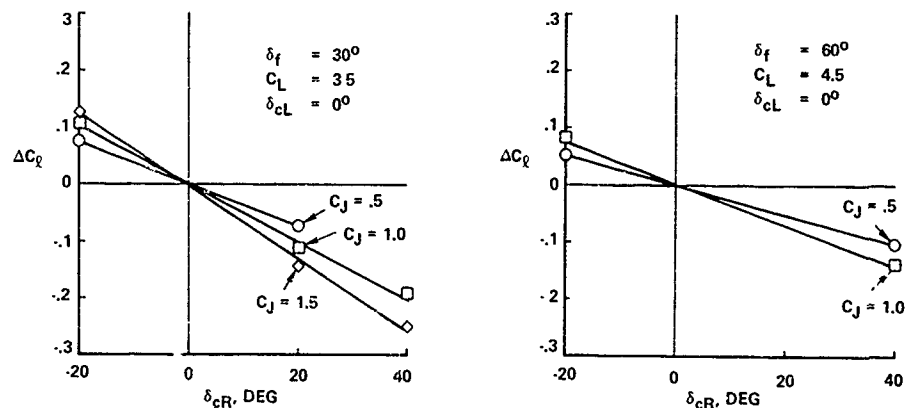
*Figure 9. Effect of Asymmetric Control-Flap Deflection
on Rolling Moment*

WING

AREA, FT^2 = 598
SPAN, FT = 68
ASPECT RATIO = 7.73
TAPER RATIO = 0.25
SWEEP (C/4), DEG = 15
MAC, IN = 118.24
ROOT CHORD, IN = 169
TIP CHORD, IN = 42

POWER PLANT

4 TF34-GE-2 TURBOFANS
BYPASS RATIO (SLS) = 6 2
FAN PRESSURE RATIO (SLS) = 1.47
AIBF DUCT LOSS   10%
INST MAX THRUST (S.L.90°F) = 6841 LB/ENG
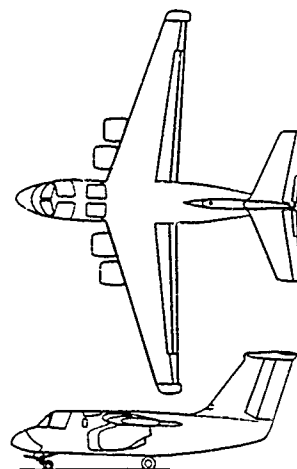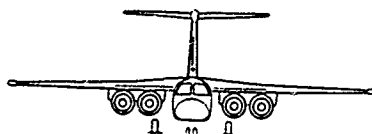
Figure 10. Configuration for AIBF Ultra-STOL Performance Study
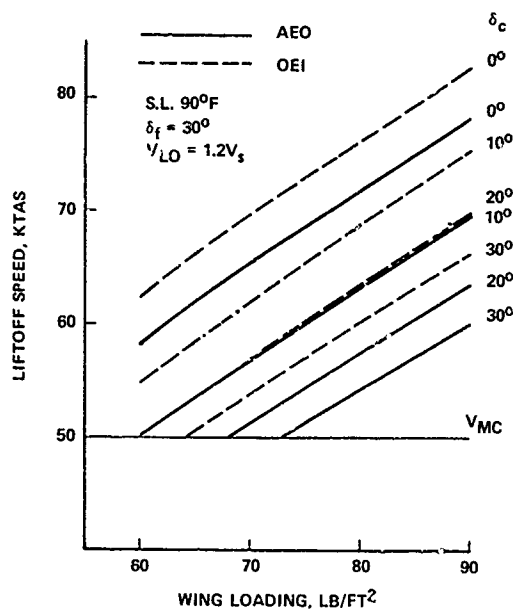
Figure 11. Effect of Control-Flap Deflection on Liftoff Speed
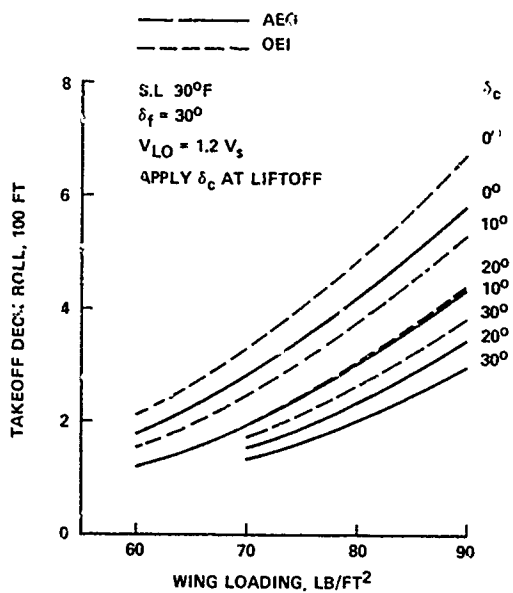
Figure 12. Effect of Control-Flap Deflection on Takeoff Deck Roll, WOD = 10 kt
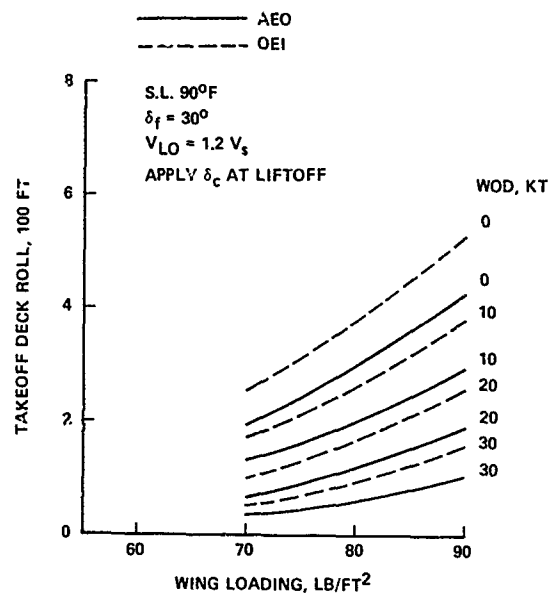
Figure 13. Effect of WOD on Takeoff Deck Roll, $\delta_c = 30^0$
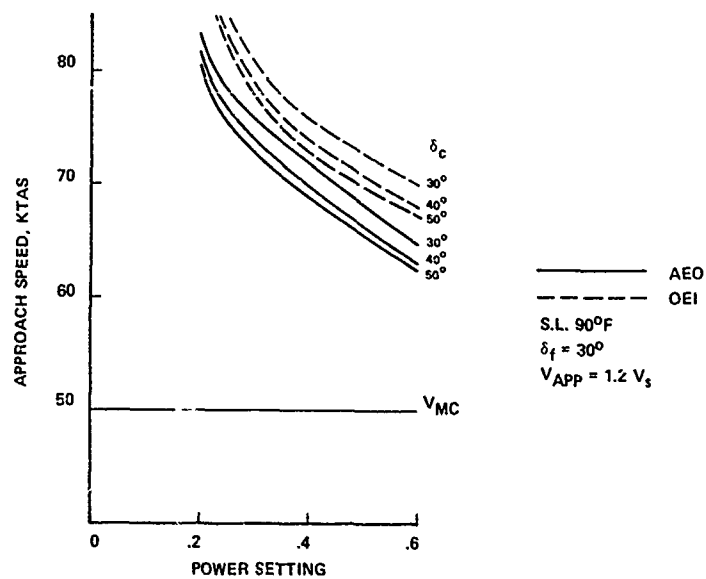
Figure 14. Effect of Control-Flap Deflection on Approach Speed, W/S = 80 lb/ft^2
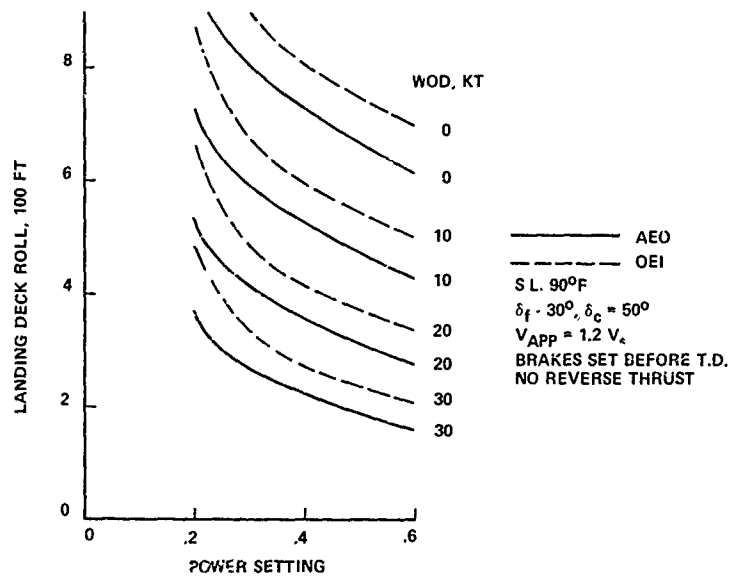
Figure 15. Effect of WOD on Landing Deck Roll, W/S = 80 lb/ft²
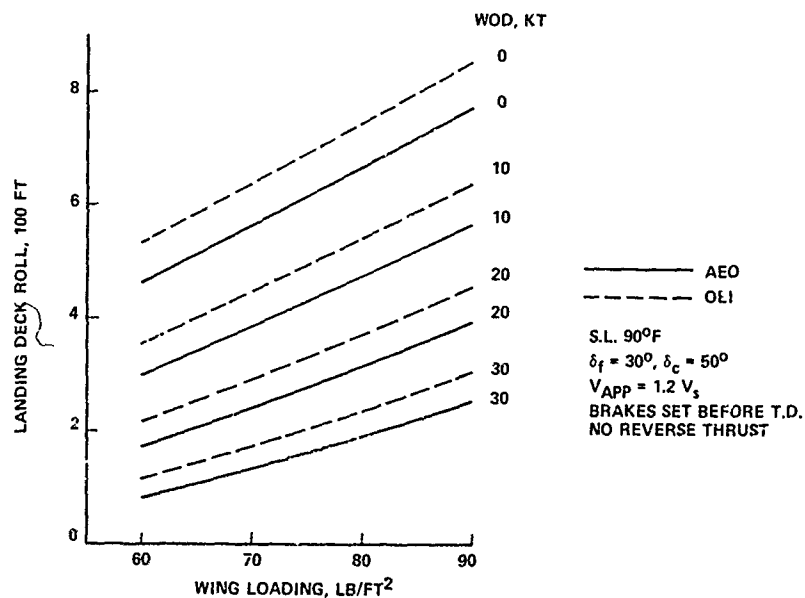
Figure 16. Effect of WOD on Landing Deck Roll, Power Setting = 0.5

S.L. 90°F, T/W = 0.58, W/S = 80 LB/FT^2
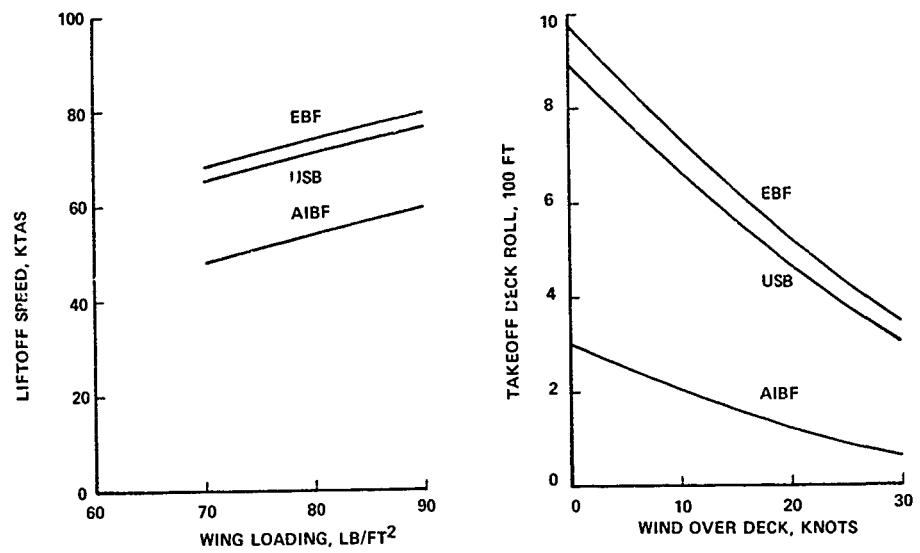
Figure 17. Comparison of Estimated Takeoff Performance

HIGH SPEED AERODYNAMIC TECHNOLOGY

FOR

VSTOL FIGHTER ATTACK AIRCRAFT

D. P. Bencze, W. P. Nelms, R. O. Bailey, D. B. Smeltzer,
M. Harper, L. Erickson and R. L. Carmichael

NASA-Ames Research Center
Moffett Field, California

ABSTRACT

The Aircraft Aerodynamics Branch at the NASA-Ames Research Center has initiated
a range of research efforts to develop aerodynamic technology for VSTOL fighter
attack aircraft. The primary emphasis is directed towards the transonic and
supersonic Mach number regimes and the propulsion/airframe interactions asso-
ciated with aircraft with a high degree of propulsion induced lift. The over-
all program consists of configuration studies, wind tunnel tests of candidate
configurations and a jet effects model employing two dimensional nozzles, tech-
nology development for the use of turbine powered propulsion simulators in small
scale wind tunnel models, top inlet tests, and the development of prediction
techniques capable of analyzing complete configurations with propulsion induced
effects. The status of each program, the accomplishments to date, and the anti-
cipated plans for the next year or two are presented herein.

INTRODUCTION

The Aircraft Aerodynamics Branch at the NASA-Ames Research Center has initiated a range of research efforts to develop aerodynamic technology for VSTOL fighter attack aircraft. The primary emphasis of the work is directed towards the transonic and supersonic Mach number regimes and the propulsion/airframe interactions associated with aircraft with a high degree of propulsion induced lift. The overall program (fig. 1) consists of: (1) configuration studies, (2) wind tunnel tests of candidate configurations and jet effects models employing two dimensional nozzles, (3) technology development for the use of turbine powered propulsion simulators in small scale wind tunnel models, (4) top inlet tests, and (5) the development of prediction techniques capable of analyzing complete configurations with propulsion induced effects.

The status of these programs is at various levels; the initial configuration studies are essentially complete while progress on the others is continuing. However, they have not reached the point of generating final results. Therefore, this paper is intended to review the status of each program, the accomplishments to date, and the anticipated plans for the next year or two.

CONFIGURATION AERODYNAMICS

A prime element in the overall program to develop aerodynamic technology for VSTOL fighter/attack aircraft anticipated in the post-1990 time period is a contractual effort jointly sponsored by Ames and the David Taylor Naval Ship Research and Development Center. The objectives of the program (fig. 2) are to generate an aerodynamic data base for Navy, NASA and industry use on a wide variety of high performance VSTOL concepts that have the potential of fulfilling the Navy fighter/attack role, to assess the computational methods of estimating the aerodynamic characteristics of these configurations, and most importantly, to identify the aerodynamic uncertainties requiring additional research.

The approach (fig. 3) adapted consisted of having each contractor define a configuration he thought appropriate and estimate the longitudinal and lateral/ directional aerodynamic characteristics associated with his proposed concept. Included was an analysis of transition from vertical to conventional flight with a definition of the control power requirements and phasing of reaction and aerodynamic controls. A general set of guidelines (fig. 4) was provided to allow the contractor to perform a conceptual aircraft analysis based upon his definition of a mission and payload. The following is a brief description of the guidelines furnished:

1. The conceptual aircraft analysis is for a high-performance VSTOL concept with potential to fulfill the Navy's fighter/attack role after 1990.

2. The aircraft shall have supersonic dash capability with a sustained Mach number capability of at least 1.6.

3. The aircraft shall be operational from land and from ships smaller than CVs without catapults and arresting gear. Good STO capability is a requirement.

The ejector diffusers are located between the fuselage and nacelles in the thick root section of the wings. For vertical takeoff and landing, the engine flow is diverted to the four ejector bays, where it is injected in both primary and diffuser nozzles. Pitch control during vertical flight is accomplished by thrust modulation of the forward and aft ejectors; yaw control is achieved by vectoring the ejector flow. Wing tip reaction controls are used for roll control. A major advantage of the ejector-diffuser lift system, of course, is its cool footprint, which could be an important factor for shipboard operation.

Grumman

The second HATOL configuration (Fig. 5, lower right hand corner) is a lift plus lift/cruise concept proposed by Grumman (Ref. 2). The configuration is a wing-canard design that employs a General Electric Remote Augmented Lift System (RALS). Grumman modified an earlier VSTOL fighter design (Model 623) by incorporating a canard and a new wing to meet the maneuver requirements in the present study. Two variable-cycle augmented turbofan study engines are used with Augmented Deflector Exhaust Nozzles (ADEN). The forward lift element is a dual burner/nozzle design. To minimize the size of this forward lift system, the ADEN nozzles are mounted at the wing trailing edge as far forward on the configuration as possible. The ADEN nozzles not only provide vertical lift for takeoff and landing, but also have in-flight thrust vectoring to enhance maneuvering.

The configuration features a high-mounted, variable incidence canard with leading and trailing-edge flaps, an advanced variable camber wing with leading and trailing edge devices, and twin vertical tails.

In conventional flight, longitudinal control is provided by incidence of the canard augmented at low speed and high angle of attack by the canard flaps; roll control is provided by asymmetric deflection of the wing trailing-edge devices; and directional control is provided by the rudder surfaces. In hover flight, pitch control is provided by flow shifting between the forward and aft nozzles; wing tip reaction controls are used for roll control; and differential lift/cruise nozzle deflections are used for yaw control.

Northrop (HATOL)

The third HATOL concept (Fig. 5, upper right hand corner) is a lift plus lift/cruise design by Northrop (Ref. 3). This design is one of two proposed by Northrop. This configuration uses a General Electric RALS concept with two variable cycle turbofan engines, ADEN nozzles and a single forward augmentor lift system with a gimbaled nozzle. The engine has a mini-afterburner (1000°F temperature rise) to provide additional thrust during combat. This augmentation is not used for vertical takeoff or landing.

4. To assure high maneuver performance, the aircraft shall have a sustained load factor (N_{Z_s}) of at least 6.2 at Mach number 0.6, 3048 m (10,000 ft) altitude at 88% VTOL gross weight.

5. The aircraft shall have a specific excess power at 1G ($P_{S_{1G}}$) of 274 m/sec (900 ft/sec) at Mach number 0.9, 3048 m (10,000 ft) altitude at 88% VTOL gross weight.

6. The aircraft weight shall be within the following boundaries:

   - VTOL gross weight = 9072 to 15876 kg (20,000 to 35,000 lb).
   - STO sea-based gross weight = VTOL gross weight plus 4536 kg (10,000 lb).

Subsequent to the aircraft definition phase, a limited number of the configurations where selected to be investigated further through a comprehensive wind tunnel program. Accordingly, the corresponding contractors were requested to design and build a wind tunnel model of their selected configurations which are to be tested in the Ames Unitary and 12-Foot Wind Tunnels. Through comparison of the predicted and measured aerodynamic characteristics, the capabilities of the present predictive techniques will be assessed.

The intent of the study is to isolate aerodynamic uncertainties associated with promising VSTOL fighter/attack concepts and to initiate wind-tunnel and computational aerodynamic investigations of these uncertainties. The intent is not to compare concepts nor company designs. This was assured by specifying only limited design requirements and permitting each contractor to define his own mission and payload on which to base his design.

Four contractors; General Dynamics, Grumman, Northrop, and Vought were selected to participate in the study and analysis phase of the effort. Three horizontal attitude takeoff and landing (HATOL) concepts and two vertical takeoff and landing (VATOL) concepts were studied (fig. 5). Northrop studied two concepts, a HATOL and a VATOL design. Each concept is briefly described in the following sections and a detailed description of each is given in References 1-5. A general review of the studies is given in Reference 6.

General Dynamics

The configuration proposed by General Dynamics (Ref. 1) is a wing-canard HATOL concept that has Alperin jet-diffuser ejectors as its vertical lift system (fig. 5, lower left corner). The design also features a Vectored-Engine-Over (VEO) wing-integrated airframe/propulsion system to achieve good transonic maneuvering and STOL performance. In this design, the full engine flow is directed over the wing aft surface to augment the aerodynamic lift through a jet flap effect. At low speeds, this is combined with spanwise blowing, which utilizes a portion of the engine exhaust at high angles of attack to produce leading-edge vortex augmentation.

The configuration is a wing-canard design with two vertical tails mounted on twin afterbodies. The clipped delta wing has variable camber, using automatically phased leading and trailing edge flaps. The canard is high mounted and all movable. Side-mounted, two-dimensional inlets are used with topside auxiliary inlet doors for takeoff. The two ADEN nozzles are mounted side-by-side on the aft fuselage centerline between two wing-mounted afterbodies.

During takeoff and hover, pitch control is provided by thrust modulation of the forward and aft nozzles; roll control by wing tip reaction controls. Yaw control is derived by lateral deflection of the forward nozzle. For conventional flight, the wing trailing-edge elevons are used for pitch and roll control and pitch stabilization. The all-movable vertical tails provide directional control and stabilization. The leading-edge flaps and canard surface are scheduled as a function of angle of attack and speed for optimum aerodynamic performance. Thrust vectoring and combined canard thrust deflection are used for manuever enhancement.

Northrop (VATOL)

The second concept studied by North-p (Ref. 4) in the present effort is a VATOL concept (Fig. 5, upper right hand corner). The configuration is a tailless design that features a wing leading edge extension (LEX) to maintain lift to high angles of attack. Top-mounted inlets are used to provide a low radar cross section as well as to free the lower surface for efficient weapon/landing gear integration and to ease mating with the alighting gantry.

Both Northrop concepts have a common wing with leading and trailing edge flaps automatically programmed to provide variable camber for optimum aerodynamic performance.

Control in the vertical takeoff and landing mode is provided by the gimbaled nozzles, which can be deflected ±30° in pitch and ±15° in yaw. Wing-tip-mounted reaction controls provide primary roll control: antisymmetric pitch deflection of the nozzles can be used for auxiliary roll control. In conventional flight, pitch and roll control is provided by the trailing-edge elevons and directional control and stabilization is provided by the all-movable vertical tail. Thrust vectoring in combination with the trailing-edge flaps is used for maneuver enhancement.

Vought - The final configuration is a VATOL concept (Fig. 5, lower center). The design features a fixed, close-coupled, high-mounted canard with trailing edge flaps, a midwing of low aspect ratio and a single vertical tail with a rudder. The wing has trailing-edge

flaps that are optimally phased to operate throughout the flight
envelope in unison with the canard flap to implement longitudinal
and lateral commands. Full-span leading-edge flaps are automat-
ically phased to maintain optimal camber for high-maneuver performance.

Axisymmetric convergent-divergent nozzles are mounted side by side
in the aft fuselage. These nozzles can be gimbaled $\pm 15°$ in pitch
and yaw to provide control during takeoff/landing, hover, transition
and in-flight maneuvering. A reaction control system in the wing
tips provides roll control for vertical takeoff and landing.

Two of the contractors, Northrop and General Dynamics, have been selected
to proceed with a second phase of the program, the design and fabrication
of wind tunnel models of their configurations. A total of four configurations
will be tested: the two Northrop configurations, the General Dynamics
ejector-diffuser/VEO configuration, and a General Dynamics RALS configu-
ration. The latter concept is similar to the ejector-diffuser/VEO concept
except the ejector-diffuser lift system has been replaced by a RALS lift
system. General Dynamics studied this configuration to provide a refer-
ence for the ejector-diffuser power concept.

The wind-tunnel program will be conducted over a Mach number range of
0.1 to 2.0 in the Ames 12-Foot and Unitary Wind Tunnels to angles of
attack of 30-degrees transonically and 90-degrees for the VATOL configu-
ration at low speed. The resulting experimental aerodynamic data base
will include untrimmed and trimmed longitudinal characteristics, lateral/
directional characteristics, and longitudinal and lateral/directional
control effectiveness. The experimental results will be compared to
estimates made by the contractors and by Ames and an assessment made as
to the adequacy of existing techniques to predict the aerodynamics of
these types of configurations.

A number of aerodynamic uncertainties related to these VSTOL fighter
concepts will be investigated in the test program. These include: (1)
lift system volume and nacelle lateral spacing effects on the drag and
aerodynamic center location, (2) effects of canard longitudinal position
and shape of the strake inboard of the engine nacelle on longitudinal
and lateral/directional stability, (3) close-coupled variable camber
wing and canard effects on aerodynamic performance, (4) effects of shape
of the wing leading-edge extension (LEX) on high angle-of-attack aero-
dynamics, (5) buffet onset and intensity, (6) forebody flow field effects
on a top-mounted inlet, (7) drag characteristics of wing-mounted after-
bodies, and (8) the effects of configuration component build-up on drag.
Control surface deflections will include wing leading- and trailing-edge
flaps, canard incidence, canard leading- and trailing-edge flaps, and
all movable vertical tails. A more detailed discussion of the aerodynamic
uncertainties, the aerodynamic predictions and the planned wind-tunnel
program is given in Reference 6.

PROPULSION INDUCED FLOWS

To expand the limited propulsion/airframe interaction data base on high performance VSTOL aircraft with particular emphasis on jet induced lift, an existing wind tunnel model (Figs. 6 and 7) has been modified for testing at Ames Research Center. The model is an 1/8-scale, twin engine, VSTOL fighter model developed for the Naval Air Propulsion Center to assess the installation aerodynamics of a number of nonaxisymmetric nozzles on a representative VSTOL fighter.

The exhaust nozzles available for testing on the model are the Augmented Deflection Exhaust Nozzle (ADEN), and Asymmetric Load Balanced Exhaust Nozzle (ALBEN), a two-dimensional convergent-divergent nozzle and a circular convergent-divergent nozzle used as a baseline. The ADEN nozzle on the wind-tunnel model can be tested in the cruise mode and in the thrust-deflection mode for in-flight maneuvering, but vertical thrust deflection is not available on this model.

Two six-component, flow-through force balances are employed in the model, one to measure total airframe forces and moments (with the exception of the vertical tails) and the other to measure forces and moments on the left-hand nozzle. The model is supported by twin vertical tails (Fig. 7), which also provide passage for high-pressure air for jet-effects testing. The model has been modified by Ames to strengthen the internal balance bellows which have caused problems in the earlier test (Refs. 7 and 8) of the model at NASA-Langley Research Center and the Arnold Engineering Development Center. In addition, to more completely define the propulsion-induced aerodynamic effects and provide pressure data for comparison with prediction methods, approximately 200 pressure taps have been installed on the wings, fuselage, external and internal nozzle surfaces, and on the aft fuselage in the vicinity of the nozzles, horizontal tail and nacelles.

Tests are planned in the Ames 11-Foot Transonic Wind Tunnel in June 1979 over a Mach number range from 0.6 to 1.4. The effects of nozzle geometry and variations in angle of attack, nozzle pressure ratio, and thrust deflection angle will be investigated.

Efforts are now underway to model this complete configuration using an advanced linear analysis technique referred to as PAN AIR which is described in a later section of the paper. PAN AIR is a surface paneling scheme, therefore the precise geometry can be modeled. An illustration of the geometry presently being used is shown in figure 8. Although, only the geometry has been modeled to date, the long term goal is to model the inlet and exhaust flows including deflected thrust and jet entrainment.

PROPULSION SIMULATION TECHNOLOGY

Inherently, VSTOL fighter/attack aircraft have large thrust to weight
ratios and significant levels of thrust deflection. These translate
into large inlet and exhaust flows and hence, significant interactions
between the airframe and the propulsion system. There is little doubt
that these interactions will be important: however, it is not clear
whether the inlet and exhaust flows are coupled such that both must be
simulated simultaneously to accurately assess the aerodynamic character-
istics. For vertical take-off and landing while in ground effect the
two flows are obviously coupled, but out of ground, through transition,
and during maneuvering flight with deflected thrust, the degree of
coupling is unknown. Because of the supercirculation induced by the
nonaxisymmetric vectoring exhaust nozzles, the geometrically close
coupled wing/canard/inlet arrangements, and the close coupling of the
inlet and nozzle, significant coupling of the inlet and exhaust flows in
these flight regimes will exist. Therefore, to determine the degree of
coupling through wind tunnel tests and to identify the important para-
meters, both the inlet and exhaust flows must be simulated simultaneously
(Fig. 9) rather than using the conventional technique of combining the
results from individual flow-through and jet-effects models.

The two potential methods for achieving this simultaneous simulation of
inlet and exhaust flows are through either turbine powered or ejector
powered simulators. Although a number of factors influence the choice
between these two alternatives such as performance, cost, versatility,
complexity, and reliability, performance is obviously the dominant
factor. A comparison of the dry power pumping characteristics of the
high pressure ratio, turbine powered Compact Multimission Aircraft
Propulsion Simulator (CMAPS) being developed by McDonnell Aircraft
Company and General Electric under contract to the Air Force Aero
Propulsion Laboratory (Ref. 9) and comparable ejector powered simulator
(Ref. 10) is presented in figure 10. Superimposed on this are the
pumping characteristics of current turbojet and low bypass ratio turbo-
fan engines. This comparison illustrates both performance advantage of
the turbine powered simulators in matching current engines and the
flexibility of the present design of providing a broad range of inlet
airflows and nozzle pressure ratios.

The operating line for the best dry power ejector powered simulator
tested and reported in reference 10 is shown in the lower left hand
corner of figure 10. It is obvious that for the dry power condition a
straight forward application of the ejector system is unsatisfactory.
The operating line can be moved to the right by bleeding the inlet but
this very rapidly leads to large bleed lines that distort the model and
result in a large support system. In addition, for engine pressure
ratios greater than 2.0, ejector powered simulators begin to develop
severe distortions in the jet total pressure profile caused by super-
sonic internal flow. For VSTOL applications, this non-uniform exit
stream could significantly effect the aerodynamic interactions being
investigated, thus leading to false conclusions. Therefore, it appears
that the turbine powered simulators are the only viable approach of

achieving simultaneous simulation of the inlet and exhaust flows that match current engines and provide the flexibility required to investigate a spectrum of aerodynamic parameters.

The primary objective of the present program described in more detail in Reference 11, is to identify the degree of coupling between the inlet and exhaust flows as a function of the flight regime and hence, determine the need for complete propulsion flow simulation. Coincident with this activity will be the development of the technology of installing, calibrating, and operating these simulators as a wind tunnel test technique. The particular program includes the acquisition of three CMAPS units and all the associated control and monitoring equipment. The CMAPS unit is a compact version of the prototype which was evaluated in a wind tunnel test program conducted by McDonnell in 1975 (Ref. 8). The CMAPS units (Fig. 11) consist of a four stage axial compressor driven by a single stage turbine. The turbine drive air is either mixed with the compressor air or bled from the unit. Through independent control of the drive and bleed flows, the compressor airflow and nozzle pressure ratio can be varied independently. The prototype unit was installed and operated statically in the Ames 9- by 7-Foot Wind Tunnel (fig. 12) to gain some experience with the unit and to identify any required facility modifi-cations.

The present focus of activity is concentrated on the definition of the first wind tunnel model designed to employ these units. The general characteristics are outlined in Figure 13. Basically, the model will be of a twin engine VSTOL configuration that has been designed to maximize the jet induced lift. This is being done to enhance the coupling of the inlet and exhaust flows to insure that a measurable level of interaction between the two flows. If a configuration with little or no interaction was used it would be impossible to ascertain whether the simulators provide any advantage over the conventional modes of testing. The model will be tested in the conventional manner which consists of a flow through and jet-effects test to provide the basic data for comparison with the data obtained using the simulator. Every attempt will be made to design the model and instrumentation to minimize any systematic errors between the conventional and simulator modes of testing.

If possible, the model will also be designed to even further increase the coupling of the inlet and exhaust flows through variations in model geometry. This may result in geometries that would be unrealistic from an aircraft configuration point of view but will help sort out the degree and importance of the coupling of the two flows.

The simulators will be nonmetric while the aero shell will be metric. This will be done to eliminate the need of obtaining detailed thrust calibrations of the simulators and developing, in the near term, methods of crossing the metric break with multiple high pressure airlines. The use of non-metric simulators may result in some distortion to the mold lines of the vehicle, however the reduced complexity of the model will allow a much earlier evaluation of the aerodynamic interactions and the propulsion simulators as a potential test technique.

Although, the initial model will be designed with nonmetric simulators, the need for metric simulators to allow realistic configurations to be tested without any modification to the mold lines is not being over-looked. To provide the detailed calibrations required to accurately reduce the thrust-minus-drag obtained from such a model, a propulsion simulator calibration facility is being constructed. Figure 14 is a schematic of the facility as presently envisioned. The facility is being designed to calibrate not only individual isolated simulators, but also to check and calibrate them when installed in the actual model. This will provide the capability of calibrating any of the inlet auxil-iary flows that may be present. The basic facility will be composed of a large tank that will be maintained at the appropriate static pressure. The drive and inlet air to each of the simulators will be individually controlled with respect to pressure and temperature and the mass flow accurately measured. The simulator or simulator model will be suspended from a metric frame which in turn is suspended from the ceiling of the tank by eight flexures and restrained to move in the horizontal plane by four load cells. With the stiffness of the load cells being significantly greater than that of the flexures, the accuracy of the load measurements in the horizontal plane should be quite good. With the model mounted with wings in the vertical plane, thrust deflecting nozzles can also be easily calibrated for both axial and normal force.

TOP MOUNTED INLETS

As a result of the configuration studies previously discussed, top mounted inlet systems (Fig. 15) have been identified as a very promising and desirable feature for VSTOL fighter aircraft. Relative to conven-tional locations, top mounted inlets offer a decreased injection of debris and hot gasses during VTOL operations, a reduction in radar cross section, improved weapons system integration, and potentially lower weight because of shorter inlet duct lengths. However, these gains are not achieved without some potential problems that require further research to avoid unacceptable performance penalties. The areas of concern include possible ingestion of distorted flows at high angles of attack resulting from canard or strake vortices, the adverse effects of operating in an expanded flow field, and the internal flow problems associated with short "S" ducts.

In light of the potential advantages of top mounted inlets and realizing the concerns, a research effort has been initiated to assess the effects of various aircraft characteristics and variations in external geometry on the performance of a representative inlet configuration. Plans include the modification of the wind tunnel model of the Northrop VATOL configuration (Fig. 15) to provide a metered inlet duct and the appro-priate engine face instrumentation (Fig. 16). In addition, provision will be made for flow field rakes at the inlet face locations. The test program, to be conducted in the Ames 11- by 11-Foot Transonic and 9- by 7-Foot Supersonic Wind Tunnels, will concentrate on variations in inlet location, the plan form of the wing leading edge extension, canard utilization, and leading edge flap deployment.

PANEL AERODYNAMICS (PAN AIR)

PAN AIR (Fig. 17) is an advanced linear analysis and design tool applicable to arbitrary configurations in steady inviscid, subsonic, or supersonic flow (refs. 12 through 14). The program is being developed by the Boeing Company under contract to NASA-Ames with support from NASA-Langley, the Air Force Flight Dynamics Lab and Aeronautical Systems Division and the Naval Coastal Systems Center. The advanced technology embodied in the code is based on higher order singularities distributed and superimposed on the actual surface of the configuration. The term higher order refers to the quadratic doublet and linear source distributions versus the linear doublet and constant source distributions employed in existing linear methods. The higher order singularities combined with the condition of continuity in singularity strength and geometry across panel edges provides an accurate and numerically stable computational method. Furthermore, a variety of boundary conditions including velocity or mass flux on the mean or actual surface, or potential on the interior of closed bodies, are available within the program.

The combination of the higher order singularities, the surface paneling, and the general boundary conditions provides a great deal of flexibility in modeling complex configurations or flow conditions. This capability is applicable to both subsonic and supersonic flow. The extension of this type of configuration modeling capability to supersonic flow represents a unique aspect of the program and a significant advancement of the state-of-the-art.

Relative to VSTOL configurations, one of the goals of the overall effort is to successfully analyze configurations and flow conditions illustrated in figure 18, with the objective of accounting for the jet induced lift effects. The actual surface geometry of the vehicle will be modeled, along with both the inlet and exhaust streams. The inlet flow is accounted for by modeling a portion of the internal geometry of the inlet and specifying the mass flow through the inlet. The exhaust flow is modeled by paneling the plume and specifying the entrainment through appropriate velocity or mass flux boundary conditions. The initial version of the method will include only an analysis capability, therefore, the shape of the exhaust plume will have to be known apriori. A planned extension of the method will include a design capability that will be directed towards determining the correct location of the plume. By modeling the actual geometry or through changes in the boundary conditions over the control surfaces, the characteristics of the control surface deflections can be easily determined.

An example of the capability of the technology embodied in the code is provided in figure 19 which shows some results obtained on a super-cruiser configuration at M = 1.2. The wing pressure distributions shown in figure 19 compare PAN AIR results with experiment and a linear theory using linearized boundary conditions. Prior to PAN AIR, this supersonic flow condition could only be analyzed using linearized boundary conditions. The PAN AIR results agree very well with the experimental data and are a definite improvement over the earlier method. It is also worth noting that the inlet located beneath the fuselage was modeled. This included capturing the inlet airflow. A number of other comparisons of PAN AIR results are contained in Reference 15.

At the present time the PAN AIR technology is contained in an operational pilot code which is available through COSMIC (fig. 20). A user oriented, well documented version of PAN AIR has been developed and is presently undergoing validation and checkout. It will be installed at the participating governmental agencies by the end of the year and should be available through COSMIC early in CY 1980. A User's Class is scheduled for early 1980.

SUMMARY

A number of programs are presently underway at NASA-Ames to develop high speed aerodynamic technology for VSTOL fighter/attack aircraft. The effort includes a spectrum of experimental programs to develop a data base on a variety of configurations, to accurately define the aerodynamic characteristics of aircraft with a large degree of propulsion/airframe interaction, and to investigate airframe effects on the potential performance of top mounted inlet systems. Parallel with this is an effort to develop prediction methods capable of analyzing complex VSTOL configurations accounting for the propulsion induced forces.

REFERENCES

1. Lummus, J. R. et al., "Study of Aerodynamic Technology for VSTOL Fighter/Attack Aircraft," NASA CR-152128, May 1978.

2. Burhans, W. R. et al., "Study of Aerodynamic Technology for VSTOL Fighter/Attack Aircraft," NASA CR-152129, May 1978.

3. Brown, S. H. et al., "Study of Aerodynamic Technology for VSTOL Fighter/Attack Aircraft - Horizontal Attitude Concept," NASA CR-152130, May 1978.

4. Gerhardt, H. A. et al., "Study of Aerodynamic Technology for VSTOL Fighter/Attack Aircraft - Vertical Attitude Concept," NASA CR-152131, May 1978.

5. Driggers, H. H. et al., "Study of Aerodynamic Technology for VSTOL Fighter/Attack Aircraft," NASA CR-152132, May 1978.

6. Nelms, W. P., "Studies of Aerodynamic Technology for V/STOL Fighter/Attack Aircraft," AIAA Paper 78-1511, August 1978.

7. Schnell, W. C., Grossman, R. L., and Hoff, G. E., "Comparison of Non-Axisymmetric and Axisymmetric Nozzles Installed on a V/STOL Fighter Model," SAE Paper 770983, November 1977.

8. Schnell, W. C. and Grossman, R. L., "Vectoring Non-Axisymmetric Nozzle Jet Induced Effects on a V/STOL Fighter Model," AIAA Paper 78-1080, July 1978.

9. Eigenmann, M. F., Bear, R. L., and Chandler, T. C., "Turbine Engine Multi-Mission Propulsion Simulator Wind Tunnel Demonstration," Air Force Aero Propulsion Laboratory TR-76-73, November 1976.

10. Smith, G. D., Matz, R. J., and Bauer, R. C., "Analytical and Experimental Investigation of Ejector-Powered Engine Simulators for Wind Tunnel Models," AEDC-TR-76-128, January, 1977.

11. Bailey, R. O., Harper, M., and Jannetta, T. J., "Evaluation of Turbo Propulsion Simulators as a Testing Technique for Fighter Aircraft," AIAA Paper 79-1149, June 1979.

12. Erickson, L. L., Johnson, F. T., and Ehlers, E. F., "Advanced Surface Paneling Method for Subsonic and Supersonic Flow," NASA CP-001, pp. 25-54, November 1976.

13. Johnson, F. T. and Rubbert, P. E., "Advanced Panel-Type Influence Coefficient Methods Applied to Subsonic Flows," AIAA Paper 75-50, January 1975.

14. Ehlers, F. E., Epton, M. A., Johnson, F. T., Magnus, A. E., and Rubbert, P. E., "A Higher Order Panel Method for Linearized Supersonic Flow," NASA CR-3062, May 1979.

15. Thomas, J. L. and Miller, D. S., "Numerical Comparisons of Panel Methods at Subsonic and Supersonic Speeds," AIAA Paper 79-0404, January 1979.

VSTOL AERODYNAMICS RESEARCH PROGRAMS

- CONFIGURATION AERODYNAMICS
- AIRFRAME/PROPULSION SYSTEM INTEGRATION
- TOP INLETS
- RAM AIR

FIGURE 1

CONFIGURATION AERODYNAMICS

OBJECTIVE

- CONFIGURATION DATA BASE
- ASSESS COMPUTATION METHODS
- IDENTIFY AERODYNAMIC UNCERTAINTIES

APPROACH — AMES/NSRDC PROGRAM

- DEFINE AIRCRAFT
- PREDICT AERODYNAMICS
- BUILD AND TEST MODELS
- ASSESS PREDICTIVE TECHNIQUES

FIGURE 2

CONFIGURATION AERODYNAMICS

PHASE I — STUDIES

- 4 CONTRACTORS
- 5 CONFIGURATIONS
- AERODYNAMIC ANALYSIS AND UNCERTAINTIES

PHASE II — TESTS

- 2 CONTRACTORS
- 4 MODELS
- UNITARY AND 12-ft WIND TUNNELS—FY 79-80

FIGURE 3

GUIDELINES

- VSTOL FIGHTER/ATTACK A/C

- SUPERSONIC DASH

- SUSTAINED M = 1.6

- OPERATE FROM SHIPS SMALLER THAN CV

- N_{Z_G} = 6.2 (M = 0.6, 10,000 ft)

- $P_{S_{IG}}$ = 900 ft/sec (M = 0.9, 10,000 ft)

- VTOL wt = 20,000 TO 35,000 lb

- STO SEA BASED wt = VTOL wt + 10,000 lb

FIGURE 4

V/STOL FIGHTER/ATTACK AIRCRAFT

MAY, 1978
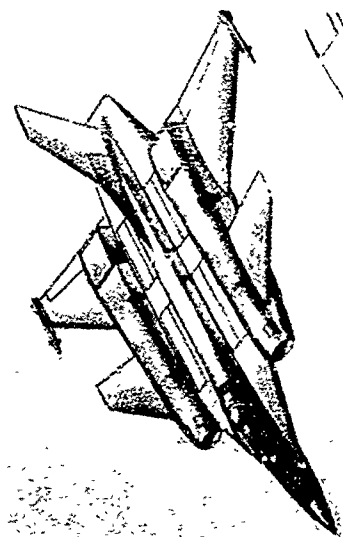
FIGURE 5

FIGURE 6 - VSTOL Fighter Jet Effects Model, Grumman 623 Configuration
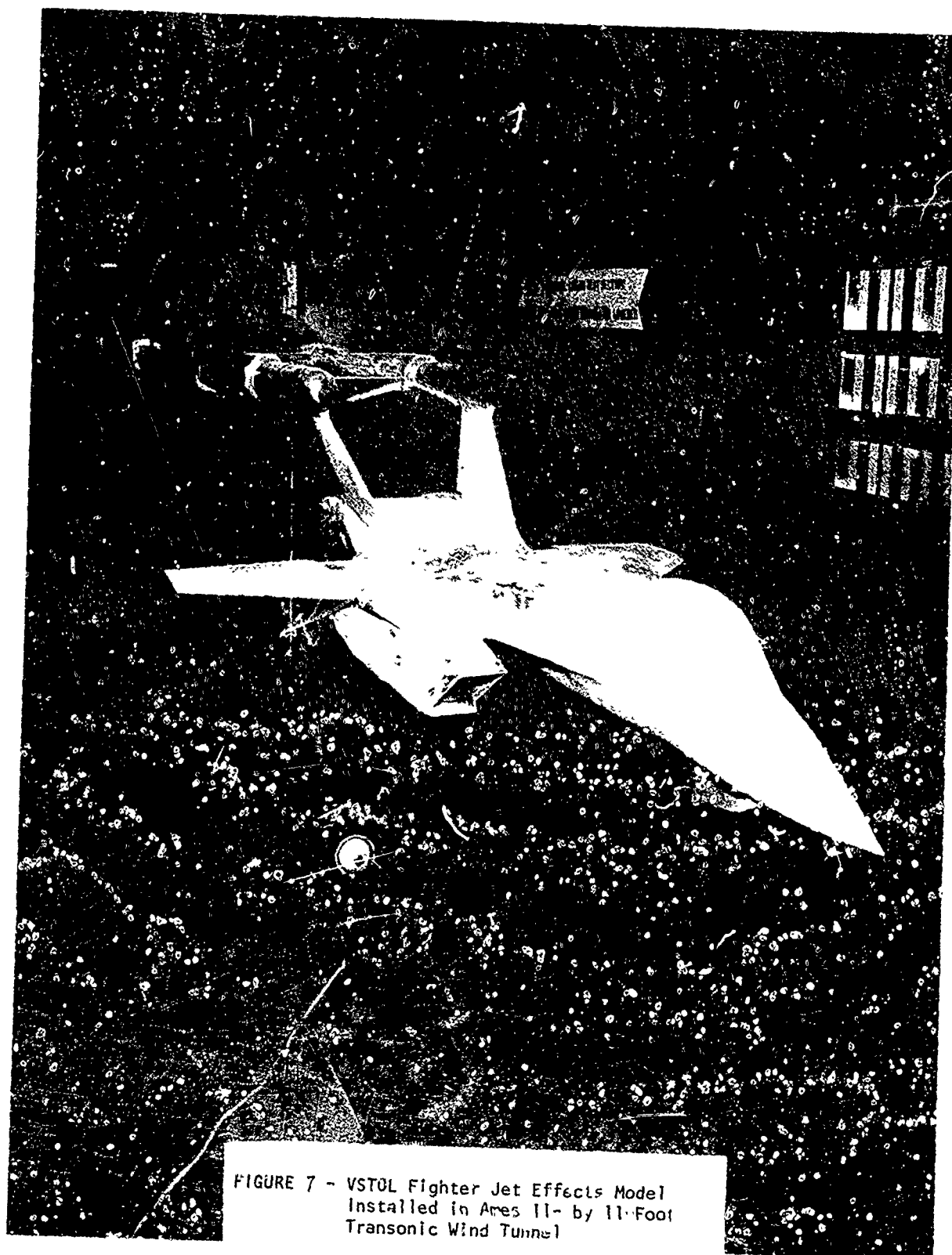
FIGURE 7 - VSTOL Fighter Jet Effects Model
Installed in Ames 11- by 11-Foot
Transonic Wind Tunnel
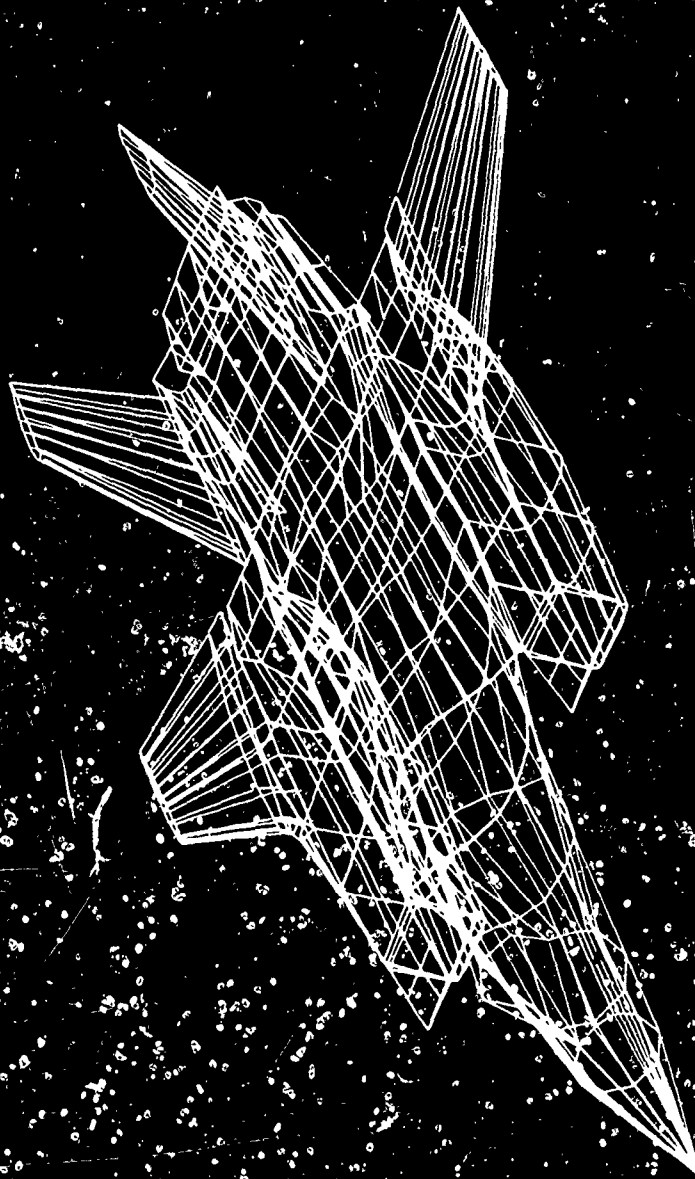
FIGURE 8 - Graphical Presentation of the Analytical Description of the VSTOL Fighter Model Geometry

VTOL AIRFRAME/ENGINE INTERACTIONS

- DEFLECTED THRUST
  T.O. AND MANEUVER

- CLOSE COUPLING OF
  INLET/NOZZLE/AIRFRAME

- LARGE T/W → LARGE A/C'S

NEED FOR
TOTAL
PROPULSION
SIMULATION

FIGURE 9

PUMPING CHARACTERISTICS OF CURRENT TURBINE & EJECTOR POWERED ENGINE SIMULATORS
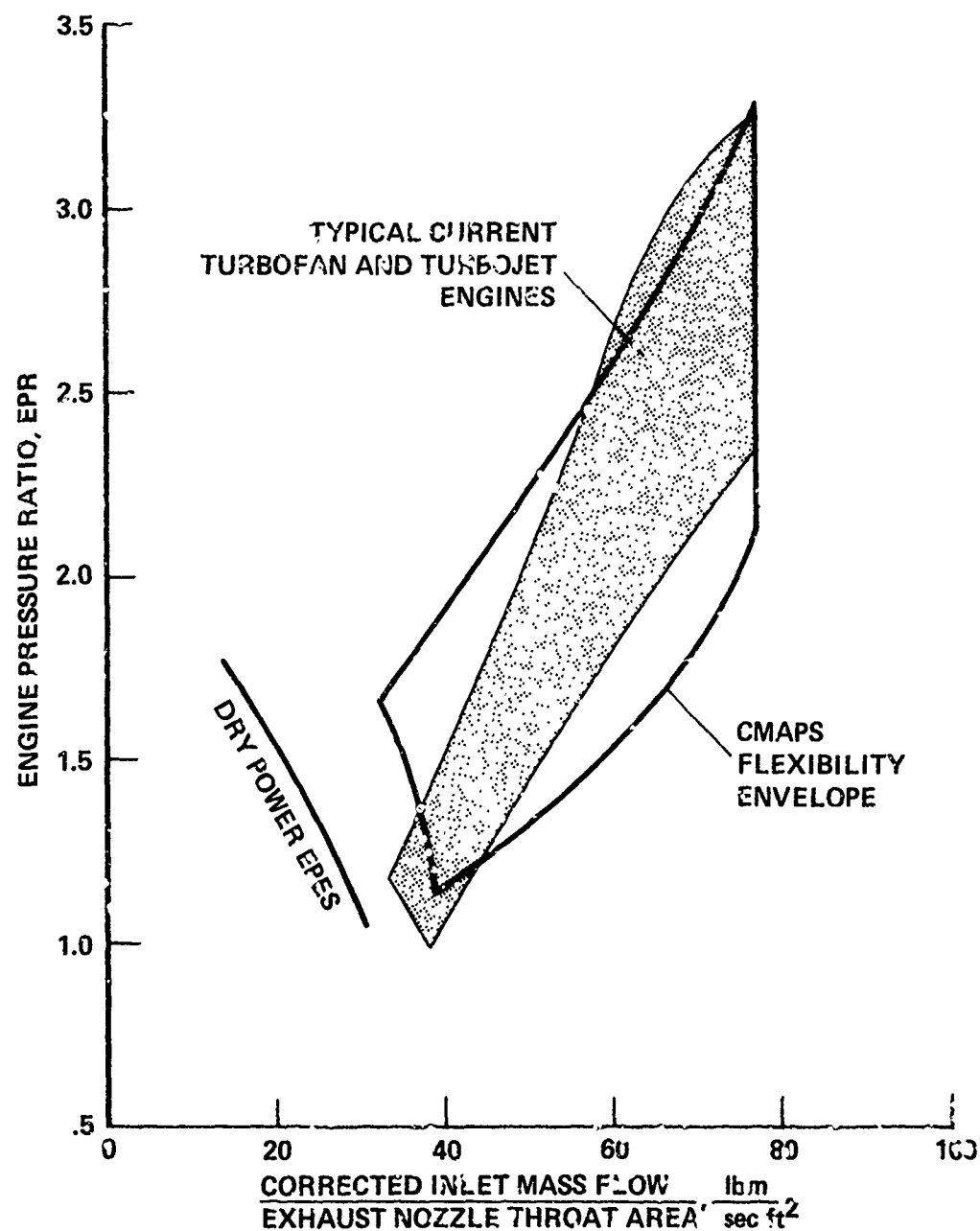
FIGURE 10

COMPARISON OF CURRENT AND COMPACT CONFIGURATIONS

CURRENT
SIMULATOR
CONFIGURATION
(MAPS)

MIXER

NOZZLE ATTACH
STATION

FORWARD MANIFOLD

16.2 in.

12.6 in.

4.3 in.

5.3 in.

COMPACT
SIMULATOR
CONFIGURATION
(C MAPS)

MIXER

BLEED AIR MANIFOLD

DRIVE AIR MANIFOLD

NOZZLE ATTACH STATION

3.9 in.

9.9 in.
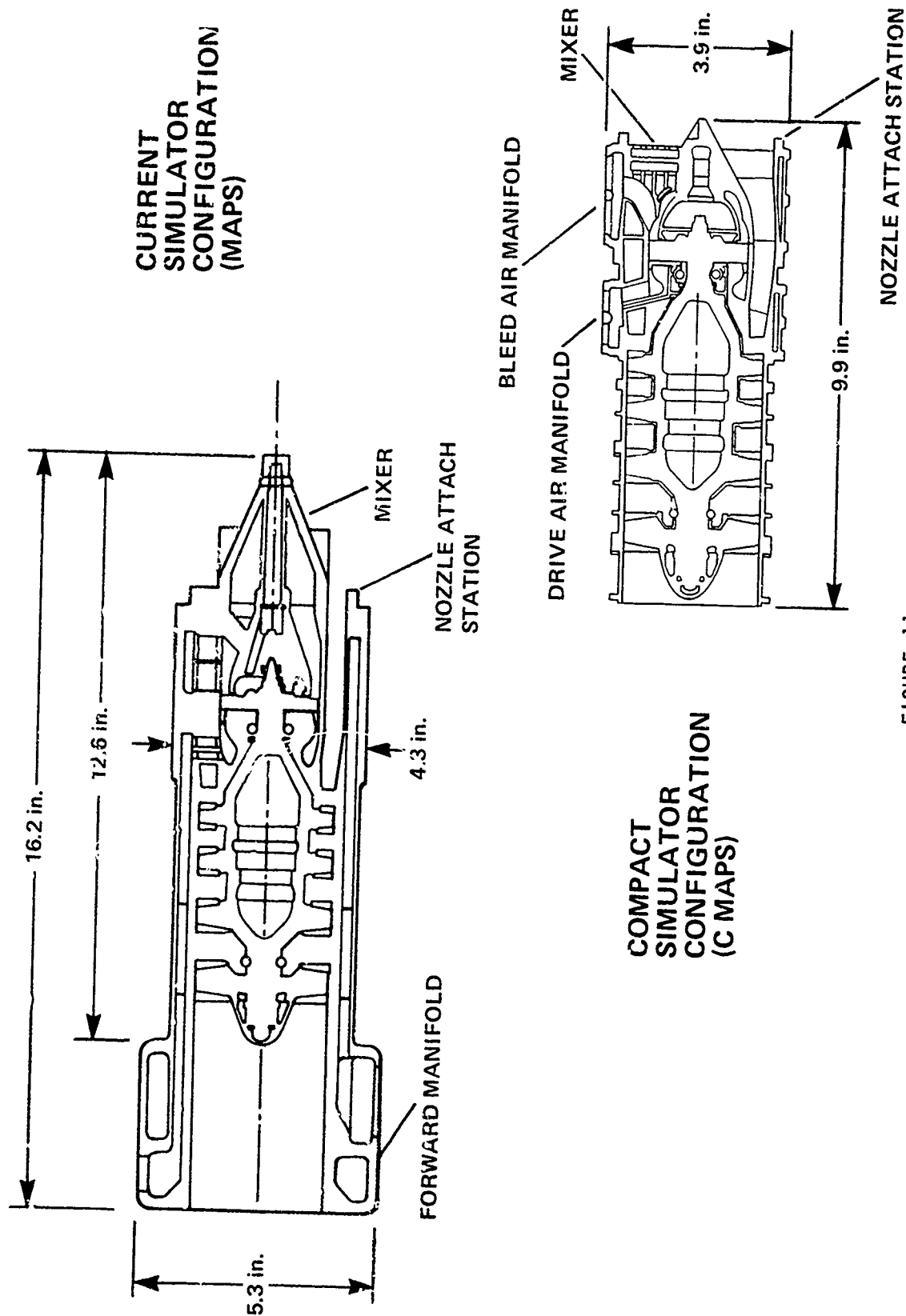
FIGURE 11

FIGURE 13 – Prototype Propulsion Simulator During Static Operations in Ames 9- by 7-Foot Supersonic Wind Tunnel

CMAPS CONFIGURATION/MODEL FEATURES

- V/STOL FIGHTER/ATTACK
- MAXIMUM PROPULSION INDUCED LIFT
- TWIN ENGINE
- NON-AXISYMMETRIC/DEFLECTABLE NOZZLES
- CMAPS NON-METRIC
- AIRFRAME SHELL METRIC
- THREE MODE TESTING
- CLOSE/CLOSER COUPLING

FIGURE 13

PROPULSION SIMULATOR CALIBRATION FACILITY

TO 1 x 3
VACUUM PUMPS

AXIAL
LOAD CELL

HIGH PRESSURE AIR LINES

VACUUM TANK

METRIC FRAME

VIEW PORT

FLEXURES
(8 ORTHOGONAL PAIRS)

TWIN ENGINED VSTOL
WIND TUNNEL MODEL

STING

ENGINE EXHAUST
EXTRACTORS

15 MAX
10 MIN

FLOOR

ENGINE INLET AIR PLENUM
INDEPENDENT SUPPLY FOR
EACH ENGINE

DIMENSIONS IN ft

≈3

≈7

TANK HEAD
HINGED FOR ACCESS
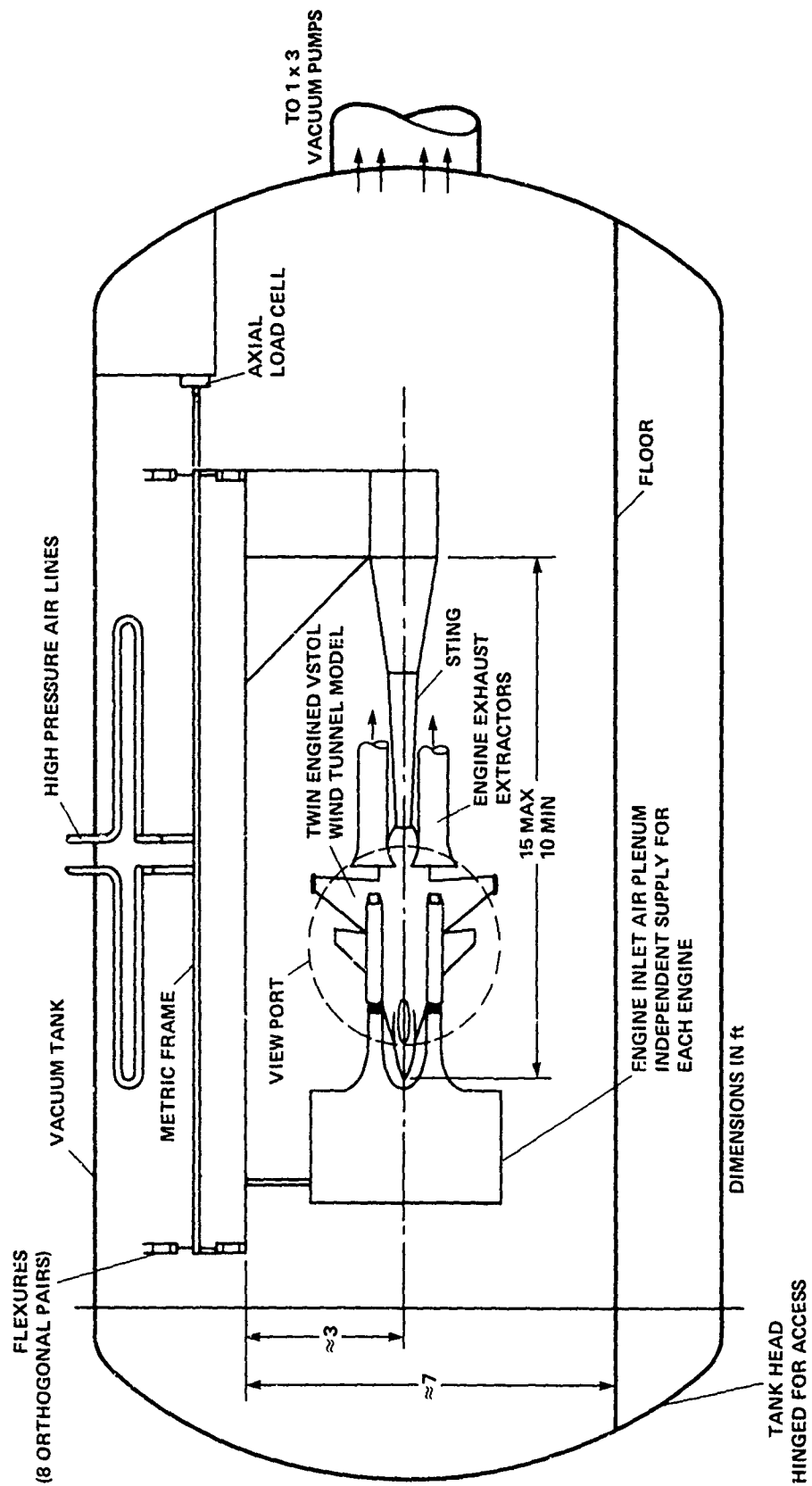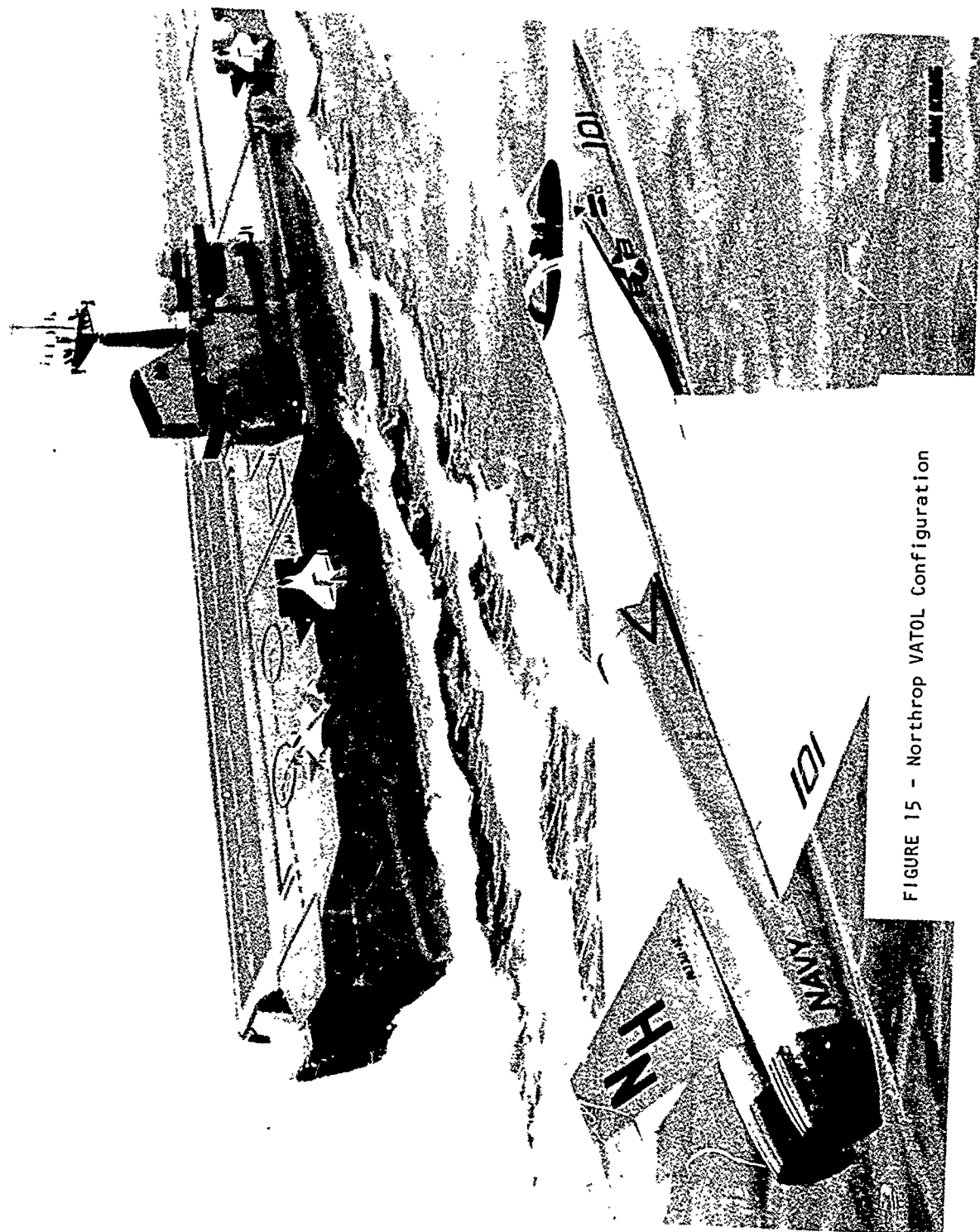
FIGURE 14

FIGURE 15 - Northrop VATOL Configuration

TOP INLET MODEL

COMPRESSOR FACE
INSTRUMENTATION

MASS FLOW CONTROL
PLUG ASSEMBLY

STRAKE AND CANARD
VARIATIONS

VARIABLE INLET POSITION
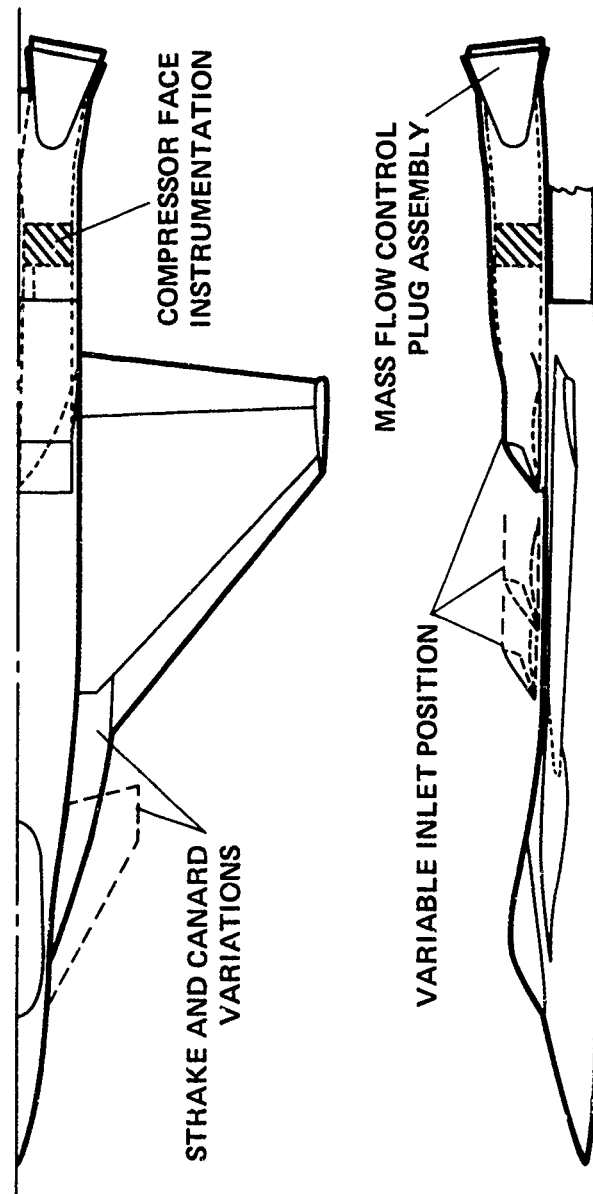
FIGURE 16

PANEL AERODYNAMICS (PAN AIR)

- ADVANCED LINEAR ANALYSIS FOR COMPLETE AIRCRAFT

- SUBSONIC AND SUPERSONIC FLOW

- PRESSURES, FORCES AND MOMENTS, STREAMLINES

FIGURE 17

AIRFRAME/PROPULSION SYSTEM MODELING

SURFACE PANELING OF ARBITRARY GEOMETRY

SPECIFIED INLET/EXHAUST MASS FLOW

CONTROL SURFACE DEFLECTIONS

SPECIFIED ENTRAINMENT

DEFLECTED THRUST
- PANELED STREAMTUBE
- ASSUMED LOCATION
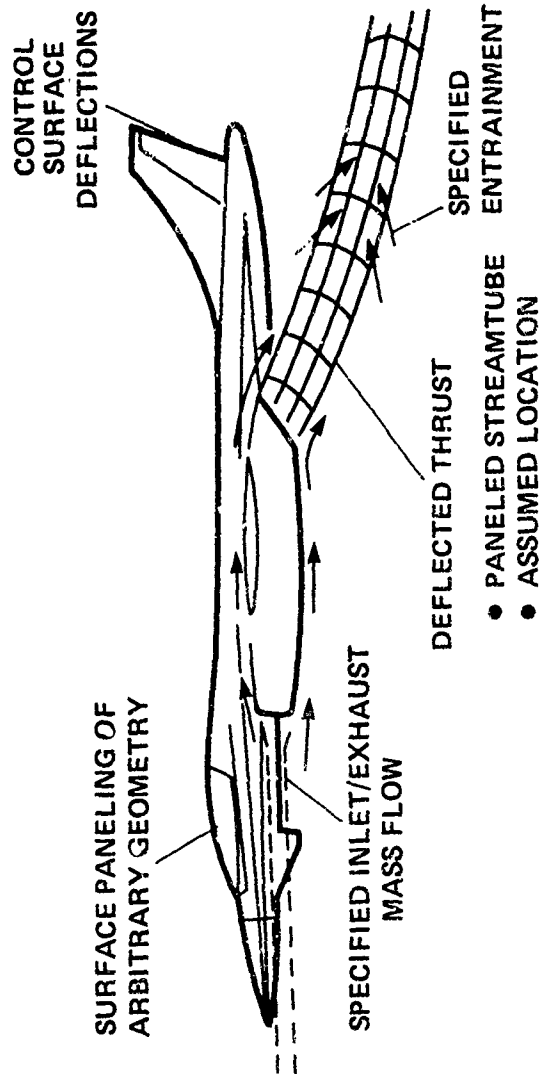
FIGURE 18

WING PRESSURE DISTRIBUTION ON SUPERCRUISER

MACH = 1.2
α = 0

SURFACE PANELING
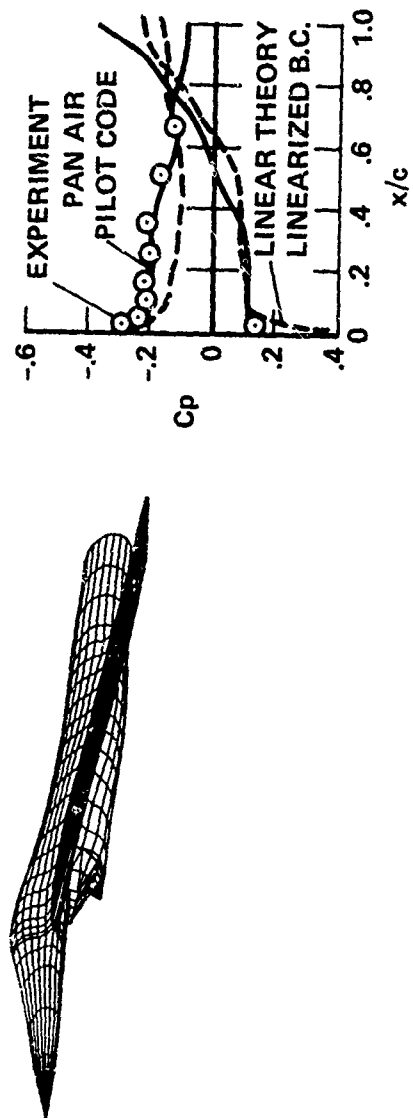
FIGURE 19

PAN AIR STATUS

- CURRENT

  - TECHNOLOGY DEMONSTRATED BY PILOT CODE
  - PROGRAM IN VALIDATION STAGE

- FUTURE

  - INSTALLATION AT FOUR GOV'T AGENCIES $\approx$ NOV. '79
  - USER'S CLASSES $\approx$ JAN. '80
  - AVAILABLE THRU COSMIC $\approx$ FEB. '80

FIGURE 20

1013

PANEL DISCUSSION

MAX PLATZER (NAVAL POSTGRADUATE SCHOOL):

As I indicated to you earlier, we'd like to have first the session chairmen, each individual session chairman, give a five to ten minute summary and after each summary we would like to open it up for additional remarks from the audience. In my estimation, that should take an hour or so.

SESSION I

K. T. YEN (NAVAL AIR DEVELOPMENT CENTER):

Session I of the workshop is on the "Flow Modelling Techniques and Prediction Methods for Transition Aerodynamics." There were seven papers in the session. I would like also to make a few comments about a paper by Professor Dan Adler which really was not in my session, but in Session III.

First of all I want to say that we are happy to have Mr. Knott from British Aerospace to come over here and give us a review of the lifting jet interference problem. We know that the AV-8 was developed over there; also it is interesting to know that Peter Wooler started his jet modelling work over there in the early 1960's.

Mr. Knott presented wind tunnel results to show that jet interference can be large and unfavorable on configurations relevant to the Navy type B aircraft. For the type A requirements he found that the configurations are more likely to have less jet interference effects. He also pointed out that not only it is possible to find ways and means to reduce adverse lift interference but also it may be possible to produce favorable lift interference. In order to optimize the lift interference, however, prediction methods are needed.

Tom Beatty (Vought) in his paper has described a computer program called "VAPE." This program has six modules, three of which are the jet models: The Wooler-Ziegler model, the Fearn-Weston model, and the Thames rectangular jet model. The "VAPE" program has been applied to a NASA V/STOL model as discussed by Tom. The agreement between the calculations and the measurements for the total forces and moments has been found to be very good at low jet velocity ratios but not very good at high velocity ratios. So it is clear that some improvements, and modifications, or even additions will be needed in order to make this program useful and practical.

One of the possible additions or improvements has been indicated by Professor McMahon of Georgia Tech. His paper is on the interference between

a lifting jet and a flap. His wind tunnel measurements show that at large flap deflection angles near the maximum lift the effective flap angle and the hinge moment are reduced significantly by the jet action. In addition, the interference effect seems to be sensitive to the location of the jet exit relative to the flap.

I want to make a few remarks about the jet models. Dr. Fearn's well-known model is basically a vortex model. Assuming the vortex properties of the jet are known, this model is intended to calculate surface pressures. It is in the VAPE program as I mentioned earlier.

I would like to compare Wooler's model with Professor Adler's. In Wooler's model three equations are used to calculate the jet velocity, jet width and the jet center line location. In Adler's work he has five unknowns and he needed five equations. In Wooler's model, he has only three unknowns assuming first of all that the jet shape is elliptic with the ratio of major axis to minor axis of four (C_p will be constant). In addition, he used only one velocity for the jet. The equation of mass conservation also has entrainment in it, but in a manner different from Adler's. The momentum equation used by Peter Wooler may also be regarded as a momentum integral equation similar to what Professor Adler had used. There is a major difference between those two models, however. Wooler is interested only in the calculation of surface pressure outside of the jet, and his model will not be able to handle anything inside the jet. He is not interested in that. On the other hand, Professor Adler's paper is intended to calculate the jet structure, but right now we have not seen any calculation for the surface pressure. It would be interesting to see that.

The paper by Perkins and Mendenhall of Nielsen Engineering is a correlation method for prediction of surface pressures. The blockage and entrainment effects of the jet are modelled by potential flow vortices and sinks. Based on measurements, the correlation factor is introduced to account for the viscous effects and they found out that in the wake and also in the lateral regions of the jet the correlation factors are very significant. One point of interest is to see if the correlation curves at a velocity ratio can be collapsed into a single curve. It would render the correlation method by Perkins and Mendenhall much more useful, but as I understand it they have not been able to do that. I think with additional development this approach may prove to be very useful.

Jerry Baker presented a numerical interaction algorithm for prediction of V/STOL jet-induced flow fields. This work is still in progress, and we hope to learn from this study something about the formation of the contra-rotating vortices near the jet exit and also the details of the entrainment mechanism of a jet in a cross flow.

We can see from the papers given in Session I, and Professor Adler's paper, different approaches have been adopted for jet modelling. The question was raised whether entrainment is important or not. There is no doubt that entrainment is important, and there appeared no disagreement on this point. However, in jet models, entrainment is accounted for in different ways. Sometimes it is really not easy to see clearly from some of the models what is meant by entrainment because the models are potential flow models. It is my impression from the workshop that some significant progress has been made in recent years in the development of prediction methods in transition aerodynamics. I am sure that more progress will be made soon and that reliable methods will be available.

MAX PLATZER (NAVAL POSTGRADUATE SCHOOL):

Thank you very much, K. T. Are there any questions or comments? No comment from Peter Wooler?

PETER WOOLER (NORTHROP CORPORATION):

It's my impression, listening in the audience, that the main problem inadequately treated at the moment is the wake region behind the jet. I don't think anybody has developed an adequate representation of the wake which can be used to calculate the flow field and hence the induced forces on adjacent surfaces.

MAX PLATZER (NAVAL POSTGRADUATE SCHOOL):

O.K., thank you. Anyone else?

TOM BEATTY (VOUGHT CORPORATION):

One thing that bothers me are the wake results that Frank Thames is getting at NASA-Langley on a flat plate and a bluff body. The primary difference between the two is that on the bluff body there is no plate behind there; it is just a jet coming out with sort of nothing around it. The structure of the vortices is entirely different, the strengths are much different and we don't know whether or not it is due to the shape of the body or due to the

fact that the flat plate could be drawing that jet down. The flat plate could possibly be adding to the wake effect that we are seeing. We do not really have a handle on that.

MAX PLATZER (NAVAL POSTGRADUATE SCHOOL):

O.K., I will turn it over to Bob Weinraub for his review of the second session.

SESSION II

ROBERT WEINRAUB (NAVAL AIR SYSTEMS COMMAND):

The second session covered aerodynamics in hovering V/STOL aircraft. I think that we have shown again that the flow field surrounding these aircraft is highly complex and not completely understood. An example of this seems to be the discrepancies in the descriptions of the fountain regions. At this time I don't think we are in a position to resolve this to anyone's satisfaction; we are just going to have to keep plugging along.

Two items in this particular area are worth highlighting. One is the indication by Foley, and Lummus and Smith from General Dynamics, of the apparent strong influence of turbulence on fountain strength. Now this is something, at least to me, that was totally unexpected. Putting on my "airplane designer's hat" I would have liked to have ignored it because it just opens up a Pandora's box on trying to determine a simple method of modelling these kinds of flow fields.

Another area where we haven't put a lot of effort, and it turns out that it might come around to burn us, though not quite as significantly as the area of turbulence, was pointed out by Bill Hill of Grumman. He did, at least to my knowledge, the first fairly systematic survey of the upper pressure region of the model. The results of his findings were that this area might warrant some attention, particularly when you go into configuration refinement for an airplane.

Another piece of work I would like to comment on was not in my session. I want to steal some of Dave Hickey's thunder. Dave Spong did a nice job in attempting to qualify optimization of fountain or jet spacing in order to get as much favorable amplification out of the fountain as possible. I think it was a good effort and it is a good first step for us in this area.

We seem to be making progress in the numerical computational types of methods, but I think we are a long way from getting any kind of practical

engineering solutions from that approach.

The last thing I would like to comment on, and please don't hit me Dick. The parametric methods. The work that Dick showed...it kind of dumbfounded me; I didn't think that we were at any kind of position to get results that good, but I would like to say that we are basing these parametric methods on wind tunnel model tests where we don't really understand the flow field. Therefore, we have to use them with a lot of caution. We are nowhere near saying that this kind of methodology is probably good beyond preliminary design application. I think in that particular stage of aicraft development this type of methodology is very useful, but I think we don't want to use this kind of thing for configuration refinements. I think, if we are not careful, we are going to get burned and burned very badly. As evidenced by some surprises we had in some of the results shown today. So, that's about all I have to say as to what my opinion of the highlights of this particular session were.

DICK KUHN - Retired (NASA-LANGLEY RESEARCH CENTER):

Yes, I agree completely with that. Any of these parametric correlations can only be used as a first-cut look at things. Before you go to fly an airplane, you have to test all of these things. I think Ted Nark showed us a lot of those kinds of things this morning.

ROBERT WEINRAUB (NAVAL AIR SYSTEMS COMMAND):

I think my comments were more directed as a warning to management; not to only depend on parametric correlations for determination of jet induced effects. Elimination of model testing may save a couple of bucks. But I think you are making a big mistake if you don't get involved in model testing once you determine the kind of configuration you are interested in pursuing. The model testing is still desirable and quite necessary.

K. T. YEN (NAVAL AIR DEVELOPMENT CENTER):

May I make a comment? At our own internal meeting, the boss was asking us: "Is there a rational, reliable method available for the prediction of lift losses? If not, do we have a plan for development of this thing?" Nobody could answer his questions.

ROBERT WEINRAUB (NAVAL AIR SYSTEMS COMMAND):

No, we were not there. We have made a couple of attempts to derive some quasi-engineering type methodology beyond the parametric stage, but we have

not been too successful. My personal opinion is that I don't foresee this coming to fruition beyond parametric types of methods in the foreseeable future. We just seem to be learning something new everyday.

WILLIAM G. HILL (GRUMMAN AEROSPACE CORPORATION):

I have not really a question but a comment. Even though I agree that it will be a long time before we can get to compute everything we want, we can use what knowledge we have now rather than waiting until the end and use it only when everything is perfect. For instance, a designer can look at the individual results and conclusions that we have come to rather than waiting for the great computer program in the sky that will calculate everything. We have already achieved a great deal of benefit to design.

ROBERT WEINRAUB (NAVAL AIR SYSTEMS COMMAND):

I agree with what you're saying, Bill. The problem is now that we have to find something bigger than a two by four to hit the designer over the head and get his attention and make sure he pays attention to the kinds of things that we have found.

DIRK RENSELAER (ROCKWELL INTERNATIONAL, LOS ANGELES):

I have a feeling that something is still left out and that is the effect of bank angles on the fountain effect; and that is really important where practical application is to be made. The effect of the fountain lift is really limited to what you can obtain in bank angles.

ROBERT WEINRAUB (NAVAL AIR SYSTEMS COMMAND):

Well, I concur wholeheartedly. And here again I'll put on my U.S. Navy aircraft designer and proposal evaluator's hat. The first thing we do when these proposals come in is look at the effect of reasonable bank angles because in severe cases the fountain can miss the airplane completely and you will get nothing from it. Also, for some configurations fountain strength may be sensitive to wind and to some degree to pitch. The work done by Rockwell also indicates some effects of jet edge placement. The work done by McDonnell also indicates that there are some dynamic considerations to be taken into account. This just complicates the problems and I think my original remarks were addressed at the simplest form of the problem.

DICK KUHN (NASA-LANGLEY-Retired):

I just want to add another thought along the line of this discussion. The kind of flows that give us the fountain effect and the favorable lift also gives, for figther-type aircraft, a very hot exhaust which could lead to hot gas ingestion problems which may be really the driving factor in the configuration of the airplane. We have to be careful in trying to optimize the fountain effect, or particularly careful in how we optimize it. Some forms of LIDs or STRAKES on the aircraft bottom may improve the fountain effect but aggravate the hot gas ingestion; whereas some other configuration arrangement may help the problem. I think really that the two problems, hot gas ingestion and the aerodynamic suckdown or fountain flows ought to be worked together because the same flows are involved and they have counteracting effects on the performance of the airplane.

ROBERT WEINRAUB (NAVAL AIR SYSTEMS COMMAND):

You're absolutely right and the only reason I confined my remarks to the force side of the problem is because that's what the session seemed to want to cover. But yes, they're synergistic except not in an additive sense, probably in a subtractive sense; so we have to be very careful about looking at the whole problem.

DICK KUHN - Retired (NASA-LANGLEY RESEARCH CENTER):

That wasn't a comment on his review; that was a comment on the state of things.

DAVE HICKEY (NASA-AMES RESEARCH CENTER):

I would like to add one or more comments in that vein and that is, the fountain flows cause buffeting on the airplane. In past airplanes that have flown, the pilots have objected to that; they don't like it. So these fellows are saying all parts of the fountain flow are not good.

MAX PLATZER (NAVAL POSTGRADUATE SCHOOL):

Any other comments? Well, I now turn it over to Dave Hickey to review Session III.

SESSION III

DAVE HICKEY (NASA-AMES RESEARCH CENTER):

I could not find a single thread through the topics in this session, so I thought I would review each paper quickly. But first, I would like to thank Professor Platzer and his NADC co-sponsor, Campbell Henderson, for organizing this workshop. I think it has been very valuable and worthwhile. Also, I would like to compliment that neglected man, the projectionist, because I can't remember him making a mistake in three days and that is really exceptional.

Dr. Erickson described the possible use of the adaptive wind tunnel wall technique for reducing or eliminating wall corrections in V/STOL tunnels. This technique has been used in two-dimensional transonic wind tunnels with some success but has not been applied to a three-dimensional case to my knowledge. Certainly, these ideas have a lot of merit. However, if you look at the plumbing involved with the simpler two-dimensional cases, the three-dimensional problem looks difficult at best. Furthermore, it would rule out the use of an external balance. Whether you have adaptive walls or not, the wave of the immediate future in V/STOL wall corrections may be a combination of flow models, measuring the important boundary conditions, and computer coupling so that you have near real time improved wall corrections.

Emmett Omar described results of tests in the Boeing nine by nine wind tunnel. This test could probably have benefited from a correction scheme like that described above. At any rate, Emmett had a very complicated powered model, and got exceptional data during the development of the Boeing Type A concept.

Culpepper and Murphy described the development of a new type of flight simulator which was the Langley Lunar Lander modified to a VTOL dynamic simulation device. If we look back a little bit in history, to see how this came about, the scheme was chosen for the XFV-12 because pilot familiarization was necessary, and if aircraft dynamics were properly simulated this would be a bonus. Furthermore, there wasn't much data on the XFV-12 that could be used as input for conventional simulators. Thus, we have a case of a unique simulator being developed for the XFV-12. It may prove to be a valuable tool and just how much it will be used will probably depend on the success of the VTOL idea and how successful other people are in providing proper inputs for more conventional simulators.

I have to agree with Bob Weinraub that Dave Spong did an excellent job in isolating the fountain forces and providing the dynamic data to simulate shipboard. The one thing that bothered me about this and all other small-scale data that I have seen before and since, is the possibility of turbulence having a major influence. It perhaps should not be a surprise because Rich Margason pointed out some time ago that when the jet profile was changed the mixing length and suckdown force was changed. And, of course, the jet profile and turbulence are interrelated. This tends to imply that the forces you measure in ground effect are a function of that profile and its turbulence. If an answer that applies to an airplane is desired then it may be necessary to simulate that airplane's exhaust profile.

Paul Bevilaqua gave the paper for Cole. They are going to start an experiment to measure jet flap thrust recovery at high momentum coefficients. I wish them luck. I think it's probably a hard job.

Joe Martin presented a case for vertical attitude take-off and landing airplanes. They are certainly very interesting, but superiority to the horizontal attitude VTOL has not been conclusively proven. However, it seems Joe has put together a technology program which will supply some of the answers and make it possible to give considered judgments as to how good the VATOL idea really is.

Jim Nichols was slipped into my session and I was glad to have him. He talked about propulsive lift with low aspect ratio wings which is probably an area that could use quite a bit of work and is relatively unstudied. In the fifties and early sixties there was a lot of work done on conventional high lift devices on low aspect ratio wings. This is how the F-4 and the F-100 series fighter aircraft were equipped with boundary layer control. But with powered lift and the higher lift loadings required for STOL application, there may be a whole different ball game. Perhaps the biggest unknown is whether we have a customer in the military for the technology.

Then, finally, Professor Adler gave his paper and K. T. Yen has discussed that and I can't add to that discussion except the observation that perhaps a way should be found to check out his jet model and carry its development further.

I would like to comment on some other aspects of the meeting, if you will bear with me for another minute. I am used to dealing with Reynolds numbers in the millions and when somebody works at a Reynolds numbers of 100 I don't know what to make of it. Solutions of the Navier-Stokes equations probably

have to be done and I realize it's beyond the computer power we have to go to high Reynolds numbers, but we must be cautious about interpretation of the results that come out of these solutions.

Another situation that gives me concern is the use of small-scale data to correct potential flow theory when we don't know whether that small-scale data is really any good. My understanding is that in the past there were wide discrepancies in small-scale data because of the flow conditions in the nozzles and so researchers concentrated on getting a clean top-hat profile jet so that there would be some consistency to the data. This approach is fine, but tends to yield academic results, because as any of you that have seen engine exhaust profiles know, they are not top-hat profiles. This can affect ground effects and jet in cross flow results. Since these are at the core of V/STOL aerodynamics we need to get into that problem and find out whether it really exists because it affects a lot of what we heard at this meeting.

MAX PLATZER (NAVAL POSTGRADUATE SCHOOL):

Thank you very much, Dave. Any comments?

DICK KUHN - Retired (NASA-LANGLEY RESEARCH CENTER):

It looks like I always have a chance to respond to Dave Hickey on some point or other. Just a comment on the problem of turbulence. You mentioned Rich Margason's work that showed a large effect of turbulence. This work involved a really major difference in turbulence and it was related to the out-of-ground effect lift losses. As I recall, and I will have to admit I want to go back and check, my recollection is that when we put those same models in ground effect we did not see anywhere near those kind of differences. I was very surprised to hear all of the comments on the turbulence here at this meeting for the ground effect case because I did not think we had that problem in ground effect—we had it in out-of-ground effect but I did not think we had it in ground effect so we need to go back and loo'- at some of the early tests.

DAVE HICKEY (NASA-AMES RESEARCH CENTER):

I think that's probably a good idea. I guess too, I am not sure it is turbulence that we are really talking about here as being the problem. We are probably talking about jet mixing, which is related to turbulence but it is not turbulence directly. I suspect you can still have a top-hat profile with a highly turbulent jet, for example.

DICK KUHN - Retired (NASA-LANGLEY RESEARCH CENTER):

In fact, Rich Margason's work showed some fairly large differences in the profile with very little difference in the entrainment and the suckdown. On the other hand there were tests without too big a difference in the profile but with different plenum chambers he got some fairly large differences. It was turbulent mixing but it wasn't classic turbulence. It was more pulsing of the jet which acted to rapidly entrain air that was occuring in those tests. So it was a very bad plenum chamber upstream of the jet that created that problem.

MIKE MENDENHALL (NIELSEN ENGINEERING):

Dave, I will agree with you on the turbulence and effects of swirl in the exhaust, but we at Nielsen have done considerable looking into these effects and we find that there is very little, good, systematic data arcund on these effects. I mean really good, high quality, systematic data in which only one parameter is changed at a time. Our recent literature searches have shown that there is almost not enough around for use to get a real good understanding of the problem, and I think that is an area that could be looked at by some of the experimental people.

K. T. YEN (NAVAL AIR DEVELOPMENT CENTER):

I just wonder about the turbulence problem. When you have a free jet, the turbulence decay and mean velocity profile really do not depend too much on the Reynolds number at the jet exit. The turbulence you are talking about may not be really turbulence in the true sense. Actually you may have larger scale disturbances. I don't think that it is turbulence. But I do agree with you that Dave Spong did a very good job. Also, I was very much interested in the moving deck problem. If you have a moving deck not only you have free jets but you also have wall jets, and the Reynolds number may become a significant parameter.

DAVE HICKEY (NASA-AMES RESEARCH CENTER):

All I am saying is the possibility is there and it is not too difficult to believe that there is a problem. We ought to do the work necessary to establish the presence or absence of the problem.

MAX PLATZER (NAVAL POSTGRADUATE SCHOOL):

Any other comments?

ROBERT WEINRAUB (NAVAL AIR SYSTEMS COMMAND):

The thing we have to be careful here is we know that these phenomena are configuration dependent and we have to be careful in drawing any kind of general conclusions from specific series of tests. Unfortunately, we are drawing on a very limited data sample and so we have to qualify any kinds of large conclusions like that on turbulence. We have to recognize the possibility that these things really do exist and can be dominating effects but let's keep things in perspective and not run off hay-wire. That's all I'm saying.

DAVE HICKEY (NASA-AMES RESEARCH CENTER):

To respond to Mike Mendenhall, part of what I was suggesting was that the appropriate people need to give this serious thought and lay out a program to answer the questions. We should avoid finding a problem when we don't have one. I think the possibility is there and that it is not too difficult to believe that there is a problem. We ought to do the work necessary to validate the existence of the problem and then lay out a program to quantify the problem and modify prediction techniques.

MAX PLATZER (NAVAL POSTGRADUATE SCHOOL):

Any other comments?

DAVE SPONG (MCDONNELL AIRCRAFT COMPANY):

To amplify what Bob Weinraub said. One thing I did not show from the moving deck test was a comparison of the supersonic and the subsonic configuration data. We found significant differences in the induced forces between the two configurations in that, relative to the static data, the subsonic configuration had improved fountain forces while the supersonic configuration had degraded suckdown forces. This seemed to correlate with the observation that the subsonic configuration induced forces were "fountain" dominated while the supersonic configuration induced forces were "suckdown" dominated.

ROBERT WEINRAUB (NAVAL AIR SYSTEMS COMMAND):

I just might add some work and I think we are just getting into this area in conjunction with Dave Hickey's people. This summer we did some tests on the 70%- scale model of McDonnell-Douglas' design and Andy Zalay from Lockheed-Huntsville brought out a laser doppler velocimeter. And although it wasn't

an objective at that time of the program we did some interesting turbulence
studies of the free jet and wall jet and fountain region and I think Andy is
going to present some of these results at the conference in Las Vegas this
summer. So I think we have made the first half-step in this area although it
wasn't our intention orginally to do that.

MAX PLATZER (NAVAL POSTGRADUATE SCHOOL):

Any other comments? Now I would like Norbert Stockman to review Session
IV.

SESSION IV

NORBERT STOCKMAN (NASA-LEWIS RESEARCH CENTER):

I plan to give summaries of each paper and then a selection of a few spe-
cific items that I thought were particularly interesting or important. I want
to emphasize that both the summaries and the selections are going to be based
on my own subjective interest because of my interest and background and, more
negatively, because of my ignorance on some of the topics that were discussed
in my session. I found three main topics or threads in my session and for
this summary I regrouped the papers according to those. The topics are:
(1) inlets, (2) nozzles and (3) forces and moments.

The first paper, my own paper, was mainly a potpourri of recent and
future applications of theoretical analysis to V/STOL inlet problems.

The second paper by Jan Syberg was a comparison of model and full-scale
inlet separation characteristics and I will go into that a little more later.

The next paper by DeLany gave the development of a tri-furcated inlet, an
inlet that has two more or less conventional inlets on the side of the fuse-
lage and then a large auxiliary inlet on the top of the fuselage. He showed
that this gives excellent static performance and satisfactory low speed per-
formance up to a moderately high angle of attack.

The next paper by Burley, Johns and Diedrich was a summary of recent
experimental tests and verified methods of achieving very high angle of
attack performance (and I will also go into that in a little more detail
shortly).

The final paper on inlets is also the first paper on nozzles. Dennis
Hawk used a simple analysis to indicate that maybe you can take the disad-
vantages, that is the distorted profiles, caused by an S-duct inlet, and

combine those with the disadvantages, mainly the distorted profile induced by a deflected nozzle, so that they partially cancel each other and give you a better distribution than either alone at the fan location.

The other nozzle paper by L. D. Miller provided an experimental data base for vented deflector nozzles. It covered a wide range of geometric variables and operating conditions.

The final two papers dealt largely with forces and moments, the one by Kress discussed the theoretical method for calculating forces and moments on V/STOL inlets and presented results for inlets at various operating conditions.

The paper by Betzina and Falarski gave experimental forces and moments on a large-scale tilt-nacelle propulsion system at various operating conditions and compared those results with annular airfoil data. I think it would be interesting to compare the theoretical results of Kress' paper with the experimental results of this paper.

Now a few detailed comments. Figure 18 of Jan Syberg's paper indicates that at some conditions the 1/3-scale model inlet gives better performance than the full-scale. This was a surprising result and I think it is a very important result, and I would like to go back to Figure 9 of Syberg's paper where he shows the conventional separation bounds for the two inlets at a couple of different freestream velocities. The thing that I think is interesting here is that the model-scale inlet curves are concave upward whereas the full-scale curves are concave downward. If you extrapolate all these curves you go into regions right on this curve where the model data looks better - more favorable - than the full-scale. So there is something different about the full-scale and we clearly need more full-scale inlet separation bounds and there is a lot more study that needs to be done here. I would also like to see some theoretical study of the boundary layer characteristics at both these scales to see if we can discover what is really happening.

Next, let's look at Figure 8 from the paper by Burley, Johns and Diedrich. I think this is an extremely important result here: This is a summary of a lot of testing that is being done at Lewis fairly recently. First of all, the flow conditions are given at the top. This is for one flow condition where it shows the angle of attack at which separation first occurs plotted versus contraction ratio. Contraction ratio is the first thing people started increasing to get high angle of attack performance and it's an easy to do but it does have a cruise penalty and what this shows is that you can achieve a lot higher angle of attack performance with other means of changing the geometry or

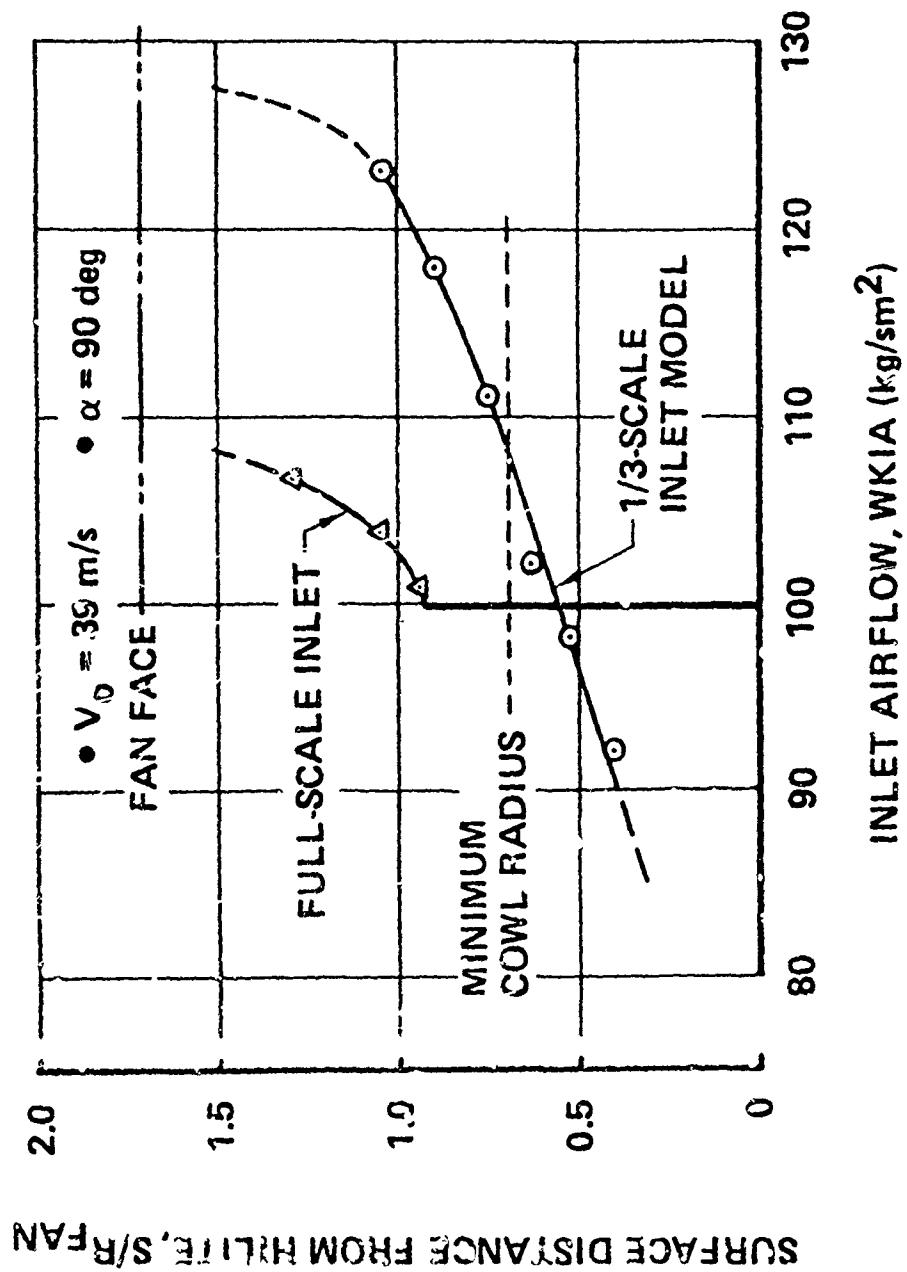FIG. 18 — DIFFUSER SEPARATION CHARACTERISTICS IN SMALL- AND LARGE-SCALE INLET MODELS

FIGURE 8 · COMPARISON OF INLETS
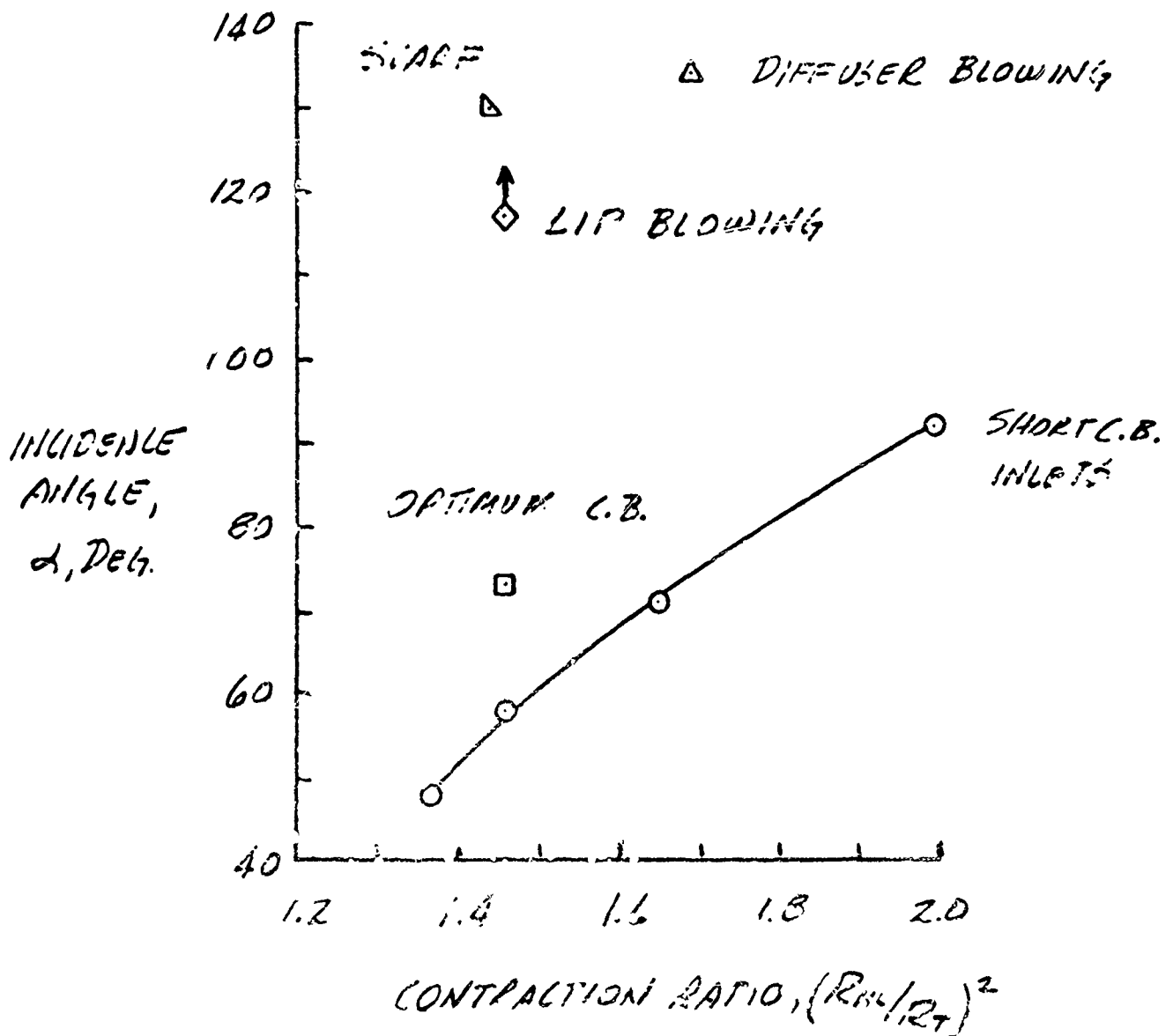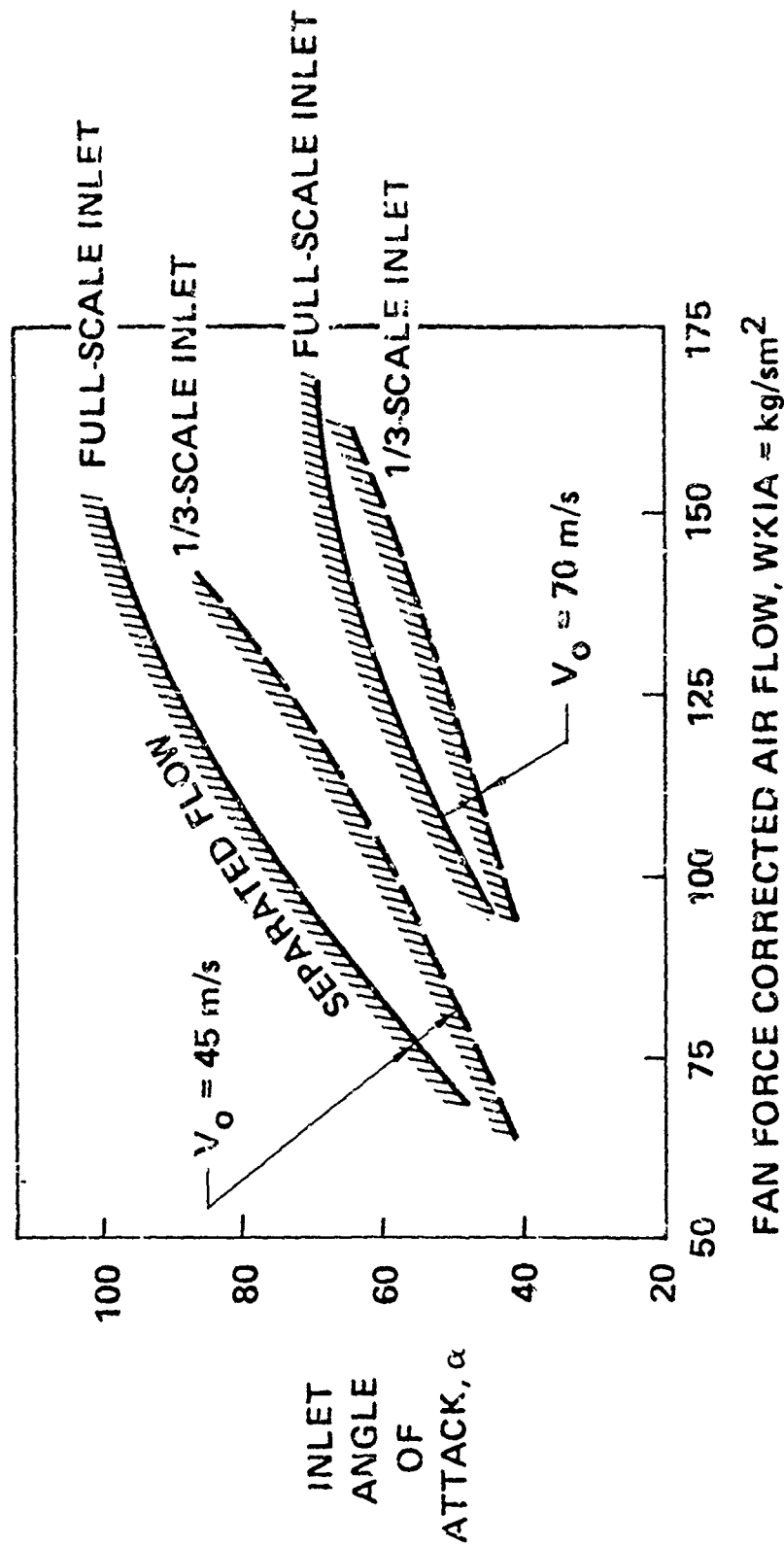
$V_0 = 41 \ m/sec \ (80 \ KT.)$

$M_T = 0.45$

FIG. 9 — SEPARATION BOUNDARIES FOR FULL-SCALE AND 1/3-SCALE TILT-NACELLE INLETS

controlling the boundary layer.

For example, a simple thing like moving the center body location until you find an optimum gives you an improvement equivalent to a much higher contraction ratio. We don't know the exact cruise penalty of all these things, but it seems to me a center body at a different location probably would not have any cruise penalty. Another thing we found out with some preliminary theoretical results on the center body study is that by getting the center body in the proper position you can eliminate diffuse separation almost completely, at least for certain flow conditions, and you can delay lip separation almost indefinitely by tripping the boundary layer to turbulent sooner than it would itself.

Now, consider the lip blowing; this is a recent test that indicates tremendous improvement. The diffuser blowing is another thing that gives tremendous improvement. Now both of these things cost you something, of course, and you don't know how to evaluate that penalty.

The scarf inlet is another very interesting one. It looks like it really has possibilities. The scarf inlet is an inlet where the lower lip, which on a tilt-nacelle would be the forward or windward lip, sticks out further than the upper lip or leeward lip. This inlet was originally conceived as a noise suppression device because it d' ects and refracts the noise upward. And when it was tested in a wind tunnel it showed surprisingly high angle of attack capability. But at any rate, that has some penalties at static operation and we don't know its cruise penalties yet.

I think what we need is some kind of a curve like this with the cruise and other penalties quantified so we can evaluate these various concepts and choose an optimum configuration.

Finally, consider Figure 6 from the paper on the forces and moments on a tilt-nacelle by Betzina and Falarski. They found that for power off the data on this nacelle - this propulsion-system agreed tremendously well with annular airfoil data. And it looks to me like it would be worthwhile to try to predict the curves with the power on just using the annular airfoil data and the jet coefficients.

MAX PLATZER (NAVAL POSTGRADUATE SCHOOL):
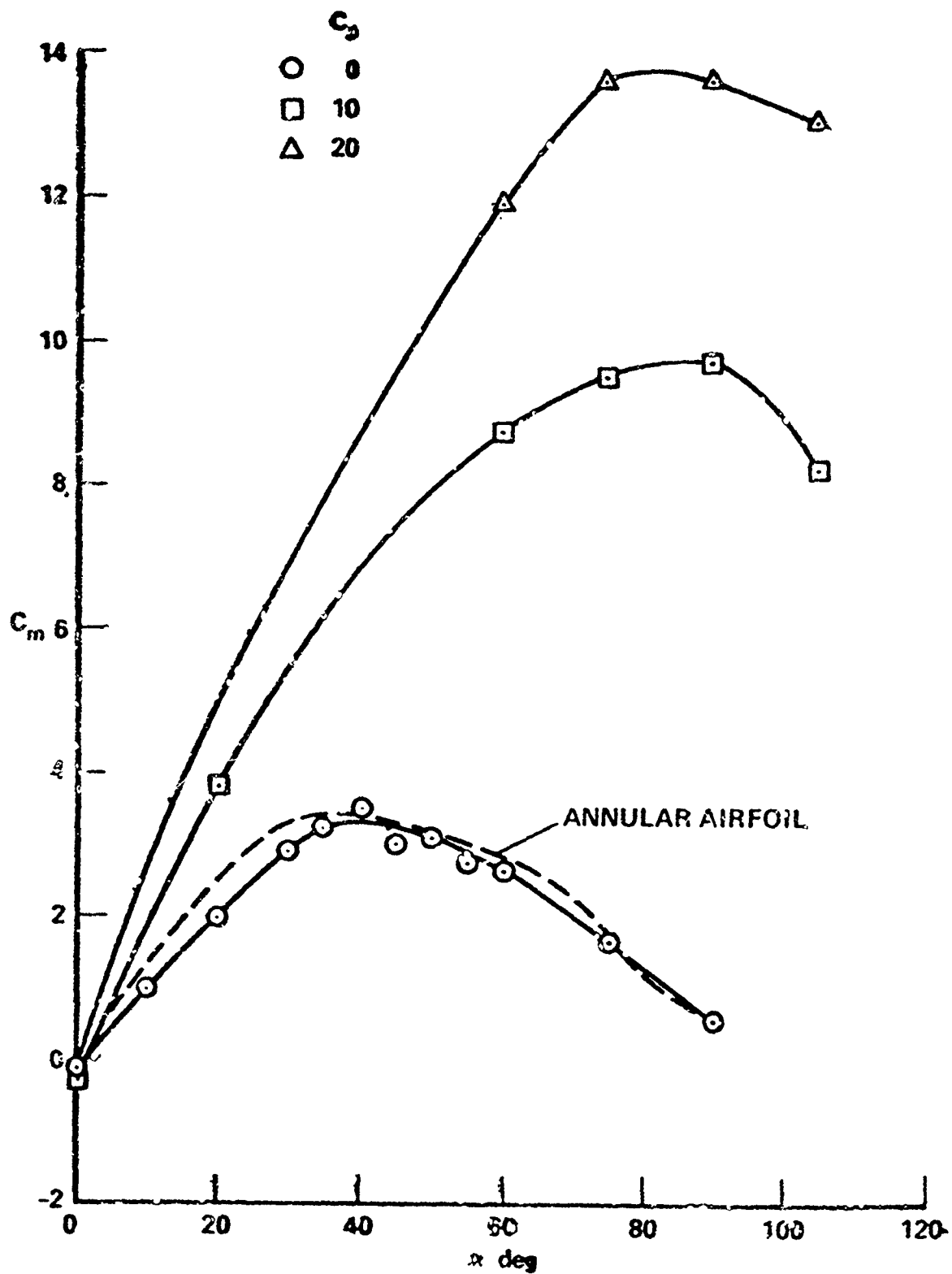
Any comments? Dick Kuhn, you are next.

Figure 6. — Pitching Moment versus Angle of Attack

DICK KUHN - Retired (NASA-LANGLEY RESEARCH CENTER):

First, Session V had several threads, or at least I have grouped the papers
in several groups. Even though Dave Hickey has already reviewed Jim Nichols'
paper, I have included it in my remarks because it ties in with a couple of
other papers. I am not going through the papers, by the way, in the order of
presentation. The first three papers I will discuss were those given by
Jim Nichols. Then I am going to review the papers by Ted Mark and Y. T. Chin
because they all relate to STOL performance and blown flap systems. Jim
pointed out the importance of the problems created by the span limitations on
Navy aircraft.

In efforts at achieving a high lift, he presented results of a plan that
is pretty comprehensive in trying to get a data base on configuration aspect
ratios of three to five using several high-lift systems, i.e., upper-surface
blowing, circulation control and double slotted flaps. The other thing he
brought in for consideration was the possibility of using tip devices for
improving the cruise efficiency as well as the high-lift performance. This is
a pretty wide open area, well worth exploring. My comment is that their effec-
tiveness is apt to be very dependent on the span load distribution on the wing,
particularly the load distribution near the tip. This has been found out in
past work and I think the fellows at David Taylor are aware of that. The
other thing he reviewed was the basic CCW wing. This is quite an impressive
program. They got some rather good field length reductions with an internally
blown system. It is a concept that can use bleed air, and therefore is
restricted, I would think, to aircraft that require pure jets or very low
bypass ratio engines; that is, engines that can supply a fairly large
quantity of bleed air. In other words it could be applicable to fighter type
aircraft. However, when you get to transport type aircraft such as the S-3
class which have bypass ratios of like 6 and fan pressure ratios like 1.5,
you can't really afford to bleed the engine. That is where we get driven
into the things like the YC-14, that Mark reviewed, and the expanding duct
flap that Y. T. Chin reviewed. Ted Mark gave us a very good review of the
practical problems of developing an airplane; the need for very careful plan-
ning and the detailed testing in the development program of the upper surface
blowing YC-14, particularly such things as the nozzle wing interaction prob-

lems. The problems of the boat tail design that are required to get the flow to turn to spread on the wing was well described.

The paper by Chin described an interesting concept in that he is trying to use very high bypass ratio engines, and take the fan flow and duct it into the flap. It needs an expanding duct on the flap to get a passage large enough to pass that air. Once the air is in and distributed across the span he gets, what I would expect, the performance of a good well-distributed internally blown flap system. My only concern is the possibility of duct loss problems when you're dealing with this kind of fan pressure ratio. This could be a problem and will have to be carefully watched.

The next two papers by Stumpfl and Falarski reviewed, what I might call, a derivative of the upper surface blowing concept for fighter aircraft. It was pointed out that for that class of aircraft they had to use a CD nozzle that has already deflected the flow a considerable amount to get the turning, but the combination of that and spanwise blowing produced fairly significant lift increases. I was particularly impressed with spanwise blowing producing about as much lift increment as the nozzle flap system itself. The resulting configuration should have a good cruise maneuverability as well as short take-off and landing capability. Maneuverability was the thing that drove the configuration at the beginning.

Falarski's review, of the 40 x 80 test of that same type of configuration verified the high lift but also indicated that the configuration at this early stage in their test program was highly unstable. They are going on to try to minimize these problems.

Then switching to the augmentors: there were three papers on augmentor concepts. Garland from De Havilland reviewed the longitudinally situated fuselage mounted augmentors. It appears that in the boiler plate configuration he tested, he achieved a very good augmentation ratio. The low interferences in transition cannot be as surprising as he was indicating because it's been shown in the past that high aspect ratio longitudinal orientation of jets does reduce the interference and, of course, the wing is quite small relative to the jet, so maybe everything is working together for us for a change.

I guess there is a concern with the practical application of these concepts as occurred in both the XV-4B and the XFV-12A. As I recall, the augmentor worked out pretty well in the boiler plate configuration, even at a large scale, but when they got to the practical airplane configuration, things

deteriorated. I think that will be the point that has to be watched very carefully and we need to go back and study what happened to those configurations to avoid those problems.

The next two papers were on the theoretical aspects (and really K. T. ought to be giving this. I'm not quite up to this area). Dillenius' and Duvvuri's work indicated to me that there's still progress being made in developing this analytical tool but it has a considerable way to go yet. One thing that impressed me was the problems that Dillenius is having in comparing his results with model tests, and his pointing out that there were separation points on the model. This reminded me that for a lot of these analytical techniques, if you are going to try to make verification tests, it is very difficult to do it on a practical airplane configuration in which all the detailed local configuration variables are built into it. What is really needed are specific models set up tailored to the analytical treatment so that you can find out that what you are dealing with is an analytical problem rather than an experimental problem. One should try to minimize the number of configuration differences that are involved in making these kinds of comparisons.

The last two papers to touch on were those by Lacy (the first paper in the session) and the NASA-Ames paper, (the last paper in the session). These papers, particularly the one by Lacey related largely to non-V/STOL aspects of fighter type of aircraft and I think serves to remind us that V/STOL capability is not an end in itself, but merely a capability to bring the airplane to the point where it can carry out a mission. Sometimes we get carried away with the problems and the details of just trying to get the V/STOL capability.

Lacey stressed the configuration's central aspects for maneuverability. These are not necessarily conflicting with V/STOL, in fact, for a lot of conditions, particularly controllability at high angle of attack maneuvering features tie in very well with V/STOL and may be a real plus.

Finally, Bencze reviewed a very comprehensive program involving several models which used propulsion simulators to look at the high-speed performance of a V/STOL fighter concept. He very rightly started out with a program to determine and demonstrate whether or not you really need these simulators. I think that their use may be very specialized. We are going to have to look very carefully at that. I think there is a lot of good work that can be done without the need for propulsion simulation techniques. I think that's really all I have to say on this session.

MAX PLATZER (NAVAL POSTGRADUATE SCHOOL):

Any questions or comments?

JIM NICHOLS (DTNRDC):

I agree whole-heartedly with all the good things you said. I just want
to comment on one thing — the bleed air situation. I think these days, par-
ticularly with avionics systems cooling requirements and other air supply
requirements, there is a strong possibility that auxiliary power units which
have to be in the aircraft anyway, all are going to be adequate to supply
the bleed-air that is needed for the CCW operation.

DICK KUHN - Retired (NASA-LANGLEY RESEARCH CENTER):

That is a good point. It also reminds me that there are some studies
going on within the engine industry looking at an engine to produce high-bleed
ratio up to 20% bleed which was unheard of a few years ago. But these are
just studies at this point. I don't know of anybody seriously going about
building one but there are possibilities to get air from other sources.

MAX PLATZER (NAVAL POSTGRADUATE SCHOOL):

Any other comments? Any other remarks by the Chairmen? Are there any
other topics within the framework of V/STOL aerodynamics that have not been
covered that you want to bring up at this point? Now is your chance.

DICK KUHN - Retired (NASA-LANGLEY RESEARCH CENTER):

I guess one of the things that impressed me at this workshop were the
several new concepts and ideas that came up. This is always good that we
are still looking for ways of doing the job right and best, but it must be
confusing to the decision makers. They are often not engineers and not
really able to follow all the reasons for all the various types of configu-
rations that are being kicked around. I think somehow we, as a community,
have to find some way to focus better on the military needs and somehow
narrow the fields of all these things that are going on. We have to try to
identify the concepts that will do the most jobs for the least risk and
concentrate more effort in that area. This was an aerodynamics workshop
and therefore we could not get much into the user's needs and so forth, but
I was wondering if maybe the proper mechanism for a future workshop of this
type is to organize around military missions. Spur fighter for one, ASW-AEW
types for another. Perhaps, we should get somebody to come in to discuss

1036

the needs in that area and then have papers that relate to that. This might be a mechanism to focus our thinking and our work and also get a little more dialogue between the users and people that are trying to develop this technology. I guess I will throw it out to see if I could get a fight started.

MAX PLATZER (NAVAL POSTGRADUATE SCHOOL):

Well, I think you'll get something from Bob Weinraub.

ROBERT WEINRAUB (NAVAL AIR SYSTEMS COMMAND):

It's a chicken or egg situation. And about the only thing I can say is that military requirements don't come down from the mountain on two tablets. It's a very iterative process; someone gets a stupid idea or brilliant idea and all of a sudden you're designing to that requirement. Based on the results of the first aircraft design the requirement may be modified in order to obtain a more attractive "compromise aircraft." It is quite a nebulous area. I don't project too much success. It's a good comment but I do not see a lot of success for it.

MAX PLATZER (NAVAL POSTGRADUATE SCHOOL):

Gentlemen, we estimated that we would finish by four o'clock. It is 3:55. Excellent planning it seems to me. I would like to thank in particular the authors for their contributions. I thank very much the session chairmen for the work they have been doing and for their summaries. In particular, further thanks to the audience for the wonderful cooperation and patience. I also thank the operator. I hope he has everything on tape. If not, I'll get a heart attack. And last by no means least, I would like to thank two ladies whom you have met and who otherwise largely stayed in the background. They have done a lot of work in making this workshop a success. They are Evelyn and Janice. They helped me in a lot of matters in preparing for the workshop and, of course, will also contribute to the editing task.

REPORT DOCUMENTATION PAGE		READ INSTRUCTIONS BEFORE COMPLETING FORM
1. REPORT NUMBER	2. GOVT ACCESSION NO.	3. RECIPIENT'S CATALOG NUMBER
4. TITLE (and Subtitle) V/STOL AIRCRAFT AERODYNAMICS, PROCEEDINGS OF A WORKSHOP VOLUME II		5. TYPE OF REPORT & PERIOD COVERED Workshop Proceedings
		6. PERFORMING ORG. REPORT NUMBER
7. AUTHOR(s) C. Henderson and M. Platzer (Editors)		8. CONTRACT OR GRANT NUMBER(s)
9. PERFORMING ORGANIZATION NAME AND ADDRESS Naval Postgraduate School Monterey, CA		10. PROGRAM ELEMENT, PROJECT, TASK AREA & WORK UNIT NUMBERS
11. CONTROLLING OFFICE NAME AND ADDRESS Naval Air Development Center Warminster, PA		12. REPORT DATE May 16 - 18, 1979
		13. NUMBER OF PAGES 471
14. MONITORING AGENCY NAME & ADDRESS(if different from Controlling Office)		15. SECURITY CLASS. (of this report) UNCLASSIFIED
		15a. DECLASSIFICATION/DOWNGRADING SCHEDULE

16. DISTRIBUTION STATEMENT (of this Report)

Unlimited

17. DISTRIBUTION STATEMENT (of the abstract entered in Block 20, if different from Report)

18. SUPPLEMENTARY NOTES

19. KEY WORDS (Continue on reverse side if necessary and identify by block number)

V/STOL Aircraft, Low Speed Aerodynamics, V/STOL Testing, Powered Lift Systems, Jet Flap, Transition Aerodynamics, Propulsion System/Airframe Interactions, Ground Interference Effects

20. ABSTRACT (Continue on reverse side if necessary and identify by block number)

This report contains the proceedings of the Workshop on V/STOL Aircraft Aerodynamics held at the Naval Postgraduate School on May 16 to 18, 1979. This workshop was sponsored by the Naval Air Development Center. The workshop participants included representatives from industry, government, universities and abroad.

DD FORM 1473 EDITION OF 1 NOV 65 IS OBSOLETE
S/N 0102-014-6601 |

GPO 693-487/48